National Library
of Canada

Bibliothèque nationale
du Canada

Canadian Theses Service

Service des thèses canadiennes

Ottawa, Canada
K1A 0N4

NOTICE

The quality of this microform is heavily dependent upon the quality of the original thesis submitted for microfilming. Every effort has been made to ensure the highest quality of reproduction possible.

If pages are missing, contact the university which granted the degree.

Some pages may have indistinct print especially if the original pages were typed with a poor typewriter ribbon or if the university sent us an inferior photocopy.

Reproduction in full or in part of this microform is governed by the Canadian Copyright Act, R.S.C. 1970, c. C-30, and subsequent amendments.

AVIS

La qualité de cette microforme dépend grandement de la qualité de la thèse soumise au microfilmage. Nous avons tout fait pour assurer une qualité supérieure de reproduction.

S'il manque des pages, veuillez communiquer avec l'université qui a conféré le grade.

La qualité d'impression de certaines pages peut laisser à désirer, surtout si les pages originales ont été dactylographiées à l'aide d'un ruban usé ou si l'université nous a fait parvenir une photocopie de qualité inférieure.

La reproduction, même partielle, de cette microforme est soumise à la Loi canadienne sur le droit d'auteur, SRC 1970, c. C-30, et ses amendements subséquents.

NL-339 (r. 88/04) c

Canada

UNIVERSITY OF ALBERTA

ENTRANCE LENGTH AND BOUNDARY LAYER GROWTH IN OPEN CHANNELS

BY

©

MARTIN JASEK

A THESIS
SUBMITTED TO THE FACULTY OF GRADUATE STUDIES AND
RESEARCH IN PARTIAL FULFILLMENT OF THE REQUIRENTS
FOR THE DEGREE OF MASTERS OF SCIENCE

DEPARTMENT OF CIVIL ENGINEERING

EDMONTON, ALBERTA
SPRING, 1992

National Library
of Canada

Bibliothèque nationale
du Canada

Canadian Theses Service

Service des thèses canadiennes

Ottawa, Canada
K1A 0N4

The author has granted an irrevocable non-exclusive licence allowing the National Library of Canada to reproduce, loan, distribute or sell copies of his/her thesis by any means and in any form or format, making this thesis available to interested persons.

The author retains ownership of the copyright in his/her thesis. Neither the thesis nor substantial extracts from it may be printed or otherwise reproduced without his/her permission.

L'auteur a accordé une licence irrévocable et non exclusive permettant à la Bibliothèque nationale du Canada de reproduire, prêter, distribuer ou vendre des copies de sa thèse de quelque manière et sous quelque forme que ce soit pour mettre des exemplaires de cette thèse à la disposition des personnes intéressées.

L'auteur conserve la propriété du droit d'auteur qui protège sa thèse. Ni la thèse ni des extraits substantiels de celle-ci ne doivent être imprimés ou autrement reproduits sans son autorisation.

ISBN 0-315-73188-5

Canadä

UNIVERSITY OF ALBERTA

RELEASE FORM

NAME OF AUTHOR Martin J. Jasek

TITLE OF THESIS Entrance Length and Boundary Layer Developement in Open Channels

DEGREE Master of Science

YEAR THIS DEGREE GRANTED Spring, 1992

Permission is hereby granted to THE UNIVERSITY OF ALBERTA LIBRARY to reproduce single copies of this thesis and to lend or sell such copies for private, scholarly or scientific research purposes only.

The author reserves other publication rights, and neither the thesis nor extensive extracts from it may be printed or otherwise reproduced without the author's written permission.

Signed : Martin Jasek

Permanent Address : 11548-139 St
Edmonton, Alberta
T5M 1R7

Date: April 15/1992

UNIVERSITY OF ALBERTA
FACULTY OF GRADUATE STUDIES AND RESEARCH

The undersigned certify that they have read, and recommend to the Faculty of Graduate Studies and Research for acceptance, a thesis entitled ENTRANCE LENGTH AND BOUNDARY LAYER GROWTH IN OPEN CHANNELS submitted by MARTIN J. JASEK in partial fulfilment of the requirements for the degree of MASTER OF SCIENCE in CIVIL ENGINEERING.

Supervisor: Late R. Gerard

N. Rajaratnam

P. Steffler

K. C. Cheng

K. C. Cheng

Date:

This thesis is dedicated in memory of

Dr. Robert Gerard (Larry)

Abstract

An experimental and an analytical investigation was conducted on the development of the turbulent boundary layer at the entrance of wide open channels.

Experiments were conducted in a wide rectangular flume to measure the boundary layer growth and the entrance length in a smooth and rough channel for subcritical flow. Velocity profiles were taken not only along the centreline but in the across-channel direction to account for the presence of strong secondary flow structures which caused the boundary layer development to vary strongly across the channel.

The analytical portion of the study consisted of the numerical solution of the Kármán Integral Equation for the turbulent boundary layer, the Bernoulli equation for the free surface, and the continuity equation for the entire flow. The effect of the bed roughness and Reynolds number on the shear stress and the shape of the velocity profile was also taken into account. The analytical investigation covered both mild and steep channels. The results for mild channels were generalized and also compared to the experimental portion of the study. The results for the steep channel were generalized and also compared with previously published data.

Acknowledgements

The author wishes to express his sincere gratitude to Dr. R. Gerard for his guidance and advice throughout the course of this study. The author would also like to thank Dr. N. Rajaratnam for providing additional supervision and financial help and Dr. P. M. Steffler for his assistance and advice in both the numerical and experimental portions of this study.

The author would also like to thank S. Lovell and S. Lodewyk for their technical help at the Graduate Hydraulics Laboratory, and his fellow graduate students who offered their opinion and advice.

Finally, I would like to thank Jan Lachoski for her patience and proof reading.

Table of contents

Page

Introduction 1

Chapter

1. Literature Review 3
    - 1.1 The Karman Integral Equation for the boundary layer 3
    - 1.2 Solutions for boundary layers with zero pressure gradients 5
        - 1.2.1 Boundary layer on a smooth plate 5
        - 1.2.2 Boundary layer on a rough plate 8
    - 1.3 Boundary layers in open channels 9
        - 1.3.1 Boundary layers in horizontal and mild channels 10
        - 1.3.2 Boundary layers in steep channels 13
    - 1.4 Secondary flow in straight open channels 18

2. Experiments in a mild channel 23
    - 2.1 Experimental arrangement and procedure 24
    - 2.2 Experimental results, analysis, and discussion 31
        - 2.2.1 Smooth channel 31
        - 2.2.2 Rough channel 38
        - 2.2.3 General discussion 44

3. Formulation of the equations for the numerical solution 100
  3.1 The boundary layer in a wide open channel 100
  3.2 Subcritical boundary condition 105
  3.3 Supercritical modifications and boundary condition . 106
  3.4 Comparison of normal depth and shear to that given by the Chezy equation 108
  3.5 Comparison of the zero pressure gradient numerical solution to known solutions 110

4. Numerical solution and results for the mild channel 127
  4.1 Solution technique 127
  4.2 Generalization of results 128
  4.3 Comparison with experiments in mild channel 137
  4.4 Comparison to pipe flow entrance lengths and other channel cross sections 138
  4.5 Sensitivity to inaccurate bed slope and tailgate matching 140

5. Numerical solutions and results for steep channels 193
  5.1 Solution technique 193
  5.2 Further consideration of upstream boundary condition 193
  5.3 Some examples of the numerical solution 197
    5.3.1 Effect of discharge 198
    5.3.2 Effect of channel bed slope 199
    5.3.3 Effect of channel bed roughness 200
  5.4 Comparison to measurements conducted

by Bauer(1954)..201
5.4.1 Bauer's smooth experiment 201
5.4.2 Bauer's rough experiment 203
5.4.3 Concluding remarks on Bauer data comparison 206
5.5 Comparison to κ-ε model by Keller et al (1977) 206
5.6 Comparison with measurements conducted by Ippen (1957) 208
5.7 Comparison to S2 type gradually varied flow profiles 210
5.8 Non-dimensional entrance lengths for depth at spillway crest near critical 213
5.9 Non-dimensional entrance lengths for depth at spillway crest controlled by a sluice gate 215

6. Conclusions and Recommendations 269
6.1 Mild channel experiment 269
6.2 Subcritical numerical solutions 271
6.3 Supercritical numerical solutions 275

References 280

Appendix 1

Experimental data for smooth mild channel 283

Appendix 2

Experimental data for rough mild channel 314

Appendix 3
Tabulation of Bauer(1954) and Delleur(1957) data 346

List of tables

Page

Table 2.1 Summary of experiments in mild channel 47

Table 2.2 Summary of entrance lengths in terms of number of depths for experiment, numerical solution, and zero pressure gradient flat plate solutions. 99

Table 2.3 Summary of entrance lengths as a percentage of the experimental average. 99

Table 3.1 Comparison of uniform flow between the Chezy relation and the numerical solution. 117

Table 3.2 Summary of input variables for the zero pressure gradient boundary layer solution. 118

Table 4.1 Summary of Set 1 numerical results. 145

Table 4.2 Summary of Set 2 numerical results. 152

Table 4.3 Summary of Set 3 numerical results. 159

Table 4.4 Summary of Set 4 numerical results. 166

Table 4.5 Summary of numerical runs to simulate inaccurate bed slope and tailgate matching. 182

Table 5.1 Summary of S2 gradually varied flow comparisons. 211

List of figures

Page

Fig. 1.1 Effect of secondary currents on the velocity distributions in the transverse direction after measurements by Delleur (1957) from his study on boundary layer development in a smooth horizontal channel. 21

Fig. 1.2 Silt deposit streaks on gravel bar left by secondary currents on the Yukon River near Dawson, 1989. 22

Fig. 2.1 Illustration of the effect of secondary flows on the boundary layer growth in the central portion of a wide channel. 46

Fig. 2.2 Experimental setup and coordinate system. 47

Fig. 2.3 Pressure transducer used for measuring velocities. 48

Fig. 2.4 Strip chart recorder used to record voltage from pressure transducer. 48

Fig. 2.5 Sample of strip chart recorder output. 49

Fig. 2.6 Dye indicating the presence of secondary flow cells. 49

Fig. 2.7 Sample of roughness mat used for the rough experiment. 50

Fig. 2.8 Flume and traverse used for the experiments. 50

Fig. 2.9 Example velocity profile showing method of obtaining the boundary layer thicknesses δ_t and δ_i. Also shown is the definition of the vertical coordinate for rough bed. 51

Fig. 2.10 The hydraulic roughness k_s was determined by regression by varying y_d at 0.5 mm intervals. 52

Fig. 2.11 The bed shear stress for the rough experiment was determined by varying u_* and y_d until the lower part of the velocity profile matched the theoretical expression. 52

Fig. 2.12a Typical velocity profiles in the developing portion of the *smooth channel* for different transverse locations. 53

Fig. 2.12b Typical velocity profiles in the developed portion of the *smooth channel* for different transverse locations. 53

Fig. 2.13a Velocity profiles in an area of downwelling (Z = 0.335 m) for different longitudinal locations. *(Smooth channel)* 54

Fig. 2.13b Velocity profiles in an area of upwelling (Z = 0.092 m) for different longitudinal locations. *(Smooth channel)* 55

Fig. 2.14 Evaluation of the Bernoulli equation to help indicate the decay of the potential core and to asses the reliability of elevation and velocity measurements. *(Smooth channel)* 56

Fig. 2.15a Boundary layer thickness based on turbulence criteria plotted in the transverse direction for different longitudinal locations. *(Smooth channel)* 57

Fig. 2.15b Boundary layer thickness based on turbulence criteria plotted in the longitudinal direction for different transverse locations. Also shown is the width averaged δ_t growth. *(Smooth channel)* 58

Fig. 2.16a Boundary layer thickness based on extrapolated intercept method plotted in the transverse direction for different longitudinal locations. *(Smooth channel)* 59

Fig. 2.16b Boundary layer thickness based on extrapolated intercept method plotted in the longitudinal direction for different transverse locations. Also shown is the width averaged δ_i growth. *(Smooth channel)* 60

Fig. 2.17a Comparison of width averaged δ_t and δ_i with the numerical solution and Schlichting's smooth flat plate solution (1934). *(Smooth channel)* 61

Fig. 2.17b Same as Fig. 2.17a except δ_t is interpolated between x=3.0 m and the average location where δ_t reaches the surface. *(Smooth channel)* 62

Fig. 2.18a Displacement thickness plotted in the transverse direction for different longitudinal locations. *(Smooth channel)* 63

Fig. 2.18b Displacement thickness plotted in the longitudinal direction for different transverse locations. Also shown is the width averaged δ_* growth and the numerical solution. *(Smooth channel)* 64

Fig. 2.19a Momentum thickness plotted in the transverse direction for different longitudinal locations. *(Smooth channel)* 65

Fig. 2.19b Momentum thickness plotted in the longitudinal direction for different transverse locations. Also shown is the width averaged θ growth and the numerical solution. *(Smooth channe)*........ 66

Fig. 2.20 Bed shear stress plotted in the transverse direction for different longitudinal locations. *(Smooth channel)* 67

Fig. 2.21 Minimum, maximum, and width averaged bed shear stress plotted in the longitudinal direction. Also shown is the numerical solution and the Schlichting's smooth flat plate solution (1934). *(Smooth channel)* 68

Fig. 2.22a Discharge per unit width as integrated from the velocity profiles plotted in the transverse direction for different longitudinal locations. *(Smooth channel)* 69

Fig. 2.22b Discharge per unit width as integrated from the velocity profiles plotted in the longitudinal direction for different transverse locations. Also shown is the width averaged unit discharge. *(Smooth channel)* 70

Fig. 2.23 Width averaged power law exponent from regressional curve fits of the boundary layer portion of the velocity profiles. Also shown is the numerical solution. *(Smooth channel)* 71

Fig. 2.24 Width averaged momentum and energy correction coefficients. Also shown is the numerical solution. *(Smooth channel)* 72

Fig. 2.25 Width averaged total energy, water surface elevation, and bed elevation. *(Smooth channel)* 73

Fig. 2.26 Width averaged maximum velocity and average velocity. Also shown is the numerical solution. *(Smooth channel)* 74

Fig. 2.27 Width averaged momentum per unit width. Also shown is the numerical solution. *(Smooth channel)* 75

Fig. 2.28a Typical velocity profiles in the developing portion of the *rough channel* for different transverse locations. 76

Fig. 2.28b Typical velocity profiles in the developed portion of the *rough channel* for different transverse locations. 76

Fig. 2.29a Velocity profiles in an area of downwelling (Z = 0.335 m) for different longitudinal locations. *(Rough channel)* 77

Fig. 2.29b Velocity profiles in an area of upwelling (Z = -0.153 m) for different longitudinal locations. *(Rough channel)* 78

Fig. 2.30 Evaluation of the Bernoulli equation to help indicate the decay of the potential core and to asses the reliability of elevation and velocity measurements. *(Rough channel)* 79

Fig. 2.31a Boundary layer thickness based on turbulence criteria plotted in the transverse direction for different longitudinal locations. *(Rough channel)* 80

Fig. 2.31b Boundary layer thickness based on turbulence criteria plotted in the longitudinal direction for different transverse locations. Also shown is the width averaged δ_t growth. *(Rough channel)* 81

Fig. 2.32a Boundary layer thickness based on extrapolated intercept method plotted in the transverse direction for different longitudinal locations. *(Rough channel)* 82

Fig. 2.32b Boundary layer thickness based on extrapolated intercept method plotted in the longitudinal direction for different transverse locations. Also shown is the width averaged δ_i growth. *(Rough channel)* 83

Fig. 2.33a Comparison of width averaged δ_t and δ_i with the numerical solution and Harrison's rough plate (1967) after Granville(1958). *(Rough channel)* 84

Fig. 2.33b Same as Fig. 2.33a except δ_t is interpolated between x=2.0 m and the average location where δ_t reaches the surface. *(Rough channel)* 85

Fig. 2.34a Displacement thickness plotted in the transverse direction for different longitudinal locations. *(Rough channel)* 86

Fig. 2.34b Displacement thickness plotted in the longitudinal direction for different transverse locations. Also shown is the width averaged δ_* growth and the numerical solution. *(Rough channel)* 87

Fig. 2.35a Momentum thickness plotted in the transverse direction for different longitudinal locations. *(Rough channel)* 88

Fig. 2.35b Momentum thickness plotted in the longitudinal direction for different transverse locations. Also shown is the width averaged θ growth and the numerical solution. *(Rough channel)* 89

Fig. 2.36 Bed shear stress plotted in the transverse direction for different longitudinal locations. *(Rough channel)* 90

Fig. 2.37 Minimum, maximum, and width averaged bed shear stress plotted in the longitudinal direction. Also shown is the numerical solution and the Granvill's rough flat plate solution (1958). *(Rough channel)* 91

Fig. 2.38a Discharge per unit width as integrated from the velocity profiles plotted in the transverse direction for different longitudinal locations. *(Rough channel)* 92

Fig. 2.38b Discharge per unit width as integrated from the velocity profiles plotted in the longitudinal direction for different transverse locations. Also shown is the width averaged unit discharge. *(Rough channel)* 93

Fig. 2.39 Width averaged power law exponent from regressional curve fits of the boundary layer portion of the velocity profiles. Also shown is the numerical solution. *(Rough channel)* 94

Fig. 2.40 Width averaged momentum and energy correction coefficients. Also shown is the numerical solution. *(Rough channel)* 95

Fig. 2.41 Width averaged total energy, water surface elevation, and bed elevation. *(Rough channel)* 96

Fig. 2.42 Width averaged maximum velocity and average velocity. Also shown is the numerical solution. *(Rough channel)* 97

Fig. 2.43 Width averaged momentum per unit width. Also shown is the numerical solution. *(Rough channel)* 98

Fig. 3.1 Definition scetch for a boundary layer in a mild channel. 114

Fig. 3.2 Definition scetch for a boundary layer in a steep channel. 115

Fig. 3.3 Modification of the Bernoulli equation for the potential core of the steep slope. 116

Fig. 3.4 Comparison of boundary shear between numerical and *smooth* flat plate solutions. 119

Fig. 3.5 Comparison of boundary layer thickness between numerical and *smooth* flat plate solutions. 120

Fig. 3.6 Comparison of displacement and momentum thickness between numerical and *smooth* flat plate solutions. 121

Fig. 3.7 Comparison of the power law exponent between numerical and *smooth* flat plate solutions. 122

Fig. 3.8 Comparison of boundary shear between numerical and *rough* flat plate solution. 123

Fig. 3.9 Comparison of boundary layer thickness between numerical and *rough* flat plate solution. 124

Fig. 3.10 Comparison of displacement and momentum thickness between numerical and *rough* flat plate solution. 125

Fig. 3.11 Comparison of the power law exponent between numerical and *rough* flat plate solution. 126

Fig. 4.1 Modified Moody Diagram showing typical solution path for the numerical solution of a boundary layer in a open channel. 144

Fig. 4.2 Modified Moody Diagram showing numerical solution paths in Set 1. 146

Fig. 4.3 Dimensionless boundary layer thicknesses for numerical solutions of Set 1. 147

Fig. 4.4 Dimensionless depths for numerical solutions of Set 1. 148

Fig. 4.5 Relative bed shear stresses for numerical solutions Set 1. 149

Fig. 4.6 Relative potential core velocities for numerical solutions Set 1. 150

Fig. 4.7 Power law exponent for numerical solutions Set 1. 151

Fig. 4.8 Modified Moody Diagram showing numerical solution paths in Set 2. 153

Fig. 4.9 Dimensionless boundary layer thicknesses for numerical solutions of Set 2. 154

Fig. 4.10 Dimensionless depths for numerical solutions of Set 2. 155

Fig. 4.11 Relative bed shear stresses for numerical solutions Set 2. 156

Fig. 4.12 Relative potential core velocities for numerical solutions Set 2. 157

Fig. 4.13 Power law exponent for numerical solutions Set 2. 158

Fig. 4.14 Modified Moody Diagram showing numerical solution paths in Set 3. 160

Fig. 4.15 Dimensionless boundary layer thicknesses for numerical solutions of Set 3. 161

Fig. 4.16 Dimensionless depths for numerical solutions of Set 3. 162

Fig. 4.17 Relative bed shear stresses for numerical solutions Set 3. 163

Fig. 4.18 Relative potential core velocities for numerical solutions Set 3. 164

Fig. 4.19 Power law exponent for numerical solutions Set 3. 165

Fig. 4.20 Modified Moody Diagram showing numerical solution paths in Set 4. 167

Fig. 4.21 Dimensionless boundary layer thicknesses for numerical solutions of Set 4. 168

Fig. 4.22 Dimensionless depths for numerical solutions of Set 4. 169

Fig. 4.23 Relative bed shear stresses for numerical solutions Set 4. 170

Fig. 4.24 Relative potential core velocities for numerical solutions Set 4. 171

Fig. 4.25 Power law exponent for numerical solutions Set 4. 172

Fig. 4.26 Dimensionless entrance length as a function of the fully developed power law exponent for numerical solutions Set 1 and Set 2. 173

Fig. 4.27 Dimensionless entrance length as a function of the fully developed power law exponent for numerical solutions Set 1, Set 2 and Set 3. 174

Fig. 4.28 Dimensionless entrance length as a function of the fully developed power law exponent for numerical solutions Set 1, Set 2 and Set 4. 175

Fig. 4.29a Dimensionless entrance length as a function of the fully developed power law exponent. 176

Fig. 4.29b Dimensionless entrance length as a function of the fully developed dimensionless Chezy coefficient. Also shown is Yalin's (1972) solution for the entrance length. 177

Fig. 4.29c Relative shear stress within the entrance region. 178

Fig. 4.30 Comparison of dimensionless entrance length as a function of the fully developed dimensionless Chezy coefficient between the numerical and the two experiments analysed in Chapter 2. 179

Fig. 4.31a Comparison of dimensionless entrance length as a function of the fully developed C_* between the numerical solution for a wide channel and pipe flow entrance lengths by Ward-Smith (1980). Pipe entrance length non dimesionalysed by the pipe radius. 180

Fig. 4.31b Comparison of dimensionless entrance length as a function of the fully developed C_* between the numerical solution for a wide channel and pipe flow entrance lengths by Ward-Smith (1980). Pipe entrance length non dimensionalysed by the hydraulic radius. 181

Fig. 4.32 The effect of inaccurate bed slope and tailgate matching on the growth of a boundary layer in a *smooth channel.* 183

Fig. 4.33 The effect of inaccurate bed slope and tailgate matching on the bed shear stress in the entrance region of a *smooth channel.* 184

Fig. 4.34 The effect of inaccurate bed slope and tailgate matching on the depth of flow in the entrance region of a *smooth channel.* 185

Fig. 4.35 The effect of inaccurate bed slope and tailgate matching on the water surface elevation in the entrance region of a *smooth channel.* 186

Fig. 4.36 The effect of inaccurate bed slope and tailgate matching on the potential core velocity in the entrance region of a *smooth channel.* 187

Fig. 4.37 The effect of inaccurate bed slope and tailgate matching on the growth of a boundary layer in a *rough channel.* 188

Fig. 4.38 The effect of inaccurate bed slope and tailgate matching on the bed shear stress in the entrance region of a *rough channel.* 189

Fig. 4.39 The effect of inaccurate bed slope and tailgate matching on the depth of flow in the entrance region of a *rough channel.* 190

Fig. 4.40 The effect of inaccurate bed slope and tailgate matching on the water surface elevation in the entrance region of a *rough channel.* 191

Fig. 4.41 The effect of inaccurate bed slope and tailgate matching on the potential core velocity in the entrance region of a *rough channel.* 192

Fig. 5.1 Diagram showing the initial depth d_i for the upstream boundary condition based on the flow going through critical in the vertical. 218

Fig. 5.2 Water surface and boundary layer thickness for the same discharge, bed roughness and slope of the channel, but different initial upstream depths. 219

Fig. 5.3 Shear stress corresponding to runs of different initial upstream depths shown in Figure 5.2. 220

Fig. 5.4 Same as Figure 5.2 but plotted to actual scale and orientation near the channel entrance. 221

Fig. 5.5 Example of an undistorted plot of water surface, boundary layer thickness, and channel bed in the entire entrance region of a steep channel. 222

Fig. 5.6 Water surface and boundary layer thicknesses for the same channel bed slope but different discharges per unit width. (*smooth channel*) 223

Fig. 5.7 Same as Figure 5.6 with a portion near the channel entrance magnified. (*smooth channel*) 224

Fig. 5.8 Water surface and boundary layer thicknesses for the same channel bed slope but different discharges per unit width. (*rough channel*) 225

Fig. 5.9 Same as Figure 5.8 with a portion near the channel entrance magnified. (*rough channel*) 226

Fig. 5.10 Water surface and boundary layer thicknesses for same discharge and a smooth bed, but different channel bed slopes. 227

Fig. 511 Bed shear stress corresponding to runs of Figure 5.10. 228

Fig. 5.12 Magnified portion of Figure 5.11 near the channel entrance. 229

Fig. 5.13 Bed shear stress non-dimesionalized by the bed shear when the boundary layer reaches the surface. Also shown is the subcritical solution in a mild channel for the same discharge and a smooth bed. 230

Fig. 5.14 Water surface and boundary layer thicknesses for the same discharge and channel bed slope but for different bed roughness. 231

Fig. 5.15 Bed shear stress corresponding to runs of Figure 5.14. 232

Fig. 5.16 Velocity profiles from Bauer's *smooth* experiment. 233

Fig. 5.17 Water surface and boundary layer thickness for Bauer's *smooth* experiment compared with the numerical solution. 234

Fig. 5.18 Potential core velocity for Bauer's *smooth* experiment compared with numerical solution. 235

Fig. 5.19 Bed shear stress for Bauer's *smooth* experiment compared with numerical solution. 236

Fig. 5.20 Power law exponent for Bauer's *smooth* experiment compared with numerical solution. 237

Fig. 5.21 Displacement and momentum thickness for Bauer's *smooth* experiment compared with numerical solution. 238

Fig. 5.22 Velocity profiles from Bauer's *rough* experiment. 239

Fig. 5.23 The channel bed roughness and bed shear stress for Bauer's *rough* experiment was determined from velocity profiles. 240

Fig. 5.24 Water surface and boundary layer thickness for Bauer's *rough* experiment compared with the numerical solution. 241

Fig. 5.25 Potential core velocity for Bauer's *rough* experiment compared with numerical solution. 242

Fig. 5.26 Bed shear stress for Bauer's *rough* experiment compared with numerical solution. 243

Fig. 5.27 Power law exponent for Bauer's *rough* experiment compared with numerical solution. 244

Fig. 5.28 Displacement and momentum thickness for Bauer's *rough* experiment compared with numerical solution. 245

Fig. 5.29 Entrance length comparison between Keller & Rostogi's k–ε model and the numerical solution. In this comparison series the same bed roughness is used and the channel bed slope and discharge is varied. 246

Fig. 5.30 Entrance length comparison between Keller & Rostogi's k–ε model and the numerical solution. In this comparison series the channel bed slope is constant and the bed roughness and discharge is varied. 247

Fig. 5.31 Water surface and boundary layer thickness from Ippen's experimental Run B. Also shown is the numerical solution and Schlichting's smooth flat plate solution. 248

Fig. 5.32 Water surface and boundary layer thickness from Ippen's experimental Run C. Also shown are two numerical solutions and Schlichting's smooth flat plate solution. 249

Fig. 5.33a Comparison between numerical solution for the water surface and the S2 backwater curve for $\phi=1$ degree and $C_*= 12.73$. Also shown is the boundary layer thickness and uniform depth. 250

Fig. 5.33b Comparison between bed shear stress given by the numerical simulation and the S2 backwater curve for $\phi=1$ degree and $C_*= 12.73$. Also shown is uniform flow shear. 251

Fig. 5.34a Comparison between numerical solution for the water surface and the S2 backwater curve for $\phi=1$ degree and $C_*= 29.70$. Also shown is the boundary layer thickness and uniform depth. 252

Fig. 5.34b Comparison between bed shear stress given by the numerical simulation and the S2 backwater curve for $\phi=1$ degree and $C_*= 29.70$. Also shown is uniform flow shear. 253

Fig. 5.35a Comparison between numerical solution for the water surface and the S2 backwater curve for $\phi=45$ degrees and $C_*= 12.73$. Also shown is the boundary layer thickness and uniform depth. 254

Fig. 5.35b Comparison between bed shear stress given by the numerical simulation and the S2 backwater curve for $\phi=45$ degrees and $C_*= 12.73$. Also shown is uniform flow shear. 255

Fig. 5.36a Comparison between numerical solution for the water surface and the S2 backwater curve for $\phi=45$ degrees and $C_*= 29.70$. Also shown is the boundary layer thickness and uniform depth. 256

Fig. 5.36b Comparison between bed shear stress given by the numerical simulation and the S2 backwater curve for ϕ=45 degrees and C*= 29.70. Also shown is uniform flow shear. 257

Fig. 5.37 Dimensionless entrance length as a function of the uniform flow C* and the slope of the channel in degrees. Also shown is the subcritical numerical solution for the mild channel. 258

Fig. 5.38 The ratio of end depth(depth at which the boundary layer reaches the surface) to normal depth as a function of the uniform flow C* and the slope of the channel in degrees. 259

Fig. 5.39 Dimensionless entrance length as a function of the uniform flow C* and the ratio of initial depth at the channel entrance to normal depth for a channel slope of 1 degree. Initial depth controlled by a sluice gate. 260

Fig. 5.40a The ratio of end depth(depth at which the boundary layer reaches the surface) to normal depth as a function of the uniform flow C* and the ratio of initial depth at the channel entrance to normal depth for a channel slope of 1 degree. Initial depth controlled by a sluice gate. 261

Fig. 5.40b Same as Figure 5.40a but also includes $d_i/d_o<1$. Slope = 1 degree. 262

Fig. 5.41 Dimensionless entrance length as a function of the uniform flow C* and the ratio of initial depth at the channel entrance to normal depth for a channel slope of 10 degrees. Initial depth controlled by a sluice gate. 263

Fig. 5.42a The ratio of end depth(depth at which the boundary layer reaches the surface) to normal depth as a function of the uniform flow C* and the ratio of initial depth at the channel entrance to normal depth for a channel slope of 10 degrees. Initial depth controlled by a sluice gate. 264

Fig. 5.42b Same as Figure 5.42a but also includes $d_i/d_o<1$. Slope = 10 degrees. 265

Fig. 5.43 Dimensionless entrance length as a function of the uniform flow C* and the ratio of initial depth at the channel entrance to normal depth for a channel slope of 45 degrees. Initial depth controlled by a sluice gate. 266

Fig. 5.44a The ratio of end depth(depth at which the boundary layer reaches the surface) to normal depth as a function of the uniform flow C* and the ratio of initial depth at the channel entrance to normal depth for a channel slope of 45 degrees. Initial depth controlled by a sluice gate. 267

Fig. 5.44b Same as Figure 5.44a but also includes $d_i/d_o<1$. Slope = 45 degrees. 268

List of symbols

Symbol	Discription
C_*	dimensionless Chezy conveyance coefficient corresponding to normal depth.
c'_f	local skin friction coefficient.
D	internal pipe diameter.
d	depth of flow measured perpendicular to channel bed.
d_{end}	depth at which the boundary layer reaches the water surface.
d_i	initial depth at channel entrance measured perpendicular to channel bed.
d_o	normal depth measured perpendicular to channel bed.
D_p	outer diameter of pitot tube.
f	friction factor.
$\mathbf{F}_o$	Froude number based on normal depth.
g	acceleration due to gravity.
k	total hydraulic roughness.
k_s	equivalent sand grain roughness.
k_v	laminar sublayer thickness.
k - ε	turbulent kinetic energy and dissipation.
L	The distance the boundary layer takes to reach the water surface, measured from channel entrance. Also referred to
as	the development length, entrance length, and distance to critical point.
M	momentum per unit width (N/m)
n	reciprocal of the power law exponent for velocity profiles.

n_o	n evaluated when $\delta = d = d_o$.
P	piezometric pressure.
p	pressure.
q	discharge per unit width.
R	hydraulic radius.
r	internal pipe radius.
$\mathbf{R}_p$	pipe Reynolds number.
$\mathbf{R}_{po}$	$\mathbf{R}_p$ evaluated when $\delta = d = d_o$.
$\mathbf{R}_\delta$	Boundary layer Reynolds number based on boundary layer thickness.
$\mathbf{R}_x$	Boundary layer Reynolds number based on the distance from the leading edge of flat plate.
S	slope if channel or spillway, $S=\sin(\phi)$.
S_f	friction slope.
S_o	slope if channel or spillway, $S=\sin(\phi)$.
u	velocity in the x direction.
$\bar{u}$	average velocity in a pipe.
u_*	shear velocity.
U	potential core velocity.
Ui	potential core velocity at channel entrance.
U_c	potential core velocity when depth passes through y_c.
U_1	potential core velocity at channel entrance.
U_{end}	potential core velocity when boundary layer reaches water surface.
U_{max}	maximum experimental velocity found in any one velocity profile.

V	depth averaged velocity in the x direction.
v	velocity in the y direction.
x	coordinate in the downstream direction.
y	coordinate in the perpendicular to the bed direction.
y_c	critical depth measured parallel with direction of gravity.
y_d	y coordinate correction for rough velocity profiles.
y_{u1}	vertical coordinate for rough boundary velocity profiles (Chp. 2)
z	coordinate in the transverse to channel direction, origin at channel centreline positive to the right looking downstream.
z_o	elevation.
α	energy correction coefficient.
β	momentum correction coefficient.
γ	specific weight of fluid.
δ	boundary layer thickness.
δ_t	boundary layer thickness based on turbulence criteria. (Chp. 2)
δ_i.	boundary layer thickness based on extrapolated intercept method. (Chp. 2)
δ_{99}	boundary layer thickness based on 0.99U criteria.
δ_*	displacement thickness.
Δx	increment in x coordinate for numerical solution.
ϕ	spillway or channel slope in degrees from horizontal.
ν	kinematic viscosity of water.
μ	viscosity of water.
θ	Momentum thickness.
ρ	density of fluid.

τ	shear stress.
τ_{end}	bed shear stress when the boundary layer reaches the surface.
τ_o	bed shear stress.

Introduction

The flow in hydraulic structures such as culverts, channels and spillways is generally analysed using fully-developed flow velocity and resistance relations. However, for short structures - say where the length is less than about 25 - 100 flow depths - the flow is likely not fully-developed and these relations may not apply. Furthermore, many experiments on the above relations assume that the flow is fully developed in the laboratory without any formal confirmation. From a broader point of view, the investigation of the boundary layer in open channels forms a better understanding of the internal mechanism of this type of flow.

To study the boundary layer and to assess the errors involved in the assumption of fully developed flow, it is desirable to be able to analyse the flow in the entrance region. (It was decided to only look at turbulent boundary layers as laminar boundary layers tend to be quite short before turning turbulent in most hydraulic structures.) The simplest option to analyse the boundary layer at the entrance of a channel might be to use the classical smooth flat plate boundary layer theory found in Schlichting (1979), or to use some later work done on rough plates; Granville (1958) and Harrison (1967). In these solutions however, the free stream velocity is a constant, while in open channels and closed conduits the potential flow outside the boundary layer is accelerating. It is for this reason that the full Kármán Integral Equation was used to find a solution for the boundary layer growth in this study. With further complications of roughness, Reynolds number effects, and coupling with the Bernoulli and continuity equations it was easier to solve the system of equations numerically, rather than analytically.

To test the adequacy of the analytical solution, experimental data was needed for both mild and steep channels on smooth and rough beds. A literature search showed that experiments conducted in mild channels were few and far between. Two experimental works were found: one by Delleur (1957) which delt with smooth horizontal channels; one by Binnie (1957) which delt with laminar boundary layers in smooth horizontal channels. Due to the lack of experimental data experiments were conducted in mild channels as part of this study. Also, as secondary flows in straight noncircular conduits are the rule rather than the exception they made the experimental results quite interesting and revealing.

There has been a lot more experimental and analytical research done on steep channels. The main point of this research was to locate the critical point on the face of the spillway. The critical point occurs when the boundary layer reaches the water surface and the turbulent eddies break through and start to entrain air. It is important to find this point because downstream of it the flow can become a water-air mixture and could follow very different flow, velocity and resistance relations. The energy losses and the air entrainment on the face of a spillway are important since they determine the design of the energy dissipation structure and the susceptibility to cavitation at any point on the spillway face.

1. Literature Review

1.1 The Karman Integral Equation for the boundary layer

Starting with the time-averaged Reynolds equations, and using order of magnitiude arguments, Prandtl derived the following simplified momentum and continuity equation for a boundary layer

$$u\frac{\partial u}{\partial x} + v\frac{\partial u}{\partial y} = -\frac{1}{\rho}\frac{dP}{dx} + \frac{1}{\rho}\frac{\partial \tau}{\partial y} \qquad (1.1)$$

$$\frac{\partial u}{\partial x} + \frac{\partial v}{\partial y} = 0 \qquad (1.2)$$

where x is the downstream direction and y is normal to the boundary, u is the velocity in the x direction, v is the velocity in the y direction, P is the piezometric pressure, ρ is the density of the fluid , and τ is the shear stress.

Flow outside the boundary layer acts essentially as inviscid and is described by the Bernoulli equation:

$$\frac{\rho U^2}{2} + \gamma z_o + p = \text{constant} \qquad (1.3)$$

where U is the free stream velocity, γ is the specific weight of the fluid, z_o is the elevation, and p is the pressure.

Combining the elevation and pressure term to a piezometric pressure P and differentiating with respect to x the Bernoulli equation becomes:

$$U \frac{dU}{dx} = - \frac{1}{\rho} \frac{dP}{dx} \tag{1.4}$$

Integrating Equation 1.1 with respect to y from y = 0 to just outside the boundary layer and using the Bernoulli equation to replace the pressure gradient term by ρU (dU/dx) where required, results in the Karman Integral Equation:

$$\frac{\tau_o}{\rho} = \frac{d}{dx} U^2\theta + U\, \delta_* \frac{dU}{dx} \tag{1.5}$$

where τ_o is the bed shear stress, and δ_* and θ are the displacement and momentum thicknesses respectively. The latter are defined by:

$$\delta_* = \int_0^{\delta_+} \left(1 - \frac{u}{U}\right) dy \tag{1.6}$$

$$\theta = \int_0^{\delta_+} \frac{u}{U}\left(1 - \frac{u}{U}\right) dy \tag{1.7}$$

1.2 Solutions for boundary layers with zero pressure gradients

1.2.1 Boundary layer on a smooth plate

A boundary layer solution on a smooth flat plate is derived in Schlichting (1934) from the similar velocity distributions found in pipes for a certain Reynolds number range. In this derivation x is the coordinate from the leading edge of the plate going downstream and y is the coordinate normal to the plate. If the velocity distribution from a pipe is used the maximum velocity in the pipe becomes the free stream velocity U of the boundary layer and the radius of the pipe becomes the boundary layer thickness δ. The velocity distribution used in this analysis is Blasius power law and takes the form:

$$\frac{u}{U} = \left(\frac{y}{\delta}\right)^{\frac{1}{n}} \tag{1.8}$$

where u is the velocity at any y and n is equal to 7.

There are two types of Reynolds numbers which are useful when talking about boundary layers, one is based on the boundary layer thickness:

$$\mathbf{R}_\delta = \frac{U\,\delta}{\nu}$$

The other is based on the distance from the leading edge:

$$\mathbf{R}_x = \frac{U\,x}{\nu}$$

The 1/7th power law velocity distribution agrees well with experiments up to $\mathbf{R}_\delta < 10^5$.

The shear stress on the pipe wall corresponding to this velocity distribution can be derived from the following:

$$\frac{\tau_0}{\rho} = \frac{1}{8} f \bar{u}^2 \tag{1.9}$$

$$f = 0.3164 \left(\frac{\bar{u} D}{\nu}\right)^{\frac{-1}{4}} = \frac{0.3164}{\mathbf{R}_p^{\frac{1}{4}}} \tag{1.10}$$

$$\frac{\bar{u}}{U} = \frac{2 n^2}{(n+1)(2n+1)} \tag{1.11}$$

where f is the friction factor, u is the average velocity in the pipe, D is the pipe diameter, and $\mathbf{R}_p$ is the pipe Reynolds number.

Equation 1.9 shows how the friction factor defines the relationship between the average velocity and wall shear. Equation 1.10 is Blasius Resistance Formula based on experiment and is applicable to smooth pipes and has shown it can also be used for boundary layers growing on smooth surfaces for certain values of Reynolds number mentioned above. Equation 1.11 is arrived at by integrating the power law velocity distribution over the area of the pipe and dividing by the area of the pipe.

Combining 1.9, 1.10, and 1.11 the final expression for the shear is:

$$\frac{\tau_0}{\rho} = 0.0225\, U^2 \left(\frac{U\,\delta}{\nu}\right)^{\frac{-1}{4}} \tag{1.12}$$

If Equation 1.8 is substituted into 1.6 and 1.7 and we integrate from 0 to δ, δ_* and θ become:

$$\delta_* = \frac{\delta}{(n + 1)} \tag{1.13}$$

$$\theta = \delta \frac{n}{(n + 1)(n + 2)} \tag{1.14}$$

The free stream velocity U in this case is a constant, therefore Equation 1.5 becomes:

$$\frac{\tau_0}{\rho} = U^2 \frac{d\theta}{dx} \tag{1.15}$$

Equating 1.12 and 1.15 we obtain:

$$0.0225 \left(\frac{U\,\delta}{\nu}\right)^{-\frac{1}{4}} = \frac{d\theta}{dx} \tag{1.16}$$

By Equation 1.14, if $n = 7$, $\theta = 7/72\ \delta$, therefore Equation 1.16 becomes:

$$0.0225 \left(\frac{U\,\delta}{\nu}\right)^{-\frac{1}{4}} = \frac{7}{72} \frac{d\delta}{dx} \tag{1.17}$$

And finally integrating from initial value $\delta = 0$ at $x = 0$ gives:

$$\delta(x) = 0.37\, x \left(\frac{U\,x}{\nu}\right)^{-\frac{1}{5}} \tag{1.18}$$

Equations 1.12 and 1.18 are Schlichtings famous solution for a boundary layer growing on a smooth flat plate.

The limitations of this solution are outlined in the following:

By equation 1.18 $\mathbf{R}_\delta < 10^5$ corresponds to $\mathbf{R}_x < 6\mathrm{x}10^6$. Also, since the boundary layer is laminar up to about $\mathbf{R}_x = 5\mathrm{x}10^5$ the range of validity for this analysis becomes:

$5\mathrm{x}10^5 < \mathbf{R}_x < 6\mathrm{x}10^6$

1.2.2 Boundary layer on a rough plate

The boundary layer solution for a rough plate is also presented in Schlichting (1934) and follows a similar type of solution as for the smooth plate. It is similar in that the measurements from rough pipes is used to describe the velocity distribution and shear stress for the boundary layer. There is a complication however since the relative roughness k_s/δ will decrease as δ increases and k_s remains constant, where in a pipe k_s/r remains constant. In addition, the velocity distribution is described by a logarithmic velocity distribution which makes equations 1.6 and 1.7 difficult to evaluate. Also, the boundary layer can go through several stages from being fully rough at the leading edge, in a transition region further downstream, and eventually hydraulically smooth further down. The details of this analysis are lengthy and will not be presented here.

The above work on rough plates was based on uniform sand grain roughened pipes. It is well known that for non-uniform roughness, as may be found on most materials, the transition curves between fully smooth to fully rough are different than for uniform sized grains. Coolebrook and White (1939) came up with these more practical transition curves for pipes and Granville (1958) applied it to boundary layers using the same methods as Schlichting. These relations however give only the coefficient of skin friction and do not give the boundary layer thickness directly. By further manipulation Harrison (1967) was able to extend the analysis further to give δ.

1.3 Boundary layers in open channels

Boundary layers in open channels can occur under many situations; they can occur on a horizontal channel in both the H1 and H2 backwater curves; in a mild channel in an M1, M2, and M3 backwater curves; in a steep channel in the S1, S2, and S3 backwater curves, and in some of the more exotic backwater curves. They can also occur in cases where there is no backwater curve at all, such as at the entrance to a mild channel flowing at normal depth, or an entrance to a steep channel where the initial depth is forced to be normal depth by a sluice gate or a nozzle.

1.3.1 Boundary layers in horizontal and mild channels

Delleur (1957) performed an experimental and analytical investigation on boundary layer development in a horizontal channel. His analysis used the full Karman momentum equation for the boundary layer(Equation 1.5) to include the effect of the accelerating potential core and he used the 1/7th Blasius power law to compute the friction and the velocity profiles. This would make his results applicable only to smooth channels with typical laboratory discharges to give a Reynolds number with the range of the Blasius power law. It also limited it to the H1 and the H2 backwater curves. He did find however, that his predicted boundary layer growth was smaller than that predicted by the zero pressure gradient solution based on Blasius's 1/7th power law (described in section **1.2.1.**). The power law exponent found from his velocity profiles ranged from 1/5.5 to 1/7.7 with a mean of 1/6.85. He did his main experimental run for subcritical flow with a high channel aspect ratio and found secondary flow structures which affected the thickness of the boundary layer significantly in the transverse direction; the width averaged boundary layer thickness however agreed well with his theory. This is much the same thing found in the experimental portion of this study on mild channels discussed in Chapter 2.

Binnie (1977) also did some similar work to Delleur but performed his experiment and analysis on a laminar boundary layer in a horizontal channel.

Yalin (1972) made a simplified attempt at solving for the entrance length. It is shown in the following:

He equated the fully developed surface velocity from the logarithmic velocity distribution to the free stream velocity for the boundary layer:

$$\frac{U}{u_*} = 2.5 \ln \frac{\delta}{k_s} + 8.5 \tag{1.19}$$

where δ and u_* vary with x. He then introduces the friction coefficient

$$c'_f = \frac{\tau_o}{\frac{1}{2} \rho U^2} \tag{1.20}$$

and using $\tau_o = \rho u_*^2$ he determines:

$$\frac{U}{u_*} = \sqrt{\frac{2}{c'_f}} \tag{1.21}$$

Equating 1.19 to 1.21 he obtains:

$$\frac{1}{c'_f} = \frac{1}{2}\left(2.5 \ln \frac{\delta}{k_s} + 8.5\right)^2 \tag{1.22}$$

For the case of a fully developed turbulent regime Schlichting gives the following expression for the variation of c'_f with the distance x:

$$\frac{1}{c'_f} = \left(1.58 \log \frac{x}{k_s} + 2.87\right)^{2.5} \qquad (1.23)$$

Equating 1.21 with 1.23 Yalin arrives at the relation between δ and x:

$$\frac{1}{2}\left(2.5 \ln \frac{\delta}{k_s} + 8.5\right)^2 = \left(1.58 \log \frac{x}{k_s} + 2.87\right)^{2.5} \qquad (1.24)$$

Now the distance L is the value of x where δ reaches the flow depth d_o. Substituting $x = L$ and $\delta = d_o$ in 1.24 and solving for L he develops an expression for the entrance length as:

$$\frac{L}{d_o} = 0.0152 \frac{k_s}{d_o} e^m \qquad \left(\text{with } m = 2.3\left[\ln 30.1 \frac{d_o}{k_s}\right]^{\frac{4}{5}}\right) \qquad (1.25)$$

Equation 1.25 may not be adequate since it does not take into account the presence of a piezometric pressure gradient. This relation will be compared later with a numerical solution which includes the presence of a pressure gradient.

With the exception of Yalin's work, surprisingly, no literature was found on mild channels. This is strange since the case where the boundary layer grows in the absence of any backwater curve is the most common and fundamental situation in a mild channel. In this case when the boundary layer reaches the surface the flow should be close to fully developed, the depth should be normal depth and the water surface and friction slope should be parallel to the bed slope.

1.3.2 Boundary layers in steep channels

The most common work found in the literature on steep slopes has to do with the prediction of the critical point on the face of the spillway which occurs when the boundary layer reaches the surface. This involves the prediction of the boundary layer in an S2 type backwater curve. Bauer (1954) took some of the first velocity profiles in the laboratory to measure the boundary layer growth for channel slopes ranging from 20° to 60° for a smooth bed and a rough bed. The roughness he used was a fly screen with a similar roughness to concrete. He discovered that the growth of the boundary layer was relatively independent of the slope and discharge, but a higher bed roughness did increase the growth rate of the boundary layer, as expected. Bauer also proposed a design method for predicting the critical point on a spillway by using the experimental data to come up with a design curve to calculate the boundary layer thickness, adding the displacement thickness to the potential flow to solve for the water surface and proceeding downstream until the boundary layer and the water surface intersected. The design curve gave δ/x as a function of x/k_s for rough flow and δ/x as a function of the Reynolds number for smooth flow. Some of the drawbacks to this design method are: the design curves do not deal with the transition between smooth and rough flow; the potential core velocity is calculated only as a function of x and not from the actual location of the water surface (ie. $U^2/2g = x \sin(\phi)$, ϕ

being the slope of the spillway in degrees), and the determination of the shape of the velocity profile to calculate the displacement thickness was not very rigorous in that it assumes a constant power law exponent. The experimental data was not width averaged to test for the possible effects of secondary flows. Further discussion of Bauer's paper is provided by Halbronn (1954).

Ippen (1957) performed some experiments to evaluate the combination of a total head tube with a capacitance type pressure transducer for measuring mean velocities and turbulence. One type of flow he investigated was boundary layer growth in high velocity streams(supercritical flow). The bed slopes he used were quite small, about 2° and 0.5°, so the results could be very different from some of the spillway data. The slopes where steep enough to categorize the channel as steep by definition for the discharges he used. The flow was controlled by a wide rectangular nozzle at the upstream end; the channel bed was smooth. It was apparent that he tried to match the bed slope, discharge, and nozzle opening to give uniform depth at the nozzle, thereby avoiding the S2 and S3 backwater curves. Ippen published two runs, the first runs showed a boundary layer growing somewhat slower than Schlichting's smooth flat plate solution and the second one closely matching it. The second run also showed a slightly increasing depth going downstream, while the first run showed a constant depth. The discussion of his results continues in Section 5.6 where the two runs are numerically modelled.

As an aside, Ippen concluded that the instrument he was investigating was reliable in giving mean velocities; root mean square values of the turbulent velocity fluctuations in the direction of the mean flow, and the scale of macro turbulence in water. A similar type of measurement device was used to measure the mean velocities in the boundary layer growth of a mild channel in this investigation. The turbulent fluctuations were not quantitatively analysed but are available in analog form for anybody wishing to do further work.

Back to spillway design, Campbell et al (1965) used the solution technique of Bauer to compute the energy losses on the face of the spillway to aid in design of energy dissipation structures occurring in situations where the length of the spillway is shorter than the distance to the critical point. Since this procedure is based on Bauer's design method, it posses some of same drawbacks mentioned earlier. Also, Campbell uses a dimensional plot in one of his design graphs making it difficult to obtain solutions for different situations. However a discussion on Campbell's paper by Cassidy (1966) nondimensionalizes this figure.

Keller and Rastogi (1975) used a k-ε model to predict the boundary layer growth on spillways with a standard crest and a vertical upstream face. They simulated the experiments by Bauer, observations of the Glenmaggie Dam, and measurements taken on the Avienmore Spillway with good agreement. The initial velocity profiles specified for their solution were based on Blasius's 1/7th power law for smooth flow and from measured profiles on rough boundaries. In 1977, Keller and Rastogi expanded their model for general design use. They developed design charts by feeding synthetic data covering a wide range of possible spillway flow situations into their k-ε model and generalizing their results through dimensional analysis. The variables chosen to influence the distance L for the boundary layer to reach the surface was the discharge per unit width q, gravitational acceleration g, spillway slope S, and spillway roughness k_s. The fluid density ρ was not included in the dimensional analysis as consideration was limited to water flows. The viscosity μ was also neglected as the Reynolds number were reasoned to be high enough for it not to be important. So in summary, $L = f(q, k_s, g, S)$, and by the Buckingham Π theorem the dimensionless combinations of these variables results:

$$\frac{L}{k_s} = f\left[\frac{q}{\left(g\,k_s^3\right)^{\frac{1}{2}}}, S\right] \tag{1.26}$$

From this relation, design curves for L/k_s as a function of $q/(g\,k_s^3)^{0.5}$ for different S where drawn. The drawback to these design curves is that as k_s gets smaller, or even zero, one is quickly out of range of the design curves as k_s is in the denominator of two of the variables. Under these situations, consideration of the viscosity or Reynolds number dependence seems necessary in order to come up with more general solutions.

Keller and Rostogi (1977) also tested the effect of the nonlinear pressure distribution on the spillway crest on the location of the critical point for flows below, at, and above the design heads. They concluded that their design charts are within 5% for flows given by 0.5 to 1.33 times the design head of the spillway for slopes more than 10^{o}, for smaller slopes the errors could be about 6% - 7%.

Wood et al (1983) try to generalize even further the Keller and Rostogi's results by assuming the boundary layer growth formula takes a general form and evaluate the coefficients by regression. Here it should be said that just because things vary subtly, they should not be simplified to the point where the physics is lost. Wood (1985) goes on to say that his simplified equation can be differentiated and applied to a spillway profile in which the slope varies gradually; he argues that the boundary layer is "close to local equilibrium".

In summary, the work done on steep slopes has still fallen short of the nature of the entire problem. The work of Keller and Rostogi seems to be adequate for spillway design in which a standard crest combined with a constant slope spillway is used with roughnesses typical of concrete. The cases of smooth spillways, high roughness spillways, slope varying spillways, and sluice gate controlled spillways still need to be investigated.

1.4 Secondary flows in straight open channels

This investigation will not go into the cause of these secondary flows, only to say that they arise from turbulent stress gradients in the transverse direction. They are known to occur in non-circular ducts (Gerard,1978) as well as open channels.

In wide channels it has been found that several secondary current cells form across the channel with each cell having an alternate direction of rotation than the cell next to it, with the size and spacing of the cells scaling on the depth. Wolman and Brush 1961, Kinoshita 1967, Ikeda and Hikkawa 1977, Muller 1982, Gulliver and Halverson 1987, found that the cell width varied from about 0.84 to 1.2 depths. Because an even integer number of cells has to occur across the width of a channel, it is evident these cell widths were the closest possible to 1.0 for the particular channel aspect ratio used by each investigator. The observations of the above investigators included both laboratory and river flows.

The impact of these secondary flows in wide channels can be quite significant on the mean longitudinal velocity distribution. The magnitude of these secondary flow velocities are generally only 2 to 4% of the mean longitudinal velocity (Gulliver and Halverson, 1987) but can cause a much larger variation in velocity or discharge between two profiles taken less than 1 depth apart from each other in the transverse direction(Ch.2). Although these transverse velocities are relatively small, they are strong enough to redistribute the momentum and cause changes in the mean flow by an order of magnitude greater than their own. As shown in Figure

1.1, Delleur(1957) found differences in unit discharge and velocity of 12.6% and 17.8% respectively. The effects of secondary currents in the experimental portion of this study were of the same order and will be discussed further in Chapter 2.

These secondary flows have an effect on the developing boundary layer as well as fully developed flow. As mentioned earlier, Delleur(1957) found secondary flows as part of his investigation. He also found secondary flows affecting the boundary layer thickness in the transverse direction for his experiments in a horizontal channel. This phenomena occurs in steep channels as well; Gulliver and Halverson (1987) say the secondary flow streaks "can be seen first-hand downstream of most spillways, where the surface foam provides an excellent surface movement tracer." It is possible that these secondary flows are responsible for the first signs of air entrainment on spillways occurring upstream of the theoretical critical point; they could be responsible for the intermittent turbulence found 1.2 δ from the bed. Nevertheless, one should keep in mind these secondary flows when analysing any boundary layer development with a 2-D analysis.

Another point is that sometimes these cells are stationary in time and space but at other times they seem to be shifting wildly. Further work is needed to see what flow conditions affect the stability of their location. It is possible that in a situation where the cells are not stable that intermittent turbulence could be easily found 1.2 δ away from the bed.

Falco (1977) found that large scale motions are also present in unrestricted boundary layers with longitudinal spacing of large scale motions equal to 2.5 times the boundary layer thickness.

These secondary flow structures in open channels can also affect the bed shear in the transverse direction. This can best be seen by evidence of sediment streaks left in natural channels and laboratory channels. An example can be seen in Figure 1.1 of silt streak deposits left on a gravel bar on the Yukon River near Dawson. These sediment streaks will not be found in every case but only when the erosional velocity of the finer sediment is in between or close to the minimum and maximum produced by the secondary flow cells.

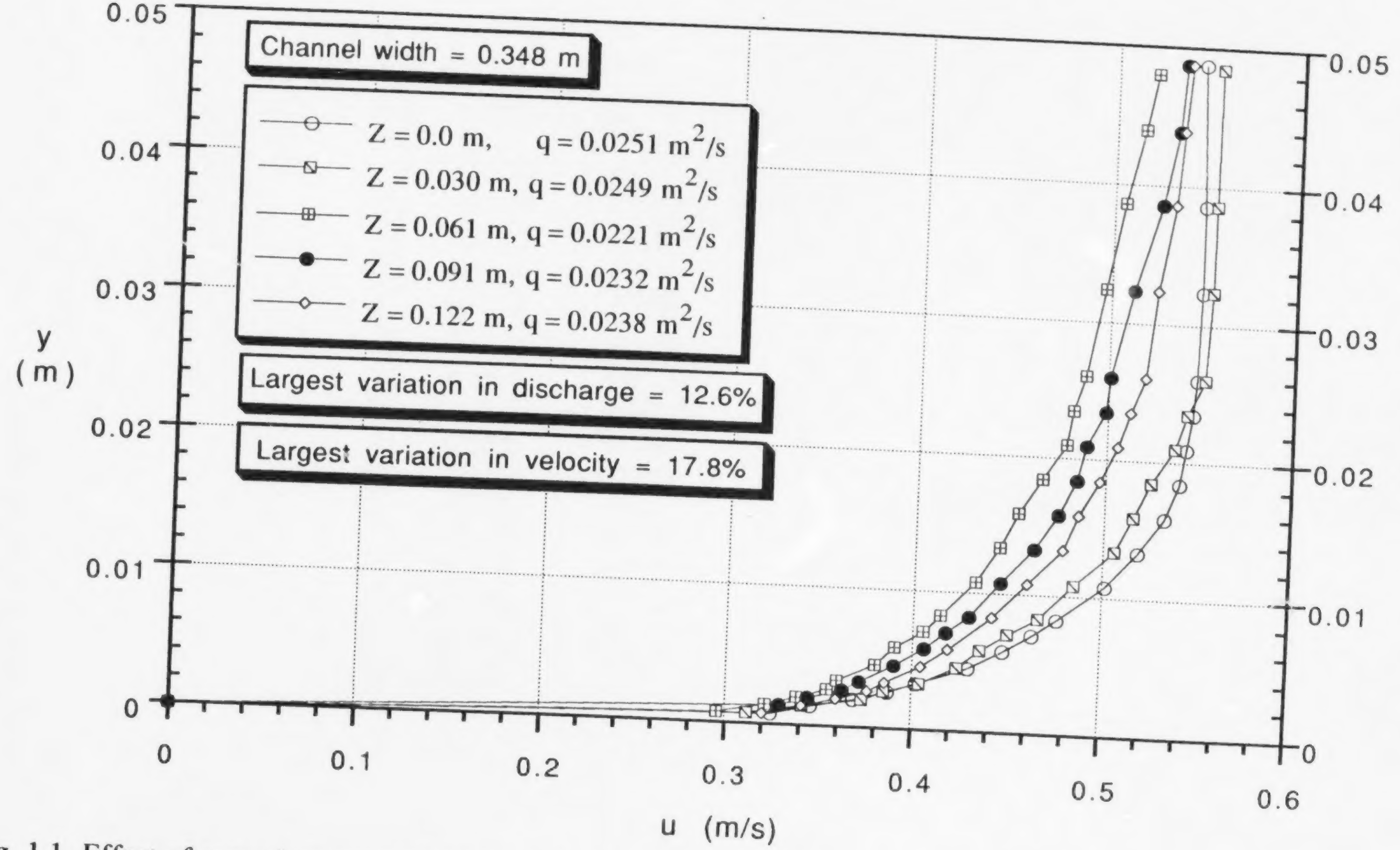

Fig. 1.1 Effect of secondary currents on the velocity distributions in the transverse direction after measurements by Delleur (1957) from his study on boundary layer development in a smooth horizontal channel.

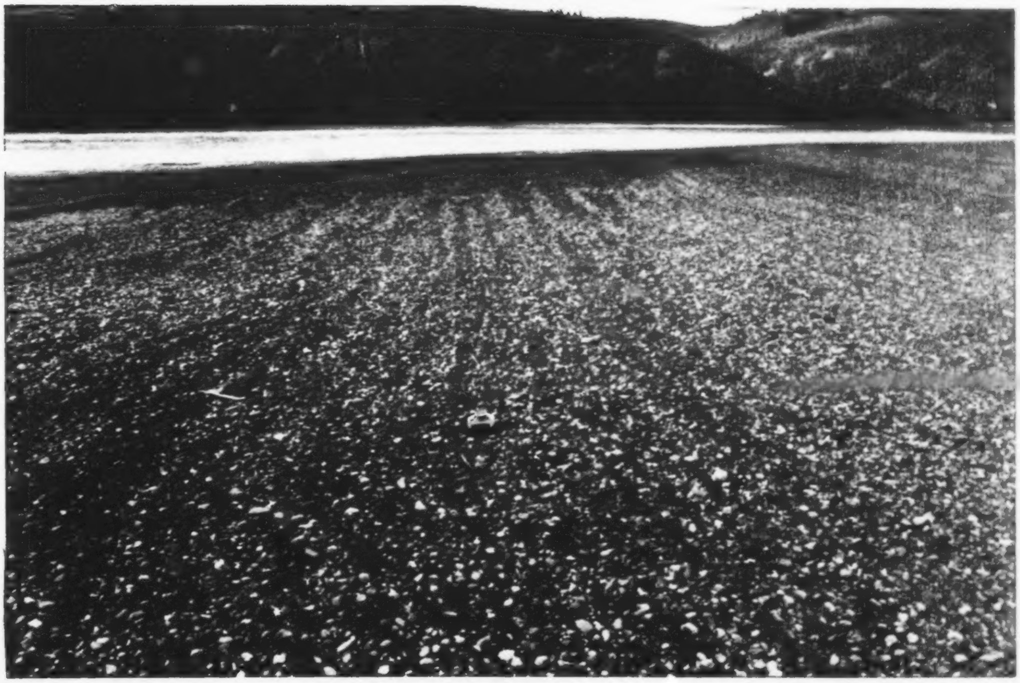

Fig. 1.2 Silt deposit streaks on gravel bar left by secondary currents on the Yukon River near Dawson, 1989.

2. Experiments in a mild channel

Experiments were conducted in a wide rectangular channel to measure the boundary layer growth and the entrance length in the case of a mild channel flowing at normal depth; the situation where there is no backwater curve. In this case, when the boundary layer reaches the surface the flow is close to fully developed, the depth is normal depth and the water surface and friction slopes are parallel to the bed slope.

As mentioned earlier, secondary flow structures caused the boundary layer development to vary strongly across the channel. Fig 2.1 shows the effect of the secondary flow structures on the boundary layer, in the central portion of a wide channel, where the measurements were taken. There is 1/4 of the channel width on each side which is not shown. The secondary flows persisted despite all efforts to avoid them by refinements to the approach flow and inlet conditions. Hence, for a reasonable comparison of the experimental results with a the two dimensional analysis the experimental data had to be width-averaged. Consequently, extensive across-channel measurements had to be carried out in addition to the traditional down-channel measurements. Because of the large number of measurements required, the experimental investigation was limited to one run for a smooth channel and one run for a rough channel.

2.1 Experimental arrangement and procedure

The experiments were conducted in a flume 18 m long, 1.22 m wide, and 0.65 m deep as shown in Figure 2.2 and Figure 2.8. The channel had an adjustable bed slope and a gate at the downstream end for tailwater control. The water leaving the flume dropped into a sump network and was returned to the head tank by a Fairbanks - Morse propeller pump through a 20 cm dia. line. The maximum discharge of the system was about 80 L/s. The head tank was 2.44 m long and 1.8 m wide and had smooth semicircular contractions from the walls and floor into the channel. Inside the head tank 10 cm dia. pipes about 1 m long were stacked to act as flow straighteners, with a synthetic hairlike material placed at the upstream and downstream ends of the pipes to reduce turbulence. The extreme turbulence generated by the water supply pipe was intercepted and controlled by a weir of masonry bricks placed upstream of the flow straighteners. The configuration of the contraction caused a strong longitudinal vortex to form and propagate down the centre of the channel. This problem was resolved by placing a sloping board at about 45 degrees to the head tank bed to intersect the curved surface of the inlet tangentially. The coordinate system set up for the velocity measurements was x in the direction of flow measured from the top of the curved portion of the channel entrance, y from the bed upwards, and z from the channel centreline positive to the right, looking downstream. (See Figure 2.1).

The experiments required measurement of the discharge, water surface profiles, depth, velocity profiles, boundary shear and for the rough channel the hydraulic roughness.

The discharge was measured by a 20 cm dia. Foxboro Magnetic flow meter. This enabled the discharge to be kept within 0.2 L/s of the desired discharge.

Velocities were measured by a United Censor 3 mm dia. pitot tube connected to a Validyne pressure transducer shown in Figure 2.3. This system allowed for the accurate measurement of relatively small velocities ranging from 0.1 to 0.5 m/s. The voltage output from the transducer was linear with velocity head and was recorded on a stripchart recorder which could be read within 0.1 mm of velocity head (See Figure 2.4 and 2.5). Each reading was averaged over 0.5 to 4 min depending on the turbulence intensity. The number of velocity readings taken ranged from about 12 - 20 for each vertical velocity profile, with the readings located closer together near the bed where high velocity gradients occur, and near the edge of the boundary layer. Measurements were confined to the central half of the channel to be away from the side wall boundary layers. It was necessary to locate the secondary flow cells in order to choose the lateral spacing of the velocity profiles. This was done by injecting a line of dye across the entire channel width on the surface and observe its behavior as it travels downstream. If there were secondary flow structures present then the line of dye would split up into several streaks as shown in Figure 2.6. As streaks formed between cells where fluid is moving downward, the distance between 2 streaks represented 2 cells. By this method it was determined that the middle half of the channel contained 4 cells. The velocity profile locations were chosen to coincide with the low and high velocities produced by these secondary flow structures: 17 vertical profiles were taken for each longitudinal location for the smooth boundary and 13 profiles for the rough boundary. The lateral distance between each profile was between 0.3 - 0.6 of the flow depth. In the longitudinal direction, the velocity profiles continued to be taken until no more change was found in the velocity profiles going downstream. There were 10 longitudinal locations for each run for a total of about 170 profiles for the smooth and about 130 profiles for the rough. The longitudinal location of the profiles for the smooth run was x = 0.43, 1, 2, 3, 4, 5, 6, 7, 9, and 11 m, for the rough run it was x = 0.5, 1, 1.5, 2, 3, 4, 5, 6, 7, and 8 m. The occasional profile was repeated and was found not to vary significantly with time.

It was thought important to look at the experimental bed shear stress distribution of the boundary layer since this is an important parameter in the analytical approach, which uses a conservation of momentum formulation. It is also of interest for any sediment transport or heat transfer study within the channel entrance length. This shear stress or shear velocity on the smooth bed was measured using a Preston tube and a formula from Haitonidis(1989) was used:

$$\mathrm{Log}\left(\frac{u_*^2\, D_p^2}{4\nu^2}\right) = -1.39 + \frac{7}{8}\,\mathrm{Log}\left(\frac{u^2 D_p^2}{8\,\nu^2}\right) \qquad (2.1)$$

where D_p is the outer diameter of the pitot tube, u is the velocity given by the pitot tube when rested on the bed, and ν is the kinematic viscosity of water. The proper formula was used based on the criteria in Springer and Verlag. To test the accuracy of this technique, the shear stress was also calculated from a few velocity profiles using:

$$\frac{u}{u_*} = 2.5 \ln\left[\frac{y\,u_*}{\nu}\right] + 5.5 \tag{2.2}$$

where u is the velocity, and u_* is the shear velocity. The two methods were found to be in excellent agreement. A variation less than 5% was found.

The bed shear stress for the rough bed was determined by analysis of the velocity profiles. The roughness used was a floor mat with very rough and stiff protrusions about 10 mm long. A sample of the mat is shown in Figure 2.7. The mat only covered half the channel length but the boundary layer reached the surface well before the end of the mat. Before the shear stress for the rough channel could be determined, the hydraulic roughness k_s of the bed had to be measured. This was determined from 13 vertical velocity profiles taken 7.0 m from the entrance where the flow was essentially fully developed. It was assumed the lower 30% of the boundary layer thickness was described by:

$$\frac{u}{u_*} = 2.5 \ln\left[\frac{y_{u1} + y_d}{k_s}\right] + 8.5 \tag{2.3}$$

where y_{u1} is the vertical coordinate measured upward from the lowest velocity reading, and y_d is the distance from the lowest velocity reading to the theoretical point of zero velocity (See Figure 2.9). The viscous sublayer in this case was much smaller than the roughnesses. The velocity u was plotted verses $\log(y_{ul}+y_d)$ as shown in Figure 2.10. The bed location correction y_d was assigned 9 values at increments of 0.5 mm for each velocity profile and a least squares fit performed on the bottom 30% of the velocity readings, this included 4 to 6 points for each profile. The regression coefficient for each curve fit was used to determine the best log fit and best value of y_d. The y intercept when u=0 can be shown to be equal to $k_s/30$. By this method an average value of k_s was found to be 30 mm with a standard deviation of 10 mm, the average value of y_d was 5.9 mm with a standard deviation of 1 mm, and the average value of the shear velocity u_* was 0.0396 m/s. Since k_s is very sensitive to small errors in y_d and u_* , k_s was fixed at the average value of 30 mm and only y_d and u_* were readjusted to obtain the best log fit when u/u_* versus $\log((y_{ul}+y_d)/k_s)$ was plotted (See Figure 2.11). For x=7.0 m this gave an average y_d of 6.1 mm with a standard deviation of 0.42 mm, and gave an average u_* of 0.0402 m/s. It can be seen that by fixing k_s the standard deviation of y_d decreased and the average value of y_d and u_* remained relatively unchanged. This method of determining u_* and y_d with a fixed k_s was employed for all other profiles and the average y_d was 6.3 mm with a standard deviation of 0.9 mm. It is worth mentioning that the hydraulic roughness k_s was about 3 times the roughness height and the value of y_d would put the point of zero velocity about 4.8 mm below the top of the roughness elements and 5.2 mm above the bottom of the roughness elements.

Normally the boundary layer thickness is defined as the point where the velocity is 99% of the potential core velocity, but this definition was found to be unsuitable for these experiments because the potential core velocity sometimes had a 1% variation in it. Two methods of obtaining the boundary layer thickness were developed. The methods are explained in the following and illustrated in Figure 2.9. The first method consisted of checking the stripchart output for the potential core to see if the level of turbulence was low enough to be potential flow.(See Figure 2.5). As we increase the y coordinate, the point where the large turbulent fluctuations disappear was almost always the point where the velocity profile became vertical. This point was named δ_t ; the boundary layer thickness based on the turbulent criteria. No intermittent turbulence was found above this point. As the boundary layer grew, the potential core disappeared and δ_t was taken as the depth of flow. The second method consisted of drawing a vertical line through the potential core velocities or through the maximum velocity in the case where δ_t was equal to the depth of flow. Then a power law curve was fitted by regression through the velocity points in the boundary layer neglecting points in the potential core and in the transition region where the profile was tending to become vertical, this was systematically done by choosing points only up to where they did not deviate significantly from the power law as shown in Figure 2.9. The point where the vertical line and the fitted power curve intersected was taken as the boundary layer thickness based on the extrapolated intercept method and was labeled: δ_i. The power law exponent for each velocity profile was noted and is presented later in the analysis to compare with the numerical solution. It is not intended here to change the definition for determining the boundary layer thickness, but rather to use these two thicknesses as a tool to help establish a lower and upper bound to the δ based on 99% of the potential core velocity (δ_{99}). In velocity profiles with well behaved potential cores, these two methods always yielded: $\delta_i < \delta_{99} < \delta_t$.

Water surface elevations and depths were taken. The water surface was quite calm and the depths and elevations were reproducible within 0.1 mm. The depth was measured at each profile location by a point gauge readable to 0.1 mm. The elevation of the water surface was determined with a survey level which could also be read within 0.1 mm. The elevation was required to allow the Bernoulli equation to be evaluated for the potential core. This provided another check on the growth of the boundary layer and on the velocity measurements. To measure the depth for the rough boundary a modified point gauge was used. It had a horizontal flat plate just above the tip of the point gauge which rested on the tops of the roughness elements, while still providing a sharp tip when the point gage was placed on the water surface.

The salient features of the two experiments are summarized in Table 2.1. Great care was taken to try and match the bed slope to the precalculated slope of the energy line for fully developed flow. To do this an effort was made to ensure a constant depth existed in the fully developed region of the channel by adjusting the bed slope and tail gate position for a given discharge. However, the undulations in the bed were found to be of the same order as the slope itself, so accurate bed and surface slope matching was difficult.

2.2 Experimental results, analysis, and discussion.

This portion of the chapter refers to many figures which can be found at the end of the chapter. They contain the analysis for both the smooth and rough experiment. The smooth experiment is contained within Figures 2.12a to 2.27 and the rough between Figures 2.28a to 2.43. The order of the figures in both the smooth and rough sections is the same and each figure caption contains the words "*Smooth channel* " or "*Rough channel* " in italics to aid the reader.

2.2.1 Smooth channel

Figures 2.12a and 2.12b show typical velocity profiles in the developing portion and the developed portion respectively. Both figures are for one x section down the channel and the differences in the velocity profiles in each figure is attributed to secondary flows. A complete set of all profiles for the smooth experiment can be found in Appendix A. Note the differences in the boundary layer thicknesses in Figure 2.12a and the surface velocities and depth integrated discharges in Figure 2.12b.

Figures 2.13a and 2.13b show typical velocity profiles in an area of downwelling and upwelling respectively for different longitudinal locations. An area of downwelling occurs where flow between two secondary flow cells is moving downward and a area of upwelling occurs where it is moving upward. Note the acceleration of the potential core in both figures. This is what makes the boundary layer grow more slowly than on a flat plate where there is a constant potential core velocity. Note also the faster boundary layer growth in the area of upwelling.

As mentioned earlier, water surface elevations were taken so that the Bernoulli equation could be evaluated by adding the width averaged water surface elevation to the maximum velocity head obtained from each velocity profile. This was not done for every profile, but rather areas of the strongest upwelling and downwelling were chosen. The areas of the strongest downwelling corresponded to z = -0.335, -0.030 to 0.030, and 0.335 m, these where referred to as the left, centre, and right downwelling respectively. The areas of strongest upwelling corresponded to z = -0.152, and 0.213 m and were referred to as the left and right upwelling respectively. The Bernoulli equation is evaluated and plotted in Figure 2.14 for the five regions of interest. The elevation of the water surface is also plotted as a reference. As one would expect, the Bernoulli equation should be constant within the potential core; as one examines Figure 2.14 closely, the areas of downwelling stay constant until about x = 9 m and the areas of upwelling to about x = 3 and 4 m. These locations where the value of the Bernoulli equation started to decrease also corresponded to the location where the turbulence or δ_t reached the surface. Note that all five curves eventually become parallel with the water surface. Not only did the evaluation of the Bernoulli equation show the decay of the potential core, but also showed that the velocity and water surface elevations where reasonably accurate. The elevation is used once again to evaluate the total energy line later in the discussion.

Figure 2.15a shows the boundary layer thickness based on turbulence criteria (δ_t) plotted in the transverse direction for different longitudinal locations. Note the effect of the secondary currents on the growth of δ_t. Figure 2.15b shows the same δ_t but from a longitudinal view point. Also shown is the width averaged δ_t and the width averaged distance where δ_t reaches the surface. Note that this distance does not correspond to where the width averaged δ_t reaches the surface. This is because as long as there is at least one δ_t less then the depth, then the average will not reach the surface. This is important later when the experiment is compared with the numerical solution.

Figure 2.16a shows the boundary layer thickness based on the extrapolated intercept method (δ_i) plotted in the transverse direction for different longitudinal locations. Again, note the effect of the secondary flows on the transverse variation of δ_i. Figure 2.16b shows the same δ_i but from a longitudinal view point. Also shown is the width averaged δ_i. Note in Figure 2.16b that δ_i rarely attains a value equal to the depth of about 0.104 m. This is due to the slight deviation from the power or log law of the top portion of the fully developed profile; the profile is more vertical near the surface than suggested by the power or log law.

Figure 2.17a shows both width averaged δ_t and δ_i along with the numerical solution and Schlichting's smooth flat plate solution(1934). Note that the growth rate of the numerical solution agrees better with the experimental data than the smooth flat plate solution. The potential core velocity used for the Schlichting's solution was the average of U_1 and U_{end}. U_1 is the initial potential core velocity at the channel entrance and U_{end} is the surface velocity when the boundary layer reaches the surface.

As mentioned earlier, there is a problem with the width averaged δ_t as it approaches the surface. This is attempted to be resolved in Figure 2.17b by only considering the width averaged values of δ_t before any individual δ_t reaches the surface. that is for x <= 3.0 m (See Figure 2.15b). A line is then interpolated between this point and the average distance δ_t takes to reach the surface for the remainder of the average δ_t growth. In this way it might be possible to predict the growth of δ_t if there where no secondary flow cells present. As δ_t is generally greater than δ_{99} it agrees well with the numerical solution. Also note in Figure 2.17a or 2.17b the undulations in the width averaged depth when compared with the nearly constant numerical solution. This is due to the undulations in the bed.

Since the numerical solution uses the definitions of displacement thickness (δ_*) and momentum thickness (θ), these two quantities were obtained from each velocity profile so a comparison could be made. Since δ_* and θ come directly from a integration process using the velocity profiles, they are a less judgmental values than δ_t and δ_i, where there is need to judge the level of turbulence or to decide which part of the boundary layer to use for the power law fit. This makes them valuable experimentally. But the trouble comes again when the individual boundary layers reach the surface and the maximum velocity for each profile is no longer constant for each x section. Since the integration procedure involves the quantity (U_{max}-u), one would expect the comparison to be valid up to about x=3.0 m for δ_* and θ.

Figure 2.18a shows the displacement thickness plotted in the transverse direction for different longitudinal locations and Figure 2.18b shows δ_* from a longitudinal view point. Also shown in 2.18b is the width averaged δ_* growth rate and the numerical δ_*. The numerical and experimental values agree well until about x = 3.0 m where the lateral difference in U_{max} starts to have an effect. The experimental fully developed width averaged displacement thickness is about 82% of that given by the numerical solution. This is due to the slight difference in the velocity profiles described earlier; the power law has a slightly higher surface velocity (U_{max}) than the actual velocity profile.

The same can be said for the momentum thickness θ as was in the above for δ_*. The difference being θ is represented in Figures 2.19a and 2.19b and experimental width averaged fully developed θ is 79% of the numerical value.

Figure 2.20 shows the bed shear stress plotted in the transverse direction for different longitudinal locations. The lateral variation of shear stress varied by 30% and was found to be consistent with the secondary flow cell structures; shear stress was high where fluid was moving downward and low where fluid was moving upward. Figure 2.21 shows the minimum, maximum, and width averaged shear stress in the longitudinal direction as well as the numerical solution and Schlichting's smooth flat plate solution. Surprisingly, the width averaged shear varies little in the longitudinal direction; it varies less than that predicted by Schlichting's smooth flat plate solution and agrees better with the numerical solution. This low variation of shear stress in the longitudinal direction can be explained by the following: the shear stress decreases with an increase in boundary layer thickness but increases with an increase in potential core velocity, so in the flat plate case where the potential core velocity is constant, and the boundary layer thickness is increasing, the shear stress has no choice but to decrease. In an open channel the effects are compensating; as the boundary layer thickens the potential core is accelerating and the shear stress tends to be evened out.

Figure 2.22a shows the discharge per unit width as integrated from the velocity profiles plotted in the transverse direction for different longitudinal locations. The trapezoidal rule was used to integrate the velocity profiles. The higher discharge occurred in areas of downwelling, the lower discharge occurred in areas of upwelling. Figure 2.22b shows q from the longitudinal viewpoint and shows that the secondary flows have a progressively increasing influence on lateral variation of discharge as the flow develops. The maximum lateral variation in unit discharge was 19%. The width averaged unit discharge remained fairly constant in the longitudinal direction;

Figure 2.23 shows the reciprocal of the width averaged power law exponent 1/n from regressional curve fits of the boundary layer portion of the velocity profiles. Also shown is the numerical solution. Considering the distortional effects of the secondary flows, they are in pretty good agreement. The experimental power law exponent decreases from about 1/6.6 at the first x section to about 1/7.1 when fully developed. The numerical curve lies somewhat lower near the entrance but is in good agreement after x = 2 m. This could be due the properties of the velocity field along the curved inlet surface having an affect on the boundary layer some distance downstream from the entrance.

Before the total energy and momentum could be calculated, the correction coefficients α and β had to be calculated from each velocity profile. Figure 2.24 shows the width averaged momentum and energy correction coefficients obtained from the velocity profiles. When width averaging the total energy and momentum, the correction coefficients for each individual velocity profile were used and than the width averaging was performed.

Figure 2.25 shows the width averaged total energy, water surface elevation and bed elevation. In general, the slope of the energy line tended to get steeper as the boundary layer developed and the slope of the water surface tended to get milder, both lines became of equal slope when the flow was fully developed. Note the bed undulations, the low points at x = 0.43 and 5 m, and the high points at x = 3 and 6 m. It was unclear if they had significant effect on the boundary layer growth but they did have an effect on the depth averaged velocity, the maximum velocity, and the longitudinal shear stress distribution. When comparing Figure 2.26 with 2.25, it can be seen that the width averaged maximum velocity and the width averaged depth averaged velocity both show variations consistent with the bed undulations. There is an higher than normal increase in V between x = 0.43 and 2 m, there is a decrease in V through the dip at x = 5 m, and a higher than normal increase in V between x = 5 and 6 m where the bed comes up slightly again. The maximum velocity U_{max} is affected in a similar fashion. When comparing the width averaged shear stress in Figure 2.21, the shear stress increases slightly at x = 6 m where there is high point on the bed. The width averaged momentum is shown in Figure 2.27 and also seems to be at the mercy of the bed undulations.

2.2.2 Rough channel

Rather than restating the same comments for each figure of the rough experiment, only the differences from the smooth will be discussed and some of the similarities stated.

Figures 2.28a and 2.28b show typical velocity profiles in the developing portion and the developed portion respectively. A complete set of all profiles for the rough experiment can be found in Appendix B. Note that there is a bigger difference in the velocity profiles in the lateral direction than for the smooth channel.(Figures 2.12a and 2.12b).

Figures 2.29a and 2.29b show typical velocity profiles in an area of downwelling and upwelling respectively for different longitudinal locations. Again, there is higher boundary layer growth rate for the upwelling and slower growth rate for the downwelling. When comparing with the smooth Figures 2.13a and 2.13b, the potential core acceleration is much greater for the rough than the smooth. This is because the channel is on a higher slope to attain uniform flow for the higher roughness.

Evaluation of the Bernoulli equation in Figure 2.30 showed similar decay of the potential core as the smooth. As expected, the potential core decayed more quickly for the rough experiment; decay started to take place at x = 4.0 m for the downwellings and x = 2.0 m for the upwellings. The areas of the strongest downwelling corresponded to z = -0.335, -0.030 to 0.0, and 0.335 m. The areas of strongest upwelling corresponded to z = -0.152, and +0.152 m.

Figure 2.31a shows the boundary layer thickness based on turbulence criteria (δ_t) plotted in the transverse direction for different longitudinal locations. Figure 2.31b shows the same δ_t but from a longitudinal view point. Also shown is the width averaged δ_t and the width averaged distance where δ_t reaches the surface. When comparing the δ_t growth with the smooth and rough, figures 2.15b and 2.31b, notice the larger effect of the secondary flows on δ_t for the smooth case. Although it was observed that the secondary flows were stronger for the rough experiment by evidence of dye and their effect on lateral shear and discharge, their effect on the boundary layer in the lateral direction was smaller. This was because the boundary layer growth was much more rapid for the rough channel so the secondary flows did not have the time or distance to create such a difference.

Figure 2.32a shows the boundary layer thickness based on the extrapolated intercept method (δ_i) plotted in the transverse direction for different longitudinal locations. Figure 2.32b shows the same δ_i but from a longitudinal view point. Also shown is the width averaged δ_i. The behavior is similar as in the smooth channel but the lateral variation is less for reasons mentioned above.

Figure 2.33a shows both width averaged δ_t and δ_i along with the numerical solution and Harrison's rough flat plate solution(1967) after Granville(1958). Note that the growth rate of the numerical solution agrees better with the experimental than the rough flat plate solution. The potential core velocity used for the Harrison's solution was the average of U_1 and U_{end}. The problem with the width averaged δ_t as it approaches the surface was resolved in Figure 2.33b by the same technique as for the smooth experiment to help predict the growth of δ_t if there where no secondary flow cells present. As δ_t is generally greater than δ_{99}, it agrees well with the numerical solution. Also note in Figure 2.33a or 2.33b the undulations in the width averaged depth when compared with the nearly constant numerical solution are again due to the undulations in the bed.

Figure 2.34a shows the displacement thickness plotted in the transverse direction for different longitudinal locations and Figure 2.34b shows δ_* from a longitudinal view point. Also shown in 2.34b is the width averaged δ_* growth rate and the numerical δ_*. The numerical and experimental values agree well until about x = 2.0 m where the lateral difference in U_{max} starts to have an effect. The experimental fully developed width averaged displacement thickness is about 69-79% of that given by the numerical solution. This is again due to the slight difference in the velocity profiles described earlier; the power law has a slightly higher surface velocity (U_{max}) than the actual velocity profile. The decrease from 79% to 69% between x = 4.0 m and x = 7.0 m is unclear and may have something to do with further adjustment of the velocity profiles after all the potential core is eliminated.

The same can be said for the momentum thickness θ as was in the above for δ_*. The difference being θ is represented in Figures 2.35a and 2.35b and experimental width averaged fully developed θ is 67-75% of the numerical value. The experimental and numerical θ in the developing portion do not agree as closely as in the smooth case.

Figure 2.36 shows the bed shear stress plotted in the transverse direction for different longitudinal locations. (The first value of shear at x=0.5 m in Figure 2.36 is suspected to be high as this location is only about 7 cm away from the leading edge of the roughness mat where it is possible to have a boundary layer growing within a boundary layer and there are less data points to match the profile in the logarithmic region for the thinner boundary layer.) The lateral variation of shear stress varied much more in the rough experiment than the smooth; a 100% variation in bed shear was found compared to 30% in the smooth. The variation was again consistent with the secondary flow cell structures. This explains the existence of sediment streaks in natural channels (Figure 1.1). Figure 2.37 shows the minimum, maximum, and width averaged shear stress in the longitudinal direction as well as the numerical solution and Granville's rough flat plate solution. Again, the width averaged shear varies little in the longitudinal direction; it varies less than that predicted by Granville's rough flat plate solution and shows the same degree of uniformity as the numerical solution. As can be seen in Figure 2.37, the numerical shear stress is about 20% lower than the experimental values and could be the result of the higher difficulty in obtaining the shear stress and depth measurements for a rough bed. It was however, theoretically impossible to find the right combination of discharge, roughness, and slope of the energy line to satisfy the experimental values of discharge, roughness, energy line slope, and depth of flow. The dimensionless Chezy equation $V/u_*=2.5 \ln(12d/k_s)$ was used along with the definition of uniform flow $u_* = (g\ d\ S_f)$^0.5. It will be left for a later time to unravel this mystery. Although there is a discrepancy between the experimental and theoretical shear stress, the relative behavior in the lateral and longitudinal direction is felt to be preserved.

Figure 2.38a shows the discharge per unit width as integrated from the velocity profiles plotted in the transverse direction for different longitudinal locations. The higher discharge again occurred in areas of downwelling, the lower discharge occurred in areas of upwelling. Figure 2.38b shows q from the longitudinal viewpoint and show again that the secondary flows have a progressively increasing influence on lateral variation of discharge as the flow develops. The maximum lateral variation in unit discharge was 26% compared to 19% in the smooth experiment. The width averaged unit discharge remained fairly constant in the longitudinal direction.

Figure 2.39 shows the reciprocal of the width averaged power law exponent 1/n from regressional curve fits of the boundary layer portion of the velocity profiles. Also shown is the numerical solution. The experimental power law exponent decreases from about 1/2 at the first x section to about 1/3.2 when fully developed. The numerical curve lies somewhat lower near the entrance but is in good agreement after $x = 2$ m. This could be due to the closeness of the leading edge of the roughness mat to the first x section, as well as the properties of the velocity field along the curved inlet surface having an effect on the boundary layer some distance downstream from the entrance. The power law exponent for uniform flow had slightly lower value of 1/3.2 compared with the numerical value of 1/2.8.

Figure 2.40 shows the width averaged momentum and energy correction coefficients obtained from the velocity profiles. Note that the values are somewhat higher than for the smooth channel in Figure 2.24.

Figure 2.41 shows the width averaged total energy, water surface elevation and bed elevation. The general behavior was even more pronounced than for the smooth channel; the slope of the energy line tended to get steeper as the boundary layer developed and the slope of the water surface tended to get milder, both lines became of equal slope when the flow was fully developed. The effect of the bed undulations have a smaller affect because relatively they are smaller when compared with the higher bed slope.

The slightly imprecise matching of Umax, V, and Momentum in Figures 2.42 and 2.43 between the measured and the numerical is due to the the difficulty in exactly modelling the uniform flow condition discussed earlier, but the general behavior is similar with the exception of some decrease in U_{max}, V, and Momentum after about x = 4.0 m. This is due to the slight increase in depth after this point due to bed imperfections and inexact tailgate settings.

2.2.3 General discussion

Now comes the difficult part in establishing what the average entrance length is for the two experiments. Since the boundary layer thickness at the inlet of the channel (x = 0.0 m) is a function of the inlet geometry, the virtual origin based on a backward extrapolation of the boundary layer thickness was used. For the smooth channel, the origin was found to be at x = -0.4 m, both for the experiment and numerical solution (See figure 2.17a or 2.17b) The origin for the rough channel was more difficult to define since the roughness mat did not start until about x = 0.43 m. Since the first section of the roughness mat was only 7 cm downstream of this leading edge, the rate of growth at the first x section would be smaller than expected for that thickness and roughness. This had an effect on the location of the origin. The origin for the experimental data was chosen to be just ahead of the roughness mat at x = 0.3 m by extrapolating the δ_t and δ_i curves to about the same starting boundary layer thickness as the numerical solution. (See Figure 2.33a or 2.33b). The origin for the numerical solution was taken at x = 0.7 m to best fit the numerical solution downstream of x = 1.0 m since it is far enough from discrepancies caused by the leading edge of the roughness mat.

The boundary layer thickness based on the turbulence criteria (δ_t) was the best way of determining the entrance length. It was thought to underpredict the entrance length slightly, since the turbulence continued to develop for about another 10 depths for the smooth experiment, and a another 5 for the rough, after δ_t reached the surface. So the average entrance length was given a range; it was between the average distance δ_t took to reach the surface plus an extra 10 and 5 depths respectively. Taking the origins into account, the entrance lengths in terms of number of depths are tabulated in Table 2.2. In addition to the average entrance lengths, the minimum and maximum entrance lengths are also presented. The minimum entrance length occurred between two secondary flow cells where fluid was moving upward and the maximum occurred between two cells where fluid was moving downward. The numerical, Schlichting, and Harrison solutions are also tabulated for comparison. Table 2.3 shows the entrance length as a percentage of the experimental average for comparison. Looking at Table 2.3 under the minimum and maximum columns, one can see the importance of width averaging when making boundary layer measurements; for the smooth channel the error in measuring the entrance length could have ranged from 44% under to 54% over; for the rough, 45% under to 39% over. For the smooth channel, the numerical solution over predicted the entrance length by 2%, and the Schlichting's smooth flat plate solution under predicted the entrance length by 15%. For the rough channel, the numerical solution under predicted the entrance length by 9%, and the Harrison's rough flat plate solution under predicted the entrance length by 40%.

The secondary flow cells were about 1.47 and 1.39 depths wide for the smooth and rough channel respectively. This differs from the range of values of 0.84 to 1.2 found by the other investigators. It was observed that the number of cells changed if the depth in the channel was changed, but there was a certain range of depths for which the number of cells did not change.

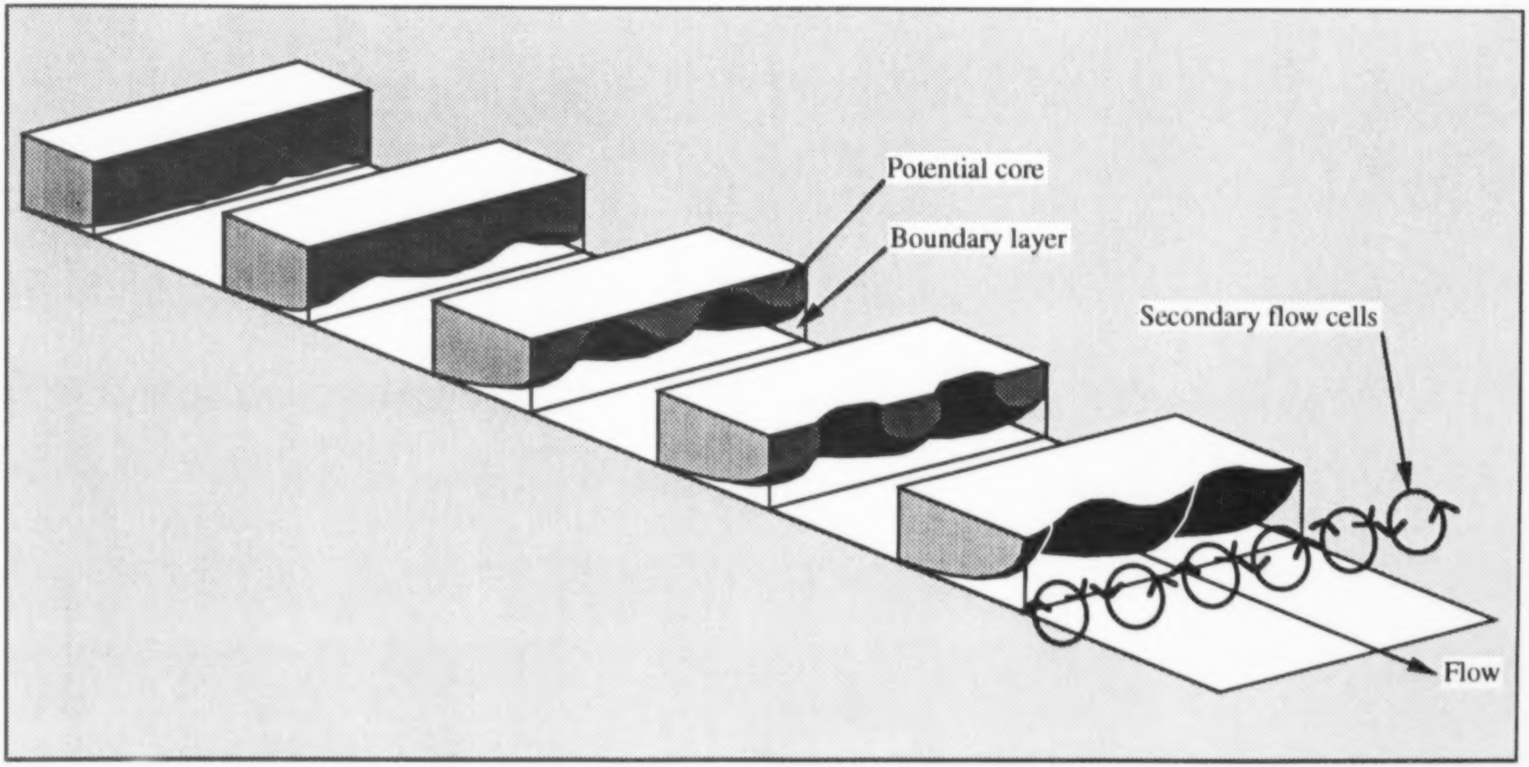
Potential core
Boundary layer
Secondary flow cells
Flow

Fig. 2.1 Illustration of the effect of secondary flows on boundary layer growth in the central portion of a wide open channel.

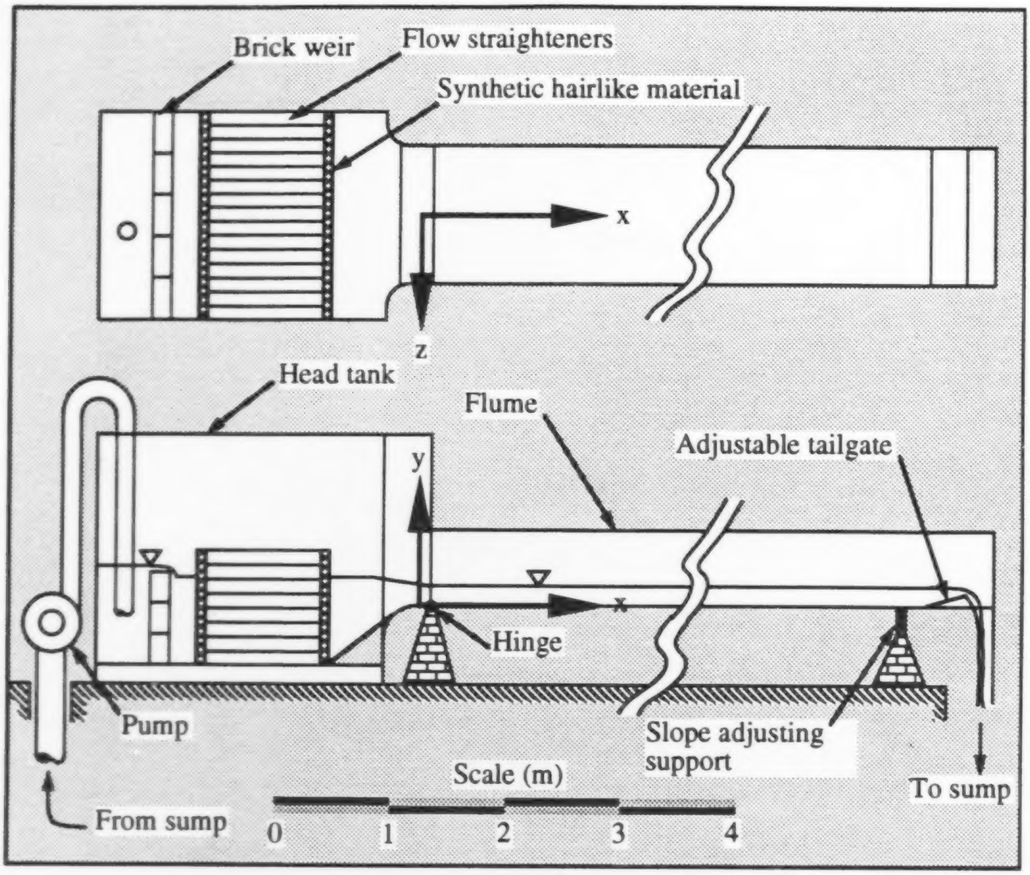
Brick weir
Flow straighteners
Synthetic hairlike material
x
z
Head tank
Flume
Adjustable tailgate
y
x
Hinge
Pump
Slope adjusting support
To sump
Scale (m)
0
1
2
3
4
From sump

Fig. 2.2 Experimental setup and coordinate system.

Run #	Bed type	q (m^2/s)	S_f	k_s (m)	d_o (m)
1	Smooth	0.038	0.00027	0	0.104
2	Rough	0.035	0.00115	0.03	0.110

Table 2.1 Summary of experiments.

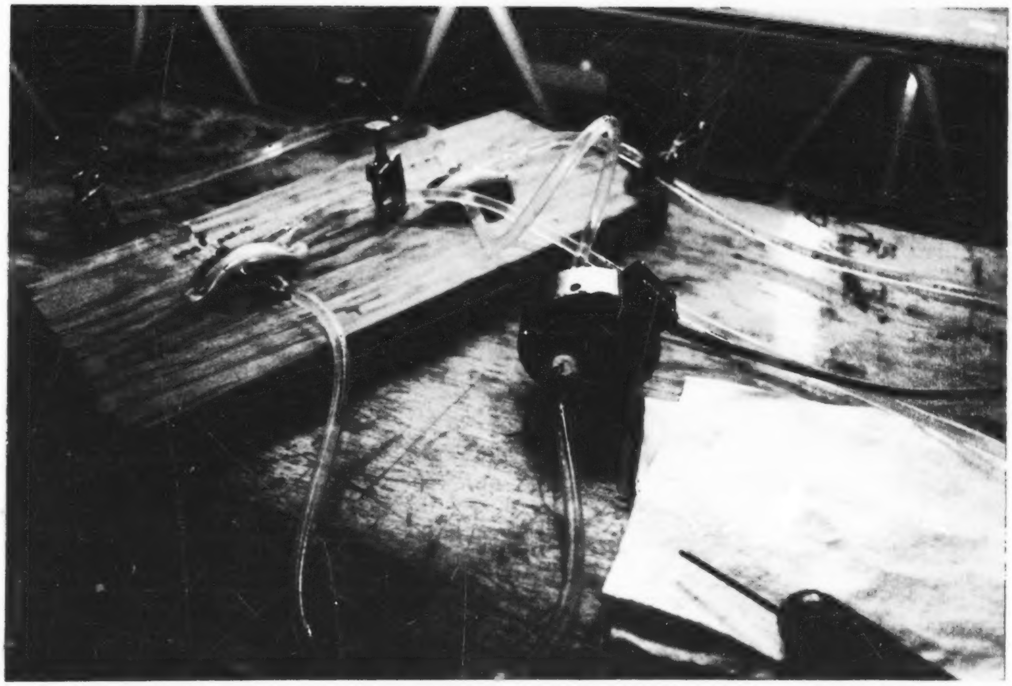

Fig. 2.3 Pressure transducer used for measuring velocities

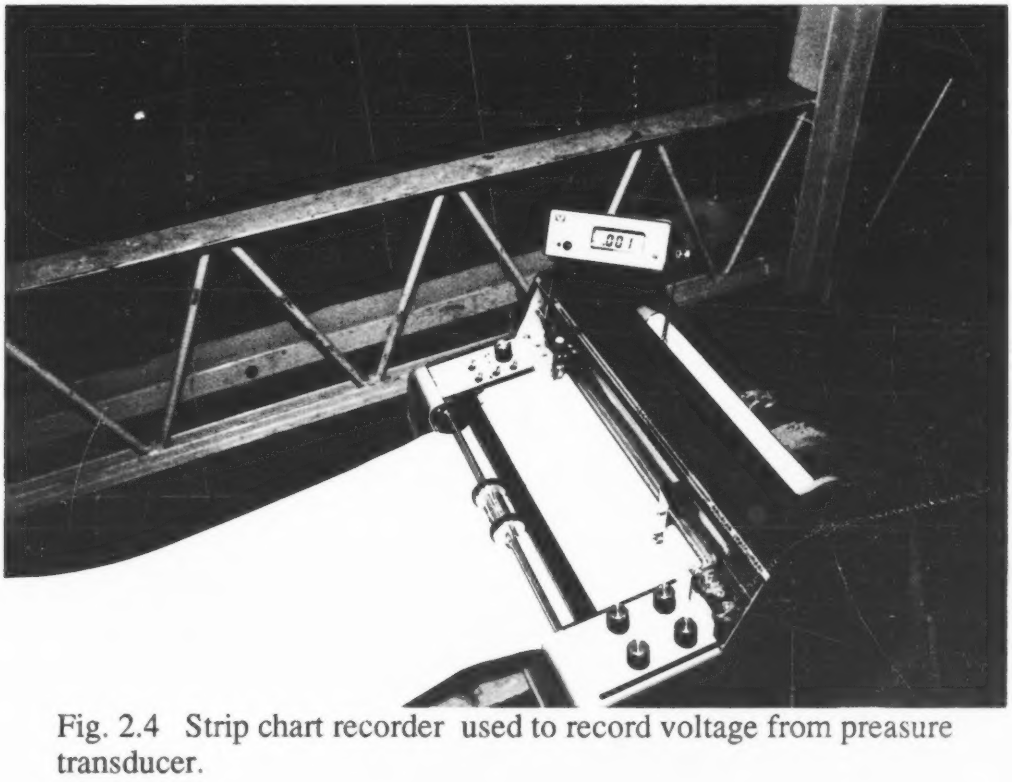

Fig. 2.4 Strip chart recorder used to record voltage from preasure transducer.

Fig. 2.5 Sample of strip chart recorder output.

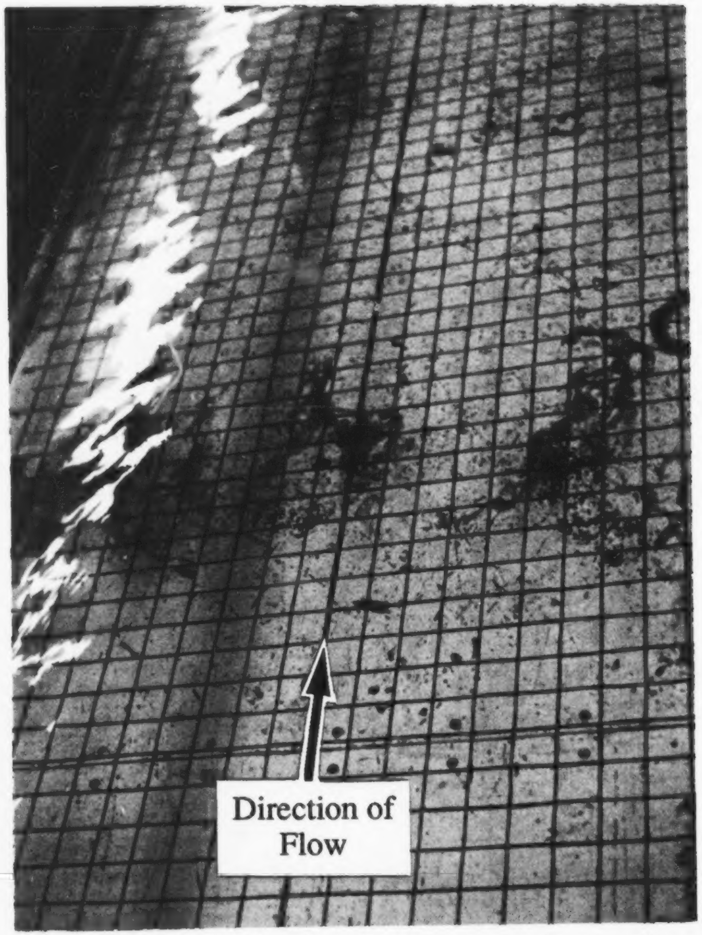
Direction of
Flow

Fig. 2.6 Dye indicating the presence of secondary flow cells

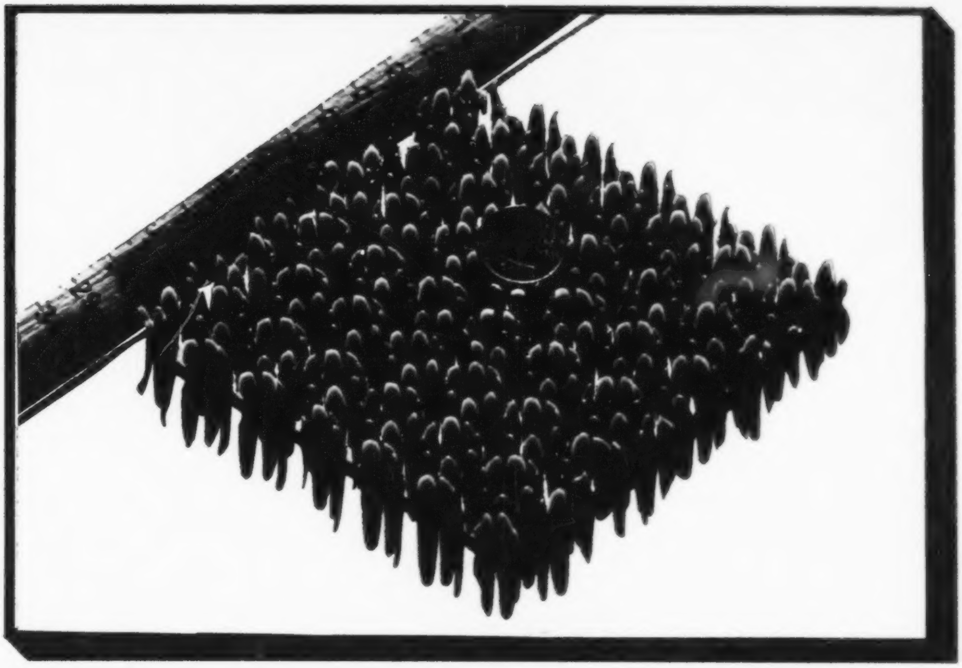

Fig. 2.9 Sample of roughness mat used for the rough experiment.

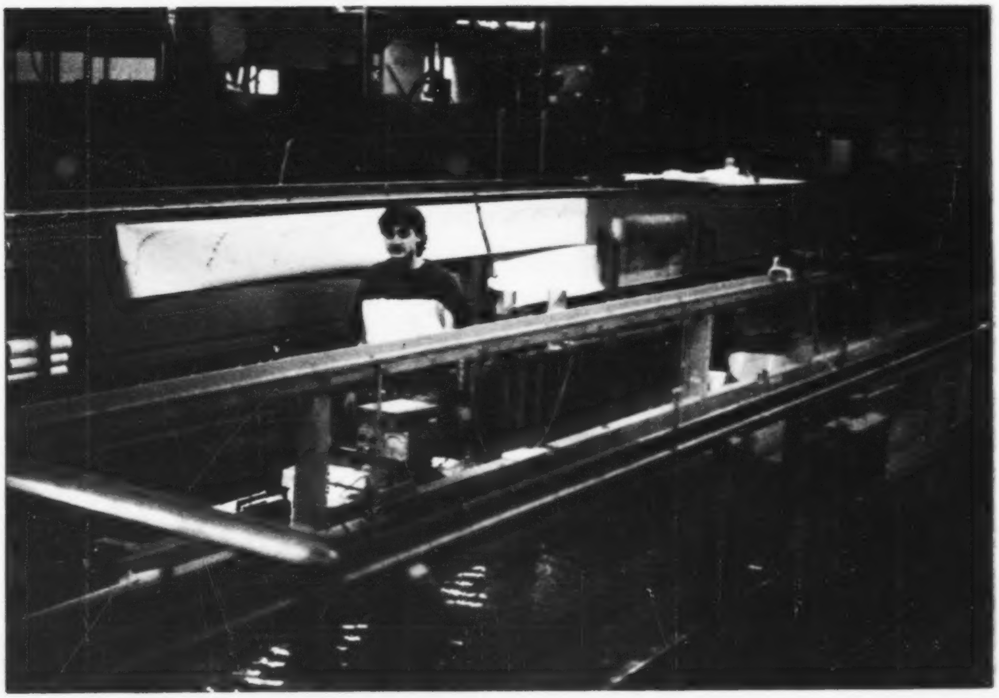

Fig. 2.8 Flume and traverse used for the experiments.

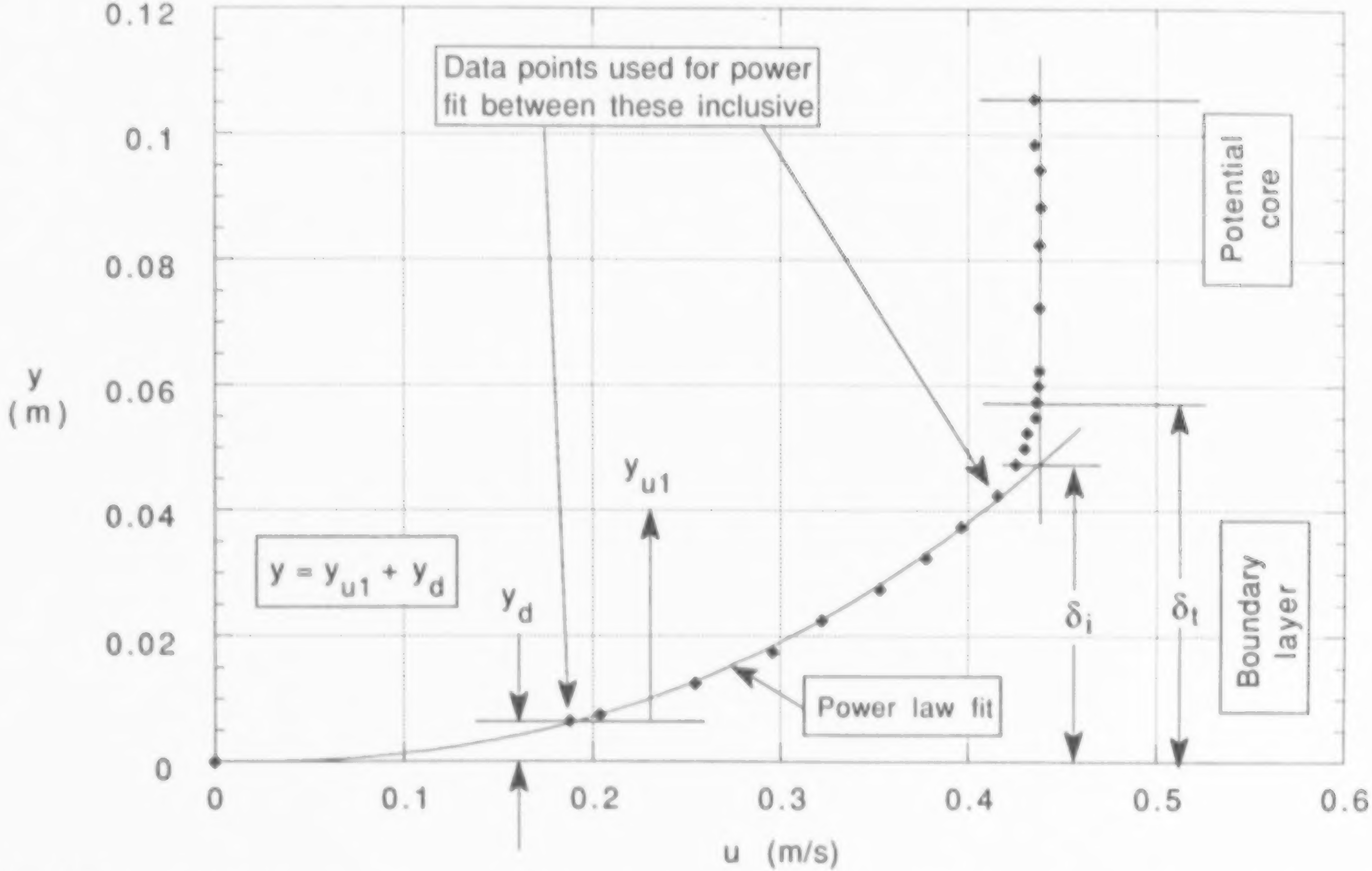

Fig. 2.9 Example velocity profile showing method of obtaining the boundary layer thicknesses δ_t and δ_i. Also shown is the definition of the vertical coordinate for rough bed.

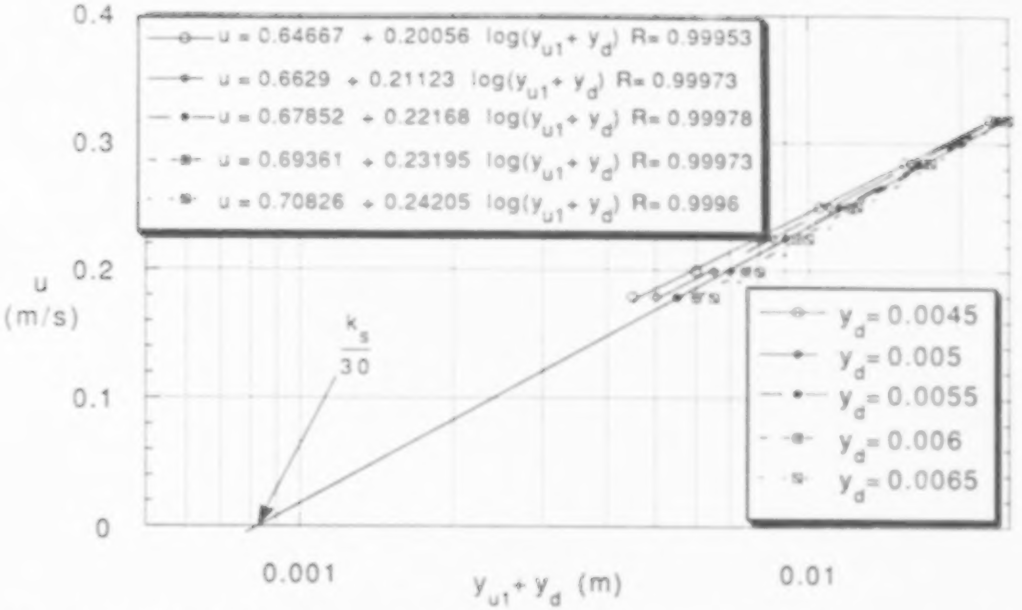

Fig. 2.10 The hydraulic roughness k_s was determined by regression by varying y_d at 0.5 mm intervals.

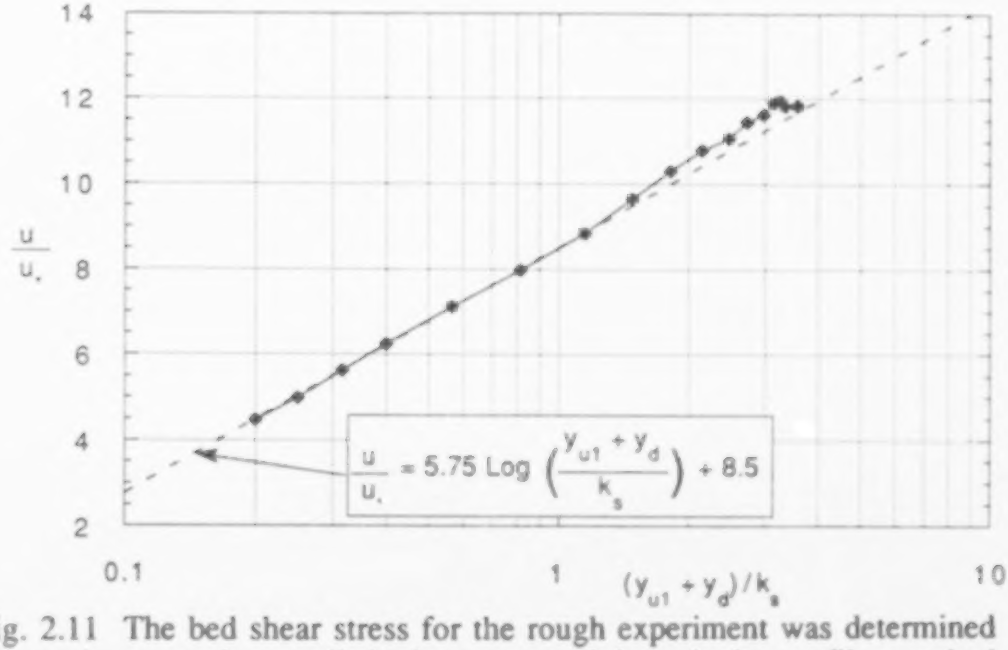

$$\frac{u}{u_*} = 5.75 \,\mathrm{Log}\left(\frac{y_{u1} + y_d}{k_s}\right) + 8.5$$

Fig. 2.11 The bed shear stress for the rough experiment was determined by varying u_* and y_d until the lower part of the velocity profile matched the theoretical expression.

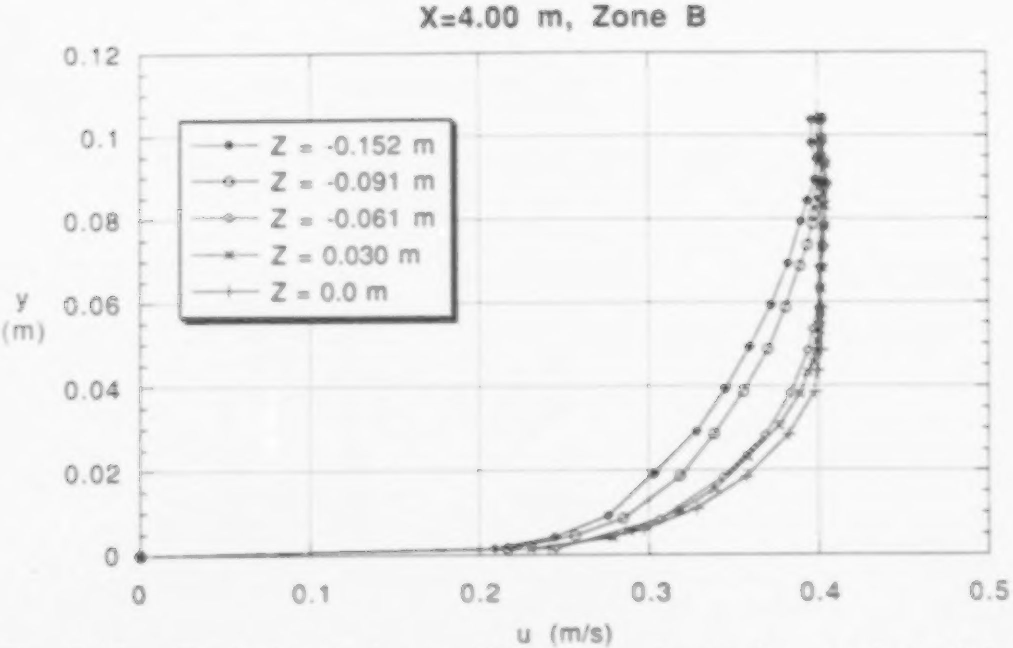

Fig. 2.12a Typical velocity profiles in the developing portion of the *smooth channel* for different transverse locations.

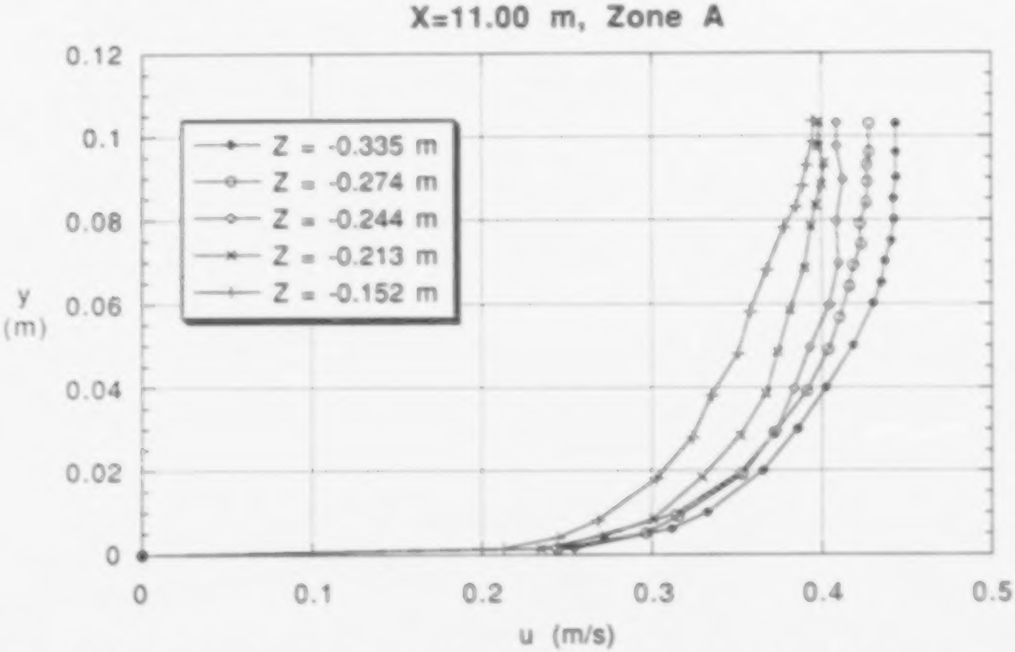

Fig. 2.12b Typical velocity profiles in the developed portion of the *smooth channel* for different transverse locations.

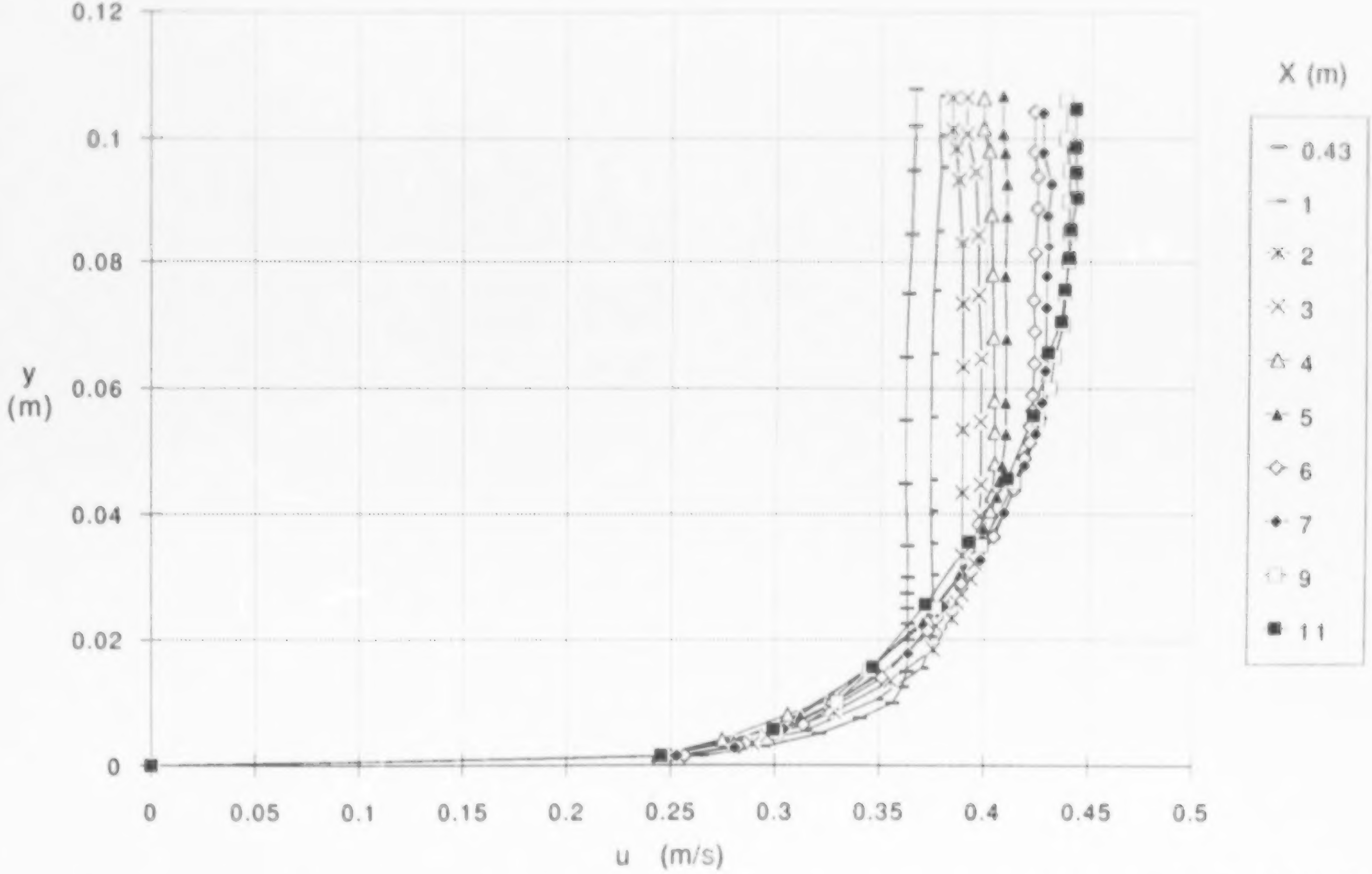

Fig. 2.13a Velocity profiles in an area of downwelling (Z = 0.335 m) for different longitudinal locations. *(Smooth channel)*

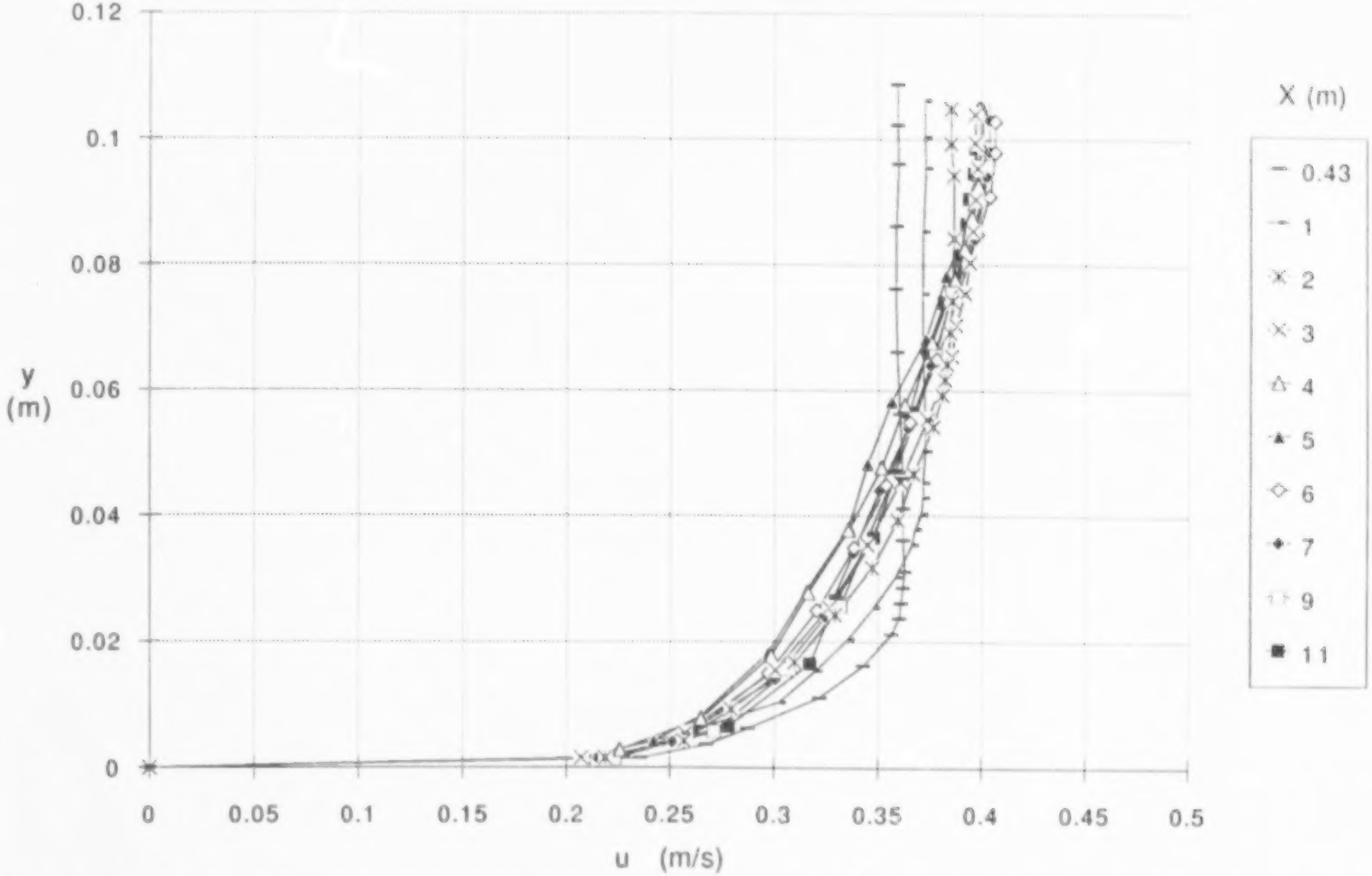

Fig. 2.13b Velocity profiles in an area of upwelling (Z = 0.092 m) for different longitudinal locations. *(Smooth channel)*

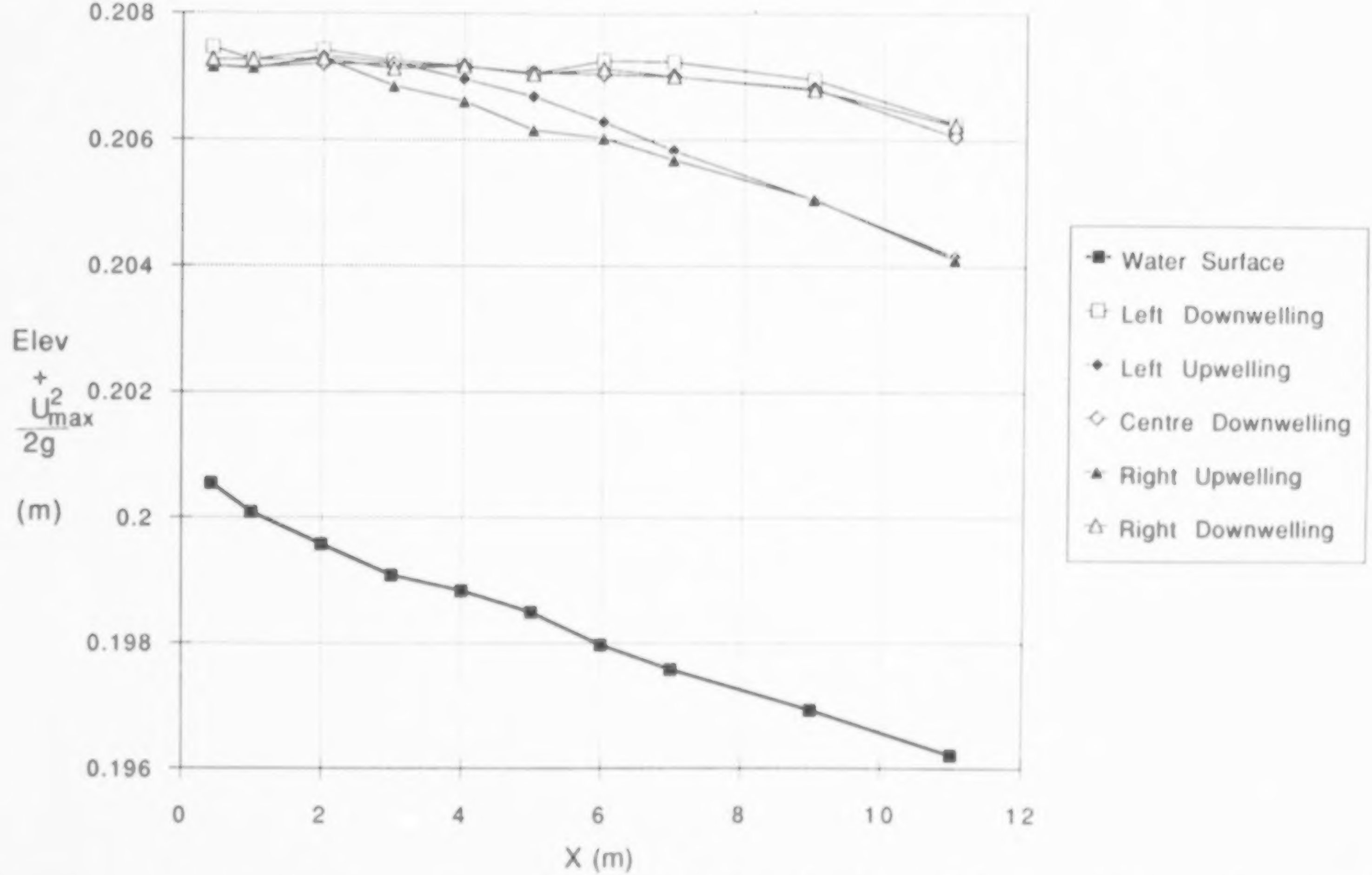

Fig. 2.14 Evaluation of the Bernoulli equation to help indicate the decay of the potential core and to asses the reliability of elevation and velocity measurements. *(Smooth channel)*

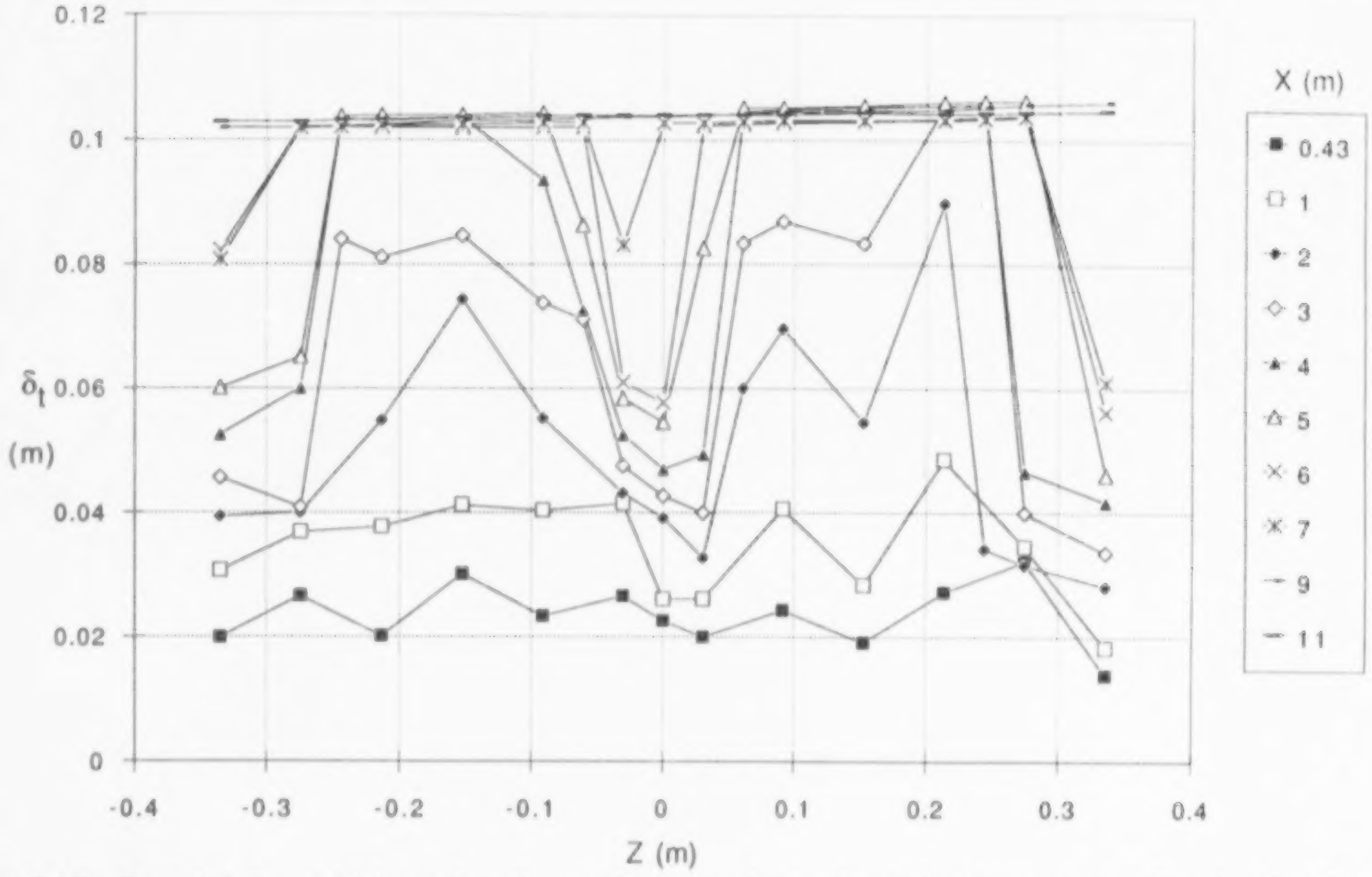

Fig. 2.15a Boundary layer thickness based on turbulence criteria plotted in the transverse direction for different longitudinal locations. *(Smooth channel)*

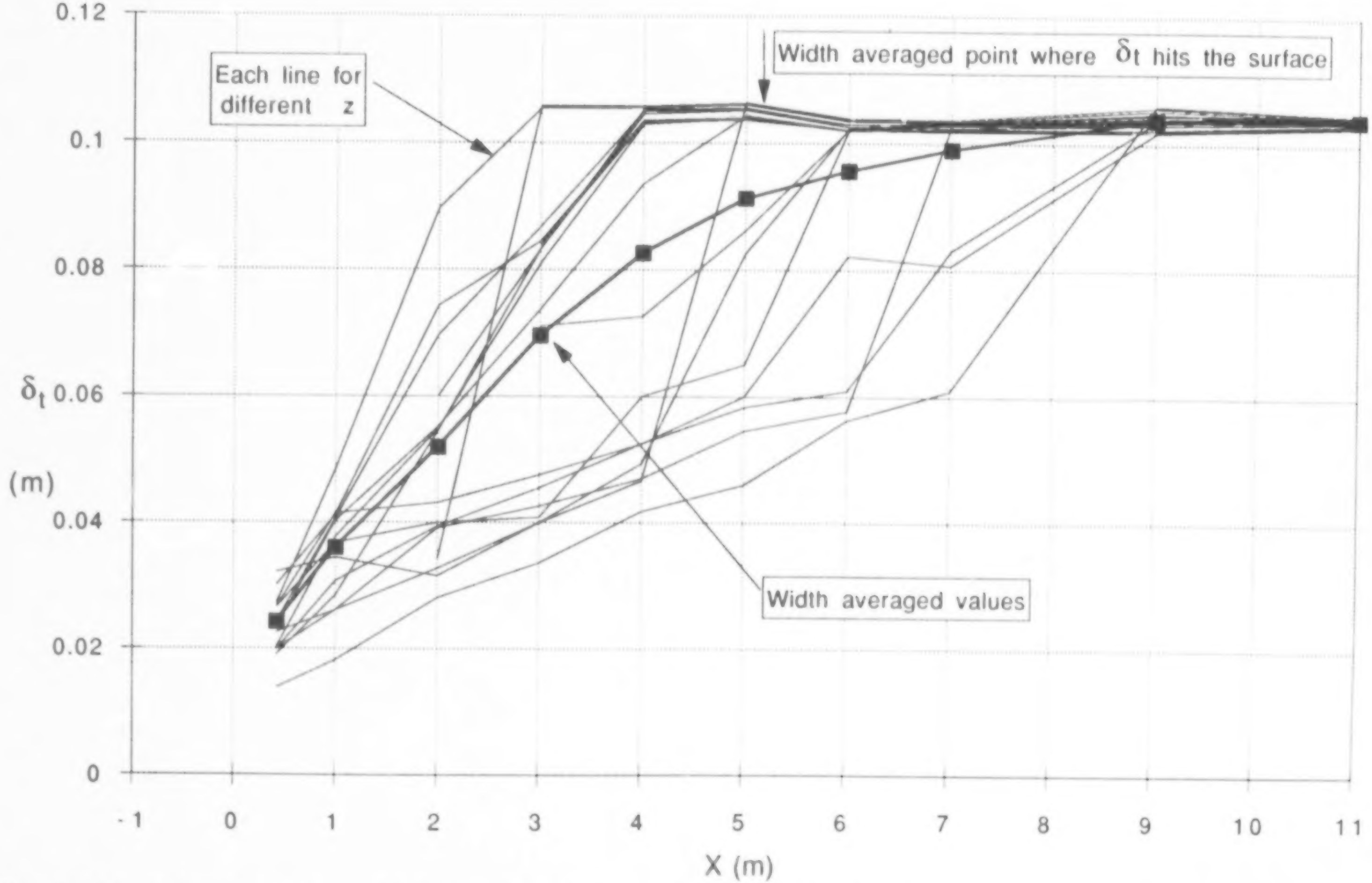

Fig. 2.15b Boundary layer thickness based on turbulence criteria plotted in the longitudinal direction for different transverse locations. Also shown is the width averaged δ_t growth. *(Smooth channel)*

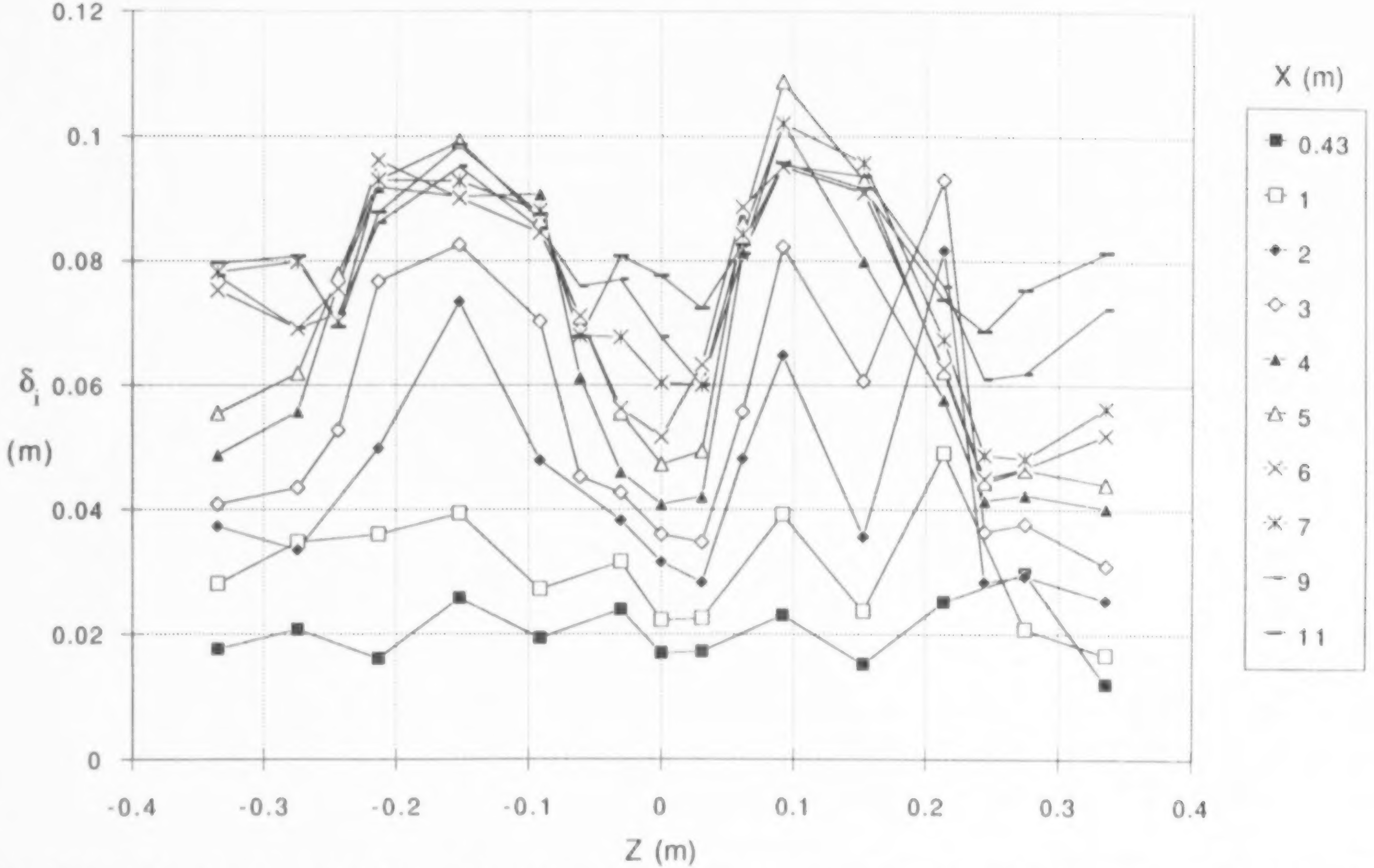

Fig. 2.16a Boundary layer thickness based on extrapolated intercept method plotted in the transverse direction for different longitudinal locations. *(Smooth channel)*

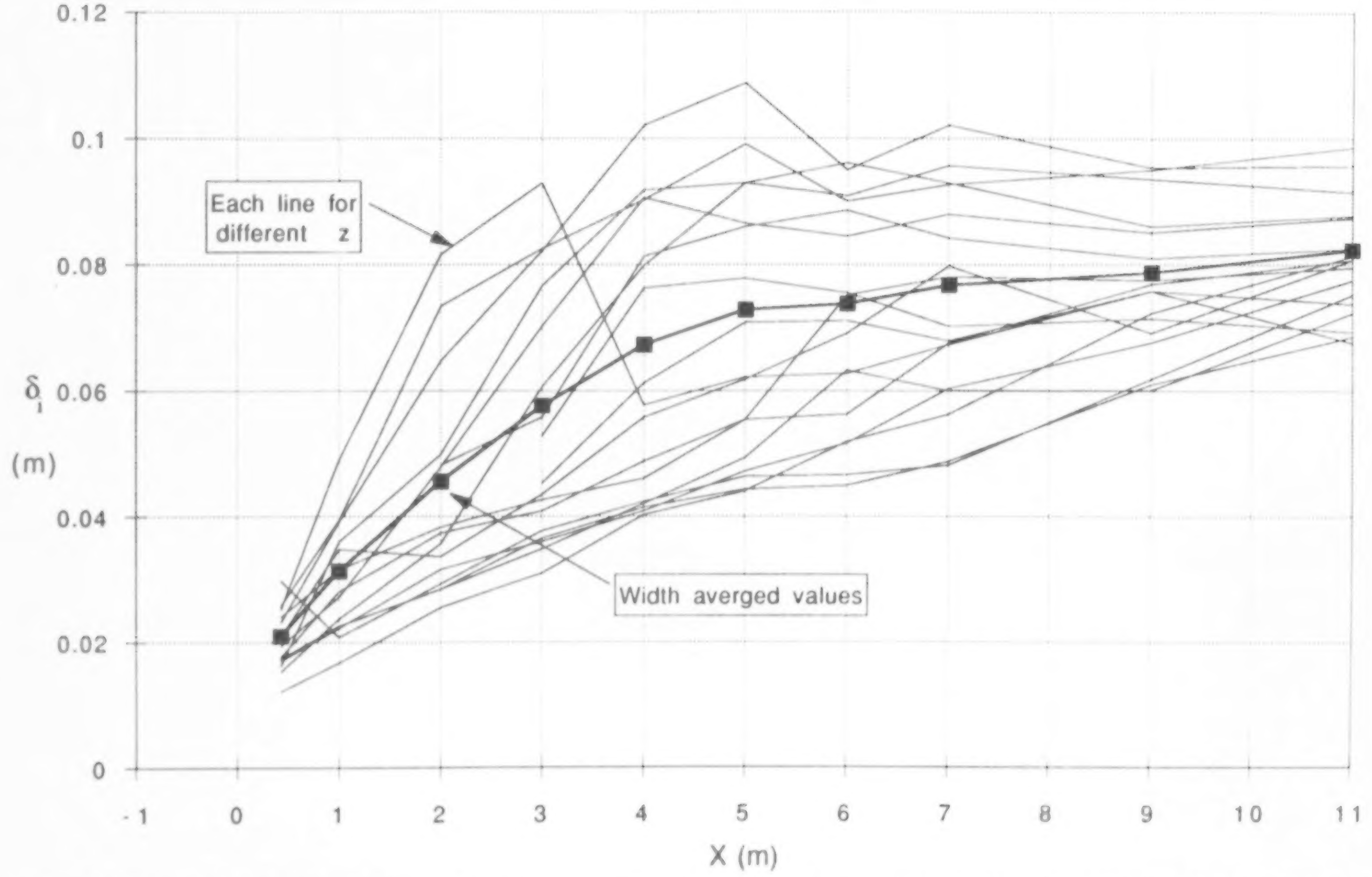

Fig. 2.16b Boundary layer thickness based on extrapolated intercept method plotted in the longitudinal direction for different transverse locations. Also shown is the width averaged δ_i growth. *(Smooth channel)*

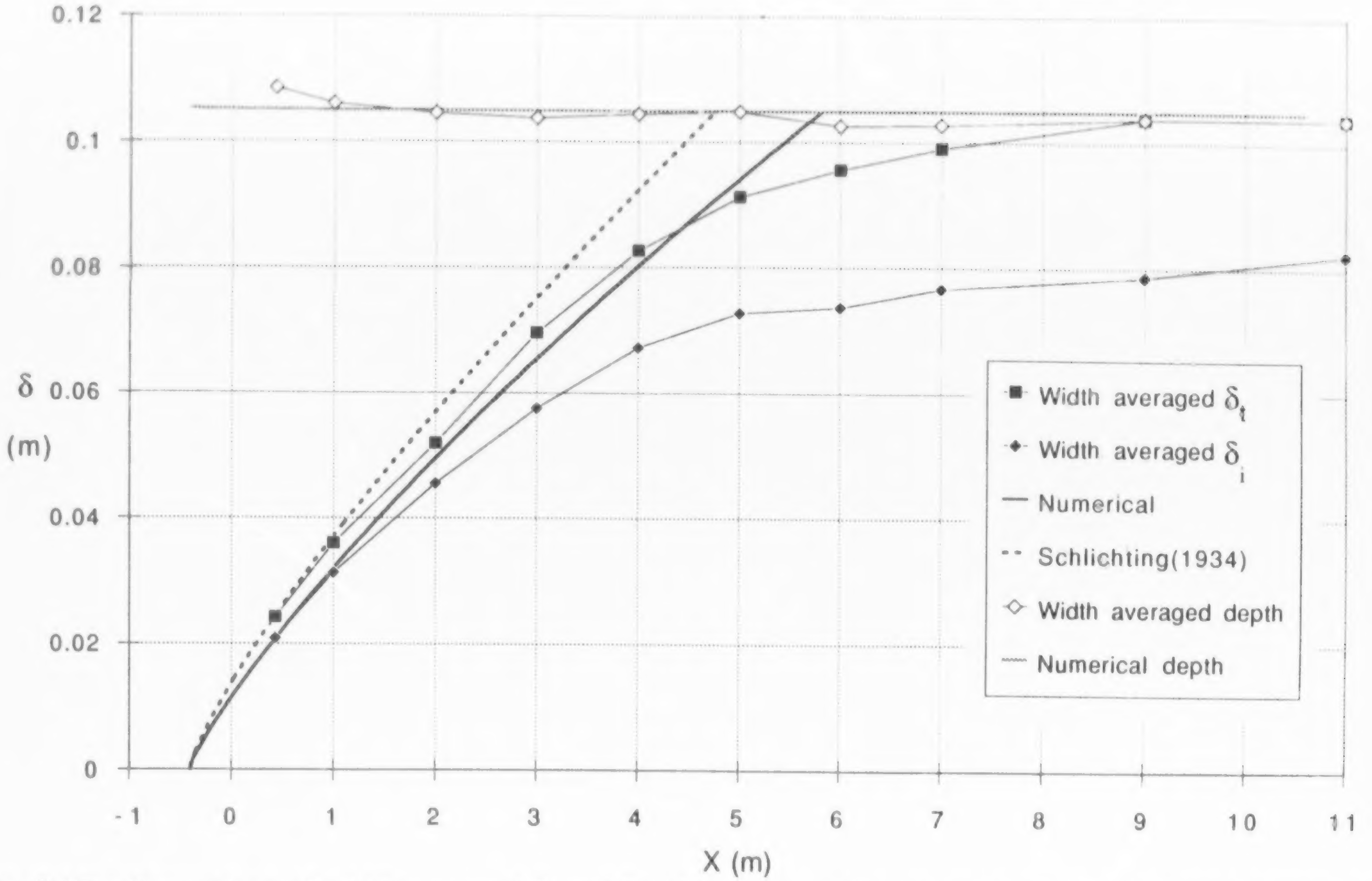

Fig. 2.17a Comparison of width averaged δ_t and δ_i with the numerical solution and Schlichting's smooth flat plate solution (1934). *(Smooth channel)*

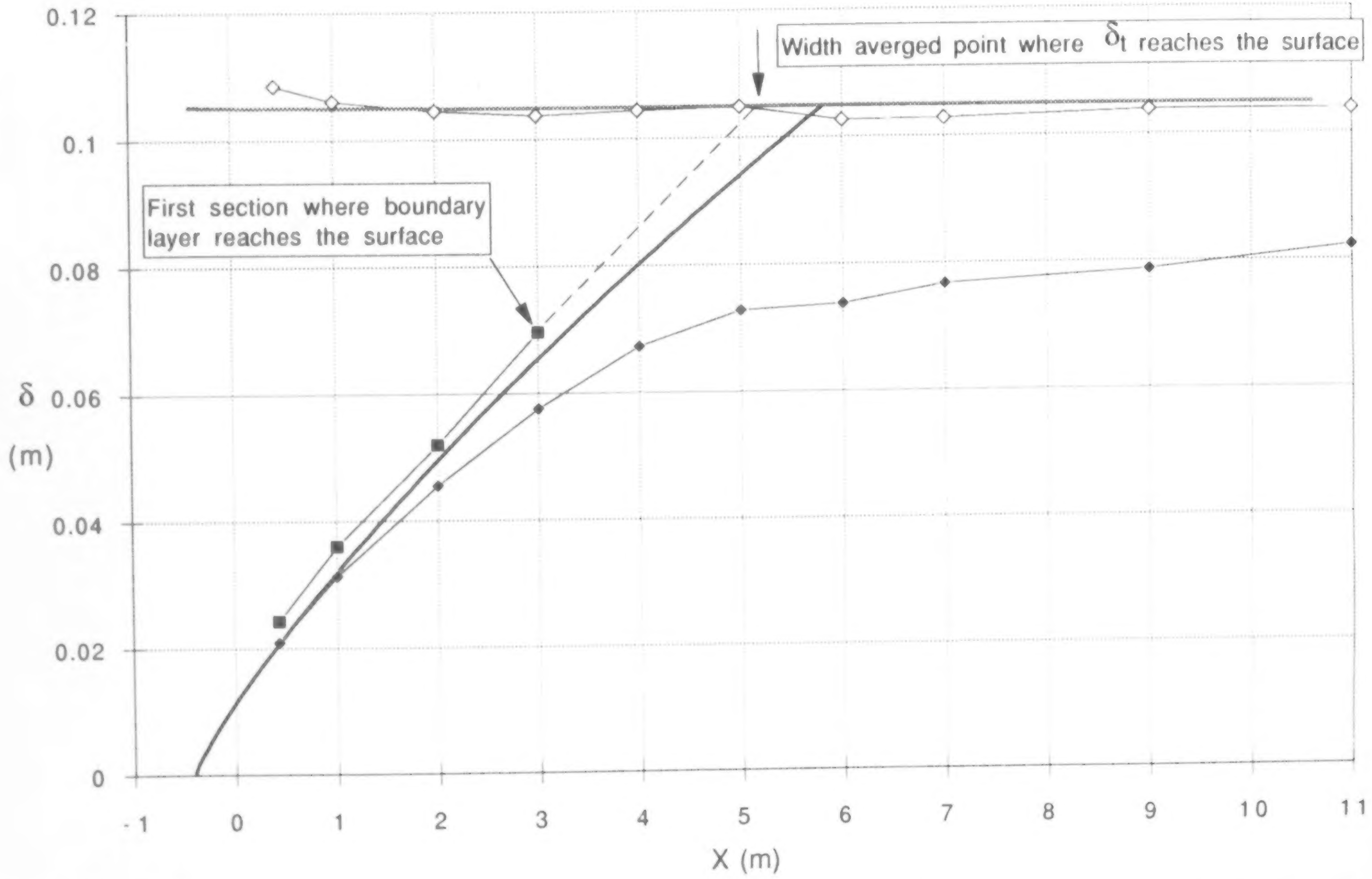

Fig. 2.17b Same as Fig. 2.17a except δ_t is interpolated between x=3.0 m and the average location where δ_t reaches the surface. *(Smooth channel)*

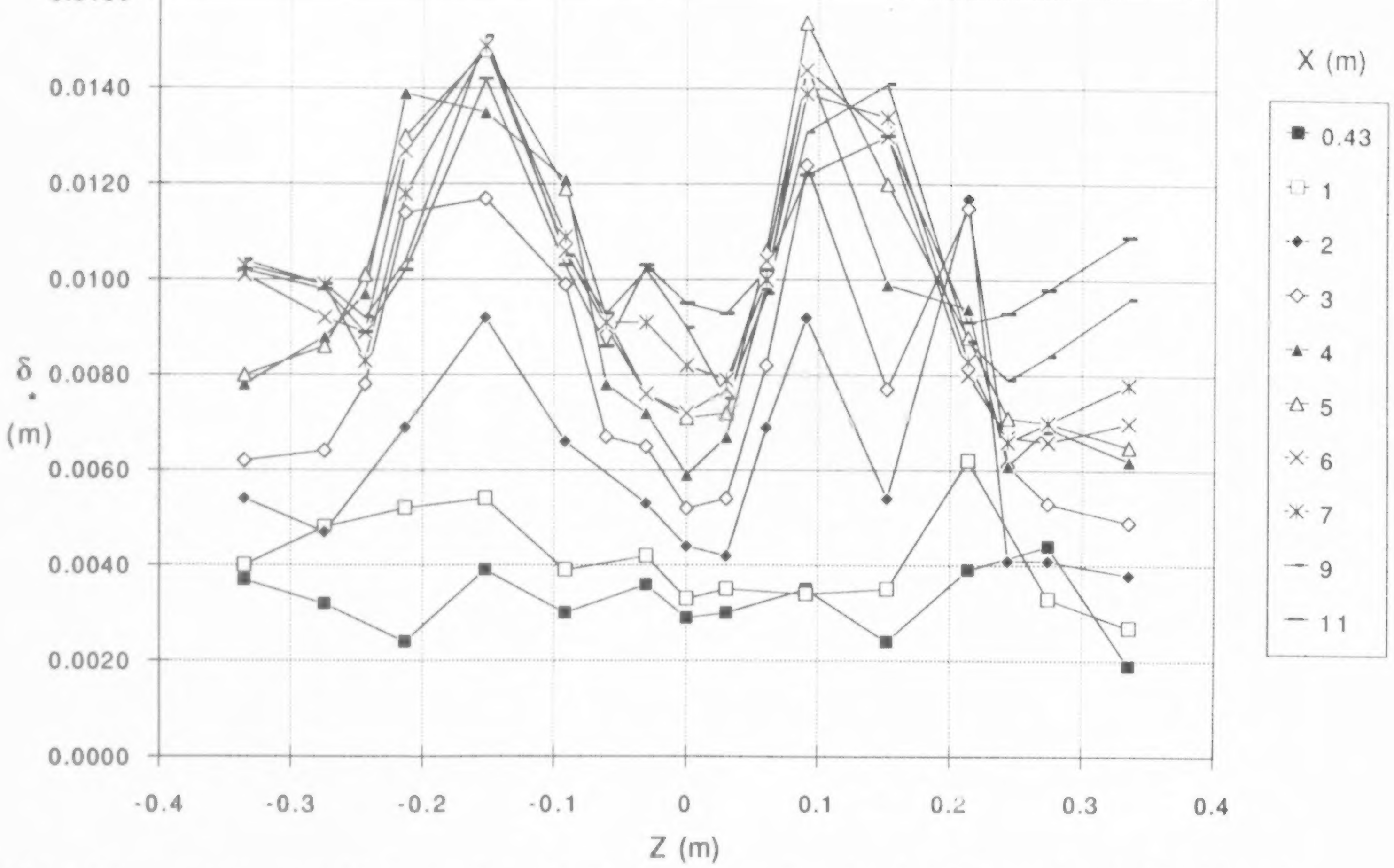

Fig. 2.18a Displacement thickness plotted in the transverse direction for different longitudinal locations. *(Smooth channel)*

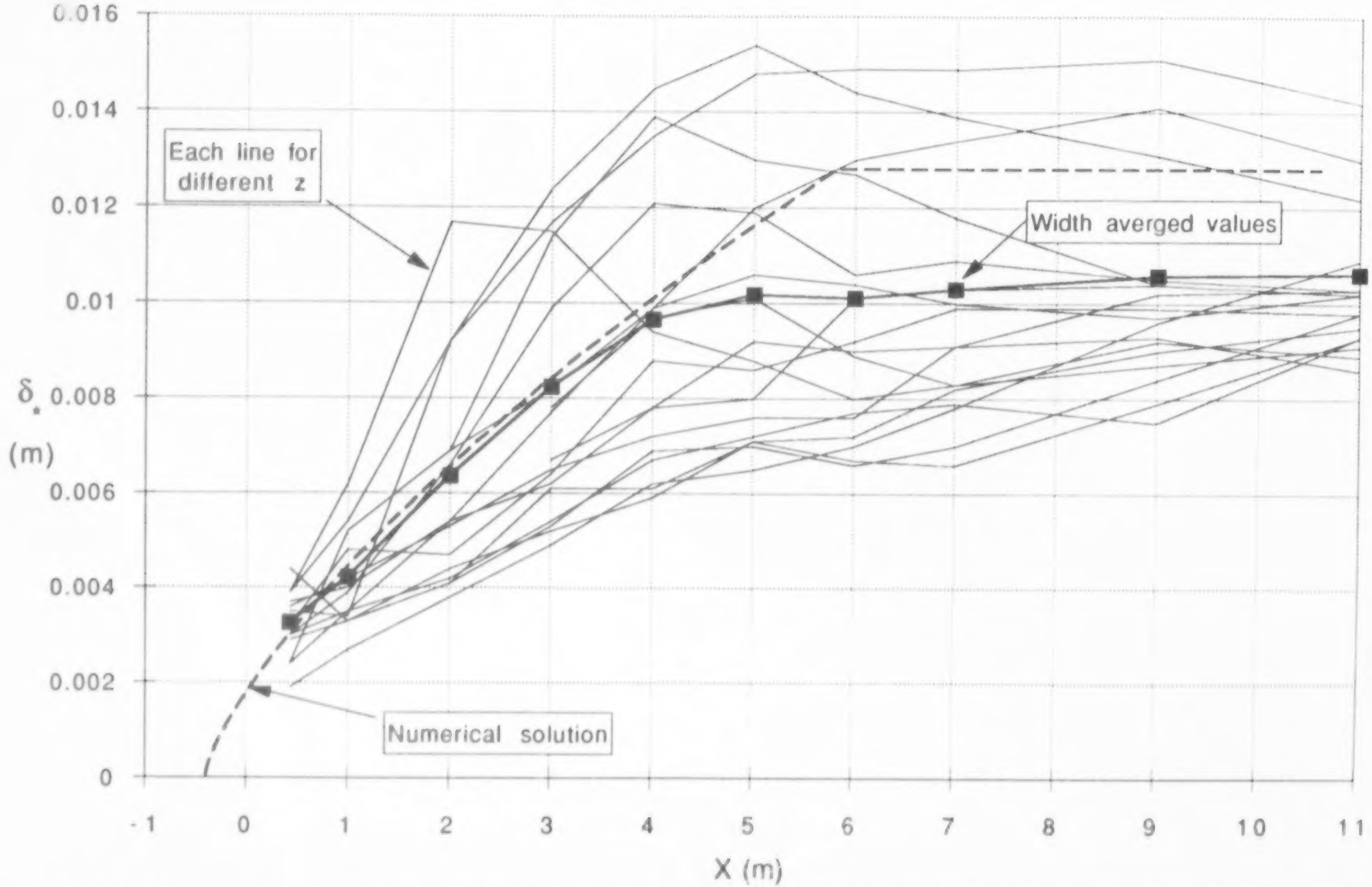

Fig. 2.18b Displacement thickness plotted in the longitudinal direction for different transverse locations. Also shown is the width averaged δ_* growth and the numerical solution. *(Smooth channel)*

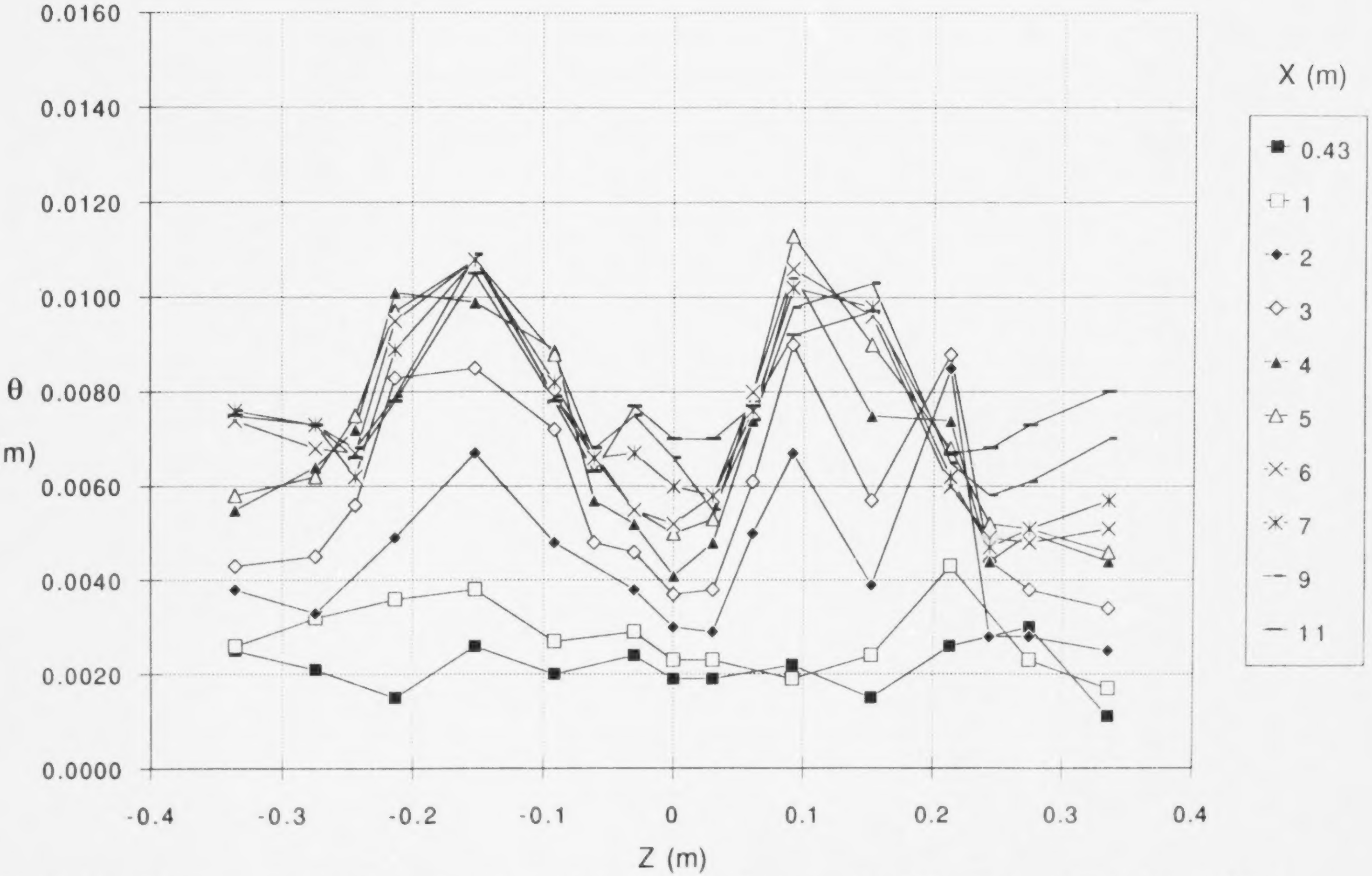

Fig. 2.19a Momentum thickness plotted in the transverse direction for different longitudinal locations. *(Smooth channel)*

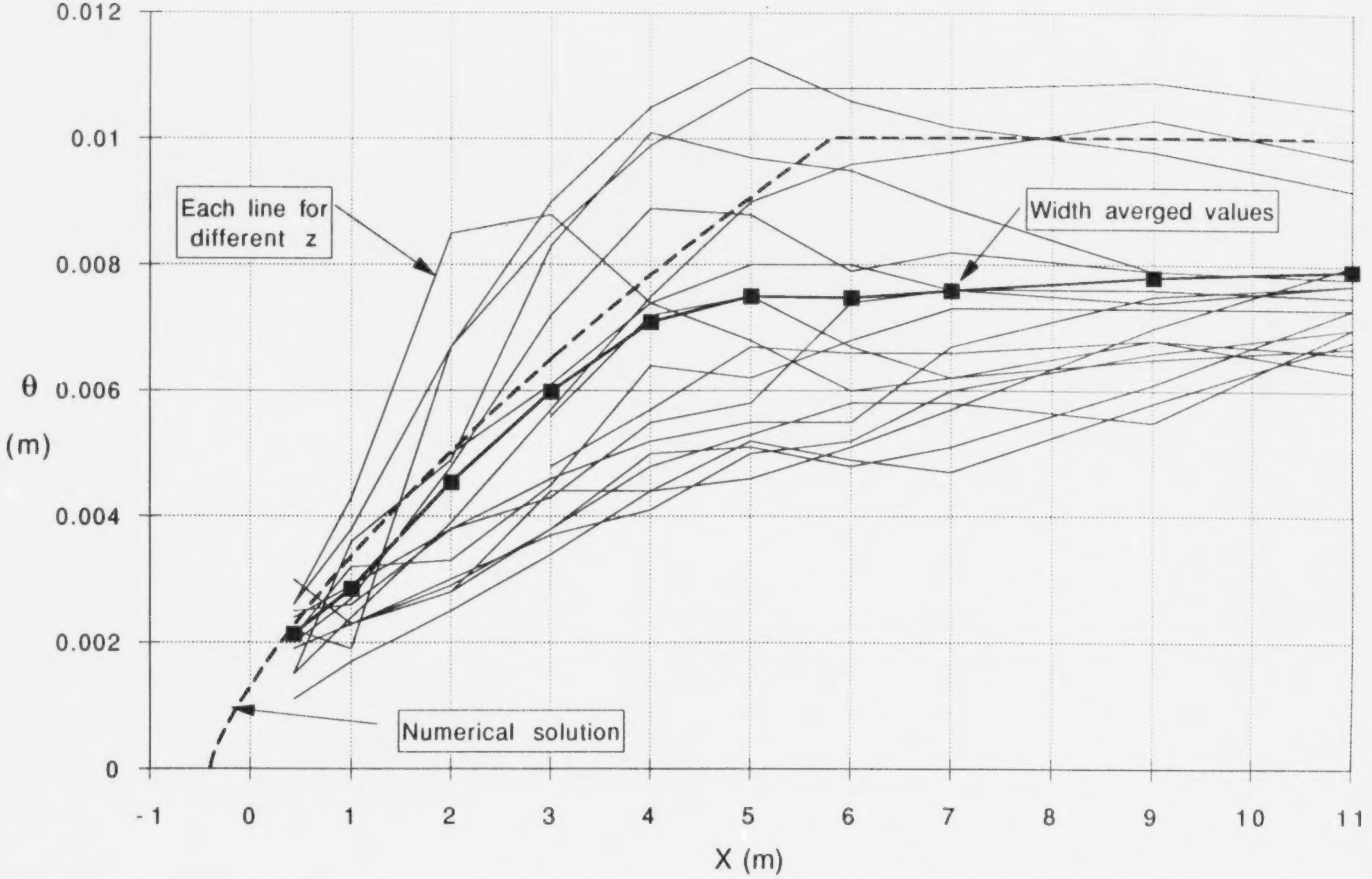

Fig. 2.19b Momentum thickness plotted in the longitudinal direction for different transverse locations. Also shown is the width averaged θ growth and the numerical solution. *(Smooth channel)*

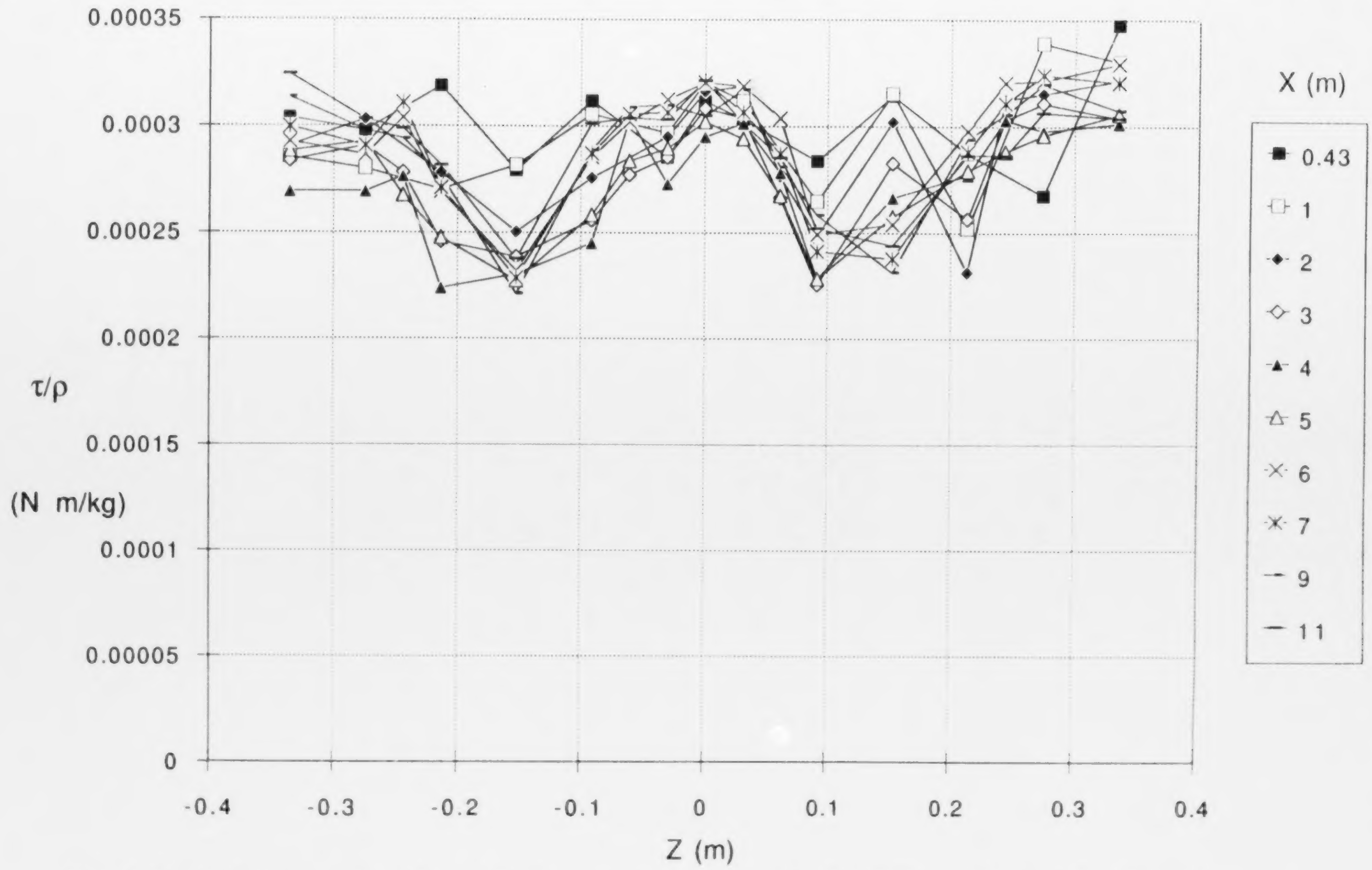

Fig. 2.20 Bed shear stress plotted in the transverse direction for different longitudinal locations. *(Smooth channel)*

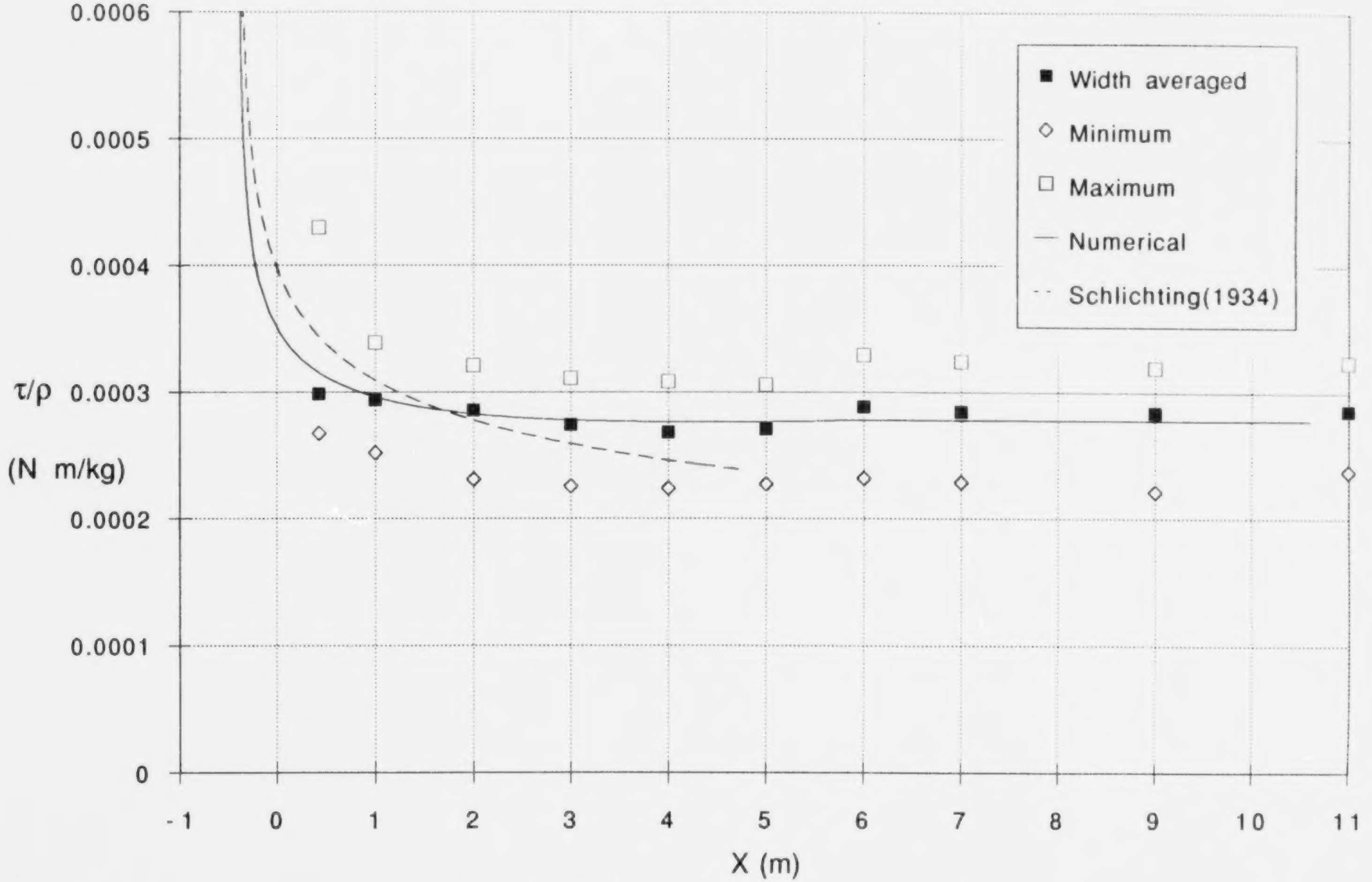

Fig. 2.21 Minimum, maximum, and width averaged bed shear stress plotted in the longitudinal direction. Also shown is the numerical solution and the Schlichting's smooth flat plate solution (1934). *(Smooth channel)*

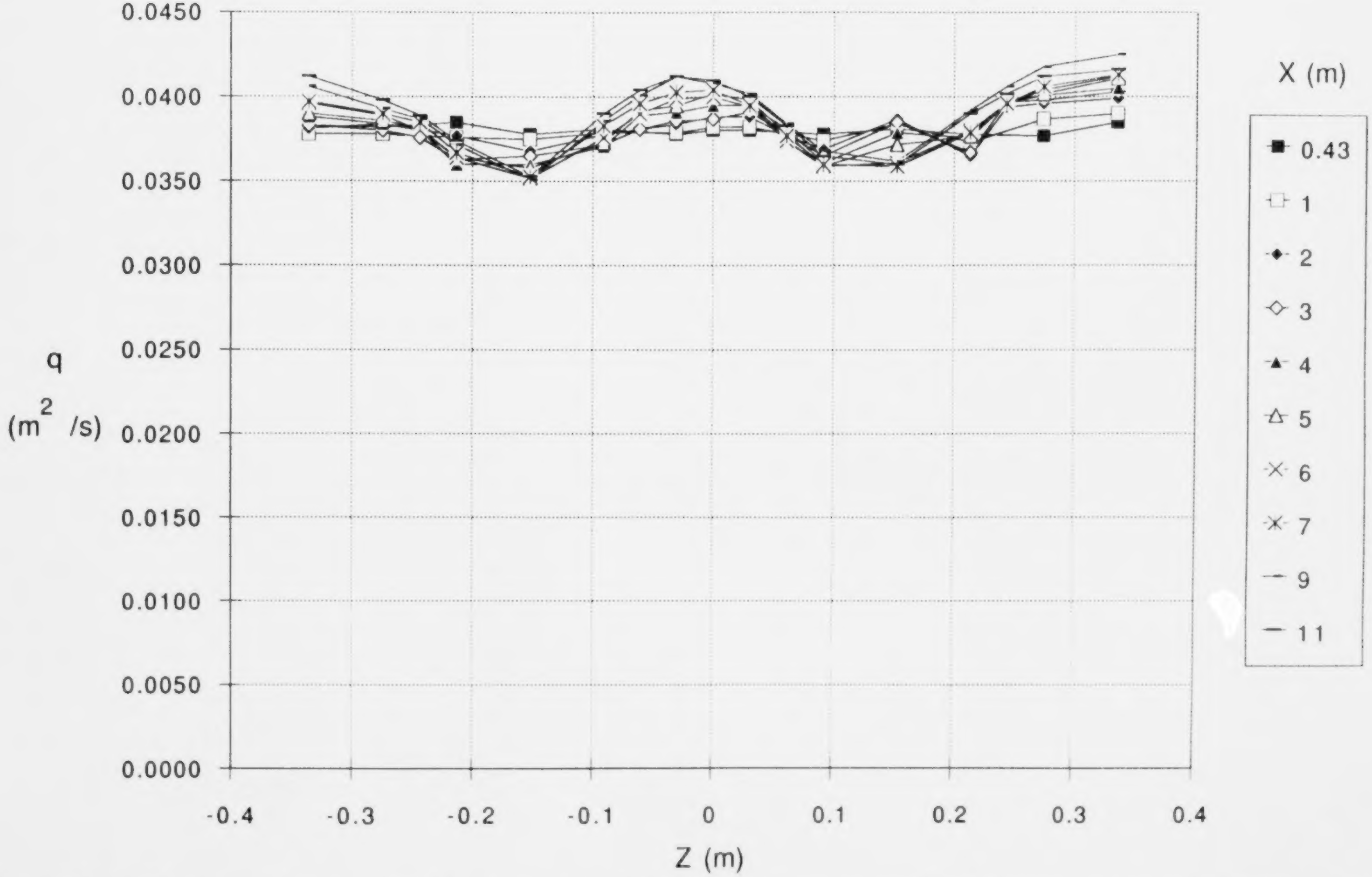

Fig. 2.22a Discharge per unit width as integrated from the velocity profiles plotted in the transverse direction for different longitudinal locations. *(Smooth channel)*

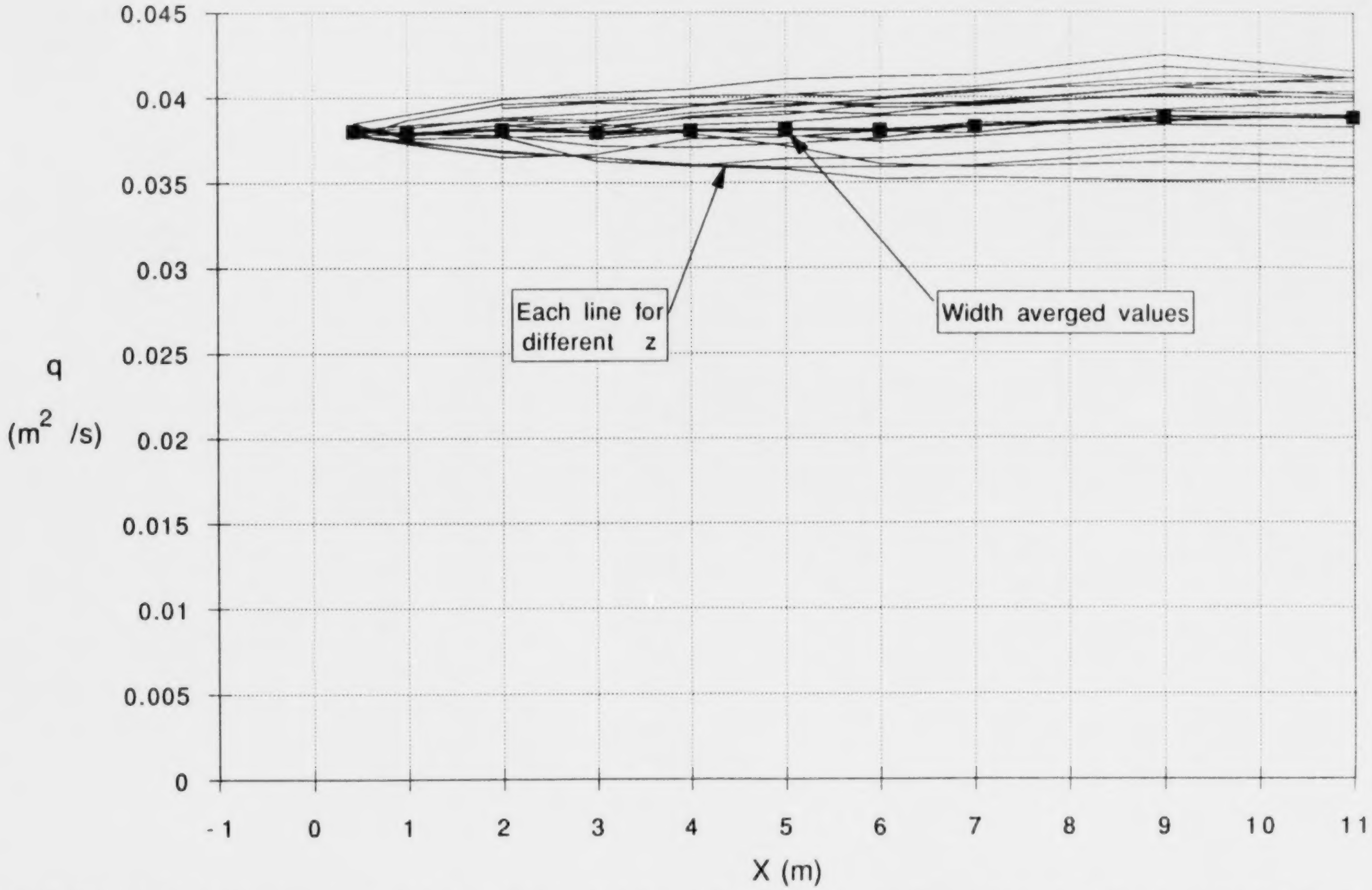

Fig. 2.22b Discharge per unit width as integrated from the velocity profiles plotted in the longitudinal direction for different transverse locations. Also shown is the width averaged unit discharge. *(Smooth channel)*

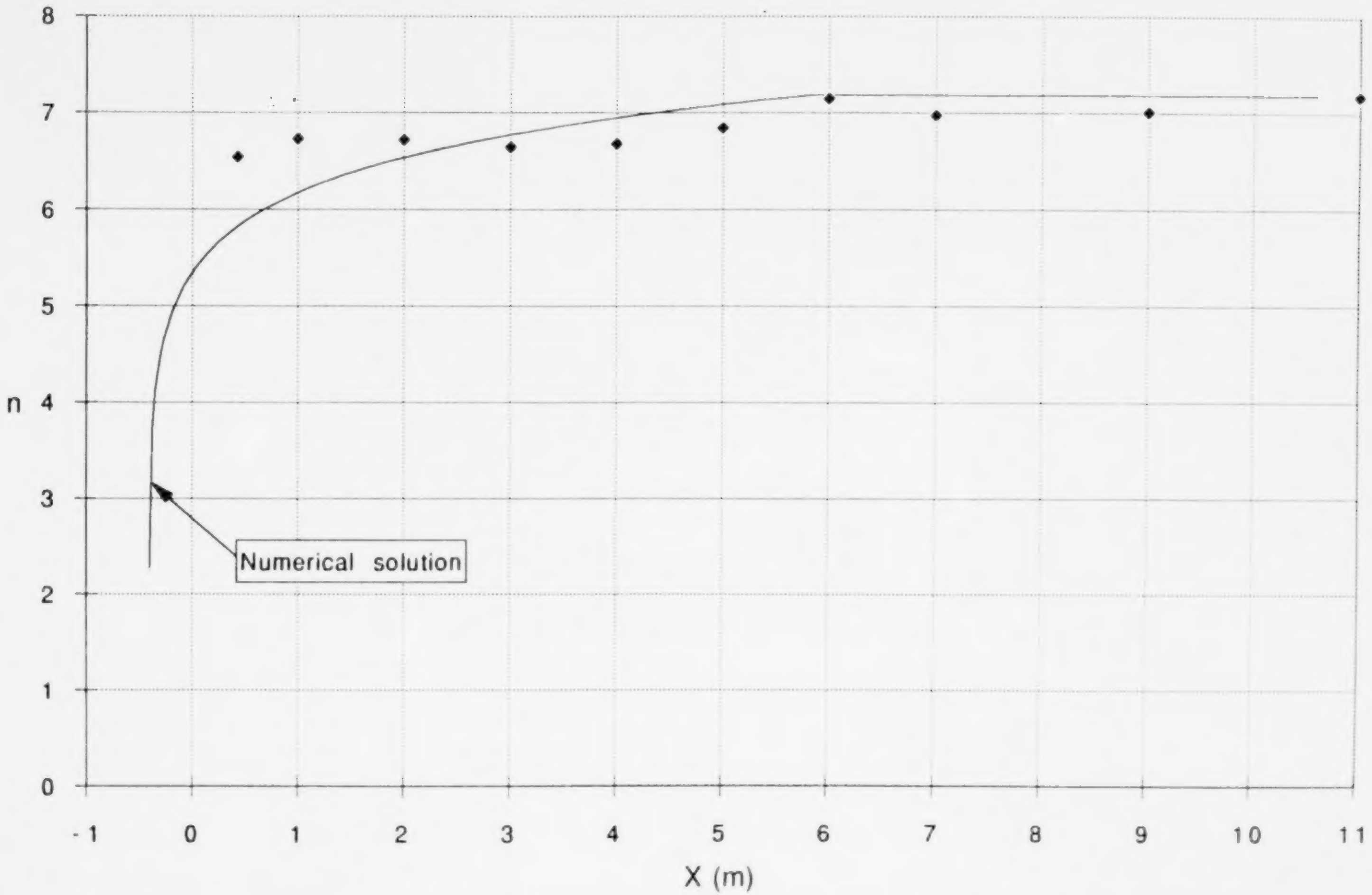

Fig. 2.23 Width averaged power law exponent from regressional curve fits of the boundary layer portion of the velocity profiles. Also shown is the numerical solution. *(Smooth channel)*

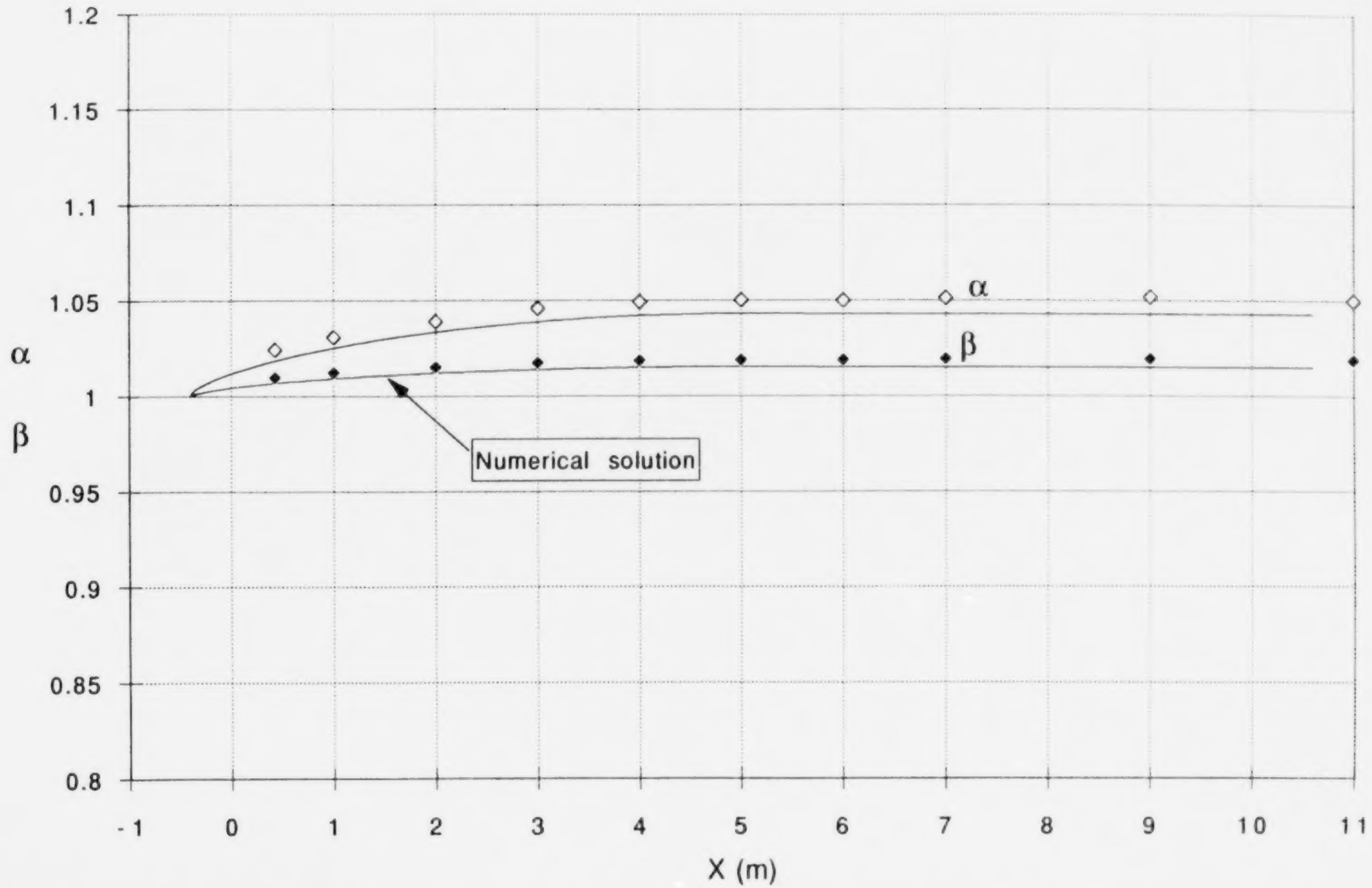

Fig. 2.24 Width averaged momentum and energy correction coefficients. Also shown is the numerical solution. *(Smooth channel)*

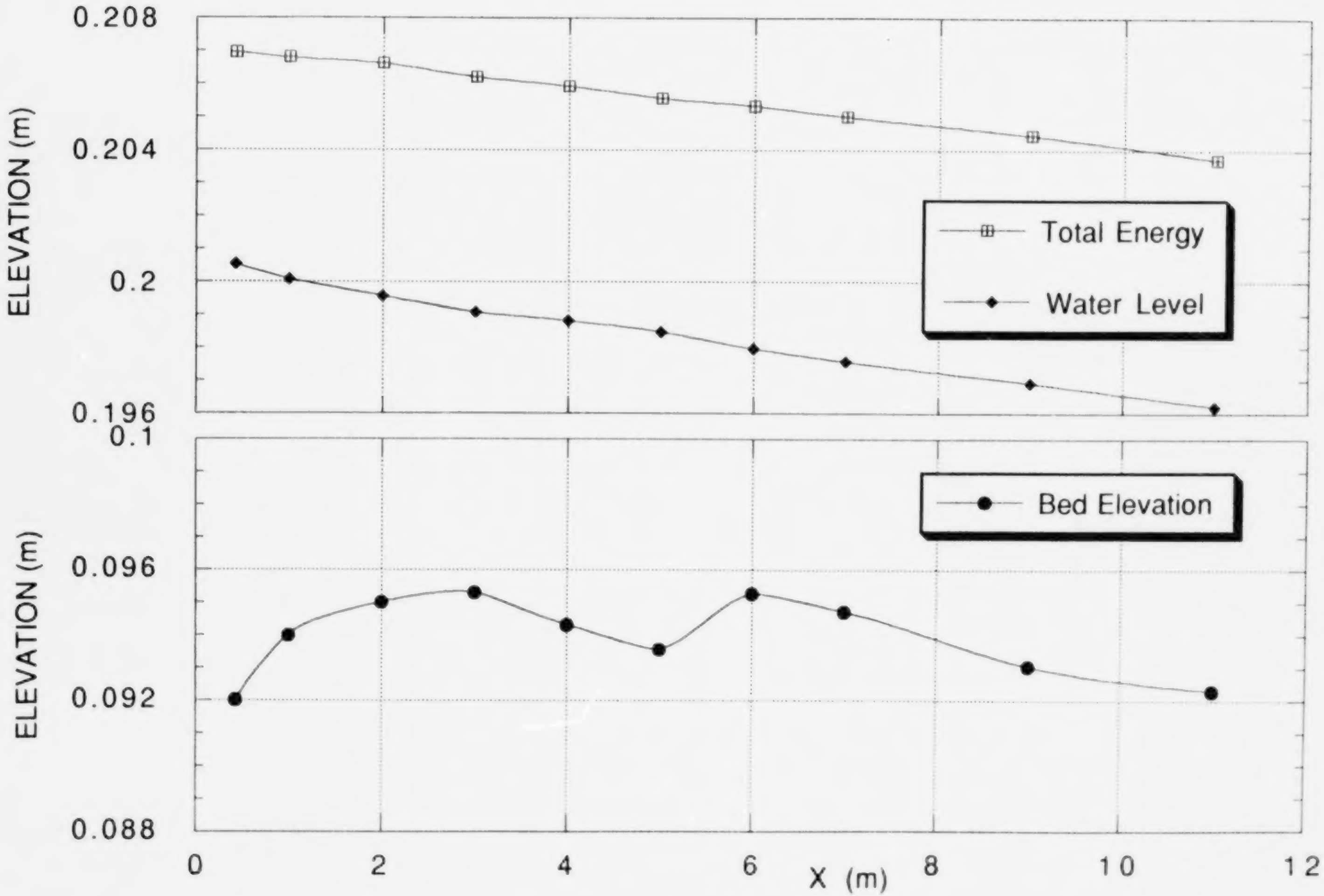

Fig. 2.25 Width averaged total energy, water surface elevation, and bed elevation. *(Smooth channel)*

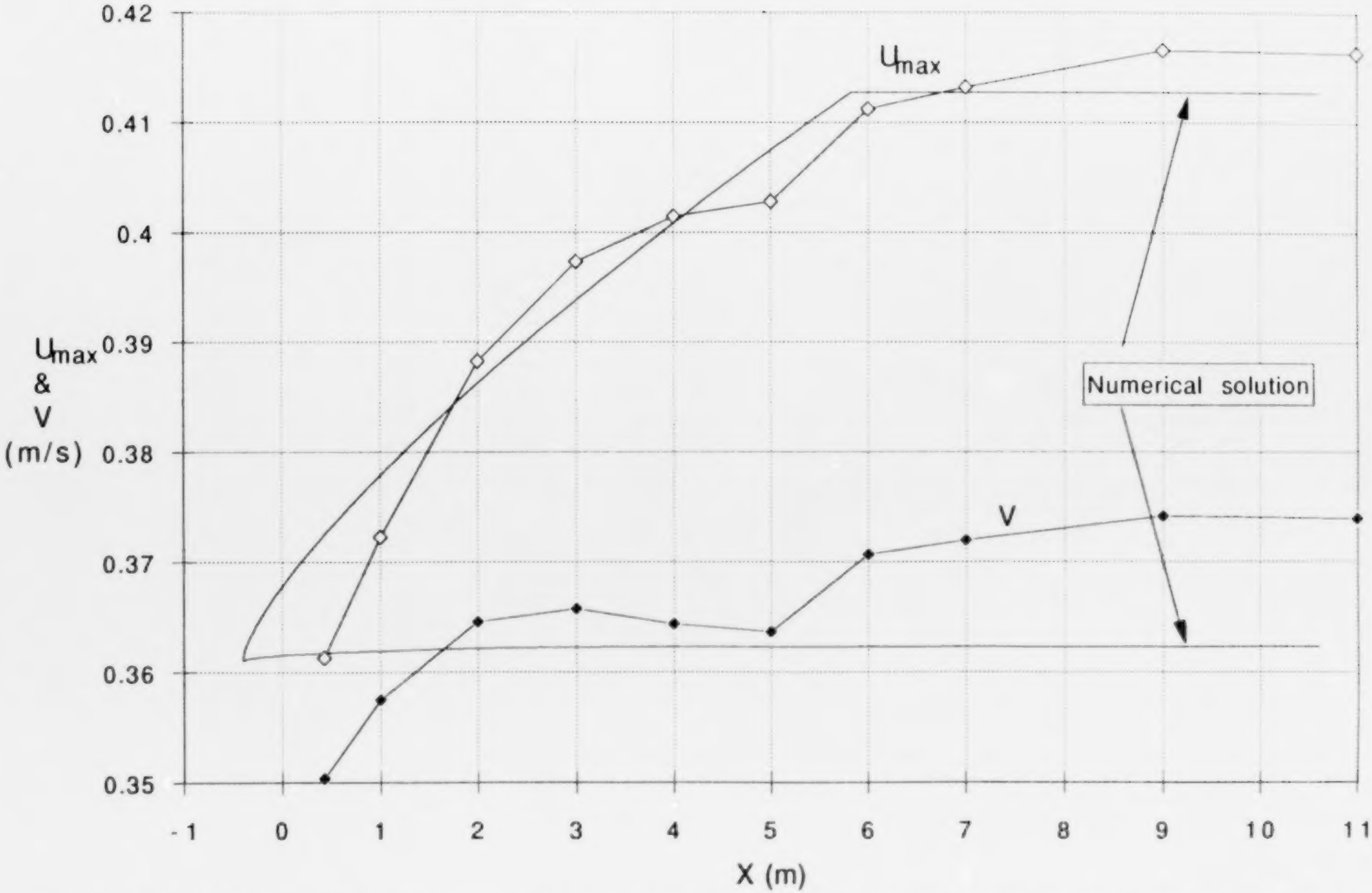

Fig. 2.26 Width averaged maximum velocity and average velocity. Also shown is the numerical solution. *(Smooth channel)*

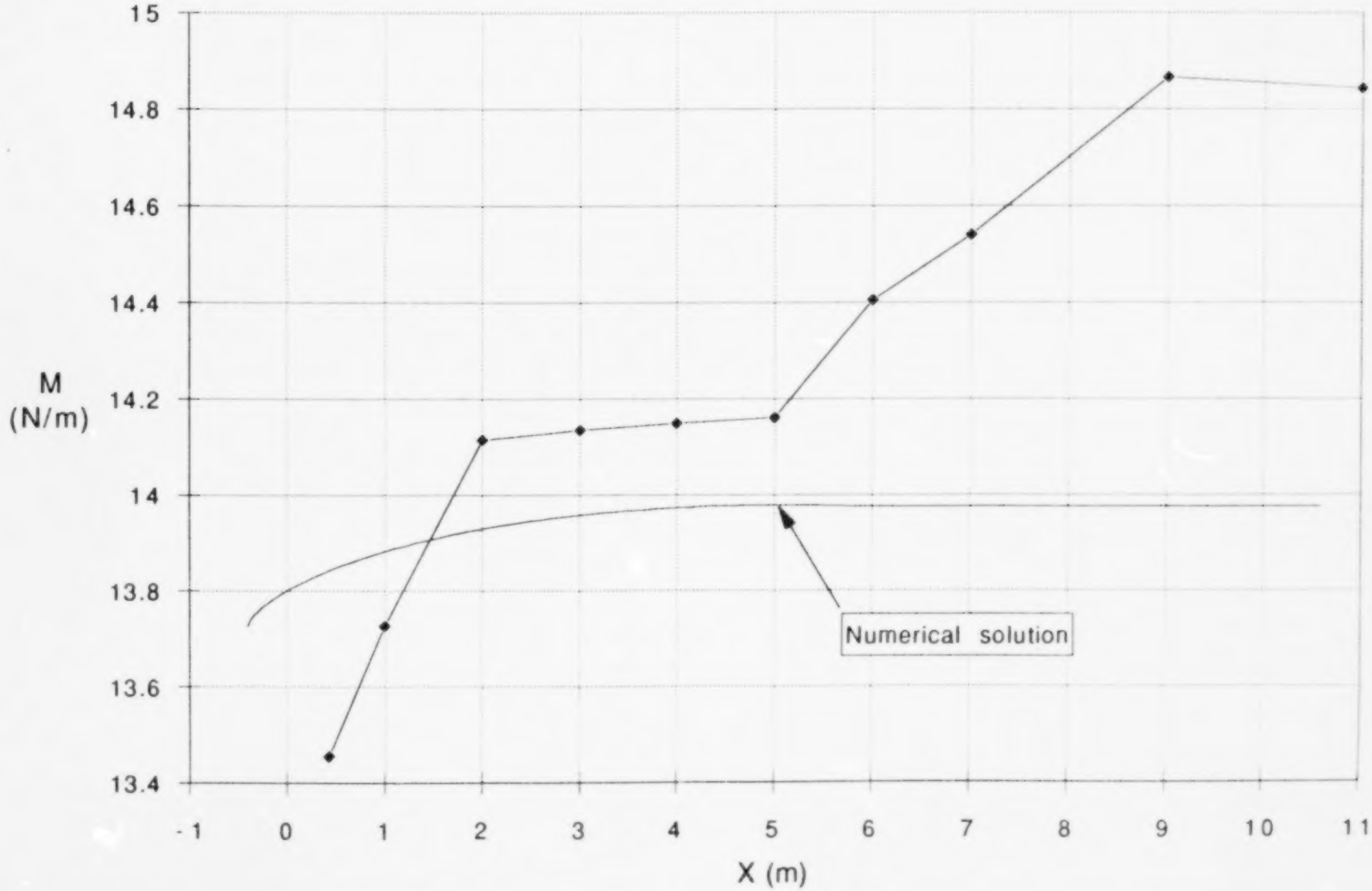

Fig. 2.27 Width averaged momentum per unit width. Also shown is the numerical solution. *(Smooth channel)*

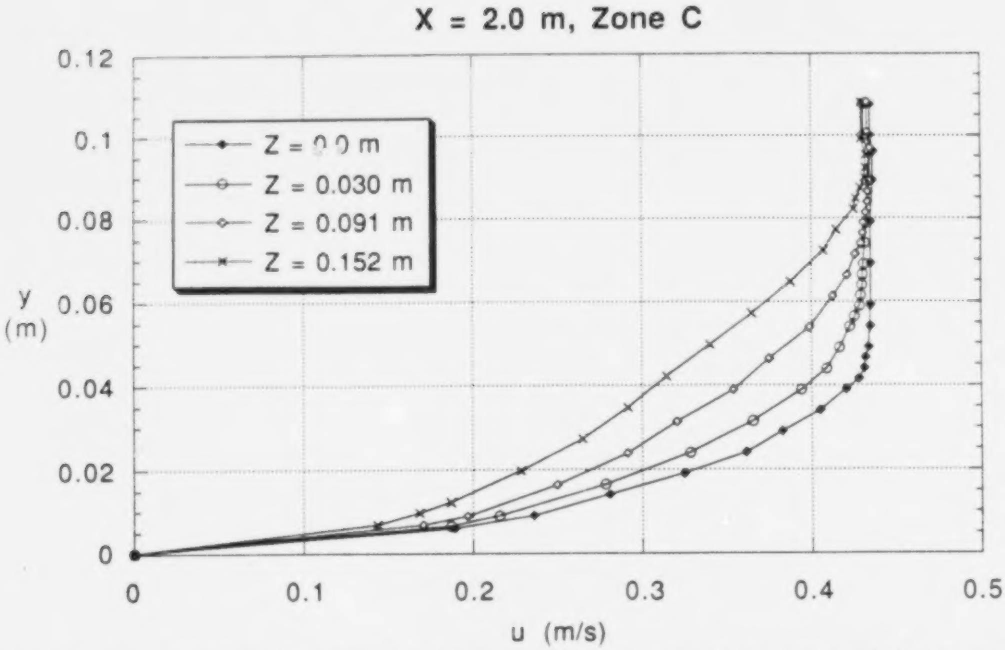

Fig. 2.28a Typical velocity profiles in the developing portion of the *rough channel* for different transverse locations.

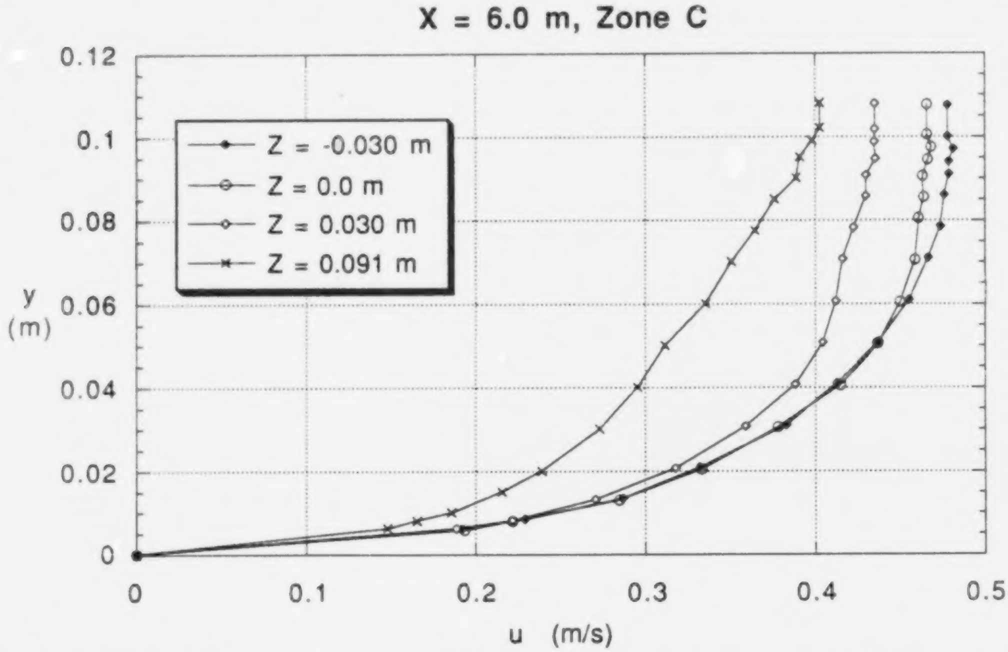

Fig. 2.28b Typical velocity profiles in the developed portion of the *rough channel* for different transverse locations.

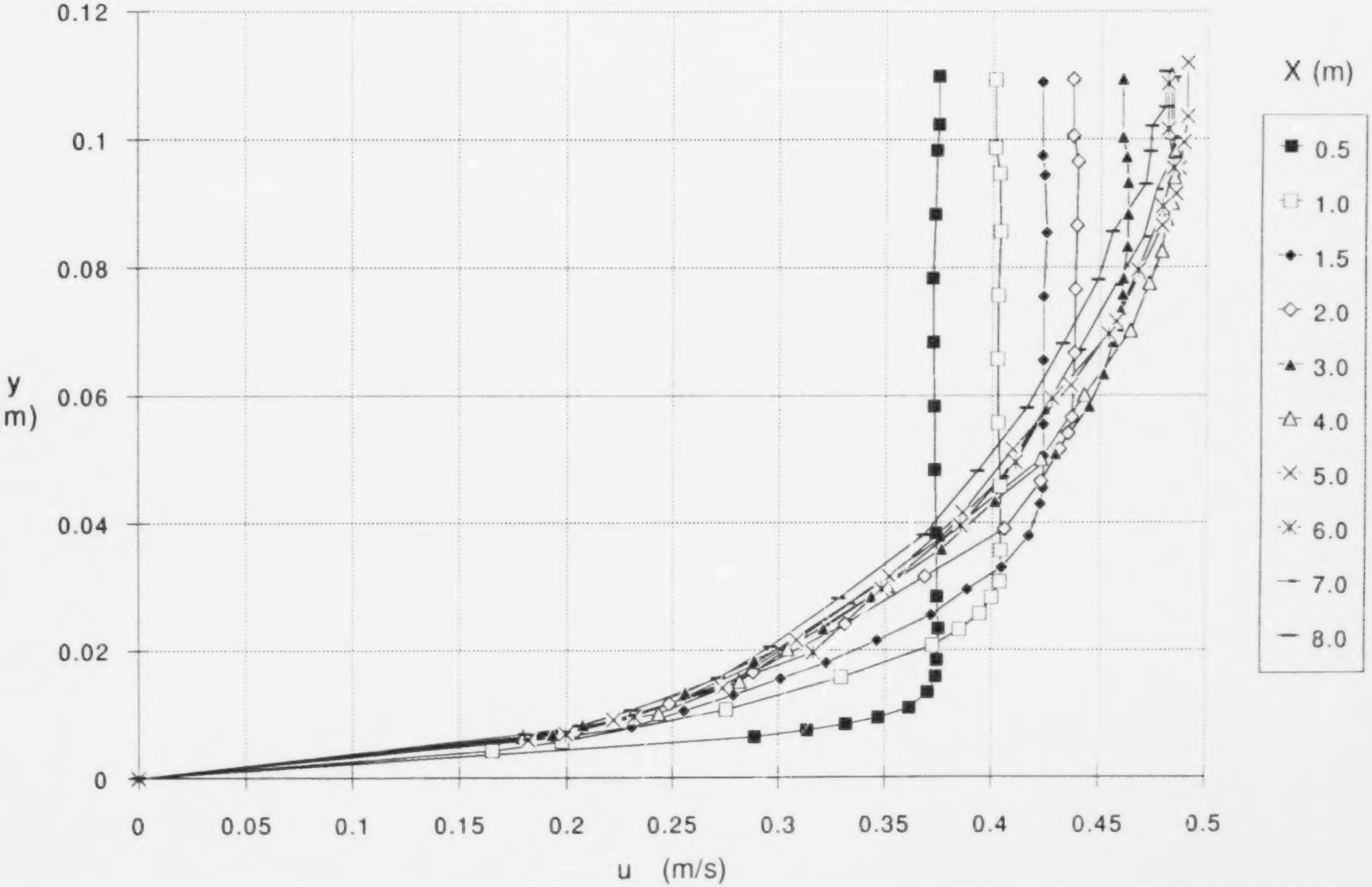

Fig. 2.29a Velocity profiles in an area of downwelling (Z = 0.335 m) for different longitudinal locations. *(Rough channel)*

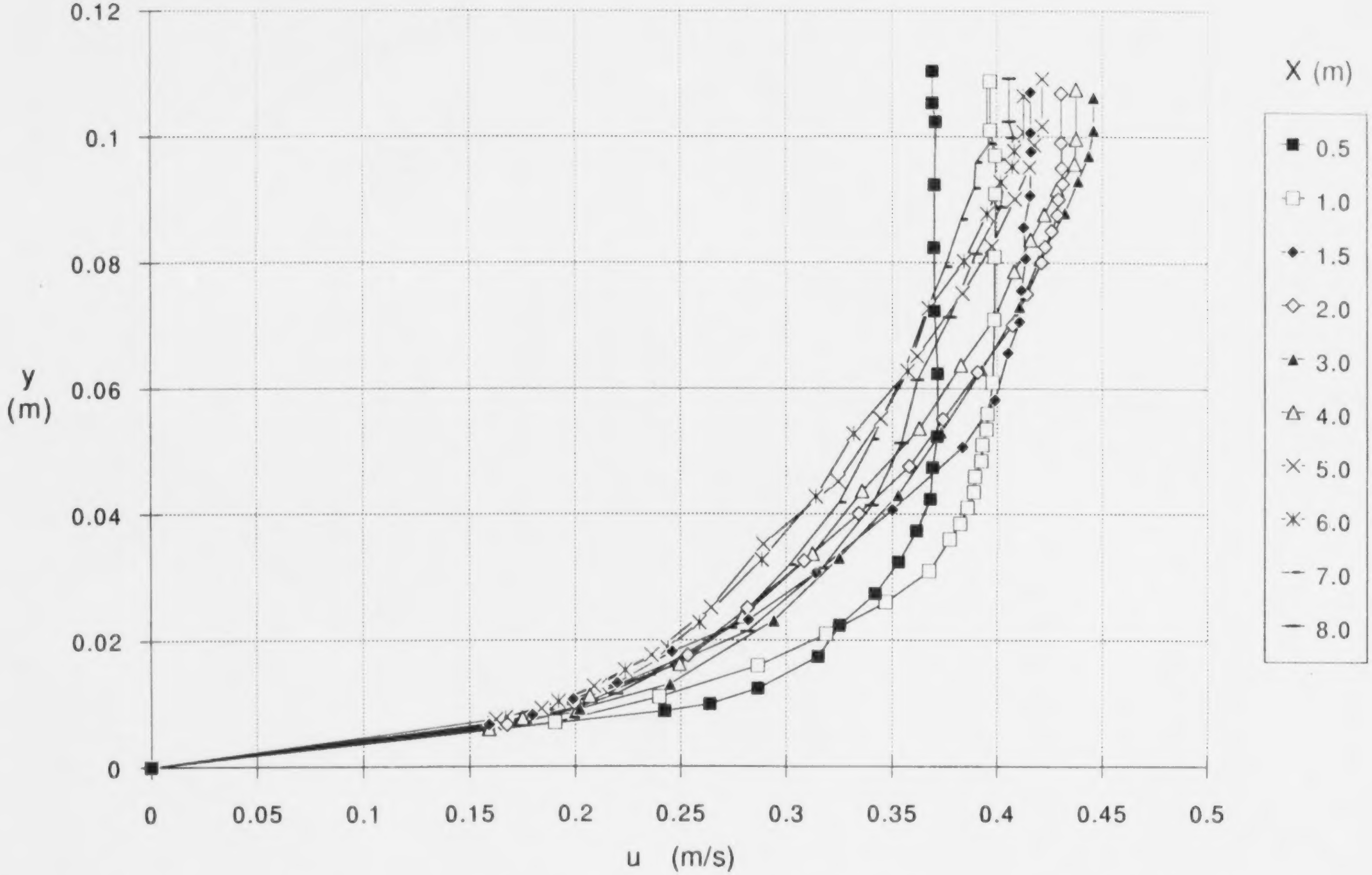

Fig. 2.29b Velocity profiles in an area of upwelling (Z = -0.153 m) for different longitudinal locations.
(Rough channel)

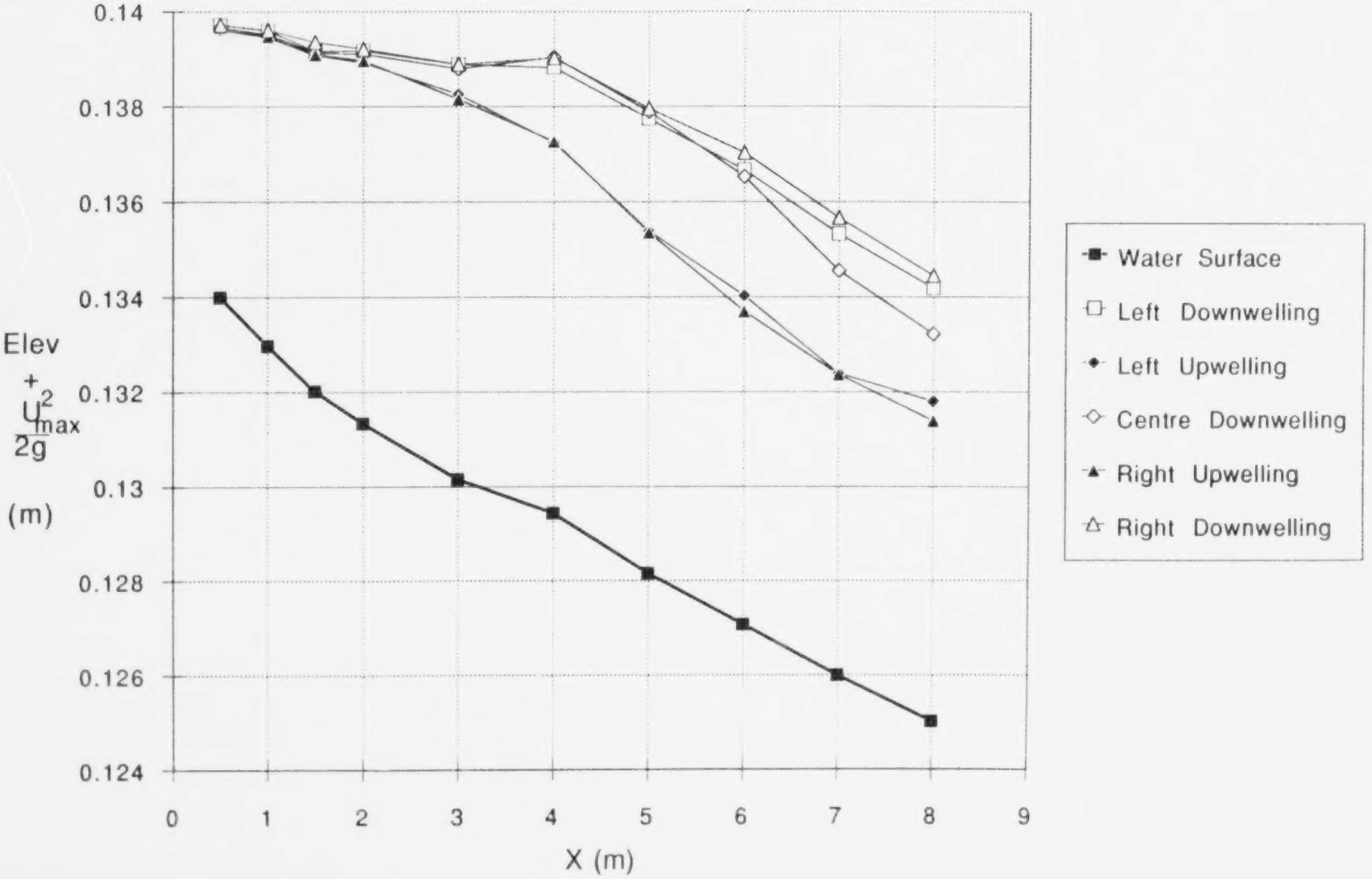

Fig. 2.30 Evaluation of the Bernoulli equation to help indicate the decay of the potential core and to asses the reliability of elevation and velocity measurements. *(Rough channel)*

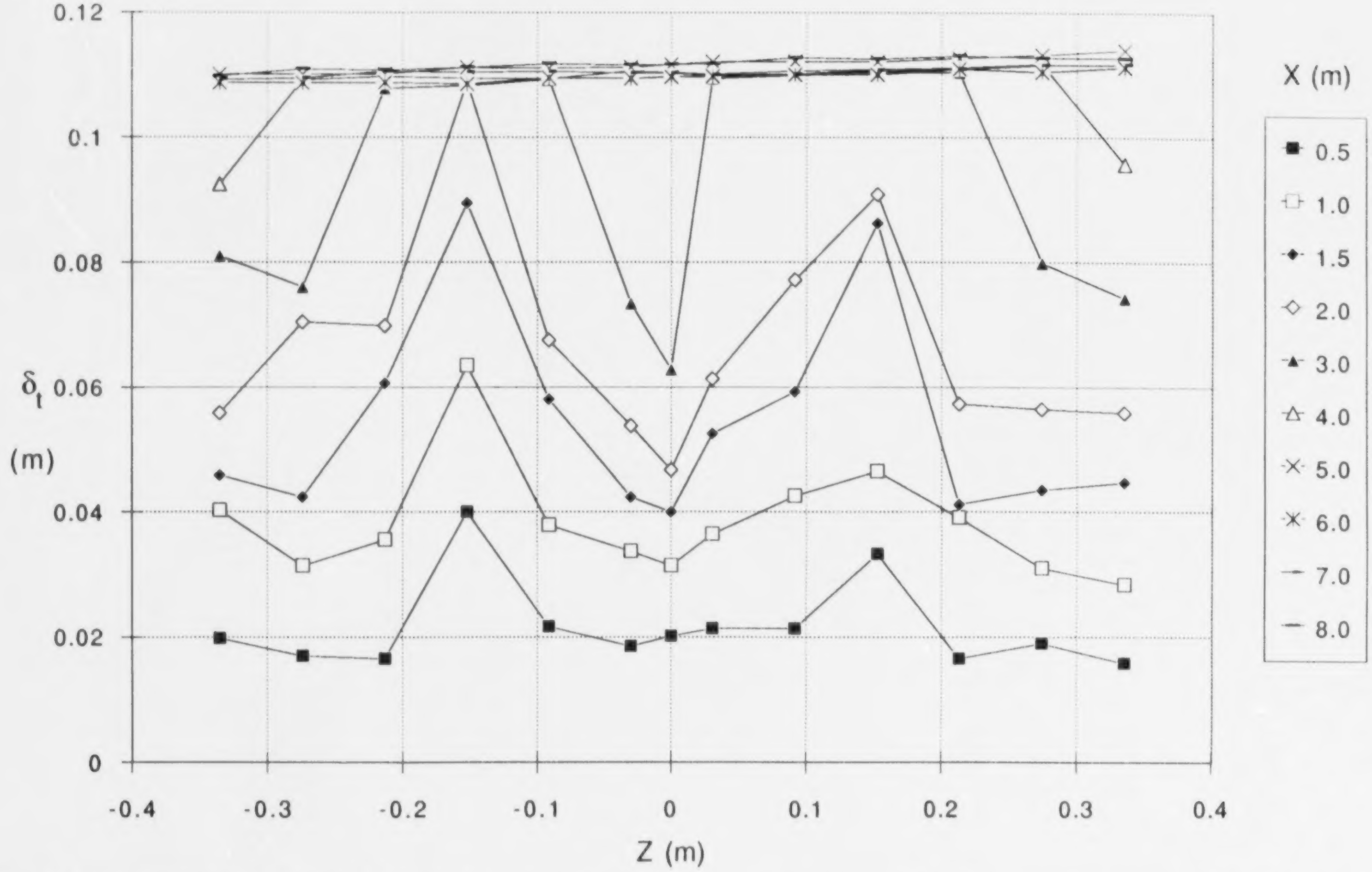

Fig. 2.31a Boundary layer thickness based on turbulence criteria plotted in the transverse direction for different longitudinal locations. *(Rough channel)*

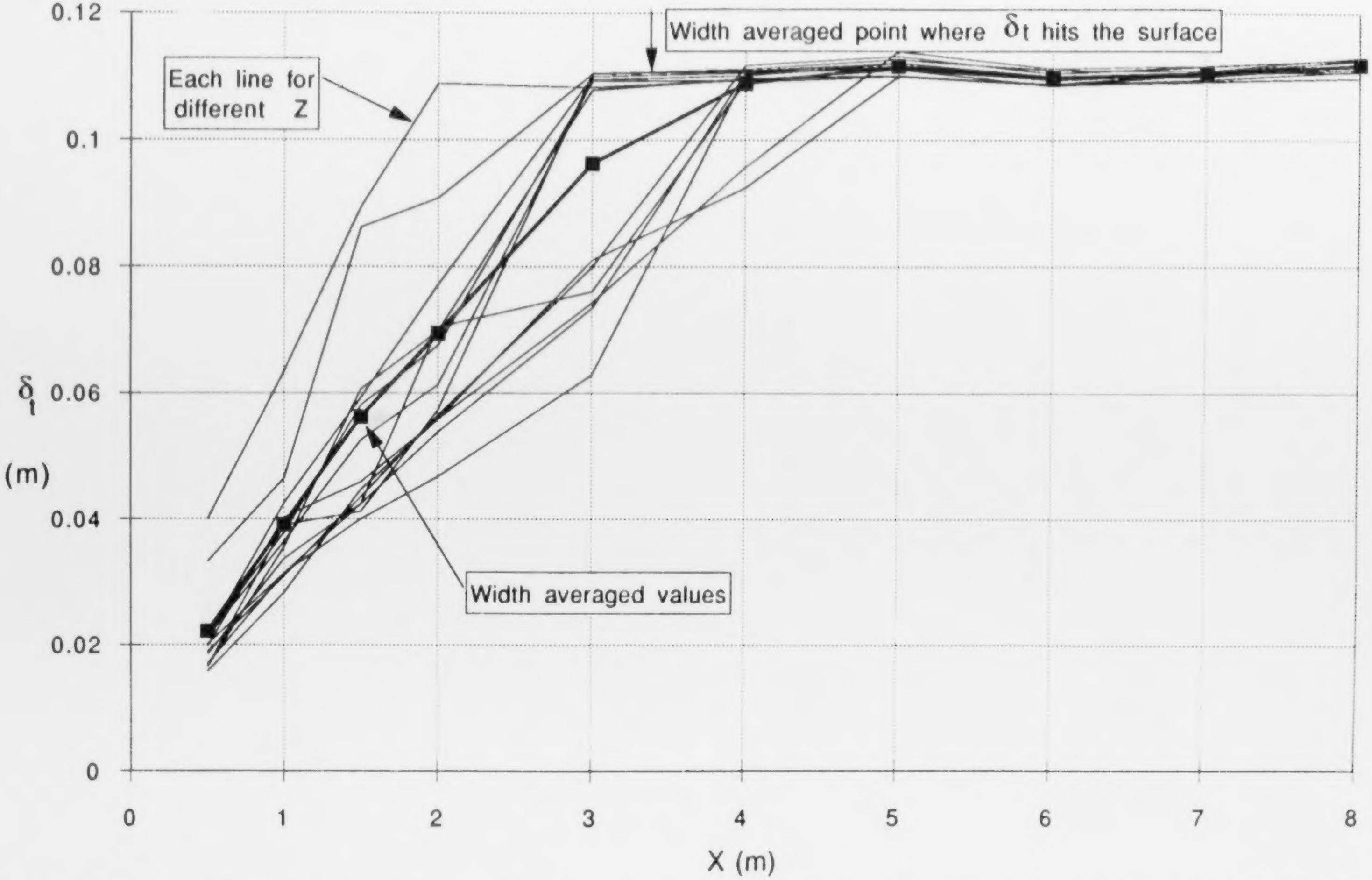

Fig. 2.31b Boundary layer thickness based on turbulence criteria plotted in the longitudinal direction for different transverse locations. Also shown is the width averaged δ_t growth. *(Rough channel)*

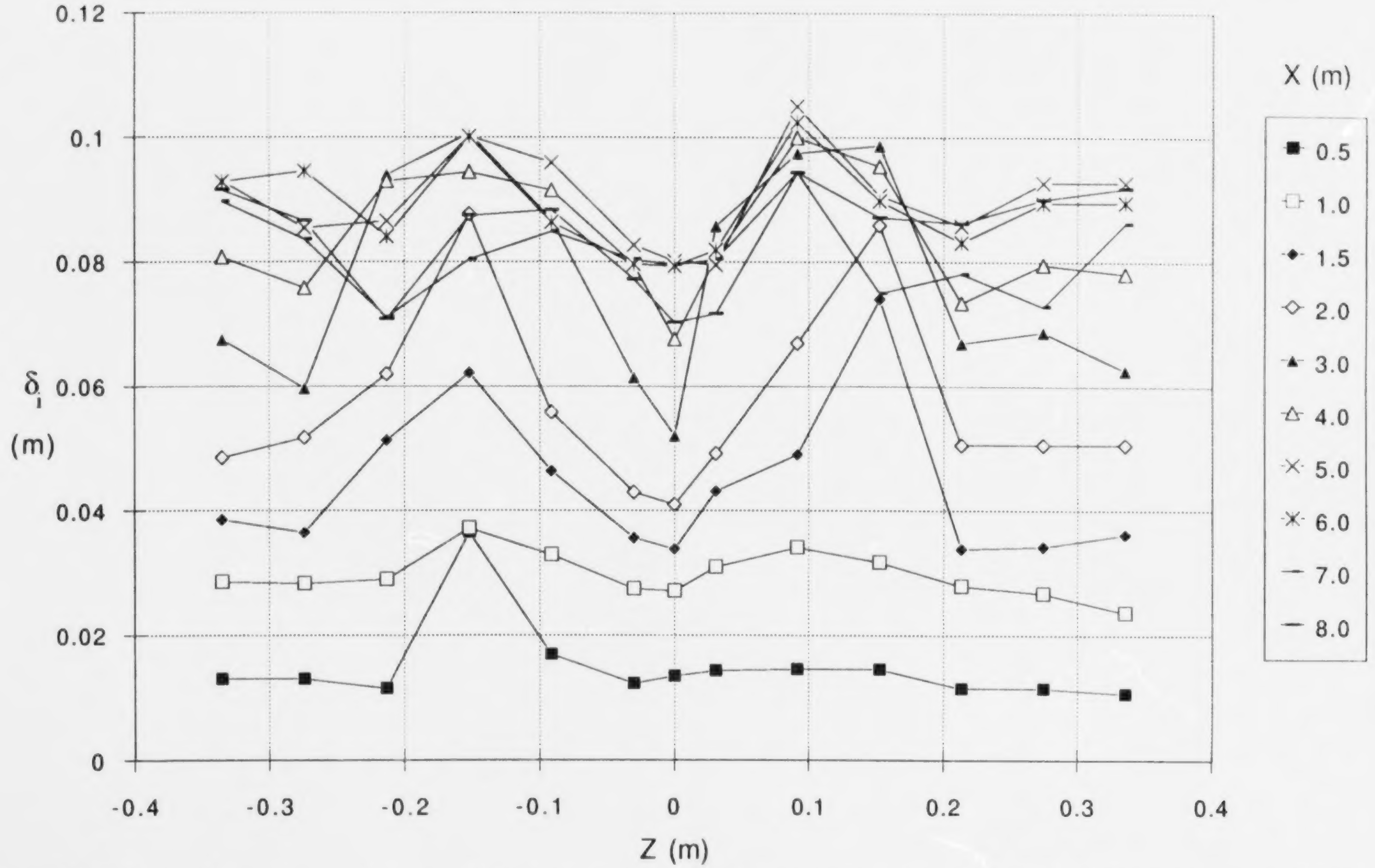

Fig. 2.32a Boundary layer thickness based on extrapolated intercept method plotted in the transverse direction for different longitudinal locations. *(Rough channel)*

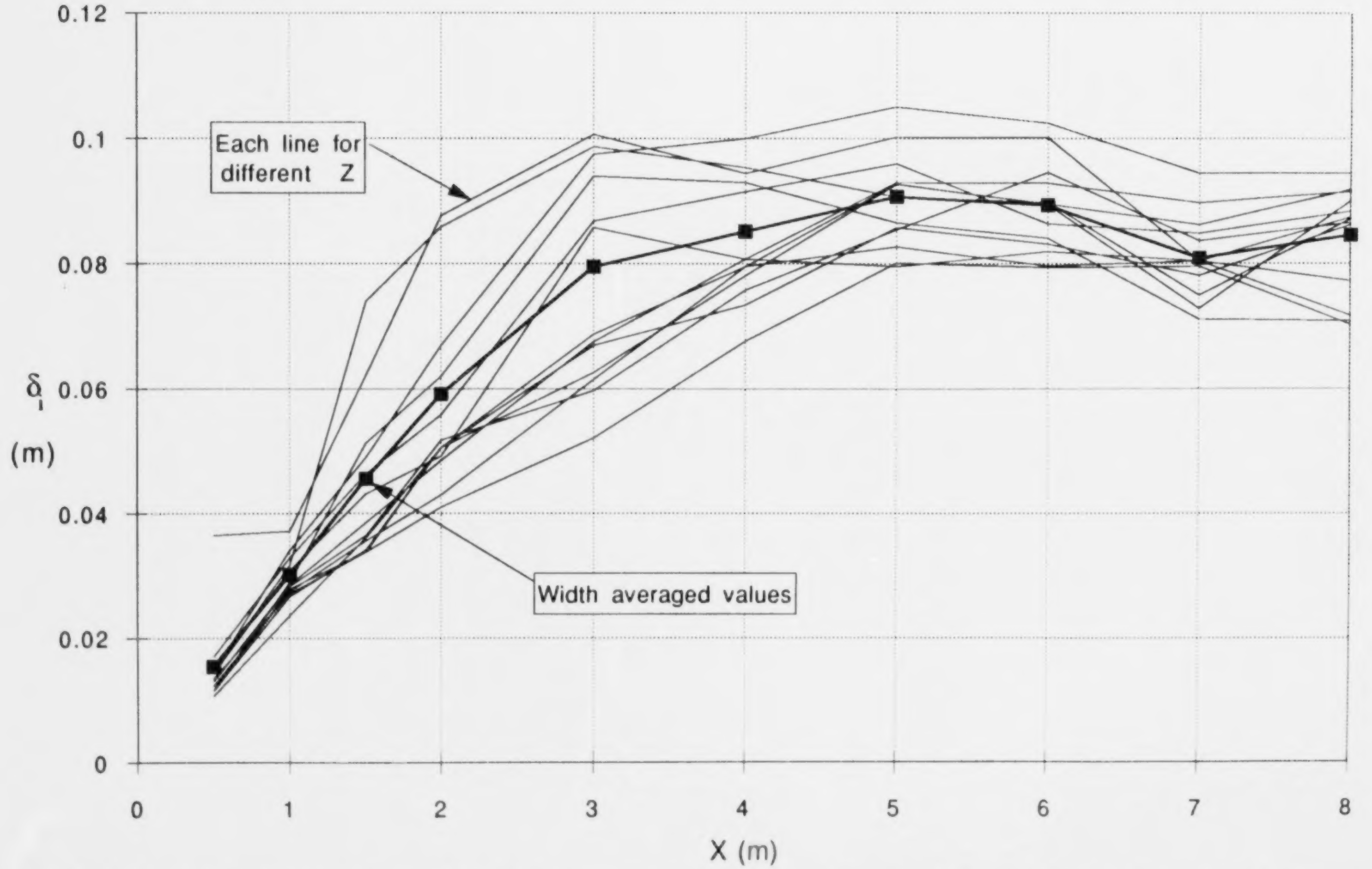

Fig. 2.32b Boundary layer thickness based on extrapolated intercept method plotted in the longitudinal direction for different transverse locations. Also shown is the width averaged δ_i growth. *(Rough channel)*

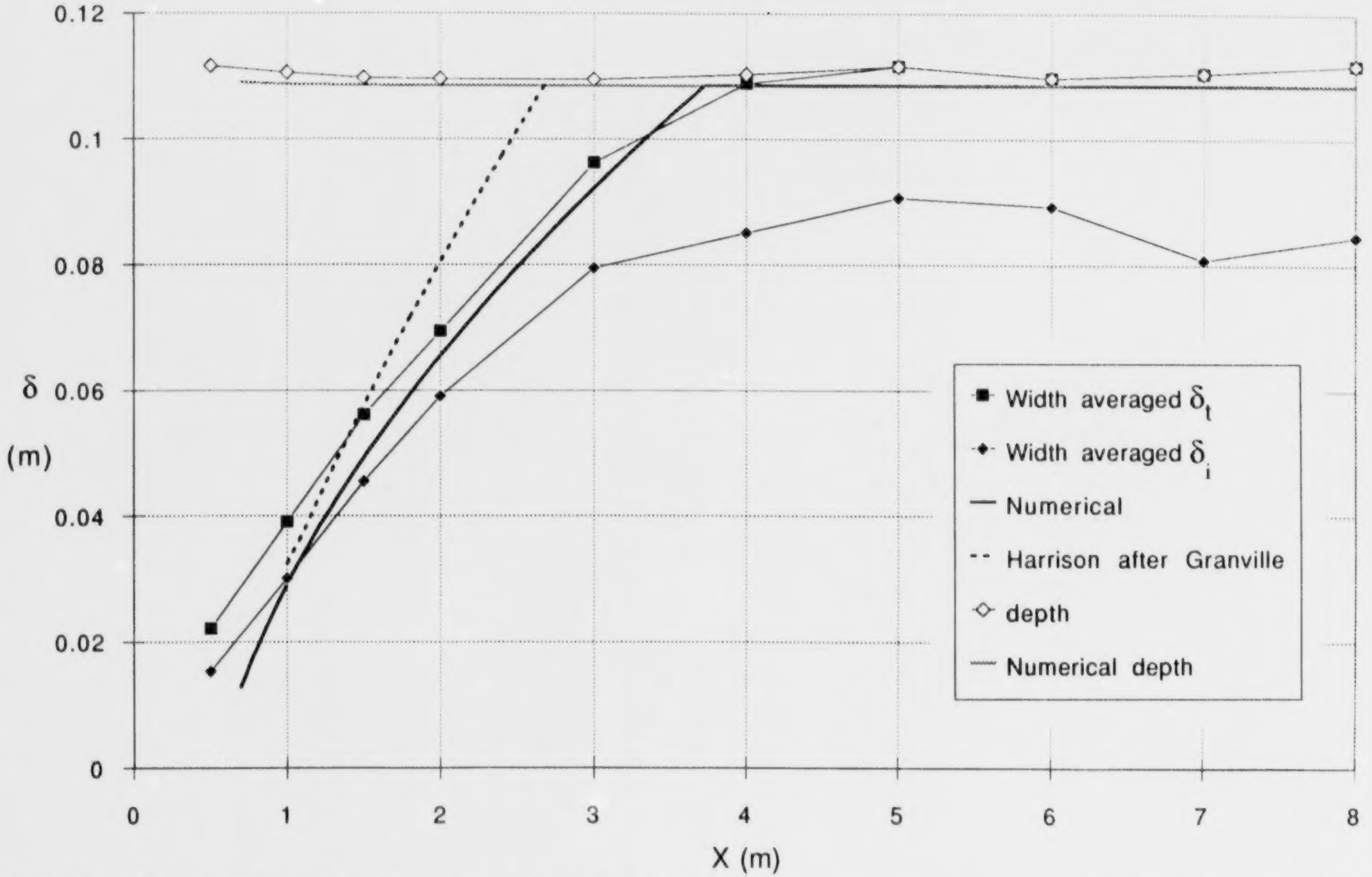

Fig. 2.33a Comparison of width averaged δ_t and δ_i with the numerical solution and Harrison's rough plate (1967) after Granville(1958). *(Rough channel)*

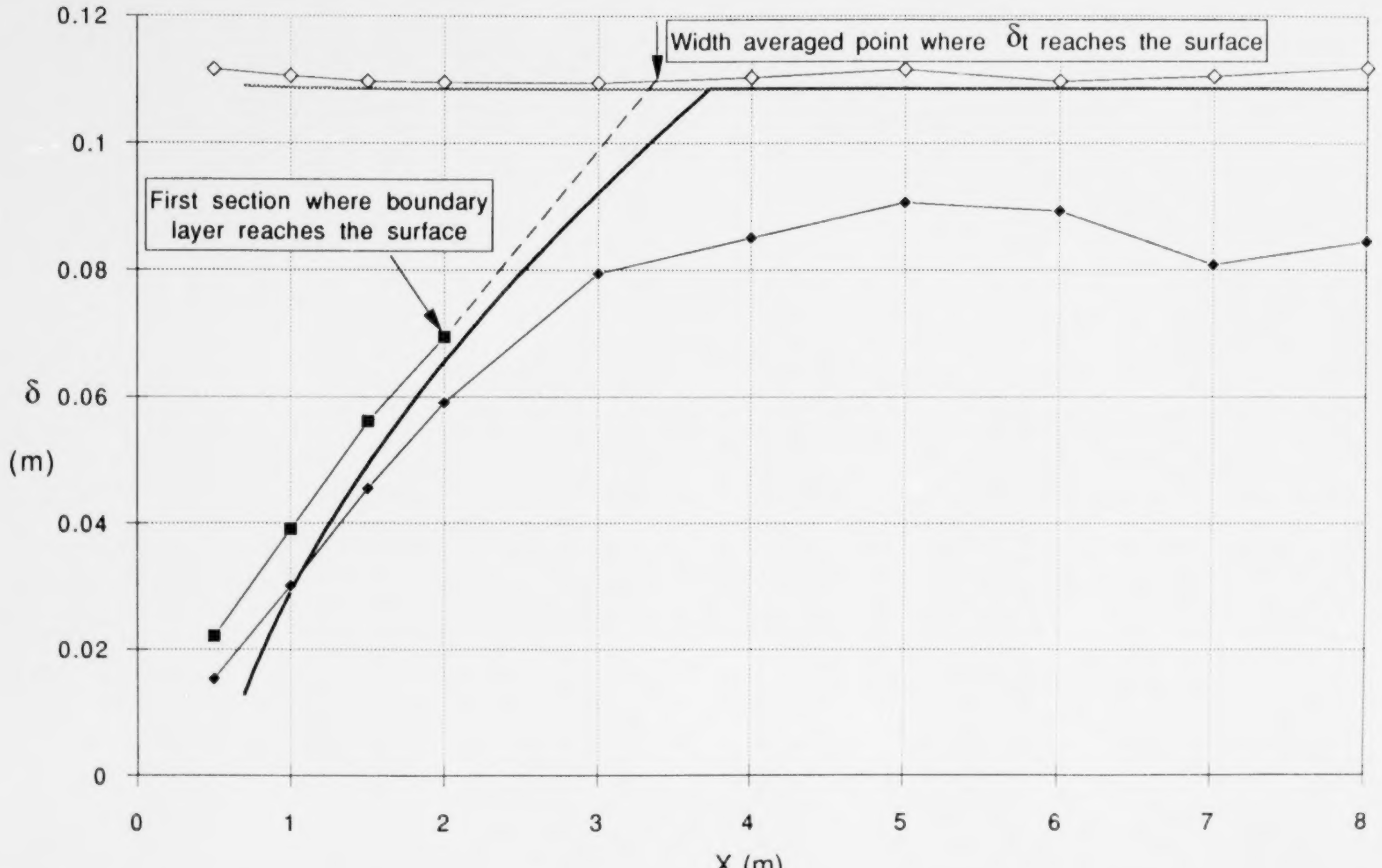

Fig. 2.33b Same as Fig. 2.33a except δ_t is interpolated between x=2.0 m and the average location where δ_t reaches the surface. *(Rough channel)*

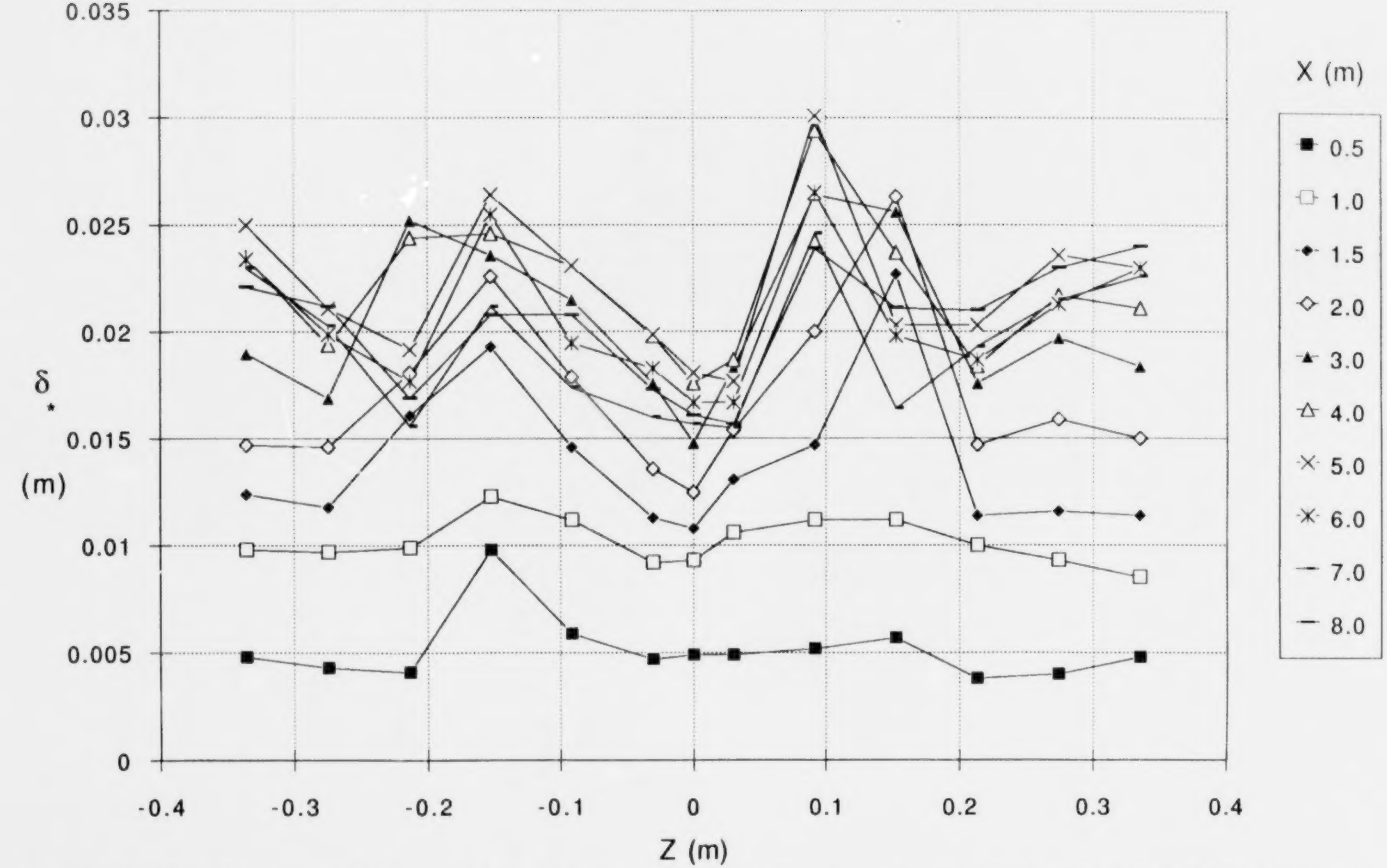

Fig. 2.34a Displacement thickness plotted in the transverse direction for different longitudinal locations. *(Rough channel)*

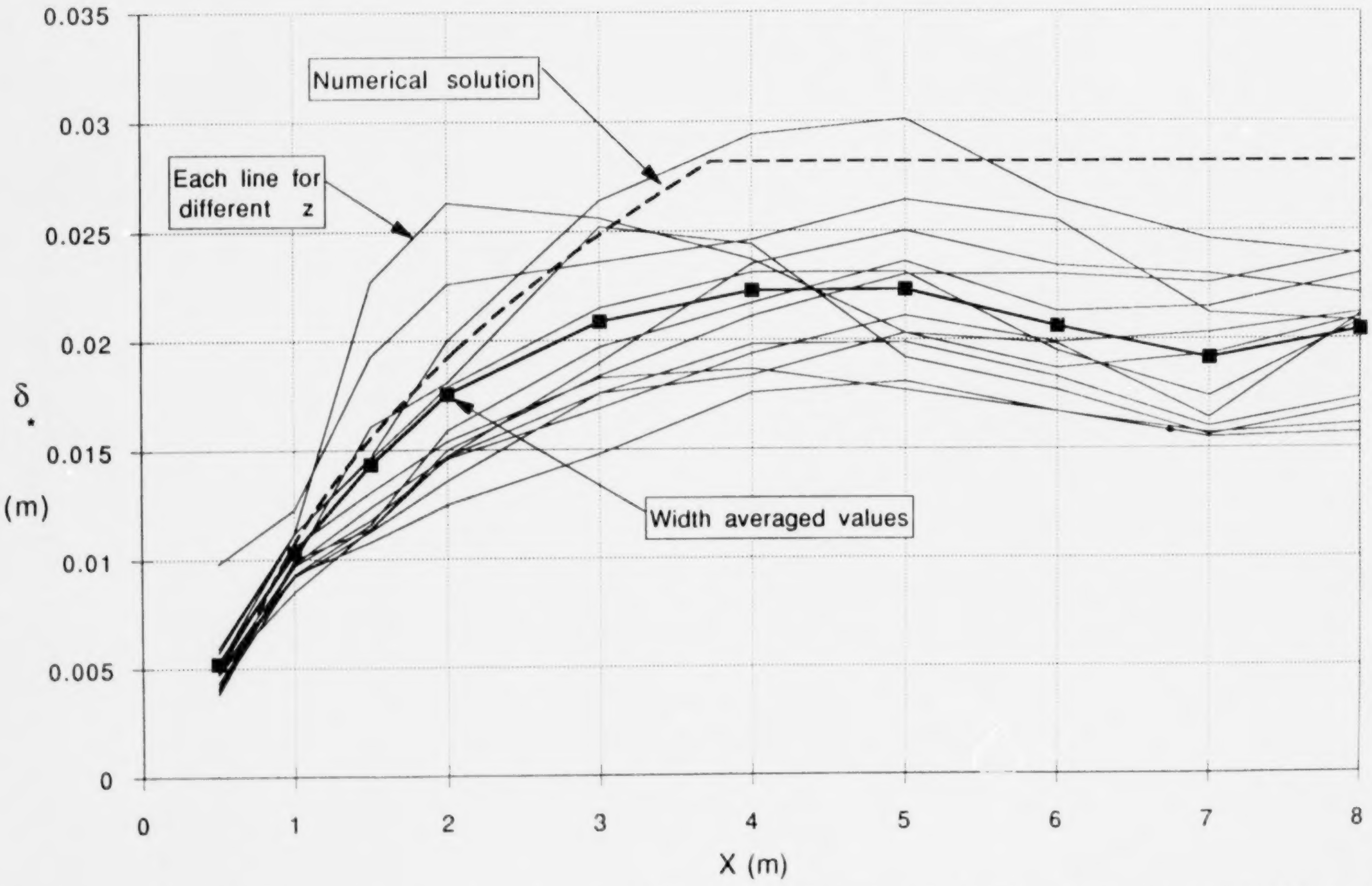

Fig. 2.34b Displacement thickness plotted in the longitudinal direction for different transverse locations. Also shown is the width averaged δ* growth and the numerical solution. *(Rough channel)*

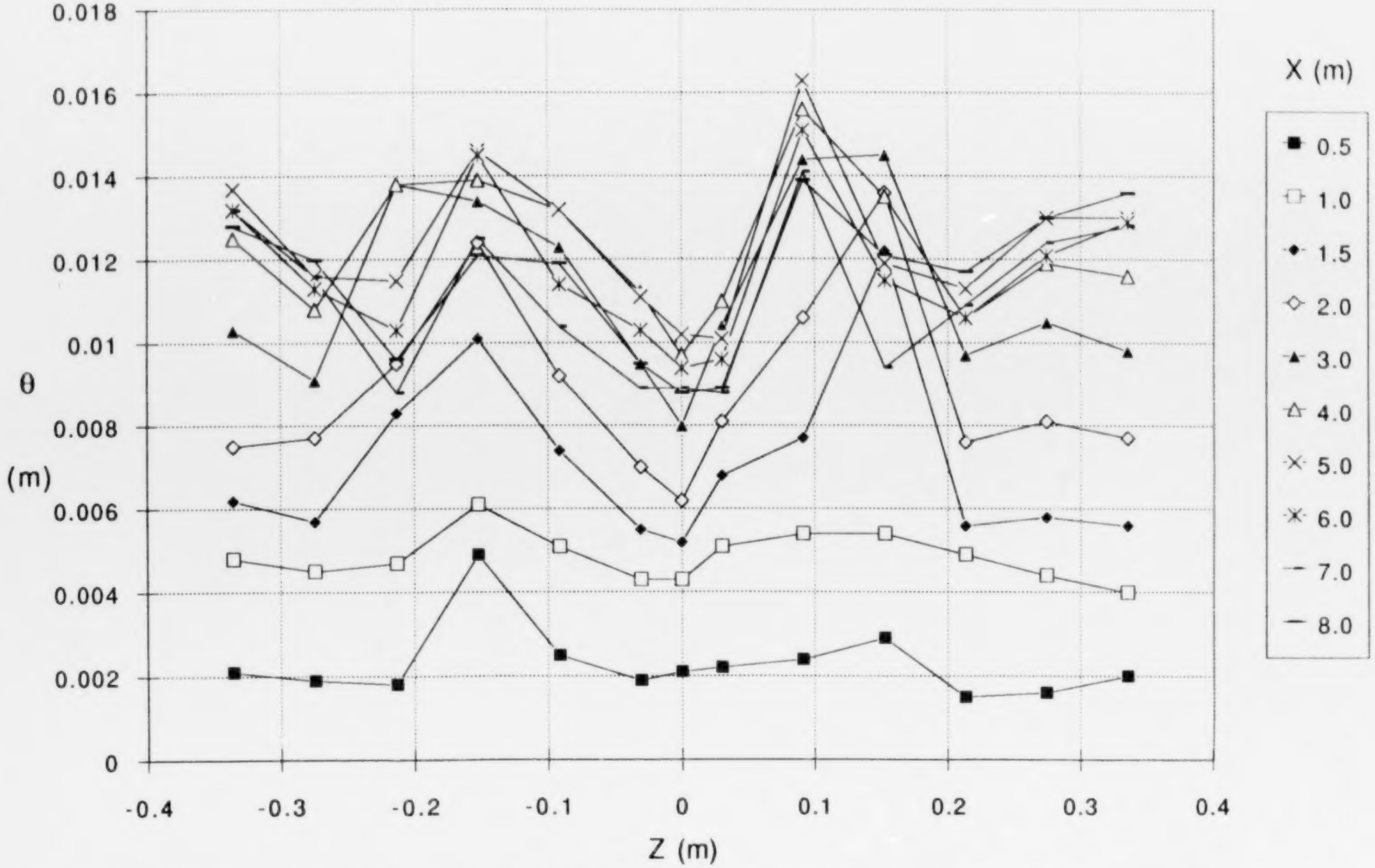

Fig. 2.35a Momentum thickness plotted in the transverse direction for different longitudinal locations. *(Rough channel)*

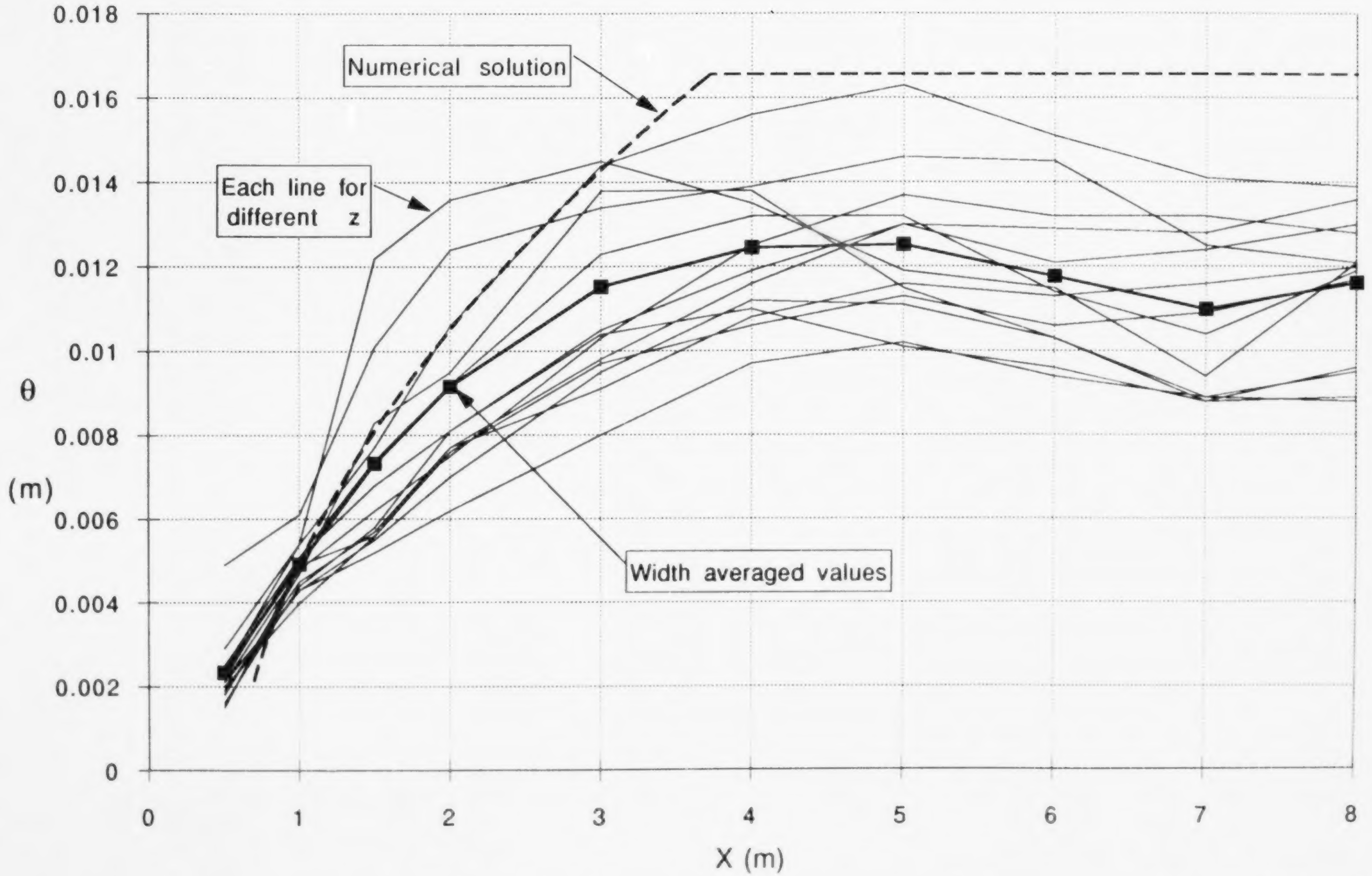

Fig. 2.35b Momentum thickness plotted in the longitudinal direction for different transverse locations. Also shown is the width averaged θ growth and the numerical solution. *(Rough channel)*

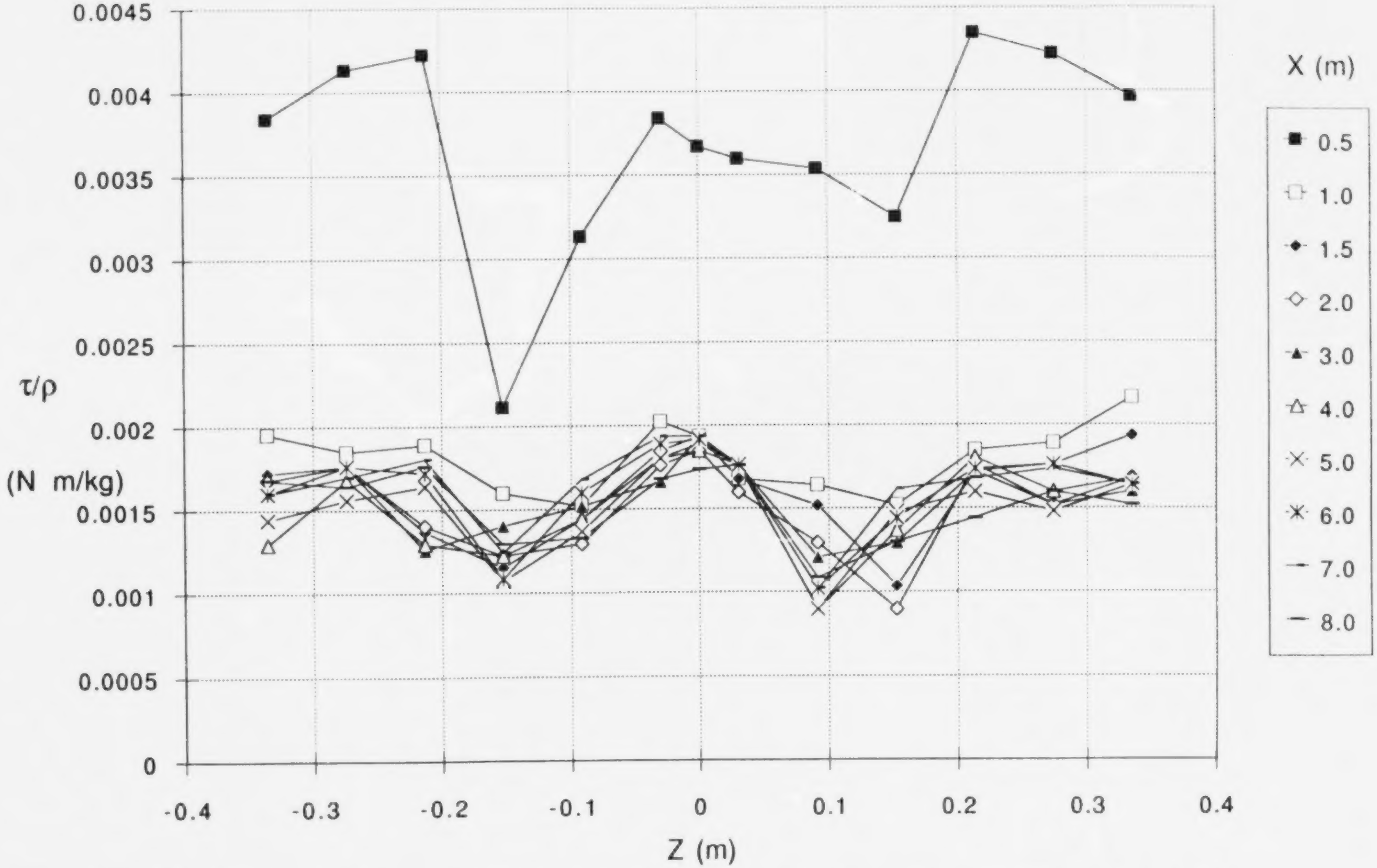

Fig. 2.36 Bed shear stress plotted in the transverse direction for different longitudinal locations. *(Rough channel)*

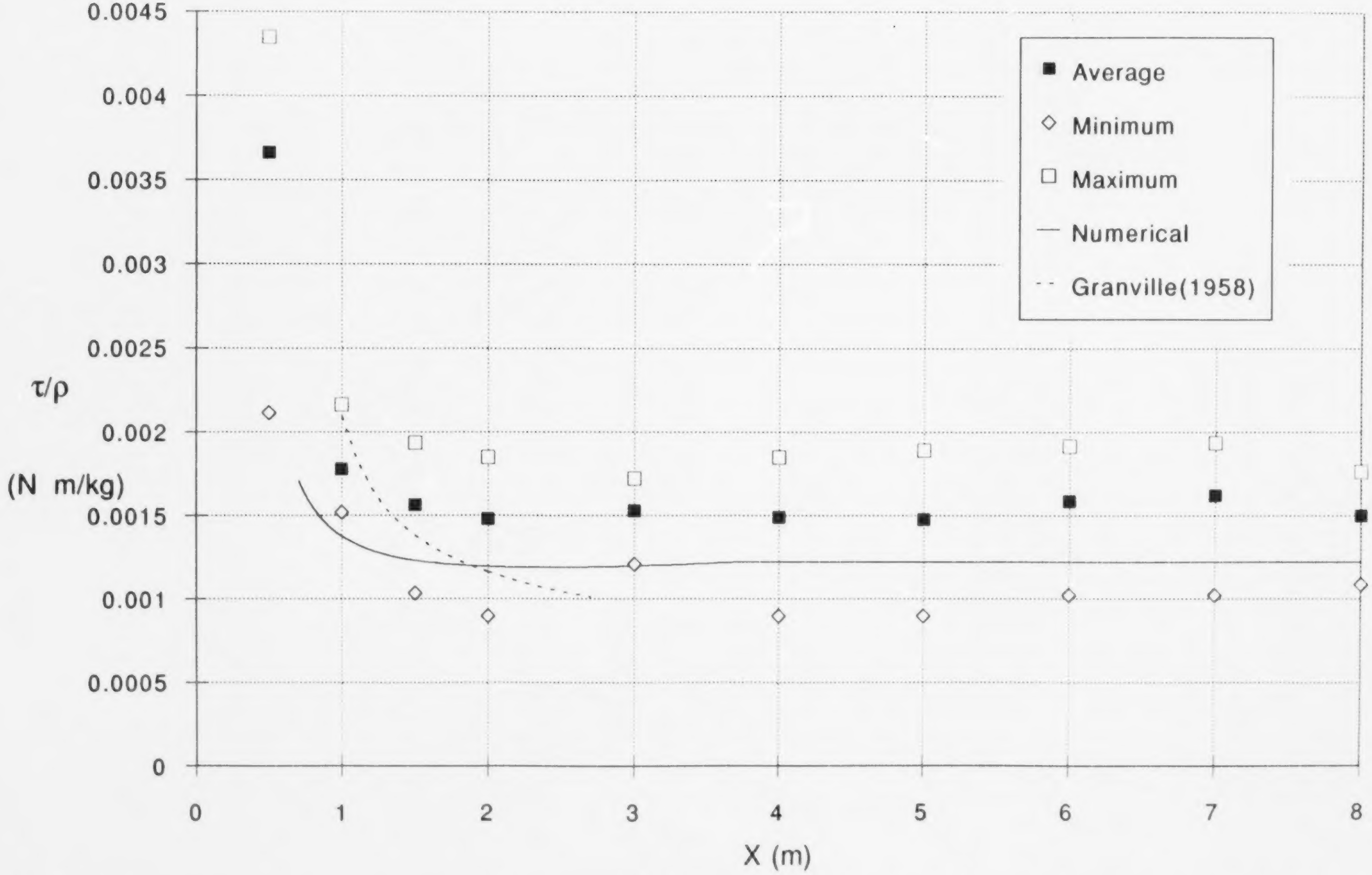

Fig. 2.37 Minimum, maximum, and width averaged bed shear stress plotted in the longitudinal direction. Also shown is the numerical solution and the Granvill's rough flat plate solution (1958). *(Rough channel)*

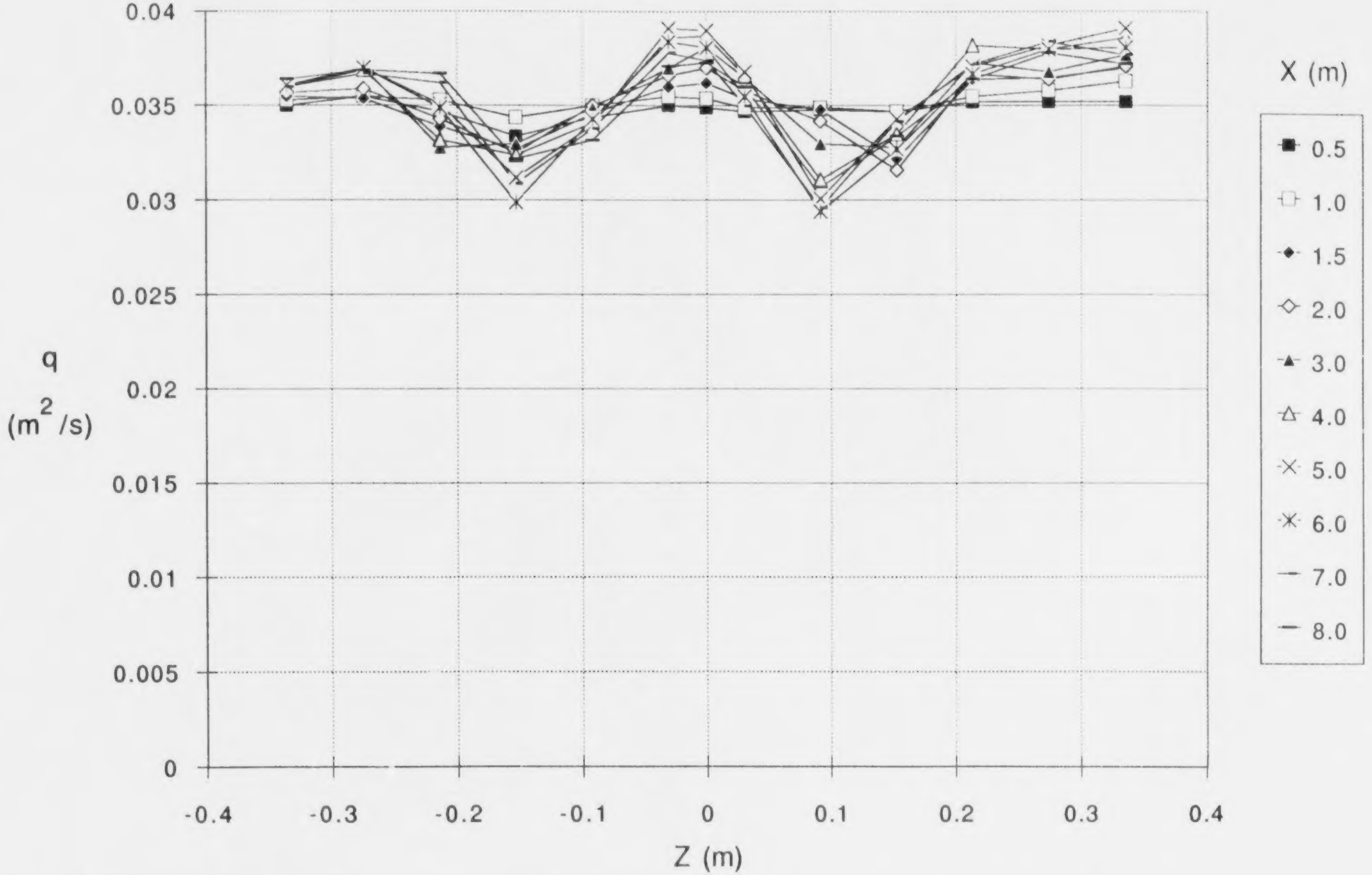

Fig. 2.38a Discharge per unit width as integrated from the velocity profiles plotted in the transverse direction for different longitudinal locations. *(Rough channel)*

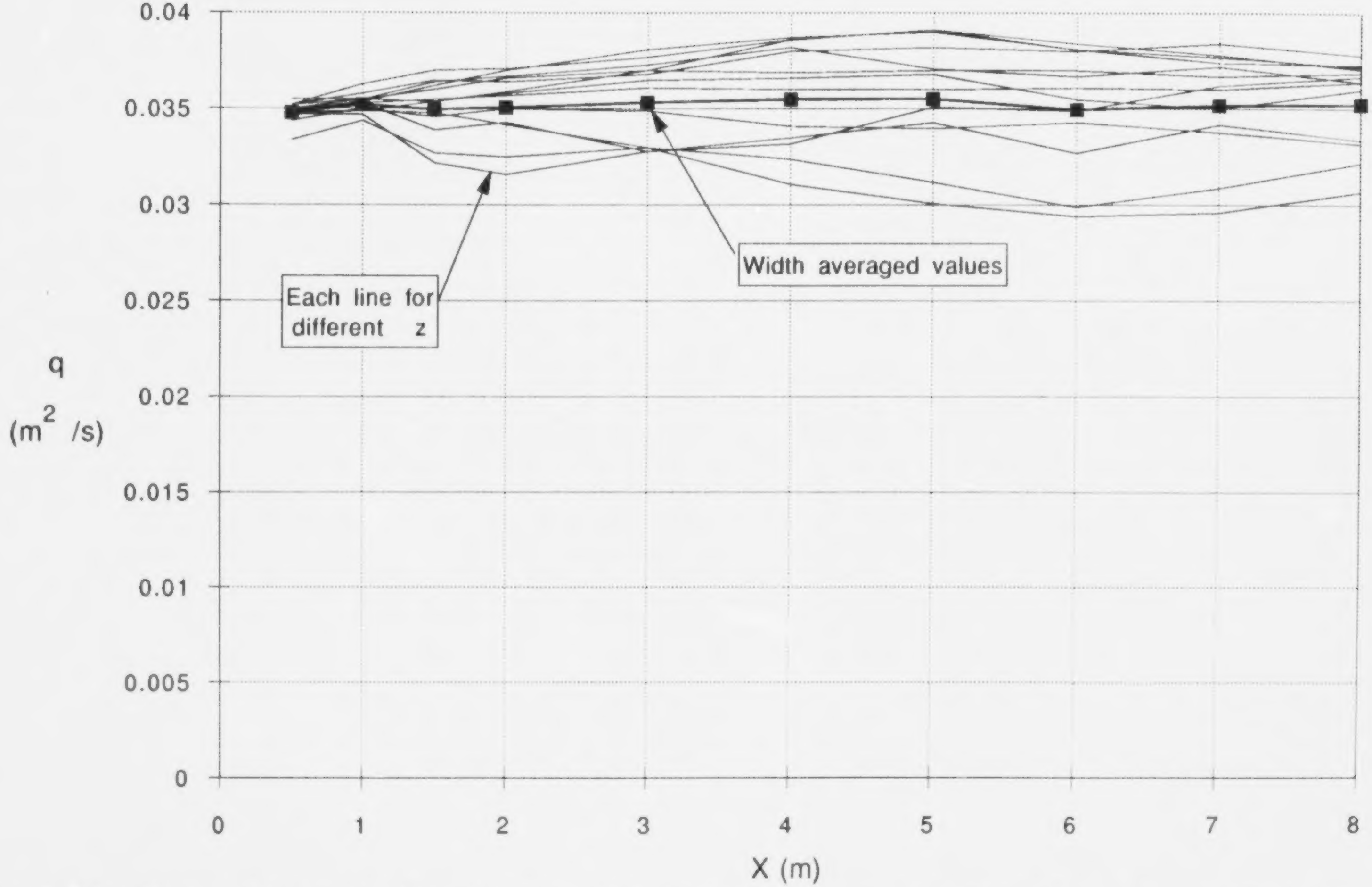

Fig. 2.38b Discharge per unit width as integrated from the velocity profiles plotted in the longitudinal direction for different transverse locations. Also shown is the width averaged unit discharge. *(Rough channel)*

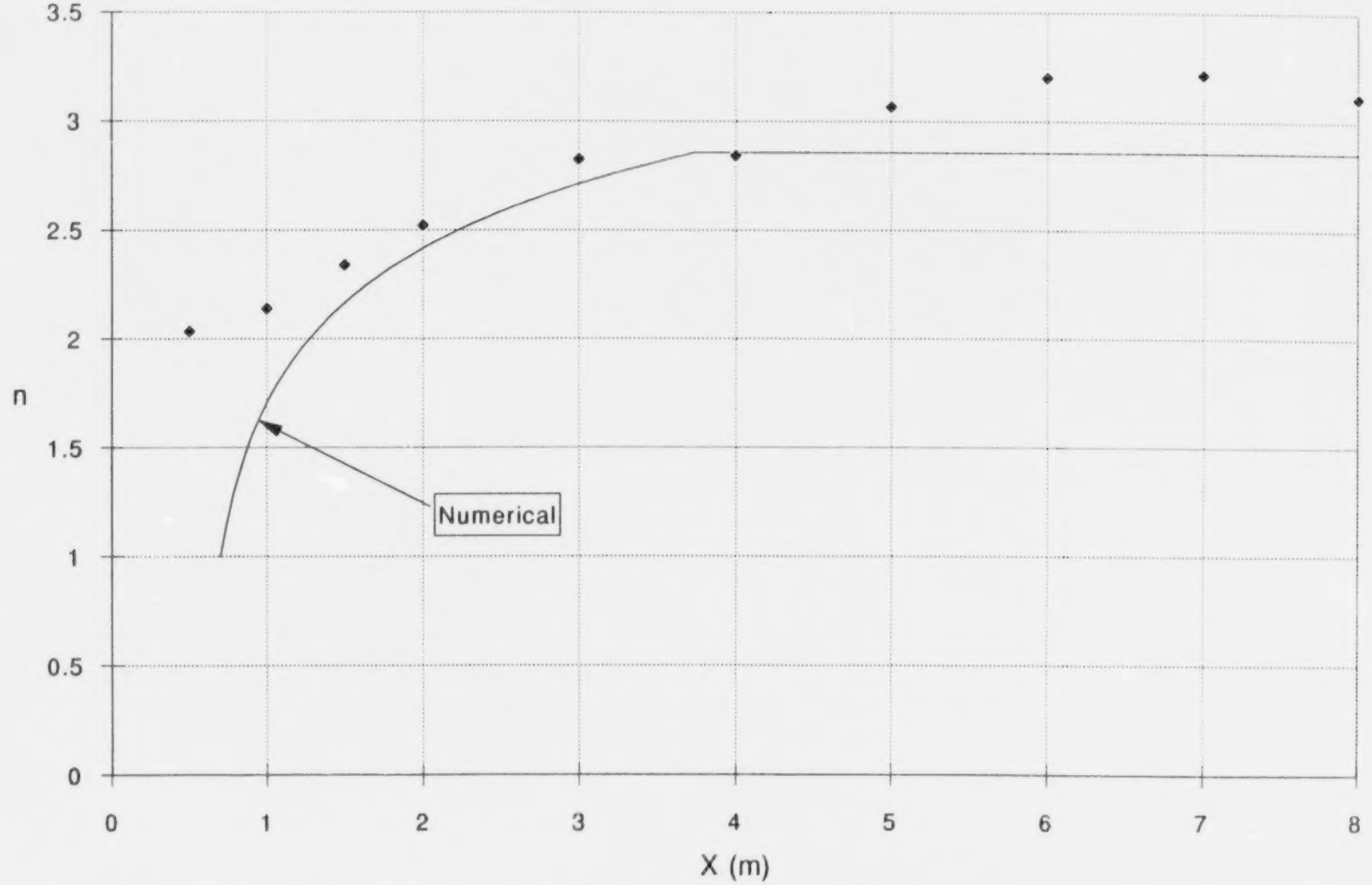

Fig. 2.39 Width averaged power law exponent from regressional curve fits of the boundary layer portion of the velocity profiles. Also shown is the numerical solution. *(Rough channel)*

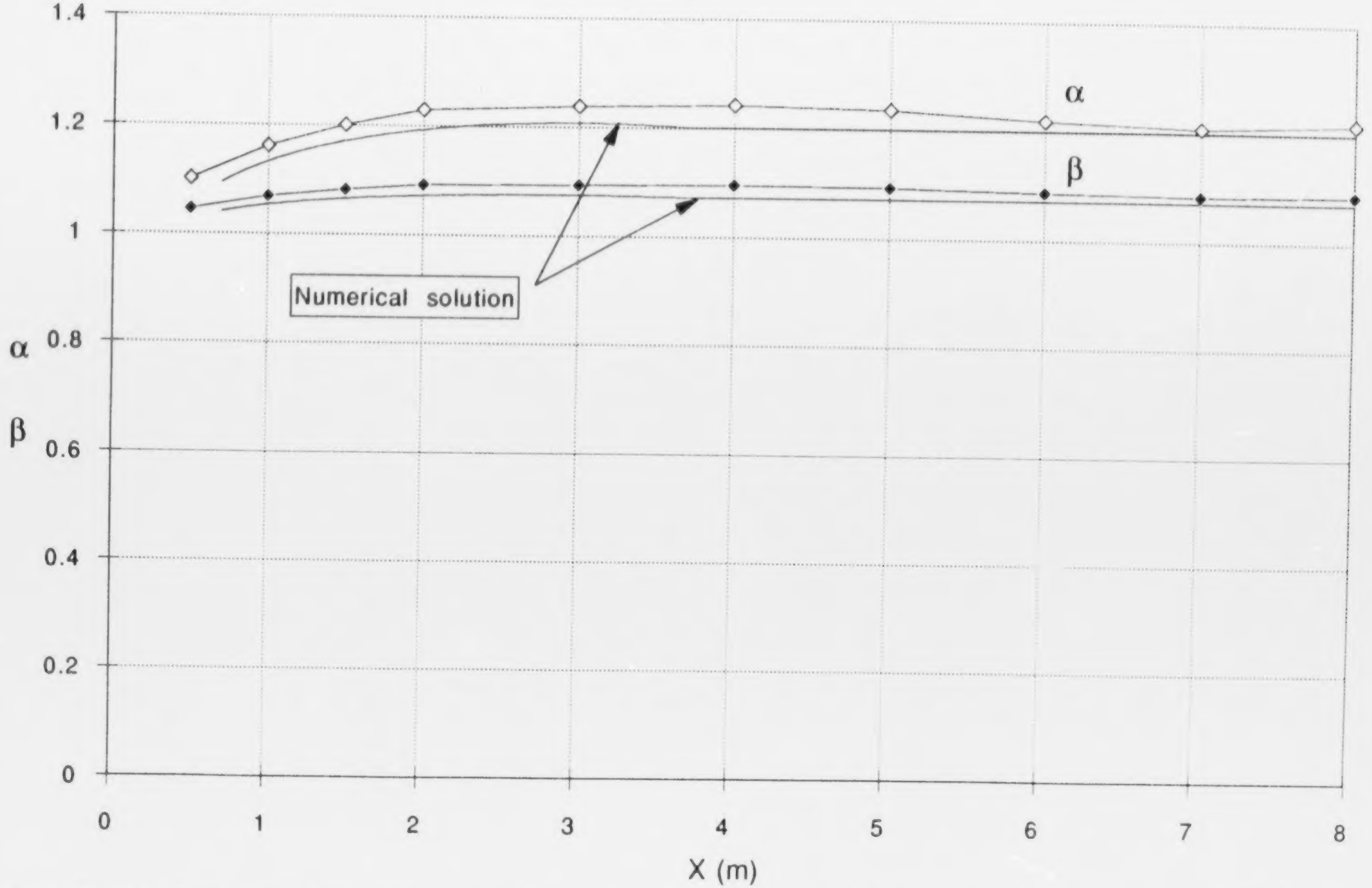

Fig. 2.40 Width averaged momentum and energy correction coefficients. Also shown is the numerical solution. *(Rough channel)*

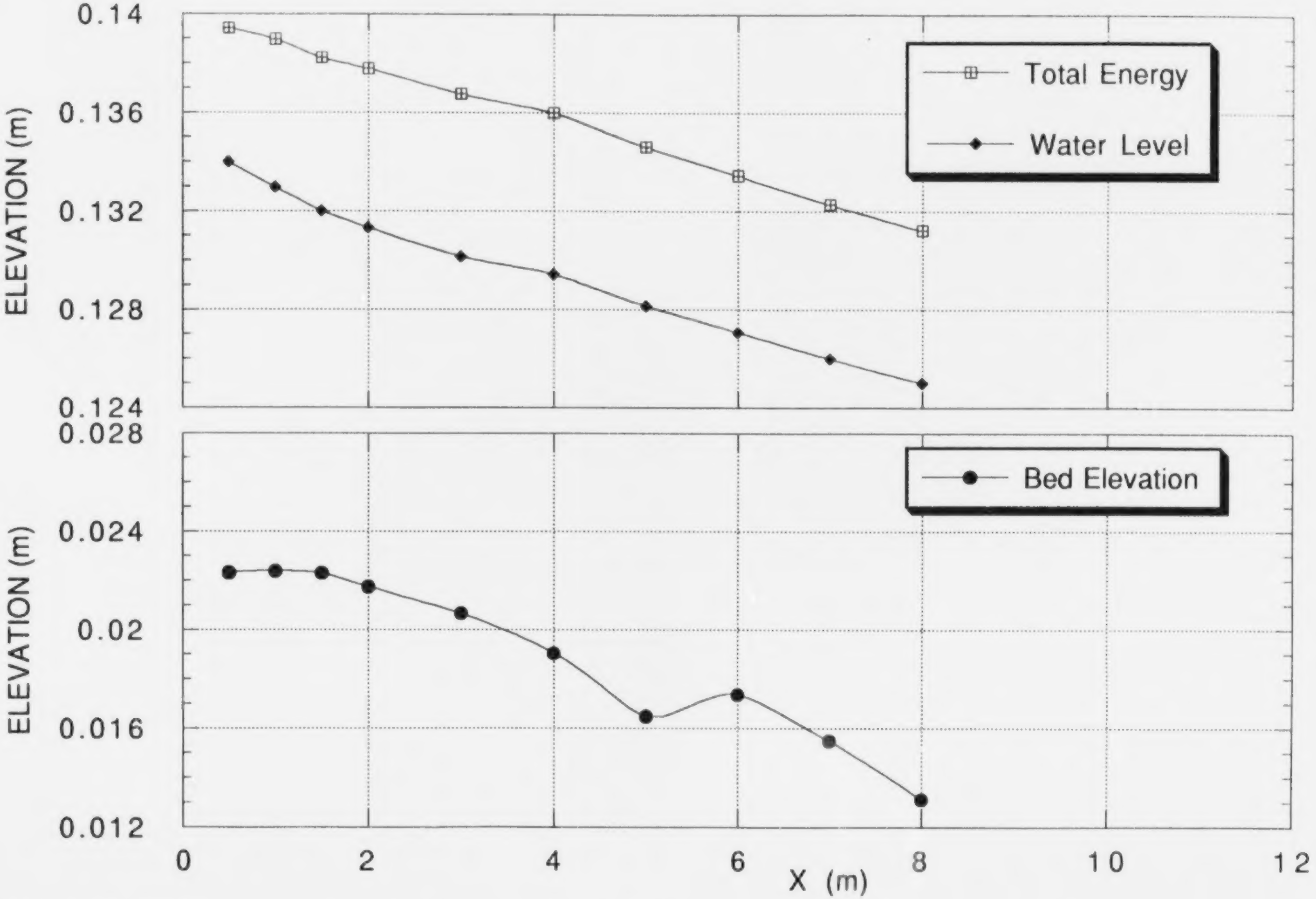

Fig. 2.41 Width averaged total energy, water surface elevation, and bed elevation. *(Rough channel)*

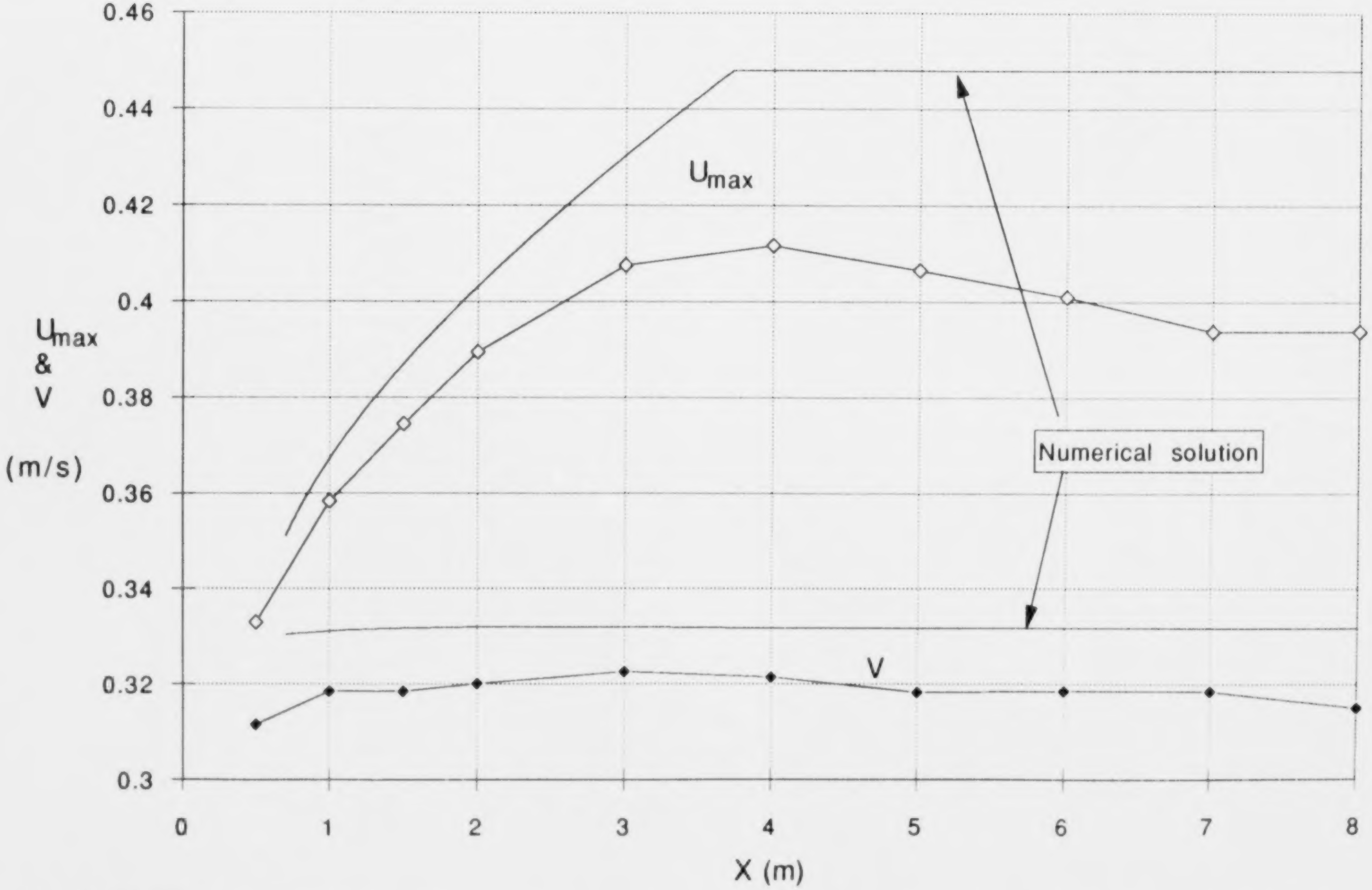

Fig. 2.42 Width averaged maximum velocity and average velocity. Also shown is the numerical solution. *(Rough channel)*

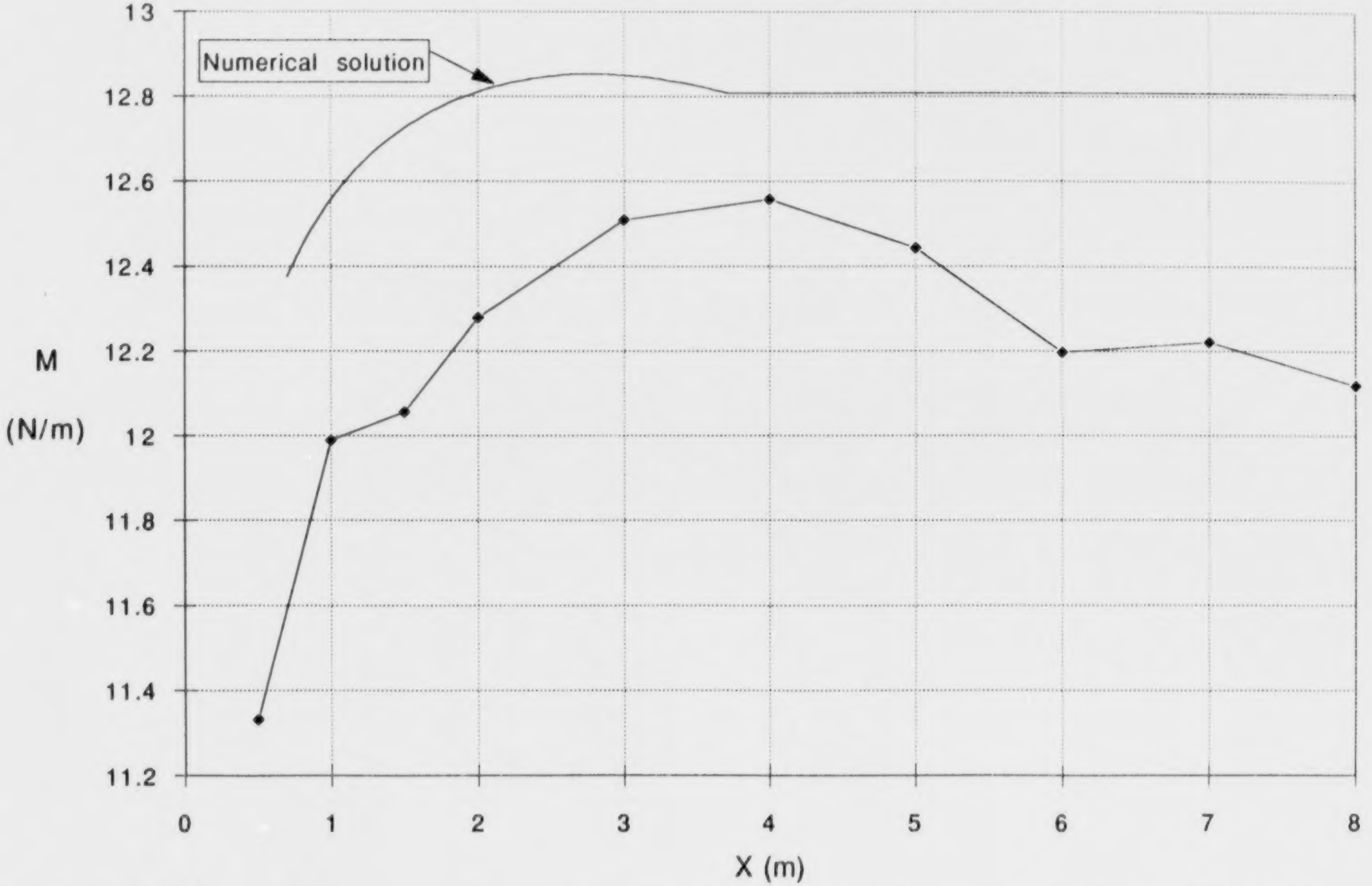

Fig. 2.43 Width averaged momentum per unit width. Also shown is the numerical solution. *(Rough channel)*

Run #	Bed type	Experimental			Numerical	From flat plate theories
		Minimum	Maximum	Average		
1	Smooth	32.5	89.9	53.2 - 63.2	59.3	* 49.2
2	Rough	15.4	42.5	28.0 - 33.0	27.9	**18.3

Table 2.2 Summary of entrance lengths in terms of number of depths for experiment, numerical solution, zero pressure gradient flat plate solutions.

* Schlichting's smooth flat plate solution based on Blasius's 1/7 th power law(1934).

** Harrison (1967) based on coefficient of skin friction after Granville (1958) and turbulent boundary layers on rough plates by Schlichting (1934).

Run #	Bed type	Experimental			Numerical	From flat plate theories
		Minimum	Maximum	Average		
1	Smooth	56	154	91 - 109	102	* 85
2	Rough	55	139	92 - 108	91	** 60

Table 2.3 Summary of entrance lengths as a percentage of the experimental average. (From Table 2.2)

3. Formulation of equations for numerical solution

3.1 The boundary layer in a wide open channel

It was decided to follow a similar solution route taken by Schlichting(Sec 1.2.1) to establish the equations for a boundary layer problem in a wide open channel. There are three additional complications to this problem then for a smooth flat plate: the presence of a pressure gradient; the effect of Reynolds number on the velocity distribution; the effect of roughness on the velocity distribution. For reasons of simplicity, the power law velocity distribution was used. It is well known that the power law exponent increases with Reynolds number and decreases with roughness (Schlichting,1979). Therefore, an expression for the power law exponent had to be developed, which included the effect of the Reynolds number and bed roughness.

Figure 3.1 helps to illustrate some of the following derivations.

For wide open channel flow with a developing boundary layer an expression for discharge per unit width q can then be written as:

$$q = \int_0^\delta u \, dy + \int_\delta^d U \, dy \tag{3.1}$$

where d is the depth of flow.

Substituting the power law velocity distribution (Equation 1.8) into 3.1, integrating, and using Equation 1.13 to simplify further, the expression for unit discharge becomes:

$$U = \frac{q}{d - \delta_*} \tag{3.2}$$

For small water surface slopes the Bernoulli equation at the free surface can be written as:

$$z_0 + d + \frac{U^2}{2g} = \text{constant} \tag{3.3}$$

where z_0 now is the bed elevation. The equivalent equation for a steep slope will be derived later.

If the bed slope is uniform Equation 3.3 can be written as:

$$- S_0\, x + d + \frac{U^2}{2g} = \text{constant} \tag{3.4}$$

where S_0 is the bed slope.

As mentioned earlier, for different Reynolds numbers, and rough boundaries, n will not be equal to 7. If it is assumed that velocity power law expressions work as well for boundary layers as they do for fully developed flow in pipes, then it is possible to use the Colebrook - White equation:

$$\frac{1}{\sqrt{f}} = 1.74 - 2\log\left(\frac{k_s}{r} + \frac{18.7}{\sqrt{f}\;\mathbf{R_p}}\right) \tag{3.5}$$

$$\mathbf{R_p} = \frac{2\,\bar{u}\,r}{\nu}$$

r = pipe radius

$\mathbf{R_p}$ = pipe Reynolds number

k_s = Equivalent sand grain roughness

The reason the coefficients used in the log expression are those for a pipe rather than that of a wide channel is because Schlichting found success in applying pipe velocity distributions in his solution. This expression applies for smooth, transition, and rough turbulent flow, and has the advantage of having an industrial type transition between the smooth turbulent and rough turbulent regimes. From this expression it is possible to derive an expression for n, using Nunners relation found in Hinze (1959) pg. 519-520.

Nunners relation states that:

$$n = \frac{1}{\sqrt{f}} \tag{3.6}$$

This relation has been experimentally shown to be valid for fully developed pipe flow for both smooth and rough boundaries.

By using Equations. 3.6 and 1.9, the friction factor f and the average velocity u can be eliminated from Equation 3.5. Also the pipe radius r can be replaced by the boundary layer thickness δ.

$$n = 1.74 - 2 \log \left(\frac{k_s}{\delta} + \frac{18.7\ n}{\mathbf{R_p}} \right) \tag{3.7}$$

$$\mathbf{R_p} = \frac{\delta\ U}{\nu} \frac{4\ n^2}{(n+1)(2\ n+1)}$$

Equations. 1.9, 1.11 and 3.6 give:

$$\frac{\tau_o}{\rho} = \frac{U^2\ n^2}{2\,(n+1)^2\,(2\ n+1)^2} \tag{3.8}$$

In Summary, the equations that describe the turbulent boundary layer in the open channel including roughness and Reynolds effects are:

$$\frac{\tau_o}{\rho} = \frac{d}{dx} U^2\theta + U\,\delta_* \frac{dU}{dx} \tag{1.5}$$

$$\delta_* = \frac{\delta}{(n+1)} \tag{1.13}$$

$$\theta = \delta \frac{n}{(n+1)(n+2)} \tag{1.14}$$

$$\frac{\tau_o}{\rho} = \frac{U^2 n^2}{2(n+1)^2(2n+1)^2} \tag{3.8}$$

$$U = \frac{q}{d - \delta_*} \tag{3.2}$$

$$-S_o x + d + \frac{U^2}{2g} = \text{constant} \tag{3.4}$$

$$n = 1.74 - 2\log\left(\frac{k_s}{\delta} + \frac{18.7\,n}{\mathbf{R}_p}\right) \tag{3.7}$$

$$\mathbf{R}_p = \frac{\delta U}{\nu} \frac{4n^2}{(n+1)(2n+1)}$$

We can now solve the above equations for U(x), d(x), n(x), δ(x).

3.2 Subcritical boundary condition

Subcritical flow is governed by a downstream boundary condition; the boundary layer thickness is equal to the depth which is equal to the normal depth,

$$\delta = d = d_o \tag{3.9}$$

and the bed shear is given by the friction or bed slope:

$$\frac{\tau_o}{\rho} = g\ d_o\ S_o \tag{3.10}$$

Define: $n_o = n$ and $\mathbf{R}_{po} = \mathbf{R}_p$ when $\delta = d = d_o$

If Equations. 3.9 and 3.10 are substituted into Equations 3.8, 3.2, 3.7 and simplified further, the downstream boundary condition reduces to:

$$d_o = \left(\frac{q^2}{2\ g\ S_o\,(2\ n_o + 1)^2} \right)^{\frac{1}{3}} \tag{3.11}$$

$$n_o = 1.74 - 2 \log \left(\frac{k_s}{d_o} + \frac{18.7\ n_o}{\mathbf{R}_{po}} \right) \tag{3.12}$$

$$\mathbf{R}_{po} = \frac{q}{\nu} \frac{4\ n_o}{(2\ n_o + 1)}$$

The downstream boundary condition is a function of discharge q, channel bed slope S_0, and bed roughness k_s only. We can now solve eqns. 28 and 29 implicitly for n_0 and d_0.

3.3 Supercritical modifications and boundary condition

Supercritical flow is governed by an upstream boundary condition; the initial depth where the boundary layer starts can be of any value, ranging from below normal depth to critical. This variation of initial depth depends on the weir geometry at the crest of the spillway or some other control such as a sluice gate. When the boundary layer reaches the water surface, the depth does not have to be equal to the normal depth as in the subcritical case, for we could have an S2 or an S1 gradually varied flow profile or be in a region of a self-aerated profile. The different depths mentioned above are shown in Figure 3.2 and will be referred to as follows:

d_o = normal depth as defined by Equations 3.11, 3.12.
d_i = initial depth at top of spillway.
d_{end} = depth when boundary layer reaches the surface.

It is necessary to modify the Bernoulli equation (Equation 3.4) for a steep slope since the direction of gravity can no longer be considered close to the perpendicular to bed direction. Figure 3.3 shows the basis for the modification and the explanation is in the following:

The elevation difference between points A and B in Figure 3.3 can be written as:

$$-\ d\cos(\phi) + x\sin(\phi) + d_i\cos(\phi) = \text{Elevation } \mathbf{A} - \text{Elevation } \mathbf{B} \qquad (3.13)$$

The difference in velocity head also has to be equal to this elevation difference:

$$\frac{U^2}{2g} - \frac{U_i^2}{2g} = \text{Elevation } \mathbf{A} - \text{Elevation } \mathbf{B} \qquad (3.14)$$

By equating Equation 3.13 to Equation 3.14, the modified Bernoulli equation for the potential core becomes:

$$x\sin(\phi) - d\cos(\phi) + \frac{U^2}{2g} = -\ d_i\cos(\phi) + \frac{U_i^2}{2g} = \text{constant} \qquad (3.15)$$

Now equations 1.5, 1.13, 1.14, 3.8, 3.2, 3.7 and 3.15 can be solved for U(x), d(x), n(x), δ(x).

3.4 Comparison of normal depth and shear to that given by the Chezy relation

It would be desirable to compare the downstream boundary condition for uniform flow (Section 3.2) to well established uniform flow relations, such as the dimensionless Chezy equation for a wide channel:

$$C_* = 2.5 \ln\left(\frac{12\,R}{k}\right) \tag{3.16}$$

where C* is the dimensionless Chezy coefficient and is defined by:

$$C_* = \frac{V}{u_*} \tag{3.17}$$

, V is the depth averaged velocity, R is the hydraulic radius, and k is the total roughness, defined by:

$$k = k_s + k_v \tag{3.18}$$

where k_v is the laminar sublayer thickness and is defined by:

$$k_v = \frac{3.3\,\nu}{u_*} \tag{3.19}$$

For uniform flow, the shear velocity can be defined by:

$$u_* = \sqrt{g\,d_o\,S_o} \tag{3.20}$$

Also, the hydraulic radius R is equal to the normal depth d_o, therefore:

$$C_* = 2.5 \ln\left(\frac{12\,d_o}{k}\right) \tag{3.21}$$

From continuity:

$$V = \frac{q}{d_o} \tag{3.22}$$

Combining Equations 3.17, 3.20, and 3.22 we obtain:

$$d_o = \left(\frac{q^2}{g\, S_o\, C_*^{\,2}}\right)^{\frac{1}{3}} \tag{3.23}$$

Combining Equations 3.18, 3.19, and 3.21 we obtain:

$$C_* = 2.5 \ln \left(\frac{12\, d_o}{k_s + \frac{3.3\, \nu}{u_*}}\right) \tag{3.24}$$

Combining Equations 3.17 and 3.22 we obtain:

$$u_* = \frac{q}{d_o\, C_*} \tag{3.25}$$

We can now solve Equations 3.23, 3.24, and 3.25 for d_o, C_*, and u_*.

Comparing Equation 3.23 with 3.11 we notice that they are very similar. If both sets of equations give the same d_o, then it follows that the relationship between the dimensionless Chezy coefficient and the power law exponent is:

$$C_* = \sqrt{2}\,(2\, n_o + 1) \tag{3.26}$$

To compare if Equations 3.11 and 3.12 give the same normal depth and bed shear stress as Equations 3.23, 3.24, and 3.25, a variety of different discharges, slopes, and bed roughnesses were chosen, and both sets of equations were solved for each flow condition. The results and percentage difference are tabulated in Table 3.1.

Table 3.1 shows that the differences between the two sets of equations is very small; errors of the order of 1% or less were found in the normal depth d_o, the bed shear stress τ_o/ρ, and C_*.

Another way to come up with a relation between C_* and n_o would be to substitute the relation between f and C_*:

$$f = \frac{8}{C_*^2} \tag{3.27}$$

into Nunners relation to obtain:

$$C_* = 2\sqrt{2}\, n_o \tag{3.28}$$

The difference between 3.26 and 3.28 could be due to the slight difference in the coefficients between log expressions for pipes and wide channels.

Another relation from Odgaurd (1986) to Zimmerman (1978) comes from equating the surface and average velocities between the log and power law expressions and yields:

$$C_* = 2.5\ n_o \qquad (3.29)$$

The difference between this equation from 3.26 or 3.28 is fairly significant. This could be due to the fact that the log expression does not accurately predict the surface velocity without the wake function component being considered. The wake function is also differant between open channels, pipes, and boundary layers.

3.5 Comparison of the zero pressure gradient numerical solution to known solutions

The first test of the numerical solution was of the zero pressure gradient case, where the potential core velocity U was constant. These tests were then compared with two known solutions; Schlichting's smooth flat plate solution and Harrison's work on rough plates after Granville's rough plate solution. Table 3.2 summarizes the details of the two comparisons. For these simulations, the potential core velocity and roughness were chosen from conditions used in the numerical simulations of the experiments in the mild channel, which included the presence of a pressure gradient (Sec 4.2.).

The first comparison of the numerical solution was the simulation of the boundary layer growth on a smooth flat plate. It was compared with both the smooth flat plate solution of Schlichting(1934)(based on Blasius's 1/7th power law) and Harrison's solution on a rough plate using a small roughness. As mentioned earlier, Harrison's work is needed to obtain boundary layer thicknesses from Granville's solution of the rough plate since Granville's solution gives only the boundary shear. The comparisons were solved for a certain length in the x direction corresponding to the limits of $\mathbf{R}_x$ where the 1/7th power law applies (Sec 1.2.1).

Figure 3.4 shows the comparison in boundary shear between the three solutions and Figure 3.5 the boundary layer thickness. All three shear stresses agree well with each other, but the boundary layer thickness differs somewhat. The boundary layer thickness seems to be a more sensitive parameter than the shear stress, making the growth of the boundary layer all that more difficult to predict. Nevertheless, the Schlichting and numerical solutions start to disagree significantly near the limit at $\mathbf{R}_x = 6 \times 10^6$, while the Harrison solution shows a somewhat lower growth rate through the entire domain. Figure 3.6 shows the comparison of the displacement and momentum thickness of the three solutions. Notice that their rate of increase is more similar than it is for the boundary layer thickness. The momentum thickness especially agrees well between all three solutions. Figure 3.7 shows the power law exponent for the three solutions and shows that the numerical solution falls above and below the constant value of n = 7 for the Sclichting solution. This is what one might expect; n should be less than 7 at the smaller Reynolds number limit and more than 7 at the upper Reynolds number limit. However, the Harrison solution falls consistently below the numerical solution by a difference in n of about 1.8. Also, it is always below 7 within the range of validity of the Schlichting formula. It is unclear what is the cause of this discrepancy.

The second comparison was for the simulation of the boundary layer growth on a rough plate using the work of Granville and Harrison mentioned earlier. Again, the shear stress was an easy match (Figure 3.8), but the boundary layer growth of the Harrison solution was somewhat lower than the numerical solution (Figure 3.9). In an opposite fashion, the displacement and momentum thickness for the numerical solution were less than that of Harrison. The power law exponent in Figure 3.11 again showed a lower power law exponent than the numerical solution; n was about 1.3 less in the Harrison solution.

Since all these solutions have been derived from the analysis and experiments conducted in pipes, further experiments are needed in evaluating this analysis in its application to boundary layers. Although this analysis seems sufficient enough for predicting skin friction or shear stress (one of the first intention of this analysis was to predict the drag on ship hulls and aircraft), it lacks the ability to accurately locate the edge of the boundary layer, and to accurately predict velocity profiles and turbulence. It was for this reason that the solution based on the Colebrook and White equation and Nunners relation was deemed as good or bad as the Harrison-Granville solution. With the added advantages of agreeing with the Schlichting power law exponent within the valid range and being of the simpler form, the solution based on the Colebrook-White relation was chosen to continue the work in the numerical analysis of boundary layers in open channels.

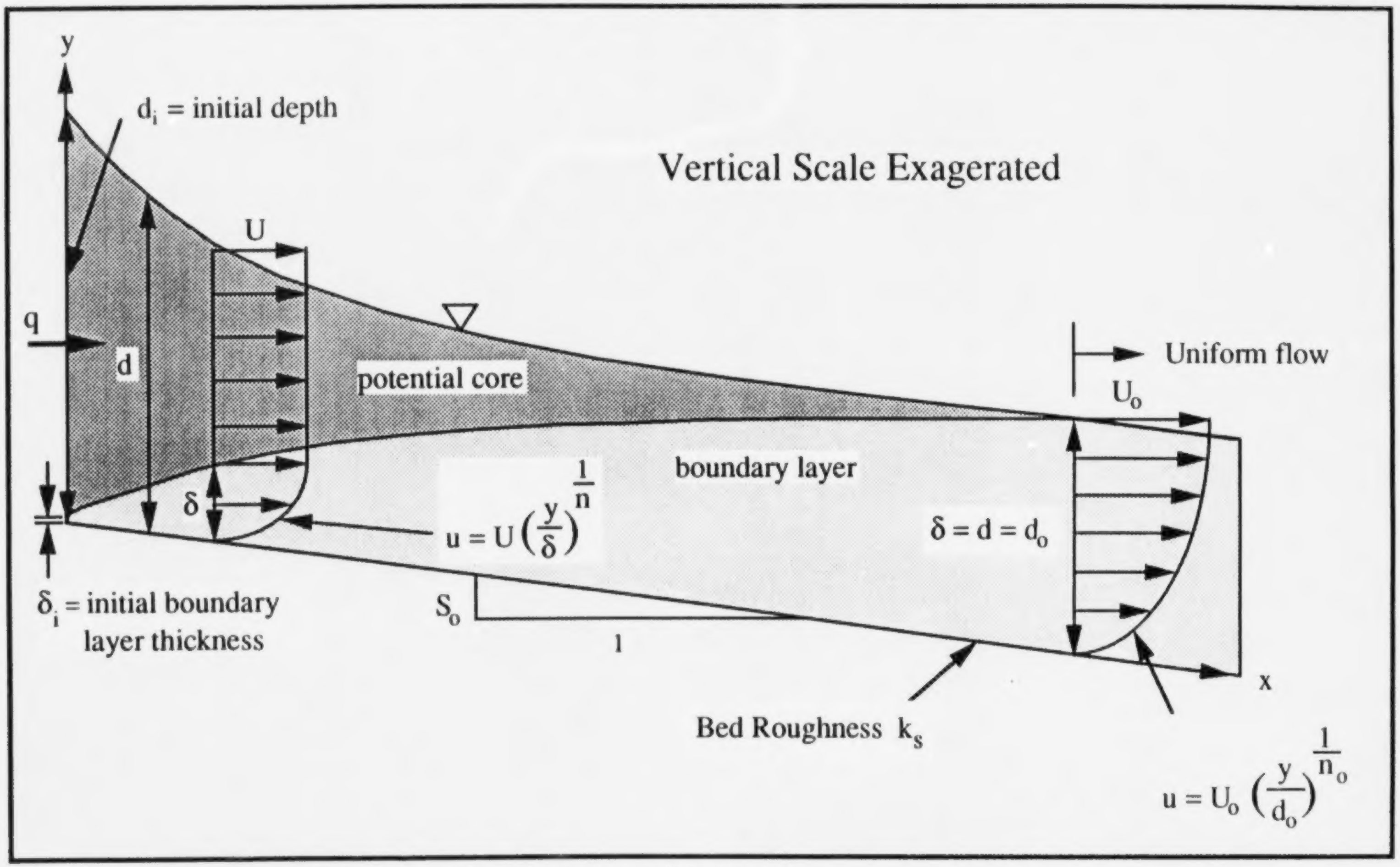
y
d_i = initial depth
Vertical Scale Exagerated
U
q
d
potential core
Uniform flow
U_o
boundary layer
δ
$u = U\left(\frac{y}{\delta}\right)^{\frac{1}{n}}$
$\delta = d = d_o$
δ_i = initial boundary layer thickness
S_o
1
x
Bed Roughness k_s
$u = U_o\left(\frac{y}{d_o}\right)^{\frac{1}{n_o}}$

Fig. 3.1 Definition scetch for a boundary layer in a mild channel.

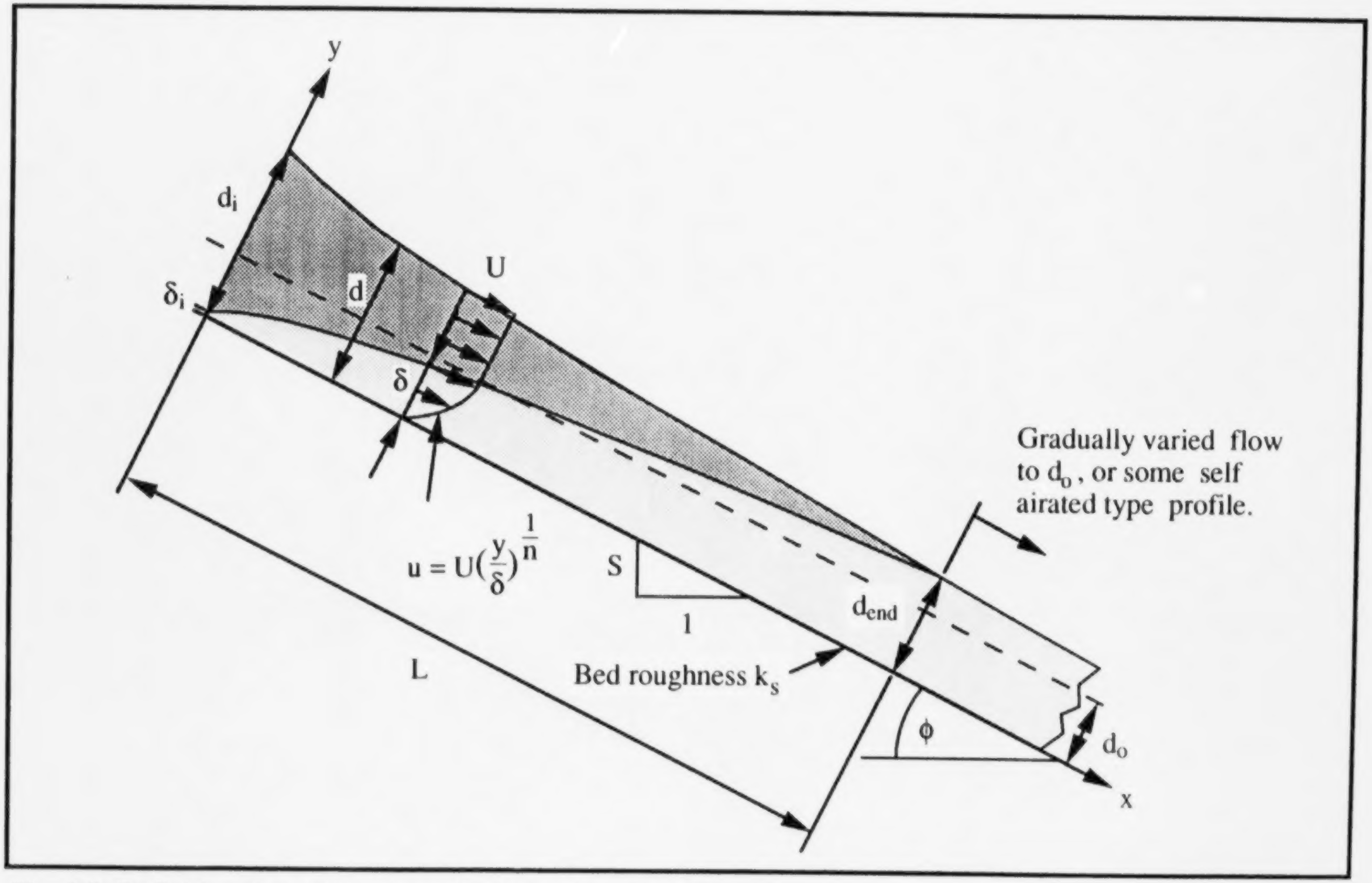
y
d_i
δ_i
d
U
δ
$u = U(\frac{y}{\delta})^{\frac{1}{n}}$
S
1
L
Bed roughness k_s
d_{end}
Gradually varied flow
to d_o, or some self
airated type profile.
ϕ
d_o
x

Fig. 3.2 Definition sketch for a boundary layer in a steep channel.

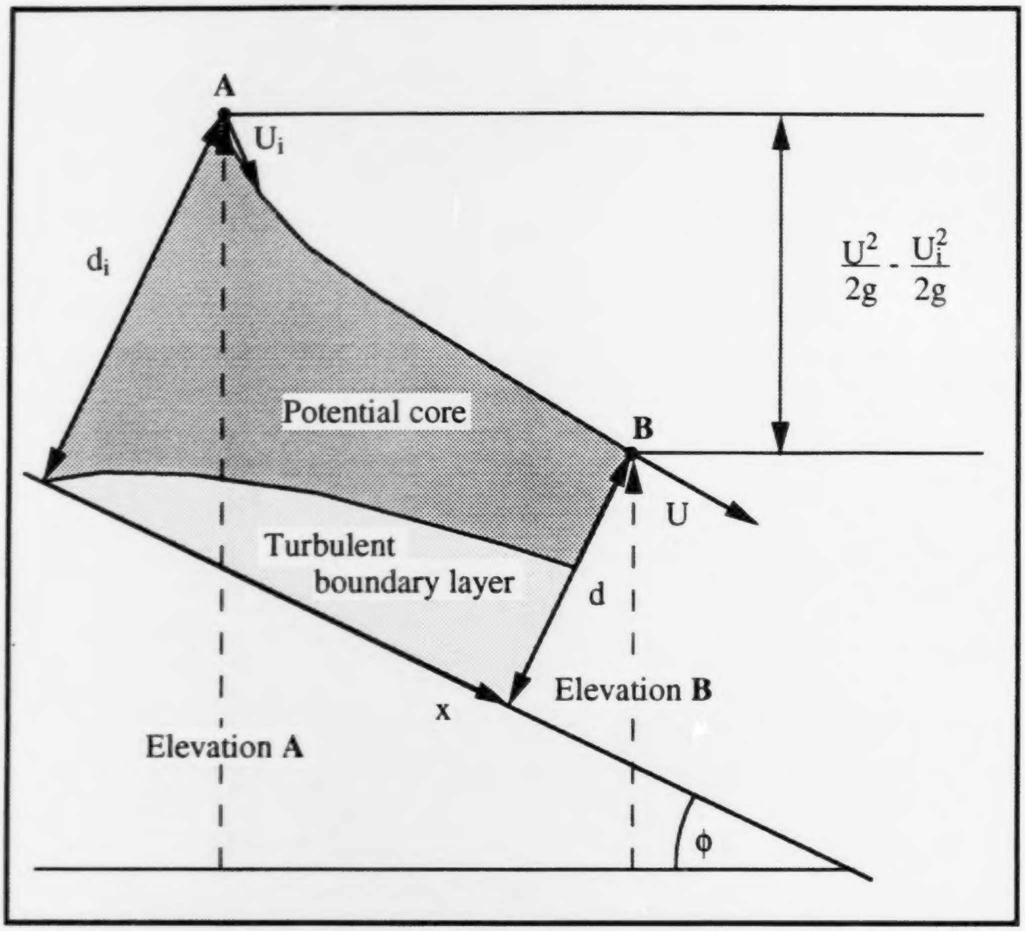
A
U_i
d_i
$\frac{U^2}{2g} - \frac{U_i^2}{2g}$
Potential core
B
U
Turbulent boundary layer
d
Elevation B
x
Elevation A
ϕ

Fig. 3.3 Modification of the Bernoulli equation for the potential core of the steep slope.

Input variables			Chezy relation (Eqns. 3.23, 3.24, 3.25)			Power law (Eqns. 3.11, 3.12)				% difference		
q (m^2/s)	So	ks (m)	do (m)	τo/ρ (N*m/kg)	C*	do (m)	τo/ρ (N*m/kg)	no	C* (Eqn. 3.25)	do	τo/ρ	C*
15.7660	0.0001	1.2735E+01	17.324	1.6988E-02	6.98	17.179	1.6846E-02	2.00	7.07	0.85	0.84	-1.28
15.7660	0.0001	3.2179E+00	13.775	1.3508E-02	9.85	13.727	1.3461E-02	3.00	9.90	0.35	0.35	-0.53
15.7660	0.0001	8.6059E-01	11.615	1.1390E-02	12.72	11.609	1.1384E-02	4.00	12.73	0.05	0.05	-0.08
15.7660	0.0001	2.3804E-01	10.140	9.9437E-03	15.59	10.156	9.9587E-03	5.00	15.56	-0.15	-0.15	0.23
15.7660	0.0001	6.7316E-02	9.059	8.8830E-03	18.47	9.085	8.9092E-03	6.00	18.38	-0.29	-0.29	0.44
15.7660	0.0001	1.9324E-02	8.226	8.0660E-03	21.34	8.259	8.0985E-03	7.00	21.21	-0.40	-0.40	0.60
15.7660	0.0001	5.5939E-03	7.561	7.4140E-03	24.22	7.598	7.4502E-03	8.00	24.04	-0.49	-0.49	0.73
15.7660	0.0001	1.6140E-03	7.016	6.8795E-03	27.09	7.055	6.9177E-03	9.00	26.87	-0.56	-0.56	0.83
15.7660	0.0001	1.0324E-04	6.170	6.0508E-03	32.85	6.211	6.0904E-03	11.00	32.53	-0.66	-0.66	0.98
15.7660	0.0001	2.6823E-14	5.835	5.7217E-03	35.72	5.875	5.7611E-03	12.00	35.36	-0.69	-0.69	1.03
0.0082	0.0001	0	0.059	5.7440E-05	18.47	0.059	5.7611E-05	6.00	18.38	-0.30	-0.30	0.44
0.0299	0.0001	0	0.126	1.2362E-04	21.34	0.127	1.2412E-04	7.00	21.21	-0.40	-0.40	0.60
0.1072	0.0001	0	0.271	2.6612E-04	24.22	0.273	2.6741E-04	8.00	24.04	-0.48	-0.48	0.72
0.3789	0.0001	0	0.584	5.7296E-04	27.09	0.588	5.7611E-04	9.00	26.87	-0.55	-0.55	0.82
1.3243	0.0001	0	1.258	1.2337E-03	29.97	1.266	1.2412E-03	10.00	29.70	-0.60	-0.60	0.90
4.5887	0.0001	0	2.710	2.6575E-03	32.85	2.728	2.6747E-03	11.00	32.53	-0.65	-0.65	0.97
15.7660	0.0001	0	5.835	5.7217E-03	35.72	5.875	5.7611E-03	12.00	35.36	-0.69	-0.69	1.03
53.8450	0.0001	0	12.567	1.2323E-02	38.60	12.657	1.2412E-02	13.00	38.18	-0.72	-0.72	1.07
0.0299	0.0001	0	0.126	1.2359E-04	21.34	0.127	1.2408E-04	7.00	21.21	-0.40	-0.40	0.60
0.0536	0.0001	1.9344E-04	0.186	1.8237E-04	21.34	0.187	1.8311E-04	7.00	21.21	-0.40	-0.40	0.60
0.1000	0.0001	4.6494E-04	0.282	2.7638E-04	21.34	0.283	2.7750E-04	7.00	21.21	-0.40	-0.40	0.60
0.3000	0.0001	1.2423E-03	0.586	5.7490E-04	21.34	0.589	5.7722E-04	7.00	21.21	-0.40	-0.40	0.60
1.0000	0.0001	2.9871E-03	1.308	1.2828E-03	21.34	1.314	1.2880E-03	7.00	21.21	-0.40	-0.40	0.60
3.0000	0.0001	6.3410E-03	2.721	2.6684E-03	21.34	2.732	2.6792E-03	7.00	21.21	-0.40	-0.40	0.60
10.0000	0.0001	1.4249E-02	6.072	5.9545E-03	21.34	6.097	5.9785E-03	7.00	21.21	-0.40	-0.40	0.60
30.0000	0.0001	2.9699E-02	12.631	1.2386E-02	21.34	12.682	1.2436E-02	7.00	21.21	-0.40	-0.40	0.60
10.0000	0.00001	1.0000E-03	10.628	1.0422E-03	29.15	10.691	1.0484E-03	9.71	28.89	-0.60	-0.60	0.89
10.0000	0.00003	1.0000E-03	7.506	2.2081E-03	28.35	7.550	2.2210E-03	9.44	28.11	-0.58	-0.58	0.87
10.0000	0.0001	1.0000E-03	5.133	5.0337E-03	27.46	5.162	5.0621E-03	9.13	27.23	-0.56	-0.56	0.84
10.0000	0.0003	1.0000E-03	3.633	1.0687E-02	26.63	3.653	1.0745E-02	8.84	26.41	-0.55	-0.55	0.81
10.0000	0.001	1.0000E-03	2.489	2.4412E-02	25.71	2.503	2.4540E-02	8.52	25.51	-0.52	-0.52	0.78
10.0000	0.003	1.0000E-03	1.765	5.1920E-02	24.87	1.774	5.2182E-02	8.23	24.68	-0.50	-0.50	0.75
10.0000	0.01	1.0000E-03	1.212	1.1883E-01	23.94	1.218	1.1940E-01	7.90	23.77	-0.48	-0.48	0.72
10.0000	0.03	1.0000E-03	0.861	2.5320E-01	23.09	0.865	2.5435E-01	7.61	22.93	-0.46	-0.46	0.68
10.0000	0.1	1.0000E-03	0.592	5.8068E-01	22.16	0.595	5.8317E-01	7.28	22.02	-0.43	-0.43	0.64
10.0000	0.3	1.0000E-03	0.421	1.2397E+00	21.31	0.423	1.2446E+00	6.99	21.19	-0.40	-0.40	0.60
10.0000	0.7	1.0000E-03	0.324	2.2265E+00	20.66	0.326	2.2350E+00	6.76	20.54	-0.38	-0.38	0.57
10.0000	0.9	1.0000E-03	0.300	2.6491E+00	20.47	0.301	2.6590E+00	6.70	20.35	-0.37	-0.37	0.56

Table 3.1 Comparison of uniform flow between the Chezy relation and the numerical solution.

	U (m/s)	k_s (m)	x_{max} (m)
Smooth plate comparisons	0.387	0.0 $*(10^{-7})$	15.5
Rough plate comparison	0.400	0.03	31.9

Table 3.2 Summary of input variables for the zero preasure gradient boundary layer solution comparisons.

* Small roughness used to simulate smooth plate using Granville and Harrison solution.

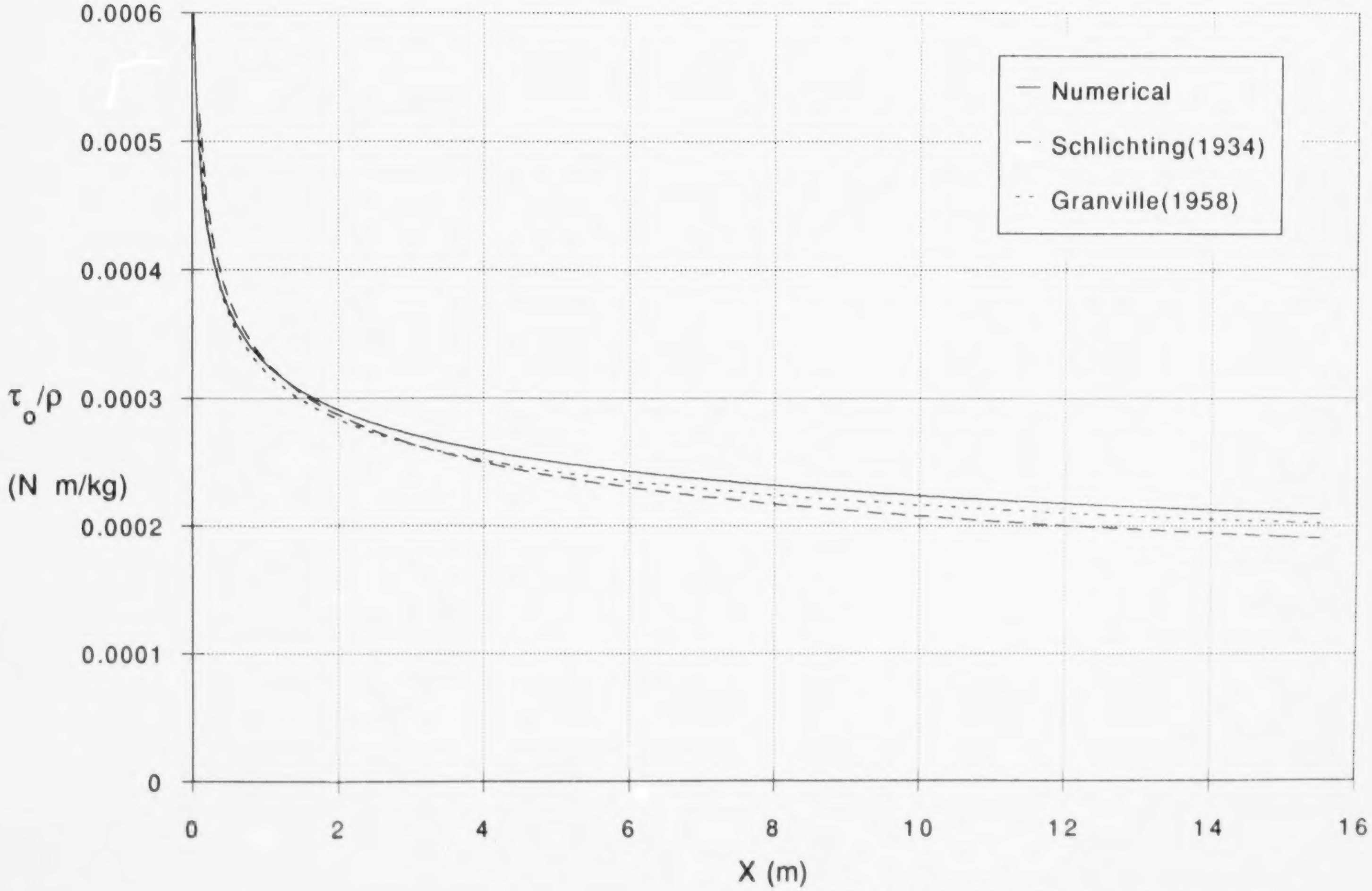

Fig. 3.4 Comparison of boundary shear between numerical and *smooth* flat plate solutions.

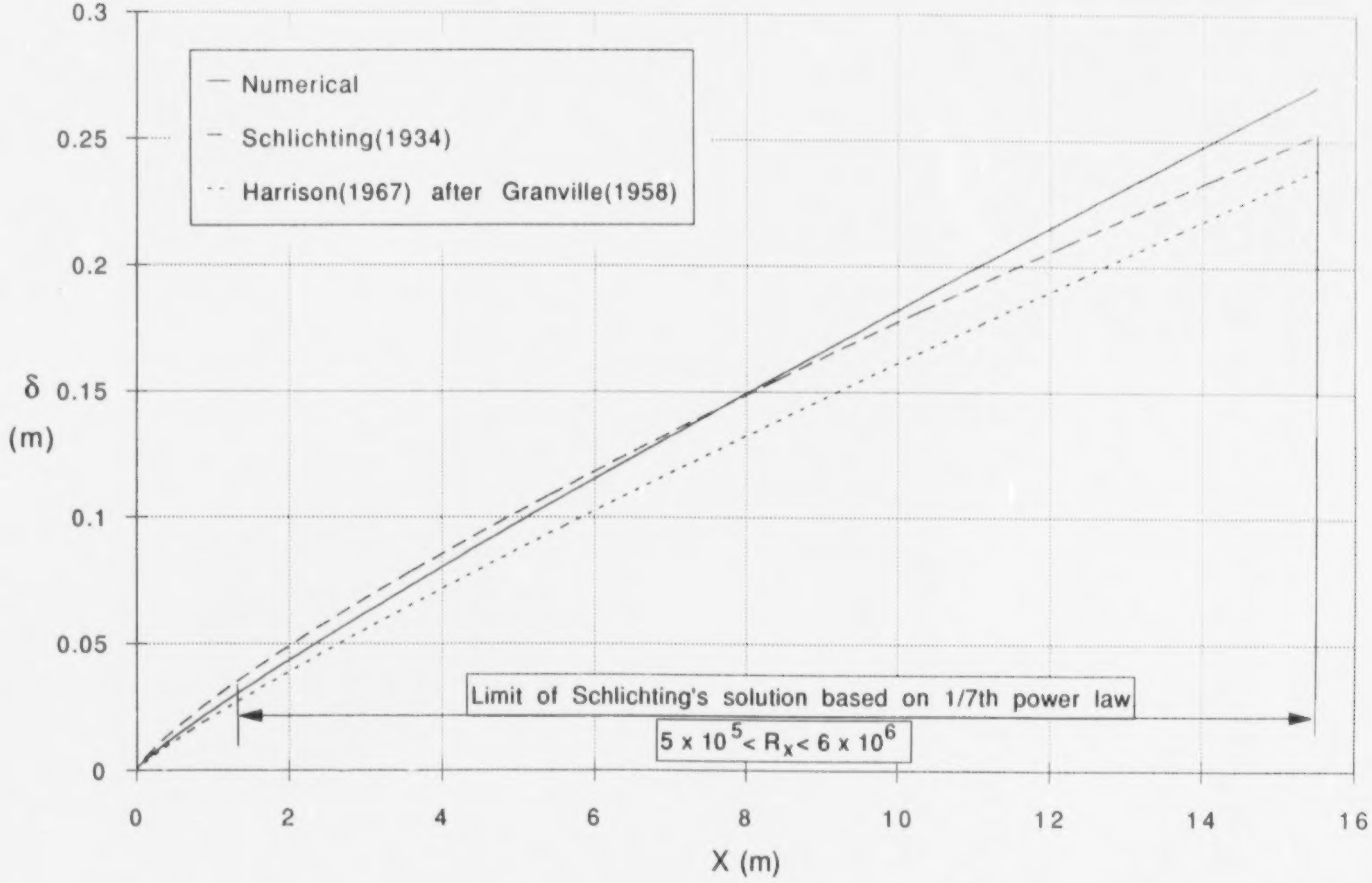

Fig. 3.5 Comparison of boundary layer thickness between numerical and *smooth* flat plate solutions.

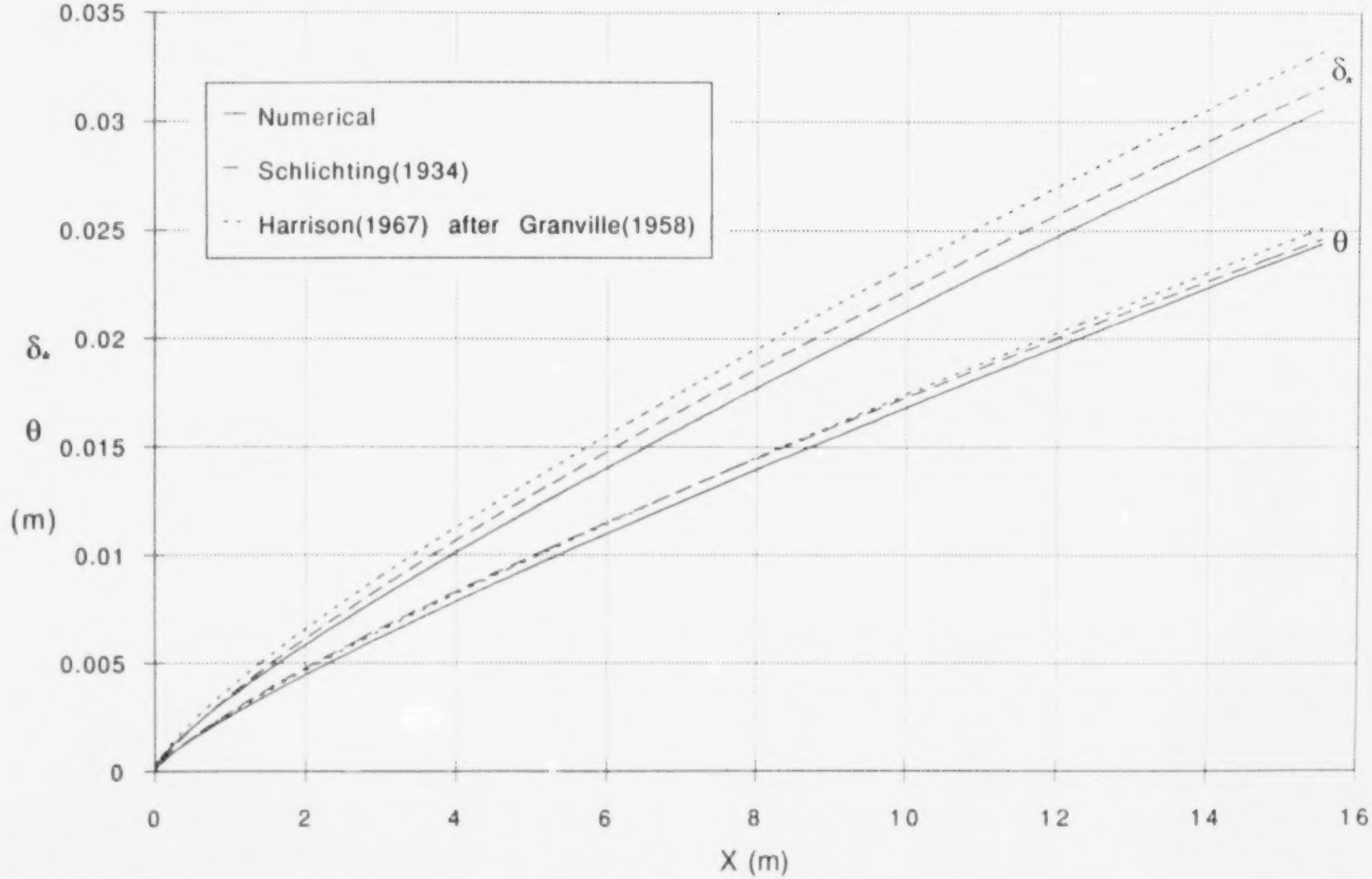

Fig. 3.6 Comparison of displacement and momentum thickness between numerical and *smooth* flat plate solutions.

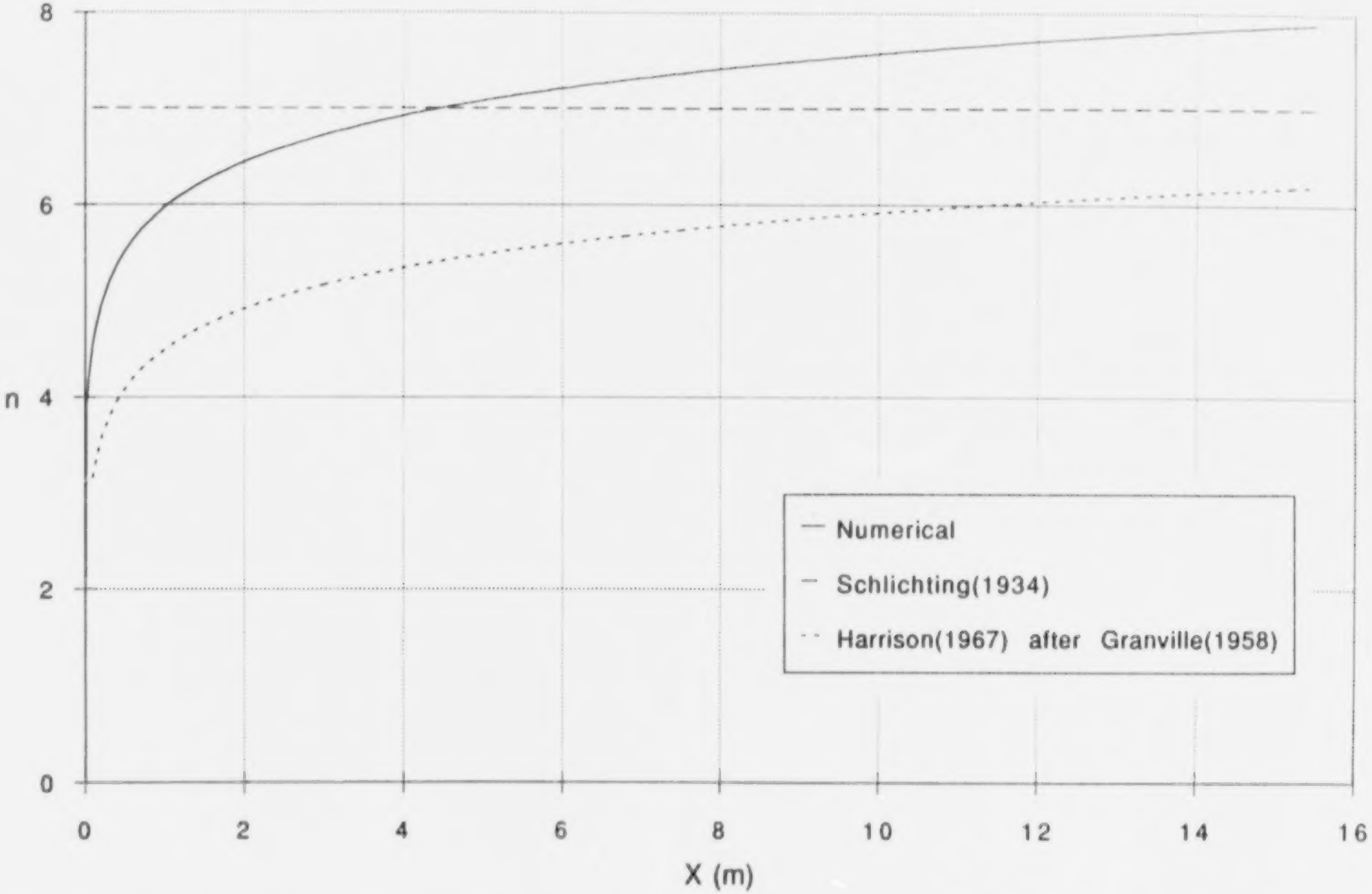

Fig. 3.7 Comparison of the power law exponent between numerical and *smooth* flat plate solutions.

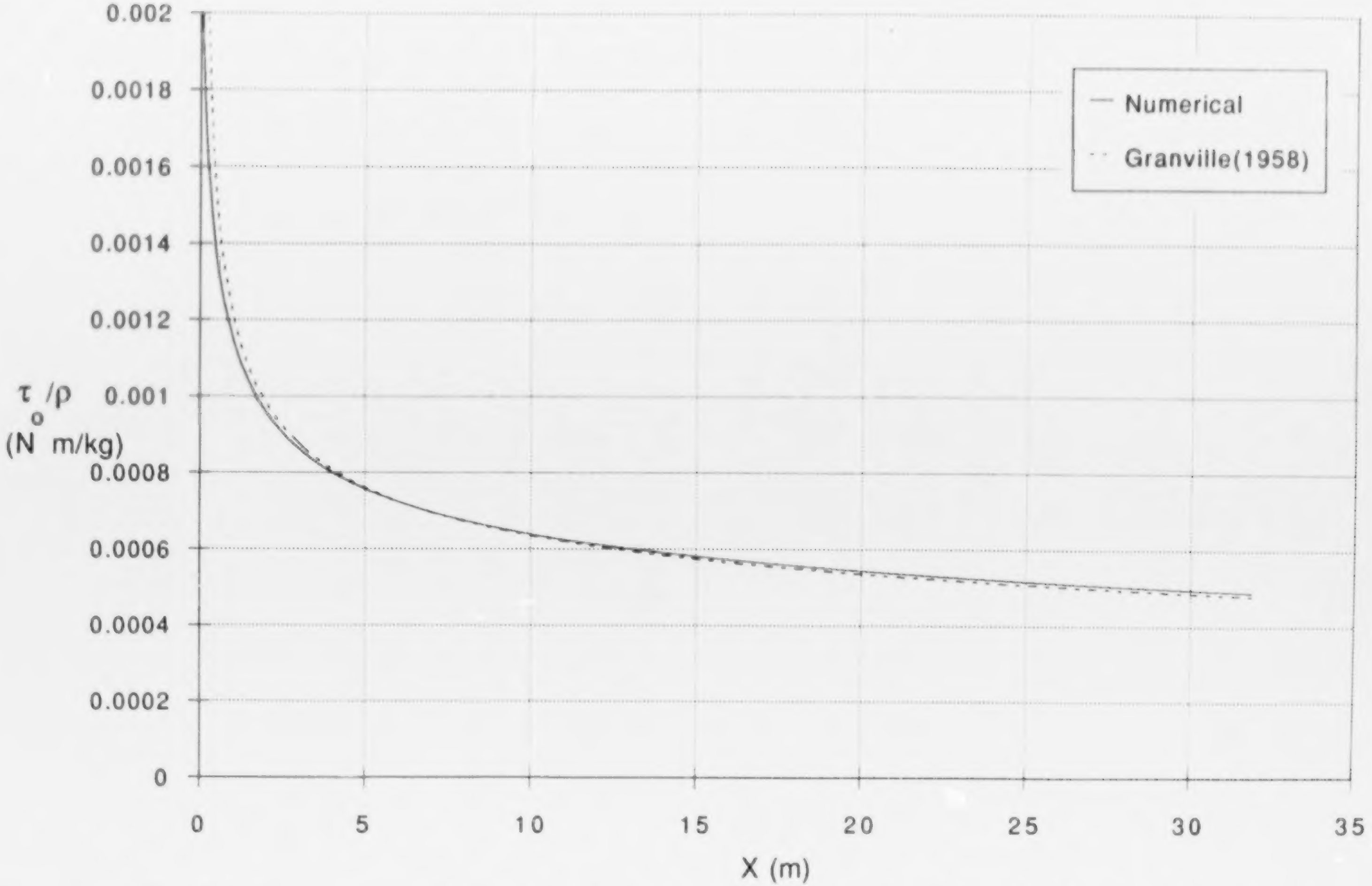

Fig. 3.8 Comparison of boundary shear between numerical and *rough* flat plate solution.

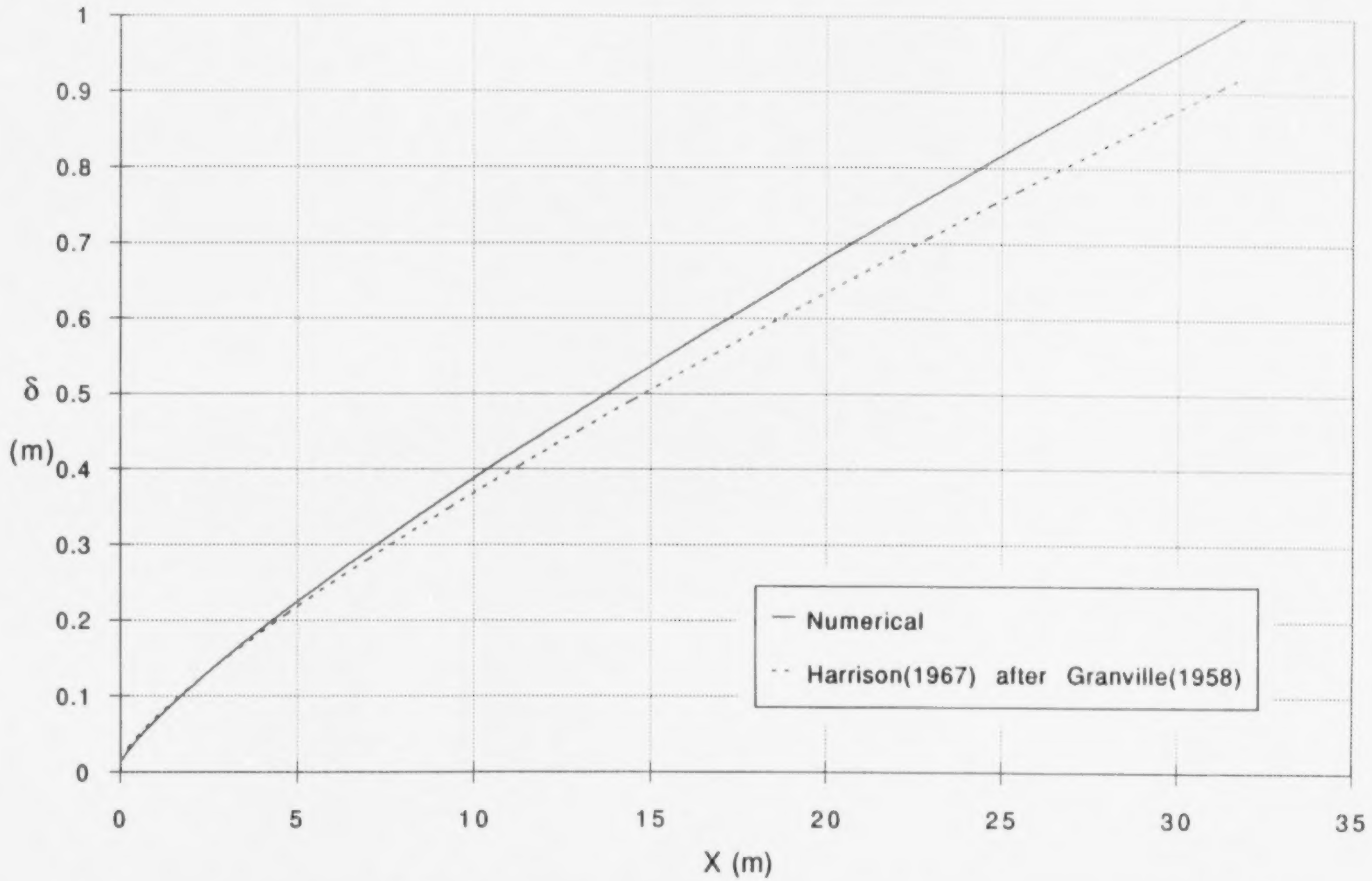

Fig. 3.9 Comparison of boundary layer thickness between numerical and *rough* flat plate solution.

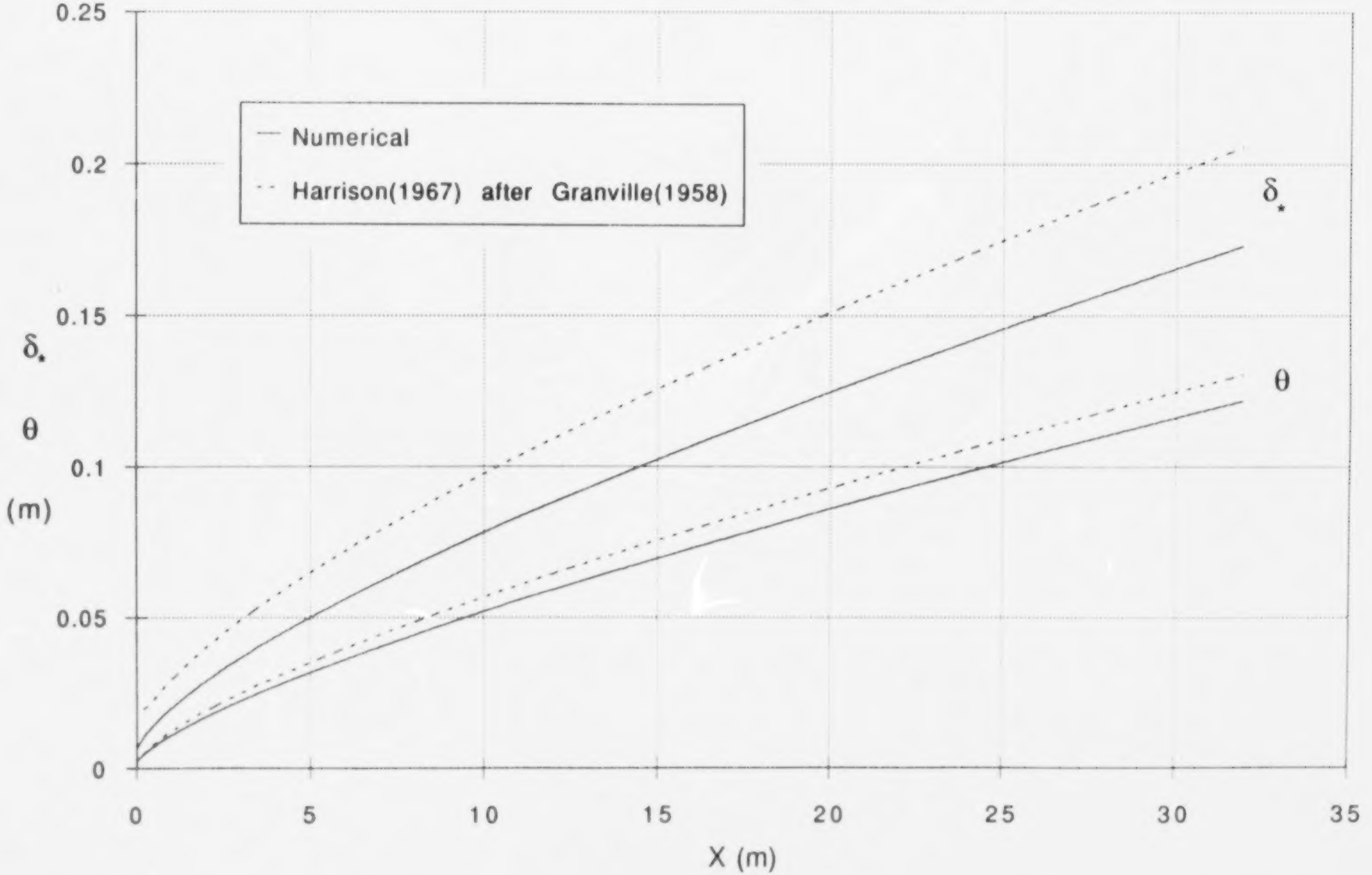

Fig. 3.10 Comparison of displacement and momentum thickness between numerical and *rough* flat plate solution.

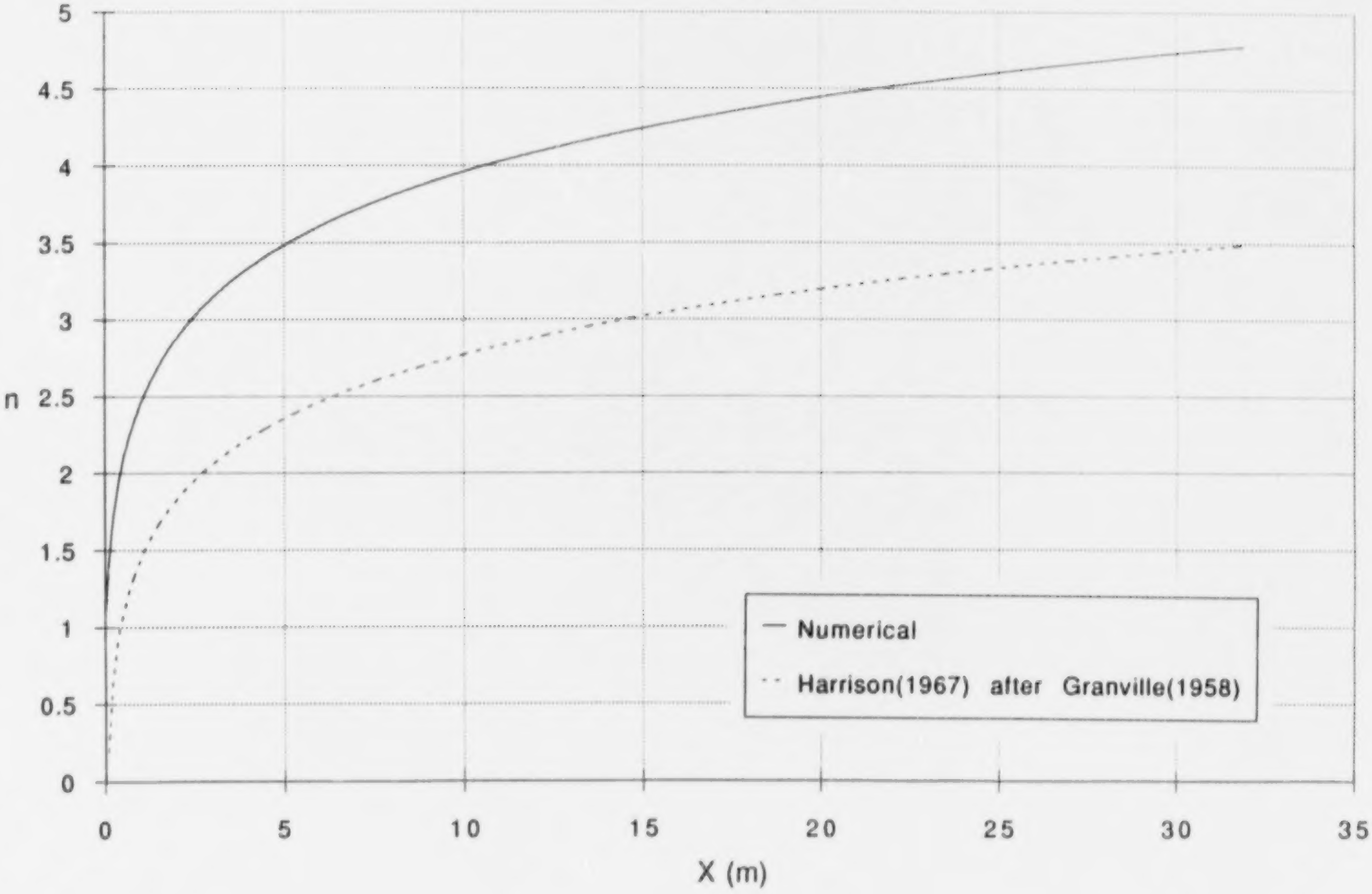

Fig. 3.11 Comparison of the power law exponent between numerical and *rough* flat plate solution.

4. Numerical solution and results for the mild channel

4.1 Solution technique

The subcritical case involved the solution of Equations 1.5, 1.13, 1.14, 3.8, 3.2, 3.4, 3.7, with downstream boundary conditions specified by Equations. 3.11, 3.12. The solution technique consisted of a simple step solution method. The descritized form of Equations 1.5, 1.13, 1.14, and 3.8 combined is:

$$\frac{\left(\dfrac{U_i^2\, n_i^2}{2\,(n_i+1)^2\,(2\,n_i+2)^2} + \dfrac{U_{i+1}^2\, n_{i+1}^2}{2\,(n_{i+1}+1)^2\,(2\,n_{i+1}+2)^2}\right)}{2} =$$

$$\frac{\left(U_{i+1}^2\,\theta_{i+1} - U_i^2\,\theta_i\right)}{\Delta x} + \frac{\left(U_{i+1}+U_i\right)}{2}\,\frac{\left(\delta_{*_{i+1}} + \delta_{*_i}\right)}{2}\,\frac{\left(U_{i+1}-U_i\right)}{\Delta x} \qquad (4.1)$$

The solution technique was as follows: First d and n were held constant and were given the values d_o and n_o for all x. The Bernoulli (Eqn. 3.4) and the equation for the power law exponent (Eqn. 3.7) were ignored for the time being. Now the Karman integral equation (Eqn. 4.1) and the continuity (Eqn. 3.2) could be solved for δ for all values of x until $\delta = d_o$ by iterating for δ moving downstream. Now all values of n_i could be calculated using Equation. 3.7. The constant in the Bernoulli equation (Eqn. 3.4) is evaluated at the node where $\delta = d_o$. Then the Bernoulli and continuity (Eqn. 3.2) could be solved for d for all x by the step method moving upstream. Now we could solve for $\delta(x)$ again moving downstream with new values of n and d. These iteration cycles continued until U(x), d(x), n(x), and $\delta(x)$ converged. Δx was chosen by decreasing its value for successive runs until no significant difference in the solutions was present.

4.2 Generalization of results

Equations 4.1,3.2,3.4, and 3.7 are in dimensional form. To obtain non-dimensional solutions, several possible non-dimensional parameters where tested.

Lets define L as the total length of channel for the flow to be fully developed, for the boundary layer to reach the surface, and non-dimensionalize it by the normal depth d_o:

$$\frac{L}{d_o} = \text{non-dimensional entrance length.}$$

The input variables for Equations 4.1,3.2,3.4, and 3.7 are q, S_o, and k_s, and the downstream boundary condition d_o and n_o can be calculated from these using Equations. 3.11 and 3.12. Preliminary runs of the numerical solution showed that n_o (the final shape of the velocity profile when the boundary layer hits the surface) was an important parameter. The parameter n_o will later be interchaged with the more familiar C_*. It is apparent from Equations 3.11 and 3.12 that n_o is a function of two parameters, the relative roughness k_s/d_o and the Reynolds number $\mathbf{R}_{po}$. These two parameters are a function of the input variables q, S_o, and k_s. It is possible that S_o is also an important parameter and should be tested.

Four sets of runs where performed to test the effect of n_o, $\mathbf{R}_{Po}$, S_o, and k_s/d_o on the entrance length:

Set 1

Test the effect of roughness induced n_o.

n_o; vary from 2 - 12 by varying k_s/d_o.

$\mathbf{R}_{Po}$; keep almost constant by keeping q constant.

S_o; keep constant.

Set 2

Test the effect of Reynolds number induced n_o.

n_o; vary from 6 - 13 by varying q.

$\mathbf{R}_{Po}$; allow to vary to be consistent with n_o

$k_s/d_o = 0$

S_o; keep constant.

Set 3

Test difference between roughness induced n_o and Reynolds number induced n_o for the same value of n_o.

n_o; keep constant.

$\mathbf{R}_{Po}$ and k_s/d_o; vary in such a way to keep n_o constant.

S_o; keep constant.

Set 4

Test the effect of slope.(or Froude number)

n_o; keep constant.

$\mathbf{R}_{Po}$; keep constant.

k_s/d_o; vary to keep n_o and $\mathbf{R}_{po}$ constant.

S_o; vary slope from small to near critical.

As the boundary layer grows n and $\mathbf{R}_p$ adjust to satisfy equation 3.7 and finally end up equal to n_o and $\mathbf{R}_{po}$ when the boundary layer is fully developed. Figure 4.1 is a modified Moody diagram showing the relation between n, $\mathbf{R}_p$, and k_s/δ. The line of solid symbols show a typical solution path for a particular solution of equations 4.1,3.2,3.4, and 3.7. Note that the upper right most point is ($\mathbf{R}_{po}$, n_o). For each set of runs the solution paths will be displayed in this way to help us make comparisons easily between different sets of runs. Also note that the initial value of n is equal to 1(the lower left most point). This is an arbitrary starting point and could be of some debate since it corresponds to a linear velocity profile. This is not of great concern as the boundary layer grows very rapidly near the beginning and n is often substantially greater than 1 at the next node. Also n equal to 1 suggests a relative roughness k_s/δ of about 2.3. Since the equivalent sand grain roughness is usually 2 to 3 times the size of roughness elements, this would suggest that the starting boundary layer thickness is somewhere near the top of the roughness elements; a reasonable assumption.

Set1

The input parameters q, S_o, k_S as well as some output values for the runs of set 1 are tabulated in Table 4.1. The output values consist of the normal depth d_o, the value of the fully developed power law exponent n_o, the dimensionless Chezy coefficient C_* of the fully developed flow (Equation 3.26), the value of the fully developed Reynolds number $\mathbf{R}_{p_o}$, the relative roughness of the fully developed flow k_s/d_o, the Froude number, the dimensionless entrance length L/d_o, and the ratio of the channel depth at the entrance to normal depth d_i/d_o.

Figure 4.2 shows the solution paths on the modified Moody diagram for the numerical solutions of set 1. Notice $\mathbf{R}_{p_o}$ is nearly constant and the relative roughness for the fully developed flow varies from about 0.74 for $n_o = 2$ to almost zero for $n_o = 12$. Figure 4.3 shows the dimensionless boundary layer growths. The entrance length varies between about 20 depths for $n_o = 2$ to almost a 100 depths for $n_o = 12$. Figure 4.4 shows the variation of relative depths within the entrance region. In all cases the depths varied little from that given by uniform flow; a variation less than 0.14% was found. With the exception of $n_o = 2$ the maximum depth occurred at the channel entrance, it then decreased to slightly below normal and than increased to normal depth as the boundary layer neared the surface. For $n_o = 2$ the depth at the channel entrance was less than normal depth, it then decreased slightly and then increased to normal depth as the boundary layer approached the surface. Notice also that the initial depth decreases with n_o. Figure 4.5 shows the bed shear relative to the fully developed shear and shows a similar trend as Figure 4.4, except the differences are more than a fraction of a percent. Still, the difference varies little from uniform flow, except near the entrance where the shear stress falls sharply. The bed shear stress will be discussed in more detail later. Figure 4.6 shows the variation of potential core velocity relative to the water surface velocity when the boundary layer reaches the surface.

Notice that the difference between the potential core velocity at the channel entrance and when the boundary layer reaches the surface is greater as n_0 decreases, or as the roughness of the channel increases. This stands to reason since, the surface velocity is higher than the average for a rough channel than for a smooth channel. Figure 4.7 shows the variation of the power law exponent within the entrance region. The power law exponent increases rapidly in the first five depths or so and then begins to level off.

Set 2

Table 4.2 shows the input and output parameters of the numerical runs of set 2. S_0 and k_s were held constant and q was varied to give different values of n_0 and $\mathbf{R}_{po}$. The runs for the smooth channel did not go below the value of $n_0 = 6$ corresponding to $\mathbf{R}_{po} = 15135$ since the flow may start to become laminar.

Figure 4.8 shows the solution paths on the modified Moody diagram for the numerical solutions of set 2. Notice all runs in set 2 overlap on the line where $k_s/\delta = 0$. The boundary layer growths shown in Figure 4.9 are almost identical to those of set 1, indicating that the value of the fully developed power law exponent is more important than what determines its value, namely, k_s/d_0 and $\mathbf{R}_{po}$. In other words, if we have two channels, one smooth, and another rough with a higher discharge(or $\mathbf{R}_{po}$) to give the same value of n_0 as the smooth channel, the dimensionless entrance length will be almost the same. The numerical solutions of set 3 investigate the differences more carefully. Figure 4.10, 4.11, 4.12, and 4.13 show the same variation in depths, bed shear, potential core velocity, and power law exponent respectively as set 2.

Set 3

As mentioned earlier, the purpose of the numerical runs of set 3 was to investigate more carefully the difference between roughness induced n_o and Reynolds number induced n_o. Table 4.3 summarizes the runs of set 3. In this set of runs n_o was held constant by varying $\mathbf{R}_{po}$ and k_s/d_o in the appropriate manner.

Figure 4.14 shows the solution paths on the modified Moody diagram. Notice n_o is always equal to 7 and $\mathbf{R}_{po}$ and k_s/d_o vary. Figure 4.15 shows almost identical boundary layer growths for all 8 runs in set 3. In addition, Figure 4.15, 4.16, 4.17, 4.18 and 4.19 show little variation in depths, bed shear, potential core velocity, and the power law exponent respectively between the runs of set 3.

Set 4

The numerical runs of set 4 were chosen to investigate the effect of the channel bed slope or Froude number. The power law exponent and $\mathbf{R}_{po}$ was kept constant by varying k_s/d_o. The slope was varied to give Froude numbers from 0.07 to 0.94 to investigate how the entrance length varied as the critical slope was approached. The runs are summarized in Table 4.4.

The modified Moody plot in Figure 4.20 shows that all runs in set 4 follow a similar solution path. Figure 4.21 shows that the boundary layer is not significantly affected by the slope until the Froude number is about 0.95; the entrance length in this case is only about 6% greater. The relative depth is significantly more affected for higher Froude numbers; for small Froude numbers the initial depth at the channel entrance is only a fraction of a percent greater than the normal depth, while for a Froude number of 0.95 it is 8% deeper(see Figure 4.22). The initial depth starts to increase significantly after about $\mathbf{F}_0 = 0.4$. Notice for $\mathbf{F}_0 = 0.95$, as the water surface approaches normal depth, it experiences some numerical instability. In fact, the numerical scheme for the mild channel which solves the boundary layer going downstream and the water surface going upstream does not work for Froude numbers greater than one. The instability for $\mathbf{F}_0 = 0.95$ is suspected to be an early sign of this condition. The relative shear stress shown in Figure 4.23 shows that the initial shear for the $\mathbf{F}_0 = 0.95$ is about 8 % lower; this is largely due to smaller potential core velocity near the channel entrance shown in Figure 4.24. Notice the dU/dx is larger for the higher $\mathbf{F}_0$ in Figure 4.24; this causes the boundary layer to develop more slowly. The power law exponent shown in Figure 4.25 shows little deviation between the runs of set 4.

Generalizations from set1, 2, 3 and 4.

The entrance length L/d_o as a function of the fully developed power law exponent is plotted in Figure 4.26 for both set 1 and set 2; there is little difference. Figure 4.27 shows a magnified portion of this diagram around $n_o = 7$ where the set 3 run results are also shown. Set 3 as expected shows a transition between the subtle difference between the entrance lengths of set 1 and set 2; the difference is about 1/2 a depth out of about 57.5 depths. The entrance length at $n_o = 7$ for the rough bed was only about 1/2 a depth shorter than the smooth; a 0.8% difference. This is probably due to the higher relative roughness near the channel entrance where the boundary layer is thin. This can be seen by a careful eye in Figure 4.15 where the boundary layers deviate slightly at the channel entrance and than become parallel further downstream. In other words, their initial growth rates are different but further downstream they are the same.

Figure 4.28 shows the same magnified portion as Figure 4.27 except set 4 rather than set 3 is plotted with set 1 and 2. Set 4 shows a greater variation in the entrance length than set 3 for the same value of n_o; a 3.5 depth difference was found, about a 6% longer entrance length for a Froude number close to 1 than a more subcritical flow.

As there seems little difference between entrance lengths for roughness induced n_o and Reynolds induced n_o for the same value of n_o, Figure 4.29a was constructed from set 1 and set 2 as a single curve to describe the entrance lengths in general as a function of the fully developed power law exponent n_o. Since it is not often customary to describe fully developed open channel flow with the power law velocity profile, Figure 4.29a was converted to Figure 4.29b by Equation 3.26. Figure 4.29b shows the entrance length as a function of the fully developed dimensionless Chezy coefficient C_*. Also shown in Figure 4.29b is Yalin's(1972) solution for the entrance length. Since Yalin's solution does not include the presence of a pressure gradient or an accelerating potential core, his entrance lengths are about 15-25 depths shorter. This error translates to about a 50% shorter entrance lengths for very rough channels, about a 30% shorter entrance lengths for typical laboratory flows in smooth flumes, and about a 25% shorter entrance lengths for high discharge flows in very smooth channels.

It is often more of an interest to know the variation of bed shear stress within the entrance region rather than the thickness of the boundary layer. This is often the case where sediment transport studies are conducted in laboratory flumes. Figure 4.29c shows this variation. Plotted in Figure 4.29c is τ_o/τ_{end} as a function of C_* and x/d_o. τ_o is the shear stress in the entrance region and τ_{end} is the fully developed shear stress when the boundary layer reaches the surface. It was demonstrated in Section 3.5 that the shear stress was more accurately predicted than the thickness of the boundary layer. Hence, greater confidence can be placed on the variation of shear stress within the entrance region than the entrance length. Figure 4.29c shows that the shear stress takes less depths to reach the fully developed shear than for the boundary layer to reach the surface. Take the example of a smooth laboratory channel with a C_* say of about 20; the boundary layer takes about 54 depths to reach the surface, while the shear stress is within 2% of the fully developed value in about 21 depths, and is equal to fully developed in about 30 depths.

4.3 Comparisons with experiments in a mild channel

Before the entrance length in the experiments could be compared to the the numerical solution, C_* for each experiment had to be calculated. This was done in two ways for each experiment. The first method consisted of taking the width averaged τ_o/ρ obtained from the velocity profiles in the fully developed portion of the channel and converting it to u_*; the width averaged depth averaged velocity V was obtained from the integration of the velocity profiles, and finally C_* was computed from $C_* = V/u_*$. The second method consisted of taking the curve fitted width averaged power law exponent in the fully developed region and converting it to C_* using Equation 3.26. For the smooth experiment, C_* had a value of 22.64 and 21.50 for the first and second method respectively. For the rough experiment, it had a value of 8.26 and 10.32. The larger variation of C_* in the rough experiment is probably the result of the difficulty encountered in the determination the shear stress and roughness to satisfy all applicable flow and resistance relations. Nevertheless, this variation was taken into account when comparing with the numerical solution. Figure 4.30 shows the comparison of the numerical solution for the entrance length compared with the two experiments of chapter 2. Note the box plotted around each experimental point in Figure 4.30. The height of the box is determined from the difference in C_* obtained between method 1 and method 2, and the width of the box is determined from the average entrance length range given in Table 2.2. The range was given since the exact entrance length could not be given due to complications of secondary flows and the difficulty in defining the boundary layer thickness.

The numerical solution showed better agreement with experiments than the zero pressure gradient theories. For the smooth channel, the numerical solution overpredicted the entrance length by 2%, and the Schlichting's smooth flat plate solution under predicted the entrance length by 15%. For the rough channel, the numerical solution under predicted the entrance length by 9%, and the Harrison's rough flat plate solution under predicted the entrance length by 40%.

Also plotted in Figure 4.30 is the effect of secondary flows on the range for the boundary layer to reach the surface. It is apparent from this that width averaged values are needed when comparing the entrance length with theory. Overall, the two points plot quite well near the experimental curve and obviously more width averaged experimental entrance lengths are needed to establish if the numerical solution is adequate.

4.4 Comparison to pipe flow entrance lengths and other channel cross sections

The numerical solution in this thesis is for wide channels. Hence, it would be desirable to investigate further the development length for other channel cross sections. As a first step one might compare to the entrance lengths for pipes since a pipe and a wide mild channel are the two extremes of all prismatic channels. In this way, one could at least get an initial idea how the entrance length varies for other channel cross sections.

Ward-Smith(1980) shows that the relationship between the entrance length and the friction factor to be:

$$\frac{L}{D} = \frac{2.44}{\sqrt{f}} \tag{4.2}$$

where D is the pipe diameter. In terms of C* this relation is:

$$\frac{L}{D} = \frac{2.44}{\sqrt{8}} C_* \tag{4.3}$$

Since the boundary layer stops growing when it reaches the channel centreline, let us use the pipe radius r as a length scale to replace the diameter:

$$\frac{L}{r} = \frac{4.88}{\sqrt{8}} C_* \tag{4.4}$$

Plotting 4.4 along with the relation for wide channels in Figure 4.31a, we see that the entrance length is shorter for a pipe than for a wide channel. This is probably due to the boundary layer growing from all sides of the pipe and having a combined effect on the small potential core in the centre. It is difficult to make predictions about other channel cross sections from these two curves since it is unclear what length scale to use for the boundary layer to reach d_0 or r in a more complicated cross section. One length scale which immediately comes to mind when thinking about this is the hydraulic radius R. Replacing D with R in Equation 4.2 we obtain:

$$\frac{L}{R} = \frac{9.76}{\sqrt{8}} C_* \qquad (4.5)$$

Figure 4.31b shows equation 4.5 plotted along with the relation for a wide channel. Now both sets of entrance lengths have the same length scale. Although the two relations are closer than in Figure 4.31a, the pipe entrance length is slightly longer. This could be due to the higher difference between the average and maximum velocity in a pipe than in a wide channel for the same profile. This could increase the dU/dx in the pipe and slow the boundary layer growth. Nevertheless, one could use Figure 4.31b to estimate the entrance lengths of other cross sections for subcritical flows.

4.5 Sensitivity to inaccurate bed slope and tailgate matching

Often in the laboratory, the depth and discharge are set to give the desired values of depth and velocity in a particular area of the flume using the tailgate and discharge setting. The flume bed slope is approximately adjusted to give a uniform depth in the area of study; sometimes it is not adjusted at all. When care is exercised in trying to match the bed slope with the water surface and the slope of the energy line, some difficulties can arise. Often for subcritical flows the slope can be very small, in fact, imperfections in the flume construction or deflections under load can be of the same order as the slope itself. In these cases and in cases where the adjustment of the bed slope is simply neglected, it would be desirable to test the effect of inaccurate bed slope and tailgate matching on the boundary layer growth and entrance length.

The two numerical solutions used to simulate the boundary layer growth of the smooth and rough experiments of Chapter 2 were tested. In addition to the original simulations, two different conditions were simulated for each of the smooth and rough channels. In one case, the bed slope was doubled and the downstream depth or boundary condition was fixed at the same value. In the other case, the bed slope was made horizontal and the downstream boundary condition was again fixed at the same depth. The notation for the simulations is as follows: $0\ S_0$ is the horizontal channel case; $1\ S_0$ is the original numerical solution where the channel bed slope is consistent with the fully developed bed shear; $2\ S_0$ is the case where the bed slope is doubled. As a matter of interest, $0\ S_0$ is the case of a boundary layer growing in an H1 backwater curve and $2\ S_0$ is the case of a boundary layer growing in M2 backwater curve. The simulations are summarized in Table 4.5.

First lets look at the smooth channel simulations; the effect on the boundary layer growth in Figure 4.32 is minimal. The horizontal channel has an entrance length which is about 3.2% longer and the double slope channel has an entrance length which is about 3.0% shorter. Figure 4.33 shows the effect on the channel bed shear. Near the channel entrance, the channel bed shear is 2.3-3.5% lower for 0 S_0 and 2.2-3.6% higher for 2 S_0. The bed shear for all three cases when the boundary layer reaches the surface is identical, as it should be since this is part of the boundary condition. As expected, the depths in Figure 4.34 are slightly deeper for 0 S_0 and slightly shallower for 2 S_0 as we get nearer to the channel entrance. Figure 4.35 shows the water surface elevation and shows that the slope of the water surface is relatively maintained even if the bed slope is varied. The total drop in elevation within the entrance region however, is greatest for the 0 S_0 case and the lowest for the 2 S_0 case. This also shows in the potential core velocities of Figure 4.36, where the largest increase in potential core velocity is for the 0 S_0 case and the lowest for the 2 S_0 case.

The results for the rough channel case are similar to the smooth channel case except the differences are larger. The differences are larger since the channel bed slope is larger and doubling or reducing the bed slope to zero is a bigger change than it was for the smooth channel. The differences in the entrance length is about 7.2% shorter for the 2 S_0 case and 8.4% longer for the 0 S_0 case(Figure 4.37). The difference in shear stress near the channel entrance was about 5.7-7.3% smaller for the 0 S_0 case and about 4.9-7.0% larger for the 2 S_0 case(Figure 4.38). Figure 4.39 shows the variation of depth. It is likely that such a high variation in depth (4 mm in 3 m) would be detected and a closer bed slope and tailgate matching would be obtained. The water surface elevation is shown in

Figure 4.40 and shows again that the water surface slope is maintained for all three cases. The potential core velocities in Figure 4.41 showed a similar behavior as the smooth solutions.

In summary, one can conclude that the effect of inaccurate bed slope and tailgate matching has little effect on the developing boundary layer and entrance length if some care and effort is made in slope adjustment and tailgate settings. This throws some confidence on the experiments of Chapter 2 where there was some difficulty in obtaining a constant depth in the fully developed portion of the channel due to bed undulations, but a sincere effort was made. However, the effect on the boundary layer can be large if the channel bed slope and tailgate position is grossly mismatched.

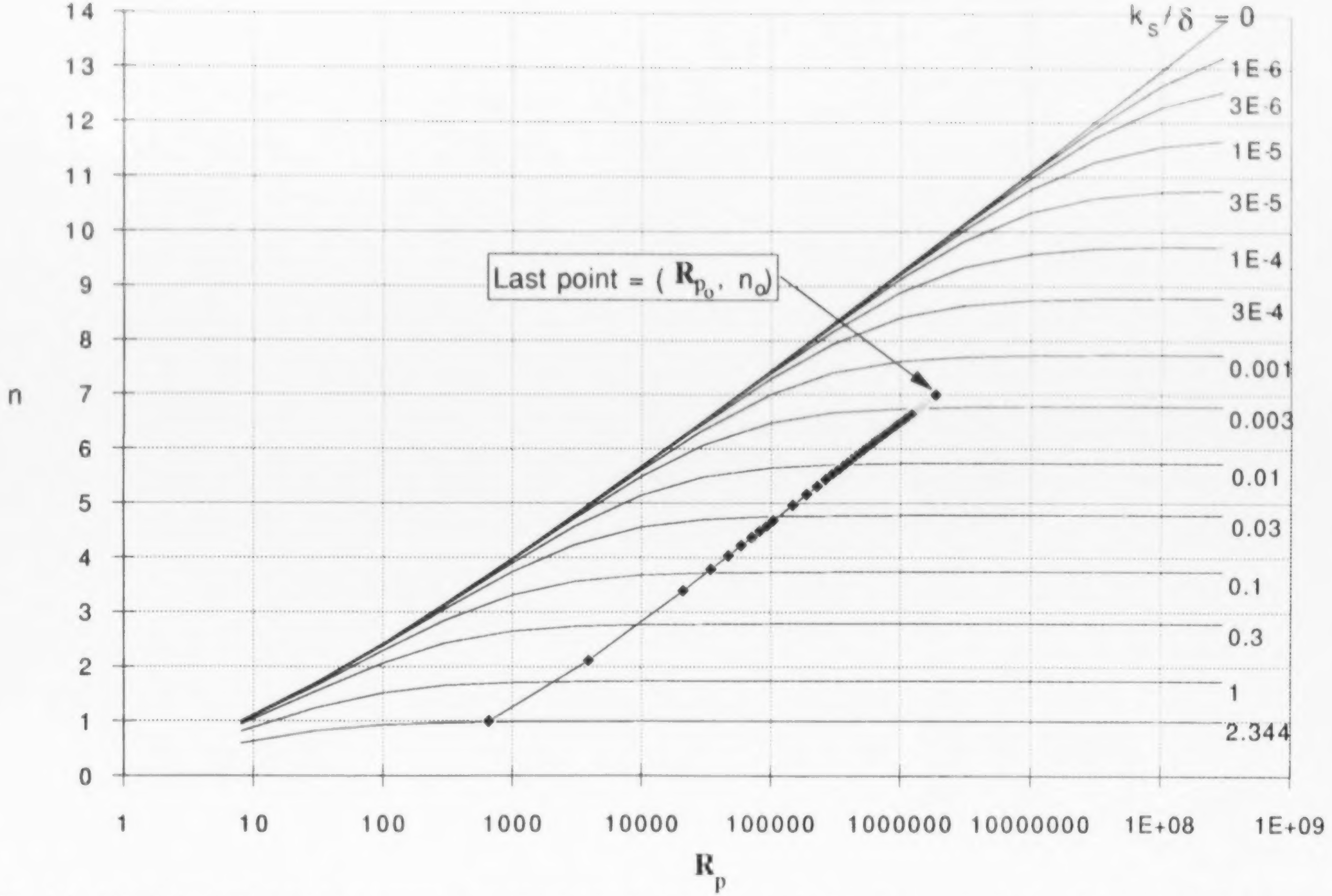

Fig. 4.1 Modified Moody Diagram showing typical solution path for the numerical solution of a boundary layer in a open channel.

q (m^2/sec)	So	ks (m)	do (m)	no	C*	Ro	ks/do	Fo	X/do	di/do
15.7660037	0.0001	12.7348231	17.179	2	7.07106781	25225606	0.74130876	0.0707	21.316	0.999869
15.7660037	0.0001	3.21789041	13.727	3	9.89949494	27027435	0.23442081	0.0990	28.835	1.000397
15.7660037	0.0001	0.86059037	11.609	4	12.7279221	28028451	0.07412836	0.1273	35.6199	1.000738
15.7660037	0.0001	0.23804089	10.156	5	15.5563492	28665461	0.02343903	0.1556	42.6408	1.000953
15.7660037	0.0001	0.06731611	9.085	6	18.3847763	29106468	0.00740925	0.1838	49.9131	1.001075
15.7660037	0.0001	0.0193236	8.259	7	21.2132034	29429874	0.00233978	0.2121	57.3984	1.001144
15.7660037	0.0001	0.00559386	7.598	8	24.0416306	29677183	0.00073627	0.2404	65.0135	1.001195
15.7660037	0.0001	0.00161401	7.055	9	26.8700577	29872428	0.00022879	0.2687	72.718	1.001245
15.7660037	0.0001	0.00044812	6.599	10	29.6984848	30030483	6.7904E-05	0.2970	80.4963	1.001287
15.7660037	0.0001	0.00010324	6.211	11	32.5269119	30161051	1.6622E-05	0.3253	88.3679	1.00133
15.7660037	0.0001	2.6823E-14	5.875	12	35.3553391	30270727	4.5656E-15	0.3536	96.4224	1.001346

Table 4.1 Summary of Set 1 numerical runs. Test the effect of roughness induced n_o.

n_o; vary from 2 - 12 by varying k_s/d_o.
$\mathbf{R}_{po}$; keep almost constant by keeping q constant.
S_o; keep constant.

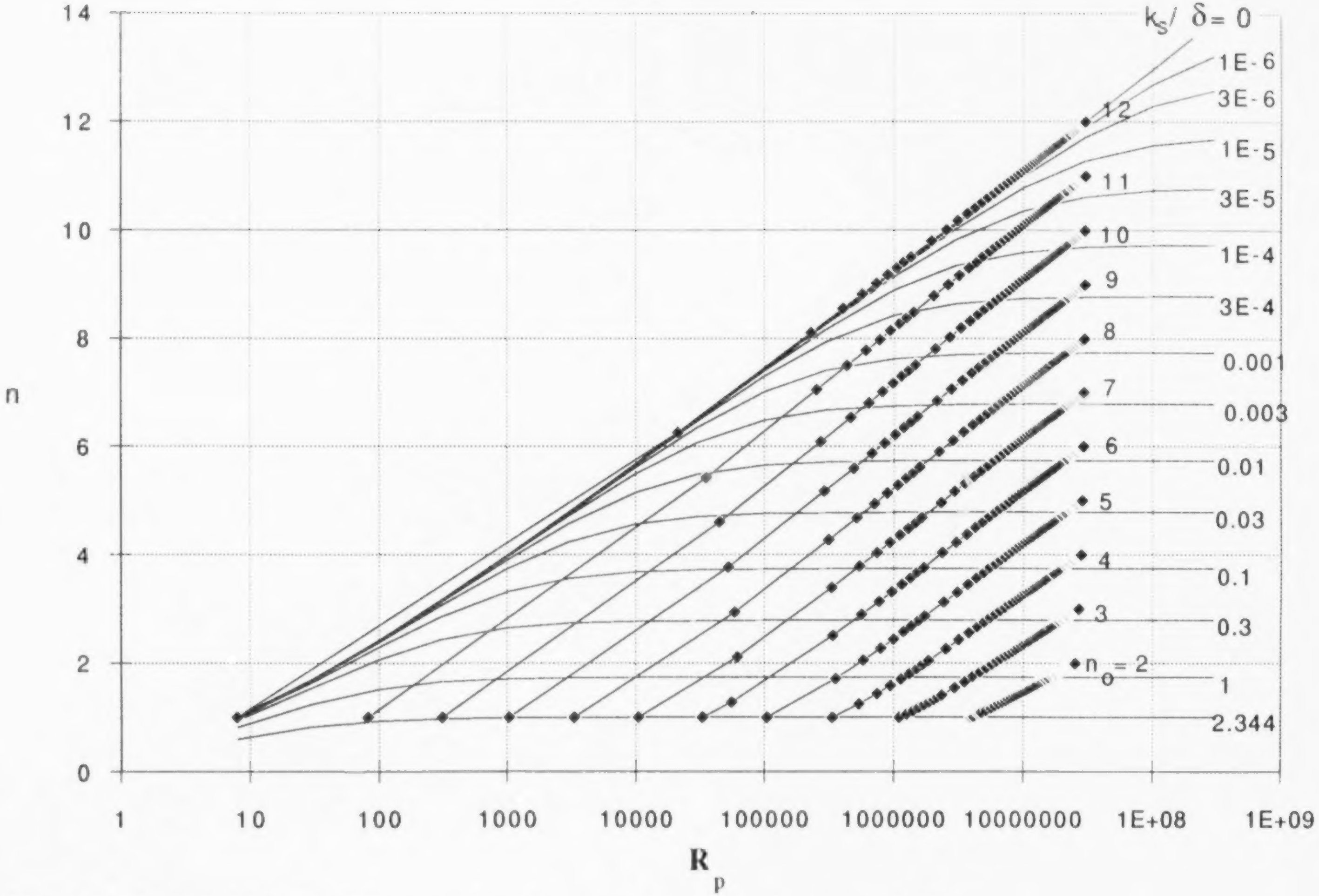

Fig. 4.2 Modified Moody Diagram showing numerical solution paths in Set 1.

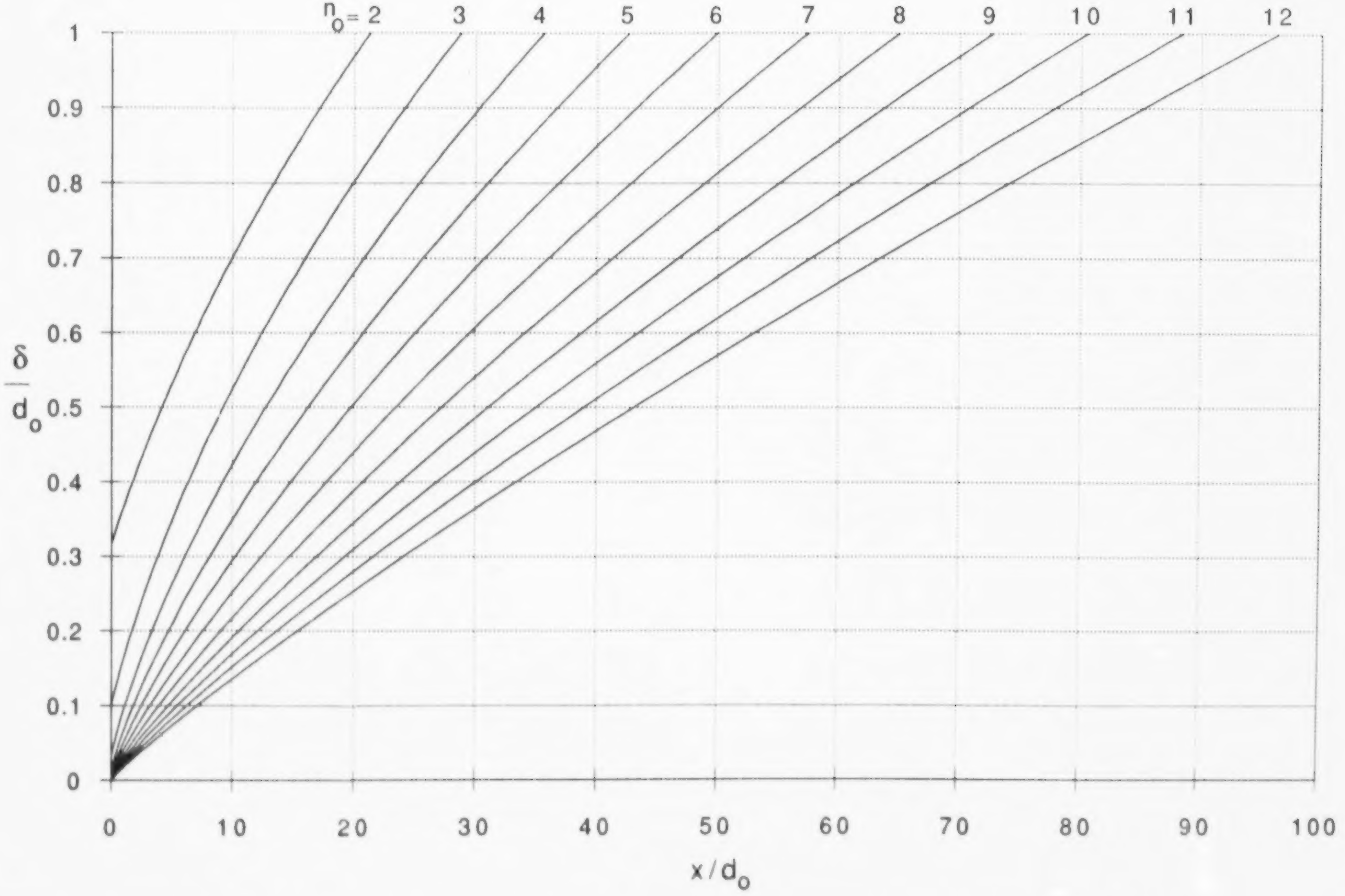

Fig. 4.3 Dimensionless boundary layer thicknesses for numerical solutions of Set 1.

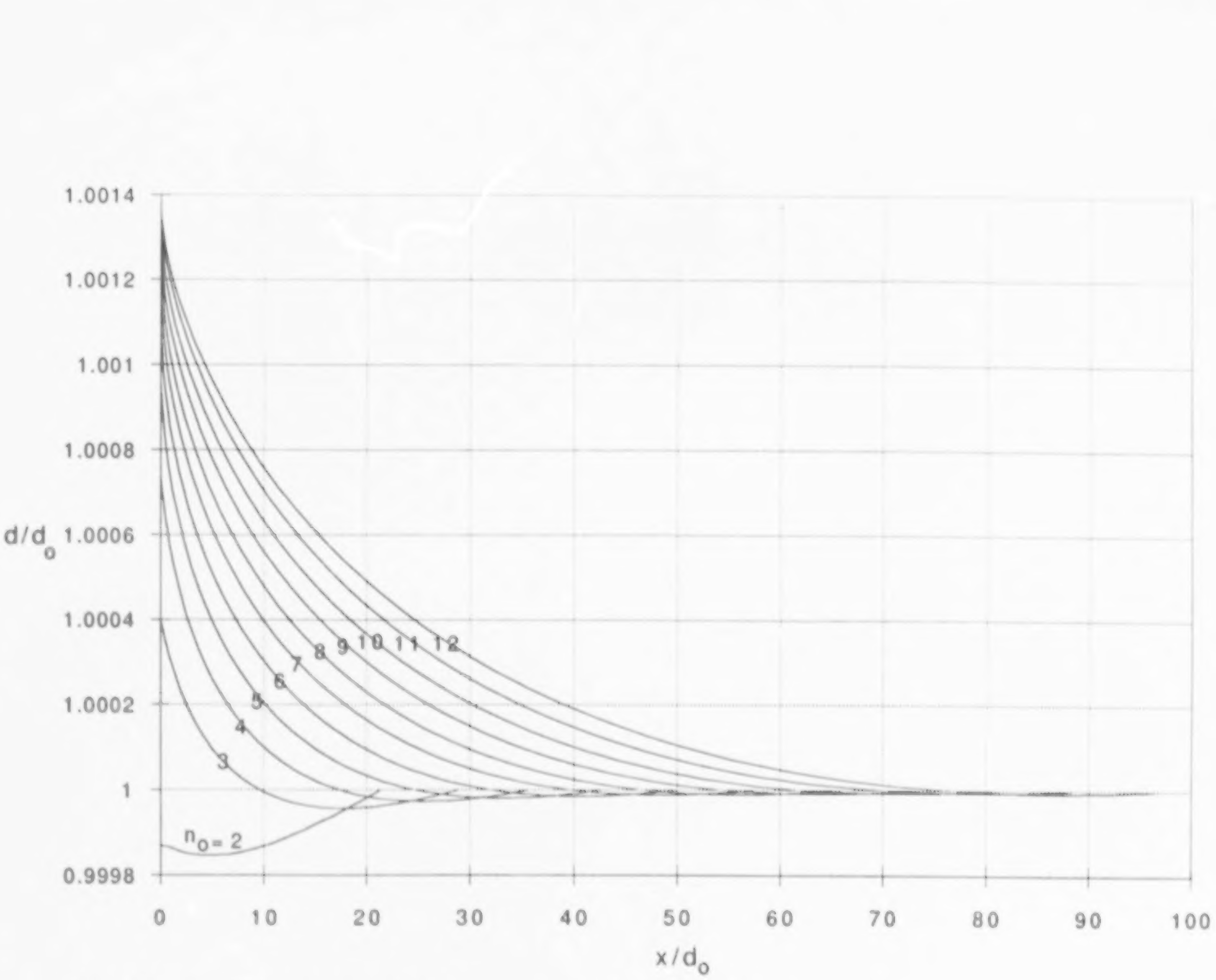

Fig. 4.4 Dimensionless depths for numerical solutions of Set 1.

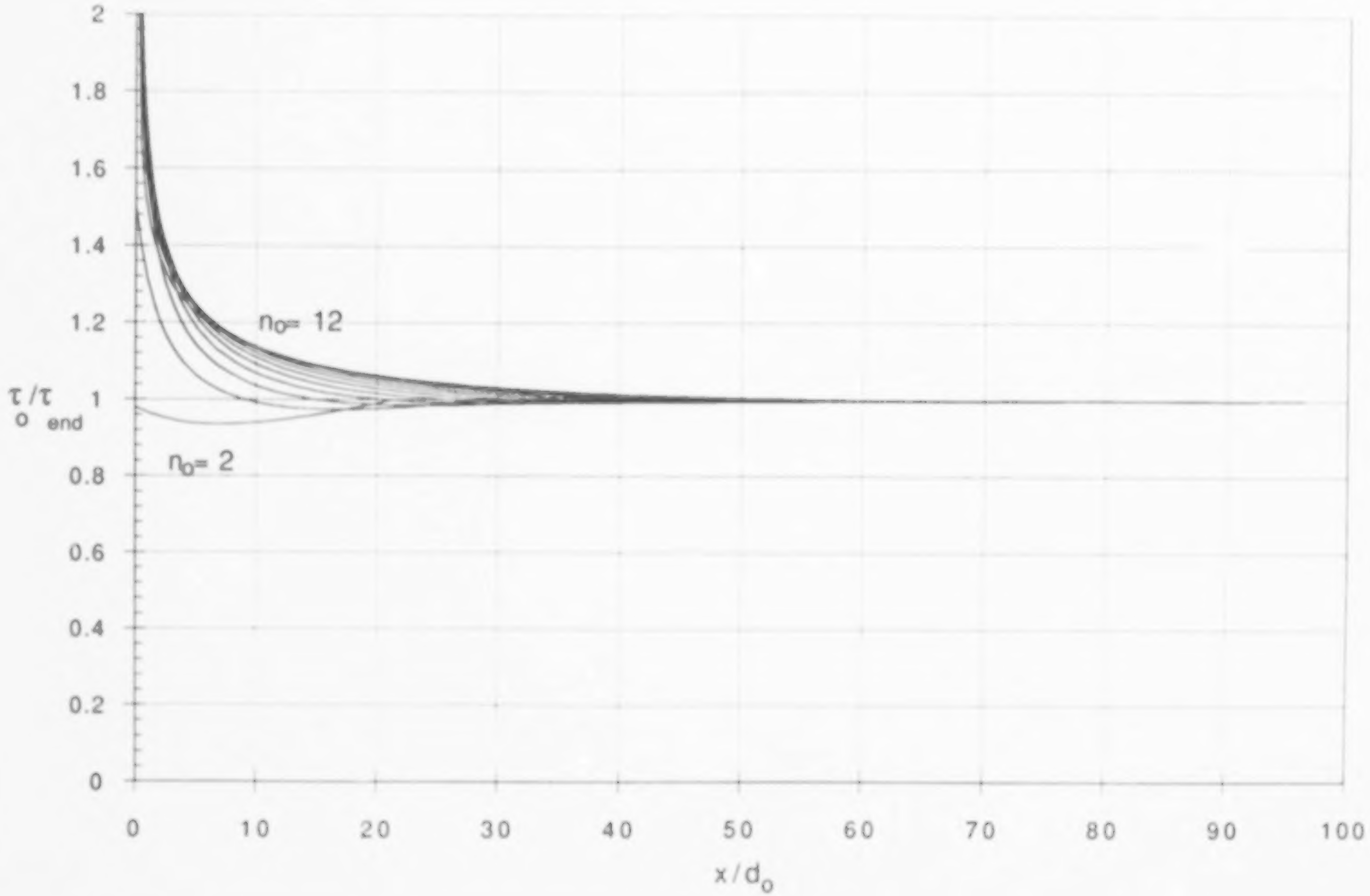

Fig. 4.5 Relative bed shear stresses for numerical solutions Set 1.

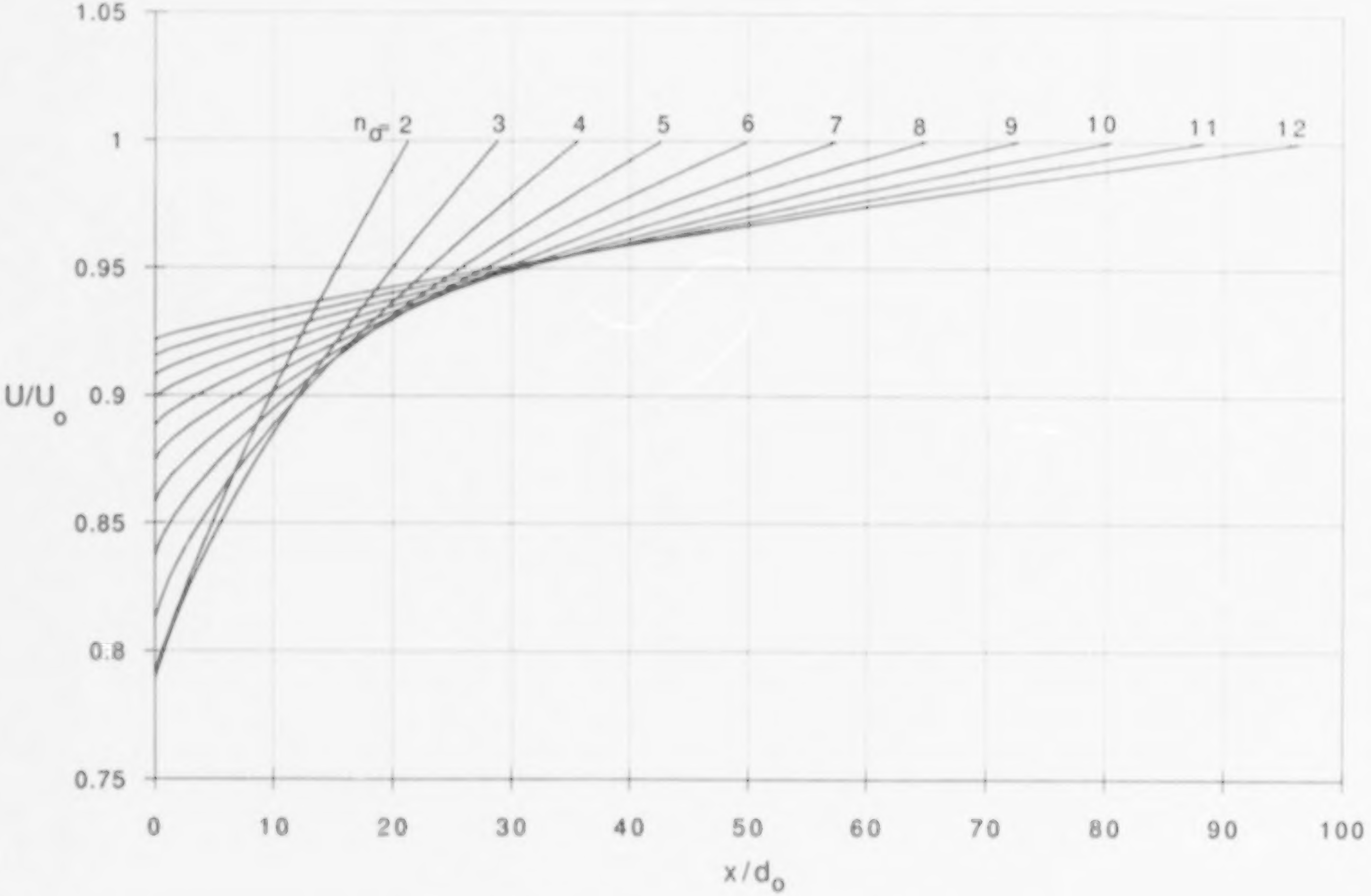

Fig. 4.6 Relative potential core velocities for numerical solutions Set 1.

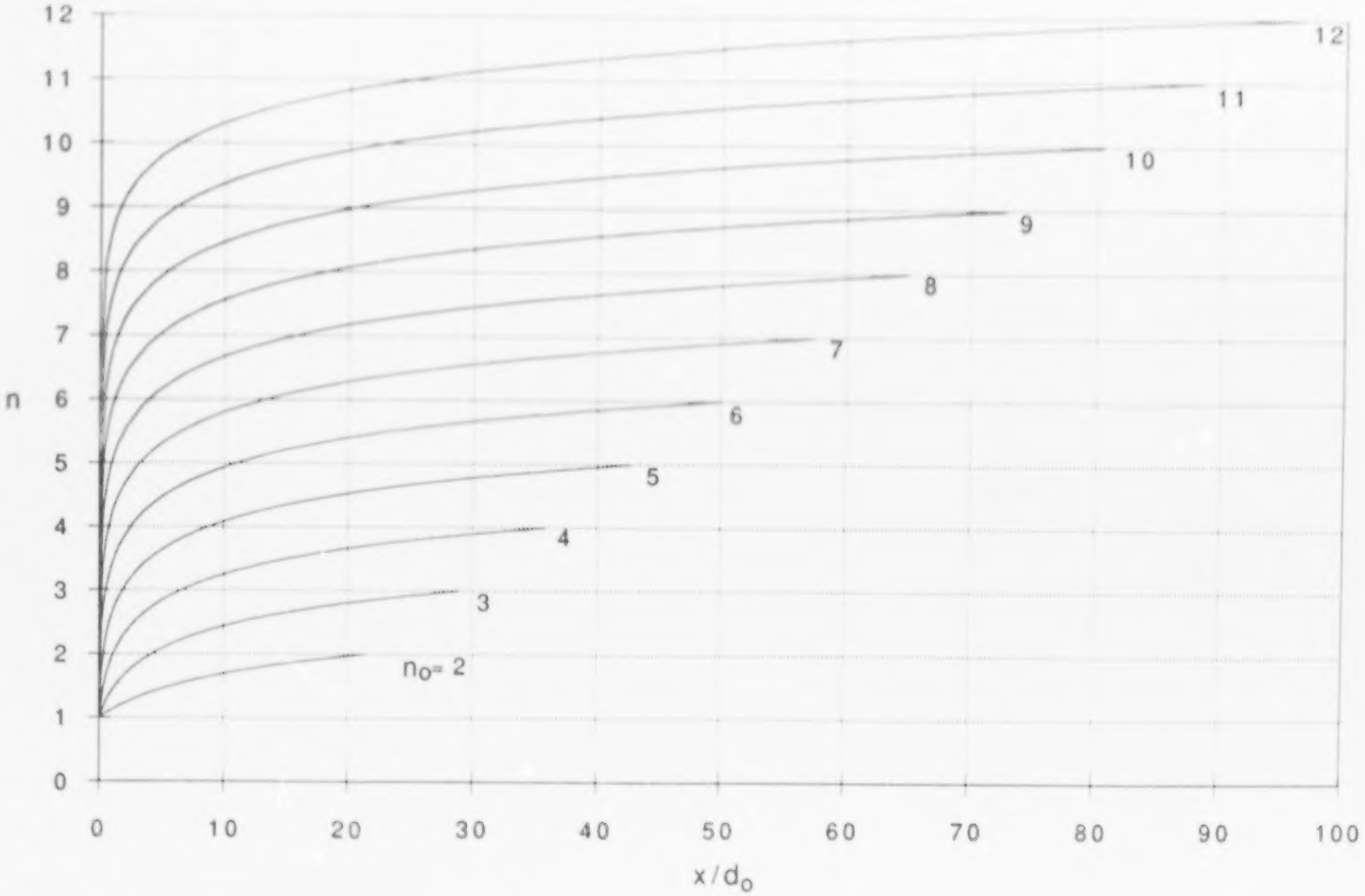

Fig. 4.7 Power law exponent for numerical solutions Set 1.

q (m^2/sec)	So	ks (m)	do (m)	no	C*	Ro	ks/do	Fo	X/do	di/do
0.00819832	0.0001	0	0.059	6	18.3847763	15135	0	0.1838	50.3878	1.001065
0.02991389	0.0001	0	0.127	7	21.2132034	55839	0	0.2121	57.8418	1.001079
0.10720883	0.0001	0	0.273	8	24.0416306	201805	0	0.2404	65.4281	1.001163
0.37890926	0.0001	0	0.588	9	26.8700577	717933	0	0.2687	73.0985	1.001217
1.32434431	0.0001	0	1.266	10	29.6984848	2522561	0	0.2970	80.8245	1.0012
4.58679628	0.0001	0	2.727	11	32.5269119	8774741	0	0.3253	88.609	1.001293
15.7660037	0.0001	0	5.875	12	35.3553391	30270727	0	0.3536	96.4224	1.001346
53.8449998	0.0001	0	12.657	13	38.1837662	103701481	0	0.3818	104.268	1.001412

Table 4.2 Summary of Set 2 numerical runs. Test the effect of Reynolds number induced n_o.

n_o; vary from 6 - 13 by varying q.
$\mathbf{R}_{po}$; allow to vary to be consistent with n_o
$k_s/d_o = 0$
S_o; keep constant.

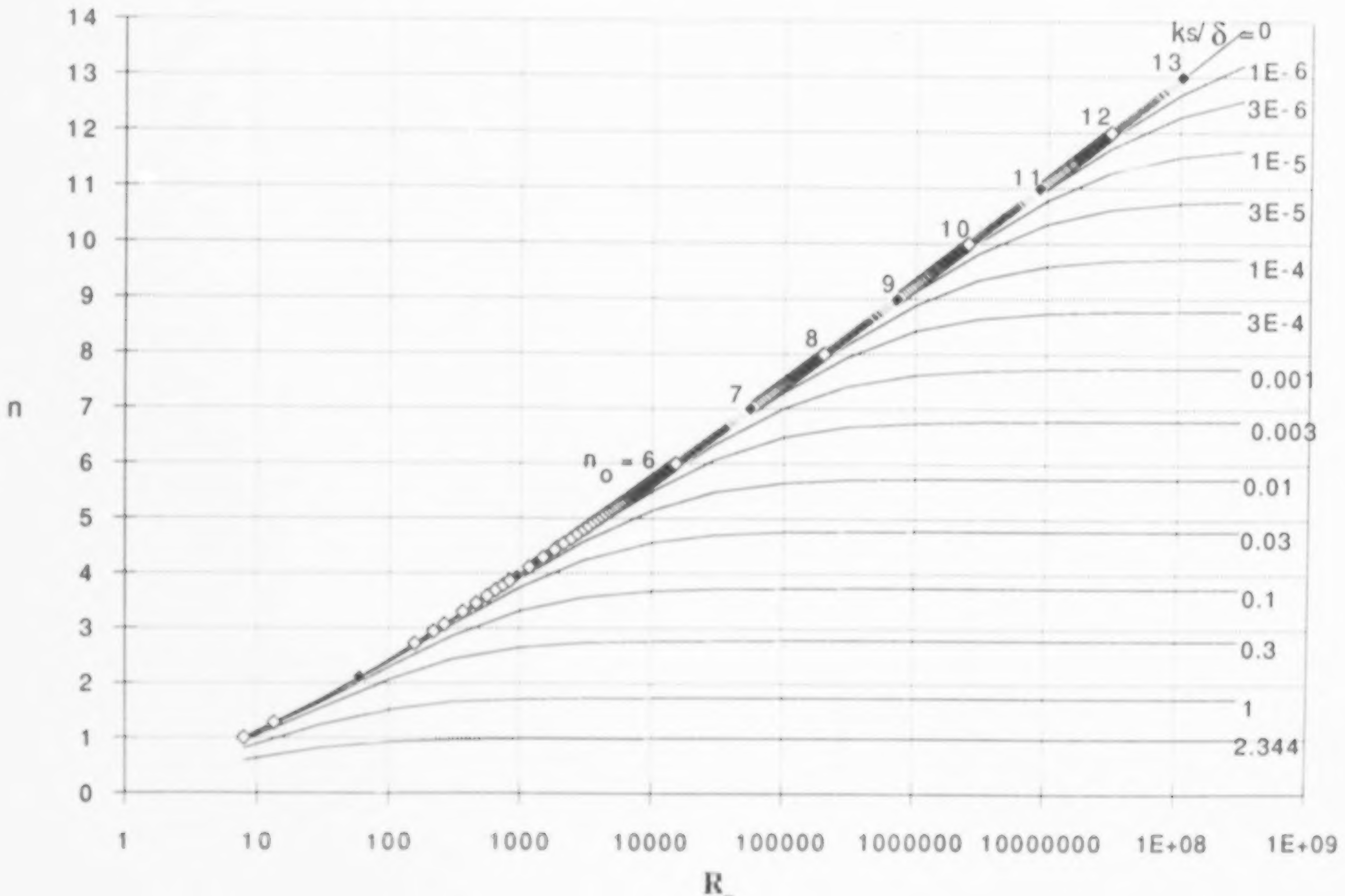

Fig. 4.8 Modified Moody Diagram showing numerical solution paths in Set 2.

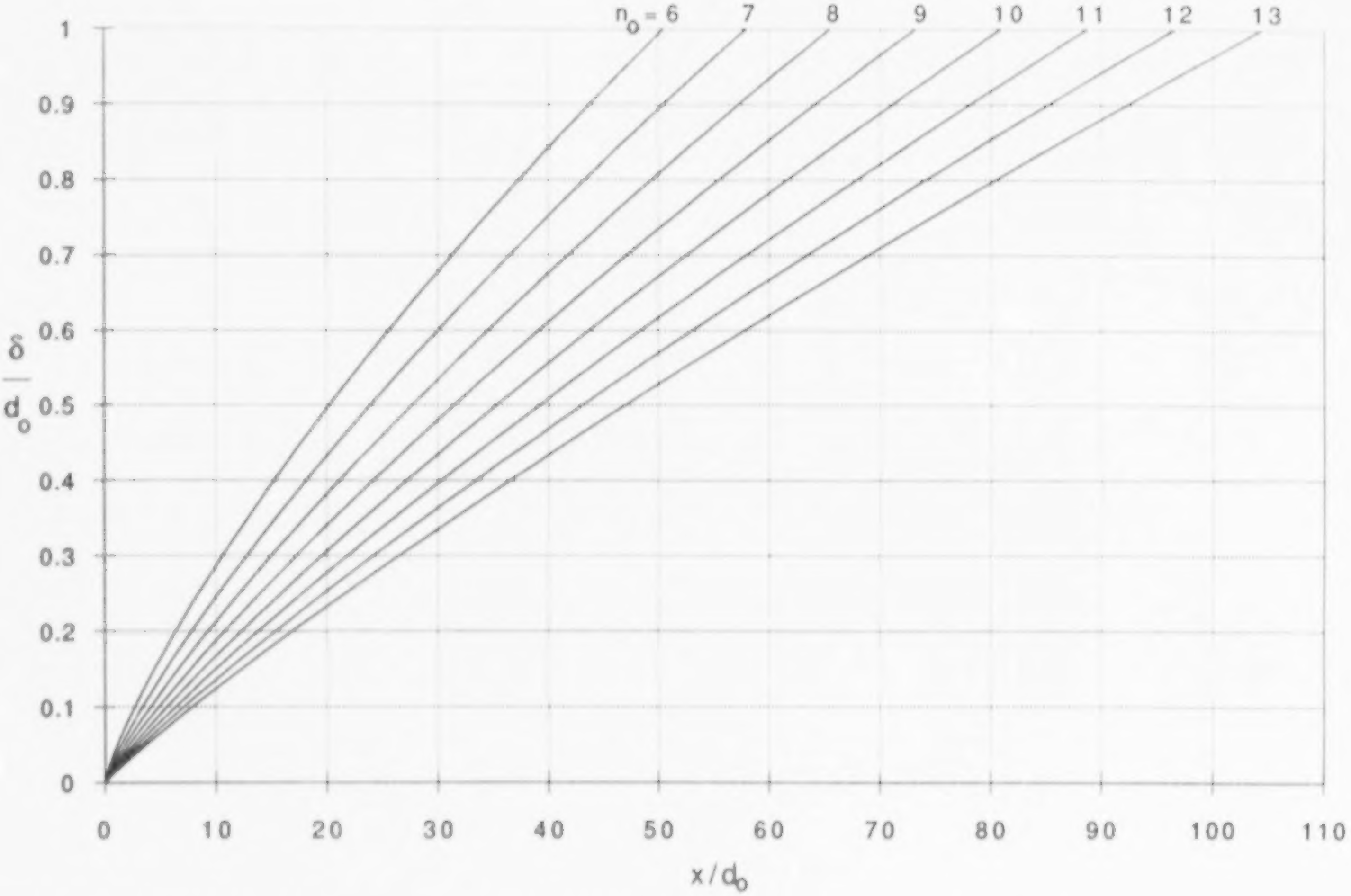

Fig. 4.9 Dimensionless boundary layer thicknesses for numerical solutions of Set 2.

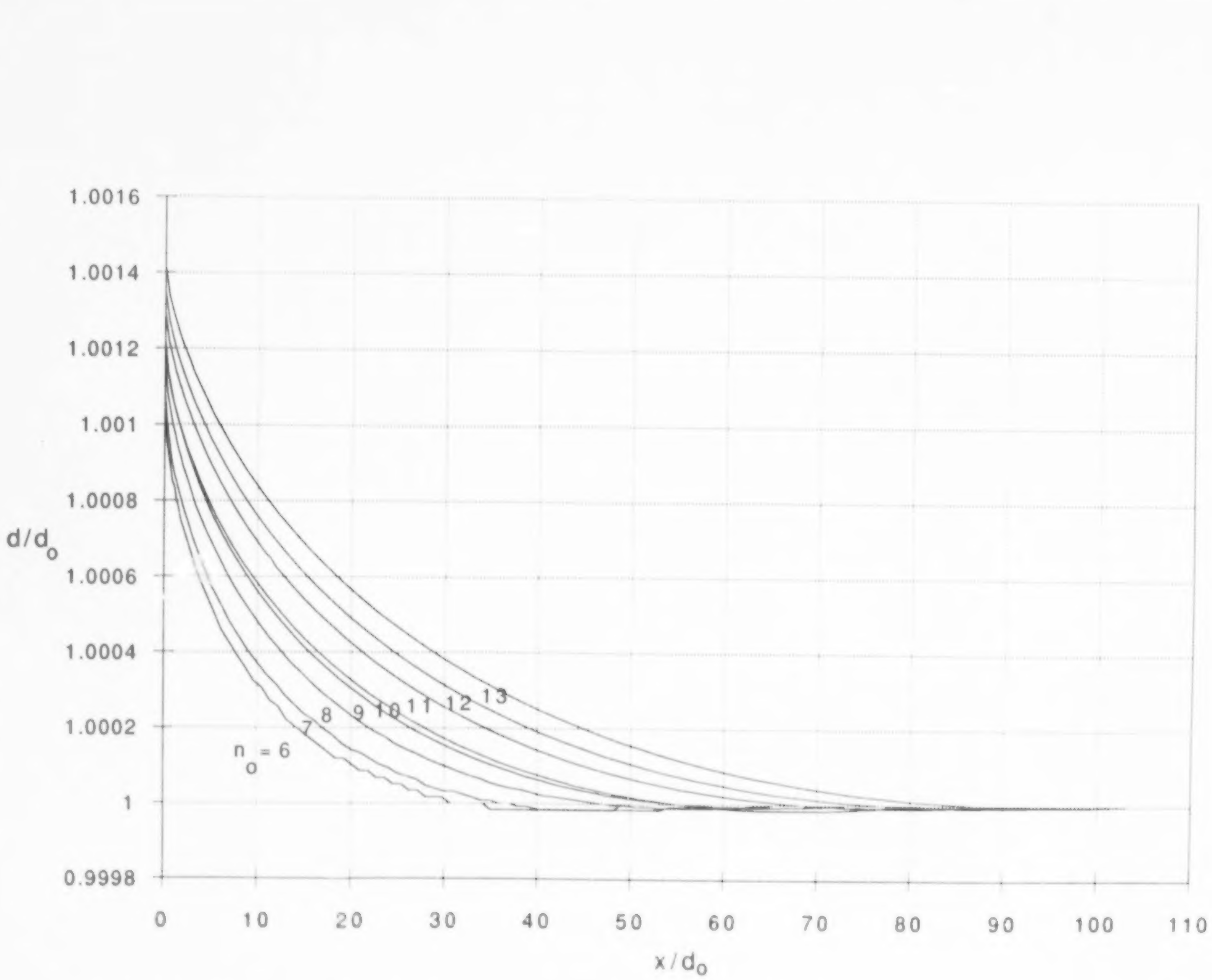

Fig. 4.10 Dimensionless depths for numerical solutions of Set 2.

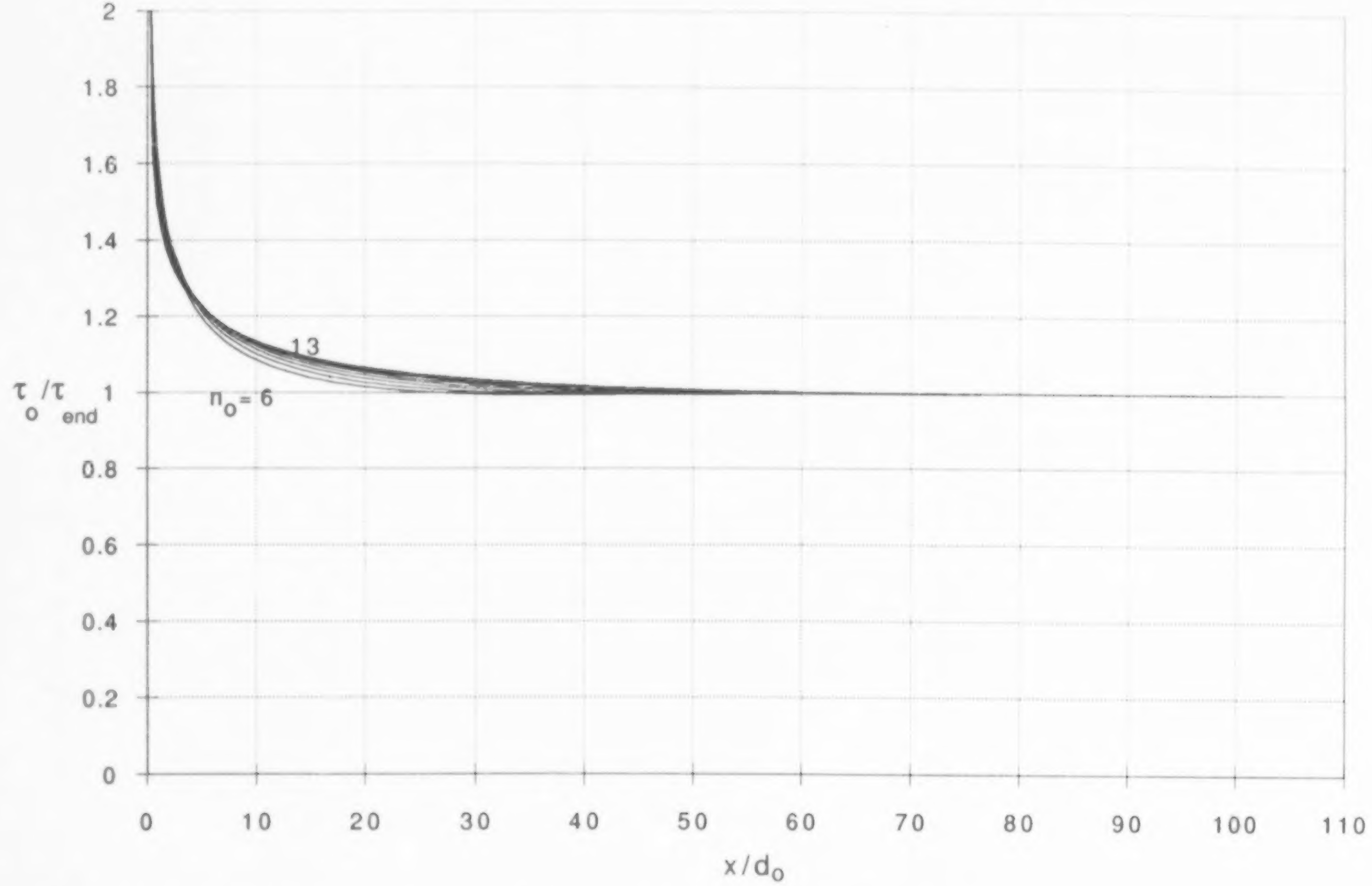

Fig. 4.11 Relative bed shear stresses for numerical solutions Set 2.

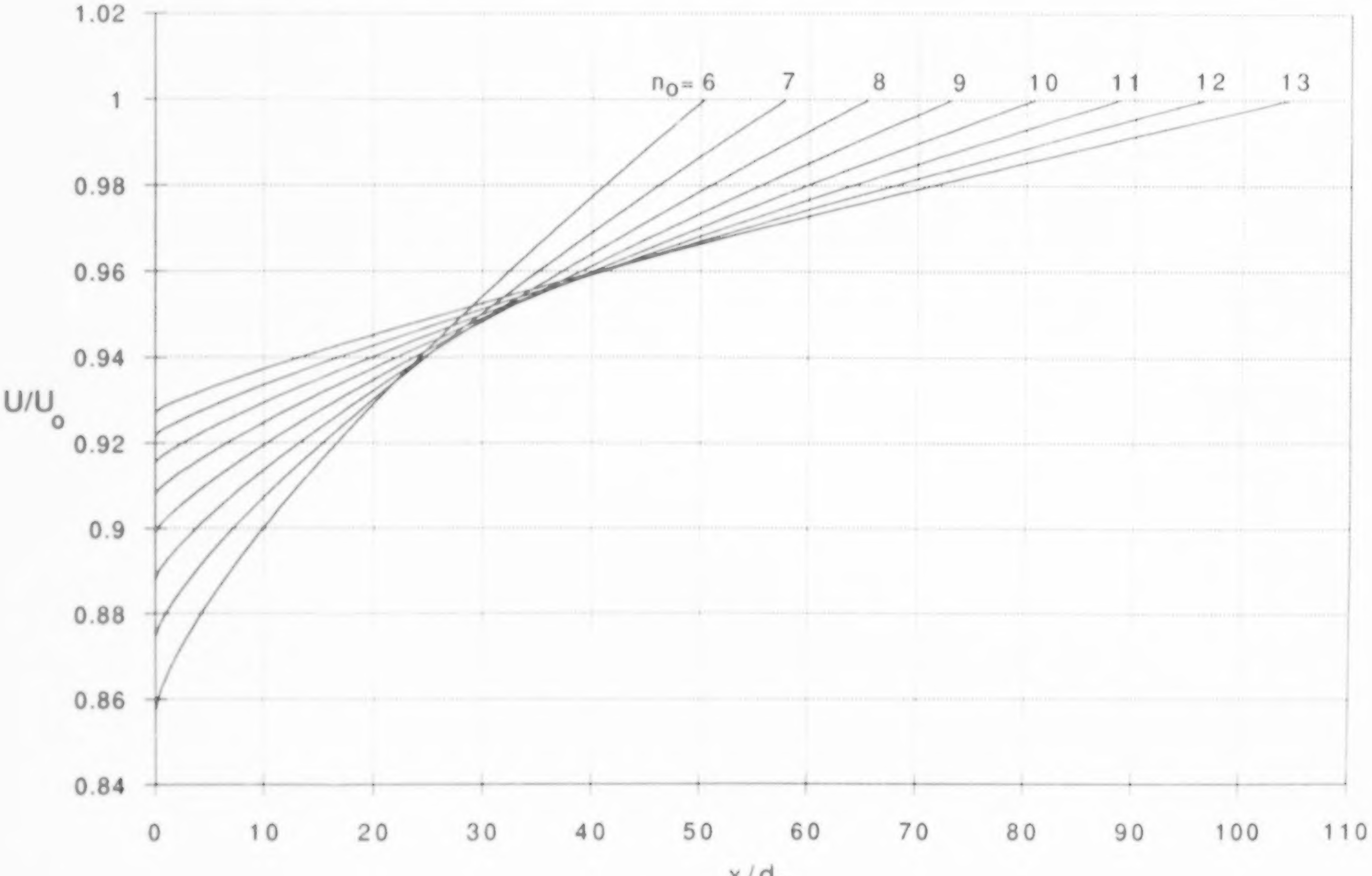

Fig. 4.12 Relative potential core velocities for numerical solutions Set 2.

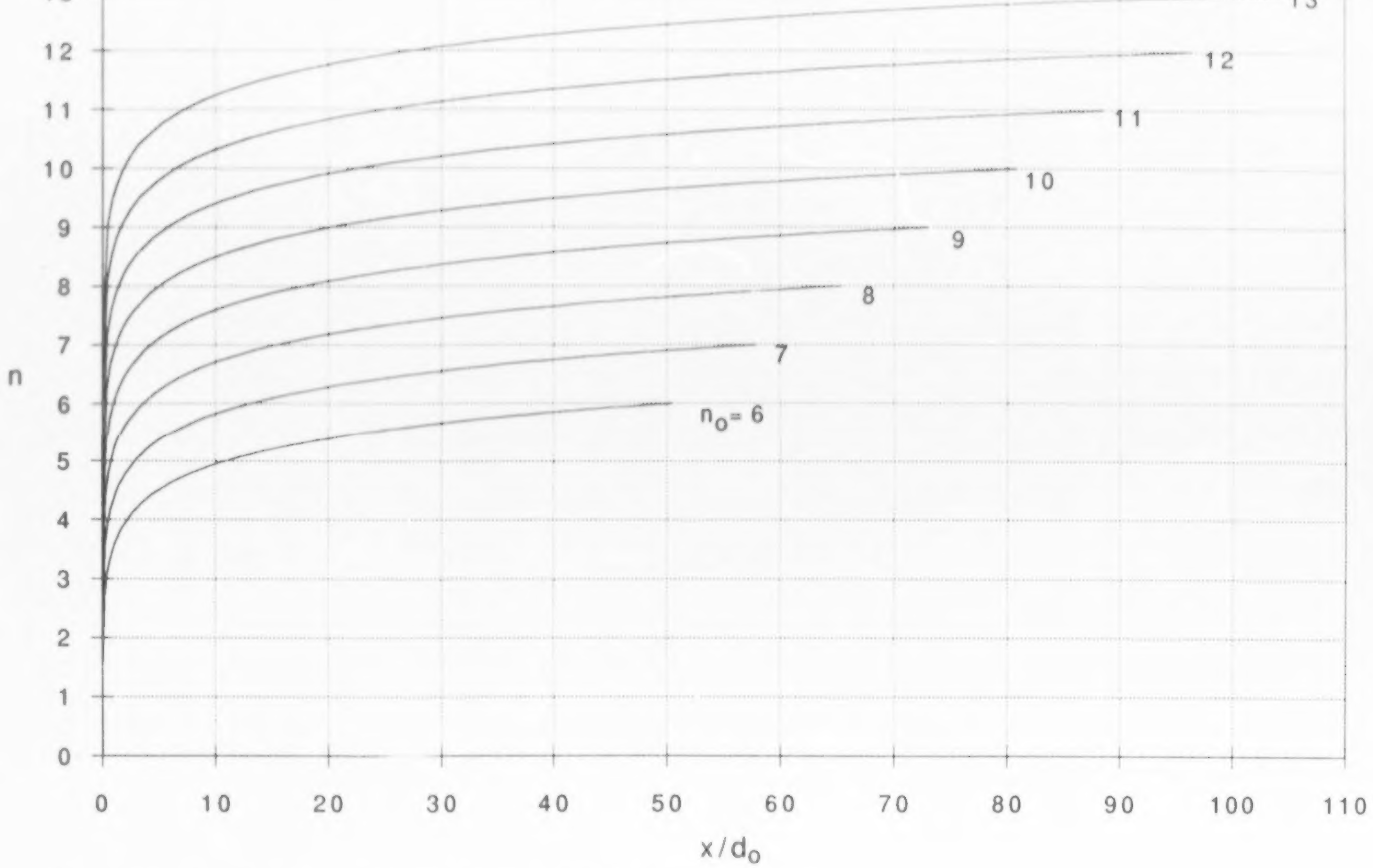

Fig. 4.13 Power law exponent for numerical solutions Set 2.

q (m^2/sec)	So	ks (m)	do (m)	no	C*	Ro	ks/do	Fo	X/do	di/do
0.0299	0.0001	0	0.127	7	21.2132034	55839	0	0.2121	57.841751	1.00107861
0.0536	0.0001	0.00019344	0.187	7	21.2132034	100053	0.00103593	0.2121	57.648361	1.00110435
0.1	0.0001	0.00046494	0.283	7	21.2132034	186667	0.00164298	0.2121	57.533478	1.00112915
0.3	0.0001	0.0012423	0.589	7	21.2132034	560000	0.00211048	0.2121	57.442764	1.00114155
1	0.0001	0.00298705	1.314	7	21.2132034	1866667	0.0022741	0.2121	57.406998	1.00109005
3	0.0001	0.00634104	2.732	7	21.2132034	5600000	0.00232085	0.2121	57.400208	1.00111961
10	0.0001	0.01424943	6.097	7	21.2132034	18666667	0.00233722	0.2121	57.398041	1.00113678
30	0.0001	0.02969929	12.682	7	21.2132034	56000000	0.00234189	0.2121	57.398132	1.00114632

Table 4.3 Summary of Set 3 numerical runs. Test difference between roughness induced n_o and Reynolds number induced n_o for the same value of n_o.

n_o; keep constant.
$\mathbf{R}_{po}$ and k_s/d_o; vary in such a way to keep n_o constant.
S_o; keep constant.

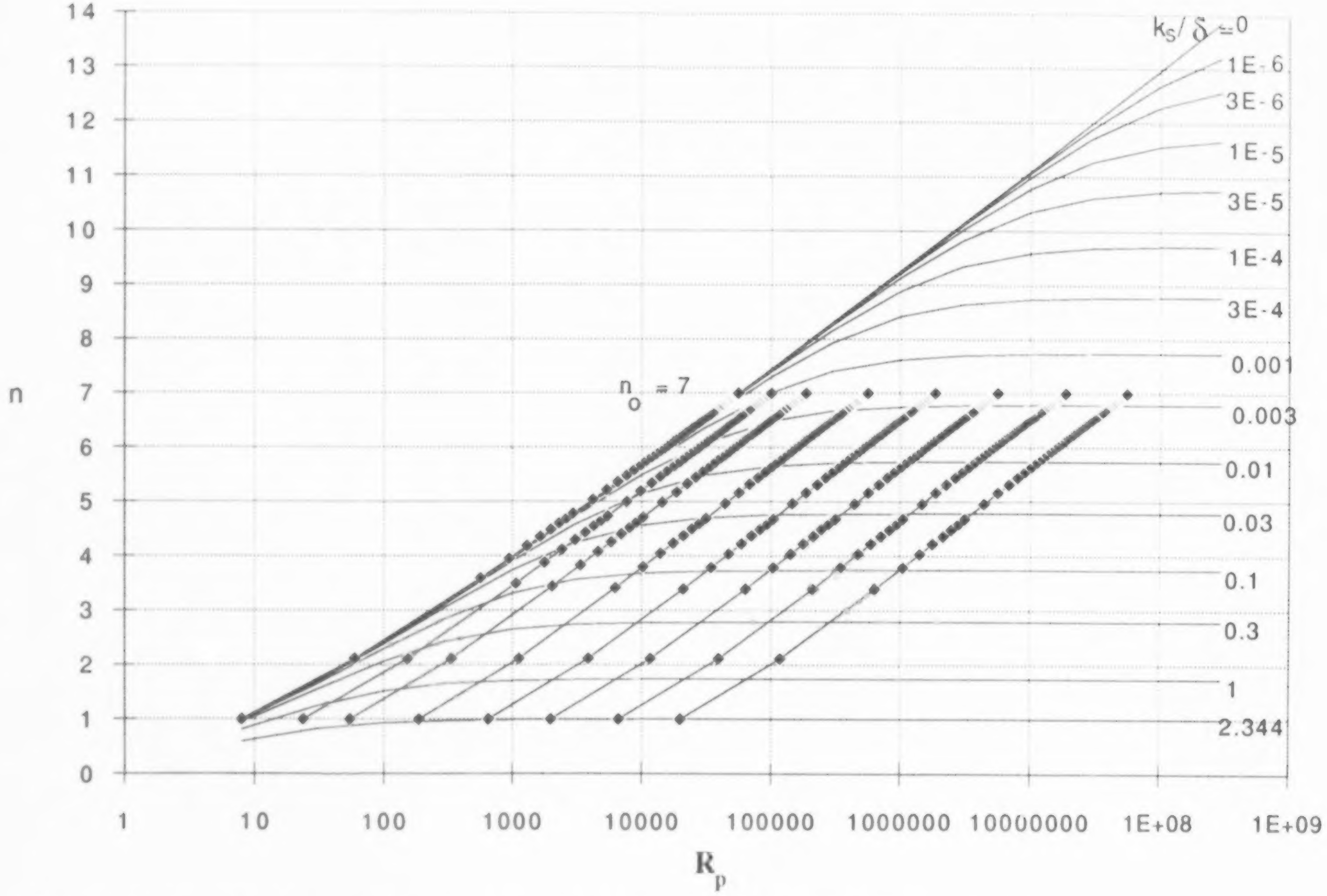

Fig. 4.14 Modified Moody Diagram showing numerical solution paths in Set 3.

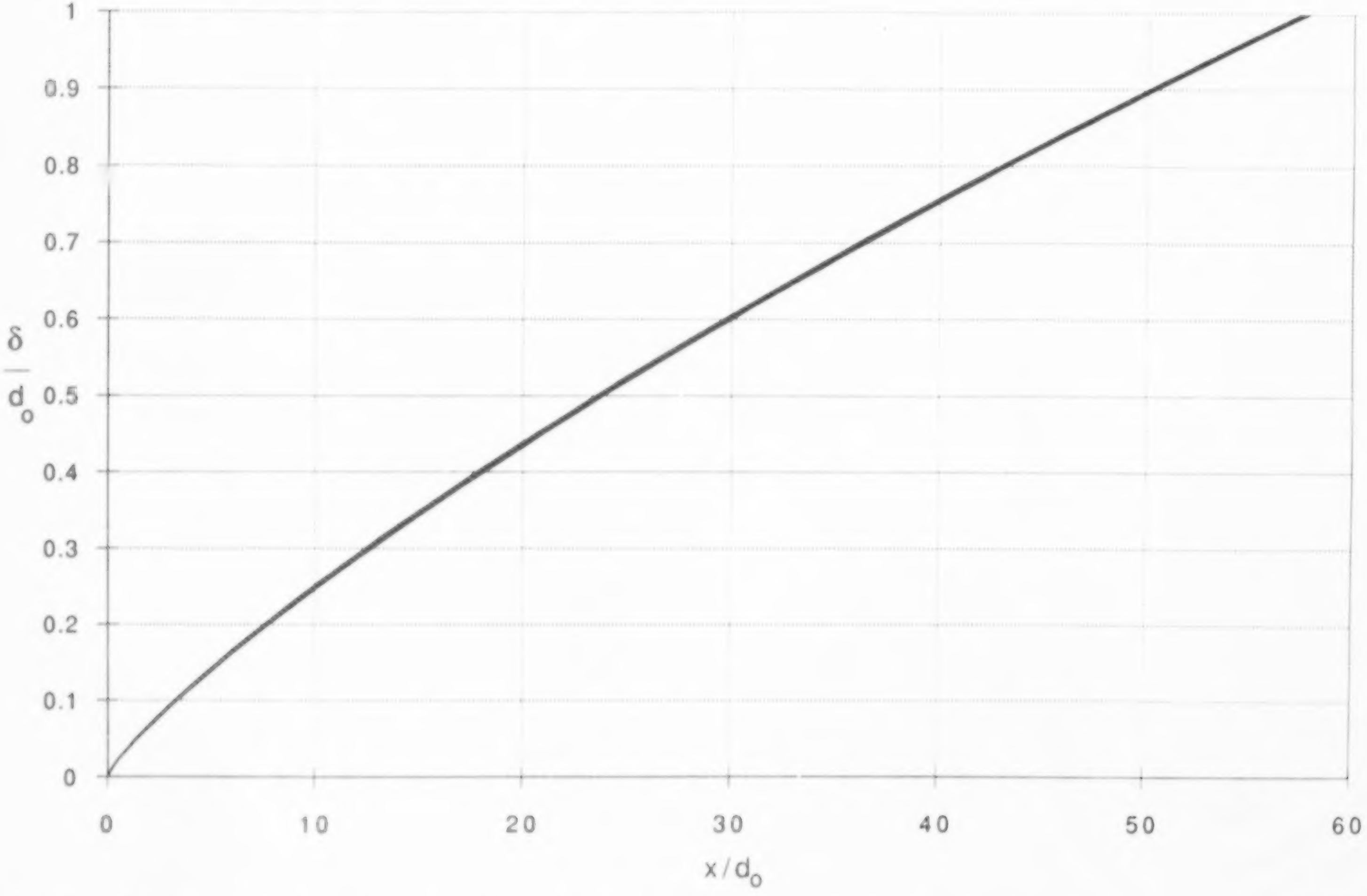

Fig. 4.15 Dimensionless boundary layer thicknesses for numerical solutions of Set 3.

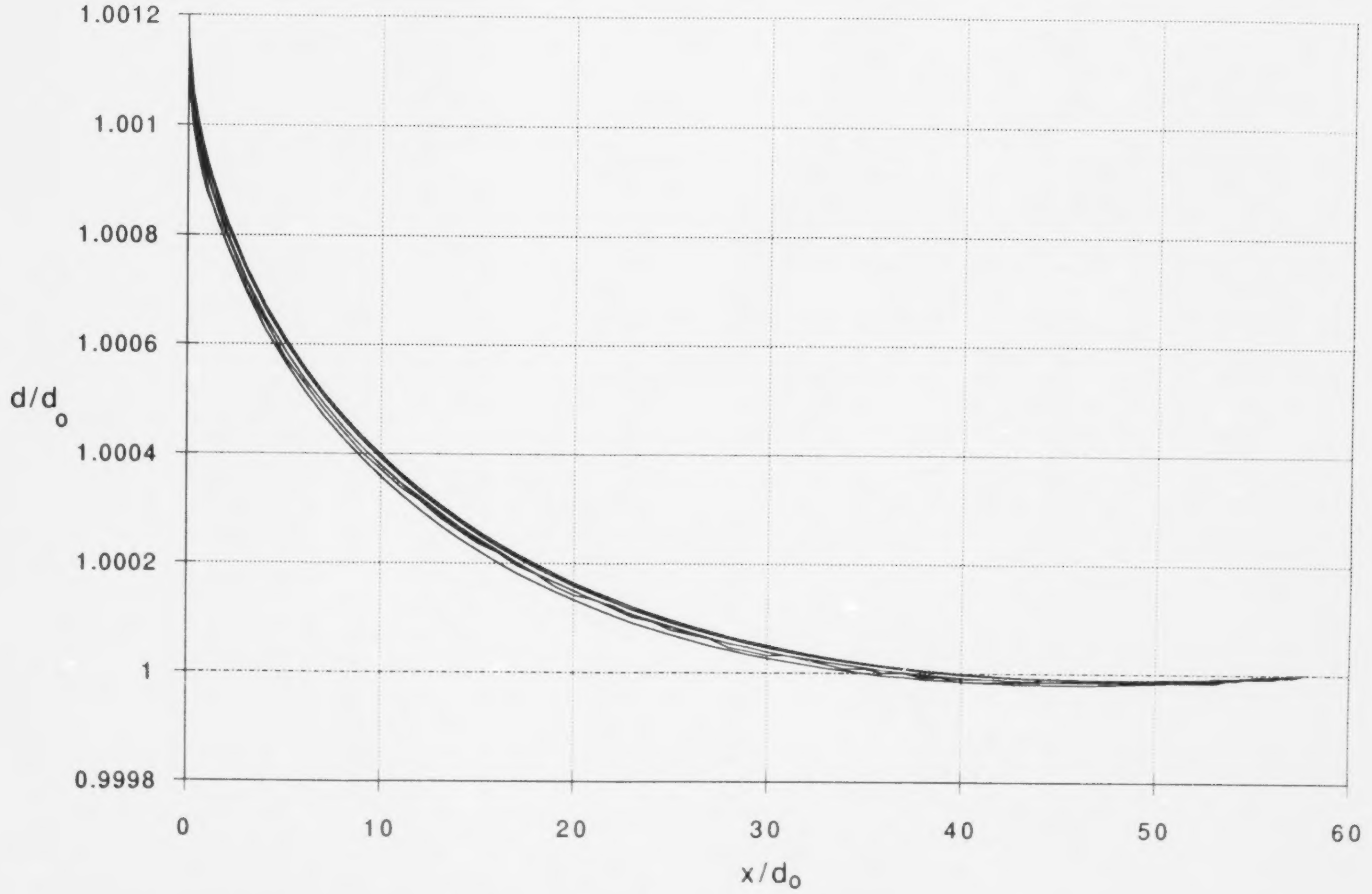

Fig. 4.16 Dimensionless depths for numerical solutions of Set 3.

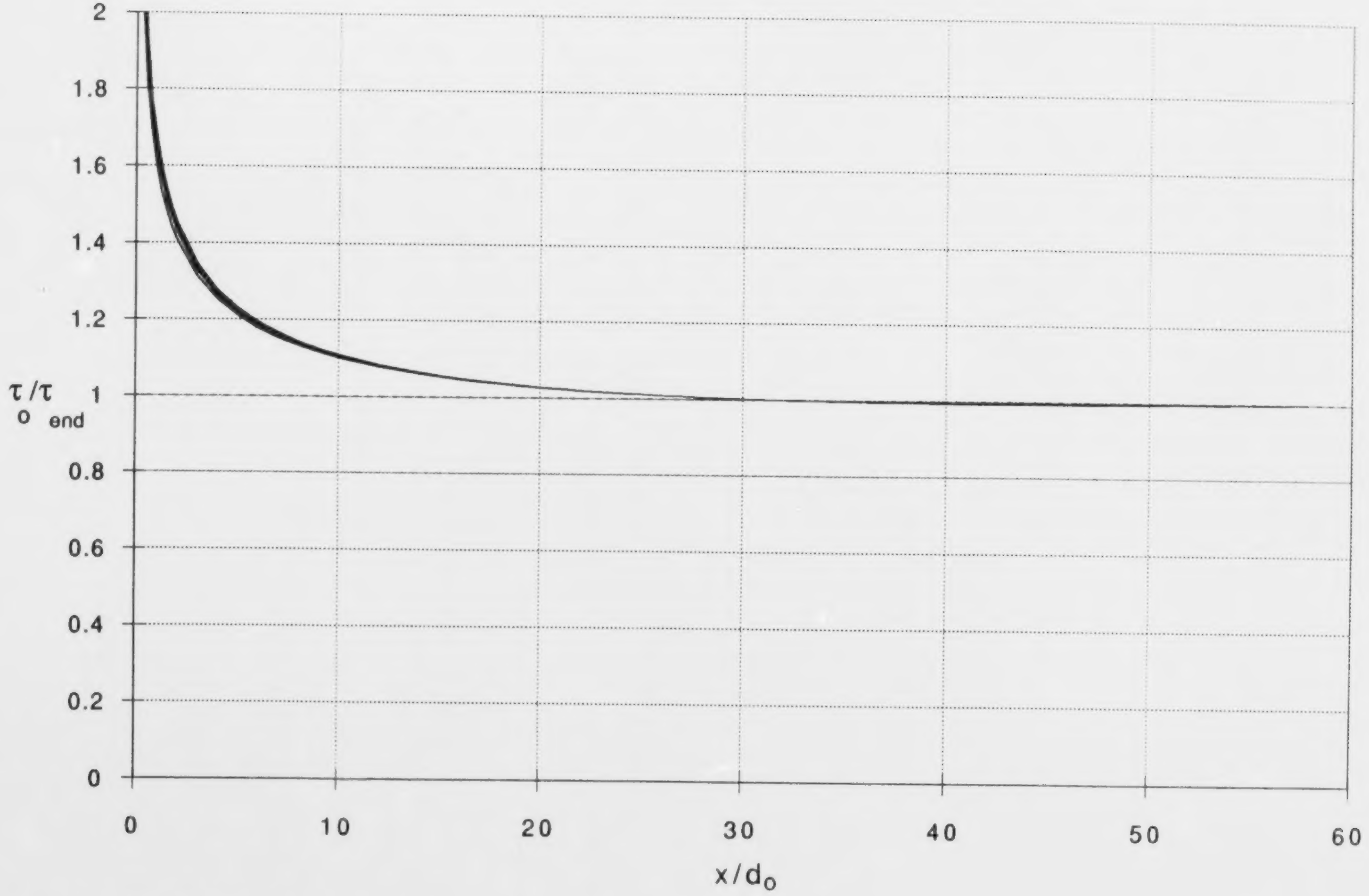

Fig. 4.17 Relative bed shear stresses for numerical solutions Set 3.

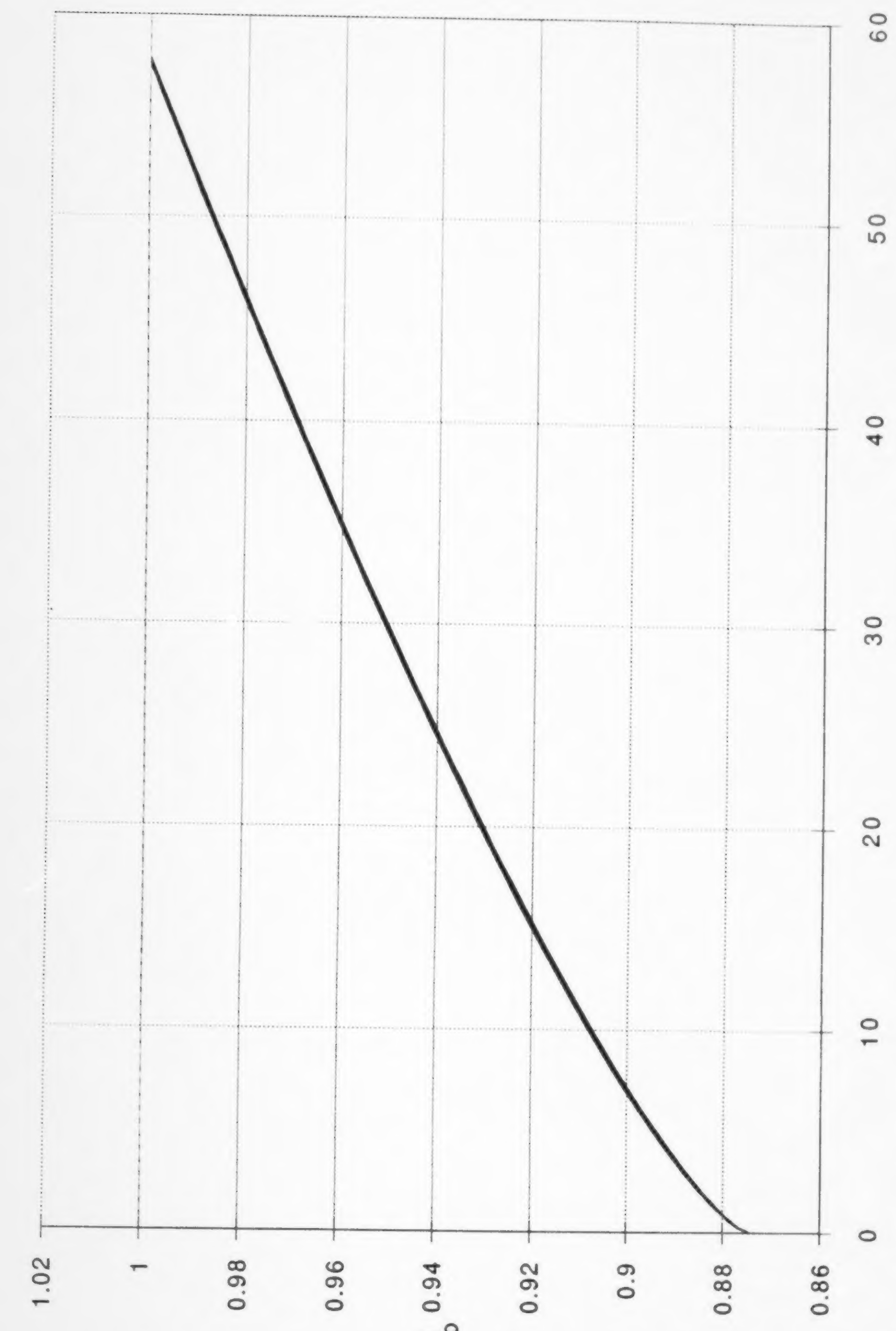

Fig. 4.18 Relative potential core velocities for numerical solutions Set 3.

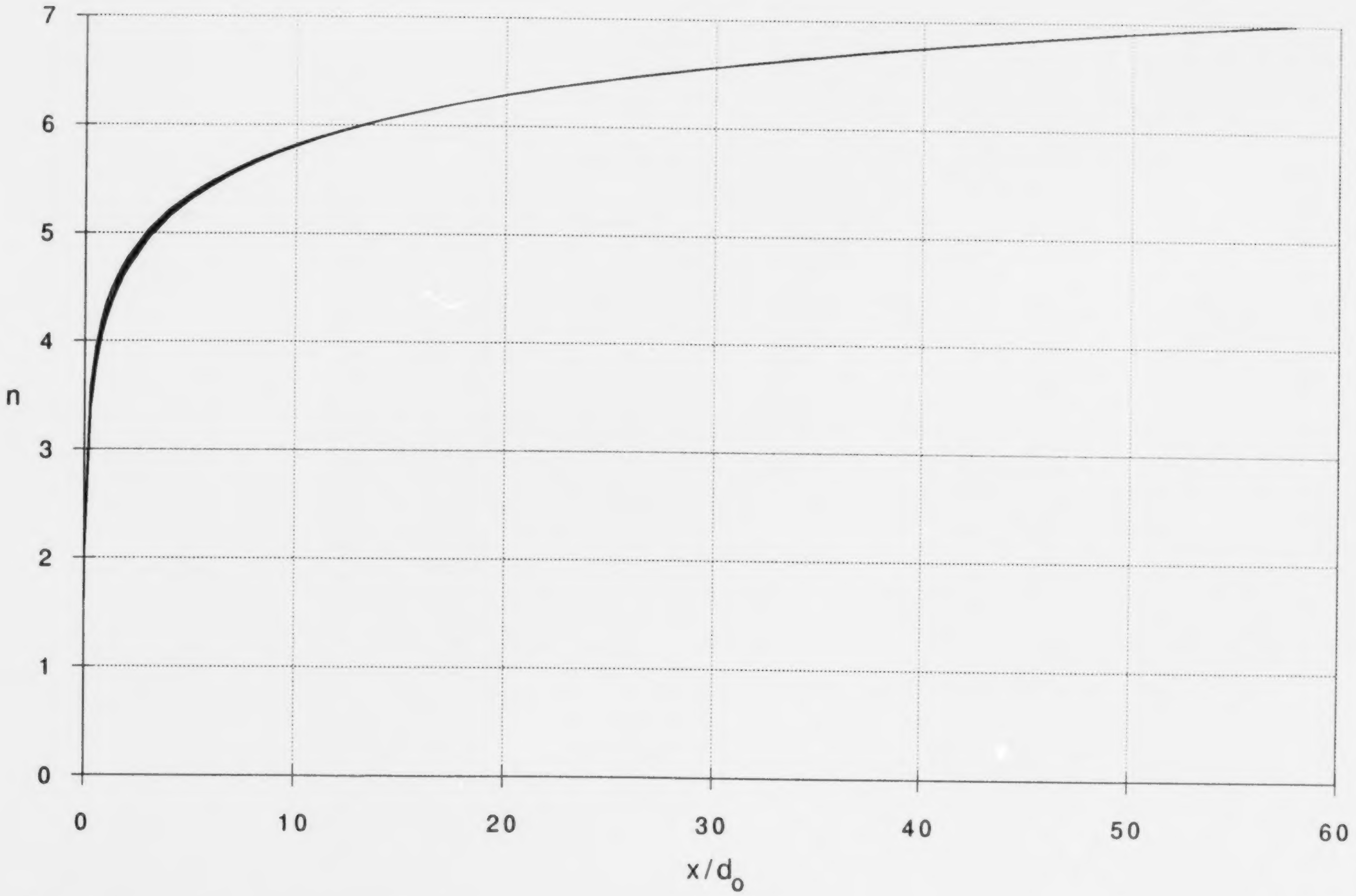

Fig. 4.19 Power law exponent for numerical solutions Set 3.

q (m^2/sec)	So	ks (m)	do (m)	no	C*	Ro	ks/do	Fo	X/do	di/do
1	0.00001	0.0064354	2.830	7	21.2132034	1866667	0.0022741	0.0671	57.372467	1.00008297
1	0.00003	0.00446206	1.962	7	21.2132034	1866667	0.0022741	0.1162	57.379684	1.00029469
1	0.0001	0.00298705	1.314	7	21.2132034	1866667	0.0022741	0.2121	57.406998	1.00109005
1	0.0003	0.0020711	0.911	7	21.2132034	1866667	0.0022741	0.3674	57.507614	1.00378036
1	0.0006	0.00164384	0.723	7	21.2132034	1866667	0.0022741	0.5196	57.690857	1.00877953
1	0.001	0.00138646	0.610	7	21.2132034	1866667	0.0022741	0.6708	58.055847	1.01[illegible]47458
1	0.0014	0.00123937	0.545	7	21.2132034	1866667	0.0022741	0.7937	58.683121	1.03[illegible]5394
1	0.002	0.00110044	0.484	7	21.2132034	1866667	0.0022741	0.9487	60.828384	1.07635579

Table 4.4 Summary of Set 4 numerical runs. Test the effect of slope.(or Froude number)

n_o; keep constant.
$\mathbf{R}_{po}$; keep constant.
k_s/d_o; vary to keep n_o and $\mathbf{R}_{po}$ constant.
S_o; vary slope from small to near critical.

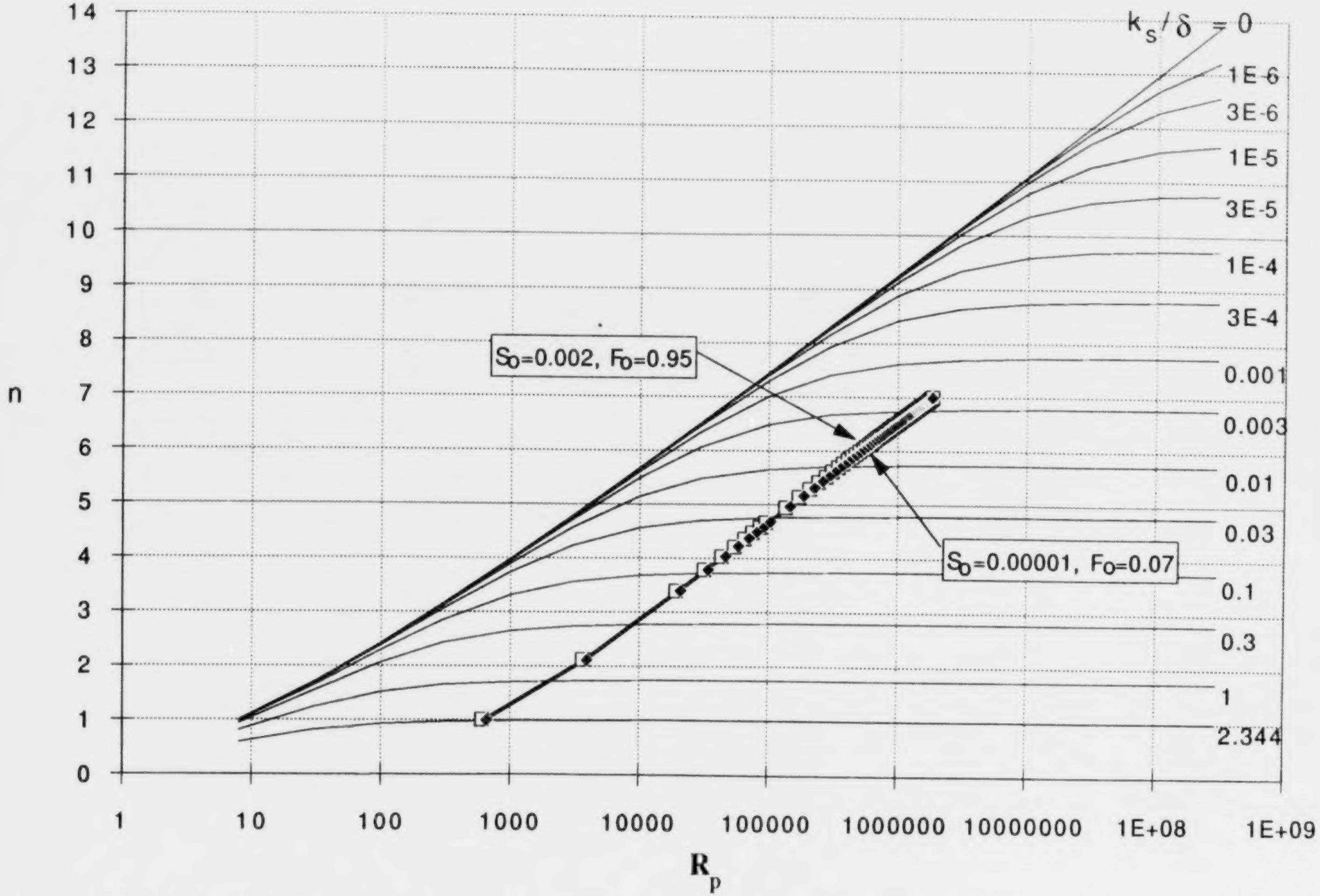

Fig. 4.20 Modified Moody Diagram showing numerical solution paths in Set 4.

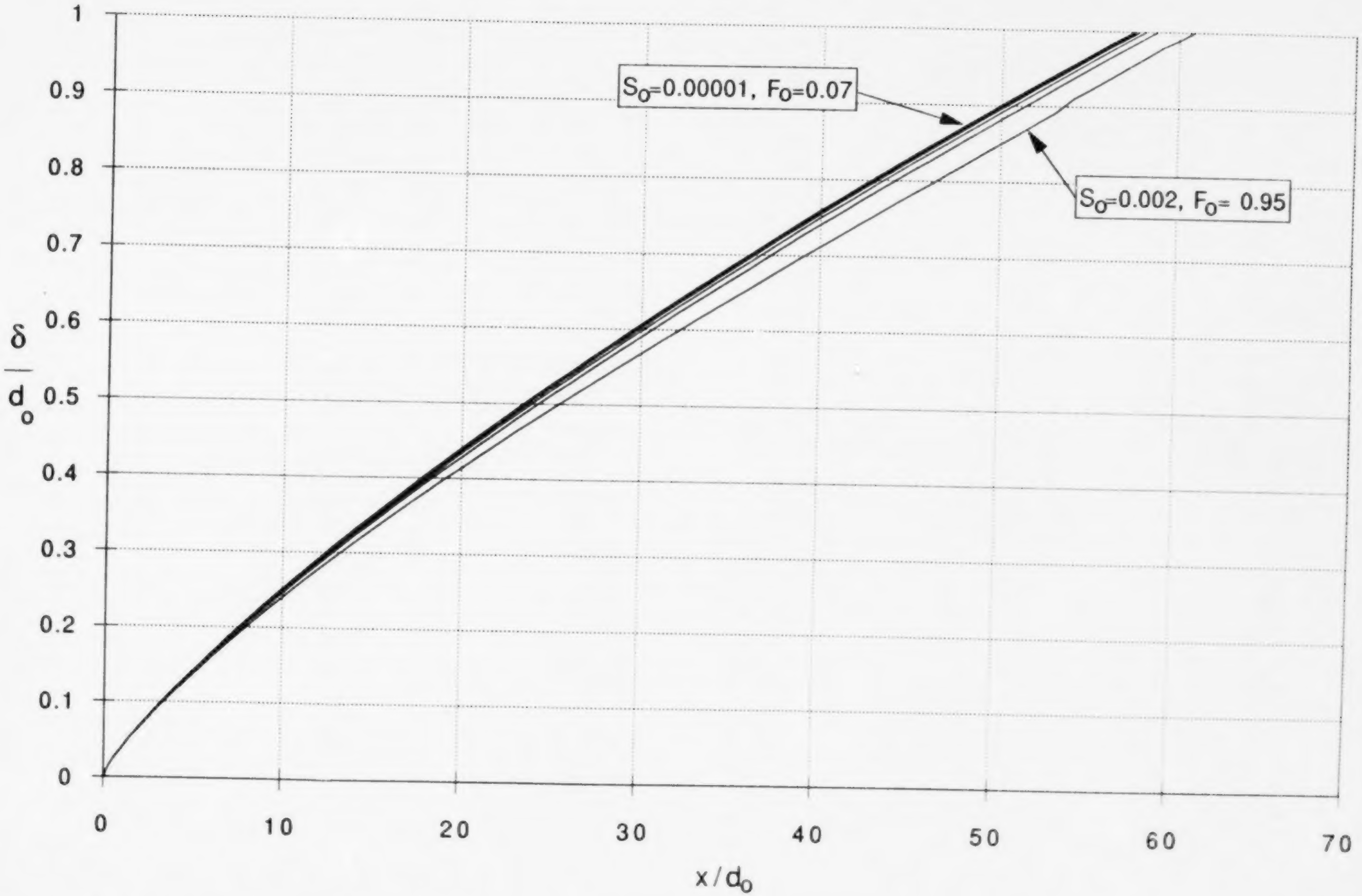

Fig. 4.21 Dimensionless boundary layer thicknesses for numerical solutions of Set 4.

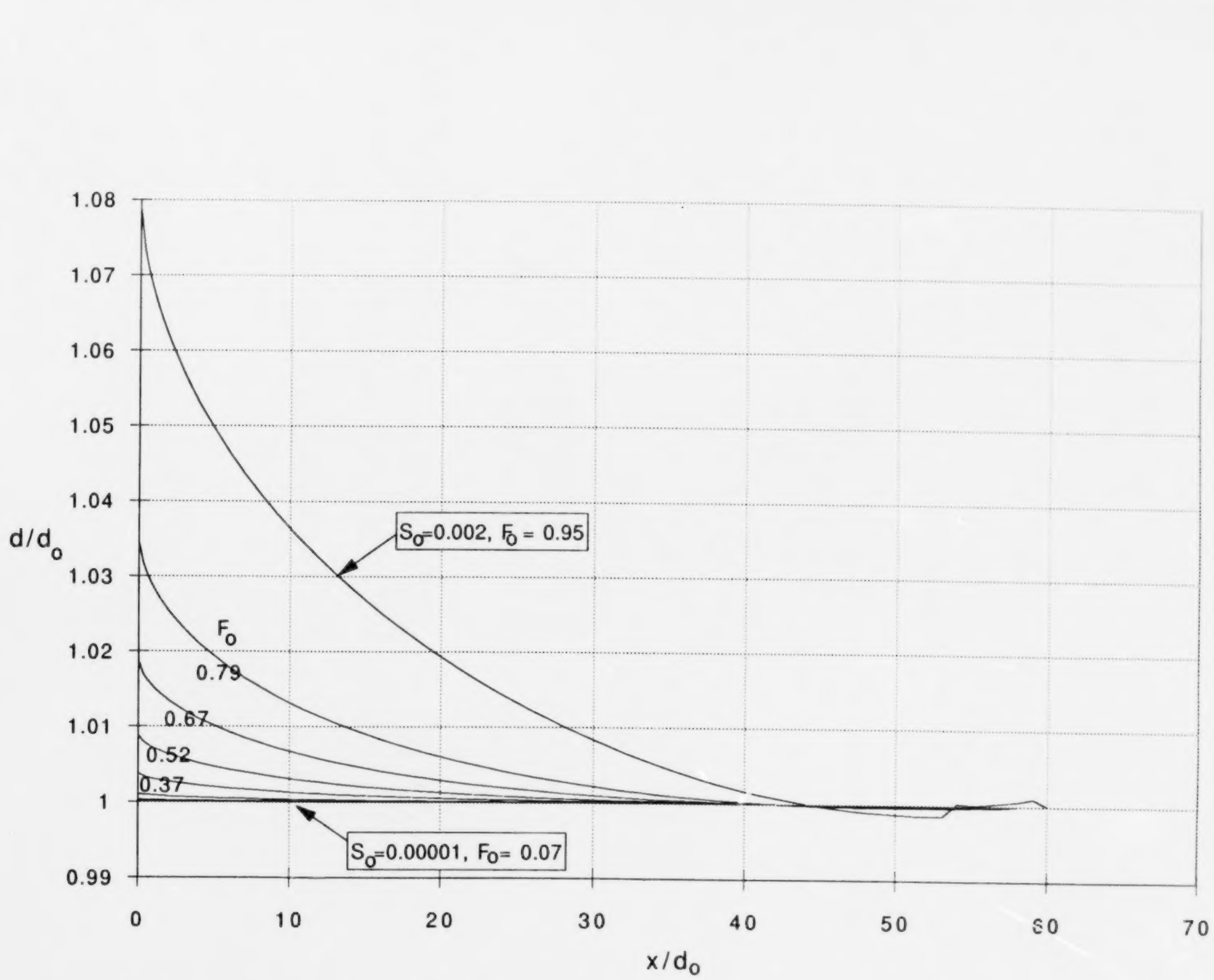

Fig. 4.22 Dimensionless depths for numerical solutions of Set 4.

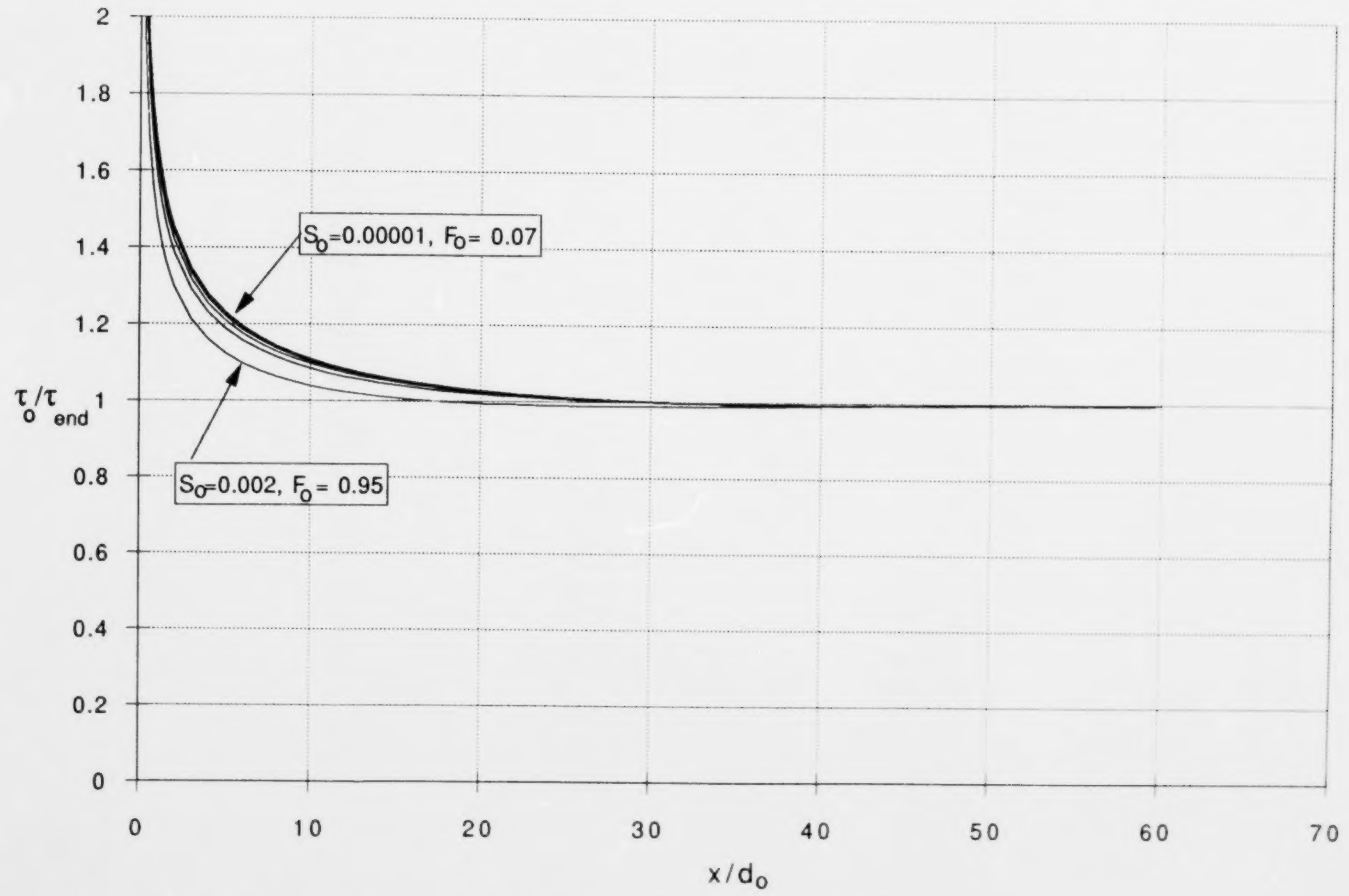

Fig. 4.23 Relative bed shear stresses for numerical solutions Set 4.

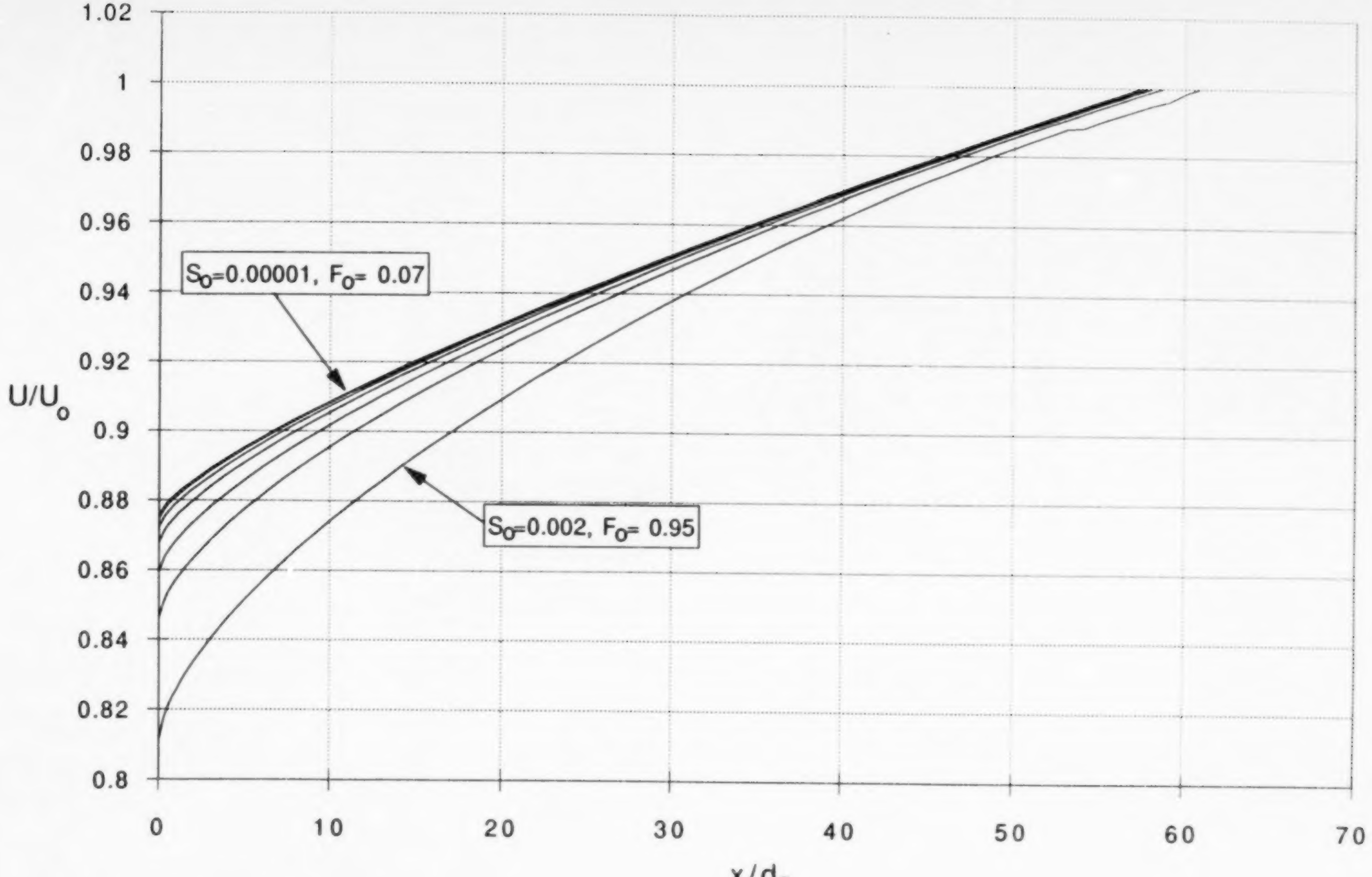

Fig. 4.24 Relative potential core velocities for numerical solutions Set 4.

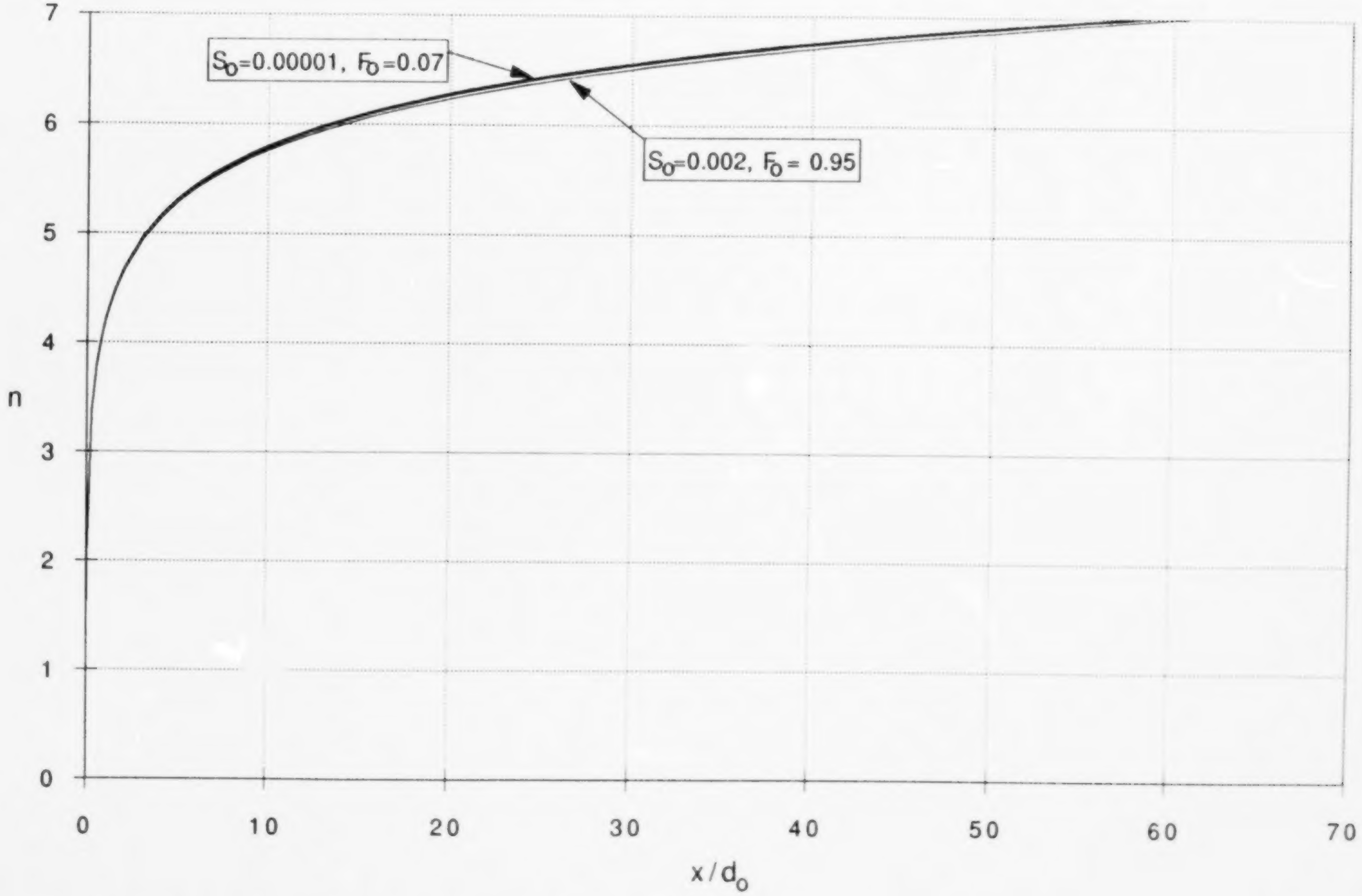

Fig. 4.25 Power law exponent for numerical solutions Set 4.

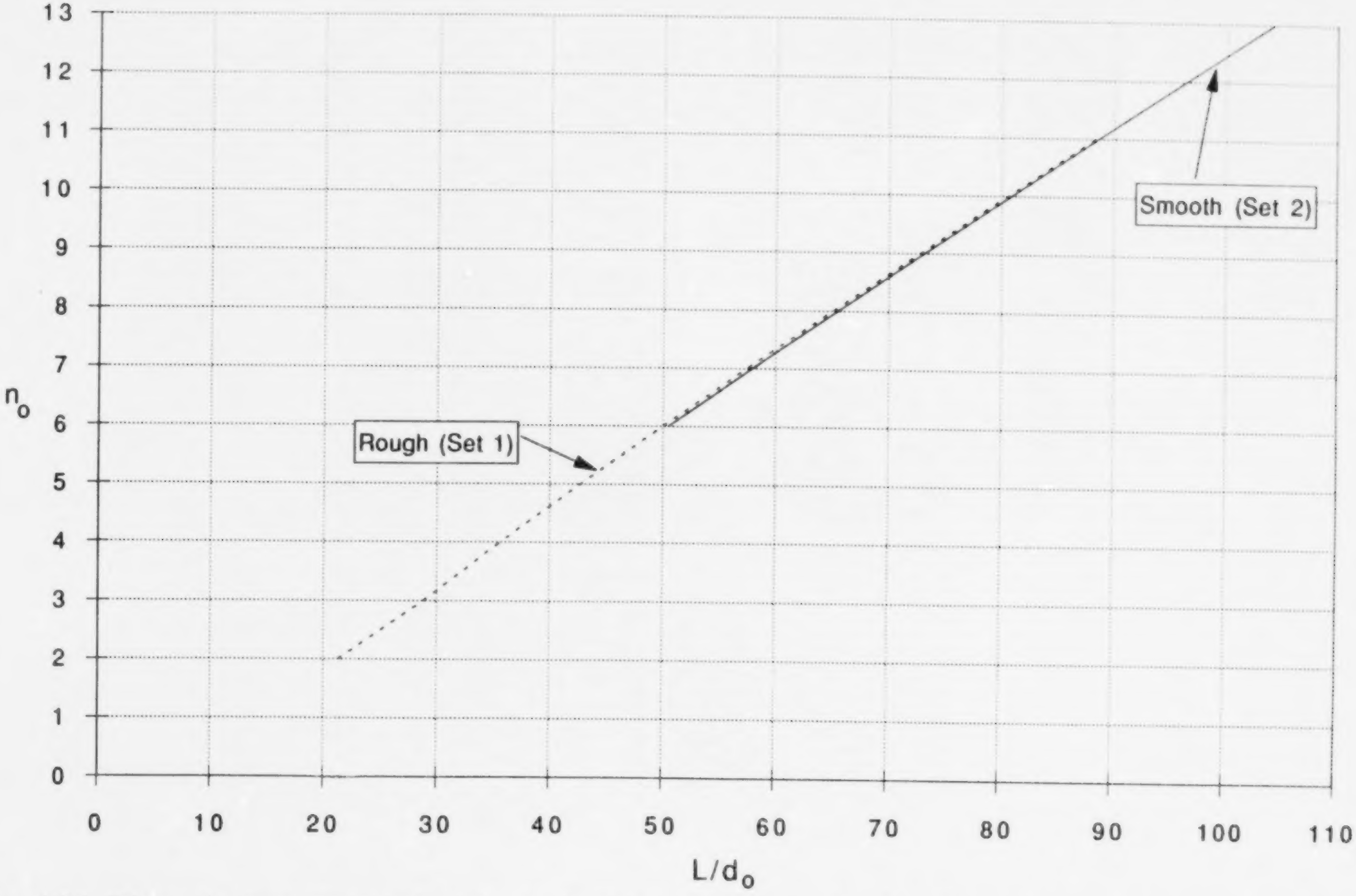

Fig. 4.26 Dimensionless entrance length as a function of the fully developed power law exponent for numerical solutions Set 1 and Set 2.

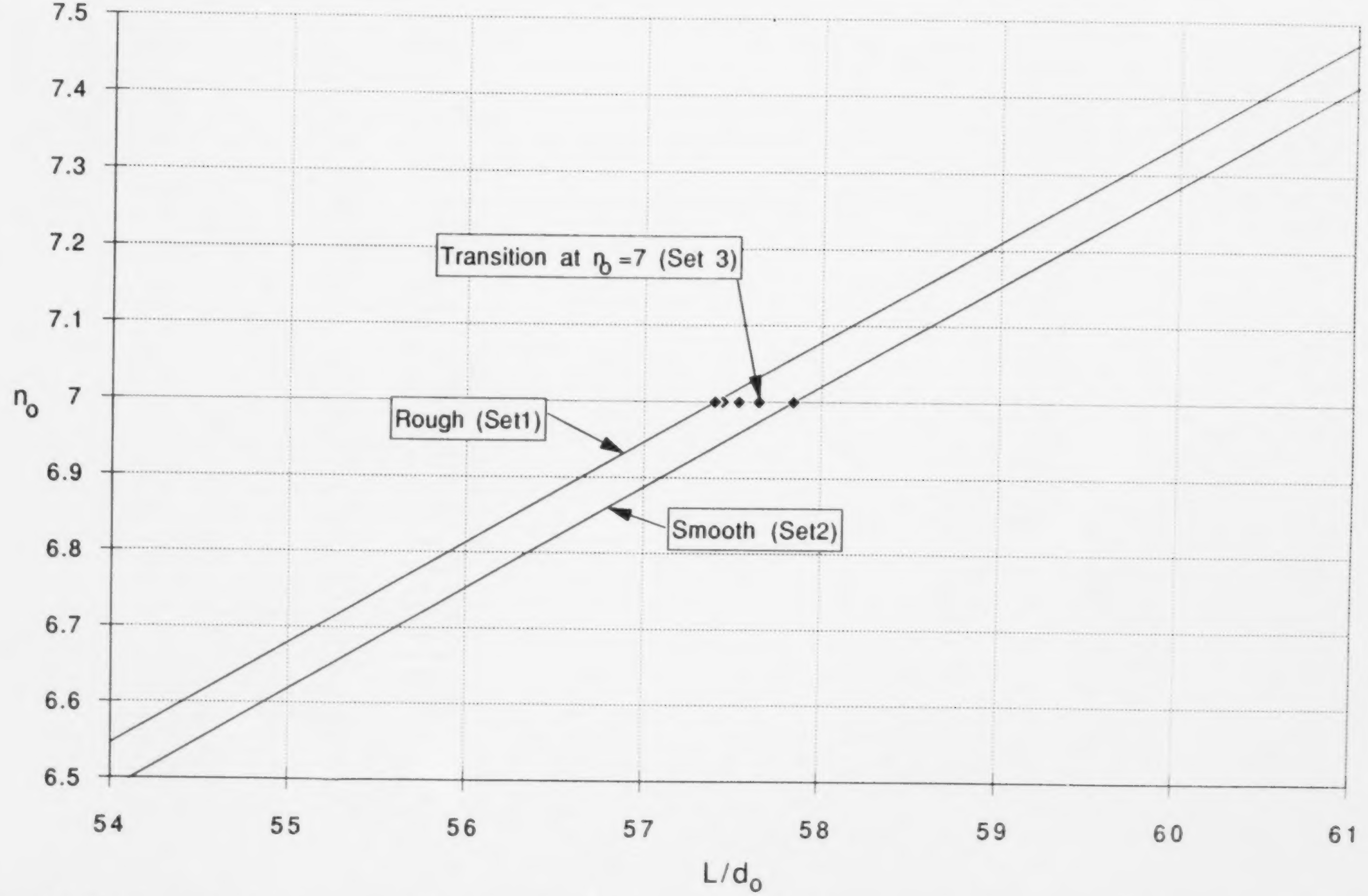

Fig. 4.27 Dimensionless entrance length as a function of the fully developed power law exponent for numerical solutions Set 1, Set 2 and Set 3.

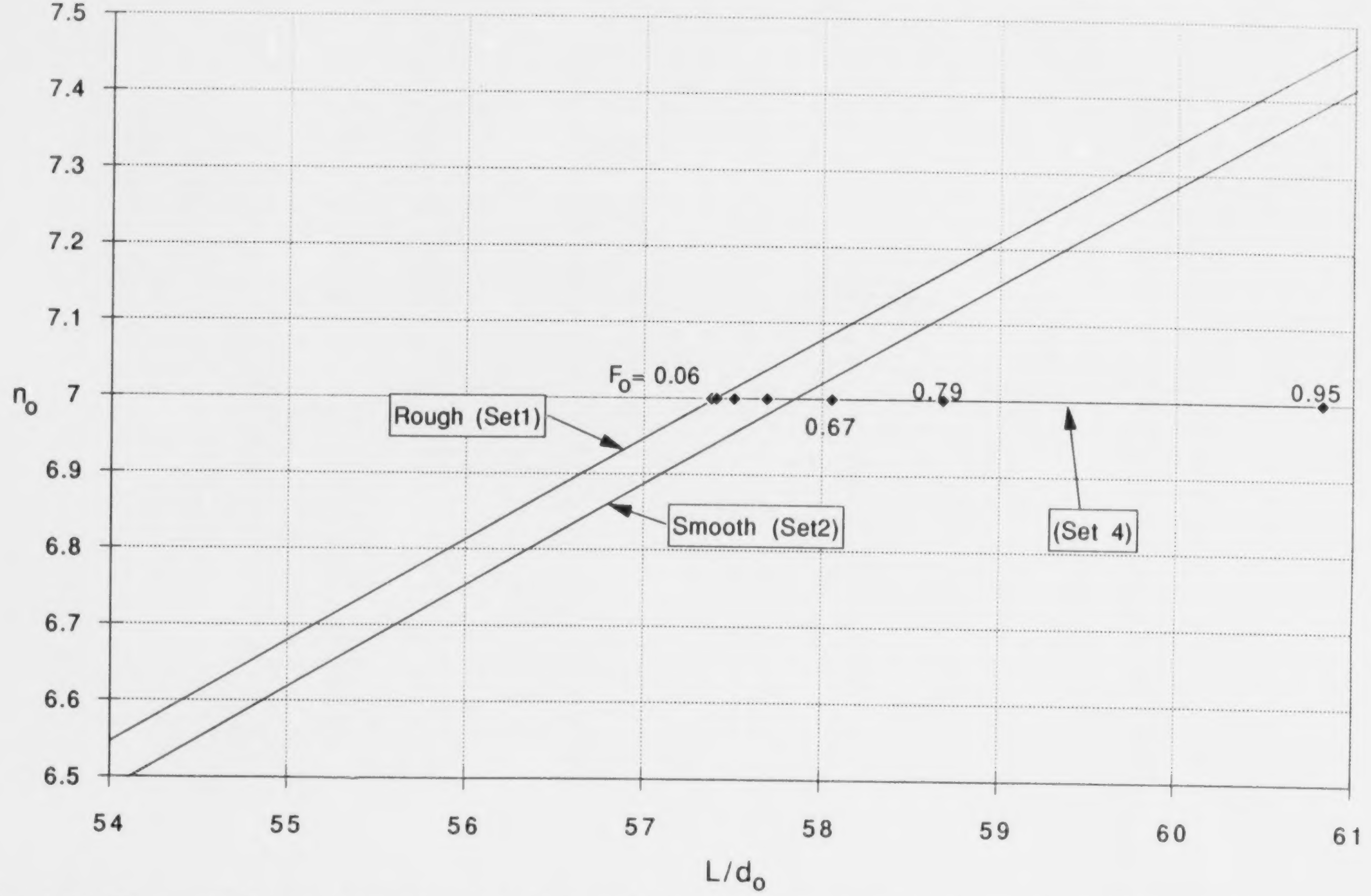

Fig. 4.28 Dimensionless entrance length as a function of the fully developed power law exponent for numerical solutions Set 1, Set 2 and Set 4.

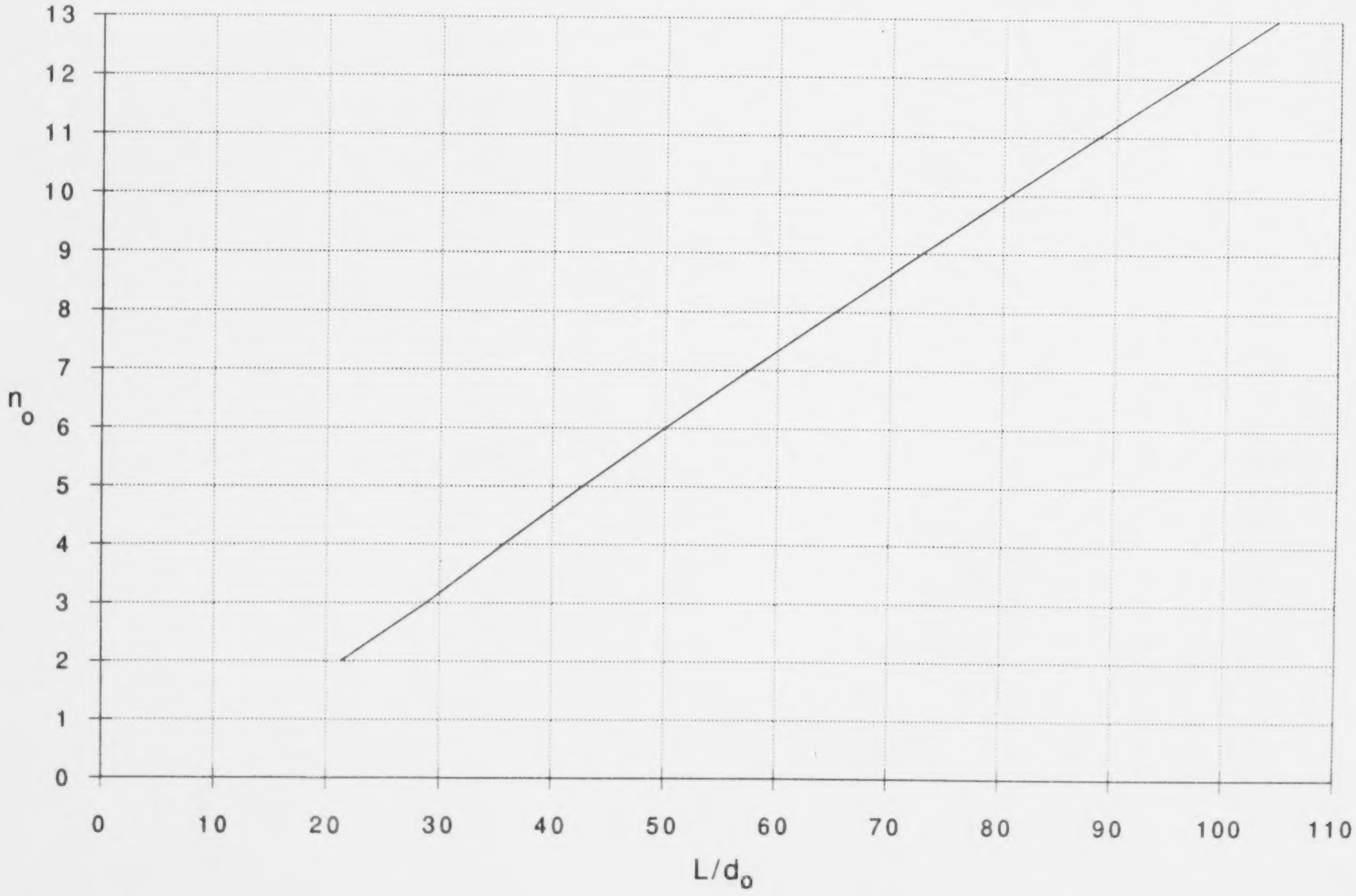

Fig. 4.29a Dimensionless entrance length as a function of the fully developed power law exponent.

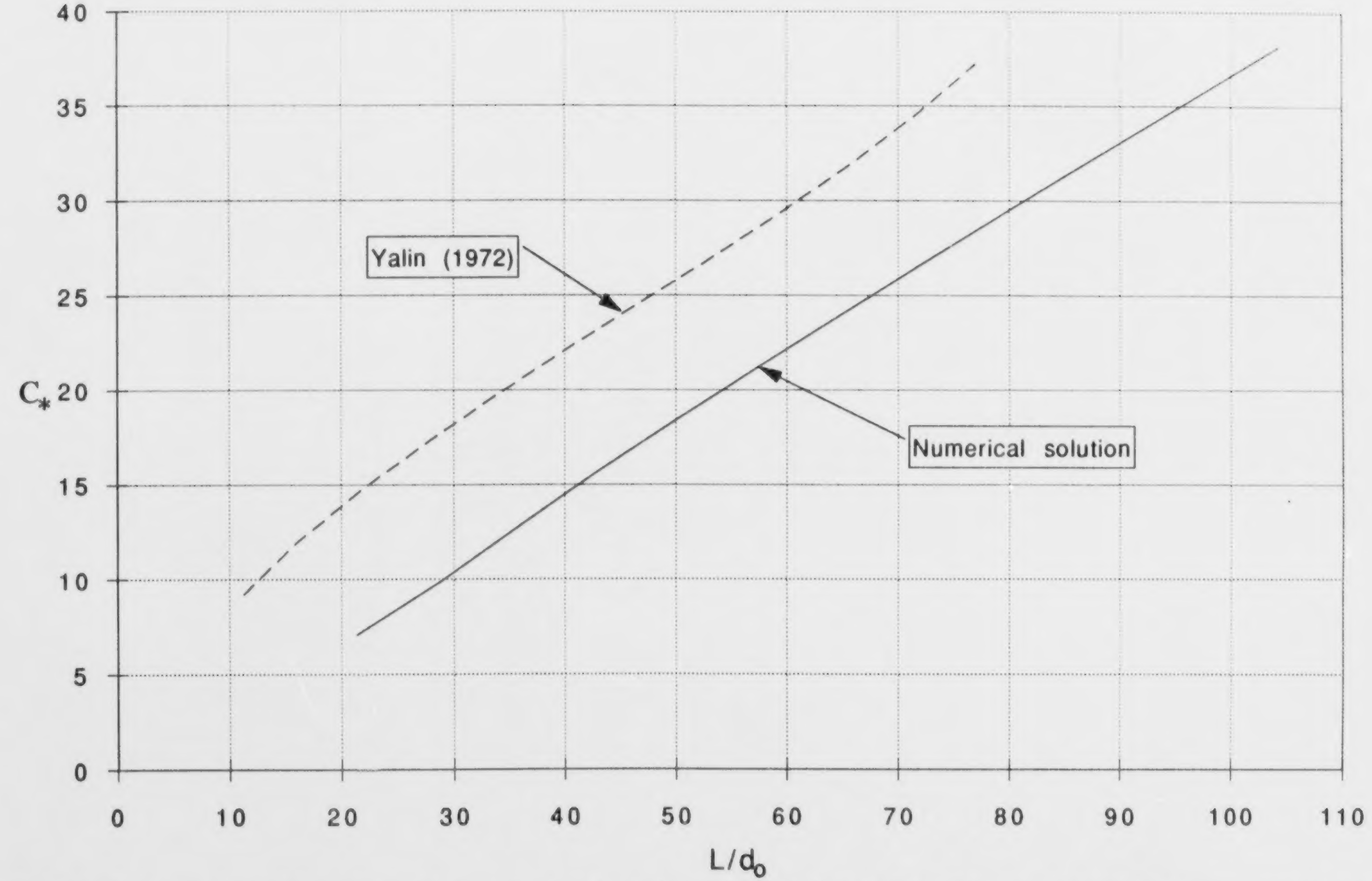

Fig. 4.29b Dimensionless entrance length as a function of the fully developed dimensionless Chezy coefficient. Also shown is Yalin's (1972) solution for the entrance length.

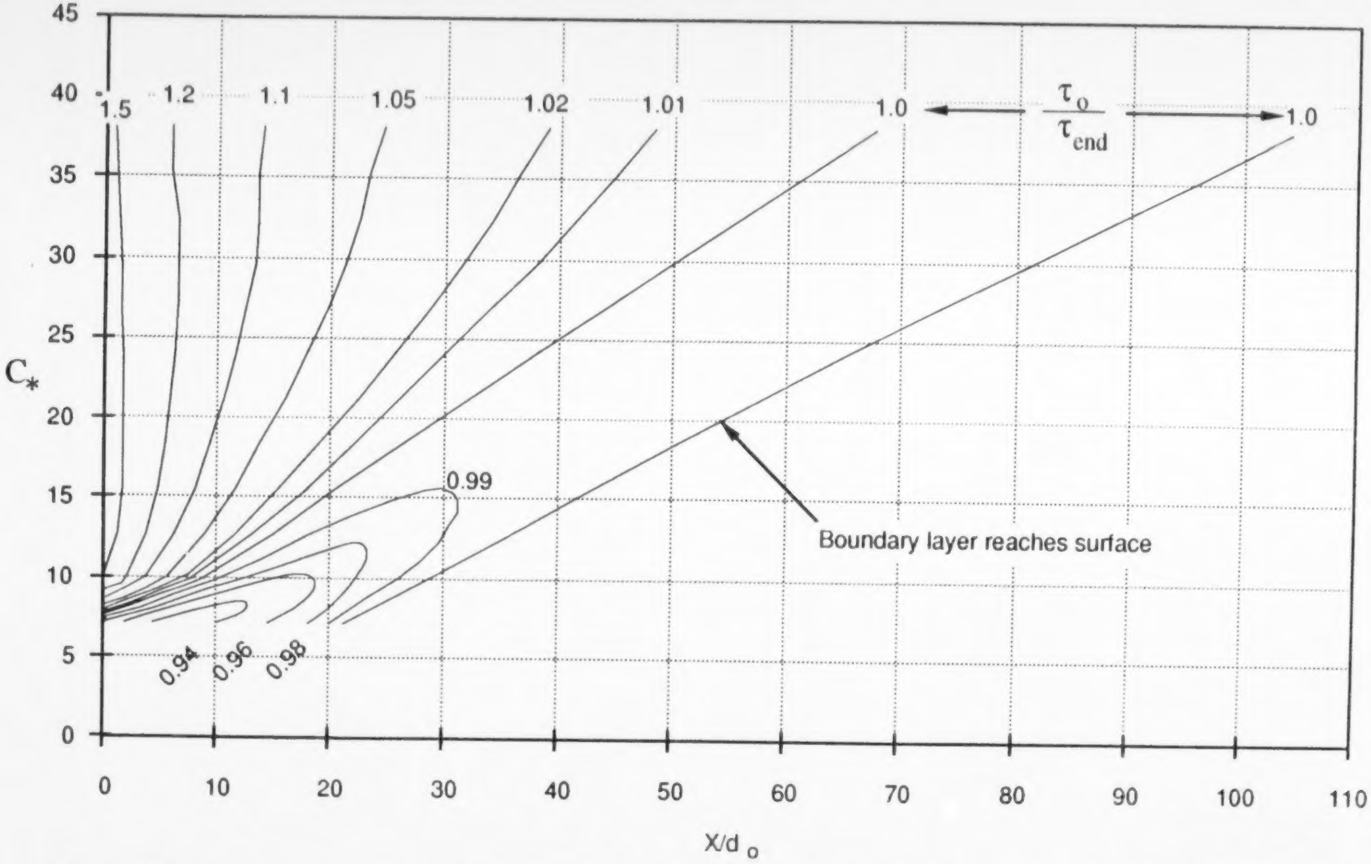

Fig. 4.29c Relative bed shear stress (τ_o/τ_{end}) within the entrance region as a function of C∗ and dimesionless distance down the channel.

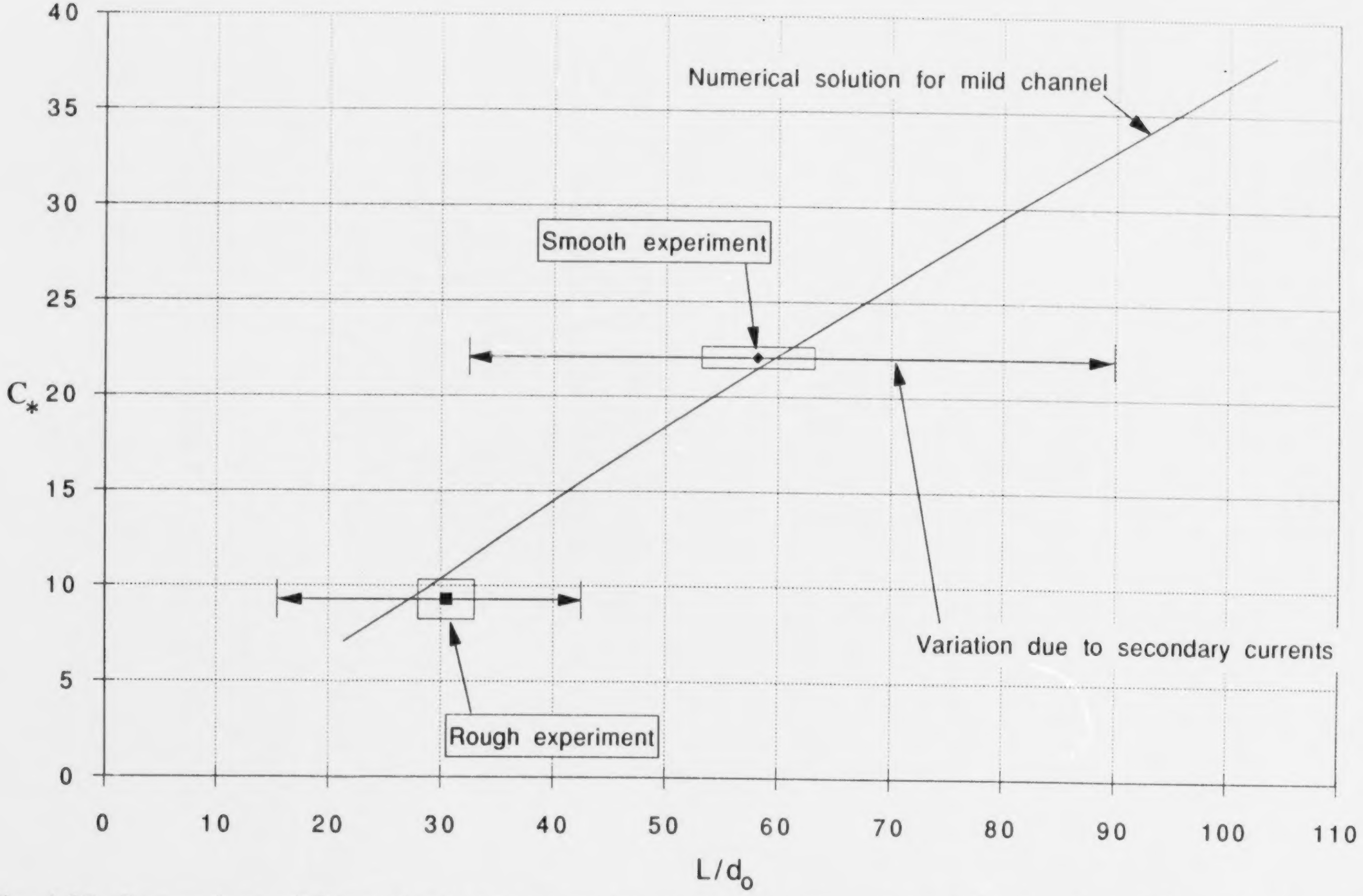

Fig. 4.30 Comparison of dimensionless entrance length as a function of the fully developed dimensionless Chezy coefficient between the numerical and the two experiments analysed in Chapter 2.

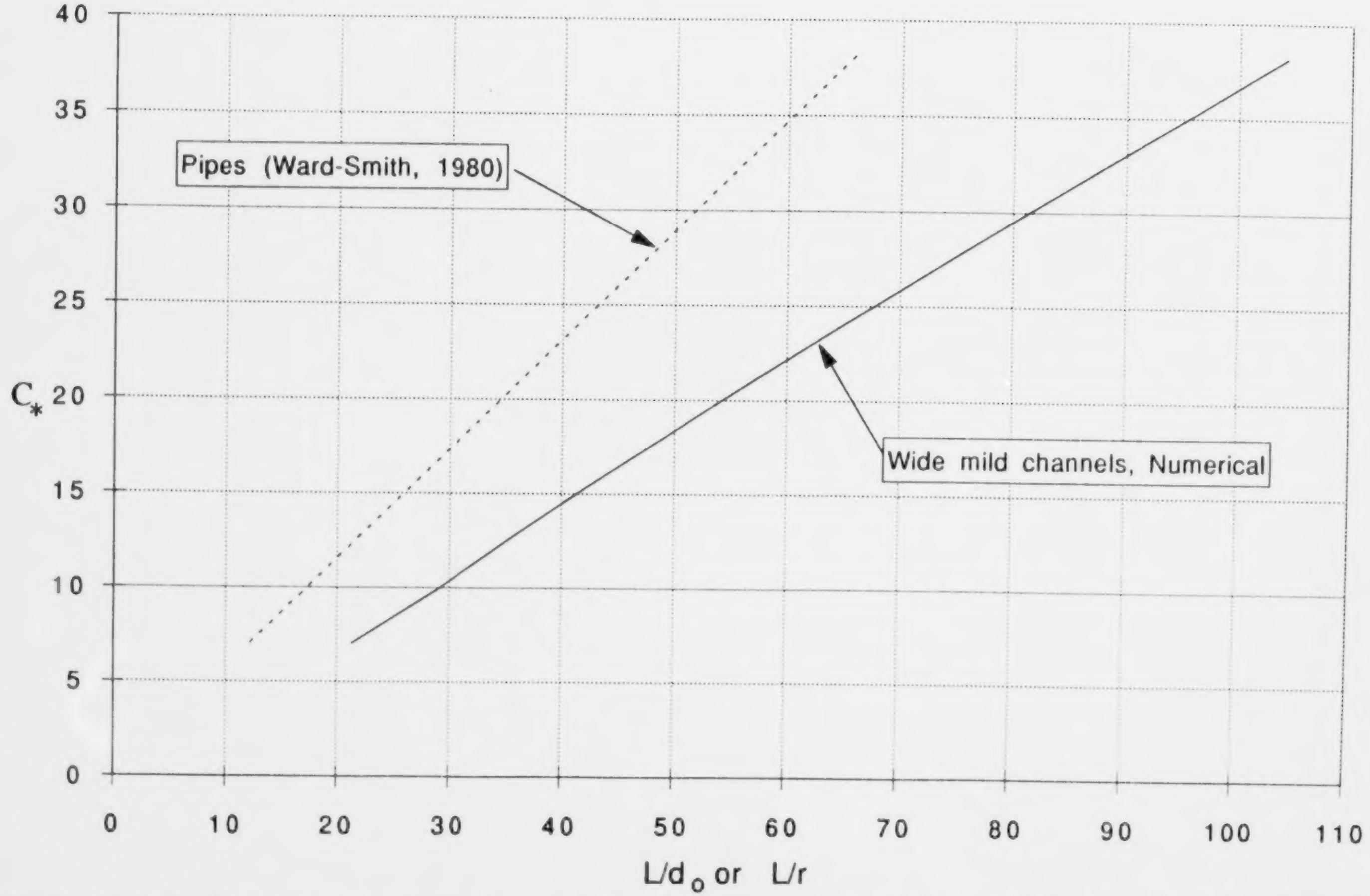

Fig. 4.31a Comparison of dimensionless entrance length as a function of the fully developed C$*$ between the numerical solution for a wide channel and pipe flow entrance lengths by Ward-Smith (1980). Pipe entrance length non dimesionalysed by the pipe radius.

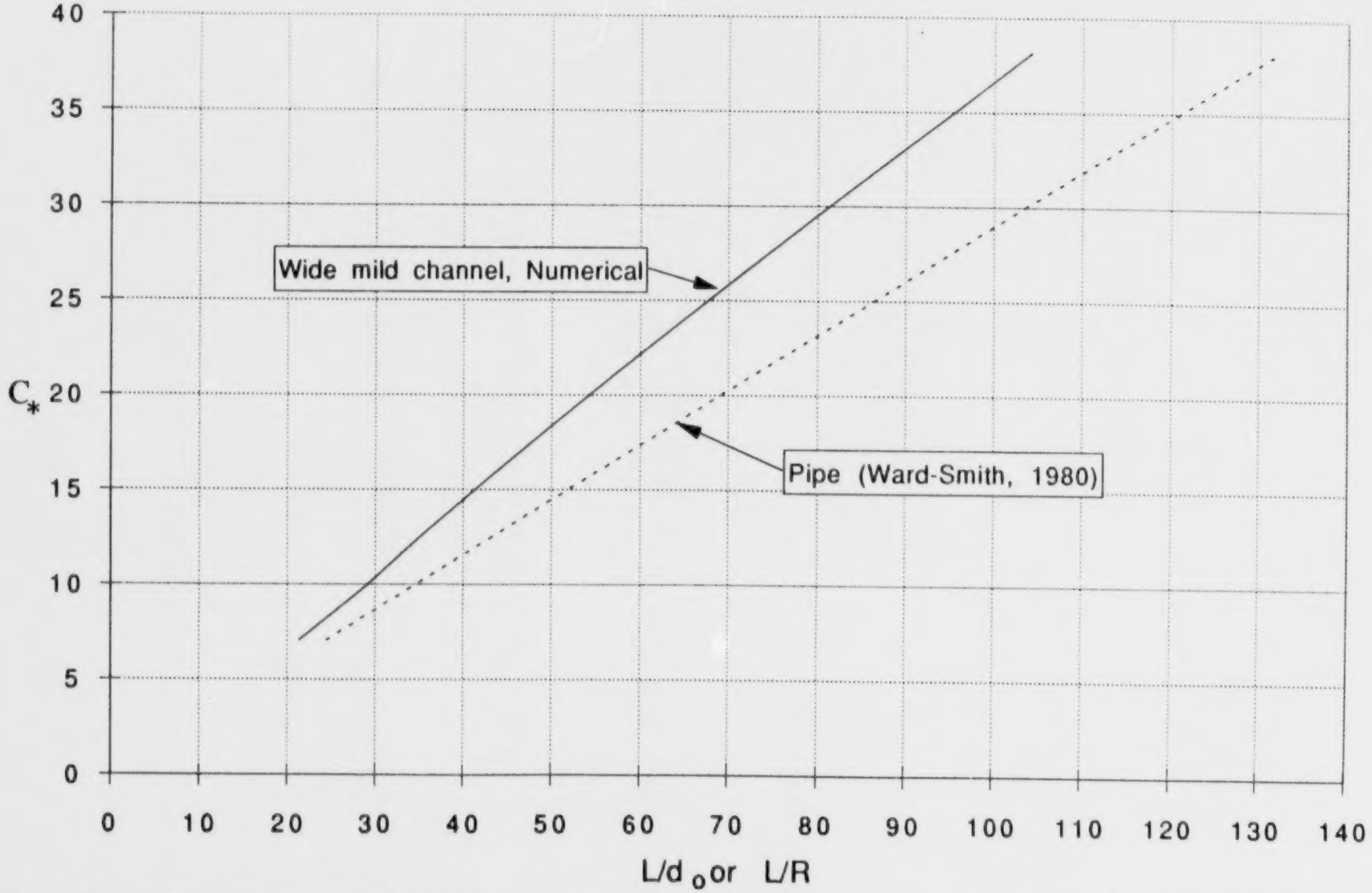

Fig. 4.31b Comparison of dimensionless entrance length as a function of the fully developed C_* between the numerical solution for a wide channel and pipe flow entrance lengths by Ward-Smith (1980). Pipe entrance length non dimensionalysed by the hydraulic radius.

	Run	S_o	d_i (mm)	$d_i - d_{end}$ (mm)	$\frac{U_i}{U_{end}}$	L/d_{end}	$\leftarrow$ % diff from $1\ S_o$
Smooth	$0\ S_o$	0	107.1	2.3	0.860	61.21	3.2
$q = 0.038\ m^3/s$	$1\ S_o$	0.00027	105.2	0.3	0.875	59.32	0
$k_s = 0$ $d_{end} = 104.9$ mm	$2\ S_o$	0.00054	103.4	-1.5	0.891	57.56	-3.0
Rough	$0\ S_o$	0	112.9	4.4	0.754	30.25	8.4
$q = 0.036\ m^3/s$	$1\ S_o$	0.00115	109.0	0.5	0.783	27.90	0
$k_s = 30$ mm $d_{end} = 108.5$ mm	$2\ S_o$	0.00230	105.5	-3.0	0.811	25.90	-7.2

Table 4.5 Summary of numerical runs to simulate inaccurate bed slope and tailgate matching.

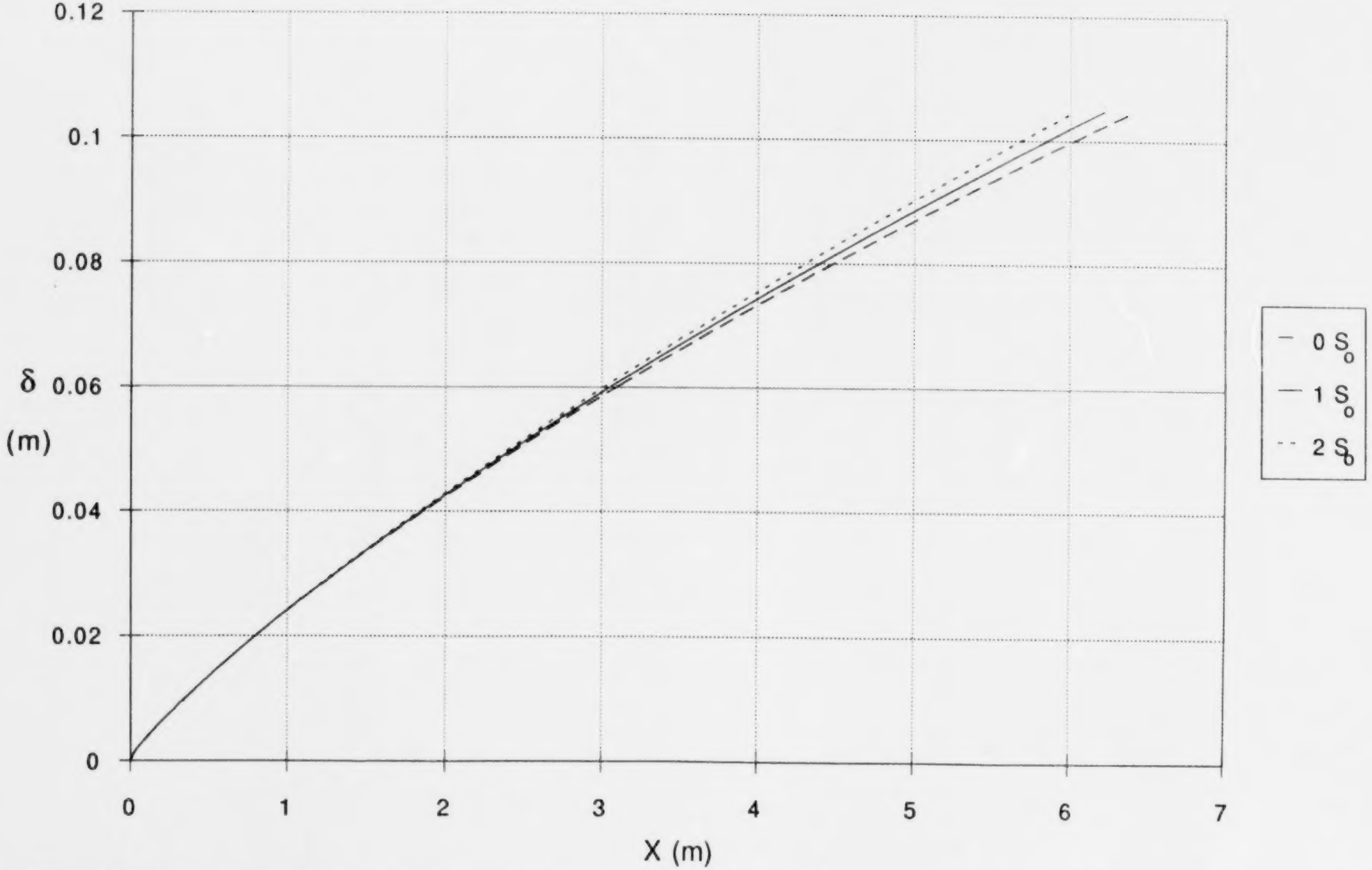

Fig. 4.32 The effect of inaccurate bed slope and tailgate matching on the growth of a boundary layer in a *smooth channel.*

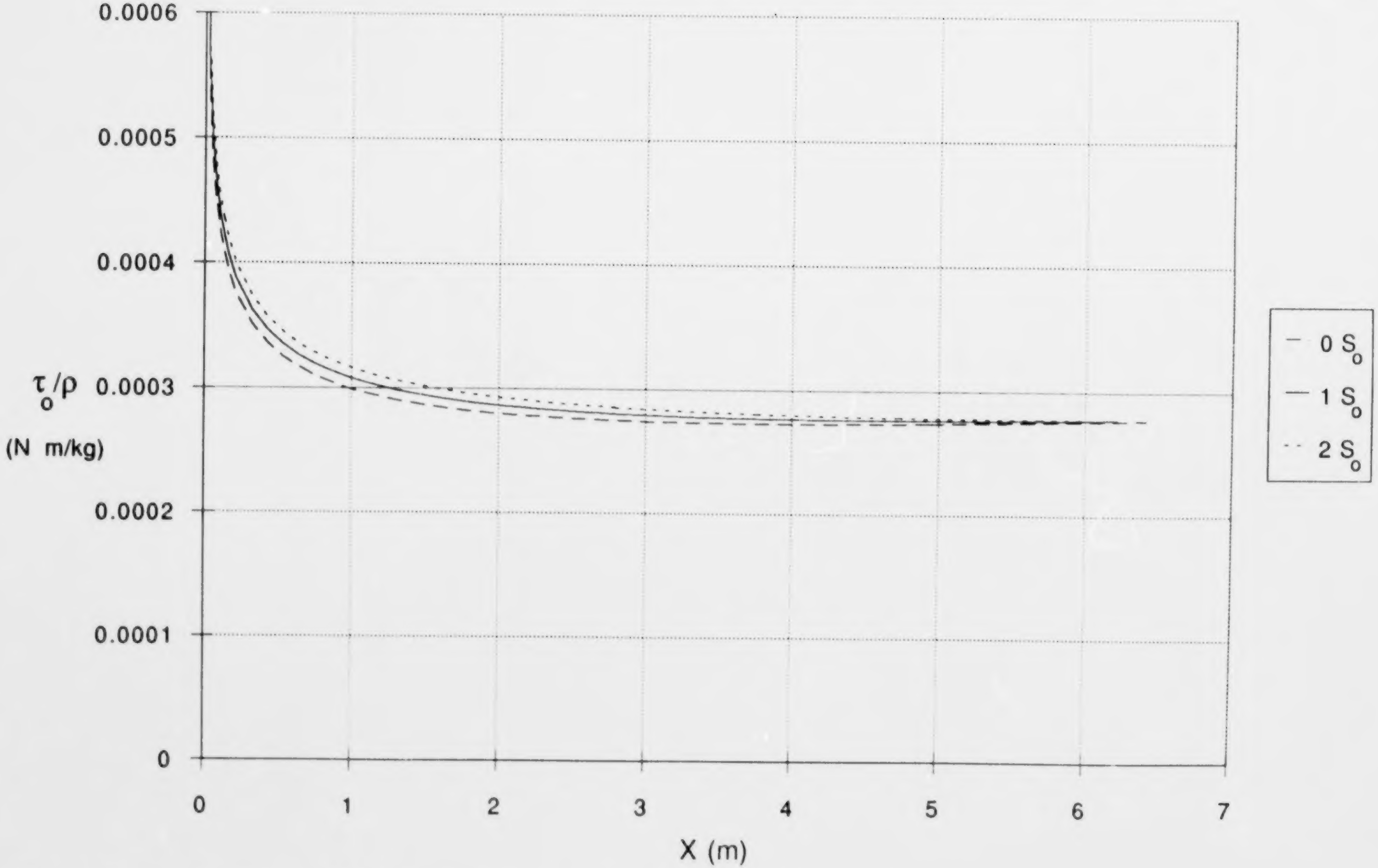

Fig. 4.33 The effect of inaccurate bed slope and tailgate matching on the bed shear stress in the entrance region of a *smooth channel.*

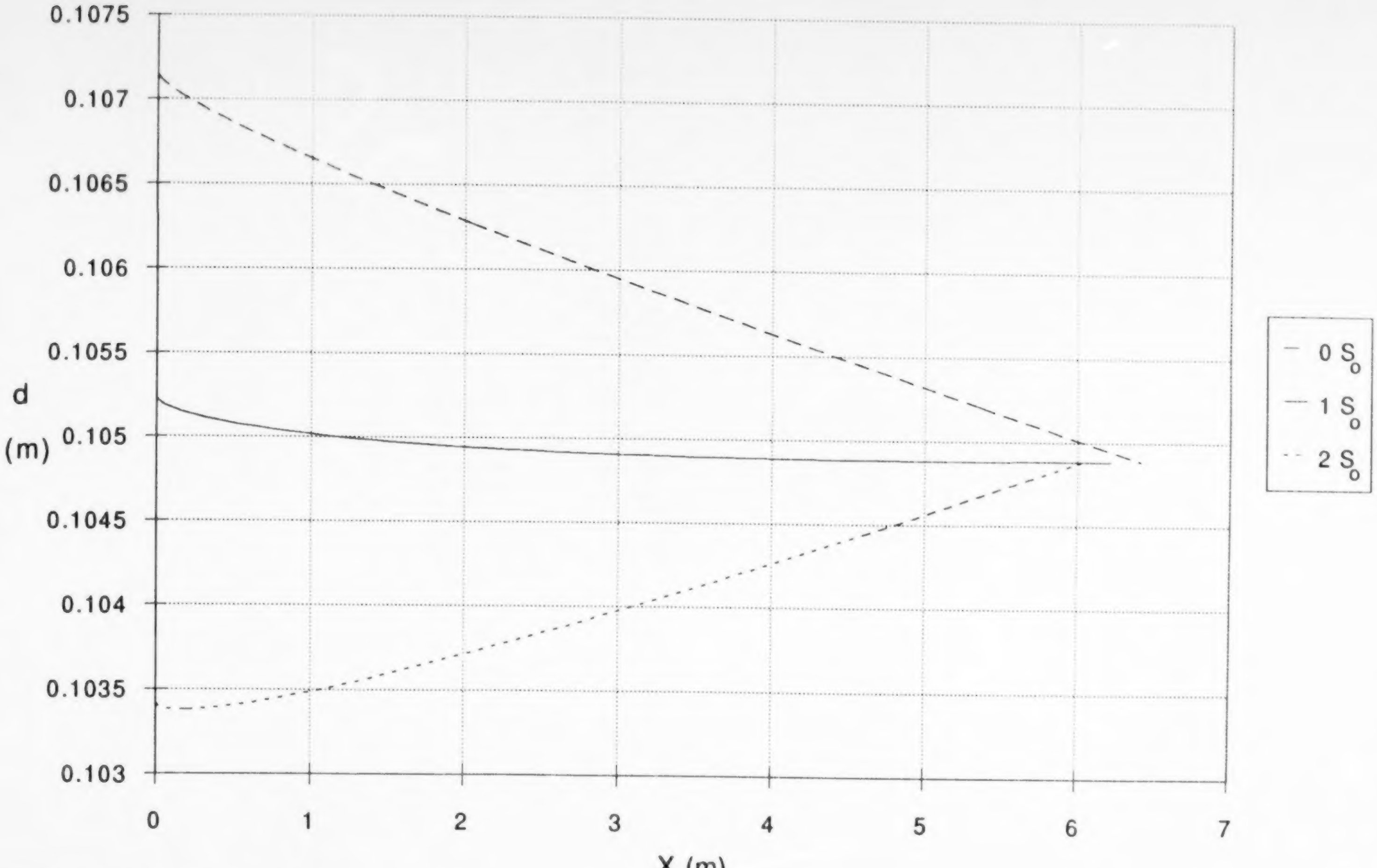

Fig. 4.34 The effect of inaccurate bed slope and tailgate matching on the depth of flow in the entrance region of a *smooth channel*.

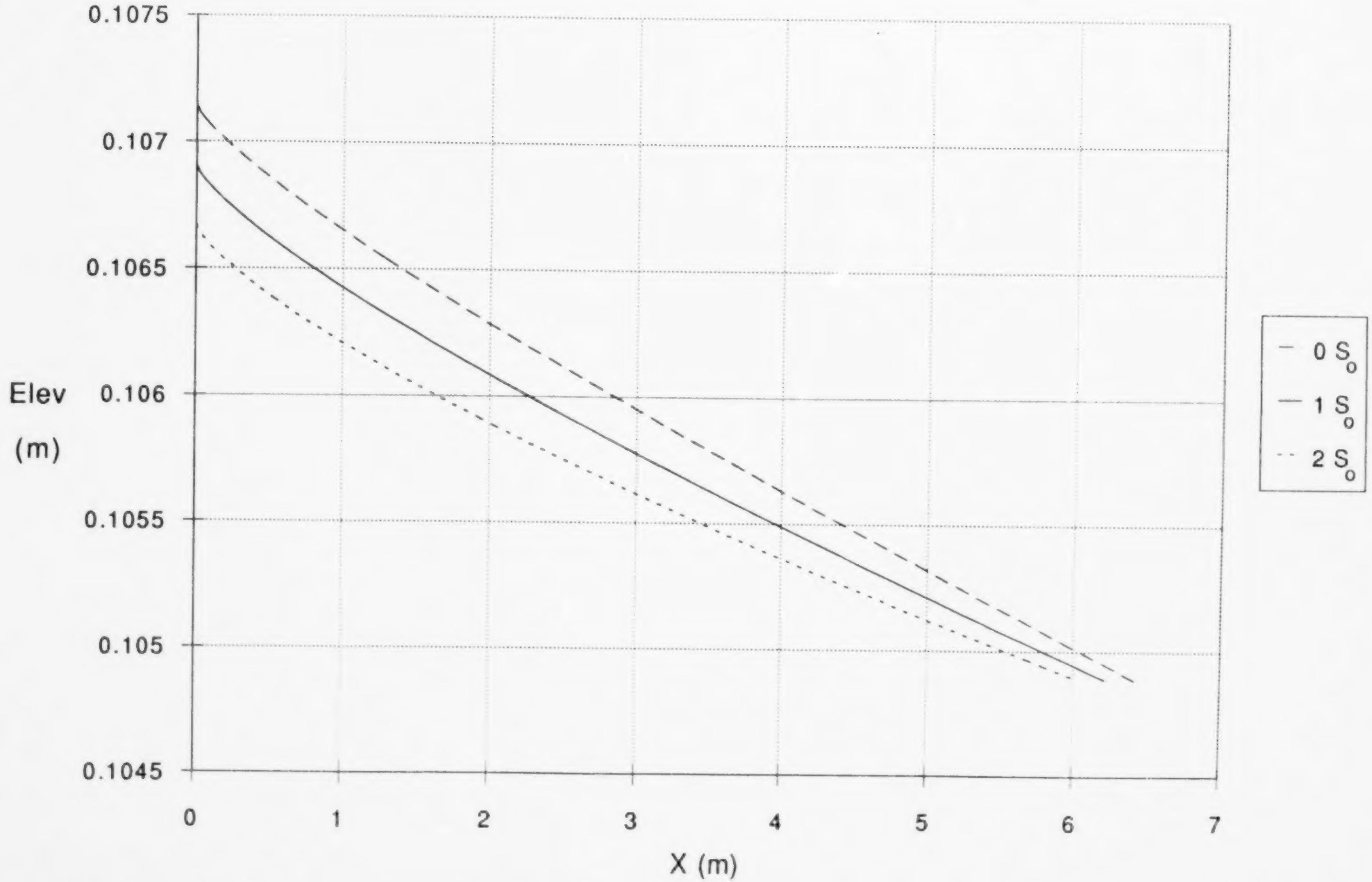

Fig. 4.35 The effect of inaccurate bed slope and tailgate matching on the water surface elevation in the entrance region of a *smooth channel*.

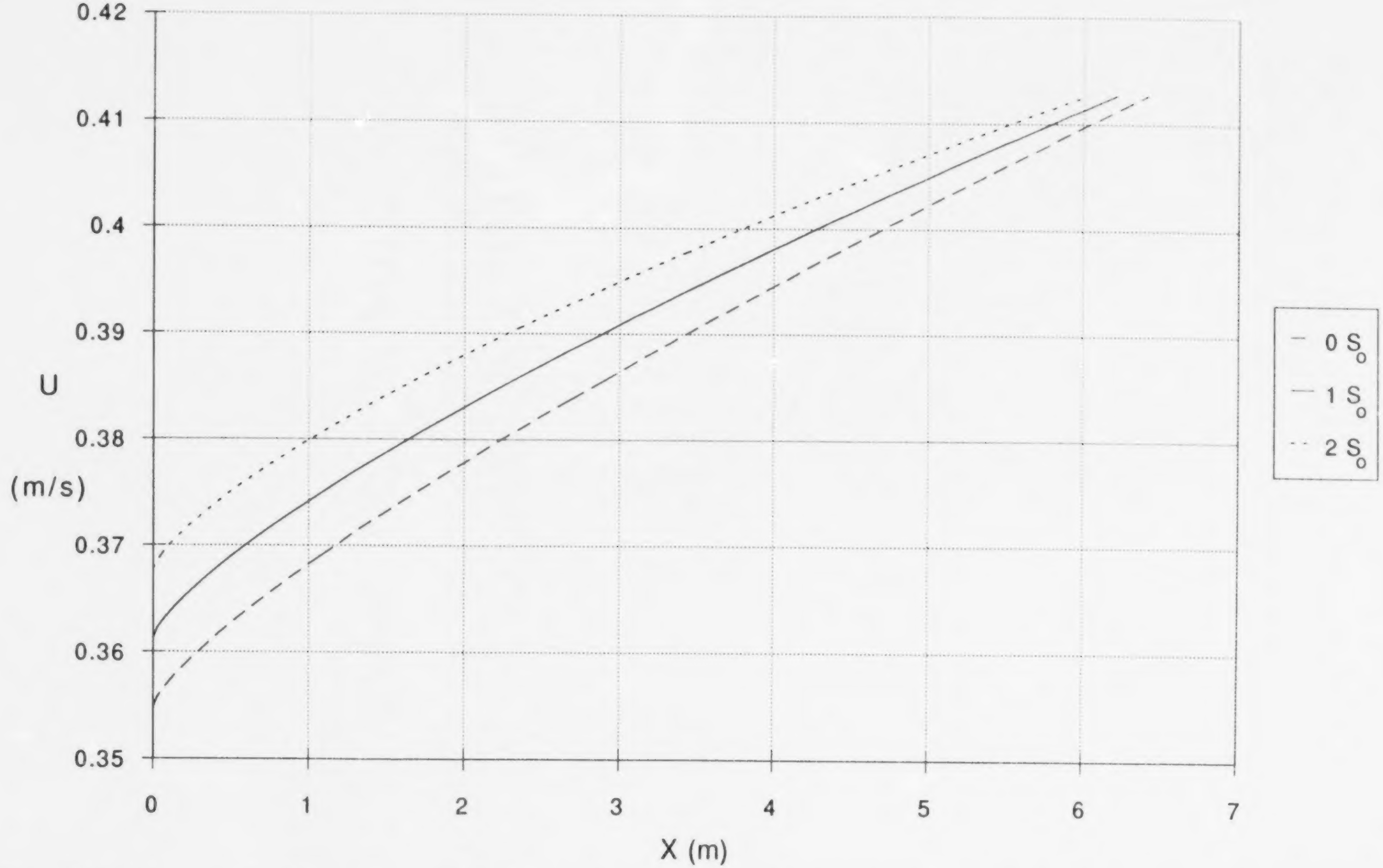

Fig. 4.36 The effect of inaccurate bed slope and tailgate matching on the potential core velocity in the entrance region of a *smooth channel*.

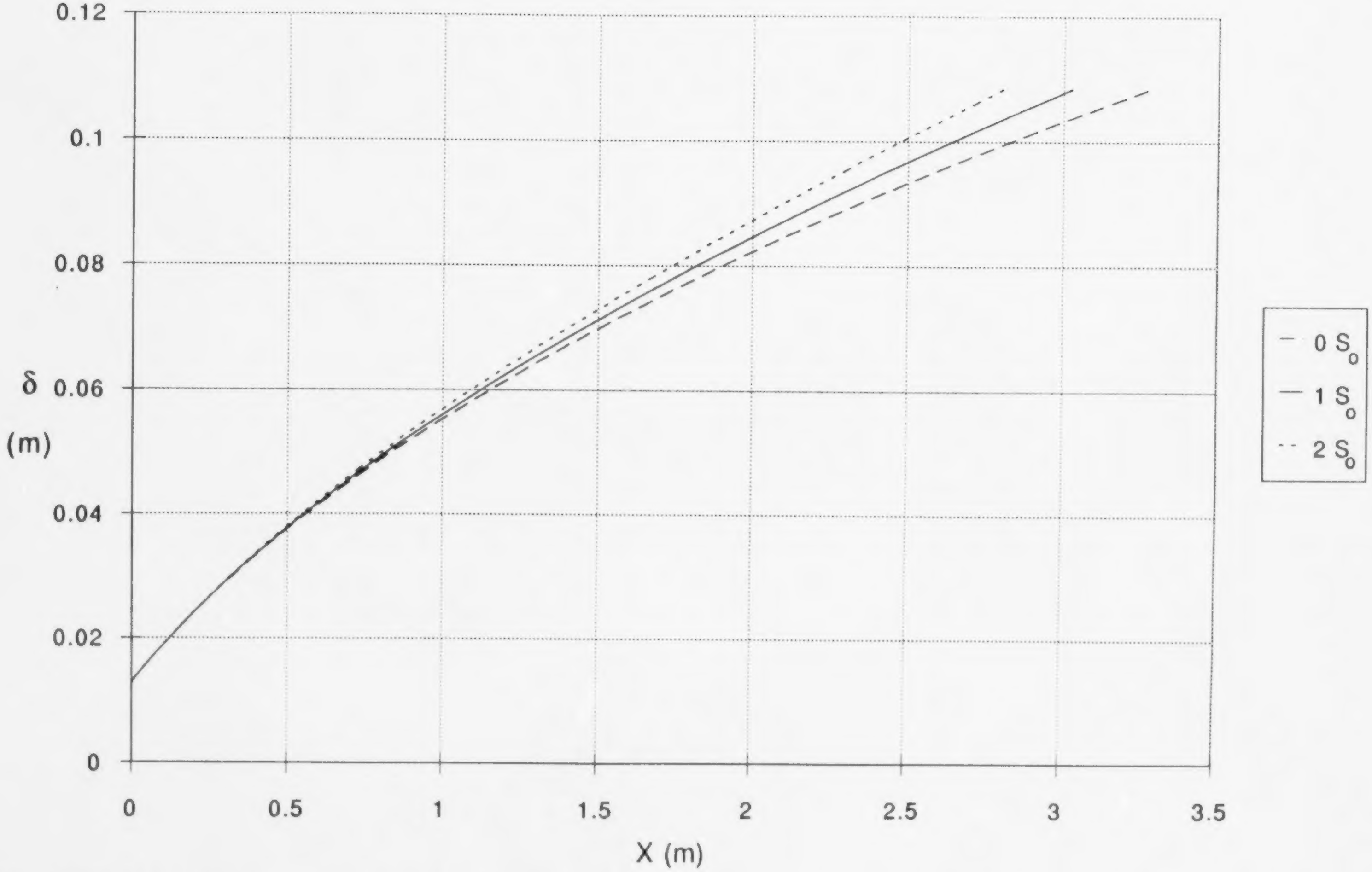

Fig. 4.37 The effect of inaccurate bed slope and tailgate matching on the growth of a boundary layer in a *rough channel.*

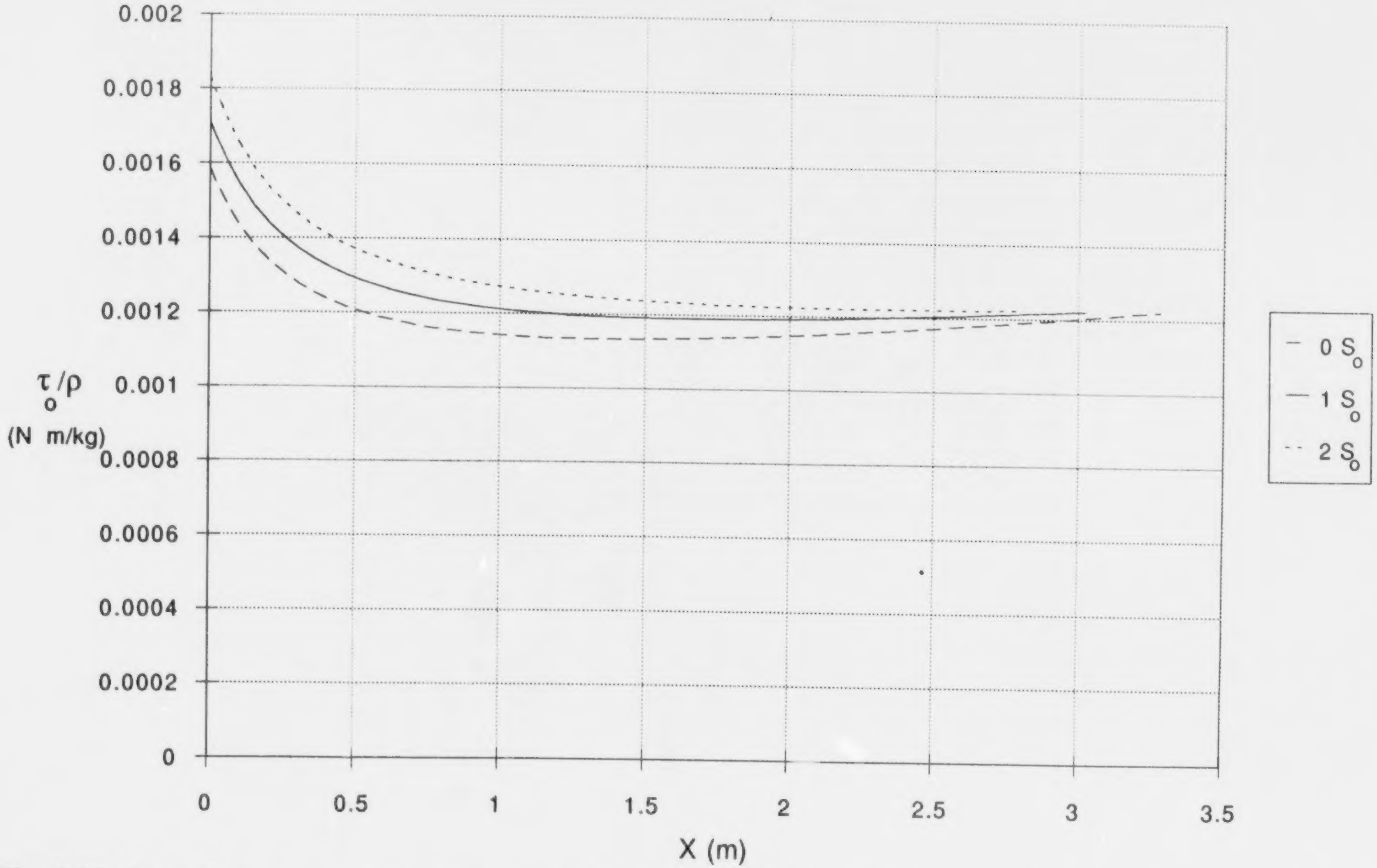

Fig. 4.38 The effect of inaccurate bed slope and tailgate matching on the bed shear stress in the entrance region of a *rough channel*.

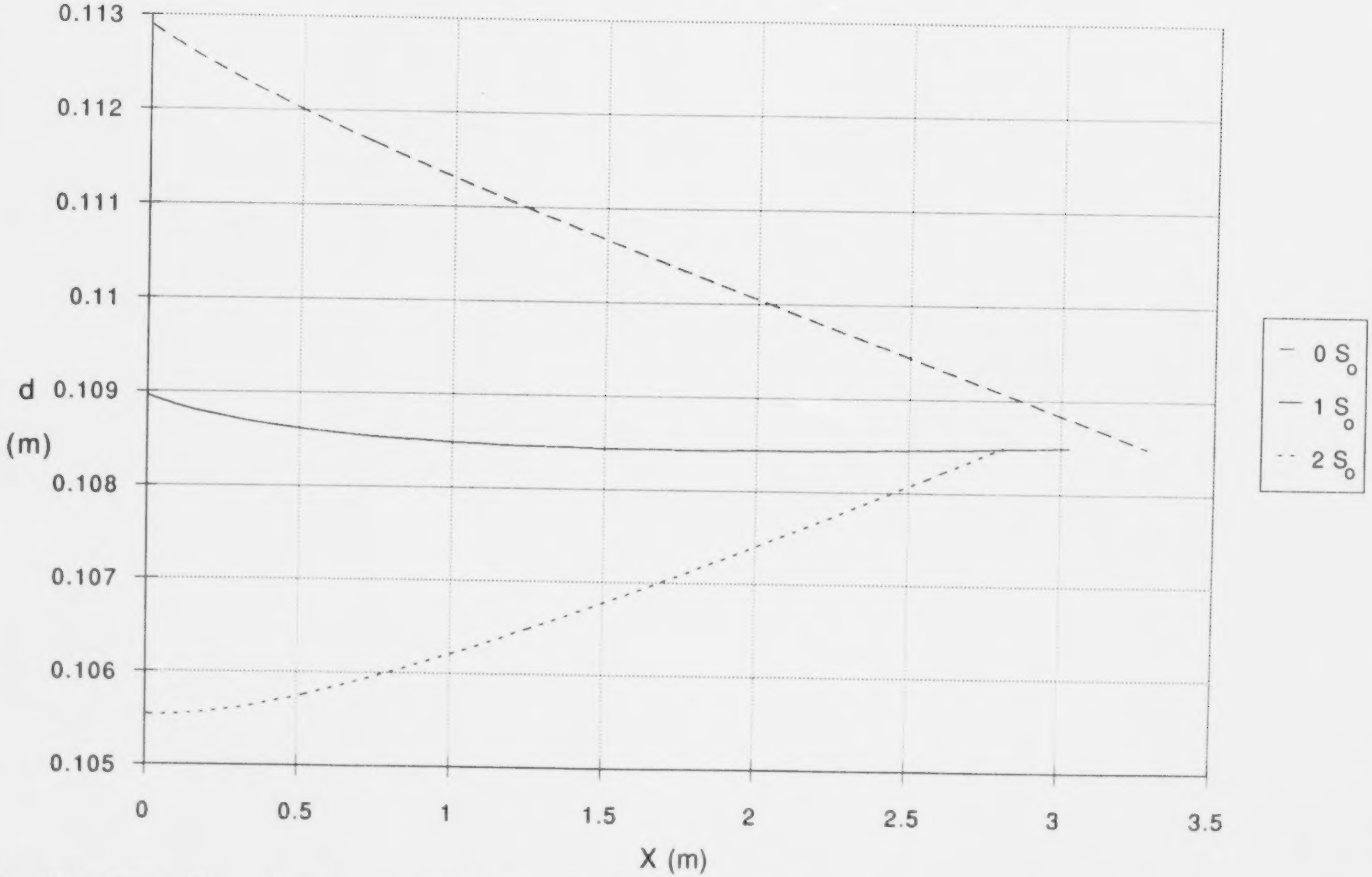

Fig. 4.39 The effect of inaccurate bed slope and tailgate matching on the depth of flow in the entrance region of a *rough channel.*

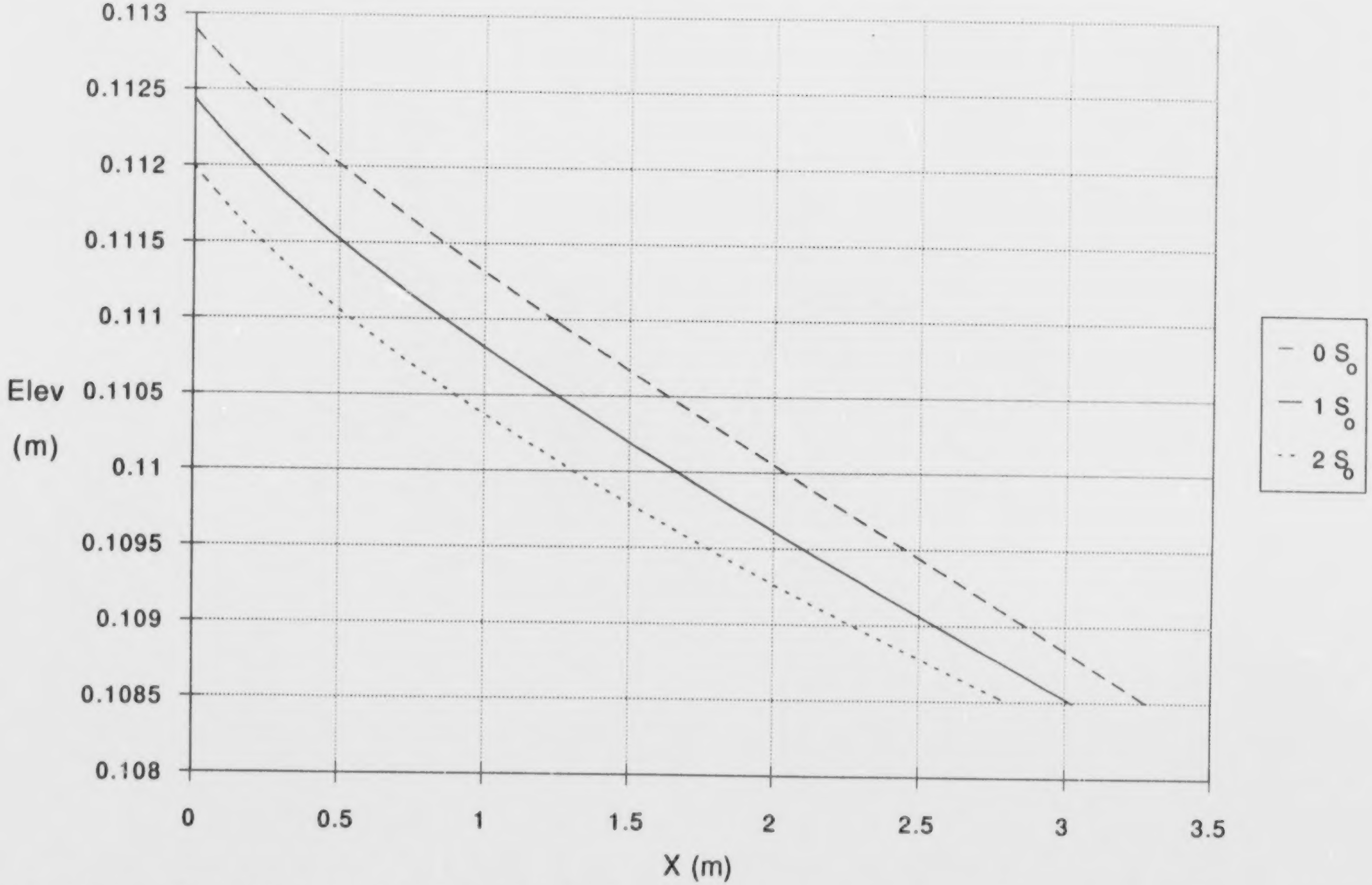

Fig. 4.40 The effect of inaccurate bed slope and tailgate matching on the water surface elevation in the entrance region of a *rough channel*.

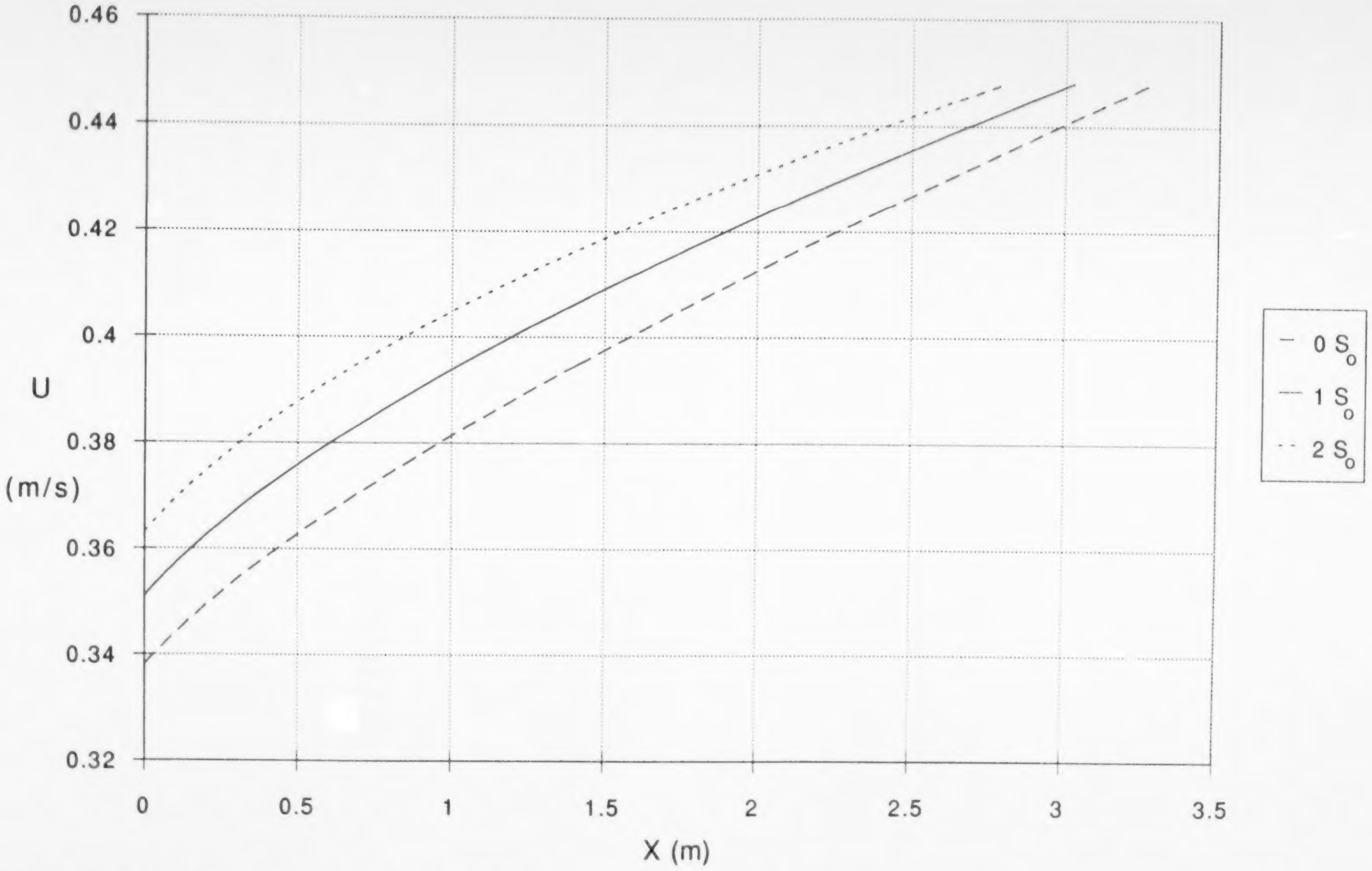

Fig. 4.41 The effect of inaccurate bed slope and tailgate matching on the potential core velocity in the entrance region of a *rough channel*.

5. Numerical solutions and results for steep channels

5.1 Solution technique

The supercritical case involved the solution of Equations 1.5, 1.13, 1.14, 3.8, 3.2, 3.7, and 3.15, with the descritized form of Equations 1.5, 1.13, 1.14, 3.8 combined being the same as the subcritical case; Equation. 4.1.

The solution technique was as follows: In this case all equations could be solved by the step method moving downstream. First d and n were held constant and δ was solved for by Equations 1.5, 1.13, 1.14, 3.8, 3.2 for one step. Then d was solved for by Equations 3.2 and 3.4 for one step. Then n was solved for by Equation 3.7 for one step. Then δ was solved for again and the iteration cycle continued until all unknowns converged for the next node. Then the unknowns could be solved for the next step. This continued until δ was equal to d.

5.2 Further consideration of the upstream boundary condition.

The upstream boundary condition or depth is very difficult to define since it depends on the weir-crest geometry. This is further complicated by non-hydrostatic pressure distributions and possible boundary layer separation if the crest of the spillway is not streamlined enough. The flow usually goes through critical depth somewhere near the spillway crest but the initial depth can also be controlled by a sluice gate.

A simplification was made for establishing the upstream boundary condition for the case of a free overflow spillway. This was justified by the relative shortness of the spillway crest when compared with the long boundary layer development region. It will be further justified by showing how the development length varies with the initial depth.

It was assumed that the flow at the crest of the spillway went through the critical depth y_c in the vertical, as shown in Figure 5.1. Assuming that the discharge is known from some weir discharge relation, the depth y_c can be calculated from:

$$y_c = \left(\frac{q^2}{g}\right)^{\frac{1}{3}} \tag{5.1}$$

Assuming that the potential core velocity is constant through this vertical and the boundary layer thickness is very small, using continuity we obtain an expression for this potential core velocity U_c:

$$U_c = \frac{q}{y_c} \tag{5.2}$$

Now for our upstream boundary condition, we are interested in an initial depth d_i measured in the perpendicular direction to the spillway face. The potential core velocity corresponding to this depth becomes:

$$U_i = \frac{q}{d_i} \tag{5.3}$$

Now suppose we write the Bernoulli between the two points shown on the water surface in Figure 5.1:

$$y_c + \frac{U_c^2}{2g} = d_i \cos \phi + \frac{U_i^2}{2g} \tag{5.4}$$

Substituting Equation 5.1, 5.2 and 5.3 into 5.4 we obtain:

$$d_i \cos \phi + \frac{q^2}{2g\, d_i^2} = \frac{3}{2}\left(\frac{q^2}{g}\right)^{\frac{1}{3}} \tag{5.5}$$

We can now solve Equation 5.5 for our upstream boundary condition or initial depth d_i.

Equation 5.5 casts some doubt since non-hydrostatic pressure distributions have been neglected. However, if the non-hydrostatic pressure distributions were carefully determined and the actual initial depth d_i was found, a problem would still remain. Since the equations for the boundary layer and water surface calculation assume a hydrostatic pressure distribution, it would be wrong to incorporate only this initial depth without the effect of the non-hydrostatic pressure distribution.

Before getting caught up further in the details of flow over a weir (a subject in itself), let us look at the effect of the initial depth on the boundary layer growth and entrance length using the solution from the numerical model. For one discharge, spillway slope, and bed roughness, a series of runs was performed for different initial upstream depths. The depth and boundary layer thickness for these runs is shown in Figure 5.2. The initial depth upstream was scaled by the normal depth d_o. It can be seen from Figure 5.2 that the entrance length increases with an increase in the initial depth but changes very slightly for $5 < d_i/d_o < 8.421$. For d_i/d_o of 5.955, d_i was determined by Equation 5.5. For $d_i/d_o = 5$ which is 16% less than that given by Equation 5.5, the entrance length is only 1.6% shorter. For $d_i/d_o = 8.421$ which is 40% greater than that given by Equation 5.5, the entrance length is only 1.4% longer. For a more detailed relation on the effect of initial depth on the entrance length for different channel bed slopes and bed roughnesses see Section 5.9. It can be seen from the above and Section 5.9 that the calculation of the initial depth does not have to be very accurate. It was therefore decided that Equation 5.5 was accurate enough to calculate the initial depth for a free overflow spillway. From hereafter (except for solutions in Section 5.9) the initial depth will be calculated using Equation 5.5. In Section 5.9 the initial depth is controlled by a sluice gate so the depth does not pass through critical in the vertical.

Let us look further at the numerical results of the above runs which investigate the effect of the initial depth on the entrance region. Figure 5.3 shows the bed shear stress for the different runs. It shows that the bed shear stress increases with a lowering of the initial depth. This is attributed to the higher velocities. Also notice that for $d_i/d_o = 1$, the shear stress distribution is very similar to the subcritical numerical solution. Figure 5.4 shows the water surface near the channel entrance plotted to actual scale and orientation for the different runs. It also shows the vertical depth y_c. One purpose of this figure is to give a feeling for curvatures in the flow likely to be encountered near the crest of the spillway. As can be seen for $d_i/d_o = 5.955$(d_i calculated by Eqn. 5.5), the curvature is relatively small. The second purpose is to see which initial depth would be visually consistent to someone who is familiar with the shape of the water surface near the crest of a spillway. Assuming the water surface goes through y_c right at the crest, $d_i/d_o = 5.955$ looks like a good candidate.

Figure 5.5 shows an undistorted plot of the water surface, boundary layer thickness, and channel bed in the entire entrance region. Its purpose is to give a feel how thin the actual flow is and how slowly the boundary layer grows.

5.3 Some examples of the numerical solution

Since the discharge, channel bed slope, and bed roughness also influences the normal depth(the length scale used for non-dimesionalizing later), it is helpful to look at some numerical runs before the non-dimesionalization is performed. This is presented here to show the effect of these three variables in a qualitative way.

5.3.1 Effect of discharge

Two sets of runs, both covering two orders of magnitude were performed for this investigation. One for a smooth bed and one for a rough bed.

Figure 5.6 shows the water surface and the boundary layer thickness in a smooth channel for 5 different discharges covering two orders of magnitude. Fig 5.7 is a magnified portion of Figure 5.6. Note the increase in boundary layer growth with increasing discharge. This disagrees with Bauer (1954). He found that the boundary layer growth was independent of discharge and therefore assumed that the same rate of growth could be inferred onto a real spillway from his laboratory experiments. The discharge range for his smooth experiment was $0.073 < q < 0.342$ m^2/s, about a 1/2 an order of magnitude. It was therefore difficult for him to discern a significant difference between boundary layer growth from the small range of discharges used in his experiment.

Figure 5.8 shows the water surface and the boundary layer thickness in a rough channel for 5 different discharges covering two orders of magnitude. Fig 5.9 is a magnified portion of Figure 5.8. Again an increase in the boundary layer growth with an increase in discharge was found. Bauer found for one roughness the rate of boundary layer growth was independent of discharge. Since his roughness was typical of concrete, he used his experiments to predict the critical point on spillways. His discharge range for his rough experiments was only 0.116

$< q < 0.342$ m^2/s. Figures 5.8 and 5.9 show it would not be very accurate to use such a small discharge to predict the boundary layer growth on a large spillway.

5.3.2 Effect of channel bed slope

Figure 5.10 shows the water surface and boundary layer growth for the same discharge and a smooth bed but different channel bed slopes. Notice that the boundary layer growth rate decreases with an increase in channel bed slope. This is due to the higher favorable pressure gradient or a higher acceleration of the potential core associated with higher bed slopes. However, notice that the entrance length decreases with an increase in channel bed slope. This is due to the rapid fall or decrease in the water surface associated with large channel bed slopes; even though the boundary layer is growing more slowly, the water depth decreases so rapidly that the boundary layer does not have to grow to a great thickness before it reaches the water surface.

Note in Figure 5.10 that the boundary layer growth rate does not vary significantly between the larger slopes of 20°, 45°, and 70°. This may have led Bauer (1954) to conclude from his experiment on channels of 20°, 40°, and 60° that the boundary layer growth rate was independent of slope.

There is some uncertainty on how the bed shear stress might vary along the length of the spillway since there are two opposing effects. On one hand, the boundary layer is getting thicker as the distance down the spillway increases, thereby decreasing the shear stress. On the other hand, the potential core is accelerating thereby increasing the shear stress. Figure 5.11 shows the bed shear stress associated with the runs of Figure 5.10. It is apparent that the acceleration of the potential core has a more significant effect on the bed shear than the growth of the boundary layer; this is true for slopes greater than about 1°. Figure 5.12 shows a magnified portion of Figure 5.11 near the channel entrance. Figure 5.12 shows that for the runs ranging from 1° - 70°, that the boundary layer effect on the bed shear is only apparent in the first 0.5 to 1 depth near the channel entrance. To see the overall variation of bed shear stress as a function of channel bed slope, Figure 5.13 was constructed. The bed shear stress in Figure 5.13 is non-dimensionalized by bed shear when the boundary layer reaches the surface and the distance x is non-dimensionalized by the development length L. Also included in this figure is the bed shear stress development for a subcritical channel. It can be seen in this figure that the boundary layer thickness plays a more important role on the bed shear stress distribution in mild channels and steep channels with small bed slopes.

5.3.3 Effect of channel bed roughness

Figure 5.14 shows the variation of water surface and boundary layer thickness for the same discharge and channel bed slope but for different bed roughnesses. As expected, the boundary layer growth is more rapid for a higher roughness and the entrance length decreases with an increase in bed roughness. Note also how the water surface is effected by the higher bed roughness; the water surface decreases somewhat slower for higher bed roughnesses. This is attributed to the higher displacement thickness attributed to rougher surfaces. Figure 5.15 shows the higher bed shear stress associated with the higher bed roughness for a given slope and discharge.

5.4 Comparison to measurements conducted by Bauer (1954)

Bauer performed 11 experiments where he obtained velocity profiles down the centerline of steep channels to measure the growth of the boundary layer. He varied the channel bed slope, discharge, and used a smooth glass bed and a rough wire mesh bed. He published complete velocity profiles for only two of his runs. Both runs were for a discharge of 0.342 m^2/s and a channel bed slope of 40°. One was for a smooth glass bed and the other was for a wire mesh bed. The numerical solution developed in this study will be compared to these two runs.

5.4.1 Bauer's smooth experiment

Figure 5.16 contains Bauer's velocity profiles for his smooth experiment. Bauer did not publish the depths for each velocity profile and stopped taking velocity measurements once he was well out of the boundary layer. However, with the discharge being known and if it is assumed that the same potential core velocity exists all the way to the surface, then the total depth at each profile can be calculated using continuity. This depth along with the boundary layer thickness is shown in Figure 5.17. Figure 5.17 shows a good agreement in boundary layer growth and the water surface profile between the numerical solution and Bauer's experimental data.

Figure 5.18 shows the experimental and potential core velocities and shows an excellent agreement between the two.

The shear stress was calculated from the velocity profiles plotted on a semi-log plot. Equation 2.2 was used:

$$\frac{u}{u_*} = 2.5 \ln\left[\frac{y\,u_*}{\nu}\right] + 5.5 \qquad (2.2)$$

The slope of the lower 30% of the velocity profile was used to determine u_*. The numerical and experimental shear stress are plotted in Figure 5.19; the agreement between the two is good.

A power law least squares fit was performed on the velocity profiles and the power law exponent compared to the numerical in Figure 5.20. It shows reasonable agreement. The experimental power law exponent ranged from 1/6.9 to 1/8.3.

The displacement and momentum thickness was calculated for each velocity profile and compared to the numerical solution in Figure 5.21. The numerical momentum thickness agrees well but the displacement thickness is a bit low. This suggests that a power law fit does not exactly match the velocity profiles. There are some arguments that the fully developed velocity profile in steep channels is not the same as in mild channels. (See Tominaga and Nezu, 1991 or 1992)

5.4.2 Bauer's rough experiment

Before a numerical simulation of Bauer's rough experiment could be performed, the roughness of his wire mesh was needed. As there was some dispute by other authors reviewing Bauer's paper on the value of k_s for his rough channel, it was decided to independently calculate the roughness from his velocity profiles. Bauer's semi-logarthmic fit gave a $k_s = 0.00064$ m, his subcritical uniform flow experiments gave him $k_s = 0.0027$ m, and a review by HalBrann (1955) gave a $k_s = 0.00016$ m.

An attempt was made to follow the same method used in Section 2.2 based on choosing a value of y_d to give the best regression coefficient for a semi-log fit to the bottom 30% of the boundary layer thickness, using the relation:

$$\frac{u}{u_*} = 2.5 \ln\left[\frac{y + y_d}{k_s}\right] + 8.5 \qquad (2.3)$$

This was not as successful as in Section 2.2 since it yielded an average value of y_d that would put the zero velocity point 1.1 mm below the midpoint of his 0.5 mm thick wire mesh, or 0.75 mm below the glass bed on which the mesh was resting on. It was noticed that the wake function is more strongly apparent in Bauer's velocity profiles than in the wake function of velocity profiles in subcritical flows measured in Section 2.2. This stronger wake function portion of the velocity profile may have had some effect on the regression performed. The roughness had to be determined differently.

Bauer's mesh was made of 0.26 mm dia. wire inter-twined to give a total mesh thickness of 0.52 mm. His datum for his velocity profiles was at the midpoint of this mesh. Since the zero velocity plane should be around this point and not 1 mm below it, it was decided to assume the same zero datum as Bauer's, therefore y_d would be chosen as 0.0. Once y_d is fixed it than becomes apparent which data points belong to the wake function and which ones to the logarithmic portion. The data points taken closest to the bed also stand out as poor fits since pitot tube measurements near a boundary have some error due to the shifting of the stagnation point on the tip of the pitot tube toward the boundary. We can now neglect these points and the ones in the wake function visually to obtain a proper semilogarthmic curve fit. This is illustrated in Figure 5.23 where all of Bauer's rough profiles are plotted. A polygon is drawn around the data points on which the regressions were performed. From the slope of these lines, the shear velocity u_* can be calculated and from the y intercept the roughness k_s determined. The average k_s found was 0.00082 m with a standard deviation of 0.00018 m. The average value of k_s is very close to what Bauer obtained from his semilog plots.

Now that the roughness is known, the experiment can be simulated numerically. Figure 5.24 shows the boundary layer thickness and water surface profile and shows good agreement between the experimental data and the numerical solution. The numerical boundary layer growth is slightly higher.

Figure 5.25 shows that the numerical potential core velocity is in excellant agreement with the experimental values.

When the roughness was being determined from Bauer's velocity profiles, the shear velocity u_* was obtained from the slope of the semi-log plots. u_* was converted to τ_o/ρ and plotted along with the numerical results in Figure 5.26. The numerical shear stress was slightly higher than the experimental. Considering the difficulty in obtaining the proper values of y_d and k_s, the results are not too bad.

Figure 5.27 shows the power law exponent n obtained by regression along with the numerical solution. The experimental power law exponent ranged between 1/4.3 to 1/4.8. and compared reasonably with numerical solution.

The displacement and momentum thickness was calculated for each velocity profile and compared to the numerical solution in Figure 5.28. The numerical momentum thickness agrees well but the displacement thickness is a bit low. This suggests that a power law fit does not exactly match the velocity profiles. This was also the case in Bauer's smooth experiment.

5.4.3 Concluding remarks on Bauer data comparison

Based on Bauer's experimental data, the numerical model works quite well for both smooth and rough surfaces. To increase the models accuracy, more data on boundary layers on steep slopes is needed to upgrade the power law velocity profile in the numerical model to a more representative semilog relation with a wake function. This data needs to cover transverse variations as Bauer's data is not conclusive since only centreline measurements were taken. Several velocity profiles are needed to be taken in the lateral direction for each longitudinal location to average out the lateral variation due to secondary currents.

5.5 Comparison to k - ε model by Keller et al (1977)

As discussed in section 1.3.2, Keller and Rastogi developed a k - ε model to predict the development of the boundary layer on the face of a spillway. They performed 90 numerical simulations covering a wide range of discharges, spillway slopes, and roughnesses typical that of concrete. They used the results of these runs along with some dimensional analysis to come up with design curves for predicting the critical point on a spillway. Some of the Keller et al's simulations are compared with the numerical model developed in this study.

Figure 5.29 shows a series of numerical runs for one spillway roughness and different discharges where the slope was varied from 5° to

75°. The difference in entrance length between the two numerical models was about 1.5-3.7% for slopes 5° - 50° and about 6.5% for 75°. The larger difference for the 75° slope can be attributed to the higher non-hydrostatic pressure distributions at the crest of such a steep spillway. Since the k - ε model had experimental upstream depth and pressure for input, the largest difference between the two models occurred on very steep slopes where the strong curvature in flow at the crest had the most effect.

Figure 5.30 shows a series of numerical runs for one spillway slope, several discharges and different roughnesses. The difference in entrance length between the two numerical models was between 2 to 3 %. Since Keller et al were interested in concrete spillways, they did not perform any numerical runs for $k_S = 0$. This also would have further complicated their non-dimensionalization since two of their dimensionless variables used k_S in the denominator. In Figure 5.30, the numerical solution of this study shows how the entrance length varies as the roughness goes to zero. It shows that a smooth spillway of 30° would have an boundary layer development region about 30% longer than the same spillway made of concrete.

In all cases, the numerical model of this study under-predicted Keller et al's k - ε model entrance lengths slightly. But, since Keller et al found that their model slightly overpredicted the entrance lengths measured in the field, the model of this study has been evaluated as suitable for predicting the boundary layer development on spillways.

5.6 Comparison to measurements conducted by Ippen (1957)

Ippen's main concern in his investigation was to test a velocity measurement technique. He performed experiments in well understood flow situations to evaluate his instrument. In one of his investigations, he measured boundary layer thicknesses by taking velocity profiles down the centreline of a channel. He expected that the boundary layer growth rate would follow the well known Schlichting's smooth flat plate solution.

As described in Section 1.3.2, Ippen made some measurements in high velocity streams on small, steep slopes. The flow originated from a wide rectangular nozzle. The nozzle height was adjustable. The channel bed was smooth. It was apparent that he tried to match the channel bed slope to give uniform depth equal to the nozzle height, thereby avoiding the S2 and S3 backwater curve profiles. However, by putting the channel on a slope, he introduced a pressure gradient or an accelerating potential core velocity. This violated the constant potential core velocity assumption in the Schlichting's smooth flat plate theory.

Ippen never stated the channel discharge directly but left enough information in his Figure 4 to calculate it; the discharge could be determined from the potential core velocity U, the displacement thickness δ_*, and the depth d from three velocity profiles for each run. Using Equation 3.2, three different discharges were calculated for each of his runs. The variation for discharge calculated by the above method varied about 6% for each run. The three discharges were averaged and used for the numerical simulations along with the given channel bed slope .

Ippen published two experiments which he called Run B and Run C.

Ippen's Run B, the numerical solution, and Schlichting's smooth flat plate solution are shown in Figure 5.31. Figure 5.31 shows that the numerical solution agrees well with the experimental values of boundary layer thickness and water surface. However, Schlichting's smooth flat plate solution shows a higher boundary layer growth than the experiment. This difference is due to the acceleration of the potential core velocity.

Figure 5.32 shows Ippen's experimental Run C, two numerical solutions, and Schlichting's smooth flat plate solution. Numerical simulation 1 used a channel bed slope presented in Ippen's paper, but the increasing water depth with the distance x could not be duplicated by the numerical solution unless a smaller value of bed slope was used. A smaller bed slope was used in numerical simulation 2. The second simulation not only matched the water surface more accurately but also provided a closer matching boundary layer growth to the experimental points.

It is unclear why the numerical solution provided a better simulation in Run B than in Run C. One reason may be that Ippen never measured the boundary layer growth across the width of the channel to average out the effect of secondary currents. Another reason may be that he expected a boundary layer growth rate which matches the Schlichting's smooth flat plate solution. Therefore, his boundary layer growth rate may be slightly biased toward the higher growth rate of the Schlichting Solution.

5.7 Comparison to S2 type gradually varied flow profiles

In backwater curve calculations, it is assumed that the shear stress or friction slope S_f is given by the same relations as in uniform flow. That is, for a given depth, discharge, and bed roughness the same resistance relations apply as if the depth was normal depth. This is a very good approximation since backwater curves are usually gradual in nature so the velocity profiles and turbulence likely have adequate time to adjust to a quasi uniform state. However, if there happens to be a developing boundary layer within a backwater curve, the bed shear or friction slope could be substantially different than if the boundary layer was equal to the depth of flow. It is therefore of interest to investigate the effect of the boundary layer on a backwater curve profile.

The most common occurrences of boundary layers within backwater curves are spillways and sluice gates. This includes the S2, S3, M3, and H2 backwater curve profiles. This investigation only deals with the S2 backwater curve profile.

A gradual varied flow calculation was performed by using the standard step method outlined in Henderson (1966). The flow resistance relation used in the standard step method was given by the dimensionless Chezy relation:

$$\frac{V}{u_*} = 2.5 \ln\left(\frac{12\,d}{k_s + \frac{3.3\,\nu}{u_*}}\right) \tag{5.6}$$

$$u_* = \sqrt{g\,d\,S_f} \tag{5.7}$$

To compare the backwater curve to the water surface profile of the numerical solution, the same initial upstream depth, discharge, spillway slope and bed roughness was used in each comparison. It was of interest to find out under what conditions did the boundary layer make the most difference; would the largest difference occur on a rough channel or a smooth channel, or would the largest difference occur on a very steep channel or a not so steep channel? Four comparisons in all were performed; a smooth and rough channel for a channel slope of 1° and a smooth and rough channel for a channel slope of 45°. The bed shear was also compared in each comparison. The four comparisons are summarized in the following table:

Run #	Uniform flow C_*	ϕ (degrees)	Figure# for depth comparison	Maximum difference in depth %	Figure# for bed shear comparison
1	12.7	1°	5.33a	5.6	5.33b
2	29.7	1°	5.34a	1.3	5.34b
3	12.7	45°	5.35a	3.8	5.35b
4	29.7	45°	5.36a	1.8	5.36b

Table 5.1 Summary of S2 gradually varied flow profile comparisons.

It can be seen from the depth comparisons that the difference in depth between the S2 profile and the numerical solution increases with an increase in the bed roughness. It also increases with a decrease in the channel bed slope. The differences in depth were not very significant. Even for the worst case, the depth was only 5.6% higher for the numerical solution than the gradual varied flow. Runs were also performed for ϕ and C_* in between the above values and showed consistant results with the above conlsusions. These results are not shown.

As expected, the numerical solution gave a higher bed shear stress near the channel entrance than the gradually varied flow solution. This was due to the small boundary layer thickness near the channel entrance. The shear stress at the channel entrance given by the numerical solution was usually about 2 to 2.5 times the shear stress given by gradual varied flow. However, as the boundary layer grew to about 1/5th of the depth, the bed shear was within a few percent of that given by gradual varied flow.

Note: The slight undulations in the numerical solution of Figure 5.33a and 5.33b is due to the instability encountered when the Froude number is close to unity.

5.8 Non-dimensional entrance lengths for depth at spillway crest at critical

The aim of this section is to come up with design curves to determine the entrance length on steep spillways when the depth at the crest goes through critical. Figure 3.2 illustrates the development of the boundary layer on a steep slope.

As in the subcritical case, the normal depth d_o was chosen as the length scale for the entrance length L. Through numerous numerical runs, two parameters were found to influence the entrance length. As in the subcritical case, one of these was the fully developed C_*, or the C_* corresponding to the normal depth. Unlike the subcritical case, the channel bed slope did have an effect on the entrance length.

In addition to the entrance length L, one may also wish to know the depth at which the boundary layer reaches the surface. It does not have to be normal depth, as in the case of subcritical flow. Let us call the depth at which the boundary layer reaches the surface d_{end} (See Figure 3.2). Again through numerous numerical runs, d_{end} was found to be a function of the same variables as the entrance length L and could be scaled by the normal depth d_o. Therefore in summary we have:

$$\frac{L}{d_o}, \frac{d_{end}}{d_o} = f\left[C_*, \phi\right] \tag{5.8}$$

The dimensionless parameters above have the advantage over the Keller and Rastogi parameters below:

$$\frac{L}{k_s} = f\left[\frac{q}{\left(g\,k_s^3\right)^{\frac{1}{2}}}, \phi\right] \tag{1.26}$$

It can be seen that the Keller and Rastogi parameters have a problem with k_s being in the denominator of two of the dimensionless variables; as k_s gets small or even zero, L/k_s and $q/(g\,k_s{}^3)^{1/2}$ go to infinity and one is quickly out of the range of the design curves generated by Keller and Rastogi's k-ε model.

Figure 5.37 contains the design curves generated by the numerical model. It shows the dimensionless entrance length L/d_o as a function of C_* and the channel bed slope ϕ in degrees. The subcritical development length relation is also plotted for comparison. The supercritical numerical model could only solve problems which had a Froude number $\mathbf{F}_o$ of more than 1.8, otherwise the solution became unstable. ($\mathbf{F}_o$ was based on the normal depth d_o). The line for $\mathbf{F}_o$=1.8 is also drawn on Figure 5.37. It is between this line and the subcritical solution line that the entrance length relations remain somewhat of a mystery.

Looking at Figure 5.37, one may lead to the wrong conclusion that the entrance length increases with channel bed slope but, in fact, it decreases. This is because the length scale d_o decreases with slope. (See Figure 5.10 for an example of how the entrance length varies with channel bed slope).

Figure 5.38 contains design curves generated by numerical model for the depth at which the boundary layer reaches the surface (d_{end}). It shows the dimensionless end depth (d_{end}/d_o) as a function of C_* and the channel bed slope ϕ in degrees. Again there are no design curves available between the subcritical solution and $\mathbf{F}_o$=1.8 due to numerical instability. For the subcritical case $d_{end} = d_o$, therefore $d_{end}/d_o = 1$. Figure 5.38 shows that d_{end}/d_o increases as the channel bed slope increases. It also shows that for any one value of slope that d_{end}/d_o increases as the channel roughness decreases. Figure 5.38 shows that the largest realistic d_{end}/d_o ratios gives an end depth around 1.4 times the normal depth.

5.9 Non-dimensional entrance lengths for depth at spillway crest controlled by a sluice gate

In some cases, there is a sluice gate at the top of a spillway for controlling discharge. In these cases, the initial upstream depth may be other than critical and the design curves in Section 5.8 can not be used. It is the aim of this section to come up with design curves for these types of spillways.

There is now a new input variable to the problem; the initial depth d_i. This initial depth is the opening measured perpendicular to the spillway face to the bottom of the gate if the approach flow is guided under the gate in such a manner as to eliminate any Vena contraction effect. It may also be considered the depth downstream of the Vena contraction.

In summary, the entrance length and end depth are given by:

$$\frac{L}{d_o}, \frac{d_{end}}{d_o} = f\left[C_* , \phi, \frac{d_i}{d_o} \right] \tag{5.9}$$

With the new input variable d_i/d_o, it is impossible to show all design curves on one plot. Therefore, three different sets of design curves where generated for three different channel bed slopes. These slopes include $\phi = 1^\circ$, 10°, and 45°.

Figure 5.39 shows the design curves for the dimensionless entrance length as a function of C_* and the d_i/d_o ratio for a spillway slope of one degree. It shows that L/d_o decreases as d_i/d_o decreases. The thick design curve farthest to the right is from Section 5.8 and shows the end limit of the design curves. On this line, the sluice gate is above the depth given by critical flow at the spillway crest and is the maximum d_i possible. It is interesting to note that that the design curve for $d_i/d_o = 1$ is identical to the subcritical solution in Figure 5.37.

Figure 5.40a contains the design curves for d_{end}/d_o as a function of C_* and the d_i/d_o ratio for a spillway slope of 1°. Figure 5.40b is the same as Figure 5.40a but also includes d_i/d_o ratios less than 1. Figure 5.40a and 5.40b show that as d_i/d_o increases d_{end}/d_o increases. They also show that for $d_i/d_o > 1$, that $d_{end} < d_i$. In other words, if the initial depth is greater than the normal depth then the depth decreases in the downstream direction. They also show that if $d_i/d_o < 1$, then $d_{end} > d_i$; if the initial depth is less than the normal depth than the depth increases in the downstream direction. This is much like the behavior of the S2 and S3 backwater curves.

Figures 5.41 to 5.44b show design curves for L/d_o and d_{end}/d_o for slopes of 10° and 45°. They show similar behavior as the 1° slope. In fact, if we superimpose the L/d_o design curves, it can be seen that they coincide almost exactly in areas which are sufficiently far away from the $d_i=d_c$ line. For example, design curves up to $d_i/d_o = 1.4$ are almost identical for slopes of 1°, 10°, and 45° and design curves up to $d_i/d_o = 2.5$ are identical for slopes 10° and 45°. Therefore, we can conclude that the spillway slope becomes a more significant parameter as the initial depth approaches critical depth.

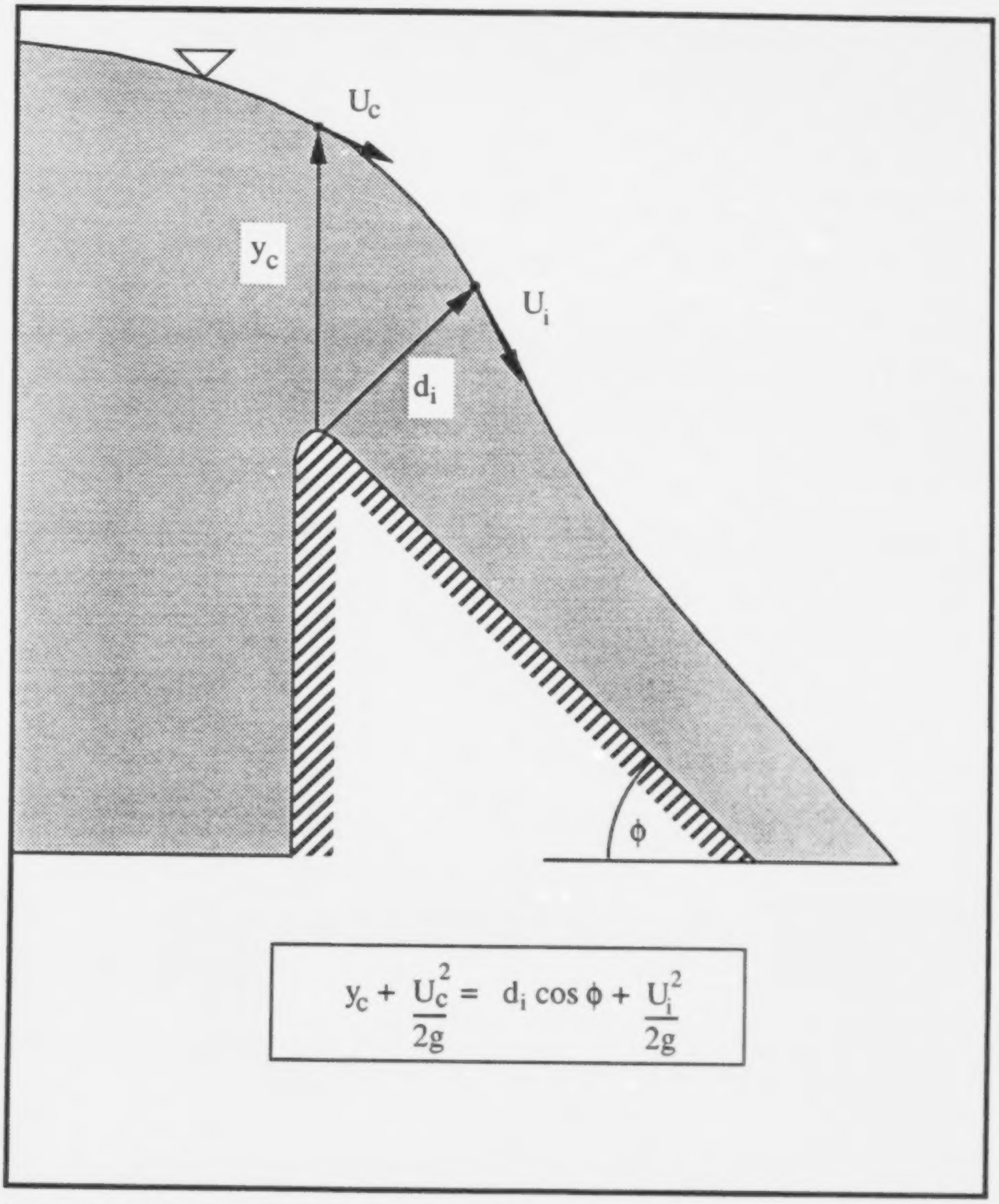

$$y_c + \frac{U_c^2}{2g} = d_i \cos\phi + \frac{U_i^2}{2g}$$

Fig. 5.1 Diagram showing the initial depth d_i for the upstream boundary condition based on the flow going through critical in the vertical.

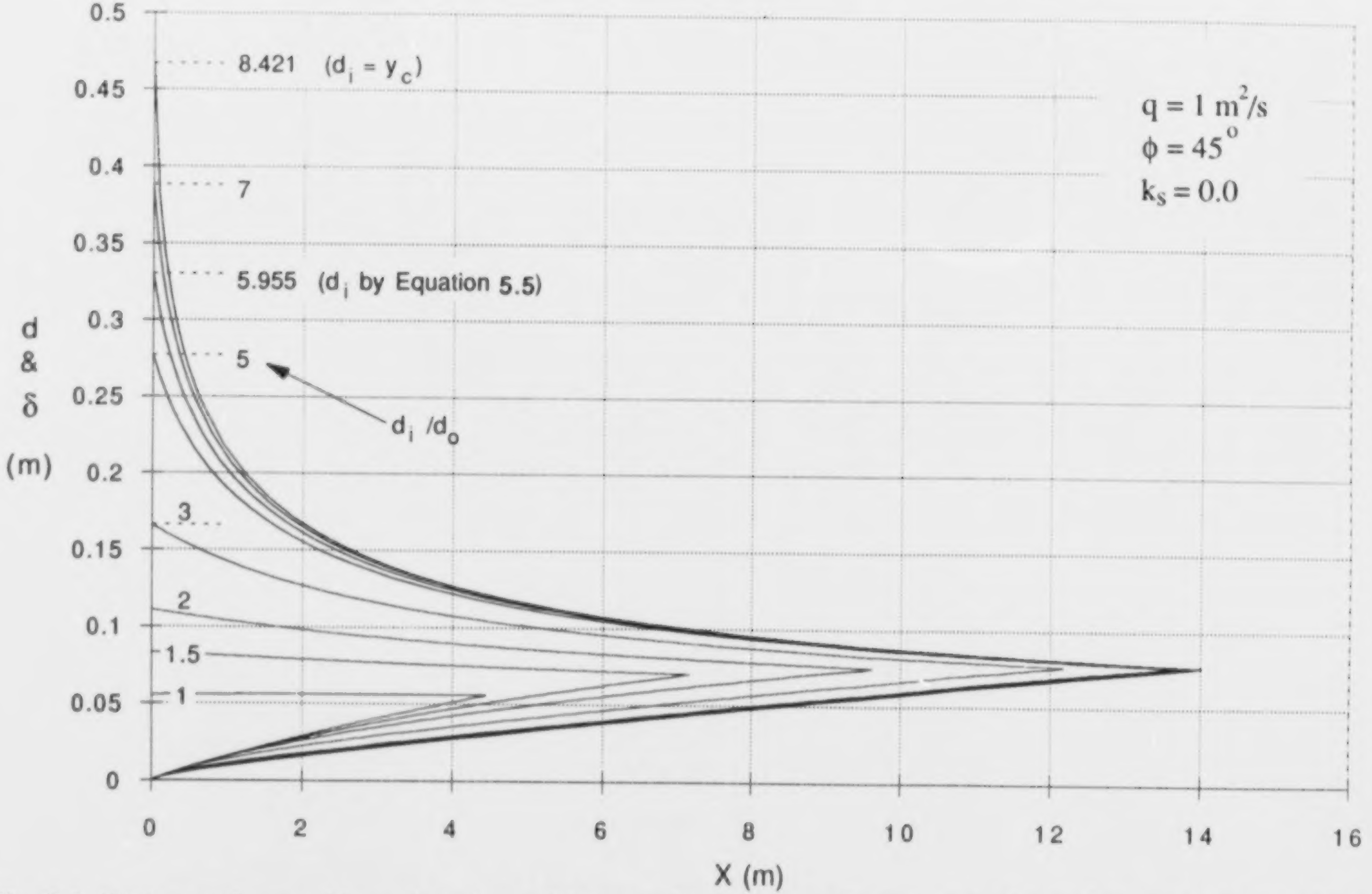

Fig. 5.2 Water surface and boundary layer thickness for the same discharge, bed roughness and slope of the channel, but different initial upstream depths.

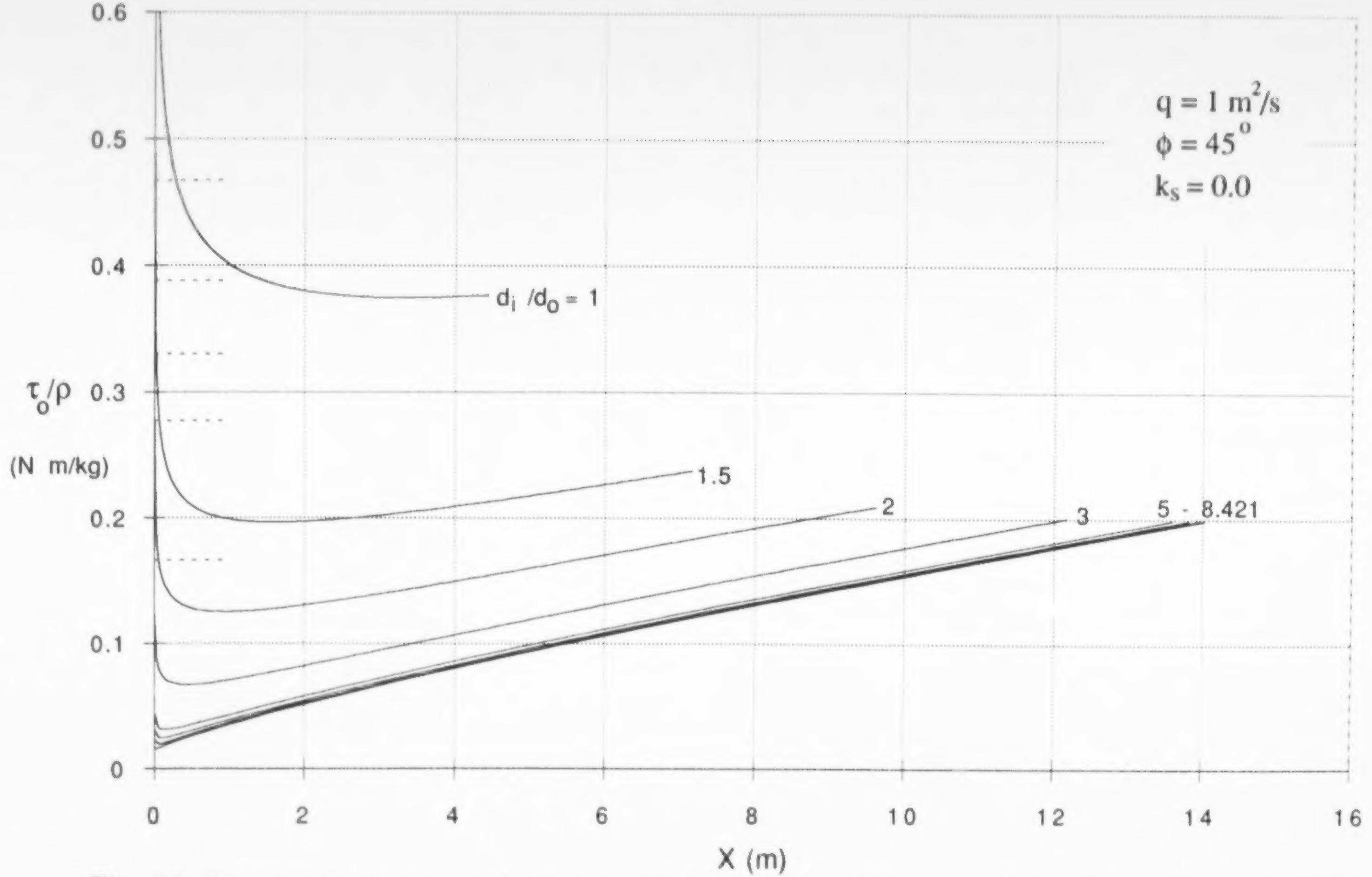

Fig. 5.3 Shear stress corresponding to runs of different initial upstream depths shown in Figure 5.2.

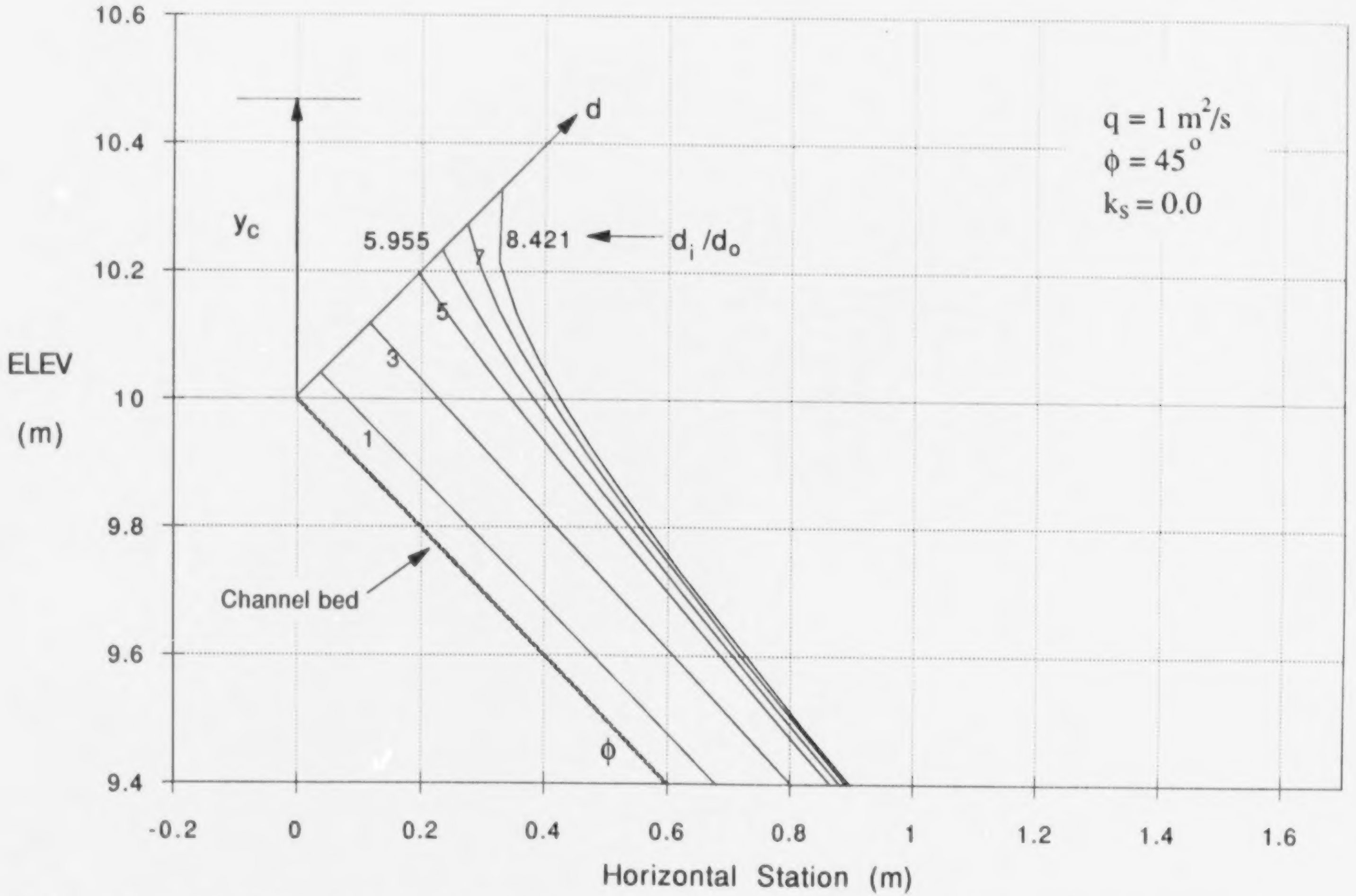

Fig. 5.4 Same as Figure 5.2 but plotted to actual scale and orientation near the channel entrance.

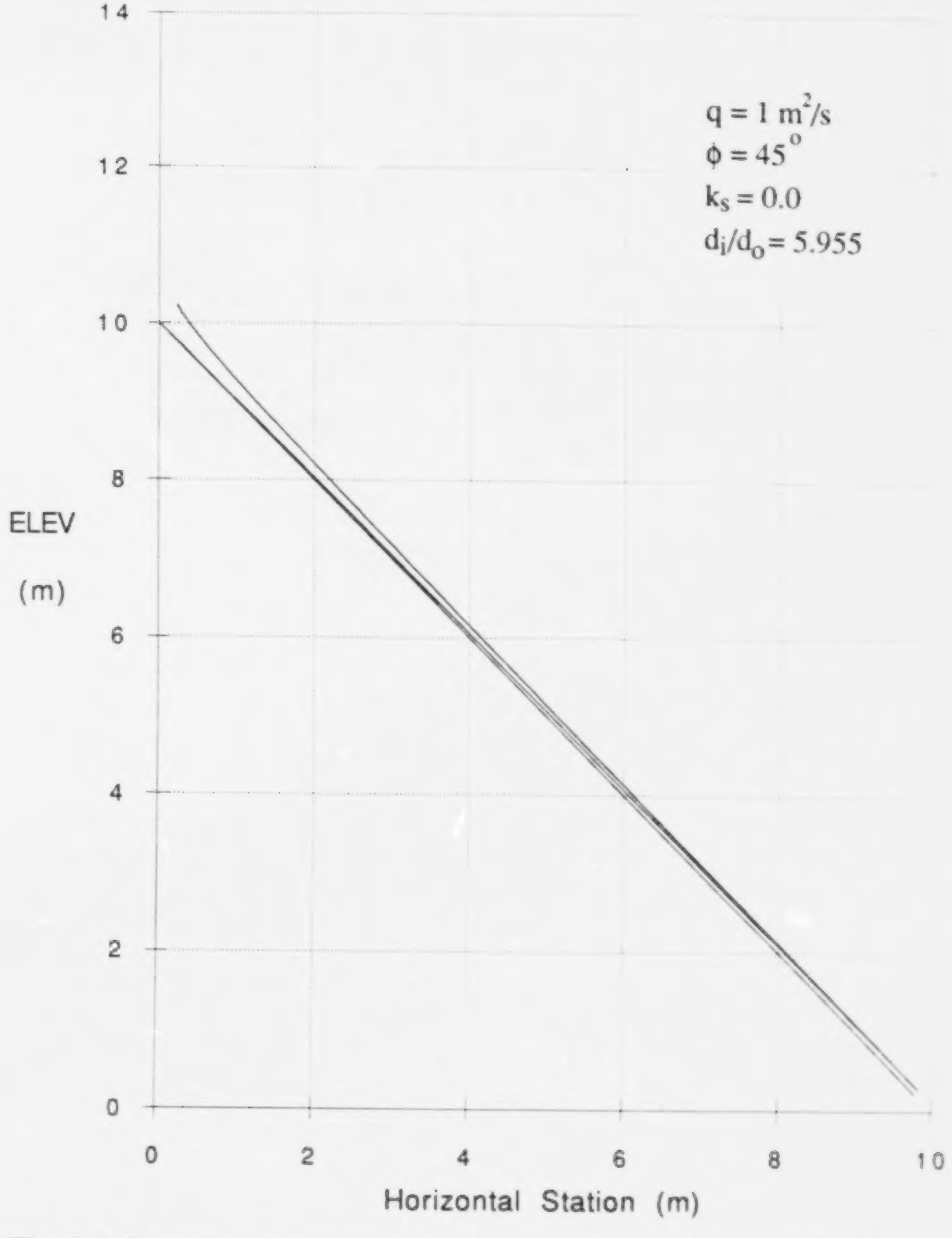

Fig. 5.5 Example of an undistorted plot of water surface, boundary layer thickness, and channel bed in the entire entrance region of a steep channel.

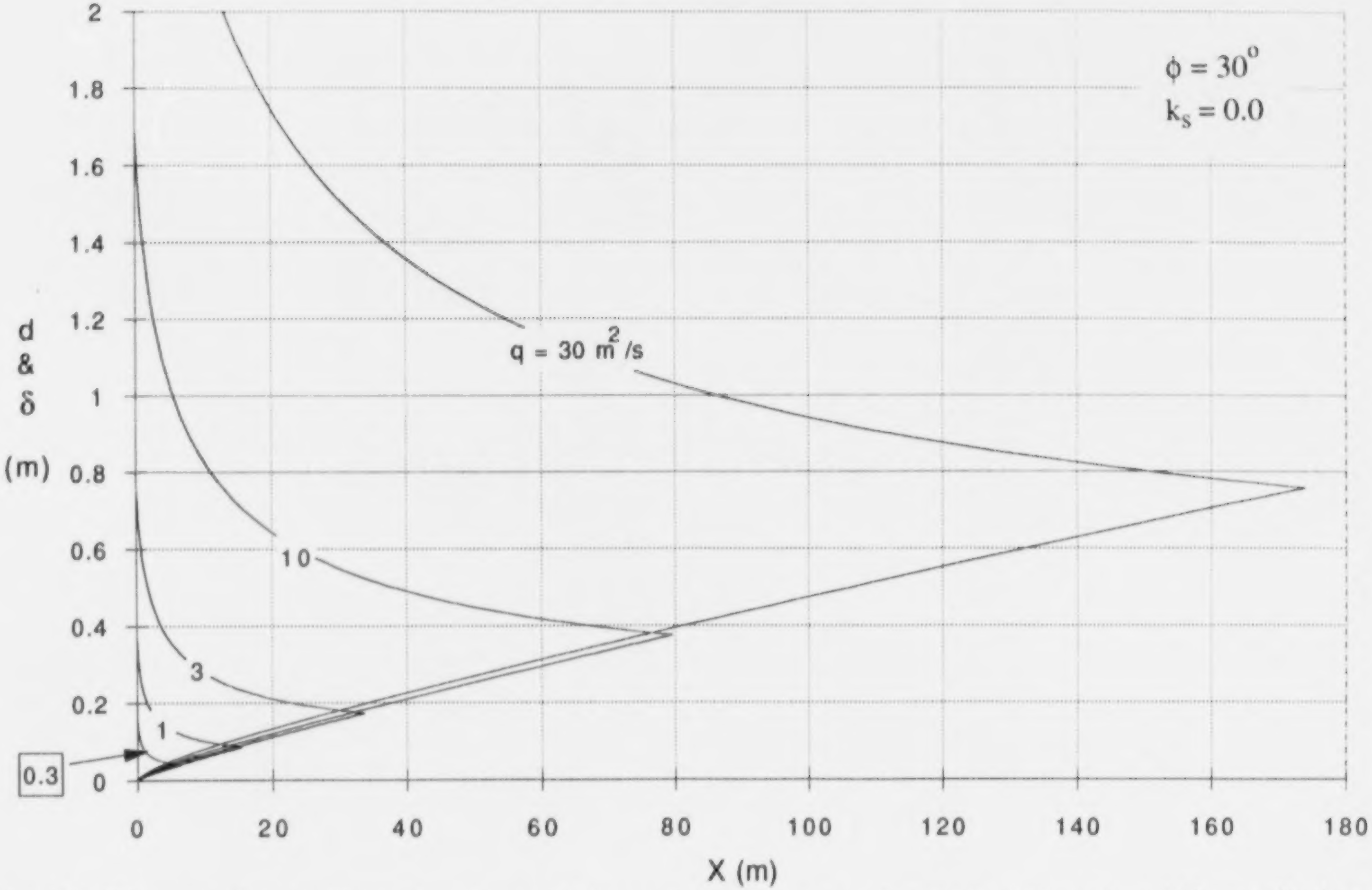

Fig. 5.6 Water surface and boundary layer thicknesses for the same channel bed slope but different discharges per unit width. (*smooth channel*)

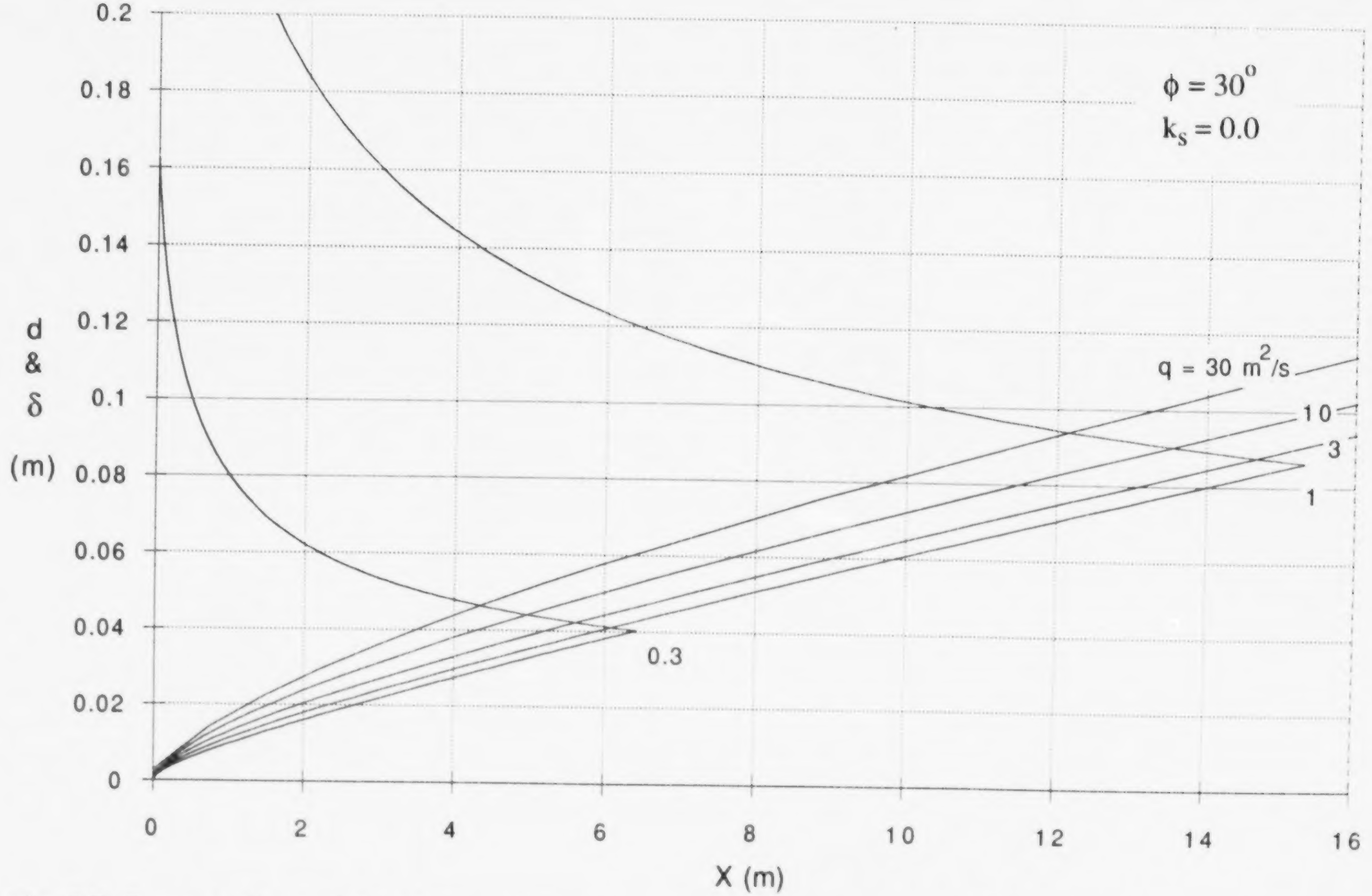

Fig. 5.7 Same as Figure 5.6 with a portion near the channel entrance magnified. (*smooth channel*)

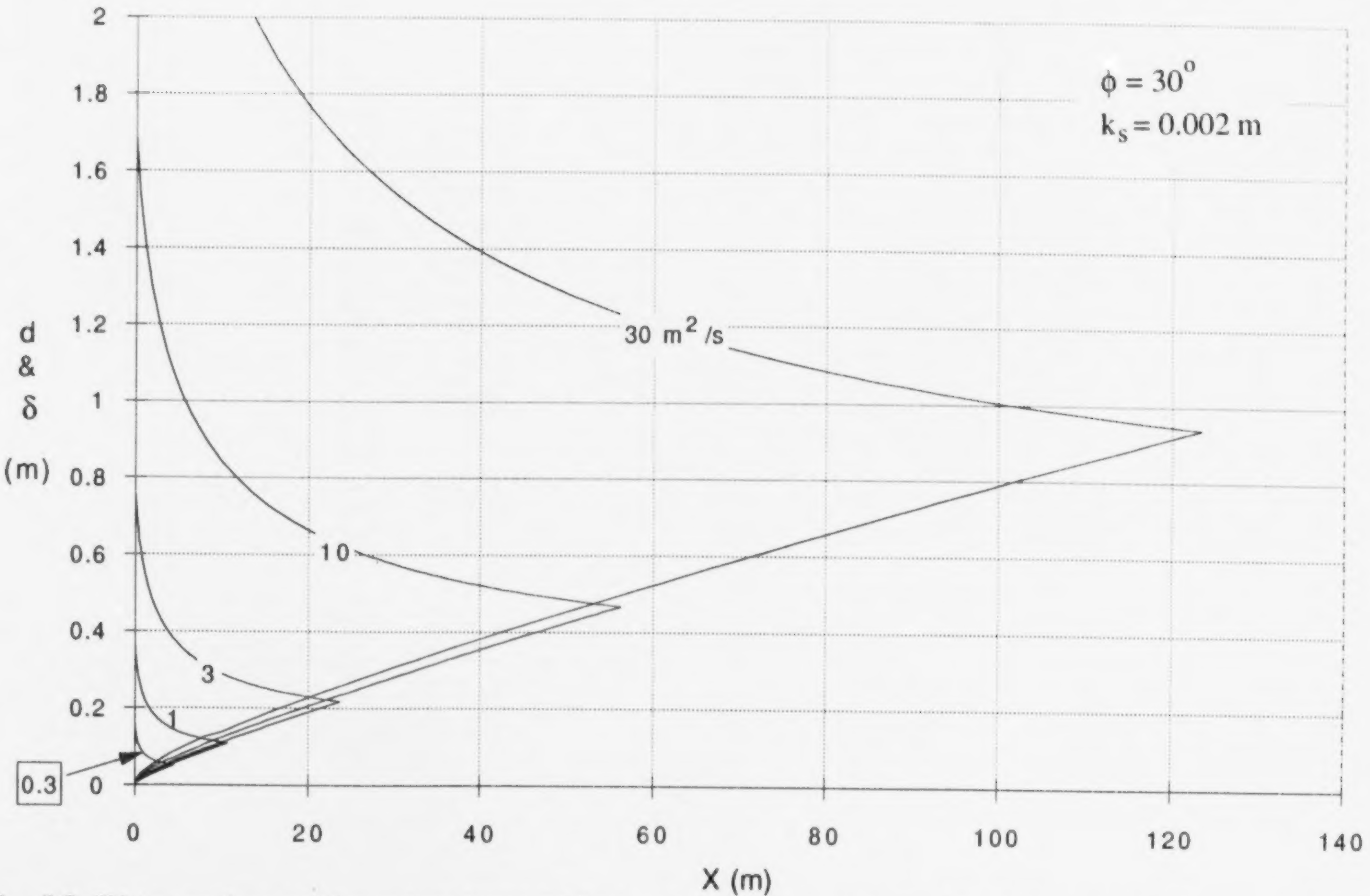

Fig. 5.8 Water surface and boundary layer thicknesses for the same channel bed slope but different discharges per unit width. (*rough channel*)

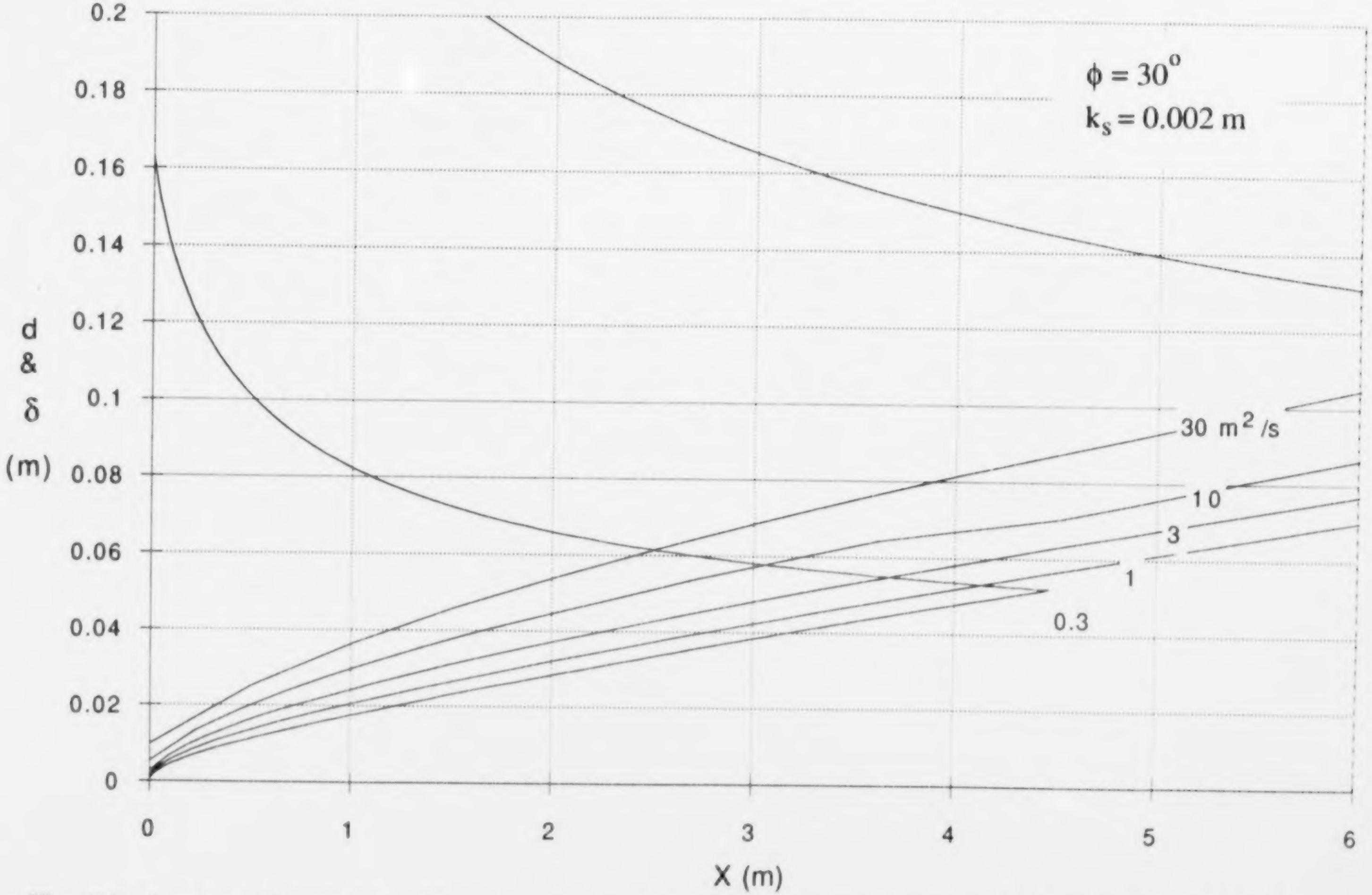

Fig. 5.9 Same as Figure 5.8 with a portion near the channel entrance magnified. (*rough channel*)

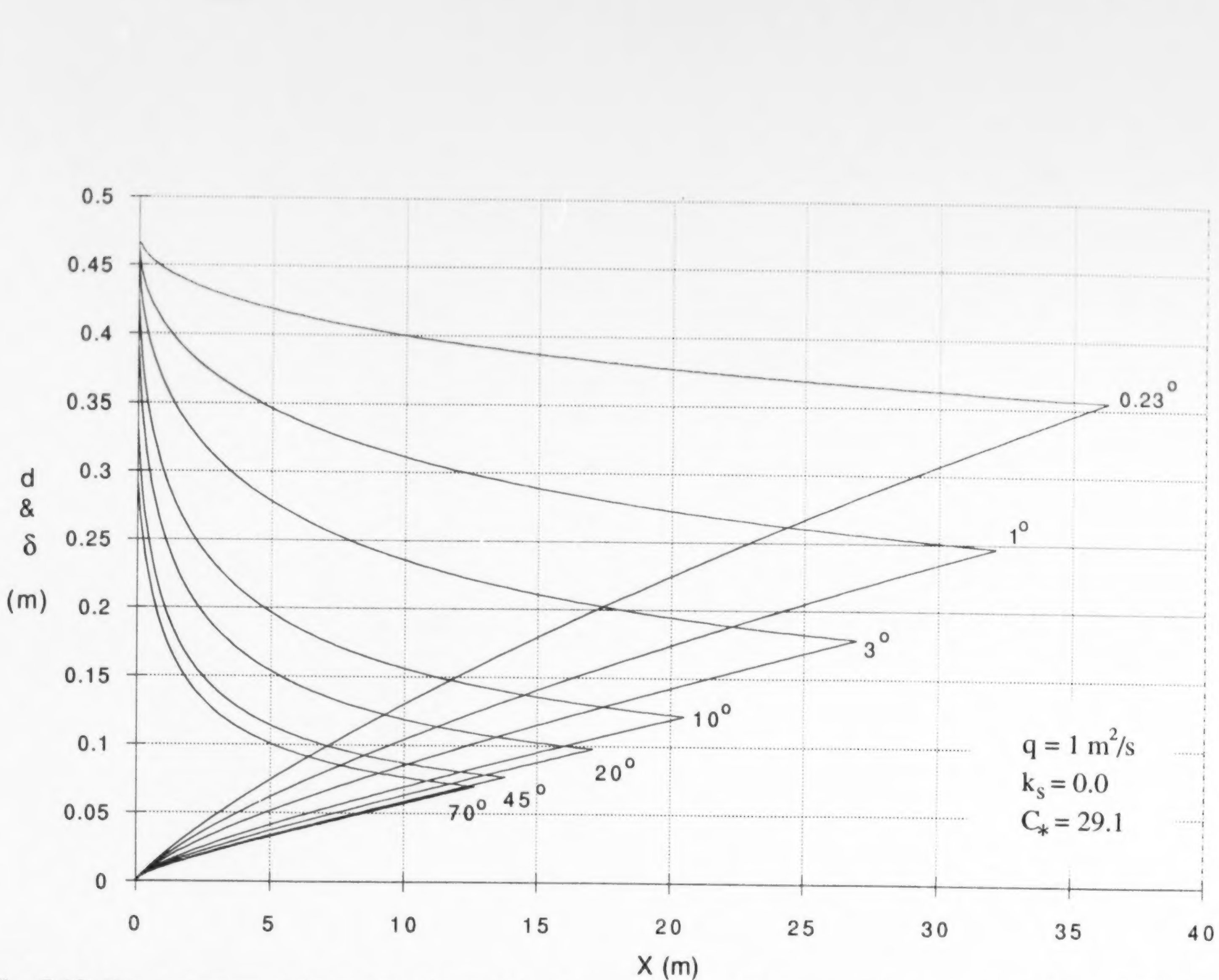

Fig. 5.10 Water surface and boundary layer thicknesses for same discharge and a smooth bed, but different channel bed slopes.

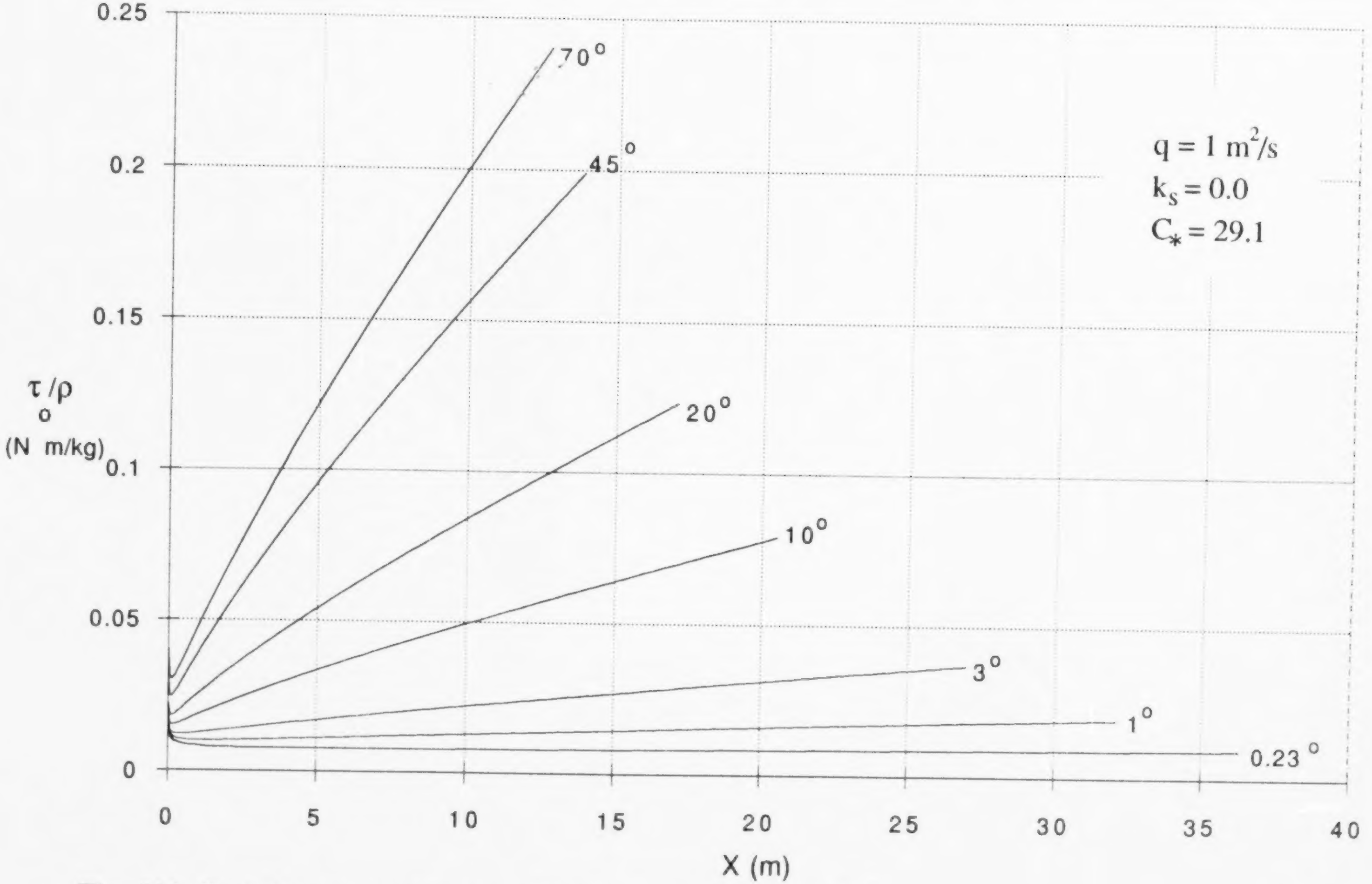

Fig. 511 Bed shear stress corresponding to runs of Figure 5.10.

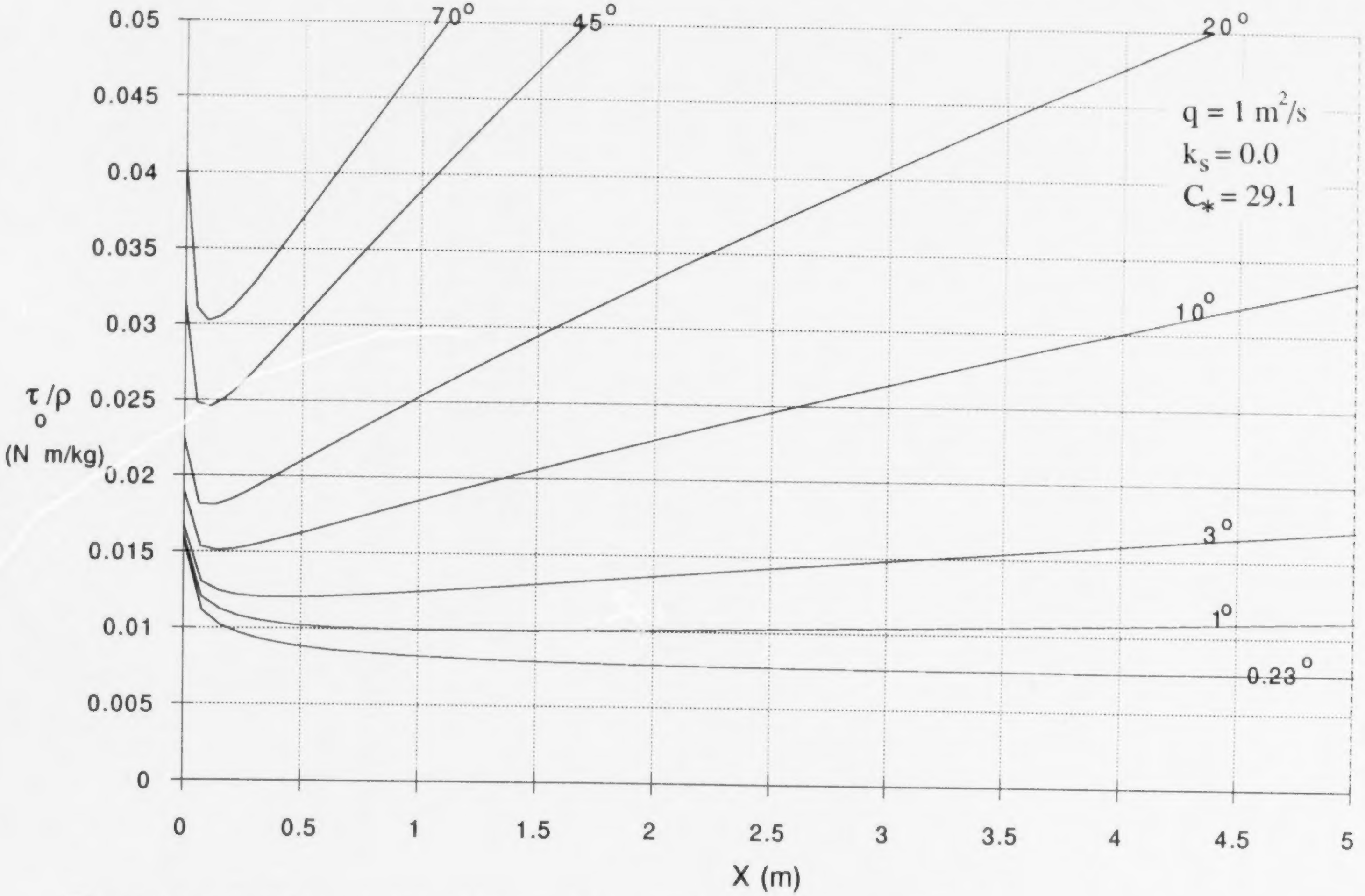

Fig. 5.12 Magnified portion of Figure 5.11 near the channel entrance.

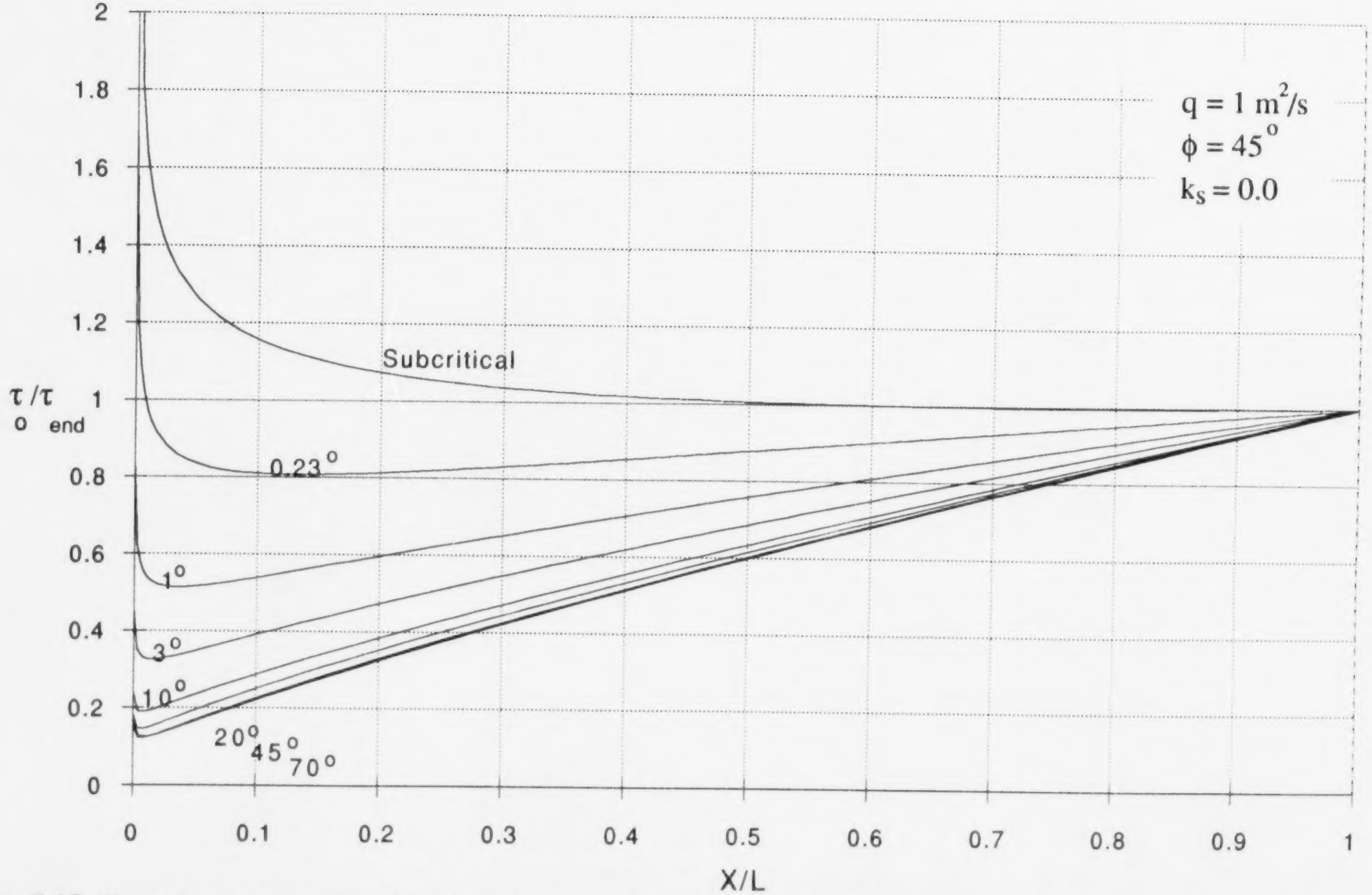

Fig. 5.13 Bed shear stress non-dimesionalized by the bed shear when the boundary layer reaches the surface. Also shown is the subcritical solution in a mild channel for the same discharge and a smooth bed.

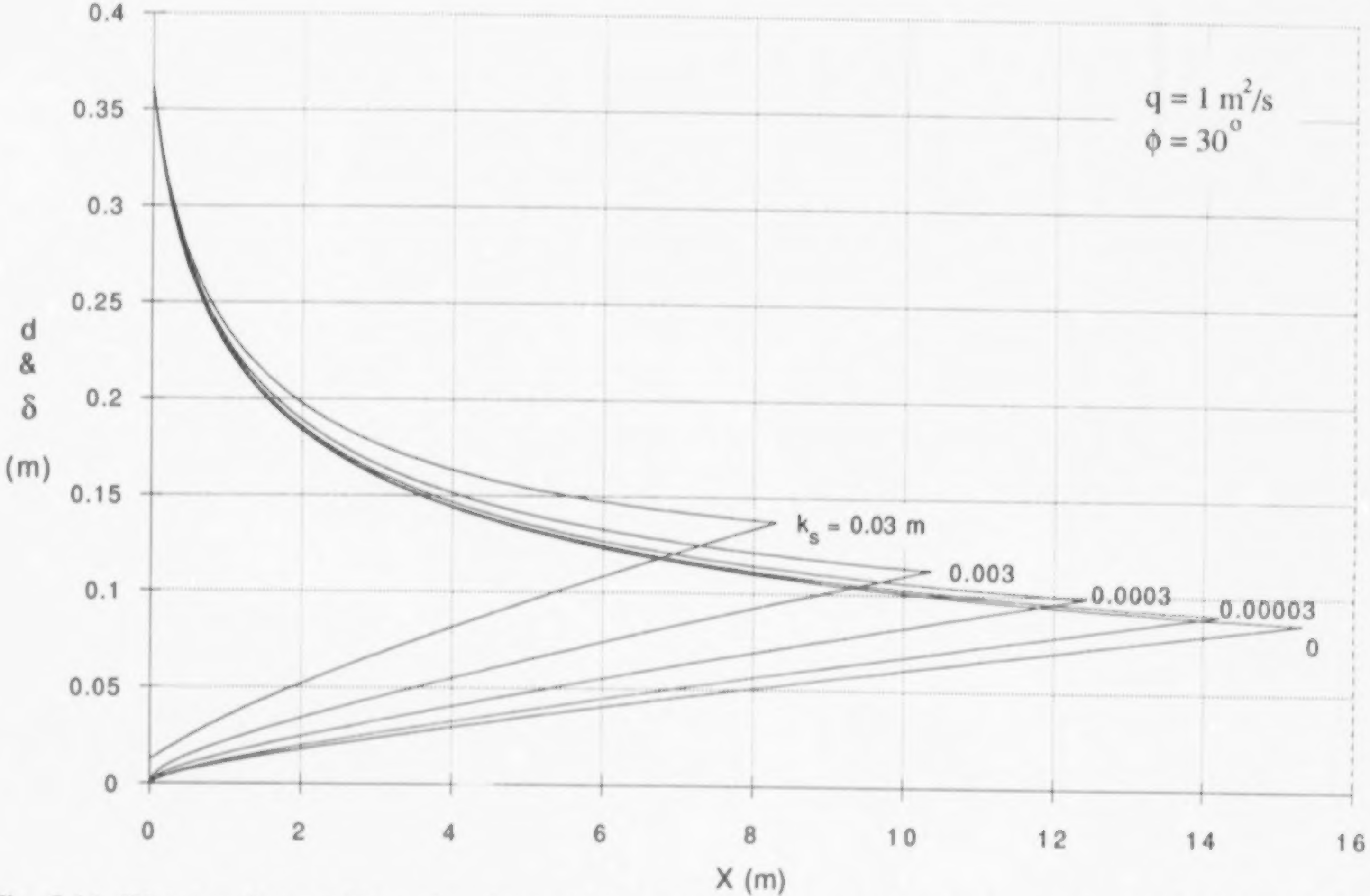

Fig. 5.14 Water surface and boundary layer thicknesses for the same discharge and channel bed slope but for different bed roughness.

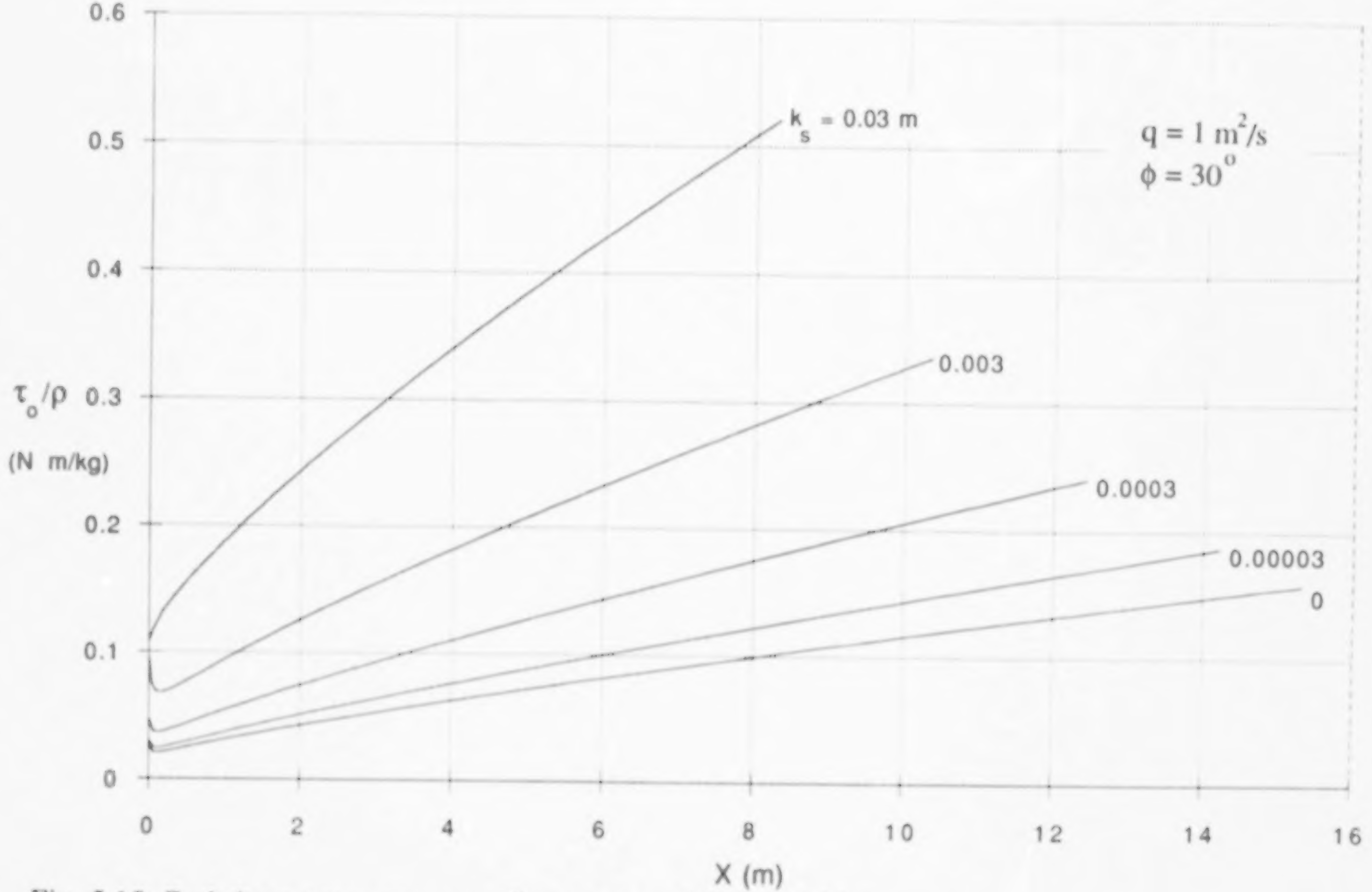

Fig. 5.15 Bed shear stress corresponding to runs of Figure 5.14.

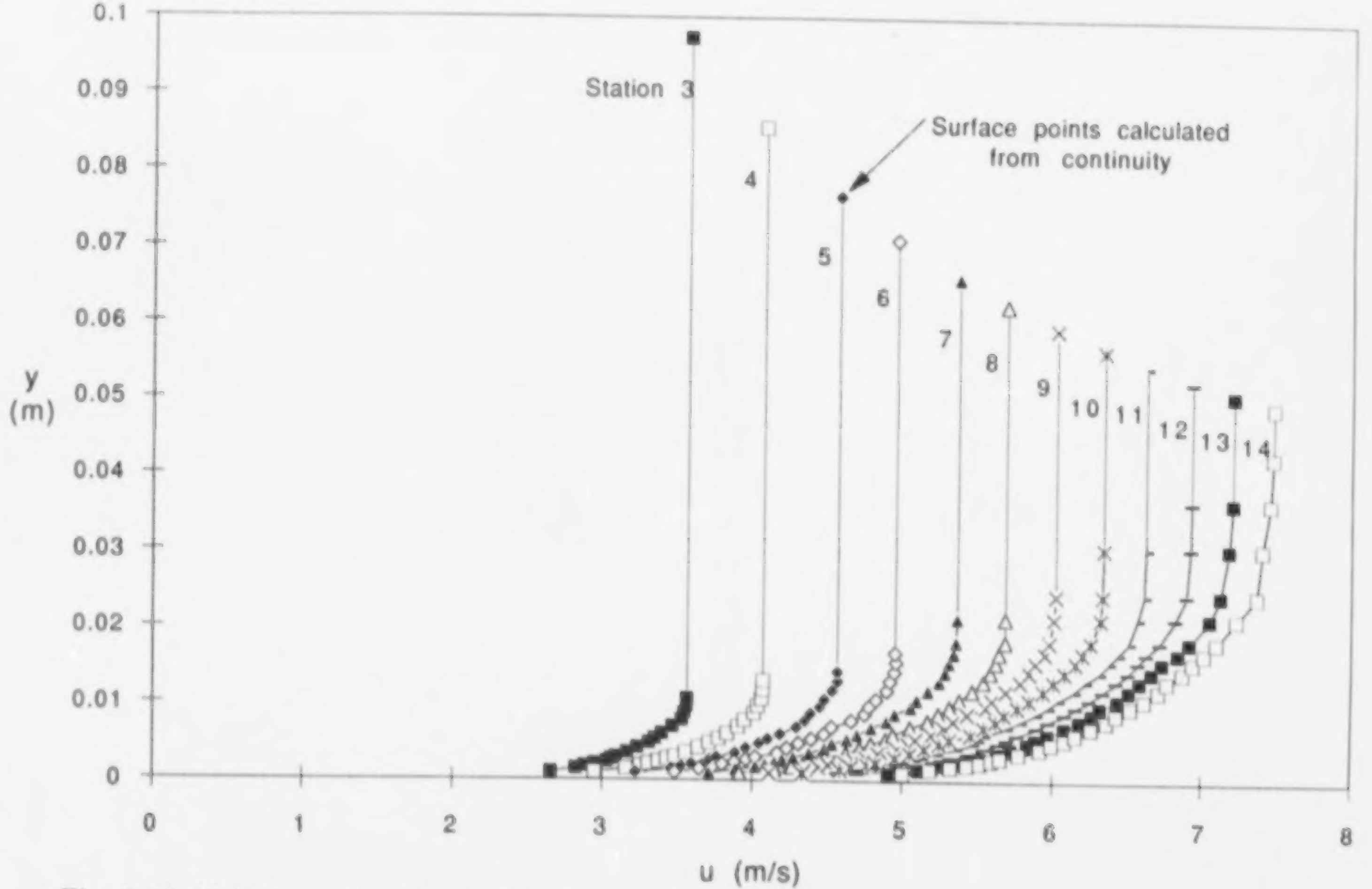

Fig. 5.16 Velocity profiles from Bauer's *smooth* experiment.

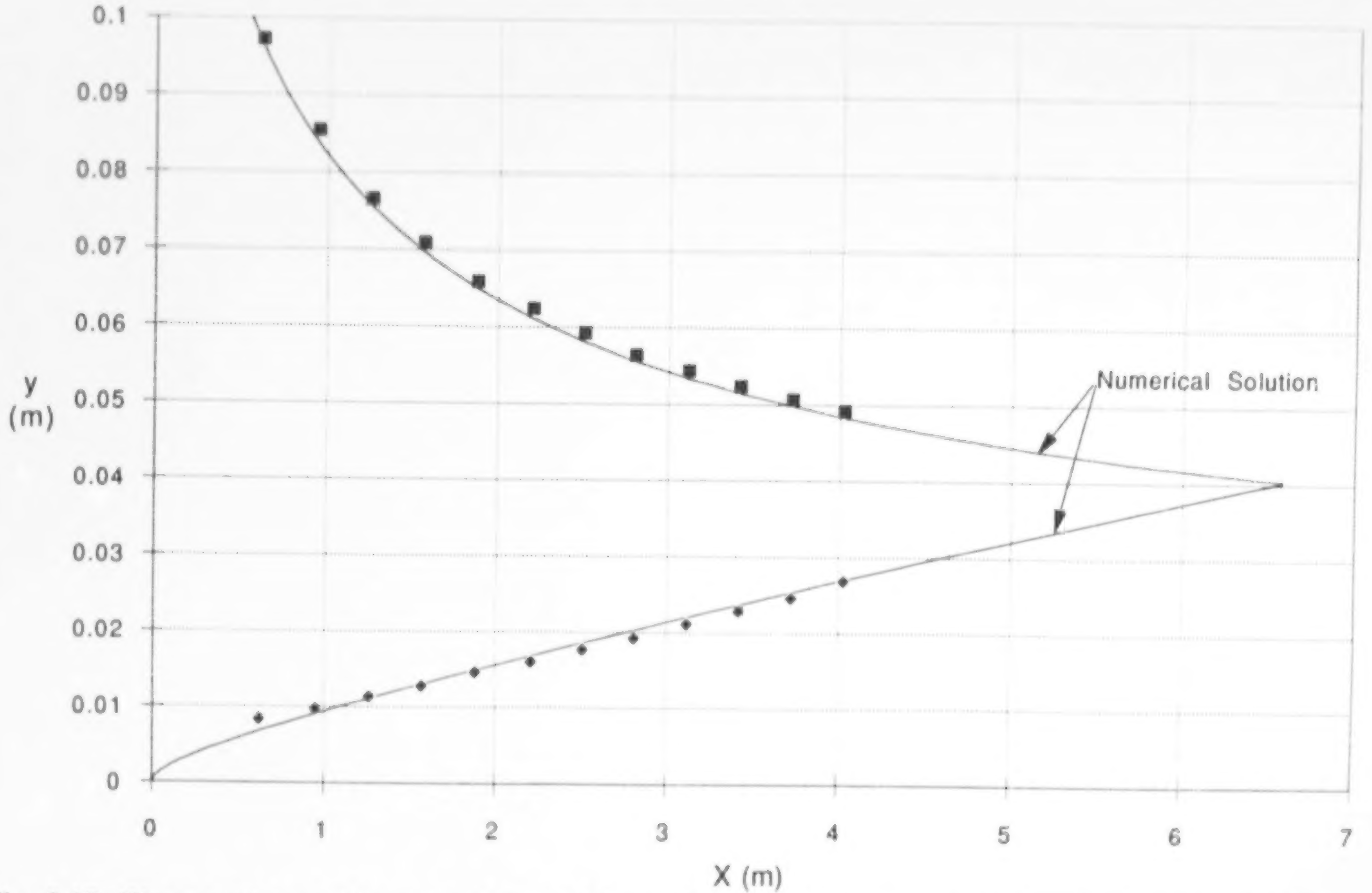

Fig. 5.17 Water surface and boundary layer thickness for Bauer's *smooth* experiment compared with the numerical solution.

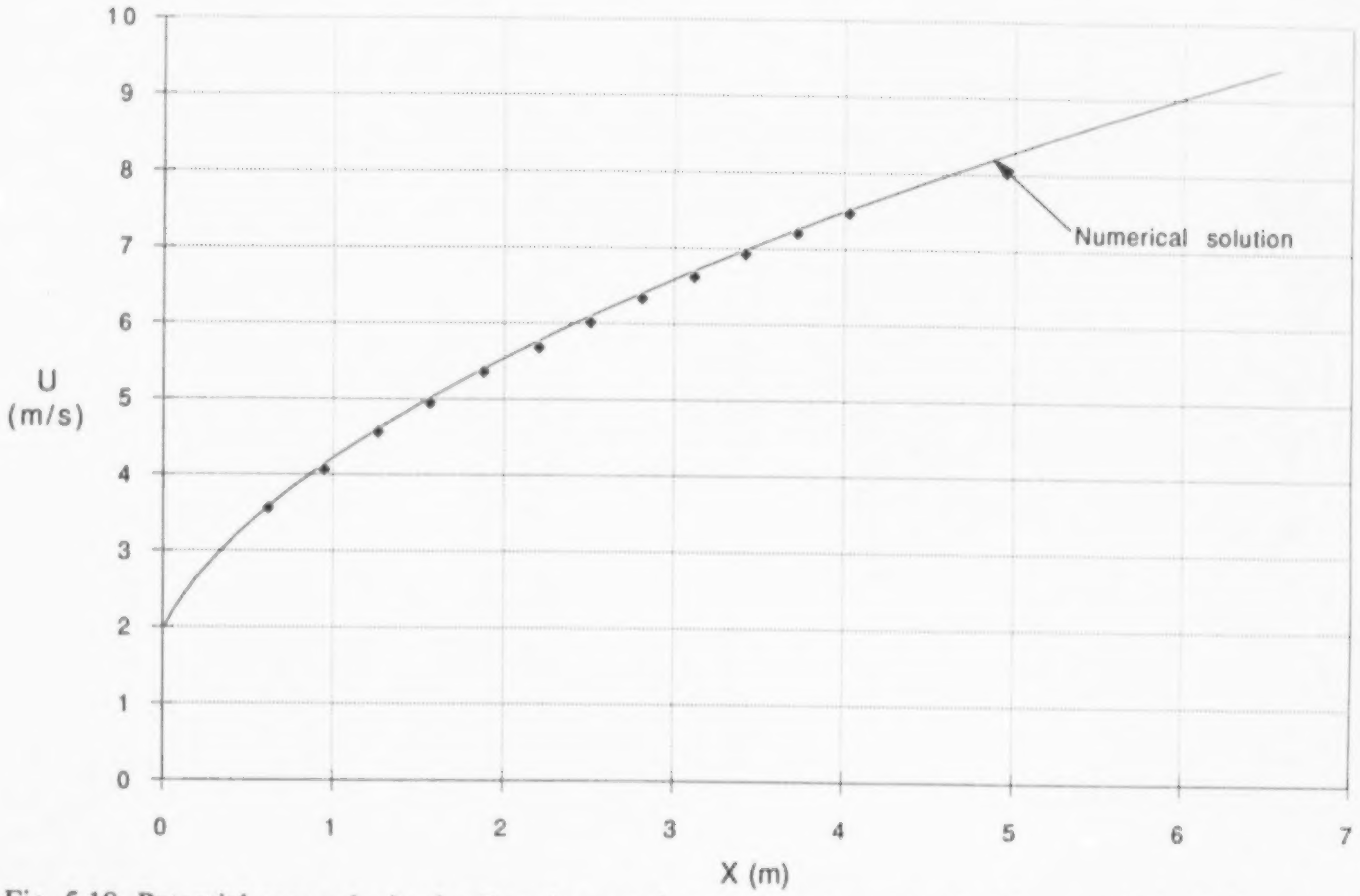

Fig. 5.18 Potential core velocity for Bauer's *smooth* experiment compared with numerical solution.

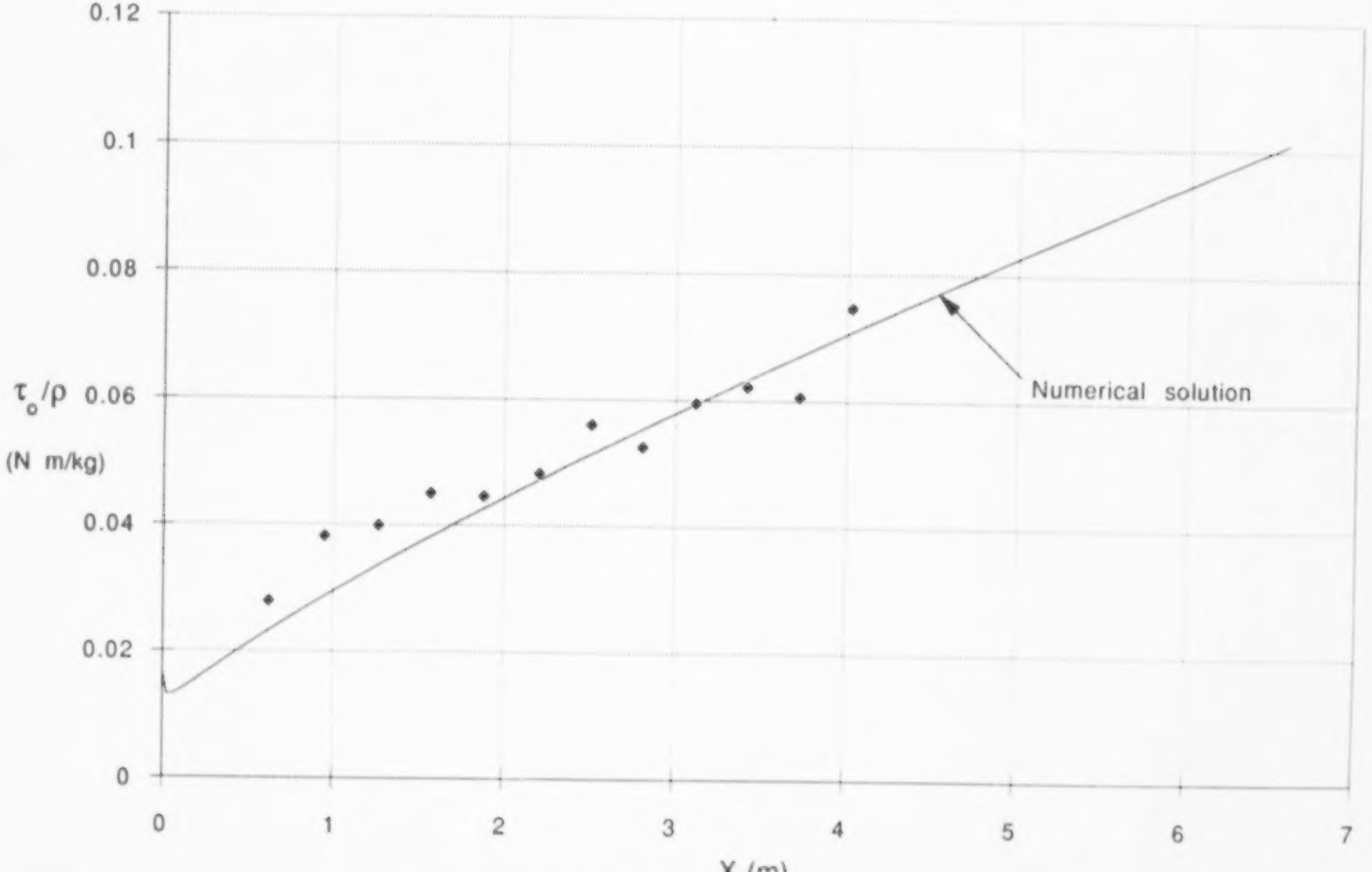

Fig. 5.19 Bed shear stress for Bauer's *smooth* experiment compared with numerical solution.

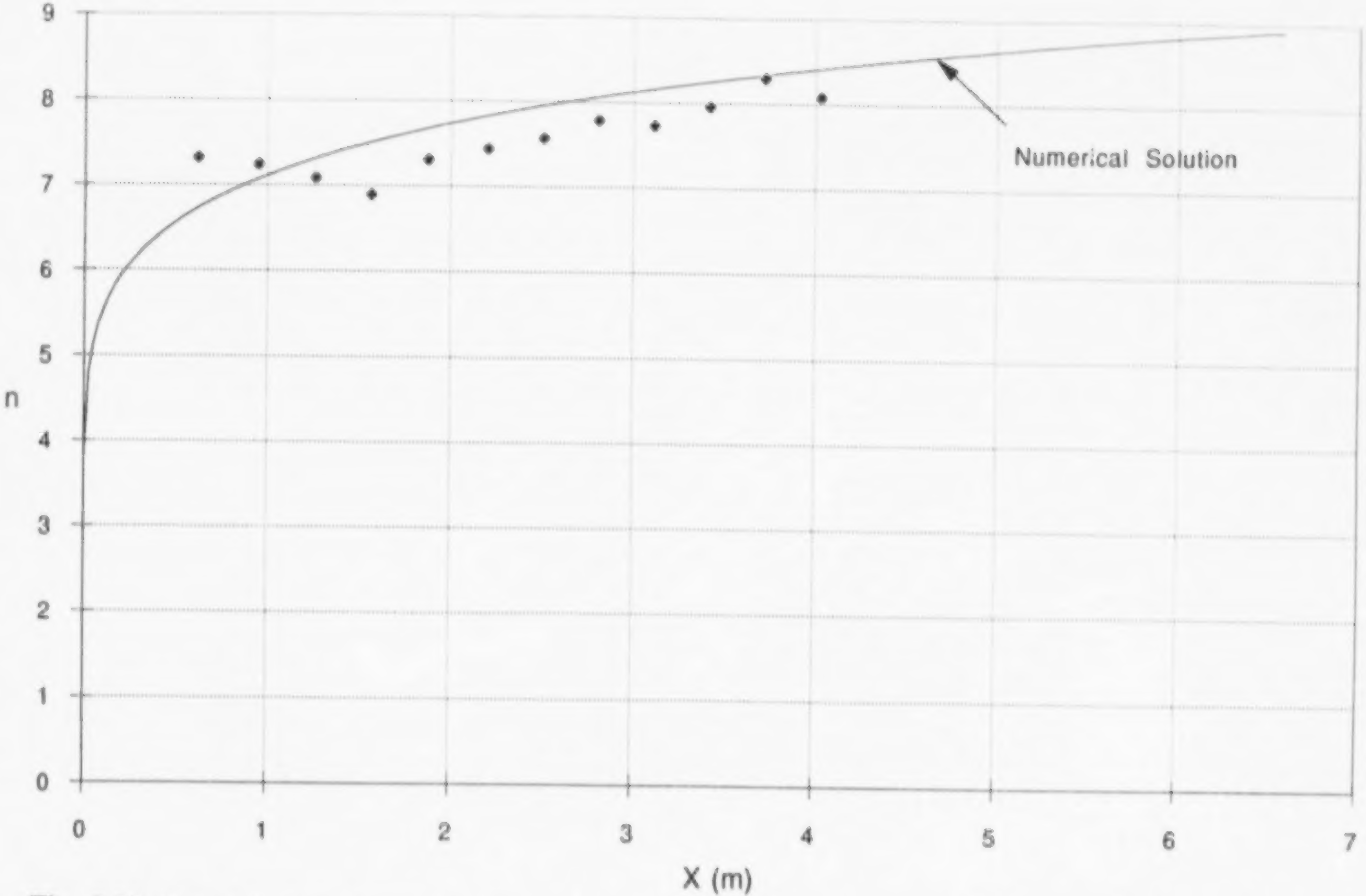

Fig. 5.20 Power law exponent for Bauer's *smooth* experiment compared with numerical solution.

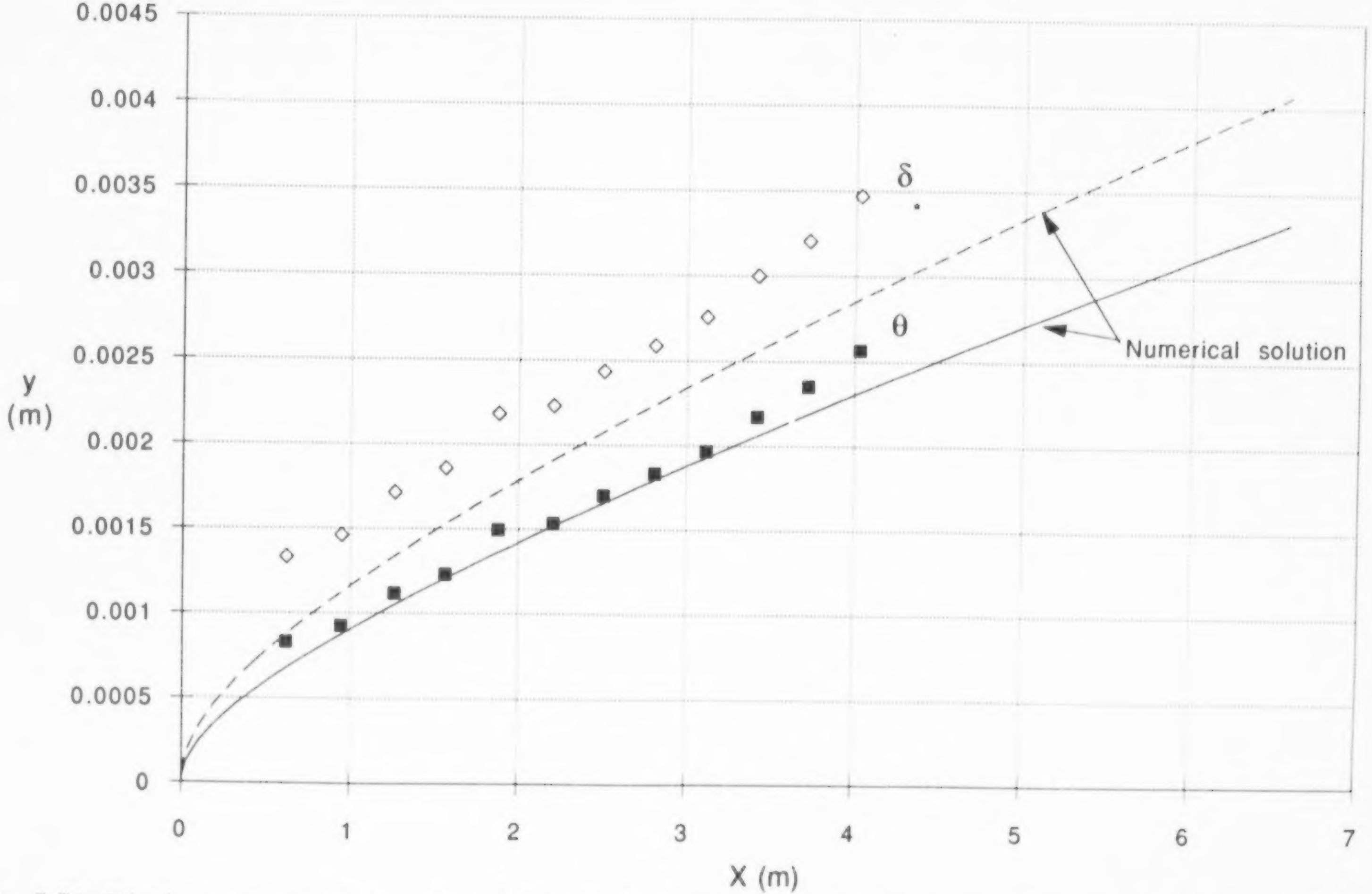

Fig. 5.21 Displacement and momentum thickness for Bauer's *smooth* experiment compared with numerical solution.

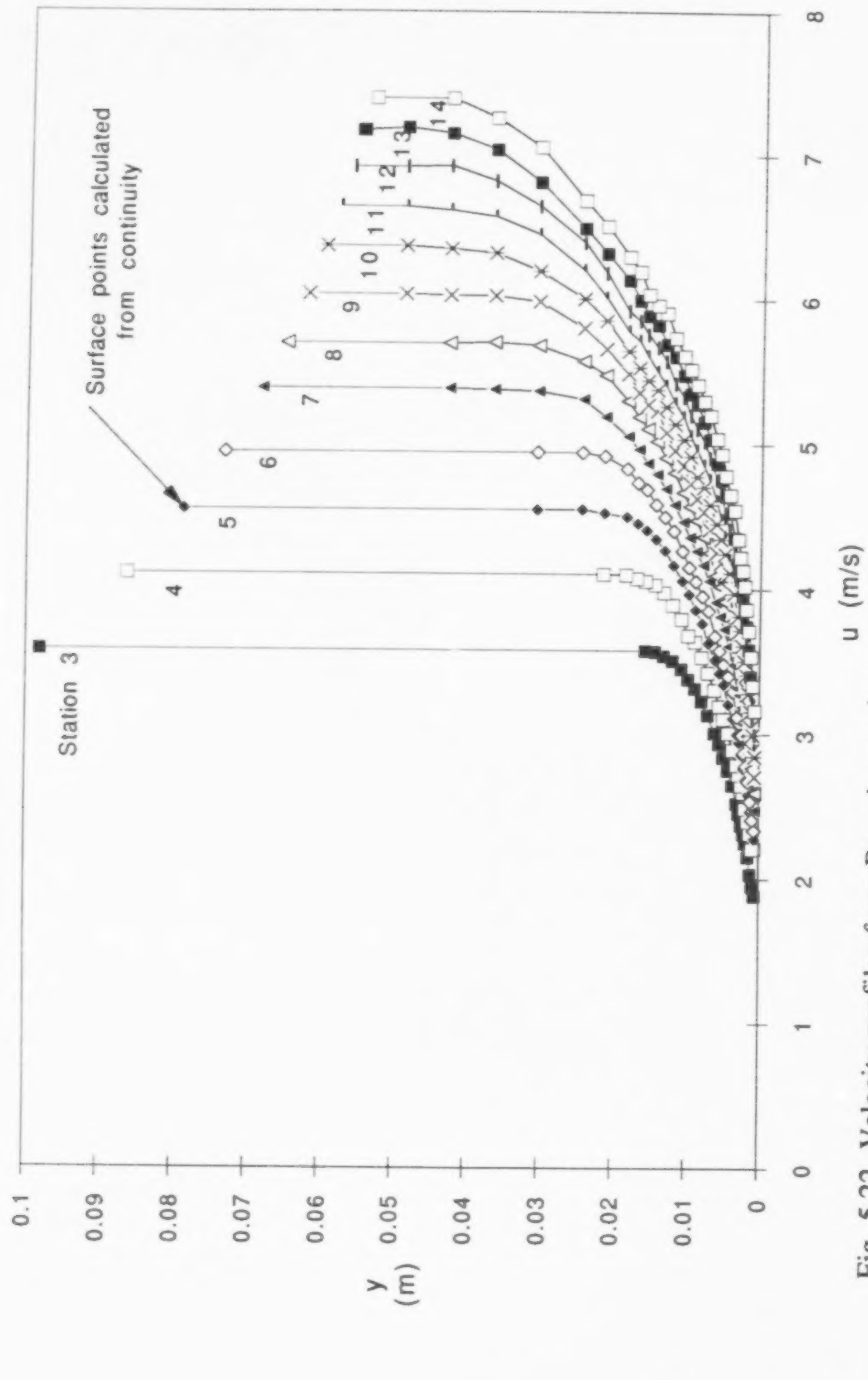

Fig. 5.22 Velocity profiles from Bauer's *rough* experiment.

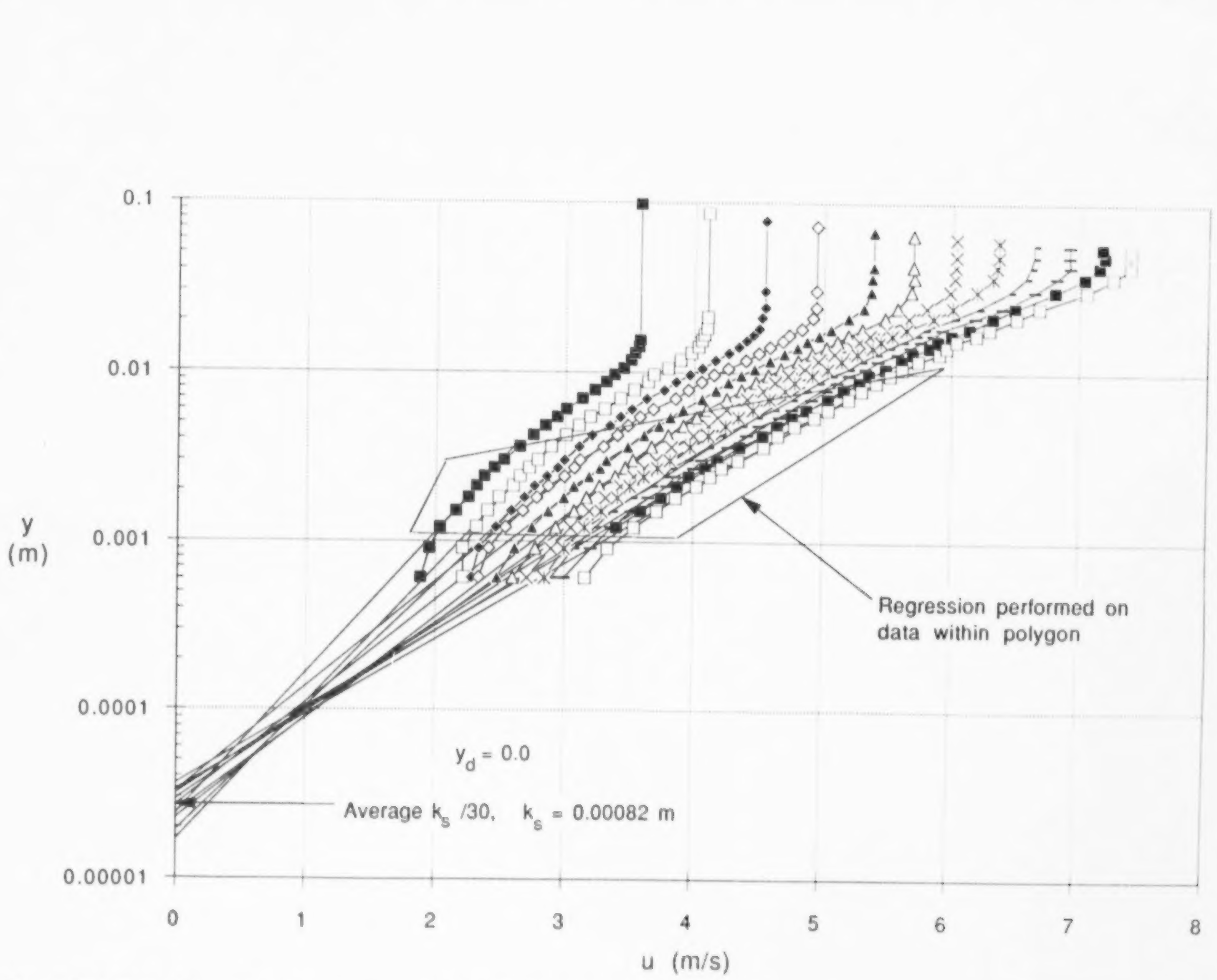

Fig. 5.23 The channel bed roughness and bed shear stress for Bauer's *rough* experiment was determined from velocity profiles.

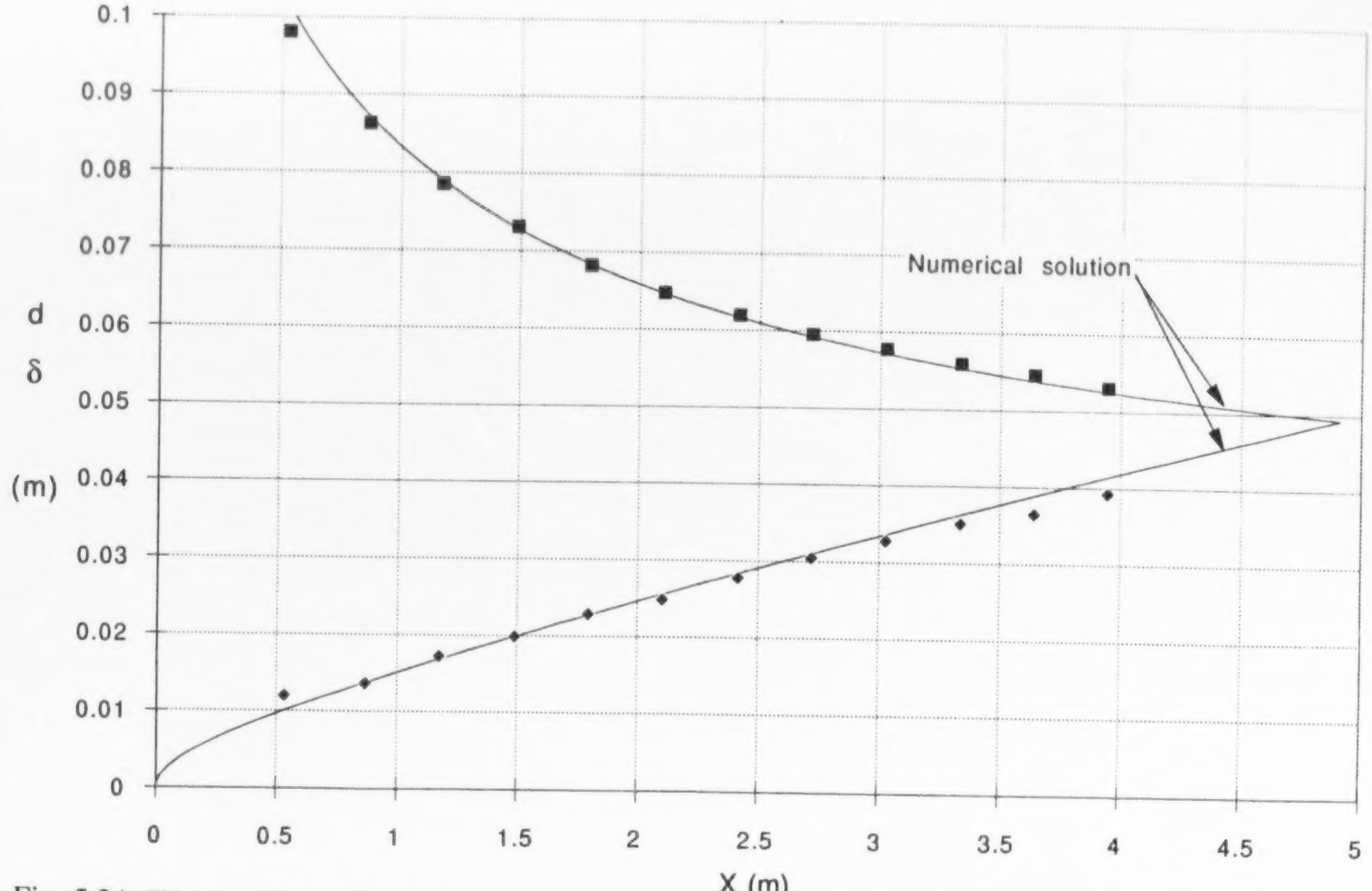

Fig. 5.24 Water surface and boundary layer thickness for Bauer's *rough* experiment compared with the numerical solution.

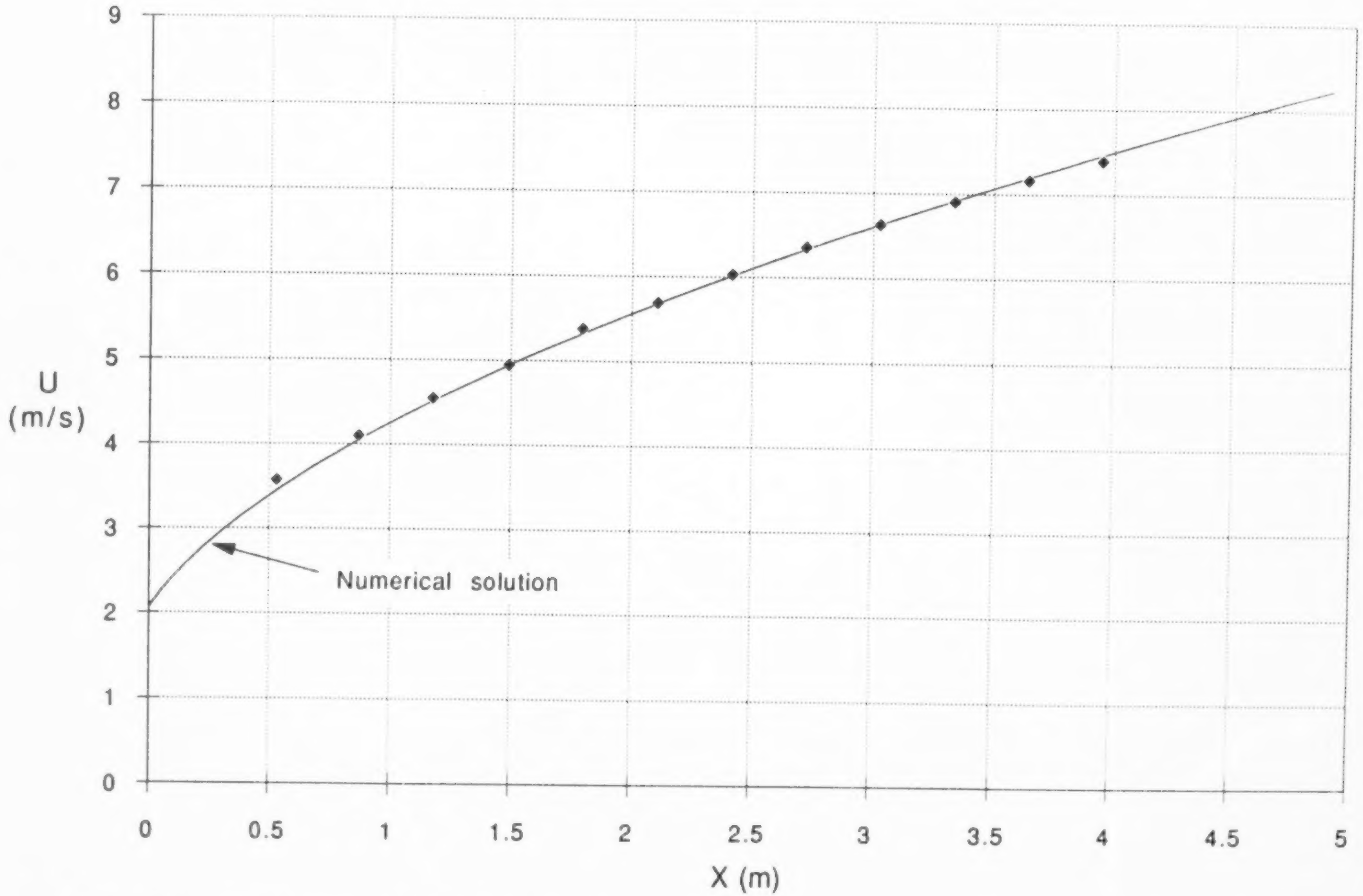

Fig. 5.25 Potential core velocity for Bauer's *rough* experiment compared with numerical solution.

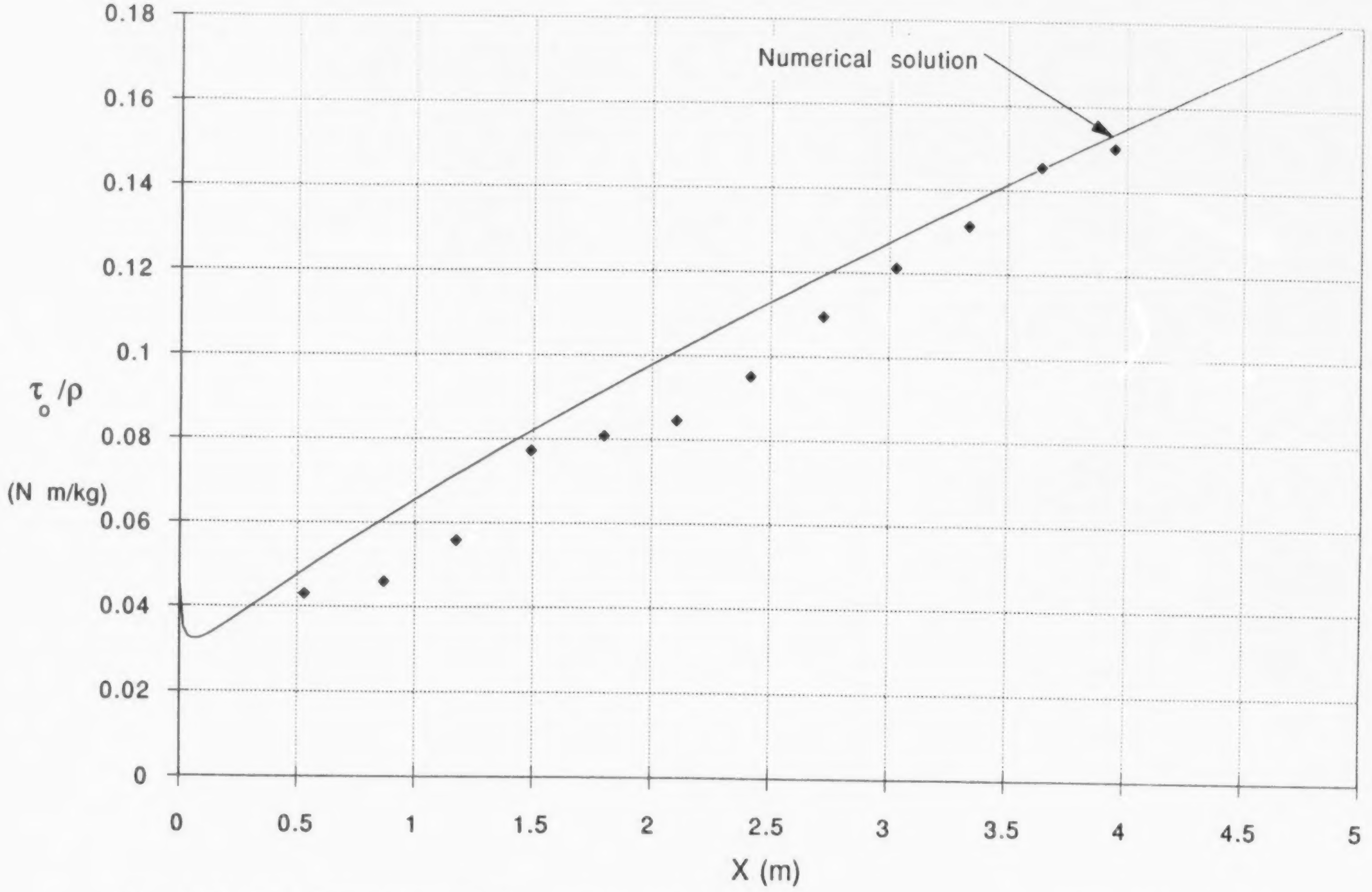

Fig. 5.26 Bed shear stress for Bauer's *rough* experiment compared with numerical solution.

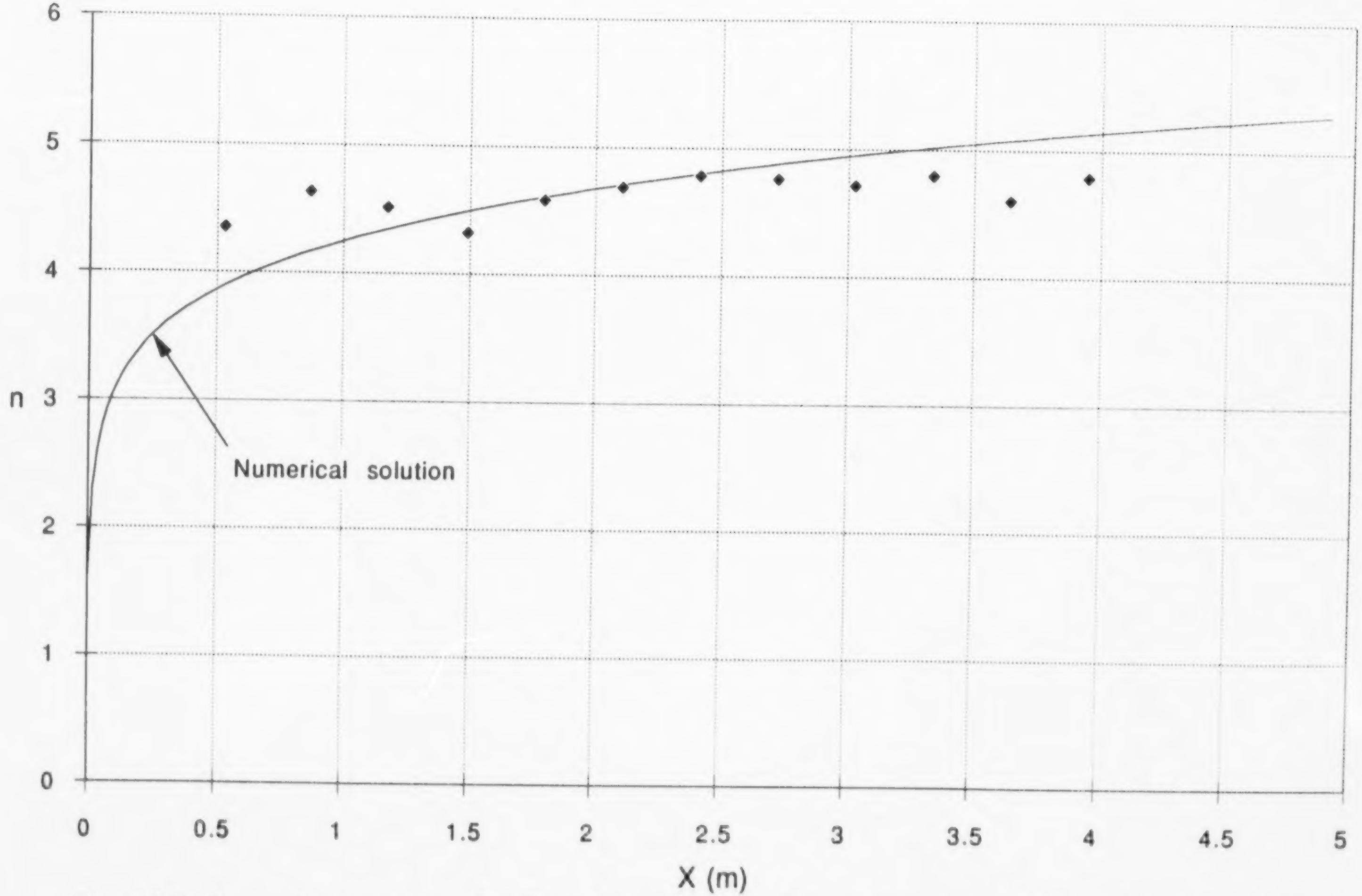

Fig. 5.27 Power law exponent for Bauer's *rough* experiment compared with numerical solution.

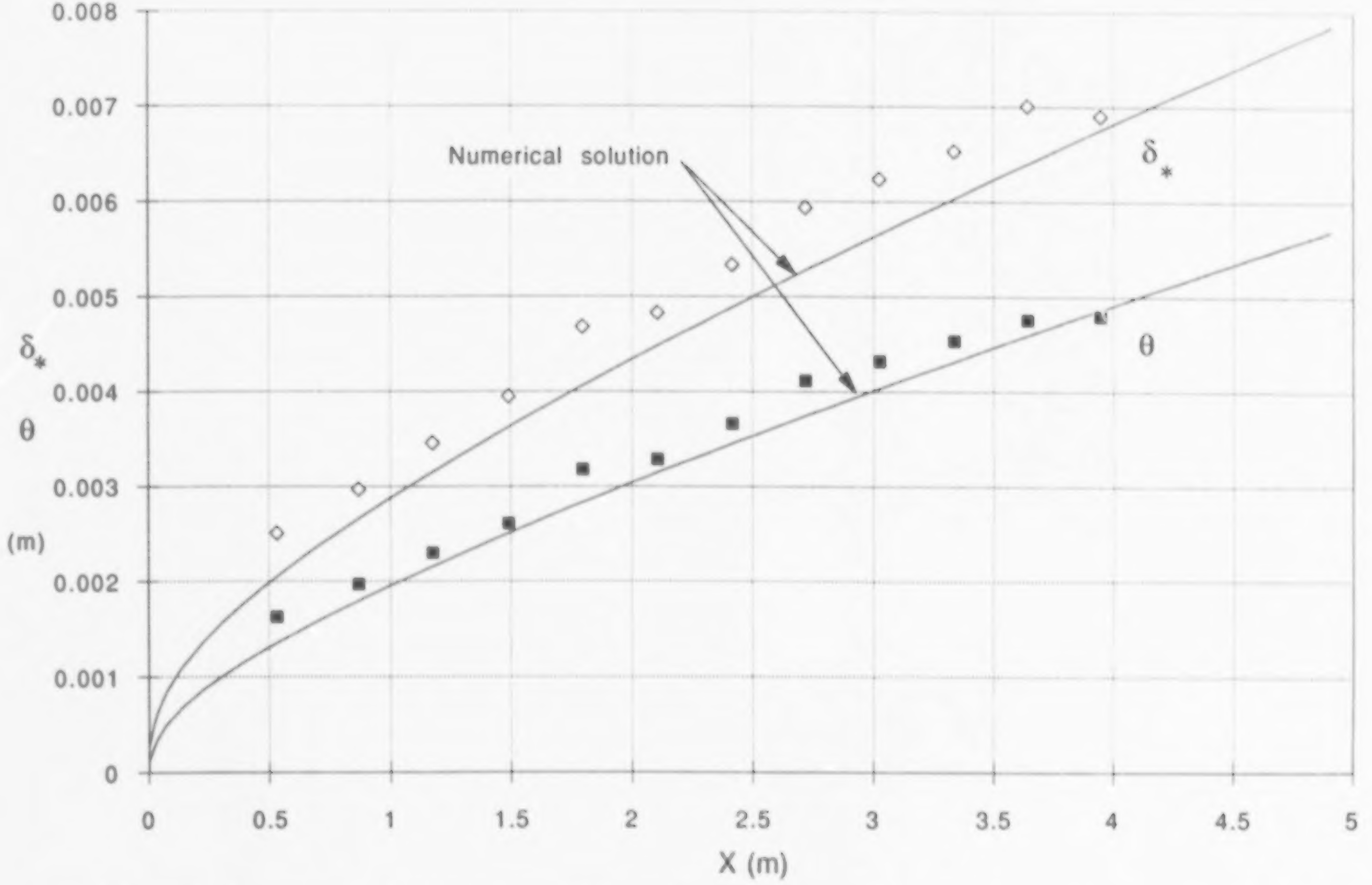

Fig. 5.28 Displacement and momentum thickness for Bauer's *rough* experiment compared with numerical solution.

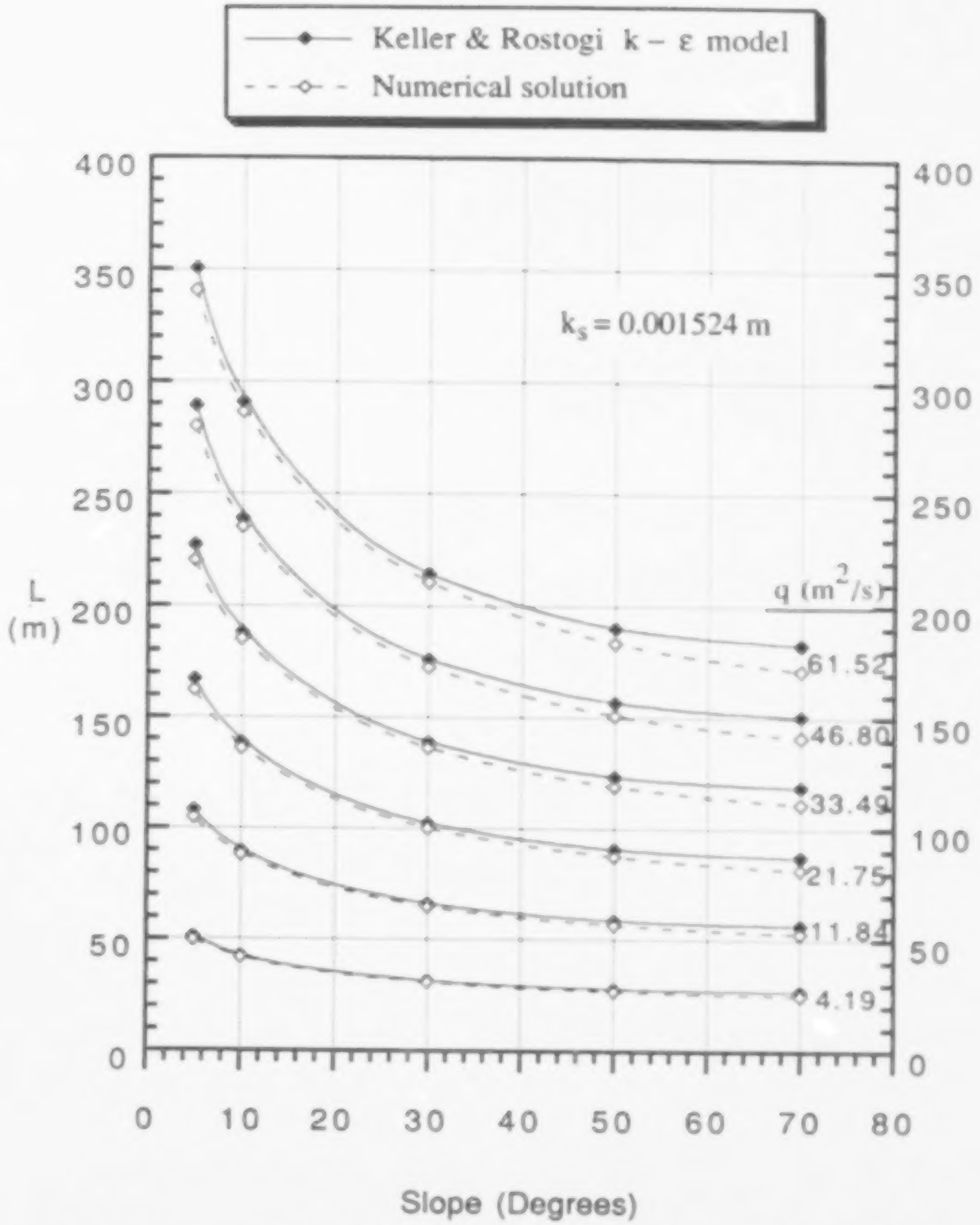

Fig. 5.29 Entrance length comparison between Keller & Rostogi's k–ε model and the numerical solution. In this comparison series the same bed roughness is used and the channel bed slope and discharge is varied.

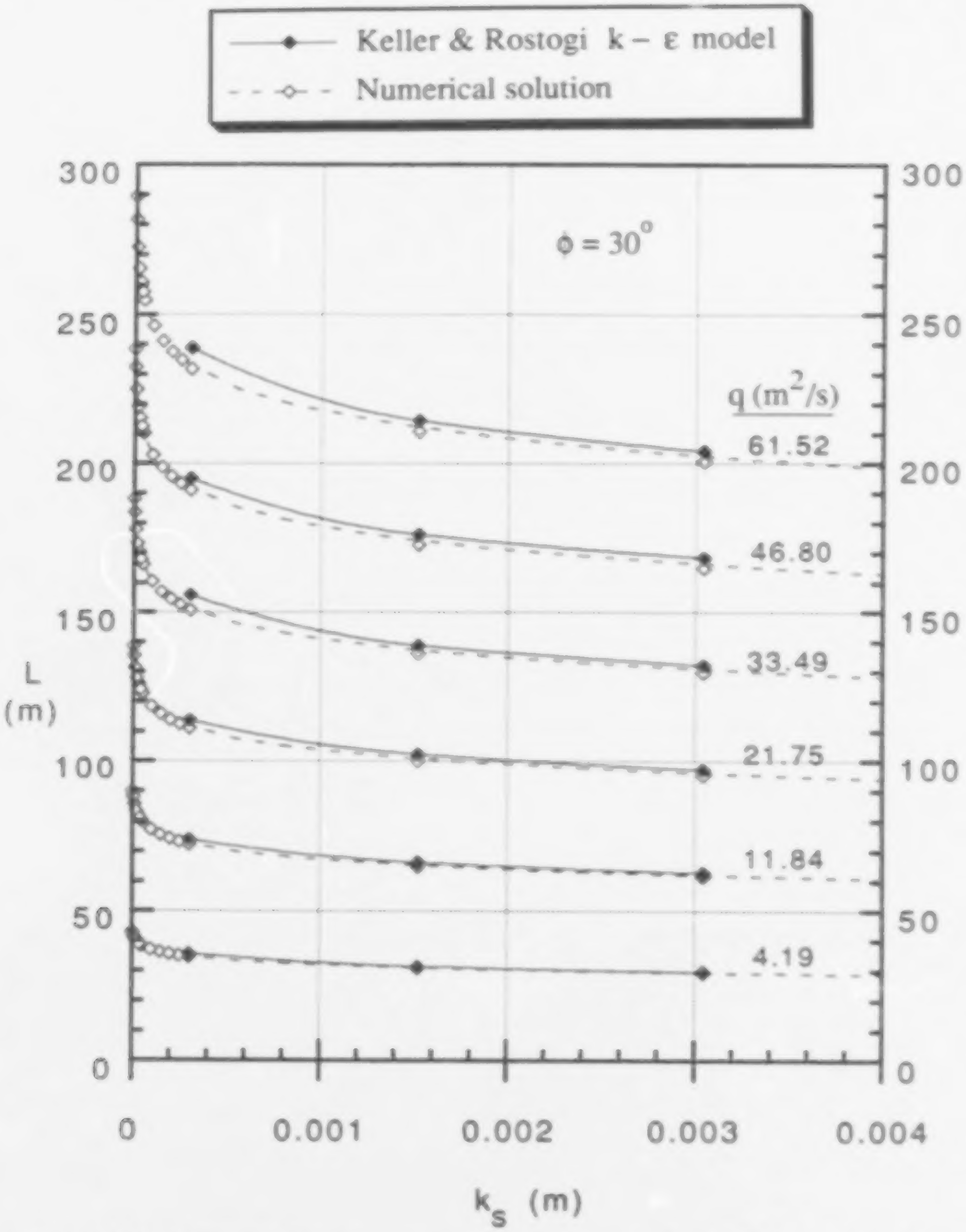

Fig. 5.30 Entrance length comparison between Keller & Rostogi's k−ε model and the numerical solution. In this comparison series the channel bed slope is constant and the bed roughness and discharge is varied.

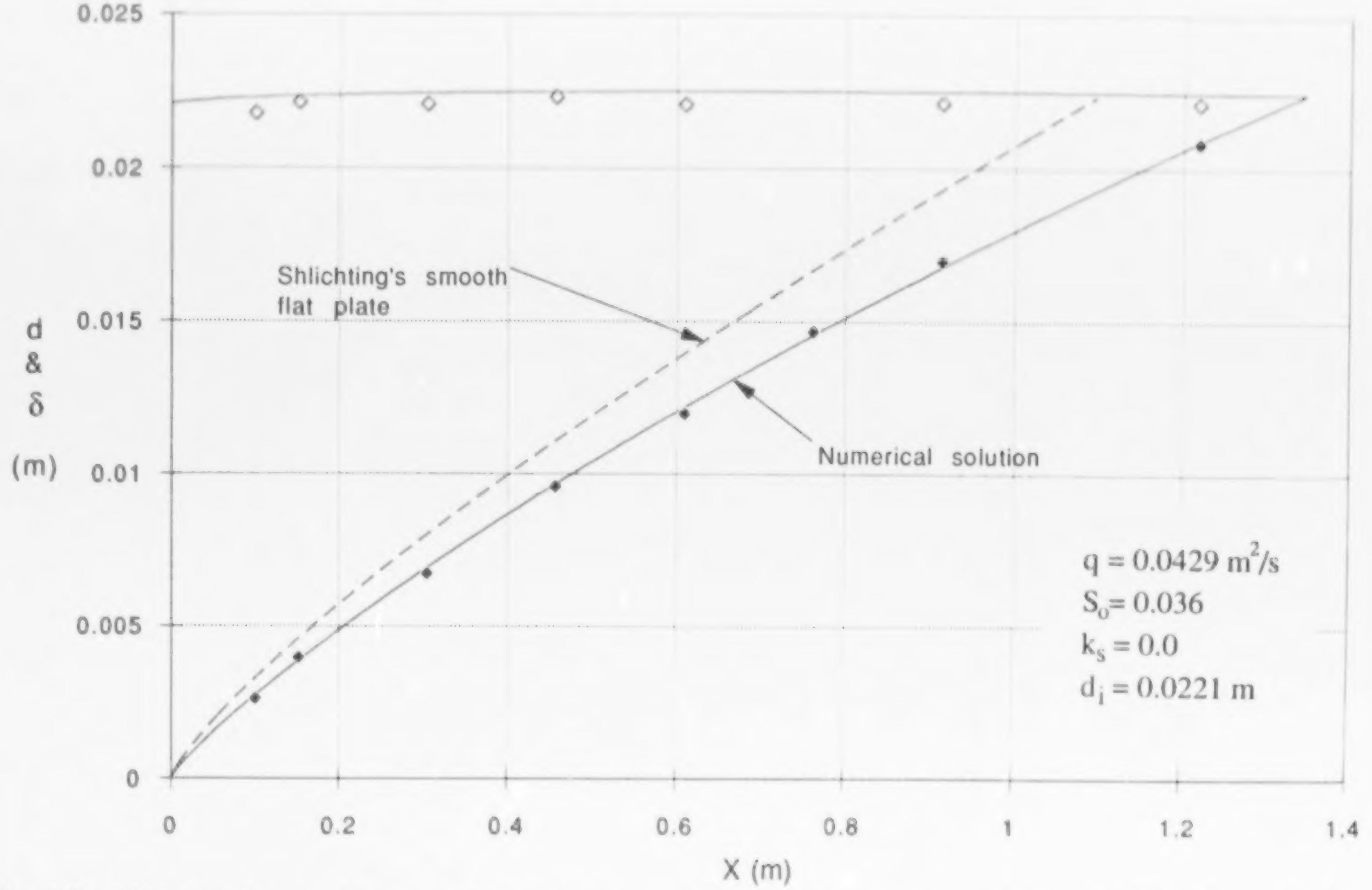

Fig. 5.31 Water surface and boundary layer thickness from Ippen's experimental Run B. Also shown is the numerical solution and Schlichting's smooth flat plate solution.

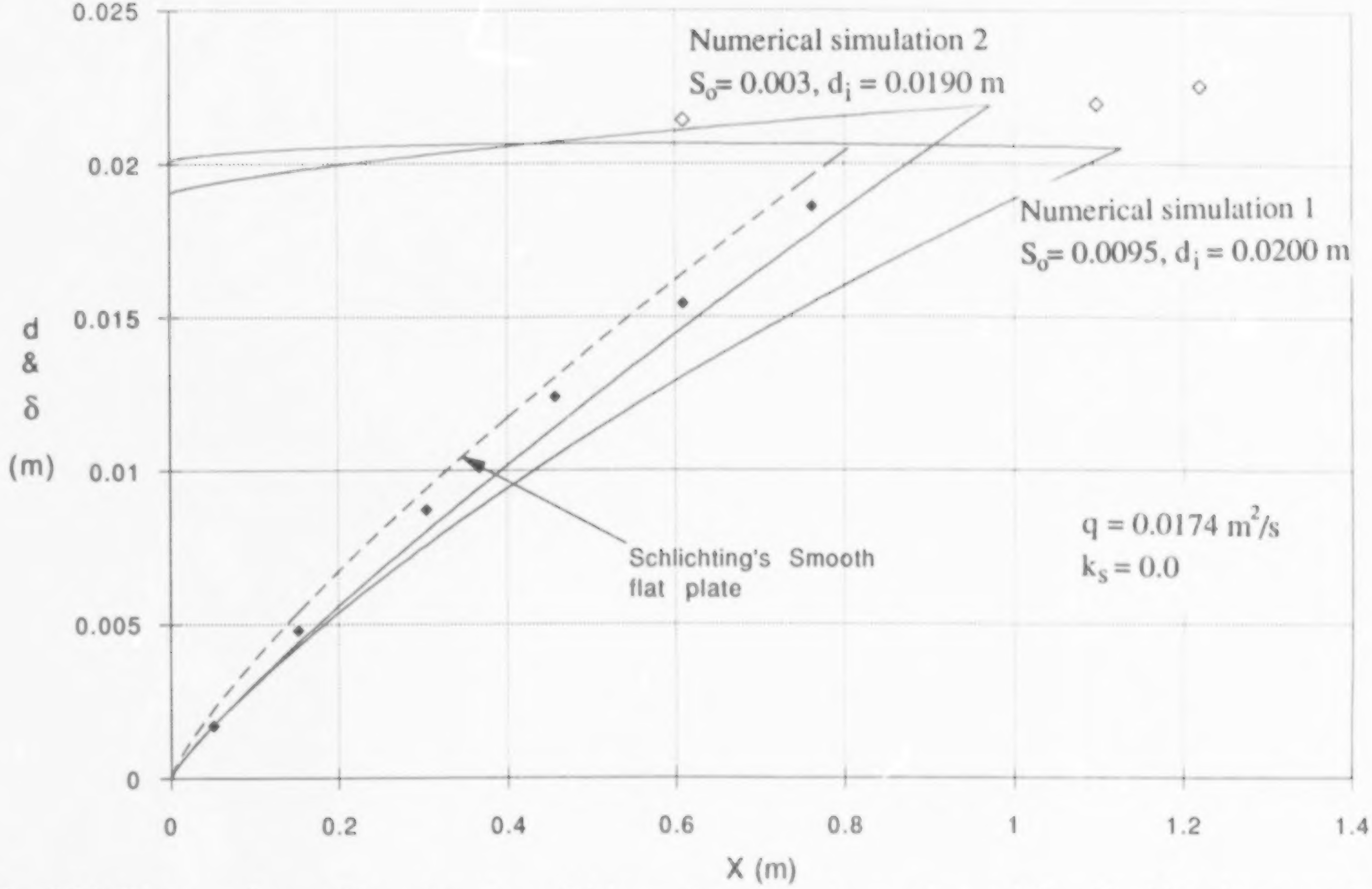

Fig. 5.32 Water surface and boundary layer thickness from Ippen's experimental Run C. Also shown are two numerical solutions and Schlichting's smooth flat plate solution.

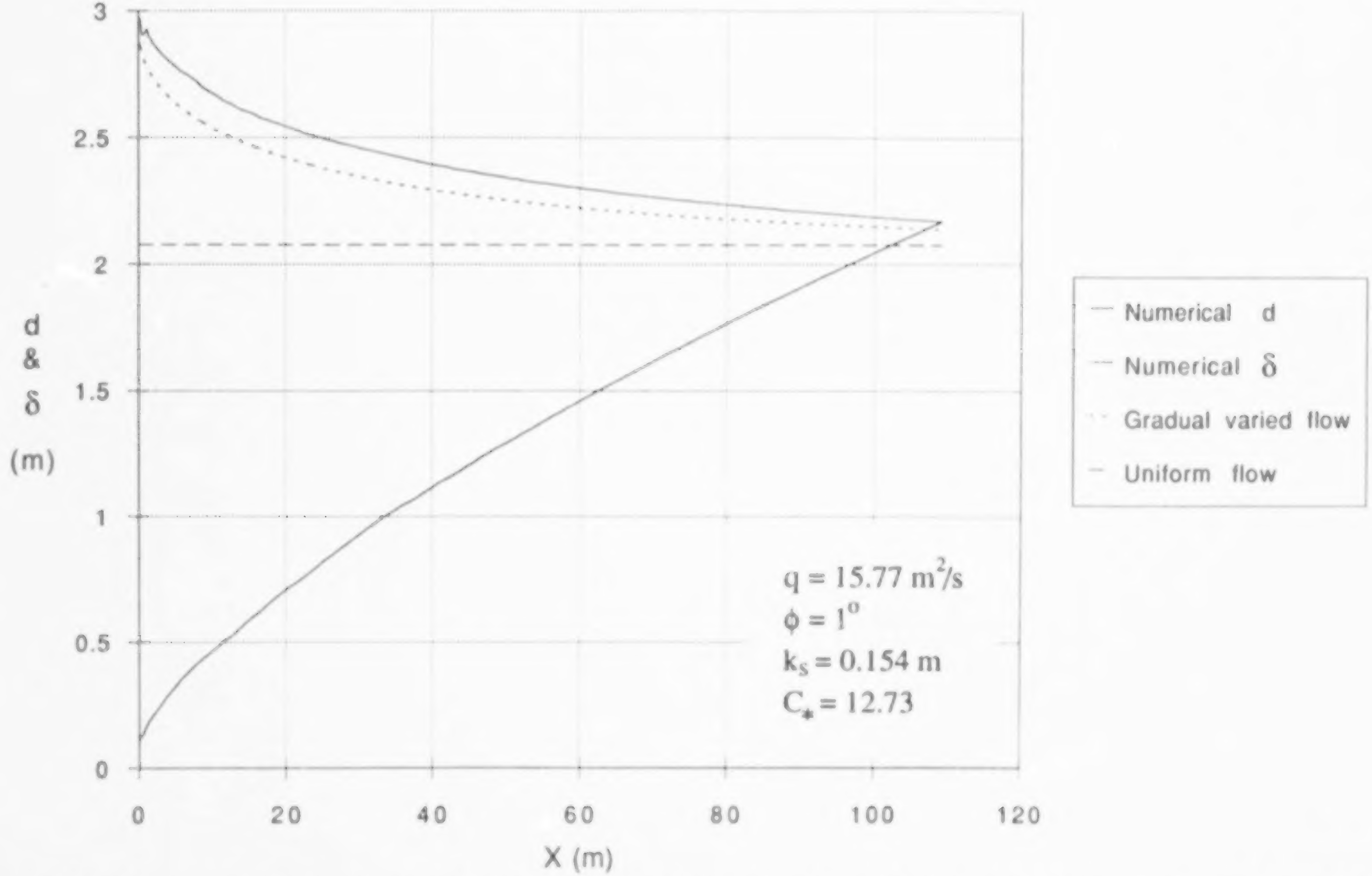

Fig. 5.33a Comparison between numerical solution for the water surface and the S2 backwater curve for $\phi=1$ degree and $C_*= 12.73$. Also shown is the boundary layer thickness and uniform depth.

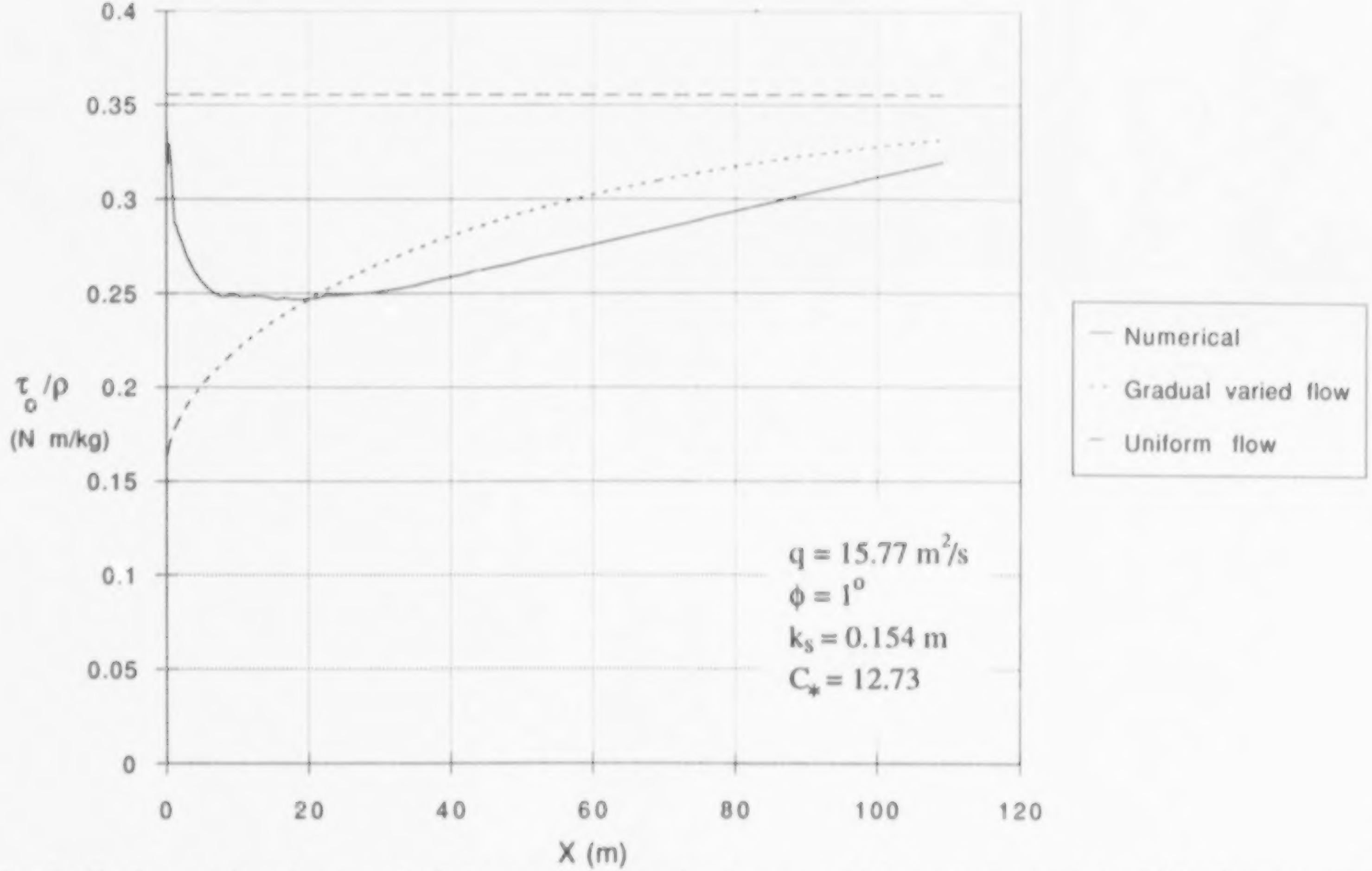

Fig. 5.33b Comparison between bed shear stress given by the numerical simulation and the S2 backwater curve for ϕ=1 degree and C_*= 12.73. Also shown is uniform flow shear.

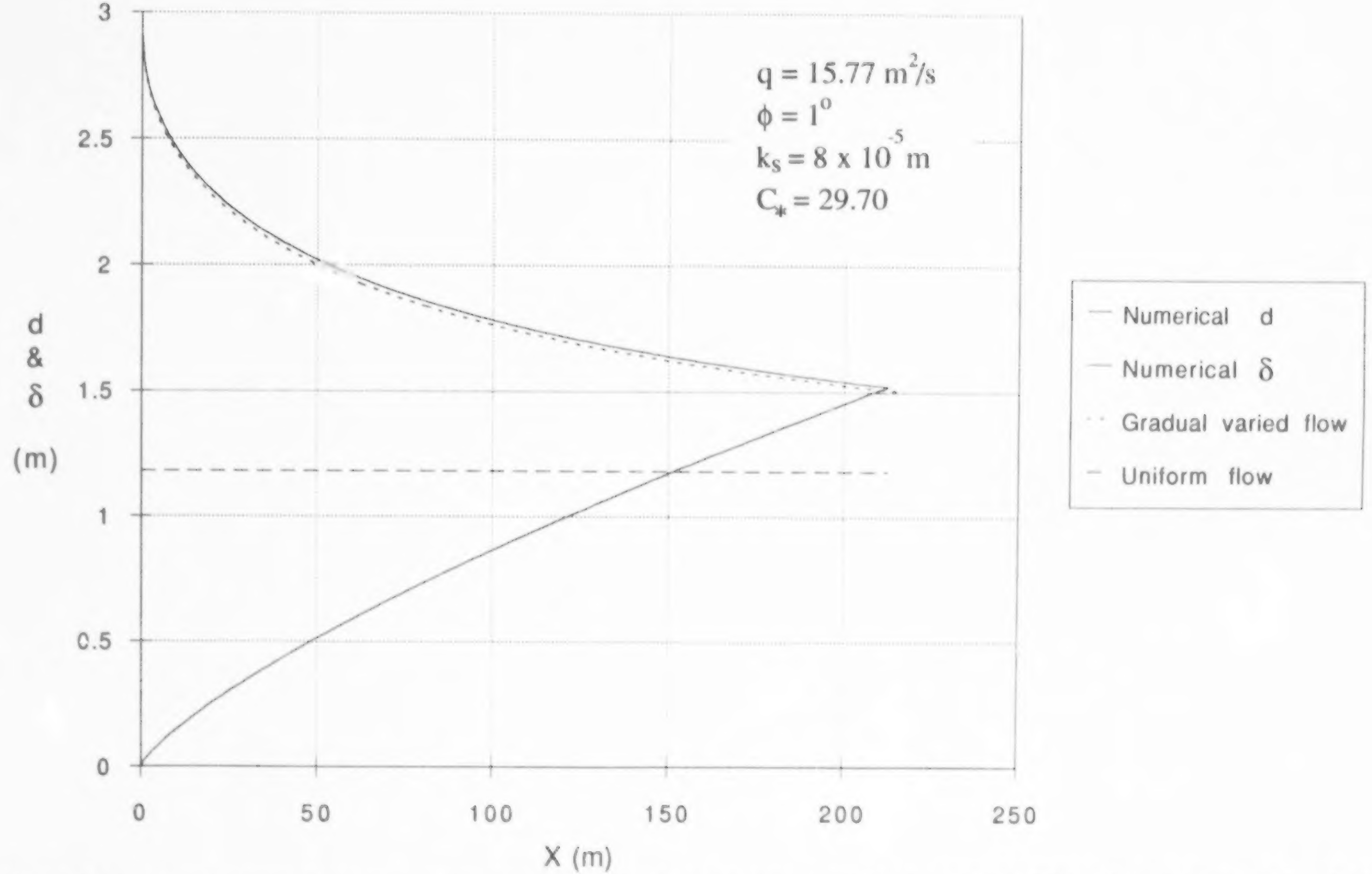

Fig. 5.34a Comparison between numerical solution for the water surface and the S2 backwater curve for $\phi=1$ degree and $C_*= 29.70$. Also shown is the boundary layer thickness and uniform depth.

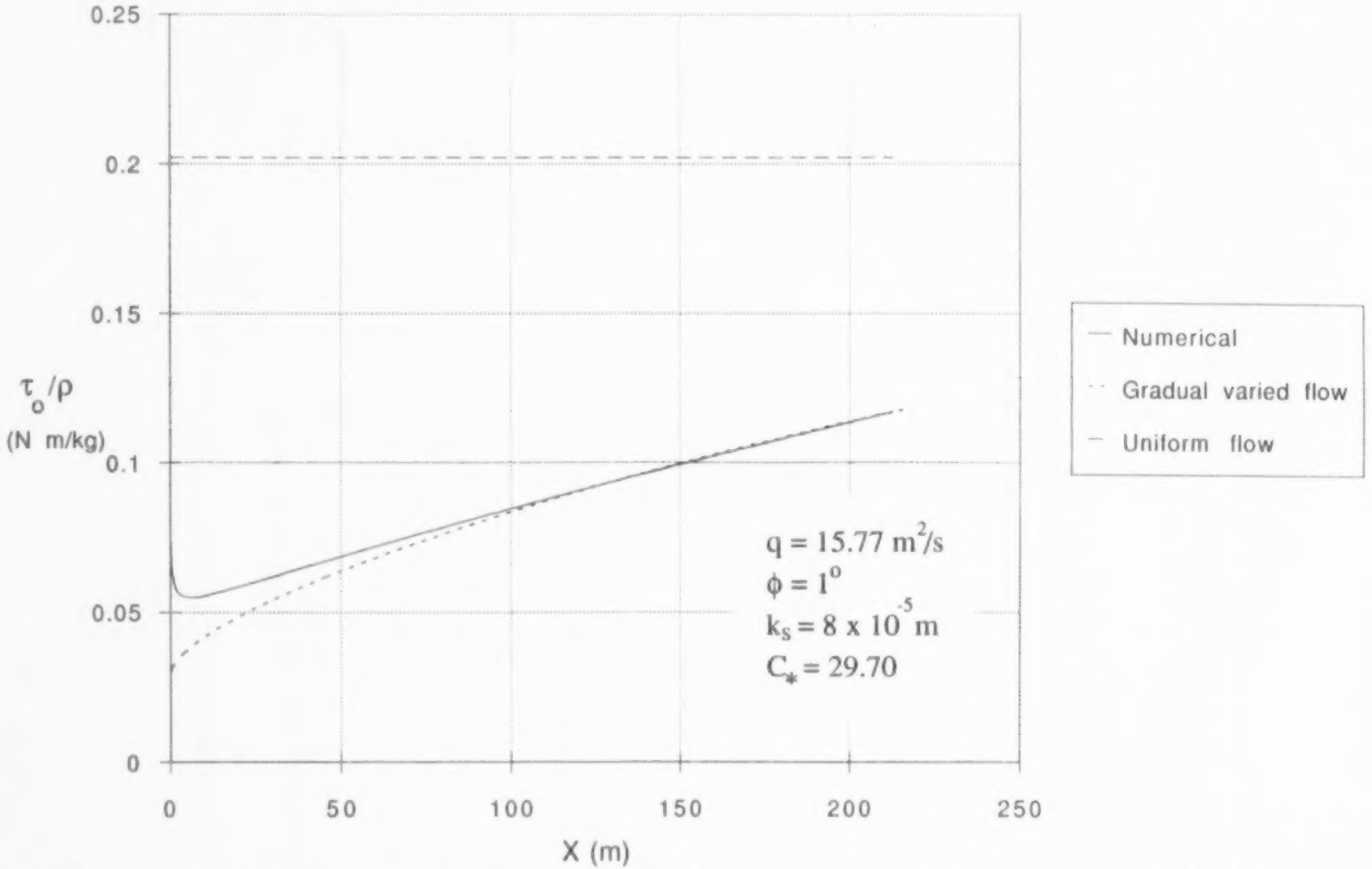

Fig. 5.34b Comparison between bed shear stress given by the numerical simulation and the S2 backwater curve for ϕ=1 degree and C∗= 29.70. Also shown is uniform flow shear.

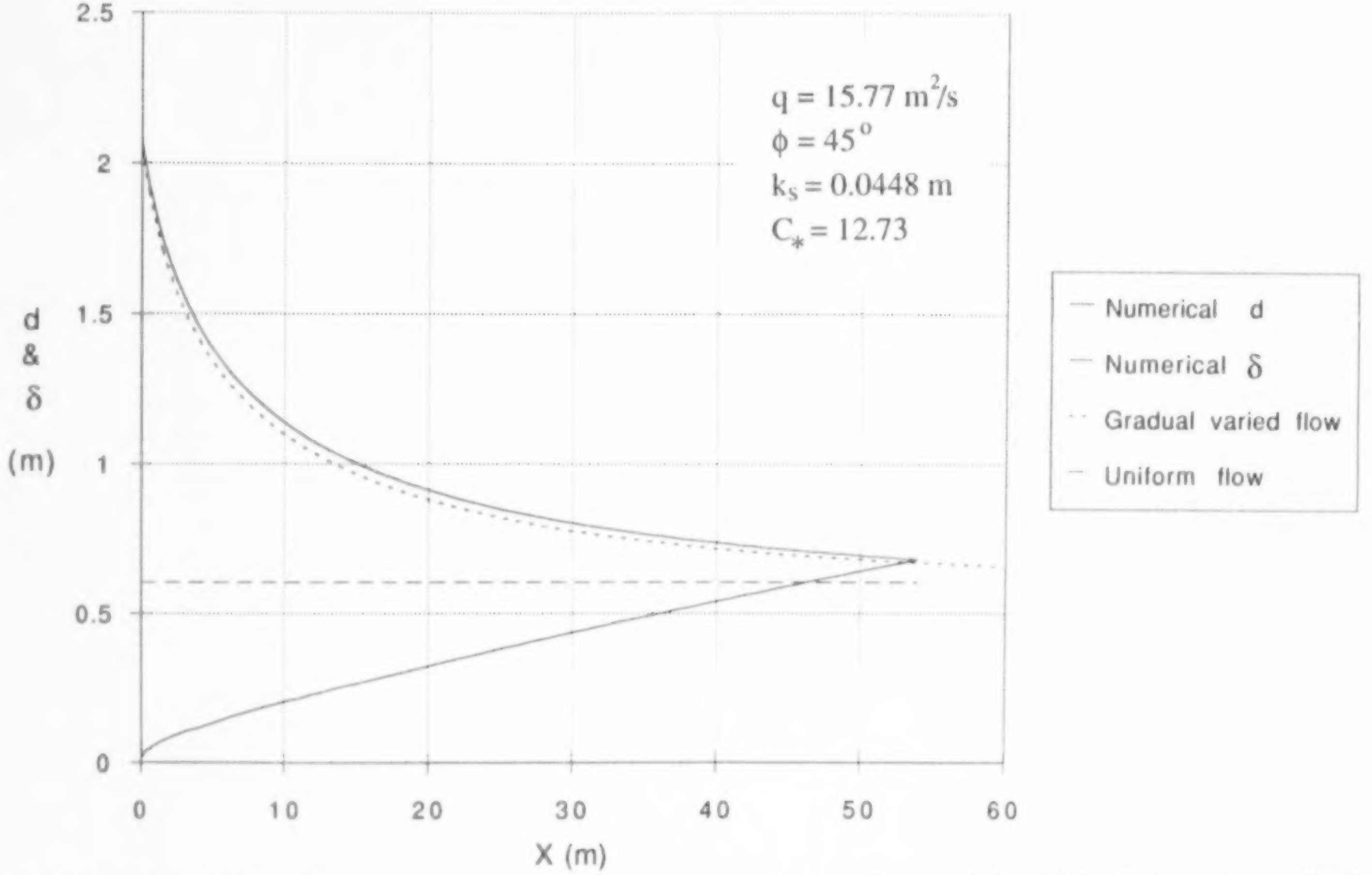

Fig. 5.35a Comparison between numerical solution for the water surface and the S2 backwater curve for $\phi=45$ degrees and $C_*= 12.73$. Also shown is the boundary layer thickness and uniform depth.

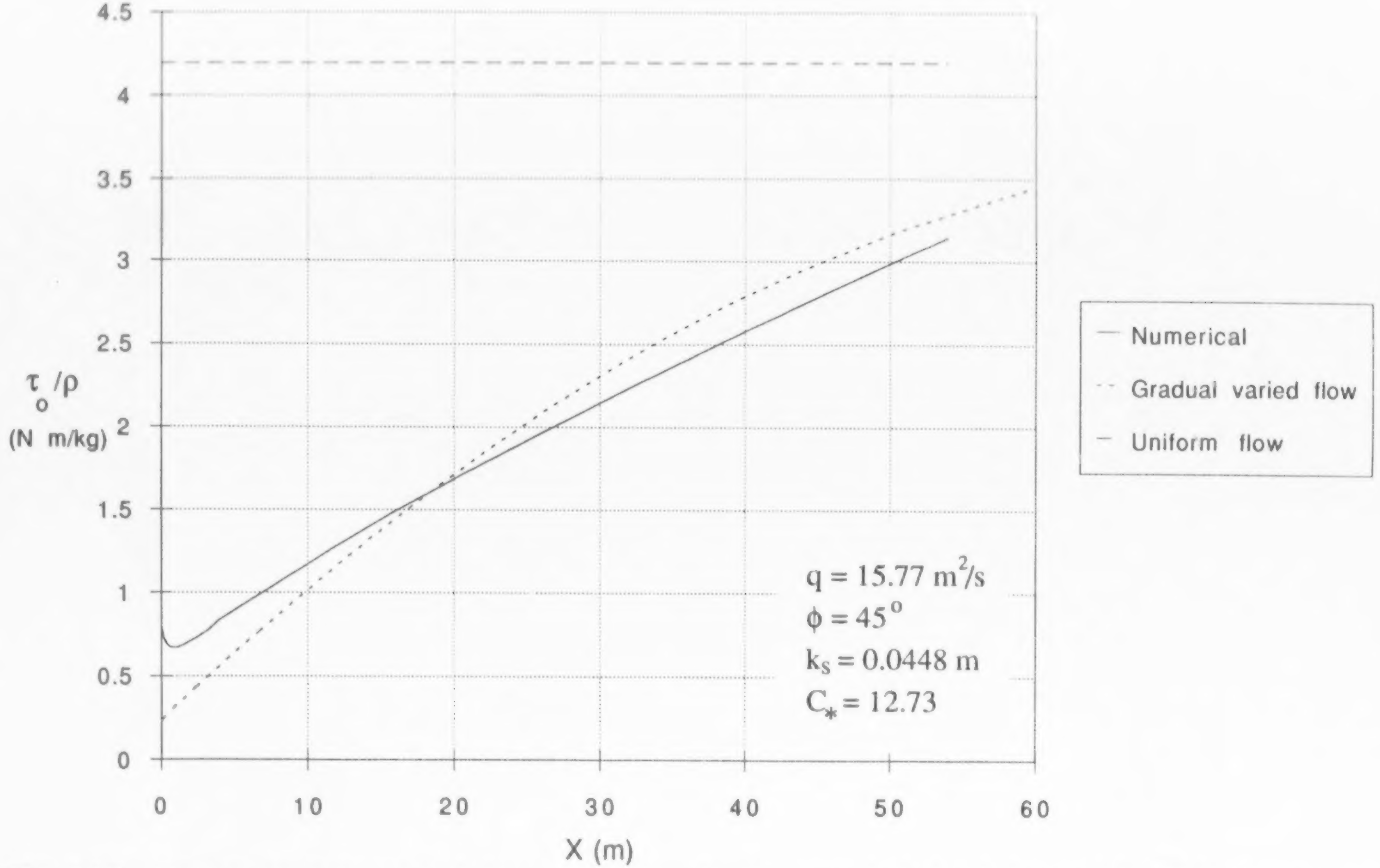

Fig. 5.35b Comparison between bed shear stress given by the numerical simulation and the S2 backwater curve for ϕ=45 degrees and C∗= 12.73. Also shown is uniform flow shear.

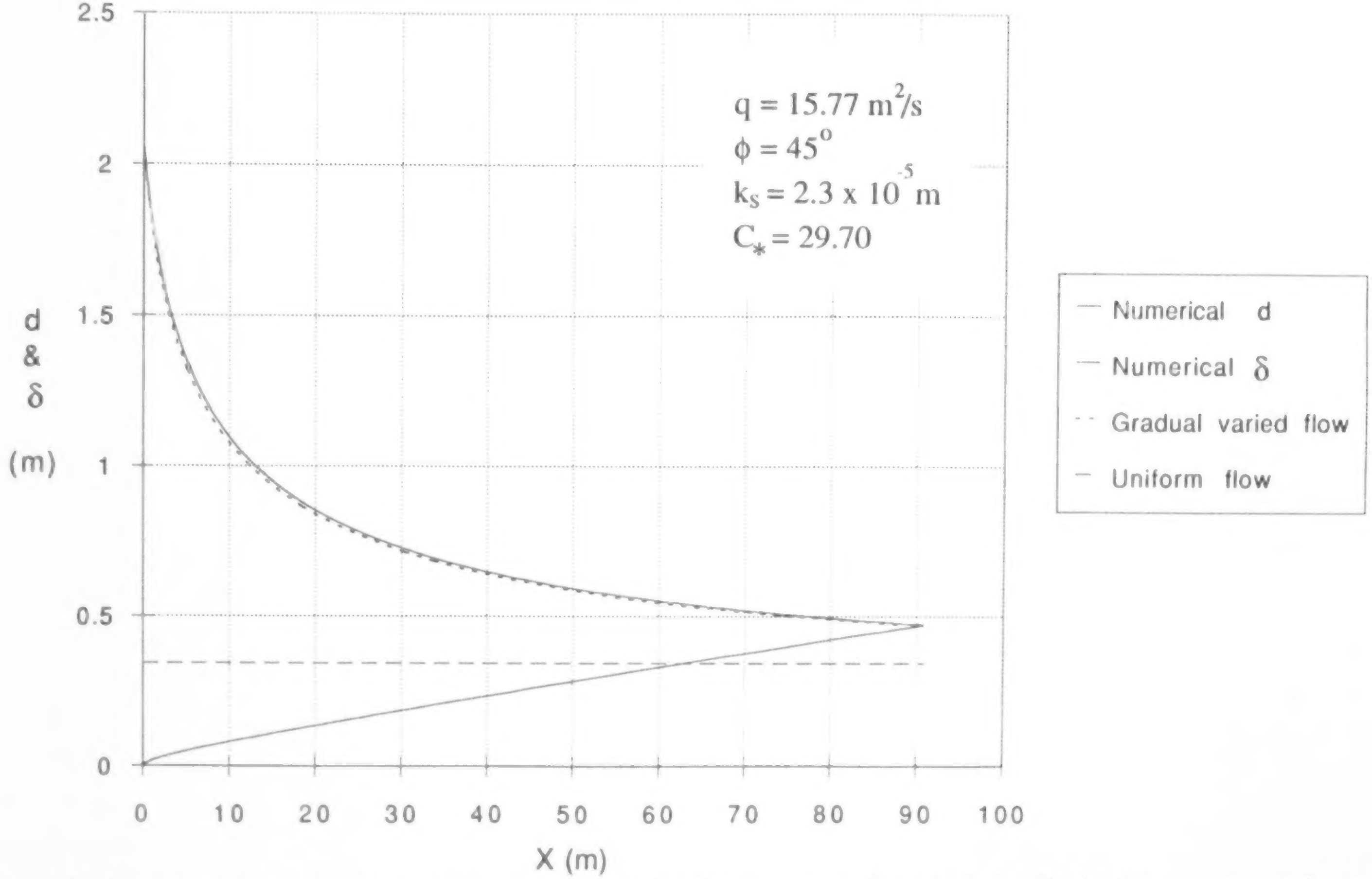

Fig. 5.36a Comparison between numerical solution for the water surface and the S2 backwater curve for $\phi=45$ degrees and $C_*= 29.70$. Also shown is the boundary layer thickness and uniform depth.

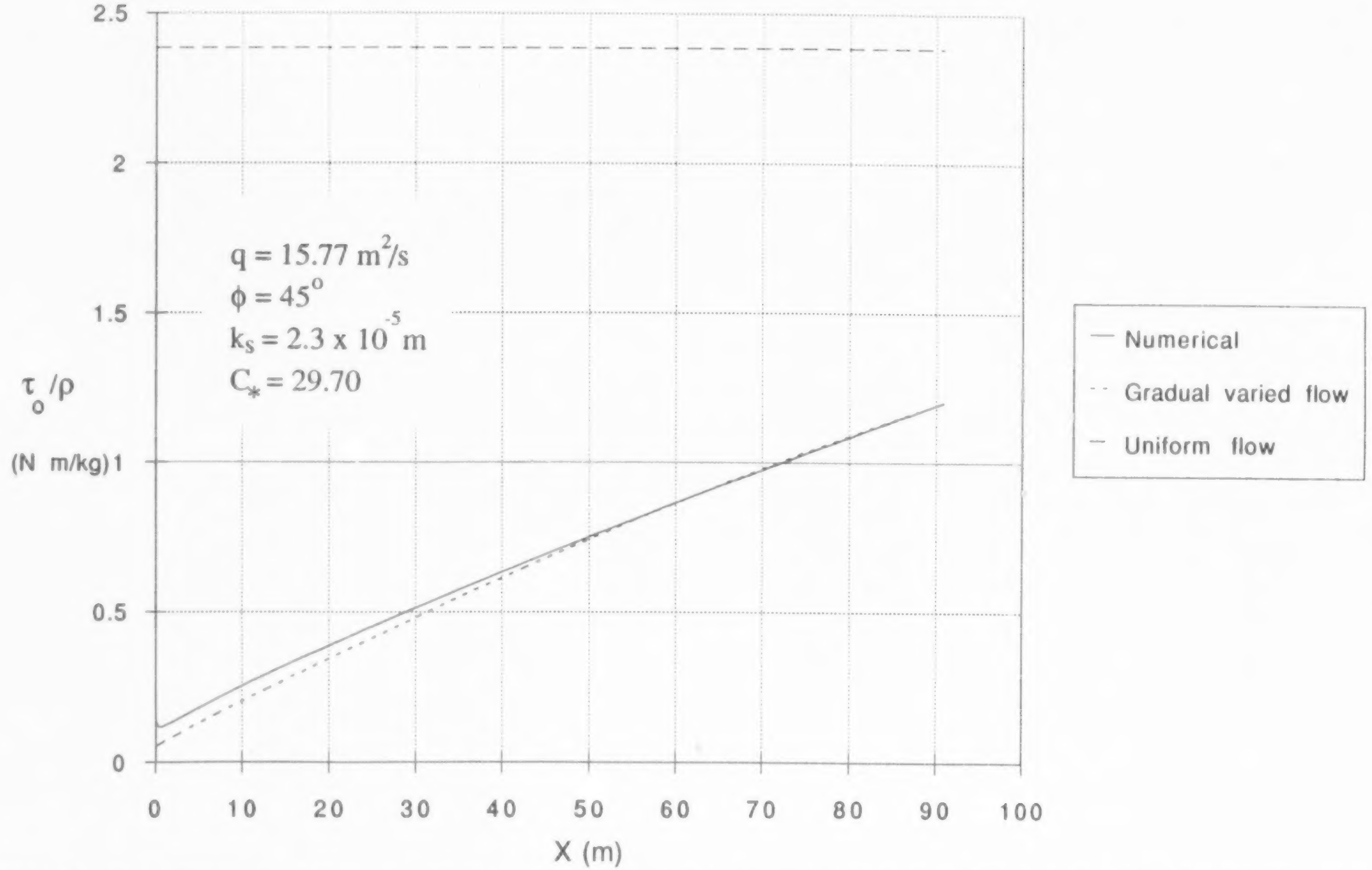

Fig. 5.36b Comparison between bed shear stress given by the numerical simulation and the S2 backwater curve for ϕ=45 degrees and C_*= 29.70. Also shown is uniform flow shear.

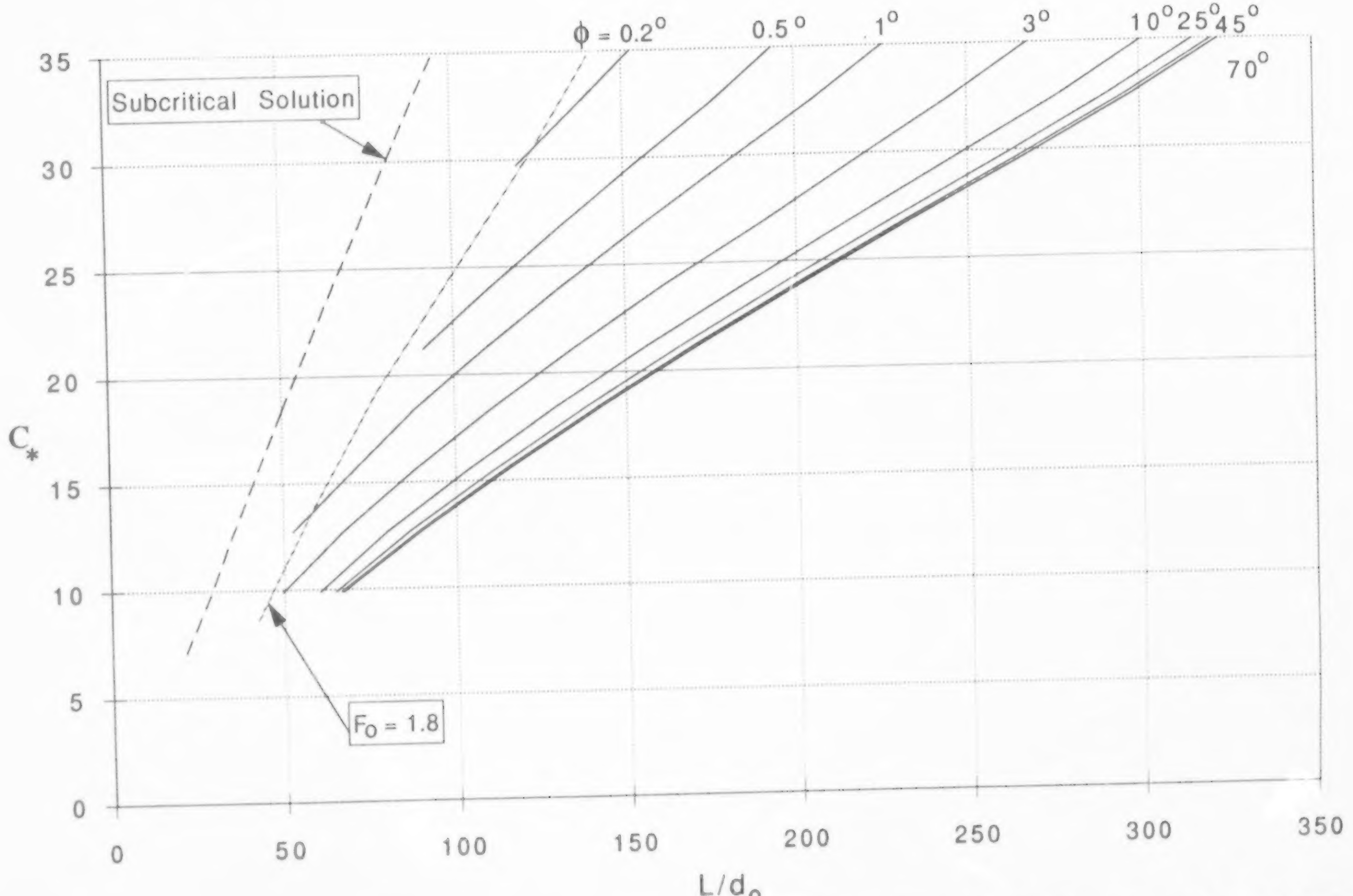

Fig. 5.37 Dimensionless entrance length as a function of the uniform flow C* and the slope of the channel in degrees. Also shown is the subcritical numerical solution for the mild channel.

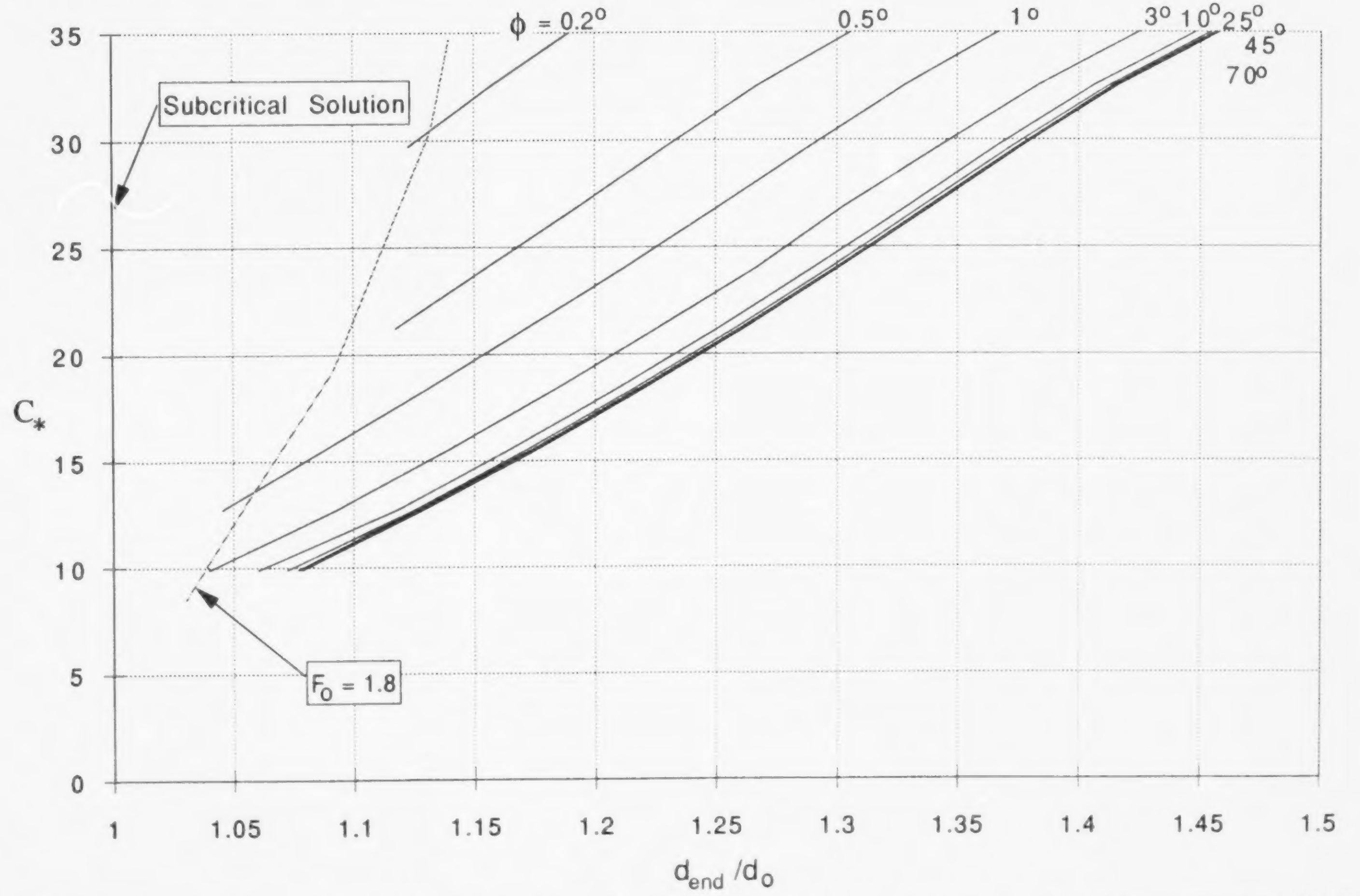

Fig. 5.38 The ratio of end depth(depth at which the boundary layer reaches the surface) to normal depth as a function of the uniform flow C∗ and the slope of the channel in degrees.

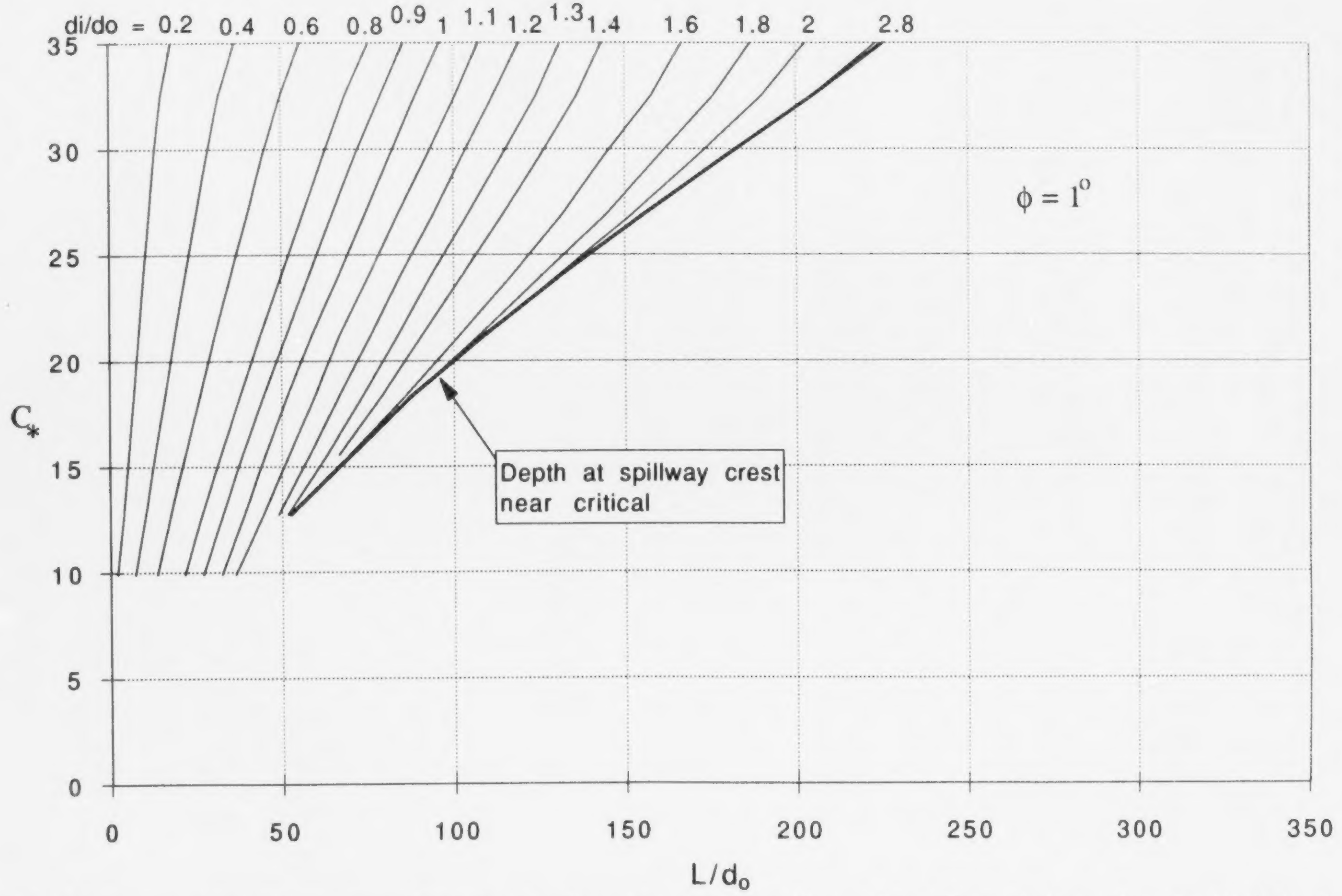

Fig. 5.39 Dimensionless entrance length as a function of the uniform flow C* and the ratio of initial depth at the channel entrance to normal depth for a channel slope of 1 degree. Initial depth controlled by a sluice gate.

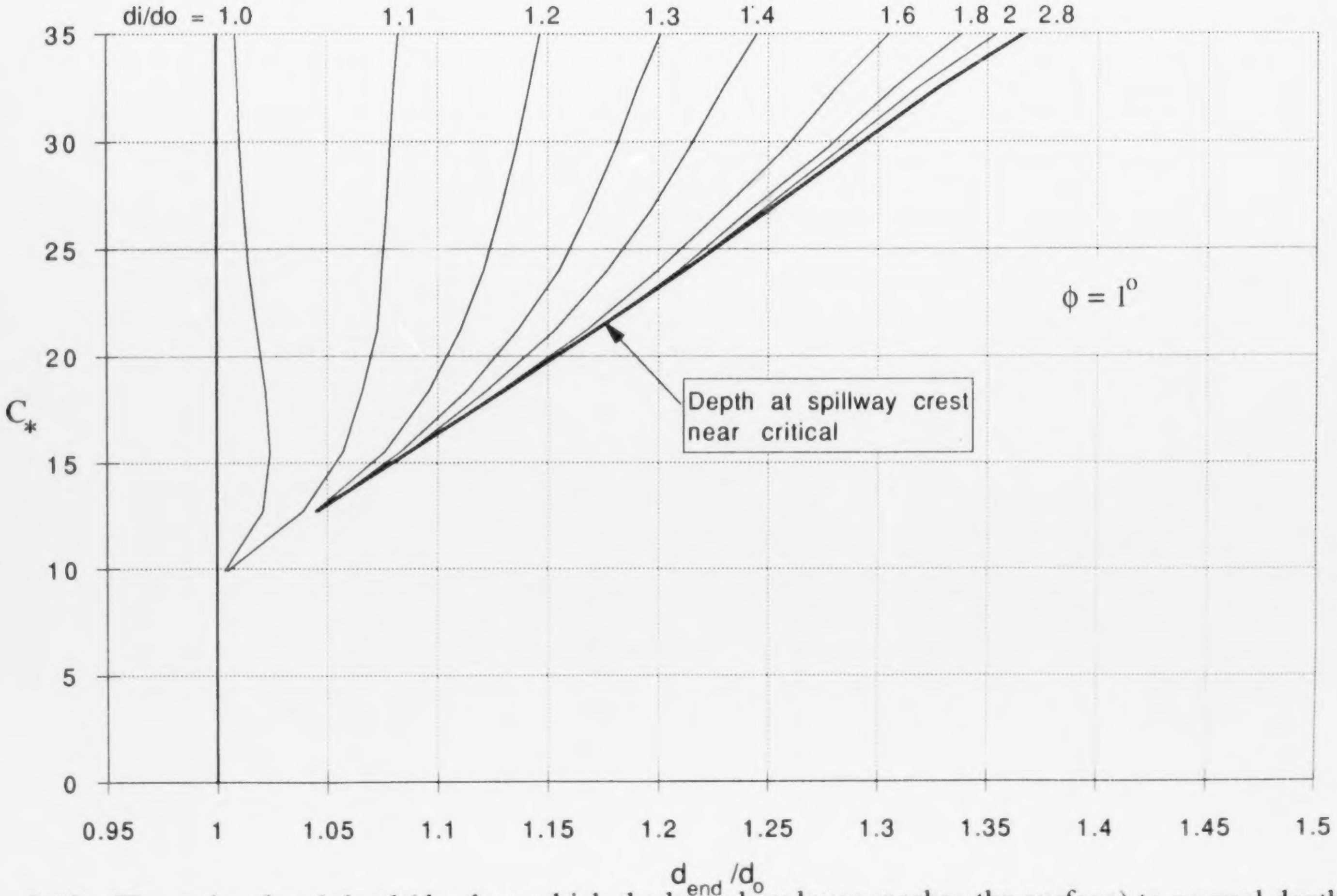

Fig. 5.40a The ratio of end depth(depth at which the boundary layer reaches the surface) to normal depth as a function of the uniform flow C* and the ratio of initial depth at the channel entrance to normal depth for a channel slope of 1 degree. Initial depth controlled by a sluice gate.

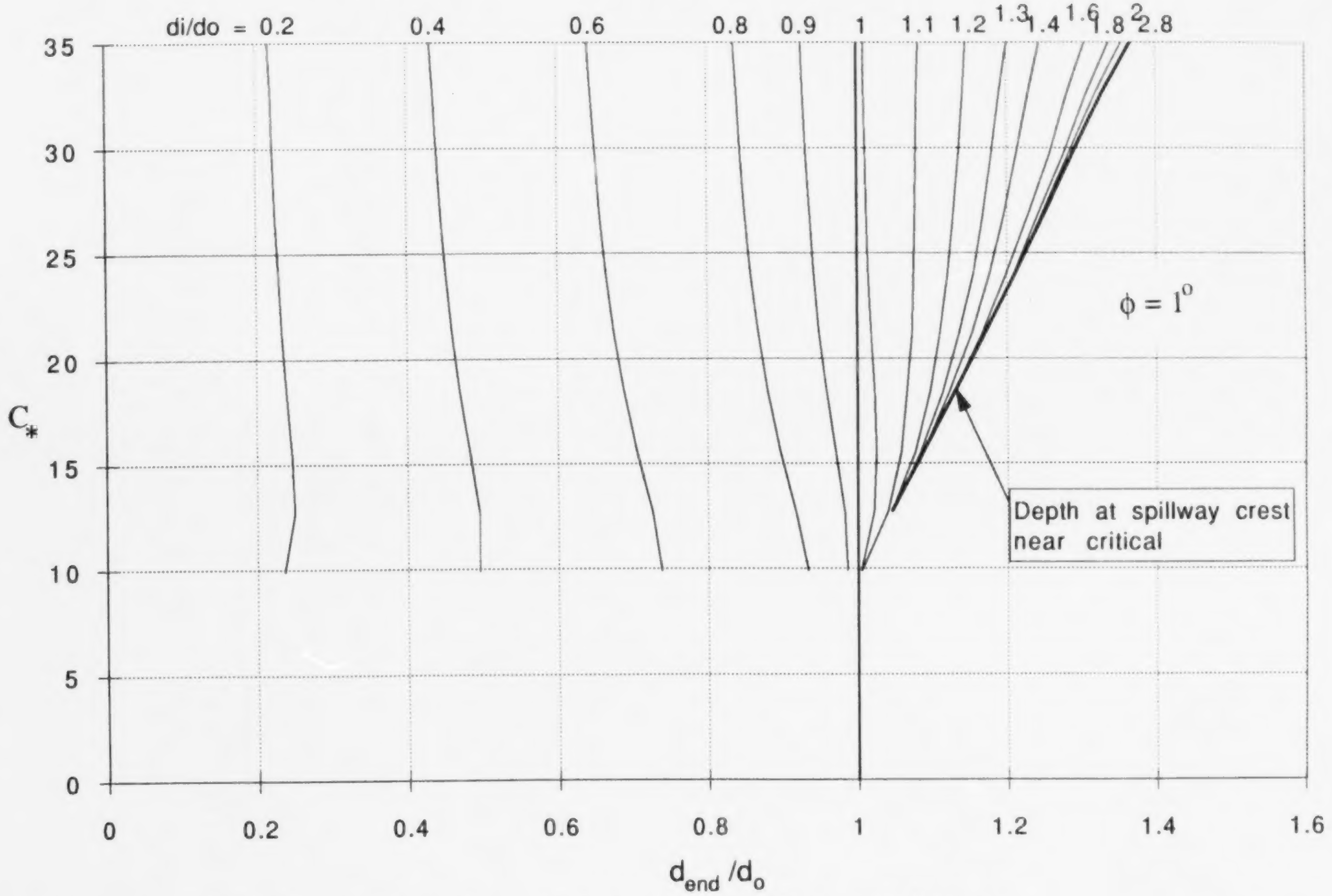

Fig. 5.40b Same as Figure 5.40a but also includes $d_i/d_o<1$. Slope = 1 degree.

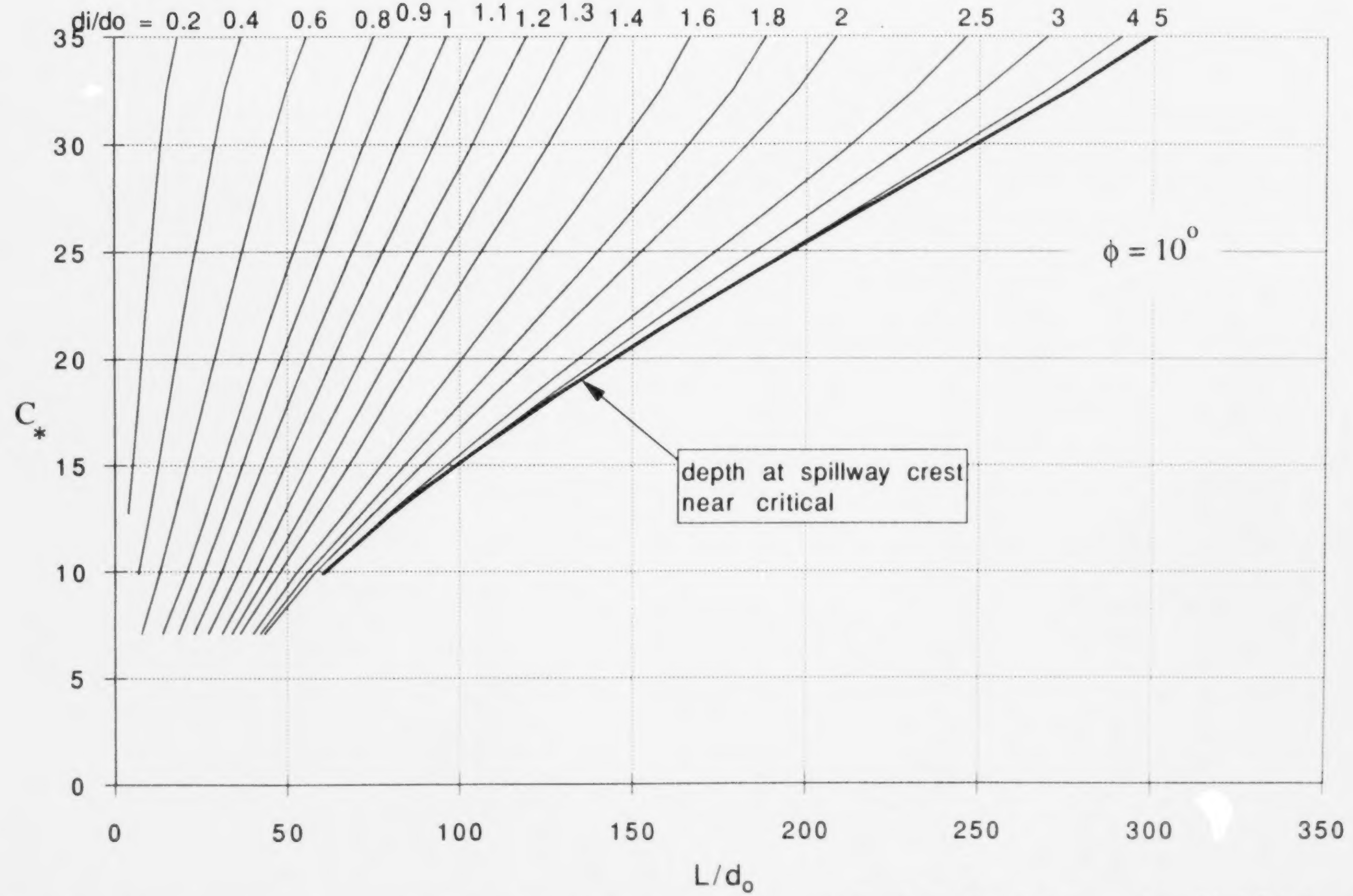

Fig. 5.41 Dimensionless entrance length as a function of the uniform flow C∗ and the ratio of initial depth at the channel entrance to normal depth for a channel slope of 10 degrees. Initial depth controlled by a sluice gate.

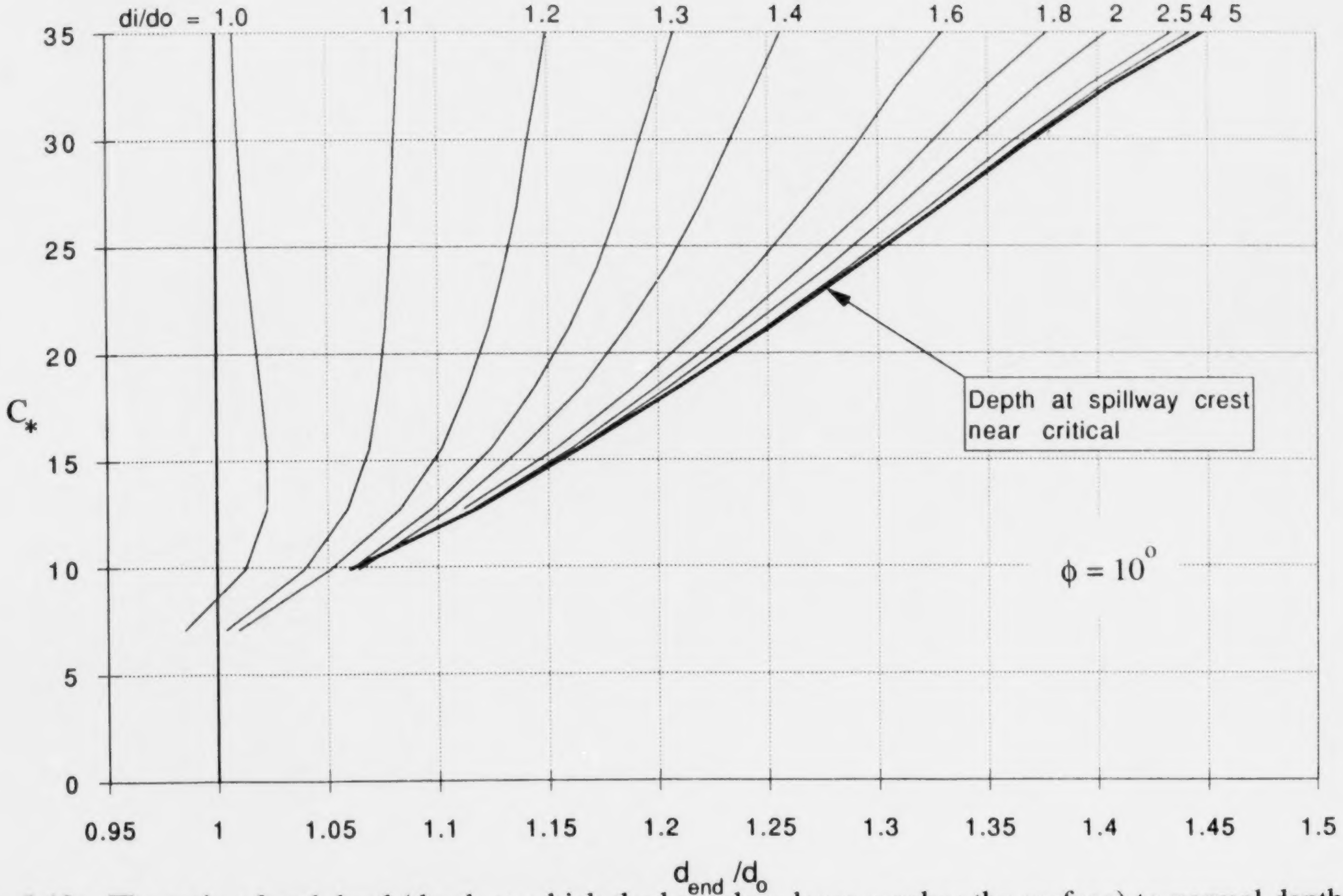

Fig. 5.42a The ratio of end depth(depth at which the boundary layer reaches the surface) to normal depth as a function of the uniform flow C_* and the ratio of initial depth at the channel entrance to normal depth for a channel slope of 10 degrees. Initial depth controlled by a sluice gate.

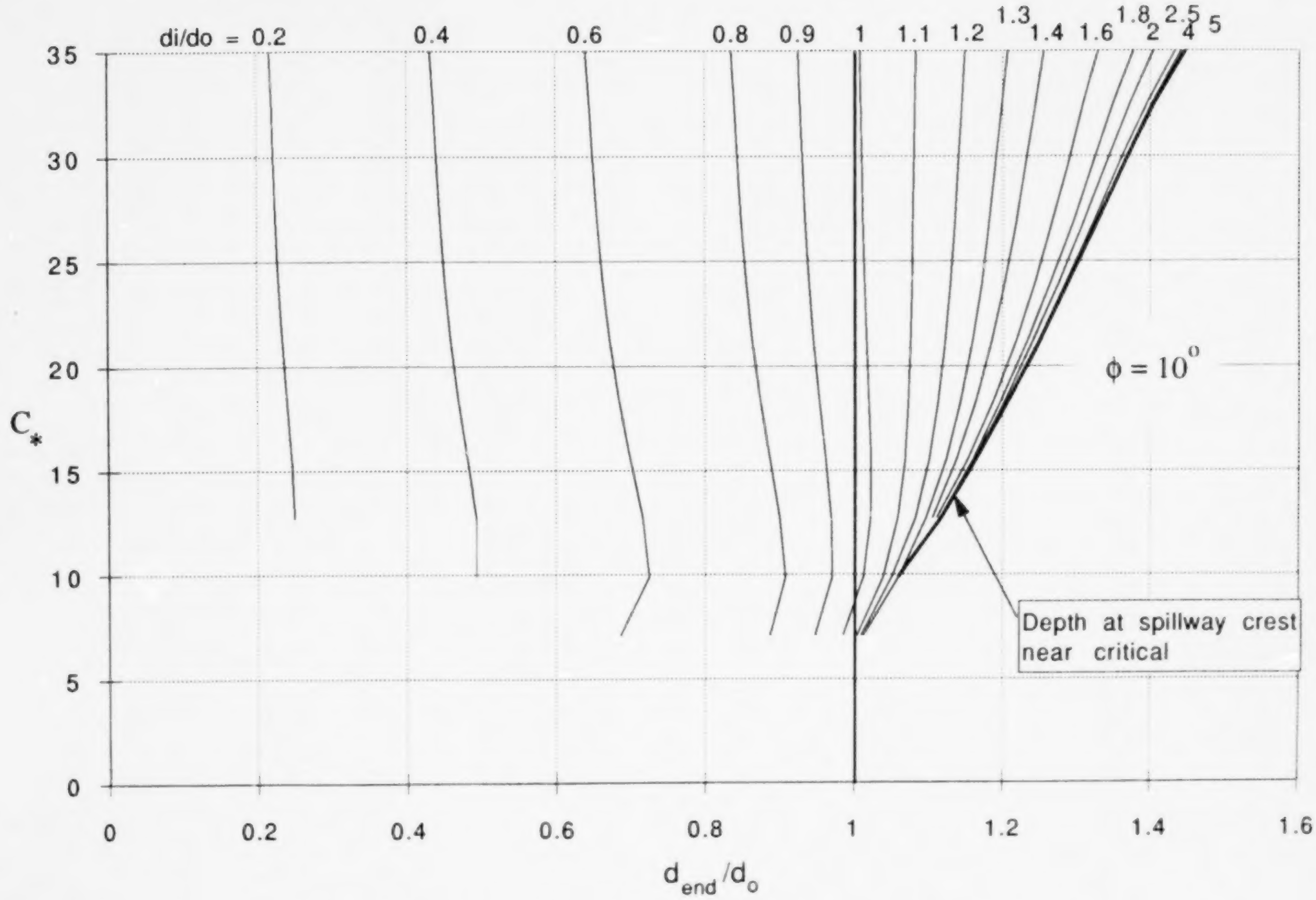

Fig. 5.42b Same as Figure 5.42a but also includes $d_i/d_o<1$. Slope = 10 degrees.

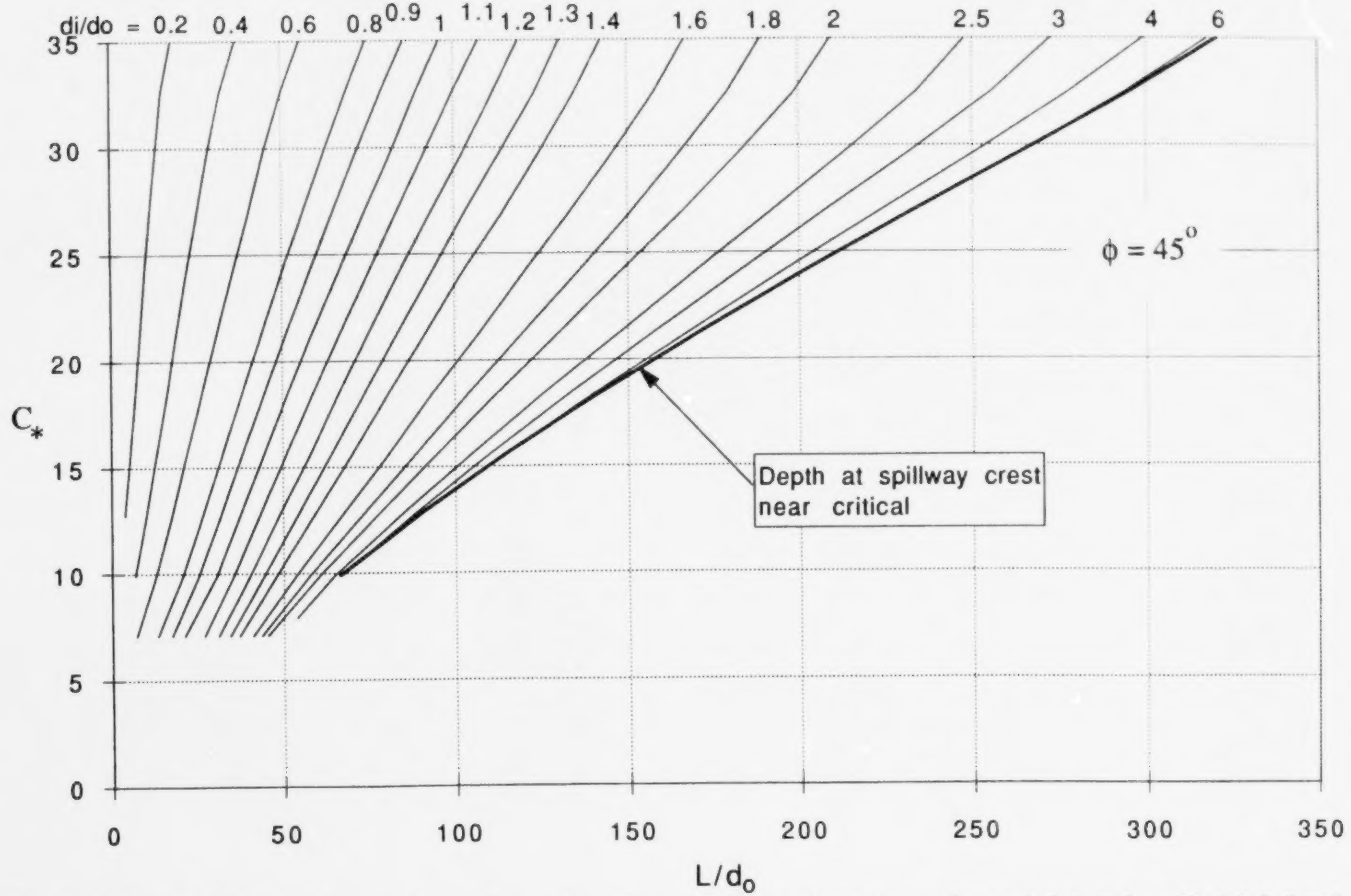

Fig. 5.43 Dimensionless entrance length as a function of the uniform flow C∗ and the ratio of initial depth at the channel entrance to normal depth for a channel slope of 45 degrees. Initial depth controlled by a sluice gate.

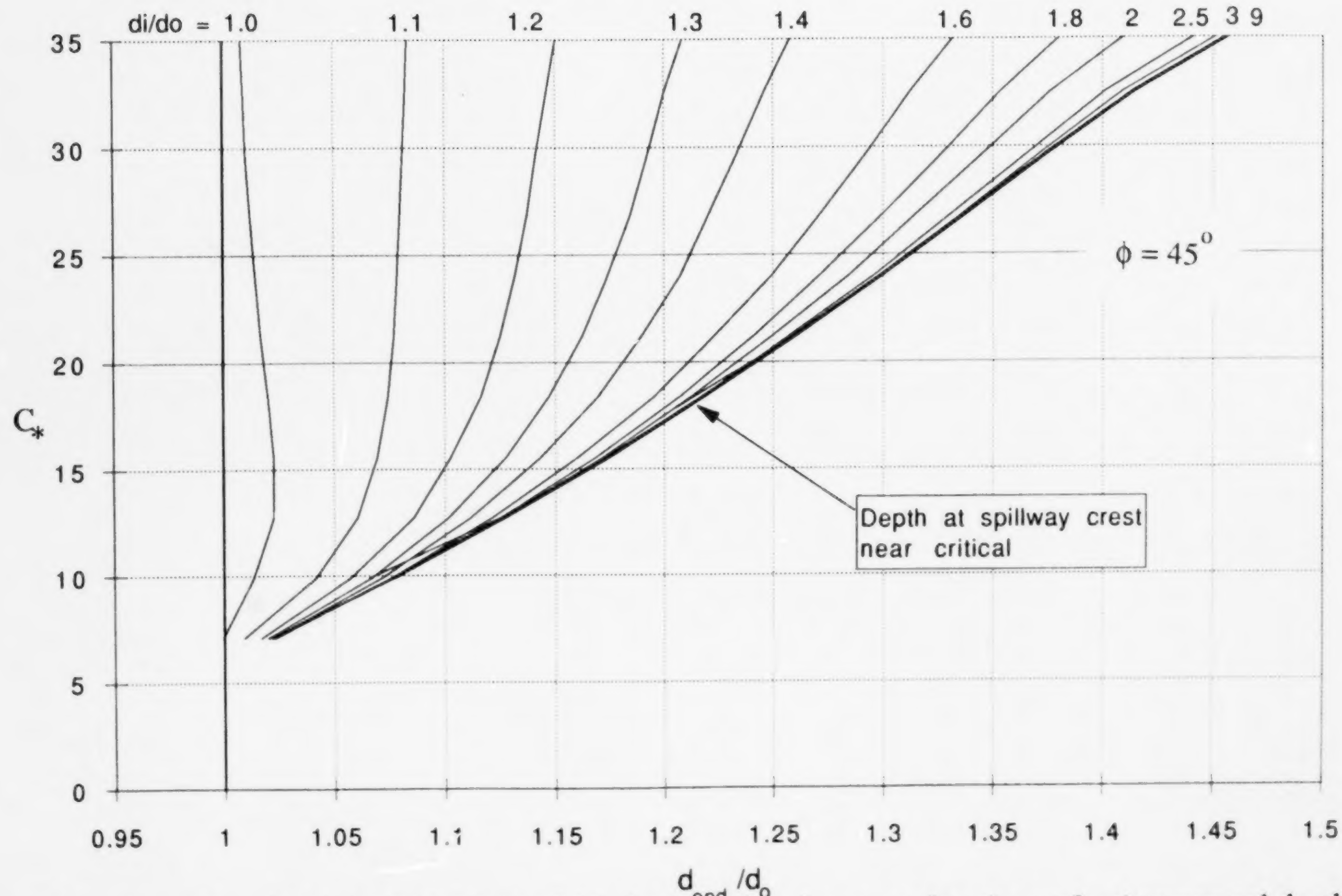

Fig. 5.44a The ratio of end depth(depth at which the boundary layer reaches the surface) to normal depth as a function of the uniform flow C* and the ratio of initial depth at the channel entrance to normal depth for a channel slope of 45 degrees. Initial depth controlled by a sluice gate.

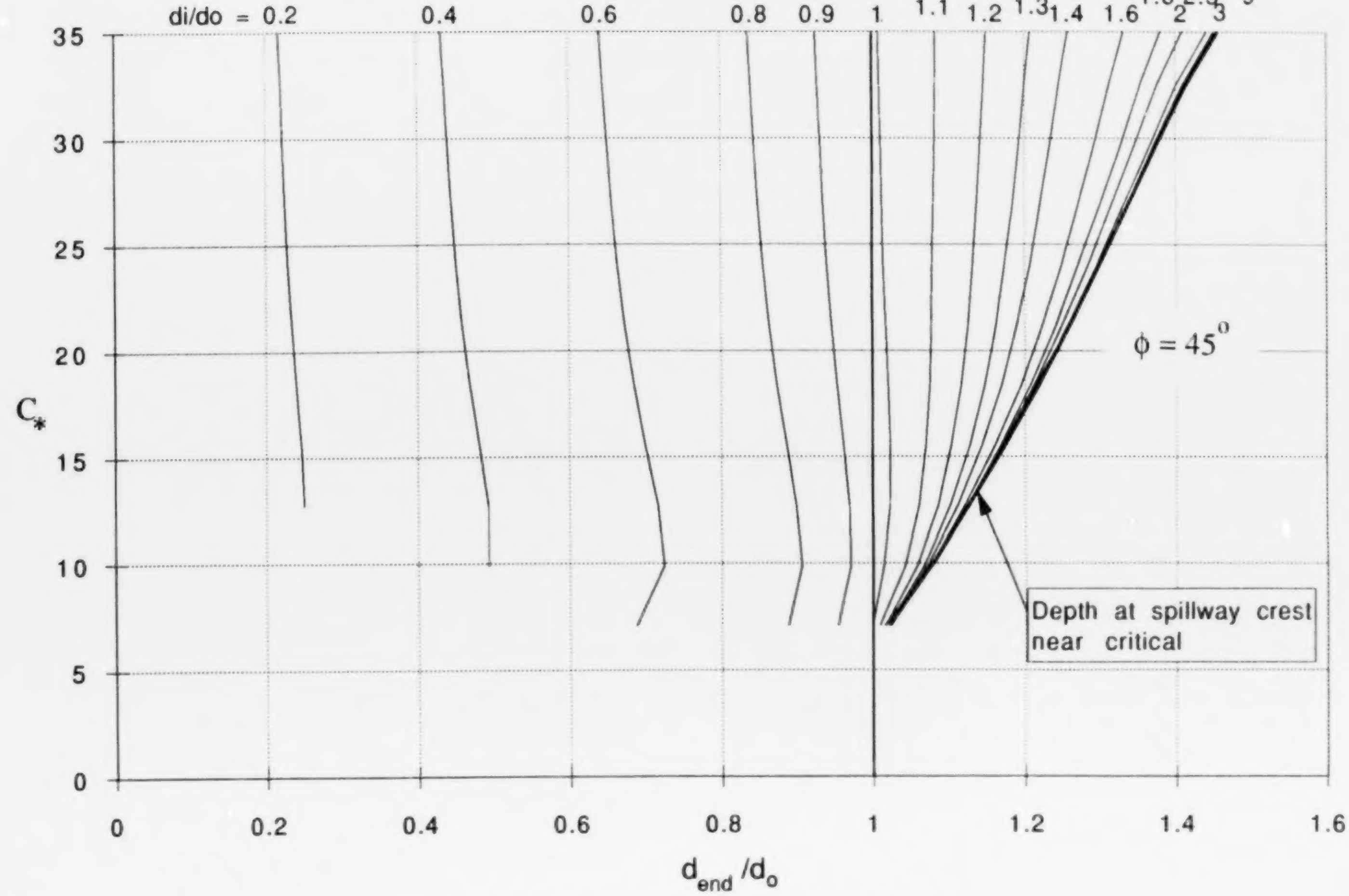

Fig. 5.44b Same as Figure 5.44a but also includes $d_i/d_o<1$. Slope = 45 degrees.

6. Conclusions and recommendations

6.1 Mild channel experiments

The experiments conducted in a wide rectangular channel to measure the boundary layer growth and the entrance length in the case of a mild channel flowing at normal depth showed some interesting results. The entrance length was longer than that predicted by zero preasure gradient solutions. The boundary layer was also strongly affected laterally by secondary currents.

The secondary currents greatly influenced the entrance length or the distance the boundary layer took to reach the surface. In the case of the smooth channel experiment, the entrance length varied anywhere from 56% to 154% of the width averaged value. In the case of the rough channel experiment, the entrance length varied anywhere from 55% to 139% of the width averaged value. It can be concluded from this variation that large errors can result in the measurement of the development length if width averaged data is not taken. The longer entrance lengths occurred between two secondary flow cells where fluid was moving downward and the shorter entrance lengths occurred between two secondary flow cells where fluid was moving upward. The entrance length difference was larger for the smooth channel despite the fact that the secondary flows were stronger in the rough experiment. This occurred because the boundary layer growth was much more rapid for the rough channel so the secondary flows did not have the time or distance to create such a difference.

The secondary flows were stronger for the rough channel by the evidence of dye and their effect on the lateral distribution of shear and discharge. The lateral variation in bed shear was 30% for the smooth channel and 100% for the rough. The lateral variation in depth integrated discharge was 19% for the smooth channel and 26% for the rough. The higher shear and discharge occurred between two secondary flow cells where fluid was moving downward and the smaller shear and discharge occurred between two secondary flow cells where fluid was moving upward.

Once the data was width averaged, the results agreed very well with the two-dimensional analysis of this study. Both the experiments and numerical results showed a longer entrance length than predicted by smooth and rough flat plate theories which neglect the effect of a pressure gradient or an accelerating potential core velocity.

The experiments and numerical solution also showed a smaller longitudinal variation in bed shear stress; it was found to be almost constant through most of the development region except for a few depths near the channel entrance. While in the smooth and rough flat plate theories, the shear stress decreased throughout the entrance region. The depth was also found to be fairly constant within the entrance region.

By measuring the water surface elevations, other features of the development region were investigated. For an instance, the Bernoulli equation was evaluated to show that the decay of the potential core was consistent with the growth of the boundary layer; the Bernoulli equation was constant until the boundary layer reached the surface. Another feature was the slope of the water surface and energy line in the entrance region. The slope of the energy line tended to get steeper as the boundary layer developed and the slope of the water surface tended to get milder; both lines became of equal slope when the flow was fully developed.

Small bed undulations in the flume bed had a small but noticeable effect on the velocity, bed shear, and depth. A small rise in bed elevation produced a slightly higher potential core acceleration than normal; a slight increase in bed shear, and a small increase in the water surface slope. The opposite effect occurred for a small fall in bed elevation. However, the bed undulations had a small effect on the boundary layer growth.

6.2 Subcritical numerical solutions

To test the analytical formulation for the numerical solution a few tests were performed on zero pressure gradient boundary layer problems. These results where compared to known solutions by Schlichting (1934), and Harrison (1967) after Granville (1958). Schlichting's solution gives the boundary shear and boundary layer thickness for the smooth plate. Granville's solution gives the boundary shear for smooth and rough plates. Harrison's solution expands on Granville's to give boundary layer thickness for smooth and rough plates.

For the smooth plate, the boundary shear agreed very well between the numerical, Schlichting and Granville solutions. For the boundary layer thickness, the numerical and Schlichting solution agreed well but the Harrison solution had somewhat of a lower growth rate. The Harrison solution also gave a power law exponent which ranged from 1/4.8 to 1/6.2 in the valid Reynolds number range for the Schlichting solution. This does not agree with the power law exponent of 1/7 from the well accepted Schlichting solution.

For the rough plate, the boundary shear agreement between the numerical and Granville solutions was excellent. However, for the boundary layer thickness the Harrison solution produced a slower growth rate than the numerical solution and again gave a lower power law exponent than the numerical solution. For an example, the Harrison solution gave a power law exponent of 1/3.5 when the numerical solution gave 1/4.8.

Since all these solutions have been derived from the analysis and experiments conducted in pipes, further experiments are needed in evaluating this analysis in its application to boundary layers. Although this analysis seems sufficient enough for predicting skin friction or shear stress (one of the first intention of these analysis was to predict the drag on ship hulls and aircraft), it lacks the ability to accurately locate the edge of the boundary layer, and to accurately predict velocity profiles and turbulence. It was for this reason that the solution based on the Colebrook and White equation and Nunners relation was deemed as good or bad as the Harrison-Granville solution. With the added advantages of agreeing with the Schlichting power law exponent within the valid range and being of the simpler form, the solution based on the Colebrook-White relation was chosen to continue the work in the numerical analysis of boundary layers in open channels.

The downstream boundary condition or uniform flow expression developed in the numerical solution using the Colebrook-White relation was tested against the well known dimensionless Chezy relation. It was discovered that the two sets of equations gave differences of less than 1% in normal depth, bed shear stress, and C_*. Altough these two sets of equations are basically the same, this excersize did support the relation developed between n_o an C_* as Equation 3.26.

From the results of the numerical simulations, the entrance length for subcritical flow in terms of the number of depths was found to be a function of the fully developed Chezy coefficient C_*; the relation is given in Figure 4.30. To help give a feel for the entrance length in mild channels, the following examples are given. A very rough channel of $k_s/d_o = 0.5$ gives a $C_* = 8$, the boundary layer takes about 25 depths to reach the surface. A smooth channel with a typical laboratory size unit discharge of say 30 L/s gives a C_* of about 20, and gives an entrance length of about 60 normal depths. A very high Reynolds number flow in a smooth channel, say about $q = 20\ m^2/s$ gives a C_* of about 37, gives an entrance length of about 100 depths.

Yalin's (1972) solution for the entrance length gave a shorter entrance length than the numerical solution since his analysis did not take into account the presence of a pressure gradient.

From the numerical runs, the entrance length for subcritical slopes was found to be independent of the channel bed slope up until the Froude number approached 1. For an example, for a channel with C_* = 21 and a Froude number of 0.94 increased the entrance length by only 6% compared to a channel with the same C_* and a Froude number of 0.07.

The bed shear stress distribution obtained from the numerical solutions for subcritical channels is shown in Figure 4.29c and shows that the bed shear approaches the fully developed value much more quickly than for the boundary layer to reach the surface. However, one has to keep in mind that secondary currents can vary the bed shear stress strongly in the transverse direction.

The two width-averaged subcritical flow experiments conducted support the entrance length relation, boundary layer growth, bed shear stress, and depth obtained from the numerical solutions. However, more width averaged experimental entrance lengths are needed to establish if the numerical solution is adequate. This is especially evident in Figure 4.30 where the two experiments plot as two single points on the numerical entrance length relation.

By comparing the numerical entrance lengths for wide channels to pipe flow entrance lengths by Ward-Smith (1980), one can make a first approximation on the entrance lengths for other channel cross-sections. The length scale for other cross-sections becomes the hydraulic radius and Figure 4.31b can be used for this purpose.

The numerical solution was used to predict the boundary layer development in a channel with less than ideal situations, such as inaccurate bed slope and tailgate matching. This is often the case in laboratory channels and can effect the entrance length. However, these effects were found out to be small and can be minimized to a few percent even if minimal care is taken to ensure a reasonably constant depth through the channel. The tailgate setting had the following effect. Setting the tailgate to high (M1 Curve) shortens the entrance length. Setting the tailgate to low (M2 Curve) lengthens it.

6.3 Supercritical numerical solutions

For a free overflow spillway, the initial depth at the spillway crest does not have to be accurately determined to obtain the upstream boundary condition for the numerical solution. It is adequate to assume that the depth goes through critical in the vertical and the equivalent depth perpendicular to the spillway face can be calculated using the Bernoulli equation. In this way, non-hydrostatic pressure distributions are neglected but, as it turns out, the boundary layer and water surface profile are very insensitive to the initial depth around the value given by the above method.(Equation 5.5)

If a sluice gate is used to decrease the initial upstream depth the boundary layer growth rate increases, the bed shear increases and the entrance length decreases. If the initial depth is lowered to normal depth, the entrance length, boundary layer growth rate, water surface, and bed shear stress are similar to the subcritical case.

The numerical model suggests that the boundary layer growth rate on a steep channel increases slightly with discharge. This contrasts Bauer's (1954) conclusion which states that the growth rate is independent of discharge. This error is due to the small range of discharges possible in a laboratory experiment. Thus it is wrong to assume that the same boundary layer growth rate will occur in the physical model and the prototype if the same roughness is used.

If the discharge is held constant and the spillway slope is increased, the boundary layer growth rate and the entrance length decreases. The boundary layer growth rate is smaller since the potential core acceleration is higher. Even though there is a smaller boundary layer growth rate, the entrance length is shorter since the depth falls much more rapidly on steeper slopes. However, if one non-dimensionalizes the entrance length by the normal depth the non-dimensional entrance length becomes longer with increasing slopes. This is because the length scale (the normal depth) decreases with an increase in the spillway slope. The change in boundary layer growth rate is most sensitive to changes in small supercritical slopes in the range <1° to 15°. For slopes 20° to 70°, the boundary layer growth rate is almost the same. This is probably the reason why Bauer (1954) concluded that the boundary layer growth rate is independent of the channel bed slope since his slopes ranged from 20° to 60°.

The bed shear on steep channels of more than 1° is mostly affected by the acceleration of the potential core; the shear stress increases going downstream. The fall in shear stress due to the thickening of the boundary layer is only apparent in the first 0.5 to 1 depth.

Based on Bauer's experimental data, the numerical model works quite well for both smooth and rough boundaries. To increase the models accuracy, more data on boundary layers on steep slopes is needed to upgrade the power law velocity profile in the numerical model to a more representative semilog relation with a wake function. This data needs to cover transverse variations as Bauer's data is not conclusive since only centreline measurements were taken. Several velocity profiles are needed to be taken in the lateral direction for each longitudinal location to average out the lateral variation due to secondary currents.

Comparing the numerical model of this study to the Keller and Rastogi (1977) k - ε model shows a difference in entrance length by a few percent. The entrance length of the numerical model always underpredicted that of Keller and Rastogi's model. But, since Keller and Rastogi found that their model slightly overpredicted the entrance lengths measured in the field, the model of this study has been evaluated as suitable for predicting the boundary layer development on spillways.

Comparing the numerical model to experiments conducted by Ippen (1957) on supercritical flows originating from a nozzle also show encouraging results despite the fact that Ippan's experiments were not width averaged.

It is unclear if secondary currents can effect supercritical flow as much as subcritical and wether width averged data is as important as it is for subcritical flow.

Using the numerical model to calculate the effect of the boundary layer on the S2 backwater curve shows that the effect is negligible. The largest difference in depth occurred on vary rough channels with small but steep slopes. The bed shear was 2 to 2.5 times larger near the channel entrance than that predicted by the gradual varied flow solution. However, as the boundary layer grew to about 1/5th of the depth the bed shear was within a few percent of that given by gradual varied flow.

Design curves for the entrance length on steep slopes when the depth at the spillway crest going through critical were constructed. It was discovered that the dimensionless entrance length L/d_o was a function of the C_* corresponding to the normal depth d_o, and the spillway slope ϕ. By using d_o as the length scale, the design curves have an advantage over the Keller and Rastogi design curves since the Keller and Rastogi design curves cannot accommodate a spillway roughness where $k_s = 0$. In addition to the entrance length L, design curves for the depth at which the boundary layer reaches the surface d_{end} were also constructed. The end depth d_{end} was also a function of C_* and and the spillway slope.

Similar design curves were constructed for spillways where the depth at the spillway crest did not go through critical or was controlled by a sluice gate. Since the initial depth d_i constituted an additional input variable, the results for L/d_o could not be represented in one graph. Therefore, three different sets of design curves where generated for three different channel bed slopes. These slopes include $\phi = 1^\circ$, 10°, and 45°. The spillway slope was a more important parameter the closer the initial depth was to critical.

References

BINNIE, A. M., 1977. Boundary layer development in open-water channel. Journal of Hydraulic Research 15, no. 3

DELLEUR, J. W., 1957. The boundary layer development in open channels. Journal of the Engineering Mechanics Division. ASCE, Vol. 83, No. EM 1, January.

CAMPBELL, F. B. and COX, R. G. and BOYD, M. B., 1965. Boundary layer development and spillway energy losses. Journal of the Hydraulics Division, ASCE, 91(HY3): 149-163

CASSIDY, J. J. and BAUER, W. J., 1966. Boundary layer development and spillway energy losses, Discussions. Journal of the Hydraulics Division, ASCE, 91(HY3): 149-163

GERARD, R. 1978. Secondary flow in noncircular conduits. Journal of the Hydraulics Division, ASCE, 104(HY5): 755-773

GRANVILLE, P. S., 1958. The frictional resistance and turbulent boundary layer of rough surfaces, Report No. 1024, David Taylor Model Basin, Washington, D.C.

GULLIVER, J. S., and HALVERSON, M. J. 1987. Measurements of large streamwise vortices in an open-channel flow. Water Resources Research Vol 23: pp. 115-123.

HINZE, J. O., 1959. Turbulence - An introduction to its mechanism and Theory. McGraw-Hill Book Company, Inc., New York, p. 518-520.

HAITONIDIS, J. H., 1989. The measurement of wall shear stress. Department of Aeronautics and Astronautics Massachusetts Institute of Technology Cambridge, MA 02139. Taken from: Lecture notes in engineering, Advances in fluid mechanics measurements, Springer - Verlag, pp. 230-261.

HARRISON, A. J. M. 1967. Boundary-layer displacement thickness on flat plates. Journal of the Hydraulics Division, ASCE, 93(HY4): 79-91.

HENDERSON, F. M. 1966. Open Channel Flow. Macmillan Publishing Co., Inc. 866 Third Avenue, New York, New York 10022.

IKEDA, S., and KIKKAWA, H. 1977. Secondary circulation in straight channels. Department of Foundation Engineering, Faculty of Engineering, University of Saitama, Saitama, Japan. Vol. 6.

IPPEN, A. T., and RAICHLEN, F. 1957. Turbulence in civil engineering: Measurements in free surface streams. Journal of the Hydraulics Division, ASCE, 83(HY5): Paper#1392, p 1-27

KELLER, J. K., and RASTOGI, K. 1975. Prediction of flow development on spillways. Journal of the Hydraulics Division, ASCE, 103(HY12): 1171-1184.

KELLER, J. K., and RASTOGI, K. 1977. Design chart for predicting critical point on spillways. Journal of the Hydraulics Division, ASCE, 101(HY9): 1417-1429.

KENNEDY, R. J. and Fulton, J. F. 1961. The effect of secondary currents upon the capacity of a straight open channel. ASME-EIC Hydraulics Conferance Paper No. 61-EIC-1.

KINOSHITA, R., 1967. An analysis of the movement of flood flows by aerial photography - concerning characteristics of turbulence and surface flow. Photogrammetry, Vol. 7, No. 1. (in Japanese).

MULLER, A., 1982. Secondary flow vortices: A structure in turbulent open channel flow, in Structure of Turbulence in Heat and Mass Transfer, edited by Z. P. Zarcic, Hemisphere Publishing, Washington, D. C.

RAJARATNAM, N., 1987. Engineering fluid mechanics. Department of Civil Engineering, University of Alberta, Edmonton, Alberta, Canada, T6G 2G7.

SCHLICHTING, H., 1979. Boundary layer theory, 7th ed., McGraw-Hill Book Co., Inc., New York, p. 596-626 and p. 635-655.

TOMINAGA, A., and NEZU, I. 1992. Velocity profiles in steep open-channel flows. Journal of Hydraulic Engineering, ASCE, 118(HY1): 73-90.

WARD-SMITH, A. J., 1980. Internal fluid flow: The fluid dynamics of flow in pipes and ducts., Oxford University Press, New York, p. 226-234.

WOLMAN, M. G. and BRUSH, L. M., 1961. Factors controlling the size and shape of stream channels in coarse noncohesive sands. Geological Survey Professional Paper, 282-G, 1961.

WOOD, I. R. and ACKERS, P. and LOVELESS, J., 1983. General method for critical point on spillways. Journal of the Hydraulics Division, ASCE, 109(HY2): 308-312.

WOOD, I. R., 1985. Air Water Flows. International Association for Hydraulics Research. Preprinted proceedings, 21st congress, Melbourne, Vol. 6, August 19-23.

YALIN, M. S., 1972. Mechanics of Sediment Transport, Pergamon Press. p. 42-46.

ZIMMERMANN, C. and KENNEDY, A. M., 1978. Transverse bed slopes in curved alluvial streams, Journal of the Hydraulics Division, ASCE, 104(HY1): 33-48.

APPENDIX 1

Experimental data for smooth mild channel

Smooth X = 0.43 m
Water Surface Elevation = 0.2005 m (5 point average)

Z = -0.335 m		Z = -0.274 m				Z = -0.213 m		Z = -0.152 m		Z = -0.091 m	
y (m)	u (m/s)	y (m)	u (m/s)			y (m)	u (m/s)	y (m)	u (m/s)	y (m)	u (m/s)
0.0000	0.0000	0.0000	0.0000			0.0000	0.0000	0.0000	0.0000	0.0000	0.0000
0.0015	0.2453	0.0015	0.2425			0.0015	0.2521	0.0015	0.2337	0.0015	0.2489
0.0050	0.2941	0.0040	0.2872			0.0034	0.2974	0.0044	0.2719	0.0040	0.2869
0.0085	0.3262	0.0080	0.3112			0.0074	0.3219	0.0069	0.2910	0.0065	0.3109
0.0135	0.3515	0.0130	0.3400			0.0124	0.3504	0.0119	0.3203	0.0115	0.3391
0.0160	0.3593	0.0180	0.3560			0.0174	0.3599	0.0169	0.3405	0.0165	0.3498
0.0185	0.3637	0.0230	0.3599			0.0199	0.3602	0.0219	0.3540	0.0190	0.3543
0.0210	0.3662	0.0255	0.3621			0.0211	0.3618	0.0244	0.3579	0.0215	0.3574
0.0235	0.3665	0.0280	0.3629			0.0224	0.3624	0.0269	0.3593	0.0240	0.3588
0.0285	0.3662	0.0305	0.3637			0.0249	0.3624	0.0294	0.3610	0.0265	0.3599
0.0335	0.3657	0.0330	0.3637			0.0274	0.3621	0.0319	0.3618	0.0290	0.3604
0.0385	0.3648	0.0380	0.3635			0.0324	0.3621	0.0369	0.3618	0.0315	0.3602
0.0485	0.3632	0.0480	0.3621			0.0374	0.3624	0.0469	0.3613	0.0365	0.3618
0.0585	0.3629	0.0580	0.3618			0.0474	0.3615	0.0569	0.3593	0.0465	0.3610
0.0685	0.3632	0.0680	0.3618			0.0574	0.3607	0.0669	0.3582	0.0565	0.3596
0.0785	0.3640	0.0780	0.3621			0.0674	0.3602	0.0769	0.3591	0.0665	0.3593
0.0885	0.3665	0.0880	0.3629			0.0774	0.3602	0.0869	0.3593	0.0765	0.3579
0.0985	0.3703	0.0980	0.3643			0.0874	0.3618	0.0969	0.3613	0.0865	0.3591
0.1015	0.3705	0.1010	0.3640			0.0974	0.3629	0.1019	0.3604	0.0965	0.3599
0.1078	0.3705	0.1030	0.3637			0.1024	0.3635	0.1089	0.3604	0.1015	0.3593
		0.1084	0.3637			0.1088	0.3635			0.1088	0.3593

Smooth X = 0.43 m
Water Surface Elevation = 0.2005 m (5 point average)

		Z = -0.030 m		Z = 0.0 m		Z = 0.030 m				Z = 0.091 m	
		y (m)	u (m/s)	y (m)	u (m/s)	y (m)	u (m/s)			y (m)	u (m/s)
		0.0000	0.0000	0.0000	0.0000	0.0000	0.0000			0.0000	0.0000
		0.0015	0.2366	0.0015	0.2489	0.0015	0.2449			0.0015	0.2358
		0.0036	0.2708	0.0037	0.2834	0.0040	0.2827			0.0037	0.2675
		0.0061	0.2974	0.0062	0.3109	0.0060	0.2974			0.0062	0.2872
		0.0111	0.3234	0.0112	0.3376	0.0110	0.3385			0.0112	0.3219
		0.0161	0.3391	0.0162	0.3532	0.0160	0.3560			0.0162	0.3426
		0.0211	0.3537	0.0212	0.3579	0.0185	0.3593			0.0212	0.3563
		0.0236	0.3585	0.0262	0.3593	0.0210	0.3613			0.0237	0.3602
		0.0261	0.3602	0.0312	0.3599	0.0235	0.3618			0.0262	0.3610
		0.0286	0.3618	0.0362	0.3602	0.0260	0.3615			0.0287	0.3621
		0.0311	0.3615	0.0462	0.3596	0.0285	0.3618			0.0312	0.3626
		0.0361	0.3610	0.0562	0.3593	0.0310	0.3613			0.0362	0.3621
		0.0461	0.3593	0.0662	0.3591	0.0360	0.3604			0.0412	0.3621
		0.0561	0.3588	0.0762	0.3593	0.0460	0.3596			0.0462	0.3618
		0.0661	0.3585	0.0862	0.3593	0.0560	0.3596			0.0562	0.3604
		0.0761	0.3588	0.0962	0.3613	0.0660	0.3593			0.0662	0.3588
		0.0861	0.3596	0.1032	0.3602	0.0760	0.3591			0.0762	0.3582
		0.0961	0.3610	0.1085	0.3602	0.0860	0.3591			0.0862	0.3585
		0.1021	0.3602			0.0960	0.3593			0.0962	0.3593
		0.1085	0.3602			0.1020	0.3582			0.1022	0.3588
						0.1085	0.3582			0.1087	0.3588

Smooth X = 0.43 m
Water Surface Elevation = 0.2005 m (5 point average)

Z = 0.152 m		Z = 0.213 m				Z = 0.274 m		Z = 0.335 m	
y (m)	u (m/s)	y (m)	u (m/s)			y (m)	u (m/s)	y (m)	u (m/s)
0.0000	0.0000	0.0000	0.0000			0.0000	0.0000	0.0000	0.0000
0.0015	0.2501	0.0015	0.2375			0.0015	0.2281	0.0015	0.2648
0.0033	0.2900	0.0056	0.2834			0.0055	0.2755	0.0030	0.2948
0.0058	0.3147	0.0106	0.3131			0.0105	0.3089	0.0050	0.3213
0.0083	0.3283	0.0156	0.3388			0.0155	0.3323	0.0075	0.3408
0.0108	0.3461	0.0206	0.3521			0.0205	0.3446	0.0100	0.3563
0.0133	0.3543	0.0231	0.3579			0.0255	0.3549	0.0125	0.3610
0.0158	0.3577	0.0256	0.3604			0.0280	0.3591	0.0150	0.3629
0.0183	0.3604	0.0281	0.3635			0.0305	0.3621	0.0175	0.3635
0.0208	0.3615	0.0306	0.3635			0.0355	0.3629	0.0200	0.3637
0.0233	0.3621	0.0356	0.3646			0.0455	0.3618	0.0225	0.3635
0.0258	0.3621	0.0456	0.3626			0.0555	0.3613	0.0250	0.3632
0.0283	0.3618	0.0556	0.3629			0.0655	0.3610	0.0275	0.3629
0.0308	0.3610	0.0656	0.3615			0.0755	0.3602	0.0300	0.3632
0.0358	0.3604	0.0756	0.3599			0.0855	0.3607	0.0350	0.3629
0.0458	0.3602	0.0856	0.3599			0.0955	0.3621	0.0450	0.3621
0.0558	0.3596	0.0956	0.3615			0.1025	0.3596	0.0550	0.3621
0.0658	0.3591	0.1026	0.3604			0.1086	0.3596	0.0650	0.3621
0.0758	0.3588	0.1084	0.3604					0.0750	0.3629
0.0858	0.3591							0.0850	0.3646
0.0958	0.3599							0.0950	0.3654
0.1028	0.3599							0.1020	0.3659
0.1083	0.3599							0.1078	0.3659

Smooth X = 1.0 m
Water Surface Elevation = 0.2001 m (5 point average)

Z = -0.335 m		Z = -0.274 m				Z = -0.213 m		Z = -0.152 m		Z = -0.091 m	
y (m)	u (m/s)	y (m)	u (m/s)			y (m)	u (m/s)	y (m)	u (m/s)	y (m)	u (m/s)
0.0000	0.0000	0.0000	0.0000			0.0000	0.0000	0.0000	0.0000	0.0000	0.0000
0.0015	0.2366	0.0015	0.2341			0.0015	0.2294	0.0015	0.2349	0.0015	0.2461
0.0050	0.2855	0.0043	0.2744			0.0067	0.2855	0.0063	0.2858	0.0059	0.2978
0.0080	0.3077	0.0073	0.2971			0.0117	0.3106	0.0113	0.3115	0.0109	0.3295
0.0130	0.3337	0.0123	0.3203			0.0167	0.3355	0.0163	0.3283	0.0159	0.3489
0.0180	0.3521	0.0173	0.3411			0.0217	0.3492	0.0213	0.3455	0.0209	0.3596
0.0230	0.3665	0.0223	0.3537			0.0267	0.3615	0.0263	0.3549	0.0259	0.3648
0.0255	0.3703	0.0273	0.3651			0.0317	0.3692	0.0313	0.3637	0.0309	0.3695
0.0280	0.3727	0.0298	0.3678			0.0342	0.3724	0.0338	0.3665	0.0334	0.3700
0.0305	0.3740	0.0323	0.3713			0.0367	0.3735	0.0363	0.3697	0.0359	0.3708
0.0330	0.3745	0.0348	0.3737			0.0417	0.3751	0.0388	0.3713	0.0384	0.3713
0.0380	0.3745	0.0373	0.3743			0.0467	0.3745	0.0413	0.3727	0.0409	0.3719
0.0480	0.3740	0.0473	0.3751			0.0567	0.3743	0.0463	0.3729	0.0459	0.3732
0.0580	0.3740	0.0573	0.3748			0.0667	0.3743	0.0563	0.3732	0.0559	0.3732
0.0680	0.3740	0.0673	0.3753			0.0767	0.3740	0.0663	0.3727	0.0659	0.3719
0.0780	0.3756	0.0773	0.3759			0.0867	0.3748	0.0763	0.3711	0.0759	0.3711
0.0880	0.3782	0.0873	0.3788			0.0967	0.3756	0.0863	0.3695	0.0859	0.3719
0.0930	0.3796	0.0973	0.3819			0.0997	0.3740	0.0963	0.3657	0.0959	0.3729
0.0980	0.3801	0.1052	0.3819			0.1057	0.3740	0.1013	0.3602	0.1009	0.3711
0.1048	0.3801							0.1063	0.3602	0.1058	0.3711

Smooth X = 1.0 m
Water Surface Elevation = 0.2001 m (5 point average)

		Z = -0.030 m		Z = 0.0 m		Z = 0.030 m				Z = 0.091 m	
		y (m)	u (m/s)	y (m)	u (m/s)	y (m)	u (m/s)			y (m)	u (m/s)
		0.0000	0.0000	0.0000	0.0000	0.0000	0.0000			0.0000	0.0000
		0.0015	0.2420	0.0015	0.2529	0.0015	0.2489			0.0015	0.2267
		0.0055	0.2910	0.0035	0.2869	0.0054	0.3008			0.0054	0.2557
		0.0105	0.3237	0.0060	0.3109	0.0104	0.3323			0.0104	0.3024
		0.0155	0.3358	0.0110	0.3417	0.0154	0.3549			0.0154	0.3200
		0.0205	0.3535	0.0160	0.3546	0.0204	0.3640			0.0204	0.3352
		0.0255	0.3602	0.0210	0.3659	0.0254	0.3703			0.0254	0.3478
		0.0305	0.3667	0.0260	0.3708	0.0279	0.3705			0.0304	0.3585
		0.0355	0.3703	0.0310	0.3713	0.0304	0.3721			0.0354	0.3662
		0.0380	0.3711	0.0360	0.3727	0.0329	0.3727			0.0379	0.3678
		0.0405	0.3713	0.0460	0.3727	0.0354	0.3729			0.0404	0.3708
		0.0455	0.3719	0.0560	0.3719	0.0379	0.3729			0.0429	0.3716
		0.0555	0.3716	0.0660	0.3719	0.0404	0.3727			0.0454	0.3716
		0.0655	0.3713	0.0760	0.3711	0.0454	0.3724			0.0504	0.3727
		0.0755	0.3719	0.0860	0.3713	0.0554	0.3719			0.0554	0.3727
		0.0855	0.3729	0.0960	0.3676	0.0654	0.3713			0.0654	0.3713
		0.0955	0.3751	0.1000	0.3681	0.0754	0.3713			0.0754	0.3711
		0.1005	0.3753	0.1060	0.3681	0.0854	0.3713			0.0854	0.3713
		0.1060	0.3753			0.0954	0.3721			0.0954	0.3727
						0.1004	0.3713			0.1004	0.3721
						0.1061	0.3713			0.1062	0.3721

Smooth X = 1.0 m
Water Surface Elevation = 0.2001 m (5 point average)

Z = 0.152 m		Z = 0.213 m				Z = 0.274 m		Z = 0.335 m	
y (m)	u (m/s)	y (m)	u (m/s)			y (m)	u (m/s)	y (m)	u (m/s)
0.0000	0.0000	0.0000	0.0000			0.0000	0.0000	0.0000	0.0000
0.0015	0.2505	0.0015	0.2205			0.0015	0.2611	0.0015	0.2572
0.0055	0.2991	0.0055	0.2682			0.0057	0.3166	0.0055	0.3141
0.0105	0.3335	0.0105	0.2941			0.0107	0.3449	0.0105	0.3486
0.0155	0.3552	0.0155	0.3153			0.0157	0.3613	0.0155	0.3703
0.0205	0.3659	0.0205	0.3271			0.0207	0.3637	0.0180	0.3732
0.0230	0.3681	0.0255	0.3391			0.0257	0.3654	0.0205	0.3745
0.0255	0.3700	0.0305	0.3509			0.0307	0.3703	0.0255	0.3756
0.0280	0.3719	0.0355	0.3588			0.0332	0.3713	0.0305	0.3748
0.0305	0.3732	0.0405	0.3651			0.0357	0.3729	0.0355	0.3745
0.0330	0.3729	0.0430	0.3678			0.0407	0.3735	0.0405	0.3743
0.0355	0.3732	0.0455	0.3705			0.0457	0.3737	0.0455	0.3740
0.0380	0.3732	0.0480	0.3719			0.0557	0.3737	0.0555	0.3740
0.0405	0.3732	0.0505	0.3724			0.0657	0.3732	0.0655	0.3743
0.0430	0.3732	0.0555	0.3729			0.0757	0.3737	0.0755	0.3748
0.0455	0.3727	0.0655	0.3732			0.0857	0.3751	0.0855	0.3764
0.0505	0.3729	0.0755	0.3735			0.0957	0.3767	0.0955	0.3785
0.0555	0.3724	0.0855	0.3743			0.1007	0.3772	0.1005	0.3775
0.0655	0.3716	0.0955	0.3759			0.1066	0.3772	0.1068	0.3775
0.0755	0.3716	0.1005	0.3761						
0.0855	0.3705	0.1065	0.3761						
0.0955	0.3684								
0.1005	0.3657								
0.1067	0.3657								

Smooth X = 2.0 m
Water Surface Elevation = 0.1996 m (5 point average)

Z = -0.335 m		Z = -0.274 m				Z = -0.213 m		Z = -0.152 m		Z = -0.091 m	
y (m)	u (m/s)	y (m)	u (m/s)			y (m)	u (m/s)	y (m)	u (m/s)	y (m)	u (m/s)
0.0000	0.0000	0.0000	0.0000			0.0000	0.0000	0.0000	0.0000	0.0000	0.0000
0.0015	0.2391	0.0015	0.2449			0.0015	0.2332	0.0015	0.2196	0.0015	0.2320
0.0045	0.2862	0.0036	0.2798			0.0040	0.2689	0.0046	0.2572	0.0032	0.2564
0.0085	0.3083	0.0076	0.3141			0.0095	0.3037	0.0091	0.2830	0.0062	0.2837
0.0160	0.3403	0.0151	0.3495			0.0170	0.3367	0.0166	0.3144	0.0137	0.3241
0.0235	0.3632	0.0226	0.3719			0.0245	0.3537	0.0241	0.3329	0.0212	0.3440
0.0285	0.3764	0.0301	0.3835			0.0320	0.3659	0.0316	0.3484	0.0287	0.3624
0.0335	0.3830	0.0351	0.3861			0.0395	0.3772	0.0391	0.3602	0.0362	0.3732
0.0360	0.3886	0.0376	0.3868			0.0445	0.3830	0.0466	0.3703	0.0437	0.3801
0.0385	0.3876	0.0401	0.3879			0.0470	0.3843	0.0516	0.3764	0.0487	0.3830
0.0410	0.3889	0.0426	0.3889			0.0495	0.3863	0.0566	0.3798	0.0512	0.3850
0.0435	0.3899	0.0476	0.3894			0.0520	0.3866	0.0616	0.3835	0.0562	0.3863
0.0485	0.3907	0.0576	0.3894			0.0570	0.3886	0.0666	0.3858	0.0662	0.3871
0.0585	0.3909	0.0676	0.3897			0.0670	0.3894	0.0766	0.3889	0.0762	0.3874
0.0685	0.3909	0.0776	0.3899			0.0770	0.3902	0.0866	0.3915	0.0862	0.3871
0.0785	0.3947	0.0876	0.3915			0.0870	0.3930	0.0916	0.3925	0.0942	0.3874
0.0885	0.3952	0.0976	0.3889			0.0920	0.3940	0.0986	0.3930	0.0982	0.3843
0.0965	0.3965	0.1032	0.3889			0.0980	0.3940	0.1037	0.3930	0.1044	0.3843
0.1026	0.3965					0.1032	0.3940				

Smooth X = 2.0 m
Water Surface Elevation = 0.1996 m (5 point average)

		Z = -0.030 m		Z = 0.0 m		Z = 0.030 m		Z = 0.061 m		Z = 0.091 m	
		y (m)	u (m/s)	y (m)	u (m/s)	y (m)	u (m/s)	y (m)	u (m/s)	y (m)	u (m/s)
		0.0000	0.0000	0.0000	0.0000	0.0000	0.0000	0.0000	0.0000	0.0000	0.0000
		0.0015	0.2412	0.0015	0.2509	0.0015	0.2521	0.0015	0.2324	0.0015	0.2187
		0.0048	0.2865	0.0058	0.3008	0.0033	0.2798	0.0055	0.2795	0.0043	0.2568
		0.0108	0.3222	0.0108	0.3355	0.0073	0.3141	0.0155	0.3280	0.0093	0.2795
		0.0183	0.3489	0.0158	0.3532	0.0148	0.3512	0.0255	0.3546	0.0168	0.3099
		0.0258	0.3676	0.0258	0.3772	0.0223	0.3761	0.0355	0.3676	0.0243	0.3292
		0.0333	0.3782	0.0308	0.3824	0.0273	0.3814	0.0455	0.3759	0.0318	0.3469
		0.0383	0.3832	0.0358	0.3850	0.0298	0.3840	0.0555	0.3824	0.0393	0.3593
		0.0408	0.3840	0.0408	0.3863	0.0323	0.3843	0.0655	0.3837	0.0468	0.3670
		0.0433	0.3853	0.0458	0.3863	0.0348	0.3853	0.0755	0.3848	0.0543	0.3764
		0.0458	0.3858	0.0558	0.3861	0.0373	0.3863	0.0855	0.3853	0.0593	0.3809
		0.0508	0.3866	0.0658	0.3863	0.0398	0.3861	0.0975	0.3835	0.0618	0.3819
		0.0558	0.3868	0.0758	0.3868	0.0448	0.3863	0.1049	0.3835	0.0643	0.3830
		0.0658	0.3863	0.0858	0.3876	0.0498	0.3863			0.0693	0.3845
		0.0758	0.3861	0.0918	0.3889	0.0548	0.3863			0.0743	0.3856
		0.0858	0.3861	0.0978	0.3866	0.0648	0.3856			0.0843	0.3863
		0.0948	0.3840	0.1048	0.3866	0.0748	0.3856			0.0943	0.3861
		0.0988	0.3811			0.0848	0.3850			0.0993	0.3848
		0.1047	0.3811			0.0948	0.3837			0.1049	0.3848
						0.1008	0.3806				
						0.1049	0.3806				

Smooth X = 2.0 m
Water Surface Elevation = 0.1996 m (5 point average)

Z = 0.152 m		Z = 0.213 m		Z = 0.244 m		Z = 0.274 m		Z = 0.335 m	
y (m)	u (m/s)	y (m)	u (m/s)	y (m)	u (m/s)	y (m)	u (m/s)	y (m)	u (m/s)
0.0000	0.0000	0.0000	0.0000	0.0000	0.0000	0.0000	0.0000	0.0000	0.0000
0.0015	0.2445	0.0015	0.2099	0.0015	0.2493	0.0015	0.2505	0.0015	0.2533
0.0040	0.2841	0.0040	0.2485	0.0052	0.3011	0.0039	0.2893	0.0035	0.2893
0.0065	0.3031	0.0140	0.2917	0.0152	0.3560	0.0089	0.3256	0.0085	0.3283
0.0140	0.3394	0.0240	0.3200	0.0252	0.3814	0.0139	0.3506	0.0135	0.3554
0.0215	0.3618	0.0340	0.3329	0.0352	0.3871	0.0189	0.3676	0.0185	0.3756
0.0290	0.3751	0.0440	0.3546	0.0452	0.3866	0.0239	0.3788	0.0235	0.3845
0.0365	0.3809	0.0540	0.3686	0.0552	0.3868	0.0264	0.3830	0.0260	0.3868
0.0440	0.3819	0.0640	0.3785	0.0652	0.3866	0.0289	0.3848	0.0285	0.3889
0.0490	0.3819	0.0690	0.3814	0.0752	0.3863	0.0314	0.3861	0.0335	0.3892
0.0515	0.3835	0.0715	0.3840	0.0852	0.3868	0.0339	0.3868	0.0435	0.3892
0.0540	0.3837	0.0740	0.3848	0.0952	0.3892	0.0389	0.3876	0.0535	0.3892
0.0590	0.3853	0.0765	0.3889	0.1002	0.3884	0.0439	0.3876	0.0635	0.3892
0.0640	0.3863	0.0790	0.3889	0.1058	0.3884	0.0539	0.3874	0.0735	0.3889
0.0740	0.3871	0.0840	0.3886			0.0639	0.3874	0.0835	0.3886
0.0840	0.3876	0.0940	0.3922			0.0739	0.3866	0.0935	0.3868
0.0940	0.3917	0.1005	0.3925			0.0839	0.3863	0.0985	0.3856
0.0995	0.3920	0.1052	0.3925			0.0939	0.3861	0.1015	0.3837
0.1049	0.3920					0.1009	0.3835	0.1065	0.3837
						0.1065	0.3835		

Smooth X = 3.0 m

Water Surface Elevation = 0.1991 m (5 point average)

Z = -0.335 m		Z = -0.274 m		Z = -0.244 m		Z = -0.213 m		Z = -0.152 m		Z = -0.091 m	
y (m)	u (m/s)	y (m)	u (m/s)	y (m)	u (m/s)	y (m)	u (m/s)	y (m)	u (m/s)	y (m)	u (m/s)
0.0000	0.0000	0.0000	0.0000	0.0000	0.0000	0.0000	0.0000	0.0000	0.0000	0.0000	0.0000
0.0015	0.2358	0.0015	0.2391	0.0015	0.2332	0.0015	0.2173	0.0015	0.2136	0.0015	0.2223
0.0045	0.2827	0.0064	0.2924	0.0082	0.2994	0.0026	0.2396	0.0069	0.2682	0.0065	0.2755
0.0095	0.3141	0.0134	0.3301	0.0182	0.3358	0.0076	0.2777	0.0169	0.3077	0.0165	0.3203
0.0145	0.3382	0.0209	0.3568	0.0282	0.3648	0.0176	0.3077	0.0269	0.3314	0.0265	0.3432
0.0195	0.3588	0.0284	0.3751	0.0382	0.3835	0.0276	0.3340	0.0369	0.3537	0.0365	0.3626
0.0270	0.3756	0.0359	0.3881	0.0482	0.3912	0.0376	0.3557	0.0469	0.3684	0.0465	0.3764
0.0345	0.3876	0.0409	0.3940	0.0582	0.3937	0.0476	0.3684	0.0569	0.3796	0.0565	0.3868
0.0395	0.3942	0.0434	0.3958	0.0682	0.3950	0.0576	0.3822	0.0669	0.3892	0.0615	0.3915
0.0420	0.3952	0.0459	0.3965	0.0782	0.3955	0.0676	0.3902	0.0769	0.3940	0.0665	0.3940
0.0445	0.3980	0.0484	0.3975	0.0882	0.3988	0.0726	0.3940	0.0819	0.3965	0.0715	0.3965
0.0495	0.3995	0.0534	0.3978	0.0962	0.3970	0.0776	0.3965	0.0869	0.3980	0.0765	0.3980
0.0595	0.3998	0.0584	0.3985	0.1021	0.3970	0.0826	0.3988	0.0919	0.3993	0.0815	0.3993
0.0695	0.4003	0.0684	0.3988			0.0876	0.3993	0.0979	0.3995	0.0865	0.3998
0.0795	0.4010	0.0784	0.3990			0.0976	0.3978	0.1030	0.3995	0.0915	0.4015
0.0875	0.4015	0.0884	0.3993			0.1024	0.3978			0.0985	0.4000
0.0925	0.4013	0.0974	0.3965							0.1030	0.4000
0.0965	0.3993	0.1018	0.3965								
0.1018	0.3993										

Smooth X = 3.0 m
Water Surface Elevation = 0.1991 m (5 point average)

Z = -0.061 m		Z = -0.030 m		Z = 0.0 m		Z = 0.030 m		Z = 0.061 m		Z = 0.091 m	
y (m)	u (m/s)	y (m)	u (m/s)	y (m)	u (m/s)	y (m)	u (m/s)	y (m)	u (m/s)	y (m)	u (m/s)
0.0000	0.0000	0.0000	0.0000	0.0000	0.0000	0.0000	0.0000	0.0000	0.0000	0.0000	0.0000
0.0015	0.2328	0.0015	0.2366	0.0015	0.2473	0.0015	0.2453	0.0015	0.2276	0.0015	0.2070
0.0064	0.2937	0.0039	0.2763	0.0039	0.2837	0.0041	0.2876	0.0059	0.2834	0.0055	0.2572
0.0164	0.3403	0.0084	0.3073	0.0089	0.3178	0.0081	0.3150	0.0159	0.3292	0.0155	0.3008
0.0264	0.3667	0.0159	0.3414	0.0164	0.3537	0.0116	0.3329	0.0259	0.3568	0.0255	0.3265
0.0364	0.3814	0.0234	0.3629	0.0264	0.3811	0.0156	0.3537	0.0359	0.3719	0.0355	0.3446
0.0464	0.3907	0.0309	0.3777	0.0364	0.3927	0.0231	0.3745	0.0459	0.3835	0.0455	0.3607
0.0564	0.3927	0.0384	0.3907	0.0464	0.3952	0.0306	0.3879	0.0559	0.3863	0.0555	0.3737
0.0664	0.3947	0.0434	0.3932	0.0564	0.3955	0.0356	0.3920	0.0659	0.3897	0.0655	0.3853
0.0764	0.3955	0.0459	0.3945	0.0664	0.3952	0.0381	0.3940	0.0759	0.3925	0.0705	0.3874
0.0864	0.3965	0.0484	0.3965	0.0764	0.3952	0.0406	0.3952	0.0859	0.3950	0.0755	0.3917
0.0964	0.3932	0.0509	0.3963	0.0864	0.3942	0.0431	0.3952	0.0929	0.3963	0.0805	0.3940
0.0984	0.3927	0.0559	0.3968	0.0934	0.3937	0.0456	0.3958	0.0989	0.3930	0.0855	0.3955
0.1031	0.3927	0.0659	0.3970	0.0984	0.3904	0.0506	0.3965	0.1037	0.3930	0.0905	0.3968
		0.0759	0.3985	0.1032	0.3904	0.0556	0.3970			0.0955	0.3978
		0.0859	0.4008			0.0656	0.3968			0.0995	0.3965
		0.0934	0.4022			0.0756	0.3975			0.1040	0.3965
		0.0984	0.4015			0.0856	0.4000				
		0.1032	0.4015			0.0956	0.4003				
						0.0986	0.4005				
						0.1033	0.4005				

Smooth X = 3.0 m
Water Surface Elevation = 0.1991 m (5 point average)

Z = 0.152 m		Z = 0.213 m		Z = 0.244 m		Z = 0.274 m		Z = 0.335 m	
y (m)	u (m/s)	y (m)	u (m/s)	y (m)	u (m/s)	y (m)	u (m/s)	y (m)	u (m/s)
0.0000	0.0000	0.0000	0.0000	0.0000	0.0000	0.0000	0.0000	0.0000	0.0000
0.0015	0.2354	0.0015	0.2227	0.0015	0.2449	0.0015	0.2485	0.0015	0.2453
0.0051	0.2830	0.0037	0.2595	0.0056	0.3011	0.0039	0.2816	0.0048	0.2964
0.0101	0.3125	0.0052	0.2723	0.0156	0.3478	0.0074	0.3099	0.0098	0.3274
0.0151	0.3340	0.0102	0.2984	0.0256	0.3782	0.0149	0.3452	0.0148	0.3518
0.0251	0.3615	0.0152	0.3122	0.0306	0.3884	0.0224	0.3695	0.0223	0.3769
0.0351	0.3732	0.0252	0.3311	0.0356	0.3927	0.0299	0.3868	0.0273	0.3892
0.0451	0.3785	0.0352	0.3420	0.0456	0.3935	0.0349	0.3925	0.0298	0.3935
0.0551	0.3837	0.0452	0.3506	0.0556	0.3917	0.0374	0.3940	0.0323	0.3952
0.0651	0.3881	0.0552	0.3591	0.0656	0.3915	0.0399	0.3952	0.0348	0.3968
0.0701	0.3897	0.0652	0.3676	0.0756	0.3912	0.0449	0.3955	0.0373	0.3973
0.0751	0.3920	0.0752	0.3772	0.0856	0.3925	0.0549	0.3960	0.0398	0.3975
0.0801	0.3937	0.0852	0.3861	0.0946	0.3965	0.0649	0.3955	0.0448	0.3980
0.0851	0.3950	0.0902	0.3889	0.0996	0.3975	0.0749	0.3947	0.0548	0.3978
0.0901	0.3952	0.0952	0.3904	0.1058	0.3975	0.0849	0.3942	0.0648	0.3980
0.0951	0.3947	0.0992	0.3892			0.0899	0.3942	0.0748	0.3965
0.0991	0.3927	0.1055	0.3892			0.0949	0.3932	0.0848	0.3963
0.1050	0.3927					0.0999	0.3894	0.0948	0.3950
						0.1060	0.3894	0.1008	0.3907
								0.1065	0.3907

Smooth X = 4.0 m
Water Surface Elevation = 0.1988 m (5 point average)

Z = -0.335 m		Z = -0.274 m		Z = -0.244 m		Z = -0.213 m		Z = -0.152 m		Z = -0.091 m	
y (m)	u (m/s)	y (m)	u (m/s)	y (m)	u (m/s)	y (m)	u (m/s)	y (m)	u (m/s)	y (m)	u (m/s)
0.0000	0.0000	0.0000	0.0000	0.0000	0.0000	0.0000	0.0000	0.0000	0.0000	0.0000	0.0000
0.0015	0.2289	0.0015	0.2289	0.0015	0.2324	0.0015	0.2060	0.0015	0.2094	0.0015	0.2169
0.0045	0.2708	0.0045	0.2678	0.0106	0.3080	0.0055	0.2576	0.0042	0.2445	0.0046	0.2568
0075	0.2941	0.0075	0.2917	0.0206	0.3400	0.0105	0.2827	0.0092	0.2763	0.0086	0.2851
0.0125	0.3172	0.0115	0.3115	0.0306	0.3618	0.0205	0.3122	0.0192	0.3034	0.0186	0.3188
0.0200	0.3452	0.0190	0.3358	0.0406	0.3809	0.0305	0.3332	0.0292	0.3283	0.0286	0.3388
0.0275	0.3654	0.0265	0.3566	0.0506	0.3889	0.0405	0.3481	0.0392	0.3452	0.0386	0.3560
0.0350	0.3830	0.0340	0.3724	0.0606	0.3925	0.0505	0.3615	0.0492	0.3596	0.0486	0.3705
0.0425	0.3932	0.0415	0.3837	0.0706	0.3988	0.0605	0.3735	0.0592	0.3724	0.0586	0.3809
0.0475	0.3983	0.0465	0.3909	0.0806	0.4000	0.0705	0.3837	0.0692	0.3824	0.0686	0.3894
0.0500	0.3998	0.0515	0.3960	0.0906	0.4037	0.0755	0.3892	0.0792	0.3899	0.0736	0.3940
0.0525	0.4013	0.0540	0.3968	0.0976	0.4057	0.0805	0.3947	0.0842	0.3940	0.0786	0.3968
0.0575	0.4027	0.0565	0.3985	0.1033	0.4057	0.0855	0.3990	0.0892	0.3985	0.0811	0.3978
0.0625	0.4037	0.0615	0.4000			0.0905	0.4020	0.0942	0.3995	0.0836	0.3990
0.0700	0.4037	0.0665	0.4010			0.0955	0.4037	0.0982	0.3965	0.0861	0.4005
0.0775	0.4042	0.0715	0.4013			0.0995	0.4025	0.1036	0.3965	0.0886	0.4015
0.0850	0.4052	0.0740	0.4015			0.1030	0.4025			0.0936	0.4040
0.0925	0.4045	0.0765	0.4017							0.0986	0.4022
0.0985	0.4015	0.0765	0.4017							0.1039	0.4022
0.1038	0.4015	0.0790	0.4020								
		0.0815	0.4017								
		0.0840	0.4027								
		0.0865	0.4042								
		0.0915	0.4064								
		0.0950	0.4055								
		0.0985	0.4050								
		0.1036	0.4050								

Smooth X = 4.0 m
Water Surface Elevation = 0.1988 m (5 point average)

Z = -0.061 m		Z = 0.030 m		Z = 0.0 m		Z = 0.030 m		Z = 0.061 m		Z = 0.091 m	
y (m)	u (m/s)	y (m)	u (m/s)	y (m)	u (m/s)	y (m)	u (m/s)	y (m)	u (m/s)	y (m)	u (m/s)
0.0000	0.0000	0.0000	0.0000	0.0000	0.0000	0.0000	0.0000	0.0000	0.0000	0.0000	0.0000
0.0015	0.2453	0.0015	0.2307	0.0015	0.2412	0.0015	0.2441	0.0015	0.2332	0.0015	0.2084
0.0083	0.3067	0.0041	0.2788	0.0060	0.2971	0.0040	0.2784	0.0079	0.2944	0.0028	0.2259
0.0183	0.3440	0.0056	0.2883	0.0110	0.3283	0.0080	0.3118	0.0179	0.3329	0.0078	0.2648
0.0283	0.3686	0.0106	0.3188	0.0185	0.3577	0.0155	0.3440	0.0279	0.3568	0.0178	0.2988
0.0383	0.3837	0.0156	0.3391	0.0285	0.3824	0.0230	0.3670	0.0379	0.3667	0.0278	0.3163
0.0483	0.3940	0.0231	0.3585	0.0385	0.3978	0.0305	0.3840	0.0479	0.3777	0.0378	0.3355
0.0533	0.3968	0.0306	0.3772	0.0435	0.3993	0.0380	0.3940	0.0579	0.3824	0.0478	0.3515
0.0583	0.4005	0.0381	0.3892	0.0485	0.4015	0.0430	0.3978	0.0679	0.3886	0.0578	0.3626
0.0633	0.4008	0.0431	0.3940	0.0485	0.4015	0.0480	0.3990	0.0779	0.3960	0.0678	0.3756
0.0683	0.4017	0.0456	0.3973	0.0585	0.4017	0.0530	0.4008	0.0829	0.3975	0.0778	0.3868
0.0733	0.4035	0.0481	0.3990	0.0685	0.4015	0.0580	0.4005	0.0879	0.4015	0.0828	0.3915
0.0783	0.4037	0.0506	0.3995	0.0885	0.4025	0.0630	0.4008	0.1049	0.4017	0.0878	0.3950
0.0883	0.4057	0.0531	0.4008	0.0955	0.4015	0.0705	0.4015	0.1046	0.4017	0.0928	0.3980
0.0993	0.4025	0.0556	0.4010	0.0985	0.3998	0.0780	0.4022			0.0993	0.3988
0.1039	0.4025	0.0581	0.4015	0.1042	0.3998	0.0855	0.4032			0.1050	0.3988
		0.0631	0.4017			0.0930	0.4040				
		0.0681	0.4022			0.1000	0.4015				
		0.0731	0.4022			0.1043	0.4015				
		0.0781	0.4037								
		0.0831	0.4040								
		0.0881	0.4042								
		0.0931	0.4042								
		0.0991	0.4017								
		0.1040	0.4017								

Smooth X = 4.0 m
Water Surface Elevation = 0.1988 m (5 point average)

Z = 0.152 m		Z = 0.213 m		Z = 0.244 m		Z = 0.274 m		Z = 0.335 m	
y (m)	u (m/s)	y (m)	u (m/s)	y (m)	u (m/s)	y (m)	u (m/s)	y (m)	u (m/s)
0.0000	0.0000	0.0000	0.0000	0.0000	0.0000	0.0000	0.0000	0.0000	0.0000
0.0015	0.2276	0.0015	0.2328	0.0015	0.2449	0.0015	0.2425	0.0015	0.2441
0.0036	0.2637	0.0036	0.2686	0.0057	0.2931	0.0037	0.2752	0.0041	0.2748
0.0076	0.2907	0.0076	0.2944	0.0127	0.3329	0.0077	0.3054	0.0081	0.3060
0.0126	0.3153	0.0126	0.3188	0.0227	0.3648	0.0127	0.3277	0.0106	0.3274
0.0176	0.3301	0.0176	0.3358	0.0327	0.3866	0.0177	0.3478	0.0156	0.3458
0.0276	0.3486	0.0276	0.3535	0.0377	0.3930	0.0252	0.3700	0.0231	0.3732
0.0376	0.3607	0.0376	0.3648	0.0427	0.3968	0.0327	0.3876	0.0306	0.3884
0.0476	0.3686	0.0476	0.3684	0.0477	0.3970	0.0377	0.3955	0.0356	0.3983
0.0576	0.3793	0.0576	0.3686	0.0527	0.3965	0.0402	0.3988	0.0381	0.3993
0.0676	0.3845	0.0676	0.3703	0.0577	0.3955	0.0427	0.3995	0.0406	0.4027
0.0776	0.3917	0.0776	0.3745	0.0627	0.3937	0.0452	0.4003	0.0431	0.4035
0.0826	0.3932	0.0876	0.3832	0.0677	0.3932	0.0477	0.4027	0.0481	0.4047
0.0876	0.3965	0.0926	0.3858	0.0727	0.3922	0.0502	0.4025	0.0531	0.4047
0.0926	0.3973	0.0976	0.3886	0.0777	0.3915	0.0577	0.4022	0.0581	0.4045
0.0976	0.3963	0.1001	0.3907	0.0827	0.3922	0.0652	0.4013	0.0681	0.4040
0.0996	0.3958	0.1056	0.3907	0.0877	0.3940	0.0727	0.4005	0.0781	0.4030
0.1053	0.3958			0.0957	0.3965	0.0802	0.4013	0.0881	0.4027
				0.1007	0.3958	0.0877	0.4015	0.0981	0.4015
				0.1058	0.3958	0.0927	0.4017	0.1016	0.3988
						0.0977	0.4015	0.1064	0.3988
						0.1002	0.4003		
						0.1061	0.4003		

Smooth X = 5.0 m
Water Surface Elevation = 0.1985 m (5 point average)

Z = -0.335 m		Z = -0.274 m		Z = -0.244 m		Z = -0.213 m		Z = -0.152 m		Z = -0.091 m	
y (m)	u (m/s)	y (m)	u (m/s)	y (m)	u (m/s)	y (m)	u (m/s)	y (m)	u (m/s)	y (m)	u (m/s)
0.0000	0.0000	0.0000	0.0000	0.0000	0.0000	0.0000	0.0000	0.0000	0.0000	0.0000	0.0000
0.0015	0.2379	0.0015	0.2400	0.0015	0.2281	0.0015	0.2182	0.0015	0.2079	0.0015	0.2236
0.0033	0.2689	0.0042	0.2715	0.0109	0.3118	0.0061	0.2686	0.0056	0.2572	0.0052	0.2652
0.0073	0.3008	0.0112	0.3125	0.0209	0.3397	0.0101	0.2907	0.0096	0.2726	0.0092	0.2869
0.0148	0.3358	0.0212	0.3446	0.0309	0.3626	0.0201	0.3160	0.0196	0.3008	0.0192	0.3225
0.0223	0.3549	0.0312	0.3673	0.0409	0.3756	0.0301	0.3329	0.0296	0.3207	0.0292	0.3440
0.0298	0.3721	0.0412	0.3871	0.0509	0.3866	0.0401	0.3489	0.0396	0.3382	0.0392	0.3585
0.0373	0.3858	0.0487	0.3955	0.0609	0.3937	0.0501	0.3599	0.0496	0.3543	0.0492	0.3676
0.0448	0.3965	0.0562	0.4008	0.0709	0.3970	0.0601	0.3729	0.0596	0.3670	0.0592	0.3775
0.0523	0.4040	0.0612	0.4032	0.0809	0.4017	0.0701	0.3819	0.0696	0.3788	0.0692	0.3884
0.0573	0.4067	0.0662	0.4050	0.0909	0.4069	0.0801	0.3920	0.0796	0.3892	0.0792	0.3965
0.0623	0.4086	0.0712	0.4047	0.0969	0.4067	0.0851	0.3980	0.0846	0.3942	0.0842	0.3993
0.0673	0.4099	0.0762	0.4055	0.1037	0.4067	0.0901	0.4010	0.0896	0.3988	0.0892	0.4015
0.0723	0.4099	0.0812	0.4062			0.0951	0.4010	0.0946	0.4013	0.0942	0.4030
0.0823	0.4099	0.0912	0.4064			0.0981	0.4003	0.0996	0.4005	0.0992	0.4015
0.0923	0.4089	0.0962	0.4047			0.1039	0.4003	0.1040	0.4005	0.1044	0.4015
0.0963	0.4064	0.0992	0.4015								
0.0983	0.4050	0.1035	0.4015								
0.1031	0.4050										

Smooth X = 5.0 m
Water Surface Elevation = 0.1985 m (5 point average)

Z = -0.061 m		Z = -0.030 m		Z = 0.0 m		Z = 0.030 m		Z = 0.061 m		Z = 0.091 m	
y (m)	u (m/s)	y (m)	u (m/s)	y (m)	u (m/s)	y (m)	u (m/s)	y (m)	u (m/s)	y (m)	u (m/s)
0.0000	0.0000	0.0000	0.0000	0.0000	0.0000	0.0000	0.0000	0.0000	0.0000	0.0000	0.0000
0.0015	0.2358	0.0015	0.2387	0.0015	0.2445	0.0015	0.2408	0.0015	0.2281	0.0015	0.2084
0.0089	0.3083	0.0045	0.2788	0.0092	0.3134	0.0044	0.2844	0.0086	0.2974	0.0043	0.2425
0.0189	0.3432	0.0110	0.3203	0.0192	0.3566	0.0084	0.3128	0.0186	0.3314	0.0083	0.2652
0.0289	0.3678	0.0185	0.3484	0.0292	0.3835	0.0109	0.3259	0.0286	0.3518	0.0183	0.2974
0.0389	0.3814	0.0260	0.3651	0.0392	0.3988	0.0159	0.3397	0.0386	0.3648	0.0283	0.3156
0.0489	0.3935	0.0335	0.3809	0.0492	0.4064	0.0234	0.3626	0.0486	0.3716	0.0383	0.3358
0.0589	0.4015	0.0410	0.3925	0.0592	0.4091	0.0309	0.3803	0.0586	0.3777	0.0483	0.3446
0.0689	0.4052	0.0485	0.3990	0.0692	0.4099	0.0384	0.3904	0.0686	0.3837	0.0583	0.3563
0.0789	0.4077	0.0535	0.4030	0.0792	0.4099	0.0459	0.3983	0.0786	0.3871	0.0683	0.3727
0.0889	0.4113	0.0560	0.4042	0.0892	0.4101	0.0509	0.4013	0.0886	0.3947	0.0783	0.3824
0.0989	0.4101	0.0585	0.4059	0.0992	0.4099	0.0559	0.4025	0.0986	0.3995	0.0883	0.3947
0.1046	0.4101	0.0635	0.4064	0.1050	0.4099	0.0609	0.4032	0.1052	0.3995	0.0933	0.3973
		0.0710	0.4069			0.0659	0.4037			0.0993	0.3998
		0.0785	0.4074			0.0709	0.4037			0.1052	0.3998
		0.0860	0.4072			0.0759	0.4042				
		0.0935	0.4064			0.0809	0.4047				
		0.0995	0.4030			0.0884	0.4062				
		0.1047	0.4030			0.0934	0.4064				
						0.0994	0.4042				
						0.1052	0.4042				

Smooth X = 5.0 m
Water Surface Elevation = 0.1985 m (5 point average)

Z = 0.152 m		Z = 0.213 m		Z = 0.244 m		Z = 0.274 m		Z = 0.335 m	
y (m)	u (m/s)	y (m)	u (m/s)	y (m)	u (m/s)	y (m)	u (m/s)	y (m)	u (m/s)
0.0000	0.0000	0.0000	0.0000	0.0000	0.0000	0.0000	0.0000	0.0000	0.0000
0.0015	0.2232	0.0015	0.2337	0.0015	0.2379	0.0015	0.2416	0.0015	0.2461
0.0042	0.2645	0.0041	0.2693	0.0085	0.3131	0.0041	0.2798	0.0039	0.2806
0.0082	0.2827	0.0081	0.2978	0.0185	0.3498	0.0081	0.3089	0.0079	0.3122
0.0182	0.3141	0.0181	0.3311	0.0285	0.3703	0.0156	0.3394	0.0154	0.3443
0.0282	0.3358	0.0281	0.3526	0.0385	0.3922	0.0231	0.3637	0.0229	0.3708
0.0382	0.3481	0.0381	0.3640	0.0485	0.3993	0.0306	0.3817	0.0304	0.3879
0.0482	0.3643	0.0481	0.3700	0.0585	0.3970	0.0381	0.3942	0.0379	0.3995
0.0582	0.3721	0.0581	0.3721	0.0685	0.3958	0.0431	0.4008	0.0429	0.4057
0.0682	0.3788	0.0681	0.3743	0.0785	0.3937	0.0481	0.4040	0.0454	0.4069
0.0782	0.3866	0.0781	0.3777	0.0885	0.3925	0.0581	0.4047	0.0479	0.4081
0.0832	0.3917	0.0881	0.3827	0.0995	0.3915	0.0681	0.4025	0.0529	0.4099
0.0882	0.3942	0.0931	0.3856	0.1063	0.3915	0.0781	0.4015	0.0579	0.4096
0.0932	0.3975	0.0981	0.3863			0.0881	0.3993	0.0679	0.4099
0.1002	0.3965	0.1011	0.3879			0.0931	0.4013	0.0779	0.4091
0.1056	0.3965	0.1061	0.3879			0.0981	0.3990	0.0879	0.4099
						0.1006	0.3983	0.0929	0.4099
						0.1064	0.3983	0.0979	0.4089
								0.1009	0.4079
								0.1068	0.4079

Smooth X = 6.0 m
Water Surface Elevation = 0.1980 m (5 point average)

Z = -0.335 m		Z = -0.274 m		Z = -0.244 m		Z = -0.213 m		Z = -0.152 m		Z = -0.091 m	
y (m)	u (m/s)	y (m)	u (m/s)	y (m)	u (m/s)	y (m)	u (m/s)	y (m)	u (m/s)	y (m)	u (m/s)
0.0000	0.0000	0.0000	0.0000	0.0000	0.0000	0.0000	0.0000	0.0000	0.0000	0.0000	0.0000
0.0015	0.2400	0.0015	0.2371	0.0015	0.2453	0.0015	0.2289	0.0015	0.2103	0.0015	0.2366
0.0058	0.2937	0.0043	0.2820	0.0086	0.3106	0.0029	0.2485	0.0019	0.2236	0.0063	0.2907
0.0108	0.3203	0.0093	0.3163	0.0186	0.3458	0.0079	0.2844	0.0069	0.2607	0.0163	0.3277
0.0208	0.3506	0.0193	0.3498	0.0286	0.3646	0.0179	0.3203	0.0169	0.2988	0.0263	0.3495
0.0308	0.3737	0.0293	0.3708	0.0386	0.3827	0.0279	0.3394	0.0269	0.3150	0.0363	0.3670
0.0408	0.3940	0.0393	0.3879	0.0486	0.3884	0.0379	0.3537	0.0369	0.3355	0.0463	0.3798
0.0508	0.4067	0.0493	0.4010	0.0586	0.3965	0.0479	0.3629	0.0469	0.3509	0.0563	0.3876
0.0608	0.4154	0.0593	0.4091	0.0686	0.3985	0.0579	0.3759	0.0569	0.3651	0.0663	0.3980
0.0658	0.4190	0.0643	0.4111	0.0786	0.4037	0.0679	0.3861	0.0669	0.3777	0.0763	0.4032
0.0708	0.4211	0.0693	0.4130	0.0886	0.4067	0.0779	0.3960	0.0769	0.3917	0.0813	0.4074
0.0758	0.4232	0.0743	0.4147	0.0966	0.4081	0.0829	0.4015	0.0869	0.3993	0.0863	0.4103
0.0808	0.4251	0.0793	0.4164	0.1021	0.4081	0.0879	0.4052	0.0919	0.4035	0.0913	0.4115
0.0858	0.4263	0.0843	0.4173			0.0929	0.4067	0.0969	0.4040	0.0973	0.4106
0.0908	0.4268	0.0893	0.4180			0.0969	0.4072	0.1020	0.4040	0.1021	0.4106
0.0978	0.4247	0.0963	0.4190			0.1020	0.4072				
0.1028	0.4247	0.1021	0.4190								

Smooth X = 6.0 m
Water Surface Elevation = 0.1980 m (5 point average)

Z = -0.061 m		Z = -0.030 m		Z = 0.0 m		Z = 0.030 m		Z = 0.061 m		Z = 0.091 m	
y (m)	u (m/s)	y (m)	u (m/s)	y (m)	u (m/s)	y (m)	u (m/s)	y (m)	u (m/s)	y (m)	u (m/s)
0.0000	0.0000	0.0000	0.0000	0.0000	0.0000	0.0000	0.0000	0.0000	0.0000	0.0000	0.0000
0.0015	0.2445	0.0015	0.2493	0.0015	0.2529	0.0015	0.2521	0.0015	0.2453	0.0015	0.2191
0.0060	0.2827	0.0055	0.2974	0.0060	0.3077	0.0052	0.3031	0.0053	0.2879	0.0050	0.2591
0.0160	0.3469	0.0155	0.3478	0.0160	0.3540	0.0152	0.3478	0.0153	0.3304	0.0150	0.2974
0.0260	0.3713	0.0255	0.3748	0.0260	0.3806	0.0252	0.3748	0.0253	0.3529	0.0250	0.3207
0.0360	0.3866	0.0355	0.3925	0.0360	0.4015	0.0352	0.3920	0.0353	0.3651	0.0350	0.3382
0.0460	0.3988	0.0430	0.4057	0.0460	0.4140	0.0452	0.4037	0.0453	0.3727	0.0450	0.3537
0.0560	0.4091	0.0505	0.4123	0.0560	0.4190	0.0502	0.4057	0.0553	0.3782	0.0550	0.3654
0.0660	0.4142	0.0555	0.4156	0.0660	0.4204	0.0552	0.4089	0.0653	0.3868	0.0650	0.3782
0.0760	0.4168	0.0580	0.4176	0.0760	0.4204	0.0677	0.4111	0.0753	0.3935	0.0750	0.3879
0.0860	0.4195	0.0605	0.4178	0.0860	0.4206	0.0752	0.4123	0.0853	0.3975	0.0850	0.3975
0.0970	0.4166	0.0630	0.4187	0.0930	0.4187	0.0802	0.4152	0.0923	0.4040	0.0910	0.4037
0.1021	0.4166	0.0655	0.4190	0.0970	0.4164	0.0852	0.4159	0.0973	0.4057	0.0980	0.4062
		0.0705	0.4202	0.1022	0.4164	0.0902	0.4168	0.1026	0.4057	0.1029	0.4062
		0.0780	0.4214			0.0972	0.4147				
		0.0855	0.4218			0.1023	0.4147				
		0.0895	0.4211								
		0.0935	0.4209								
		0.0975	0.4178								
		0.1022	0.4178								

Smooth X = 6.0 m
Water Surface Elevation = 0.1980 m (5 point average)

Z = 0.152 m		Z = 0.213 m		Z = 0.244 m		Z = 0.274 m		Z = 0.335 m	
y (m)	u (m/s)	y (m)	u (m/s)	y (m)	u (m/s)	y (m)	u (m/s)	y (m)	u (m/s)
0.0000	0.0000	0.0000	0.0000	0.0000	0.0000	0.0000	0.0000	0.0000	0.0000
0.0015	0.2214	0.0015	0.2425	0.0015	0.2529	0.0015	0.2533	0.0015	0.2568
0.0047	0.2603	0.0047	0.2872	0.0048	0.2974	0.0045	0.3008	0.0030	0.2827
0.0147	0.3031	0.0147	0.3314	0.0148	0.3475	0.0095	0.3311	0.0065	0.3137
0.0247	0.3250	0.0247	0.3591	0.0248	0.3729	0.0170	0.3577	0.0140	0.3512
0.0347	0.3411	0.0347	0.3732	0.0348	0.3965	0.0245	0.3811	0.0215	0.3732
0.0447	0.3540	0.0447	0.3835	0.0448	0.4045	0.0320	0.3940	0.0290	0.3889
0.0547	0.3673	0.0547	0.3856	0.0548	0.4086	0.0395	0.4077	0.0365	0.4045
0.0647	0.3790	0.0647	0.3889	0.0648	0.4064	0.0445	0.4113	0.0440	0.4140
0.0747	0.3897	0.0747	0.3904	0.0748	0.4040	0.0495	0.4152	0.0490	0.4190
0.0847	0.3973	0.0847	0.3922	0.0848	0.4040	0.0545	0.4156	0.0515	0.4214
0.0907	0.4013	0.0907	0.3960	0.0918	0.4035	0.0645	0.4147	0.0540	0.4214
0.0977	0.4015	0.0977	0.3978	0.0978	0.4045	0.0745	0.4132	0.0565	0.4225
0.1030	0.4015	0.1035	0.3978	0.1037	0.4045	0.0845	0.4118	0.0590	0.4228
						0.0895	0.4118	0.0640	0.4235
						0.0945	0.4115	0.0690	0.4235
						0.0985	0.4096	0.0740	0.4230
						0.1039	0.4096	0.0815	0.4235
								0.0890	0.4247
								0.0940	0.4247
								0.0980	0.4232
								0.1043	0.4232

Smooth X = 7.0 m
Water Surface Elevation = 0.1976 m (5 point average)

Z = -0.335 m		Z = -0.274 m		Z = -0.244 m		Z = -0.213 m		Z = -0.152 m		Z = -0.091 m	
y (m)	u (m/s)	y (m)	u (m/s)	y (m)	u (m/s)	y (m)	u (m/s)	y (m)	u (m/s)	y (m)	u (m/s)
0.0000	0.0000	0.0000	0.0000	0.0000	0.0000	0.0000	0.0000	0.0000	0.0000	0.0000	0.0000
0.0015	0.2433	0.0015	0.2391	0.0015	0.2485	0.0015	0.2298	0.0015	0.2084	0.0015	0.2375
0.0039	0.2869	0.0039	0.2770	0.0076	0.3051	0.0041	0.2663	0.0063	0.2588	0.0055	0.2869
0.0089	0.3178	0.0079	0.3041	0.0176	0.3452	0.0071	0.2907	0.0163	0.2941	0.0155	0.3283
0.0139	0.3364	0.0179	0.3440	0.0276	0.3705	0.0171	0.3222	0.0263	0.3163	0.0255	0.3560
0.0189	0.3546	0.0279	0.3713	0.0376	0.3858	0.0271	0.3449	0.0363	0.3301	0.0355	0.3713
0.0289	0.3756	0.0379	0.3856	0.0476	0.3940	0.0371	0.3552	0.0463	0.3484	0.0455	0.3822
0.0389	0.3950	0.0479	0.3980	0.0576	0.3995	0.0471	0.3678	0.0563	0.3621	0.0555	0.3915
0.0489	0.4089	0.0579	0.4101	0.0676	0.4040	0.0571	0.3759	0.0663	0.3780	0.0655	0.3998
0.0589	0.4187	0.0679	0.4156	0.0776	0.4084	0.0671	0.3840	0.0763	0.3897	0.0755	0.4062
0.0639	0.4247	0.0729	0.4183	0.0876	0.4103	0.0771	0.3920	0.0813	0.3942	0.0805	0.4079
0.0689	0.4282	0.0779	0.4204	0.0966	0.4103	0.0821	0.3990	0.0863	0.3980	0.0855	0.4128
0.0739	0.4305	0.0829	0.4214	0.1021	0.4103	0.0871	0.4032	0.0923	0.4015	0.0915	0.4164
0.0764	0.4316	0.0879	0.4225			0.0921	0.4045	0.0973	0.4025	0.0975	0.4164
0.0789	0.4328	0.0919	0.4235			0.0971	0.4055	0.1025	0.4025	0.1028	0.4164
0.0814	0.4337	0.0949	0.4211			0.1023	0.4055				
0.0839	0.4351	0.1019	0.4211								
0.0889	0.4353										
0.0959	0.4335										
0.1015	0.4335										

Smooth X = 7.0 m
Water Surface Elevation = 0.1976 m (5 point average)

Z = -0.061 m		Z = -0.030 m		Z =0.0 m		Z = 0.030 m		Z = 0.061 m		Z = 0.091 m	
y (m)	u (m/s)	y (m)	u (m/s)	y (m)	u (m/s)	y (m)	u (m/s)	y (m)	u (m/s)	y (m)	u (m/s)
0.0000	0.0000	0.0000	0.0000	0.0000	0.0000	0.0000	0.0000	0.0000	0.0000	0.0000	0.0000
0.0015	0.2461	0.0015	0.2465	0.0015	0.2529	0.0015	0.2465	0.0015	0.2375	0.0015	0.2150
0.0055	0.2827	0.0049	0.2954	0.0053	0.3008	0.0044	0.2903	0.0047	0.2809	0.0041	0.2513
0.0155	0.3391	0.0149	0.3426	0.0153	0.3463	0.0144	0.3394	0.0147	0.3304	0.0141	0.3008
0.0255	0.3708	0.0249	0.3729	0.0253	0.3764	0.0244	0.3692	0.0247	0.3478	0.0241	0.3247
0.0355	0.3907	0.0349	0.3932	0.0353	0.3993	0.0344	0.3899	0.0347	0.3678	0.0341	0.3379
0.0455	0.4050	0.0449	0.4079	0.0453	0.4130	0.0444	0.4035	0.0447	0.3809	0.0441	0.3506
0.0555	0.4106	0.0524	0.4164	0.0553	0.4214	0.0544	0.4084	0.0547	0.3811	0.0541	0.3646
0.0655	0.4180	0.0599	0.4228	0.0653	0.4249	0.0644	0.4118	0.0647	0.3845	0.0641	0.3751
0.0755	0.4223	0.0649	0.4251	0.0753	0.4268	0.0744	0.4142	0.0747	0.3965	0.0741	0.3843
0.0855	0.4232	0.0699	0.4258	0.0853	0.4258	0.0794	0.4144	0.0847	0.3993	0.0841	0.3965
0.0975	0.4225	0.0749	0.4272	0.0913	0.4261	0.0844	0.4156	0.0927	0.4040	0.0941	0.4020
0.1028	0.4225	0.0799	0.4282	0.0973	0.4232	0.0894	0.4152	0.0977	0.4050	0.0981	0.4035
		0.0849	0.4300	0.1028	0.4232	0.0944	0.4161	0.1030	0.4050	0.1032	0.4035
		0.0899	0.4291			0.0984	0.4118				
		0.0949	0.4282			0.1028	0.4118				
		0.0974	0.4261								
		0.1028	0.4261								

Smooth X = 7.0 m
Water Surface Elevation = 0.1976 m (5 point average)

Z = 0.152 m		Z = 0.213 m		Z = 0.244 m		Z = 0.274 m		Z = 0.335 m	
y (m)	u (m/s)	y (m)	u (m/s)	y (m)	u (m/s)	y (m)	u (m/s)	y (m)	u (m/s)
0.0000	0.0000	0.0000	0.0000	0.0000	0.0000	0.0000	0.0000	0.0000	0.0000
0.0015	0.2132	0.0015	0.2379	0.0015	0.2485	0.0015	0.2545	0.0015	0.2529
0.0040	0.2461	0.0045	0.2701	0.0035	0.2816	0.0032	0.2820	0.0028	0.2809
0.0140	0.2937	0.0095	0.3109	0.0135	0.3394	0.0062	0.3083	0.0058	0.3044
0.0240	0.3194	0.0145	0.3250	0.0235	0.3727	0.0107	0.3295	0.0103	0.3301
0.0340	0.3358	0.0245	0.3563	0.0335	0.3915	0.0182	0.3621	0.0178	0.3637
0.0440	0.3529	0.0345	0.3716	0.0435	0.4040	0.0257	0.3824	0.0253	0.3806
0.0540	0.3659	0.0445	0.3824	0.0535	0.4091	0.0332	0.3998	0.0328	0.3980
0.0640	0.3782	0.0545	0.3876	0.0635	0.4089	0.0382	0.4084	0.0403	0.4091
0.0740	0.3858	0.0645	0.3920	0.0735	0.4089	0.0432	0.4115	0.0478	0.4190
0.0790	0.3927	0.0745	0.3925	0.0835	0.4081	0.0482	0.4164	0.0528	0.4242
0.0840	0.3935	0.0795	0.3940	0.0915	0.4069	0.0532	0.4178	0.0553	0.4270
0.0890	0.3968	0.0845	0.3950	0.0985	0.4067	0.0582	0.4190	0.0578	0.4272
0.0940	0.3998	0.0895	0.3980	0.1035	0.4067	0.0632	0.4183	0.0603	0.4286
0.0990	0.4000	0.0945	0.3988			0.0682	0.4192	0.0628	0.4286
0.1032	0.4000	0.0995	0.3975			0.0732	0.4183	0.0653	0.4289
		0.1033	0.3975			0.0782	0.4166	0.0728	0.4291
						0.0832	0.4152	0.0778	0.4291
						0.0882	0.4140	0.0828	0.4300
						0.0932	0.4149	0.0878	0.4296
						0.0982	0.4140	0.0928	0.4312
						0.1038	0.4140	0.0978	0.4272
								0.1040	0.4272

Smooth X = 9.0 m
Water Surface Elevation = 0.1969 m (5 point average)

Z = -0.335 m		Z = -0.274 m		Z = -0.244 m		Z = -0.213 m		Z = -0.152 m		Z = -0.091 m	
y (m)	u (m/s)	y (m)	u (m/s)	y (m)	u (m/s)	y (m)	u (m/s)	y (m)	u (m/s)	y (m)	u (m/s)
0.0000	0.0000	0.0000	0.0000	0.0000	0.0000	0.0000	0.0000	0.0000	0.0000	0.0000	0.0000
0.0015	0.2497	0.0015	0.2425	0.0015	0.2408	0.0015	0.2324	0.0015	0.2046	0.0015	0.2383
0.0050	0.2991	0.0040	0.2858	0.0085	0.3083	0.0034	0.2652	0.0068	0.2595	0.0064	0.2998
0.0090	0.3197	0.0080	0.3080	0.0185	0.3455	0.0074	0.2961	0.0168	0.2961	0.0164	0.3340
0.0190	0.3591	0.0180	0.3449	0.0285	0.3676	0.0174	0.3280	0.0268	0.3153	0.0264	0.3591
0.0290	0.3863	0.0280	0.3724	0.0385	0.3863	0.0274	0.3484	0.0368	0.3329	0.0364	0.3745
0.0390	0.3988	0.0380	0.3879	0.0485	0.3995	0.0374	0.3676	0.0468	0.3449	0.0464	0.3843
0.0490	0.4161	0.0480	0.4040	0.0585	0.4052	0.0474	0.3727	0.0568	0.3588	0.0564	0.3920
0.0590	0.4284	0.0580	0.4137	0.0685	0.4115	0.0574	0.3827	0.0668	0.3708	0.0664	0.3993
0.0690	0.4378	0.0630	0.4164	0.0785	0.4161	0.0674	0.3932	0.0768	0.3811	0.0764	0.4084
0.0740	0.4385	0.0680	0.4223	0.0885	0.4140	0.0774	0.3963	0.0818	0.3894	0.0814	0.4118
0.0790	0.4412	0.0730	0.4228	0.0965	0.4125	0.0824	0.4013	0.0868	0.3950	0.0864	0.4161
0.0840	0.4435	0.0780	0.4261	0.1022	0.4125	0.0874	0.4040	0.0918	0.3968	0.0924	0.4156
0.0890	0.4435	0.0830	0.4235			0.0924	0.4037	0.0978	0.3993	0.0984	0.4154
0.0950	0.4428	0.0880	0.4263			0.0974	0.4047	0.1031	0.3993	0.1032	0.4154
0.1019	0.4428	0.0920	0.4270			0.1024	0.4047				
		0.0955	0.4249								
		0.1020	0.4249								

Smooth X = 9.0 m
Water Surface Elevation = 0.1969 m (5 point average)

Z = -0.061 m		Z = -0.030 m		Z = 0.0 m		Z = 0.030 m		Z = 0.061 m		Z = 0.091 m	
y (m)	u (m/s)	y (m)	u (m/s)	y (m)	u (m/s)	y (m)	u (m/s)	y (m)	u (m/s)	y (m)	u (m/s)
0.0000	0.0000	0.0000	0.0000	0.0000	0.0000	0.0000	0.0000	0.0000	0.0000	0.0000	0.0000
0.0015	0.2477	0.0015	0.2481	0.0015	0.2457	0.0015	0.2513	0.0015	0.2345	0.0015	0.2236
0.0068	0.3073	0.0060	0.3021	0.0063	0.3083	0.0058	0.3089	0.0065	0.2964	0.0057	0.2712
0.0168	0.3417	0.0160	0.3506	0.0163	0.3478	0.0158	0.3469	0.0165	0.3329	0.0157	0.3077
0.0268	0.3761	0.0260	0.3767	0.0263	0.3727	0.0258	0.3729	0.0265	0.3563	0.0257	0.3317
0.0368	0.3922	0.0360	0.3965	0.0363	0.3968	0.0358	0.3937	0.0365	0.3711	0.0357	0.3437
0.0468	0.4062	0.0460	0.4106	0.0463	0.4111	0.0458	0.4037	0.0465	0.3817	0.0457	0.3566
0.0568	0.4142	0.0560	0.4242	0.0563	0.4242	0.0558	0.4103	0.0565	0.3879	0.0557	0.3676
0.0668	0.4187	0.0660	0.4307	0.0663	0.4275	0.0658	0.4161	0.0665	0.3915	0.0657	0.3775
0.0768	0.4223	0.0710	0.4351	0.0763	0.4307	0.0758	0.4166	0.0765	0.3980	0.0757	0.3853
0.0868	0.4242	0.0760	0.4371	0.0863	0.4305	0.0808	0.4166	0.0865	0.4027	0.0857	0.3963
0.0978	0.4258	0.0810	0.4376	0.0933	0.4307	0.0858	0.4166	0.0935	0.4057	0.0907	0.3993
0.1035	0.4258	0.0860	0.4403	0.0983	0.4282	0.0918	0.4166	0.0985	0.4062	0.0957	0.4022
		0.0920	0.4396	0.1038	0.4282	0.0978	0.4168	0.1043	0.4062	0.0987	0.4003
		0.0980	0.4374			0.1040	0.4168			0.1046	0.4003
		0.1037	0.4374								

Smooth X = 9.0 m
Water Surface Elevation = 0.1969 m (5 point average)

Z = 0.152 m		Z = 0.213 m		Z = 0.244 m		Z = 0.274 m		Z = 0.335 m	
y (m)	u (m/s)	y (m)	u (m/s)	y (m)	u (m/s)	y (m)	u (m/s)	y (m)	u (m/s)
0.0000	0.0000	0.0000	0.0000	0.0000	0.0000	0.0000	0.0000	0.0000	0.0000
0.0015	0.2099	0.0015	0.2408	0.0015	0.2461	0.0015	0.2525	0.0015	0.2469
0.0058	0.2618	0.0057	0.2914	0.0061	0.3008	0.0057	0.2984	0.0051	0.3011
0.0158	0.2961	0.0157	0.3394	0.0161	0.3452	0.0157	0.3526	0.0101	0.3298
0.0258	0.3203	0.0257	0.3613	0.0261	0.3759	0.0257	0.3801	0.0151	0.3455
0.0358	0.3329	0.0357	0.3780	0.0361	0.3889	0.0357	0.3985	0.0251	0.3767
0.0458	0.3504	0.0457	0.3879	0.0461	0.4017	0.0457	0.4128	0.0351	0.3985
0.0558	0.3621	0.0557	0.3945	0.0561	0.4099	0.0557	0.4202	0.0451	0.4140
0.0658	0.3764	0.0657	0.4000	0.0661	0.4156	0.0607	0.4261	0.0551	0.4254
0.0758	0.3850	0.0757	0.4017	0.0761	0.4156	0.0657	0.4279	0.0601	0.4309
0.0808	0.3899	0.0807	0.4040	0.0861	0.4164	0.0707	0.4272	0.0651	0.4330
0.0858	0.3932	0.0857	0.4069	0.0951	0.4161	0.0757	0.4277	0.0701	0.4371
0.0908	0.3975	0.0907	0.4074	0.1001	0.4144	0.0807	0.4270	0.0751	0.4376
0.0958	0.3988	0.0957	0.4077	0.1054	0.4144	0.0857	0.4291	0.0801	0.4394
0.0993	0.3995	0.0997	0.4079			0.0907	0.4284	0.0851	0.4399
0.1048	0.3995	0.1049	0.4079			0.0957	0.4261	0.0901	0.4396
						0.1007	0.4291	0.0951	0.4399
						0.1058	0.4291	0.1001	0.4383
								0.1061	0.4383

Smooth X = 11.0 m
Water Surface Elevation = 0.1962 m (5 point average)

Z = -0.335 m		Z = -0.274 m		Z = -0.244 m		Z = -0.213 m		Z = -0.152 m		Z = -0.091 m	
y (m)	u (m/s)	y (m)	u (m/s)	y (m)	u (m/s)	y (m)	u (m/s)	y (m)	u (m/s)	y (m)	u (m/s)
0.0000	0.0000	0.0000	0.0000	0.0000	0.0000	0.0000	0.0000	0.0000	0.0000	0.0000	0.0000
0.0015	0.2545	0.0015	0.2449	0.0015	0.2429	0.0015	0.2349	0.0015	0.2132	0.0015	0.2441
0.0061	0.3118	0.0051	0.2964	0.0096	0.3137	0.0045	0.2726	0.0041	0.2449	0.0035	0.2788
0.0101	0.3329	0.0091	0.3160	0.0196	0.3521	0.0085	0.3011	0.0081	0.2686	0.0075	0.3044
0.0201	0.3657	0.0191	0.3537	0.0296	0.3735	0.0185	0.3298	0.0181	0.3028	0.0175	0.3420
0.0301	0.3861	0.0291	0.3721	0.0396	0.3840	0.0285	0.3523	0.0281	0.3237	0.0275	0.3651
0.0401	0.4030	0.0391	0.3915	0.0496	0.3930	0.0385	0.3673	0.0381	0.3352	0.0375	0.3806
0.0501	0.4185	0.0491	0.4042	0.0596	0.4045	0.0485	0.3743	0.0481	0.3506	0.0475	0.3897
0.0601	0.4305	0.0566	0.4106	0.0696	0.4101	0.0585	0.3814	0.0581	0.3579	0.0575	0.3963
0.0651	0.4351	0.0641	0.4161	0.0796	0.4091	0.0685	0.3902	0.0681	0.3678	0.0675	0.3993
0.0701	0.4371	0.0691	0.4187	0.0896	0.4128	0.0785	0.3940	0.0781	0.3780	0.0775	0.4106
0.0751	0.4410	0.0741	0.4232	0.0976	0.4089	0.0835	0.3968	0.0831	0.3850	0.0825	0.4115
0.0801	0.4426	0.0791	0.4225	0.1031	0.4089	0.0885	0.4000	0.0881	0.3889	0.0875	0.4137
0.0851	0.4424	0.0841	0.4265			0.0935	0.4017	0.0931	0.3915	0.0925	0.4173
0.0901	0.4442	0.0891	0.4272			0.0975	0.3983	0.0986	0.3950	0.0985	0.4115
0.0961	0.4437	0.0931	0.4268			0.1033	0.3983	0.1036	0.3950	0.1038	0.4115
0.1029	0.4437	0.0961	0.4282								
		0.1029	0.4282								

Smooth X = 11.0 m
Water Surface Elevation = 0.1962 m (5 point average)

Z = -0.061 m		Z = -0.030 m		Z = 0.0 m		Z = 0.030 m		Z = 0.061 m		Z = 0.091 m	
y (m)	u (m/s)	y (m)	u (m/s)	y (m)	u (m/s)	y (m)	u (m/s)	y (m)	u (m/s)	y (m)	u (m/s)
0.0000	0.0000	0.0000	0.0000	0.0000	0.0000	0.0000	0.0000	0.0000	0.0000	0.0000	0.0000
0.0015	0.2453	0.0015	0.2449	0.0015	0.2533	0.0015	0.2441	0.0015	0.2366	0.0015	0.2205
0.0078	0.3172	0.0032	0.2806	0.0072	0.3137	0.0038	0.2844	0.0072	0.2951	0.0066	0.2781
0.0178	0.3535	0.0072	0.3147	0.0172	0.3535	0.0068	0.3064	0.0172	0.3379	0.0166	0.3172
0.0278	0.3809	0.0172	0.3549	0.0272	0.3790	0.0168	0.3498	0.0272	0.3568	0.0266	0.3295
0.0378	0.3925	0.0272	0.3785	0.0372	0.3963	0.0268	0.3724	0.0372	0.3703	0.0366	0.3478
0.0478	0.4062	0.0372	0.3960	0.0472	0.4089	0.0368	0.3866	0.0472	0.3780	0.0466	0.3579
0.0578	0.4164	0.0472	0.4103	0.0572	0.4214	0.0468	0.4000	0.0572	0.3863	0.0566	0.3651
0.0678	0.4204	0.0572	0.4214	0.0672	0.4282	0.0568	0.4089	0.0672	0.3937	0.0666	0.3735
0.0778	0.4237	0.0672	0.4309	0.0772	0.4305	0.0668	0.4137	0.0772	0.4010	0.0741	0.3814
0.0878	0.4228	0.0772	0.4351	0.0872	0.4339	0.0718	0.4147	0.0872	0.4059	0.0816	0.3889
0.0988	0.4218	0.0822	0.4360	0.0982	0.4330	0.0768	0.4161	0.0992	0.4081	0.0866	0.3925
0.1039	0.4218	0.0872	0.4374	0.1040	0.4330	0.0818	0.4183	0.1041	0.4081	0.0906	0.3937
		0.0912	0.4387			0.0868	0.4187			0.0946	0.3960
		0.0952	0.4396			0.0908	0.4221			0.0986	0.3968
		0.0992	0.4360			0.0948	0.4216			0.1042	0.3968
		0.1039	0.4360			0.0983	0.4159				
						0.1041	0.4159				

Smooth X = 11.0 m
Water Surface Elevation = 0.1962 m (5 point average)

Z = 0.152 m		Z = 0.213 m		Z = 0.244 m		Z = 0.274 m		Z = 0.335 m	
y (m)	u (m/s)	y (m)	u (m/s)	y (m)	u (m/s)	y (m)	u (m/s)	y (m)	u (m/s)
0.0000	0.0000	0.0000	0.0000	0.0000	0.0000	0.0000	0.0000		0.0000
0.0015	0.2164	0.0015	0.2371	0.0015	0.2371	0.0015	0.2465	0.0015	0.2453
0.0064	0.2611	0.0062	0.2934	0.0067	0.3008	0.0061	0.3067	0.0057	0.2991
0.0164	0.3064	0.0162	0.3355	0.0167	0.3526	0.0161	0.3478	0.0157	0.3469
0.0264	0.3268	0.0262	0.3621	0.0267	0.3703	0.0261	0.3759	0.0257	0.3719
0.0364	0.3420	0.0362	0.3803	0.0367	0.3897	0.0361	0.3922	0.0357	0.3927
0.0464	0.3481	0.0462	0.3894	0.0467	0.4015	0.0461	0.4111	0.0457	0.4106
0.0564	0.3635	0.0562	0.3965	0.0567	0.4115	0.0561	0.4195	0.0557	0.4232
0.0664	0.3700	0.0662	0.4015	0.0667	0.4166	0.0611	0.4244	0.0657	0.4300
0.0764	0.3782	0.0712	0.4022	0.0767	0.4190	0.0661	0.4277	0.0707	0.4362
0.0814	0.3848	0.0762	0.4037	0.0867	0.4192	0.0711	0.4289	0.0757	0.4376
0.0864	0.3879	0.0812	0.4062	0.0947	0.4230	0.0761	0.4293	0.0807	0.4396
0.0904	0.3925	0.0862	0.4084	0.0997	0.4202	0.0811	0.4323	0.0857	0.4405
0.0944	0.3917	0.0902	0.4094	0.1044	0.4202	0.0861	0.4321	0.0907	0.4435
0.0984	0.3937	0.0942	0.4079			0.0901	0.4328	0.0947	0.4430
0.1045	0.3937	0.0982	0.4099			0.0941	0.4351	0.0987	0.4428
		0.1043	0.4099			0.0981	0.4342	0.1047	0.4428
						0.1045	0.4342		

APPENDIX 2

Experimental data for rough mild channel

Rough X = 0.5 m
Water Surface Elevation = 0.1340 m (5 point average)

Z = -0.335 m		Z = -0.274 m		Z = -0.213 m		Z = -0.152 m		Z = -0.091 m	
y (m)	u (m/s)	y (m)	u (m/s)	y (m)	u (m/s)	y (m)	u (m/s)	y (m)	u (m/s)
0.0000	0.0000	0.0000	0.0000	0.0000	0.0000	0.0000	0.0000	0.0000	0.0000
0.0055	0.2646	0.0043	0.2346	0.0043	0.2378	0.0088	0.2425	0.0073	0.2738
0.0064	0.2841	0.0053	0.2697	0.0054	0.2738	0.0099	0.2641	0.0083	0.2961
0.0079	0.3172	0.0068	0.3048	0.0064	0.3048	0.0124	0.2867	0.0103	0.3246
0.0089	0.3322	0.0093	0.3461	0.0089	0.3440	0.0174	0.3153	0.0153	0.3522
0.0114	0.3511	0.0118	0.3644	0.0114	0.3585	0.0224	0.3254	0.0203	0.3654
0.0164	0.3684	0.0143	0.3715	0.0139	0.3671	0.0274	0.3422	0.0253	0.3695
0.0189	0.3718	0.0168	0.3748	0.0164	0.3705	0.0324	0.3533	0.0303	0.3711
0.0214	0.3735	0.0193	0.3755	0.0189	0.3701	0.0374	0.3616	0.0403	0.3715
0.0264	0.3745	0.0243	0.3751	0.0214	0.3691	0.0424	0.3681	0.0503	0.3708
0.0314	0.3735	0.0293	0.3745	0.0239	0.3691	0.0474	0.3691	0.0603	0.3698
0.0414	0.3728	0.0393	0.3738	0.0264	0.3695	0.0524	0.3715	0.0703	0.3698
0.0514	0.3721	0.0493	0.3735	0.0289	0.3691	0.0624	0.3718	0.0803	0.3691
0.0614	0.3725	0.0593	0.3731	0.0339	0.3705	0.0724	0.3701	0.0903	0.3701
0.0714	0.3728	0.0693	0.3731	0.0389	0.3705	0.0824	0.3698	0.1003	0.3705
0.0814	0.3728	0.0793	0.3735	0.0489	0.3711	0.0924	0.3701	0.1033	0.3688
0.0914	0.3731	0.0893	0.3738	0.0589	0.3708	0.1024	0.3708	0.1097	0.3688
0.0984	0.3721	0.0973	0.3745	0.0689	0.3705	0.1054	0.3691		
0.1014	0.3708	0.1003	0.3731	0.0789	0.3705	0.1104	0.3691		
0.1097	0.3708	0.1104	0.3731	0.0889	0.3718				
				0.0979	0.3721				
				0.1009	0.3711				
				0.1086	0.3711				

Rough X = 0.5 m
Water Surface Elevation = 0.1340 m (5 point average)

Z = -0.030 m		Z = 0.0 m		Z = 0.030 m		Z = 0.091 m		Z = 0.152 m	
y (m)	u (m/s)	y (m)	u (m/s)	y (m)	u (m/s)	y (m)	u (m/s)	y (m)	u (m/s)
0.0000	0.0000	0.0000	0.0000	0.0000	0.0000	0.0000	0.0000	0.0000	0.0000
0.0062	0.2828	0.0057	0.2603	0.0050	0.2394	0.0049	0.2341	0.0042	0.2046
0.0073	0.3093	0.0079	0.3105	0.0070	0.2884	0.0068	0.2828	0.0061	0.2535
0.0088	0.3370	0.0104	0.3440	0.0095	0.3303	0.0098	0.3359	0.0086	0.3052
0.0113	0.3550	0.0129	0.3554	0.0120	0.3472	0.0138	0.3595	0.0111	0.3363
0.0163	0.3684	0.0179	0.3691	0.0170	0.3647	0.0168	0.3654	0.0161	0.3515
0.0188	0.3711	0.0204	0.3721	0.0195	0.3698	0.0193	0.3711	0.0211	0.3623
0.0213	0.3731	0.0229	0.3728	0.0220	0.3721	0.0218	0.3731	0.0261	0.3654
0.0238	0.3745	0.0279	0.3745	0.0270	0.3741	0.0243	0.3748	0.0311	0.3701
0.0288	0.3741	0.0379	0.3735	0.0370	0.3735	0.0268	0.3751	0.0336	0.3721
0.0388	0.3735	0.0479	0.3728	0.0470	0.3721	0.0318	0.3741	0.0361	0.3741
0.0488	0.3725	0.0579	0.3721	0.0570	0.3711	0.0368	0.3738	0.0411	0.3755
0.0588	0.3715	0.0679	0.3715	0.0670	0.3708	0.0468	0.3731	0.0461	0.3755
0.0688	0.3715	0.0779	0.3718	0.0770	0.3705	0.0568	0.3721	0.0561	0.3741
0.0788	0.3721	0.0879	0.3721	0.0870	0.3708	0.0668	0.3708	0.0661	0.3725
0.0888	0.3728	0.0979	0.3728	0.0970	0.3708	0.0768	0.3701	0.0761	0.3718
0.0988	0.3728	0.1019	0.3718	0.1000	0.3698	0.0868	0.3705	0.0861	0.3721
0.1028	0.3715	0.1095	0.3718	0.1094	0.3698	0.0968	0.3705	0.0961	0.3725
0.1097	0.3715					0.1008	0.3695	0.1001	0.3711
						0.1094	0.3695	0.1096	0.3711

Rough X = 0.5 m
Water Surface Elevation = 0.1340 m (5 point average)

Z = 0.213 m		Z = 0.274 m		Z = 0.335 m	
y (m)	u (m/s)	y (m)	u (m/s)	y (m)	u (m/s)
0.0000	0.0000	0.0000	0.0000	0.0000	0.0000
0.0039	0.2276	0.0047	0.2520	0.0064	0.2889
0.0049	0.2603	0.0057	0.2854	0.0074	0.3137
0.0059	0.2897	0.0067	0.3089	0.0084	0.3318
0.0074	0.3318	0.0077	0.3250	0.0094	0.3472
0.0084	0.3472	0.0092	0.3447	0.0109	0.3616
0.0109	0.3664	0.0117	0.3599	0.0134	0.3701
0.0134	0.3721	0.0142	0.3688	0.0159	0.3738
0.0159	0.3755	0.0167	0.3725	0.0184	0.3745
0.0209	0.3755	0.0192	0.3748	0.0234	0.3751
0.0259	0.3751	0.0217	0.3751	0.0284	0.3745
0.0309	0.3745	0.0267	0.3751	0.0384	0.3738
0.0359	0.3738	0.0367	0.3735	0.0484	0.3731
0.0459	0.3725	0.0467	0.3725	0.0584	0.3728
0.0559	0.3711	0.0567	0.3705	0.0684	0.3725
0.0659	0.3701	0.0667	0.3701	0.0784	0.3721
0.0759	0.3698	0.0767	0.3705	0.0884	0.3731
0.0859	0.3715	0.0867	0.3711	0.0984	0.3738
0.0959	0.3721	0.0967	0.3715	0.1024	0.3748
0.0999	0.3718	0.1007	0.3698	0.1099	0.3748
0.1095	0.3718	0.1098	0.3698		

Rough X = 1 m
Water Surface Elevation = 0.1330 m (5 point average)

Z = -0.335 m		Z = -0.274 m		Z = -0.213 m		Z = -0.152 m		Z = -0.091 m	
y (m)	u (m/s)	y (m)	u (m/s)	y (m)	u (m/s)	y (m)	u (m/s)	y (m)	u (m/s)
0.0000	0.0000	0.0000	0.0000	0.0000	0.0000	0.0000	0.0000	0.0000	0.0000
0.0060	0.1990	0.0060	0.1900	0.0065	0.2021	0.0070	0.1907	0.0070	0.1881
0.0080	0.2260	0.0110	0.2559	0.0110	0.2608	0.0110	0.2399	0.0106	0.2303
0.0110	0.2669	0.0160	0.3093	0.0160	0.3129	0.0160	0.2867	0.0156	0.2863
0.0140	0.3044	0.0210	0.3557	0.0210	0.3511	0.0210	0.3192	0.0206	0.3265
0.0170	0.3265	0.0250	0.3807	0.0260	0.3768	0.0260	0.3472	0.0256	0.3613
0.0220	0.3582	0.0285	0.3955	0.0285	0.3863	0.0310	0.3678	0.0281	0.3755
0.0270	0.3778	0.0310	0.4002	0.0310	0.3927	0.0360	0.3775	0.0306	0.3863
0.0320	0.3914	0.0335	0.4021	0.0335	0.3955	0.0385	0.3824	0.0331	0.3920
0.0345	0.3949	0.0360	0.4027	0.0360	0.3952	0.0410	0.3859	0.0356	0.3958
0.0370	0.3996	0.0385	0.4033	0.0385	0.3986	0.0435	0.3888	0.0381	0.3993
0.0395	0.4014	0.0410	0.4027	0.0410	0.4002	0.0460	0.3895	0.0406	0.4002
0.0420	0.4017	0.0510	0.4027	0.0510	0.4017	0.0485	0.3923	0.0506	0.4014
0.0520	0.4030	0.0610	0.4017	0.0610	0.4011	0.0510	0.3930	0.0606	0.4005
0.0620	0.4030	0.0710	0.4014	0.0710	0.4005	0.0535	0.3949	0.0706	0.4002
0.0720	0.4030	0.0810	0.4017	0.0910	0.4017	0.0560	0.3955	0.0806	0.4002
0.0820	0.4027	0.0910	0.4027	0.0970	0.4021	0.0610	0.3980	0.0906	0.3999
0.0920	0.4027	0.0960	0.4024	0.1010	0.4008	0.0710	0.3986	0.0986	0.4005
0.0970	0.4011	0.1000	0.4008	0.1083	0.4008	0.0810	0.3990	0.1026	0.3990
0.1010	0.3986	0.1083	0.4008			0.0910	0.3993	0.1089	0.3990
0.1079	0.3986					0.0970	0.3993		
						0.1010	0.3968		
						0.1088	0.3968		

Rough X = 1 m
Water Surface Elevation = 0.1330 m (5 point average)

Z = -0.030 m		Z = 0.0 m		Z = 0.030 m		Z = 0.091 m		Z = 0.152 m	
y (m)	u (m/s)	y (m)	u (m/s)	y (m)	u (m/s)	y (m)	u (m/s)	y (m)	u (m/s)
0.0000	0.0000	0.0000	0.0000	0.0000	0.0000	0.0000	0.0000	0.0000	0.0000
0.0057	0.1933	0.0060	0.1939	0.0055	0.1736	0.0052	0.1640	0.0052	0.1610
0.0092	0.2495	0.0093	0.2425	0.0088	0.2232	0.0082	0.2135	0.0076	0.1971
0.0142	0.2969	0.0143	0.3011	0.0138	0.2779	0.0132	0.2608	0.0126	0.2559
0.0192	0.3483	0.0193	0.3447	0.0188	0.3168	0.0182	0.3089	0.0176	0.3003
0.0242	0.3758	0.0243	0.3755	0.0238	0.3543	0.0232	0.3400	0.0226	0.3440
0.0267	0.3859	0.0268	0.3888	0.0288	0.3791	0.0282	0.3654	0.0276	0.3688
0.0292	0.3920	0.0293	0.3949	0.0313	0.3863	0.0332	0.3846	0.0326	0.3859
0.0317	0.3977	0.0318	0.3983	0.0338	0.3927	0.0357	0.3911	0.0351	0.3911
0.0342	0.3993	0.0343	0.3999	0.0363	0.3986	0.0382	0.3946	0.0376	0.3955
0.0392	0.4005	0.0393	0.4011	0.0388	0.4002	0.0407	0.3974	0.0401	0.3955
0.0442	0.4008	0.0493	0.4005	0.0488	0.4002	0.0432	0.3986	0.0426	0.3977
0.0492	0.3999	0.0593	0.3996	0.0588	0.3999	0.0482	0.3996	0.0451	0.3980
0.0592	0.4002	0.0693	0.3999	0.0688	0.3993	0.0582	0.4005	0.0476	0.3986
0.0692	0.3999	0.0793	0.3999	0.0788	0.3993	0.0682	0.3999	0.0576	0.4002
0.0792	0.4002	0.0893	0.4002	0.0888	0.4002	0.0782	0.3993	0.0676	0.3996
0.0892	0.4017	0.0963	0.4011	0.0968	0.3999	0.0882	0.3990	0.0776	0.3996
0.0972	0.4017	0.1003	0.3993	0.1008	0.3986	0.0962	0.3986	0.0876	0.4005
0.1012	0.3996	0.1083	0.3993	0.1082	0.3986	0.1002	0.3974	0.0956	0.4005
0.1083	0.3996					0.1088	0.3974	0.0996	0.3999
								0.1083	0.3999

Rough X = 1 m
Water Surface Elevation = 0.1330 m (5 point average)

Z = 0.213 m		Z = 0.274 m		Z = 0.335 m	
y (m)	u (m/s)	y (m)	u (m/s)	y (m)	u (m/s)
0.0000	0.0000	0.0000	0.0000	0.0000	0.0000
0.0042	0.1506	0.0045	0.1655	0.0043	0.1655
0.0065	0.1996	0.0062	0.1926	0.0057	0.1978
0.0115	0.2646	0.0112	0.2678	0.0107	0.2752
0.0165	0.3160	0.0162	0.3207	0.0157	0.3295
0.0215	0.3476	0.0212	0.3582	0.0207	0.3725
0.0265	0.3765	0.0262	0.3866	0.0232	0.3850
0.0315	0.3888	0.0287	0.3949	0.0257	0.3946
0.0340	0.3949	0.0312	0.3993	0.0282	0.3999
0.0365	0.3958	0.0362	0.4024	0.0307	0.4036
0.0390	0.3986	0.0462	0.4021	0.0357	0.4039
0.0415	0.3996	0.0562	0.4008	0.0457	0.4036
0.0440	0.4005	0.0662	0.4005	0.0557	0.4027
0.0465	0.4008	0.0762	0.3999	0.0657	0.4024
0.0515	0.4005	0.0862	0.4008	0.0757	0.4027
0.0565	0.4024	0.0952	0.3999	0.0857	0.4036
0.0665	0.4008	0.0992	0.3977	0.0947	0.4033
0.0765	0.4005	0.1090	0.3977	0.0987	0.4011
0.0865	0.4014			0.1093	0.4011
0.0945	0.4014				
0.0985	0.4005				
0.1088	0.4005				

Rough X = 1.5 m
Water Surface Elevation = 0.1320 m (5 point average)

Z = -0.335 m		Z = -0.274 m		Z = -0.213 m		Z = -0.152 m		Z = -0.091 m	
y (m)	u (m/s)	y (m)	u (m/s)	y (m)	u (m/s)	y (m)	u (m/s)	y (m)	u (m/s)
0.0000	0.0000	0.0000	0.0000	0.0000	0.0000	0.0000	0.0000	0.0000	0.0000
0.0060	0.1861	0.0063	0.1920	0.0060	0.1648	0.0067	0.1594	0.0065	0.1841
0.0074	0.2058	0.0071	0.2094	0.0081	0.1933	0.0082	0.1799	0.0079	0.1959
0.0099	0.2367	0.0096	0.2325	0.0106	0.2164	0.0107	0.1990	0.0099	0.2117
0.0149	0.2779	0.0121	0.2608	0.0156	0.2540	0.0132	0.2198	0.0124	0.2394
0.0224	0.3322	0.0171	0.2965	0.0206	0.2927	0.0182	0.2460	0.0174	0.2792
0.0299	0.3751	0.0221	0.3411	0.0281	0.3203	0.0232	0.2823	0.0224	0.3097
0.0374	0.4024	0.0271	0.3678	0.0356	0.3585	0.0307	0.3141	0.0299	0.3451
0.0424	0.4137	0.0321	0.3942	0.0431	0.3850	0.0407	0.3501	0.0374	0.3817
0.0449	0.4161	0.0371	0.4085	0.0506	0.4045	0.0507	0.3833	0.0449	0.4011
0.0474	0.4179	0.0396	0.4131	0.0556	0.4128	0.0582	0.3990	0.0499	0.4103
0.0524	0.4187	0.0421	0.4158	0.0581	0.4137	0.0657	0.4051	0.0524	0.4119
0.0624	0.4185	0.0446	0.4170	0.0606	0.4158	0.0707	0.4106	0.0549	0.4140
0.0724	0.4185	0.0471	0.4173	0.0656	0.4167	0.0757	0.4119	0.0599	0.4158
0.0824	0.4193	0.0521	0.4176	0.0706	0.4170	0.0807	0.4137	0.0699	0.4155
0.0924	0.4187	0.0621	0.4176	0.0796	0.4173	0.0857	0.4128	0.0799	0.4161
0.0974	0.4182	0.0721	0.4176	0.0806	0.4176	0.0907	0.4158	0.0899	0.4170
0.1004	0.4158	0.0821	0.4179	0.0896	0.4187	0.0977	0.4164	0.0969	0.4167
0.1074	0.4158	0.0921	0.4185	0.0906	0.4196	0.1007	0.4161	0.0999	0.4152
		0.0961	0.4173	0.0956	0.4190	0.1071	0.4161	0.1074	0.415[illegible]
		0.1001	0.4158	0.0996	0.4179				
		0.1067	0.4158	0.1068	0.4179				

Rough X = 1.5 m
Water Surface Elevation = 0.1320 m (5 point average)

Z = -0.030 m		Z = 0.0 m		Z = 0.030 m		Z = 0.091 m		Z = 0.152 m	
y (m)	u (m/s)	y (m)	u (m/s)	y (m)	u (m/s)	y (m)	u (m/s)	y (m)	u (m/s)
0.0000	0.0000	0.0000	0.0000	0.0000	0.0000	0.0000	0.0000	0.0000	0.0000
0.0065	0.1996	0.0067	0.2112	0.0050	0.1655	0.0065	0.1854	0.0047	0.1253
0.0073	0.2100	0.0075	0.2181	0.0070	0.2021	0.0077	0.1952	0.0067	0.1514
0.0093	0.2425	0.0095	0.2435	0.0090	0.2238	0.0092	0.2170	0.0092	0.1799
0.0118	0.2631	0.0145	0.2957	0.0140	0.2646	0.0142	0.2608	0.0117	0.1996
0.0143	0.2893	0.0195	0.3363	0.0190	0.3015	0.0192	0.2910	0.0167	0.2346
0.0168	0.3085	0.0245	0.3657	0.0240	0.3329	0.0267	0.3288	0.0242	0.2655
0.0203	0.3329	0.0295	0.3946	0.0315	0.3721	0.0342	0.3637	0.0317	0.2931
0.0243	0.3616	0.0345	0.4073	0.0390	0.3952	0.0417	0.3898	0.0417	0.3318
0.0283	0.3791	0.0370	0.4109	0.0440	0.4070	0.0492	0.4051	0.0517	0.3578
0.0318	0.3930	0.0395	0.4152	0.0465	0.4106	0.0542	0.4119	0.0617	0.3859
0.0368	0.4085	0.0420	0.4158	0.0490	0.4140	0.0567	0.4152	0.0692	0.4008
0.0393	0.4128	0.0445	0.4167	0.0515	0.4158	0.0592	0.4158	0.0742	0.4088
0.0418	0.4146	0.0495	0.4167	0.0540	0.4161	0.0617	0.4149	0.0792	0.4140
0.0443	0.4164	0.0595	0.4164	0.0590	0.4170	0.0642	0.4164	0.0817	0.4167
0.0493	0.4173	0.0695	0.4158	0.0690	0.4167	0.0692	0.4167	0.0842	0.4185
0.0593	0.4170	0.0795	0.4161	0.0790	0.4170	0.0792	0.4167	0.0867	0.4199
0.0693	0.4170	0.0895	0.4164	0.0890	0.4173	0.0892	0.4170	0.0917	0.4214
0.0793	0.4173	0.0975	0.4158	0.0970	0.4170	0.0972	0.4167	0.0957	0.4208
0.0893	0.4187	0.1005	0.4137	0.1000	0.4158	0.1002	0.4146	0.0987	0.4199
0.0973	0.4182	0.1079	0.4137	0.1081	0.4158	0.1082	0.4146	0.1082	0.4199
0.1003	0.4167								
0.1077	0.4167								

Rough X = 1.5 m
Water Surface Elevation = 0.1320 m (5 point average)

Z = 0.213 m		Z = 0.274 m		Z = 0.335 m	
y (m)	u (m/s)	y (m)	u (m/s)	y (m)	u (m/s)
0.0000	0.0000	0.0000	0.0000	0.0000	0.0000
0.0045	0.1514	0.0047	0.1633	0.0065	0.1996
0.0055	0.1779	0.0057	0.1799	0.0080	0.2309
0.0080	0.2106	0.0072	0.2015	0.0105	0.2555
0.0105	0.2500	0.0097	0.2388	0.0130	0.2788
0.0155	0.2994	0.0122	0.2646	0.0155	0.3011
0.0205	0.3396	0.0172	0.3117	0.0180	0.3227
0.0255	0.3708	0.0222	0.3447	0.0215	0.3465
0.0305	0.3930	0.0272	0.3721	0.0255	0.3718
0.0355	0.4119	0.0322	0.4014	0.0295	0.3885
0.0380	0.4167	0.0372	0.4149	0.0330	0.4045
0.0405	0.4199	0.0397	0.4196	0.0380	0.4170
0.0430	0.4211	0.0422	0.4220	0.0430	0.4223
0.0455	0.4223	0.0447	0.4229	0.0455	0.4235
0.0505	0.4217	0.0497	0.4235	0.0505	0.4238
0.0555	0.4217	0.0547	0.4232	0.0555	0.4238
0.0605	0.4217	0.0647	0.4226	0.0655	0.4238
0.0655	0.4211	0.0747	0.4226	0.0755	0.4238
0.0755	0.4211	0.0847	0.4229	0.0855	0.4249
0.0855	0.4217	0.0937	0.4226	0.0945	0.4241
0.0905	0.4220	0.0967	0.4205	0.0975	0.4229
0.0945	0.4211	0.1082	0.4205	0.1090	0.4229
0.0975	0.4199				
0.1080	0.4199				

Rough X = 2 m
Water Surface Elevation = 0.1313 m (5 point average)

Z = -0.335 m		Z = -0.274 m		Z = -0.213 m		Z = -0.152 m		Z = - 0.091 m	
y (m)	u (m/s)	y (m)	u (m/s)	y (m)	u (m/s)	y (m)	u (m/s)	y (m)	u (m/s)
0.0000	0.0000	0.0000	0.0000	0.0000	0.0000	0.0000	0.0000	0.0000	0.0000
0.0065	0.1881	0.0070	0.2033	0.0080	0.1978	0.0067	0.1678	0.0065	0.1648
0.0075	0.2040	0.0093	0.2341	0.0123	0.2336	0.0101	0.1996	0.0109	0.2123
0.0125	0.2550	0.0123	0.2622	0.0198	0.2845	0.0176	0.2535	0.0159	0.2559
0.0175	0.2961	0.0173	0.3019	0.0273	0.3254	0.0251	0.2819	0.0234	0.3036
0.0225	0.3223	0.0223	0.3333	0.0348	0.3501	0.0326	0.3085	0.0309	0.3385
0.0275	0.3533	0.0298	0.3674	0.0423	0.3807	0.0401	0.3344	0.0384	0.3768
0.0325	0.3778	0.0373	0.3920	0.0473	0.3920	0.0476	0.3582	0.0459	0.3986
0.0375	0.3968	0.0423	0.4085	0.0523	0.4051	0.0551	0.3741	0.0509	0.4073
0.0425	0.4161	0.0473	0.4140	0.0573	0.4170	0.0626	0.3907	0.0559	0.4187
0.0475	0.4258	0.0523	0.4244	0.0623	0.4261	0.0701	0.4076	0.0584	0.4229
0.0500	0.4305	0.0548	0.4285	0.0648	0.4287	0.0751	0.4143	0.0609	0.4270
0.0525	0.4319	0.0573	0.4313	0.0673	0.4308	0.0801	0.4211	0.0634	0.4287
0.0550	0.4362	0.0598	0.4322	0.0698	0.4325	0.0826	0.4229	0.0659	0.4313
0.0575	0.4368	0.0623	0.4345	0.0723	0.4328	0.0851	0.4261	0.0684	0.4322
0.0600	0.4377	0.0673	0.4354	0.0748	0.4339	0.0876	0.4287	0.0709	0.4325
0.0625	0.4382	0.0723	0.4374	0.0773	0.4348	0.0901	0.4293	0.0759	0.4328
0.0725	0.4382	0.0823	0.4377	0.0823	0.4348	0.0926	0.4313	0.0809	0.4348
0.0825	0.4382	0.0923	0.4371	0.0923	0.4354	0.0951	0.4308	0.0909	0.4362
0.0885	0.4391	0.0963	0.4368	0.0973	0.4348	0.0991	0.4305	0.0979	0.4348
0.0945	0.4385	0.0993	0.4357	0.1003	0.4322	0.1069	0.4305	0.1009	0.4339
0.0985	0.4357	0.1063	0.4357	0.1062	0.4322			0.1077	0.4339
0.1057	0.4357								

Rough X = 2 m
Water Surface Elevation = 0.1313 m (5 point average)

Z = -0.030 m		Z = 0.0 m		Z = 0.030 m		Z = 0.091 m		Z = 0.152 m	
y (m)	u (m/s)	y (m)	u (m/s)	y (m)	u (m/s)	y (m)	u (m/s)	y (m)	u (m/s)
0.0000	0.0000	0.0000	0.0000	0.0000	0.0000	0.0000	0.0000	0.0000	0.0000
0.0055	0.1750	0.0060	0.1894	0.0065	0.1874	0.0068	0.1707	0.0068	0.1438
0.0090	0.2309	0.0090	0.2362	0.0089	0.2158	0.0088	0.1971	0.0097	0.1685
0.0140	0.2770	0.0140	0.2810	0.0164	0.2783	0.0163	0.2500	0.0122	0.1874
0.0190	0.3129	0.0190	0.3250	0.0239	0.3284	0.0238	0.2914	0.0197	0.2287
0.0240	0.3465	0.0240	0.3613	0.0314	0.3654	0.0313	0.3207	0.0272	0.2650
0.0290	0.3731	0.0290	0.3827	0.0389	0.3942	0.0388	0.3540	0.0347	0.2919
0.0340	0.3920	0.0340	0.4051	0.0439	0.4091	0.0463	0.3751	0.0422	0.3149
0.0390	0.4091	0.0390	0.4205	0.0489	0.4167	0.0538	0.3990	0.0497	0.3403
0.0440	0.4223	0.0415	0.4279	0.0539	0.4226	0.0613	0.4128	0.0572	0.3650
0.0490	0.4293	0.0440	0.4311	0.0564	0.4255	0.0663	0.4211	0.0647	0.3879
0.0515	0.4316	0.0465	0.4319	0.0589	0.4285	0.0713	0.4258	0.0722	0.4073
0.0540	0.4328	0.0490	0.4337	0.0614	0.4293	0.0738	0.4293	0.0772	0.4149
0.0590	0.4345	0.0540	0.4345	0.0639	0.4299	0.0763	0.4305	0.0822	0.4249
0.0640	0.4339	0.0590	0.4348	0.0664	0.4302	0.0788	0.4308	0.0847	0.4264
0.0690	0.4337	0.0690	0.4348	0.0689	0.4308	0.0813	0.4322	0.0872	0.4293
0.0740	0.4345	0.0790	0.4348	0.0739	0.4316	0.0838	0.4334	0.0897	0.4316
0.0790	0.4357	0.0890	0.4362	0.0789	0.4325	0.0863	0.4337	0.0922	0.4322
0.0810	0.4357	0.0960	0.4365	0.0889	0.4334	0.0888	0.4345	0.0952	0.4325
0.0870	0.4371	0.1000	0.4348	0.0959	0.4345	0.0968	0.4348	0.0992	0.4296
0.0890	0.4379	0.1075	0.4348	0.0999	0.4308	0.1008	0.4331	0.1081	0.4296
0.0970	0.4385			0.1077	0.4308	0.1081	0.4331		
0.1000	0.4365								
0.1074	0.4365								

Rough X = 2 m
Water Surface Elevation = 0.1313 m (5 point average)

Z = 0.213 m		Z = 0.274 m		Z = 0.335 m	
y (m)	u (m/s)	y (m)	u (m/s)	y (m)	u (m/s)
0.0000	0.0000	0.0000	0.0000	0.0000	0.0000
0.0077	0.2117	0.0070	0.1900	0.0073	0.2046
0.0099	0.2419	0.0115	0.2362	0.0116	0.2485
0.0174	0.2957	0.0190	0.2927	0.0166	0.2880
0.0249	0.3411	0.0265	0.3366	0.0241	0.3314
0.0324	0.3761	0.0340	0.3735	0.0316	0.3688
0.0399	0.4045	0.0415	0.4014	0.0391	0.4058
0.0474	0.4235	0.0465	0.4176	0.0466	0.4226
0.0524	0.4299	0.0490	0.4226	0.0516	0.4313
0.0549	0.4316	0.0515	0.4287	0.0541	0.4354
0.0574	0.4339	0.0540	0.4337	0.0566	0.4371
0.0599	0.4345	0.0565	0.4342	0.0616	0.4377
0.0624	0.4351	0.0590	0.4348	0.0666	0.4382
0.0649	0.4357	0.0615	0.4357	0.0766	0.4385
0.0674	0.4357	0.0665	0.4365	0.0866	0.4391
0.0699	0.4365	0.0765	0.4371	0.0966	0.4396
0.0724	0.4371	0.0865	0.4382	0.1006	0.4374
0.0774	0.4374	0.0955	0.4391	0.1094	0.4374
0.0874	0.4377	0.0992	0.4377		
0.0964	0.4377	0.1088	0.4377		
0.0999	0.4357				
0.1085	0.4357				

Rough X = 3 m
Water Surface Elevation = 0.1302 m (5 point average)

Z = -0.335 m		Z = -0.274 m		Z = -0.213 m		Z = -0.152 m		Z = -0.091 m	
y (m)	u (m/s)	y (m)	u (m/s)	y (m)	u (m/s)	y (m)	u (m/s)	y (m)	u (m/s)
0.0000	0.0000	0.0000	0.0000	0.0000	0.0000	0.0000	0.0000	0.0000	0.0000
0.0062	0.1854	0.0066	0.1990	0.0068	0.1655	0.0085	0.1996	0.0055	0.1663
0.0094	0.2175	0.0086	0.2226	0.0085	0.1933	0.0091	0.2021	0.0080	0.2070
0.0144	0.2650	0.0136	0.2734	0.0125	0.2243	0.0131	0.2450	0.0105	0.2336
0.0194	0.2961	0.0236	0.3348	0.0225	0.2747	0.0231	0.2944	0.0205	0.2876
0.0269	0.3322	0.0336	0.3791	0.0325	0.3093	0.0331	0.3250	0.0305	0.3295
0.0344	0.3609	0.0411	0.4079	0.0425	0.3425	0.0431	0.3529	0.0405	0.3661
0.0419	0.3888	0.0486	0.4305	0.0525	0.3701	0.0531	0.3731	0.0505	0.3892
0.0494	0.4152	0.0561	0.4436	0.0625	0.3952	0.0631	0.3927	0.0605	0.4064
0.0569	0.4374	0.0636	0.4519	0.0725	0.4173	0.0731	0.4106	0.0705	0.4270
0.0644	0.4486	0.0686	0.4536	0.0800	0.4348	0.0806	0.4199	0.0780	0.4379
0.0694	0.4550	0.0736	0.4571	0.0875	0.4456	0.0881	0.4322	0.0855	0.4469
0.0719	0.4580	0.0786	0.4590	0.0925	0.4508	0.0931	0.4385	0.0905	0.4517
0.0744	0.4596	0.0836	0.4599	0.0975	0.4539	0.0971	0.4436	0.0955	0.4541
0.0769	0.4601	0.0886	0.4609	0.0995	0.4536	0.1011	0.4458	0.0995	0.4519
0.0794	0.4617	0.0936	0.4612	0.1059	0.4536	0.1063	0.4458	0.1073	0.4519
0.0844	0.4628	0.0986	0.4590						
0.0894	0.4636	0.1066	0.4590						
0.0944	0.4631								
0.0984	0.4607								
0.1061	0.4607								

Rough X = 3 m
Water Surface Elevation = 0.1302 m (5 point average)

Z = -0.030 m		Z = 0.0 m		Z = 0.030 m		Z = 0.091 m		Z = 0.152 m	
y (m)	u (m/s)	y (m)	u (m/s)	y (m)	u (m/s)	y (m)	u (m/s)	y (m)	u (m/s)
0.0000	0.0000	0.0000	0.0000	0.0000	0.0000	0.0000	0.0000	0.0000	0.0000
0.0057	0.1772	0.0060	0.1990	0.0070	0.2064	0.0075	0.1750	0.0067	0.1663
0.0067	0.1939	0.0085	0.2357	0.0089	0.2226	0.0110	0.2082	0.0092	0.2015
0.0107	0.2455	0.0100	0.2540	0.0109	0.2450	0.0160	0.2430	0.0142	0.2404
0.0157	0.2743	0.0150	0.2969	0.0159	0.2957	0.0210	0.2588	0.0192	0.2683
0.0232	0.3292	0.0200	0.3333	0.0209	0.3211	0.0310	0.3019	0.0292	0.2910
0.0307	0.3582	0.0275	0.3698	0.0309	0.3623	0.0410	0.3303	0.0392	0.3273
0.0382	0.3892	0.0350	0.4017	0.0409	0.4017	0.0510	0.3543	0.0492	0.3479
0.0457	0.4140	0.0425	0.4290	0.0509	0.4161	0.0610	0.3827	0.0592	0.3698
0.0532	0.4342	0.0500	0.4436	0.0609	0.4252	0.0710	0.4042	0.0667	0.3820
0.0607	0.4461	0.0550	0.4492	0.0684	0.4345	0.0785	0.4232	0.0742	0.4005
0.0657	0.4514	0.0600	0.4547	0.0759	0.4394	0.0860	0.4351	0.0817	0.4143
0.0682	0.4522	0.0625	0.4555	0.0809	0.4456	0.0910	0.4425	0.0892	0.4316
0.0707	0.4563	0.0650	0.4569	0.0859	0.4506	0.0950	0.4475	0.0932	0.4382
0.0732	0.4571	0.0675	0.4571	0.0909	0.4541	0.0980	0.4517	0.0962	0.4405
0.0757	0.4588	0.0700	0.4574	0.0949	0.4552	0.1010	0.4517	0.0992	0.4430
0.0782	0.4590	0.0725	0.4585	0.0979	0.4571	0.1080	0.4517	0.1084	0.4430
0.0807	0.4599	0.0750	0.4580	0.1009	0.4544				
0.0832	0.4599	0.0775	0.4590	0.1075	0.4544				
0.0857	0.4601	0.0800	0.4599						
0.0882	0.4604	0.0850	0.4596						
0.0907	0.4607	0.0900	0.4601						
0.0957	0.4601	0.0955	0.4596						
0.0997	0.4582	0.0995	0.4547						
0.1074	0.4582	0.1075	0.4547						

Rough X = 3 m
Water Surface Elevation = 0.1302 m (5 point average)

Z = 0.213 m		Z = 0.274 m		Z = 0.335 m	
y (m)	u (m/s)	y (m)	u (m/s)	y (m)	u (m/s)
0.0000	0.0000	0.0000	0.0000	0.0000	0.0000
0.0060	0.1861	0.0070	0.1799	0.0068	0.1933
0.0083	0.2175	0.0090	0.2221	0.0084	0.2076
0.0133	0.2697	0.0140	0.2559	0.0134	0.2559
0.0183	0.3007	0.0190	0.2871	0.0184	0.2884
0.0283	0.3476	0.0240	0.3081	0.0234	0.3211
0.0383	0.3892	0.0315	0.3461	0.0284	0.3436
0.0483	0.4167	0.0390	0.3788	0.0359	0.3765
0.0558	0.4348	0.0465	0.4048	0.0434	0.4011
0.0633	0.4461	0.0540	0.4255	0.0509	0.4293
0.0683	0.4514	0.0615	0.4402	0.0584	0.4450
0.0733	0.4541	0.0665	0.4506	0.0634	0.4519
0.0783	0.4555	0.0715	0.4547	0.0684	0.4560
0.0833	0.4571	0.0740	0.4571	0.0709	0.4585
0.0883	0.4588	0.0765	0.4582	0.0734	0.4596
0.0923	0.4593	0.0790	0.4593	0.0759	0.4607
0.0963	0.4590	0.0815	0.4601	0.0784	0.4609
0.0993	0.4580	0.0840	0.4609	0.0834	0.4626
0.1085	0.4580	0.0865	0.4615	0.0884	0.4628
		0.0890	0.4617	0.0934	0.4628
		0.0930	0.4626	0.0974	0.4620
		0.0970	0.4620	0.1004	0.4604
		0.1000	0.4607	0.1095	0.4604
		0.1086	0.4607		

Rough X = 4 m
Water Surface Elevation = 0.1294 m (5 point average)

Z = -0.335 m		Z = -0.274 m		Z = -0.213 m		Z = -0.152 m		Z = -0.091 m	
y (m)	u (m/s)	y (m)	u (m/s)	y (m)	u (m/s)	y (m)	u (m/s)	y (m)	u (m/s)
0.0000	0.0000	0.0000	0.0000	0.0000	0.0000	0.0000	0.0000	0.0000	0.0000
0.0074	0.1799	0.0068	0.1939	0.0064	0.1602	0.0060	0.1594	0.0063	0.1663
0.0109	0.2117	0.0087	0.2198	0.0078	0.1861	0.0077	0.1750	0.0080	0.2052
0.0159	0.2505	0.0137	0.2646	0.0128	0.2325	0.0112	0.2070	0.0105	0.2204
0.0209	0.2836	0.0187	0.3048	0.0178	0.2603	0.0162	0.2495	0.0155	0.2612
0.0284	0.3276	0.0262	0.3403	0.0253	0.2914	0.0237	0.2792	0.0230	0.2961
0.0359	0.3522	0.0362	0.3788	0.0353	0.3288	0.0337	0.3125	0.0330	0.3337
0.0434	0.3791	0.0462	0.4045	0.0453	0.3472	0.0437	0.3359	0.0430	0.3578
0.0509	0.4079	0.0537	0.4279	0.0553	0.3731	0.0537	0.3630	0.0530	0.3755
0.0584	0.4290	0.0612	0.4399	0.0653	0.3907	0.0637	0.3827	0.0630	0.3990
0.0659	0.4405	0.0687	0.4541	0.0753	0.4091	0.0712	0.3986	0.0730	0.4187
0.0734	0.4558	0.0762	0.4609	0.0828	0.4270	0.0787	0.4082	0.0805	0.4322
0.0784	0.4626	0.0812	0.4655	0.0903	0.4334	0.0837	0.4161	0.0880	0.4430
0.0834	0.4711	0.0862	0.4676	0.0953	0.4430	0.0877	0.4226	0.0930	0.4453
0.0859	0.4735	0.0902	0.4690	0.1003	0.4453	0.0917	0.4285	0.0970	0.4489
0.0884	0.4761	0.0942	0.4700	0.1077	0.4453	0.0957	0.4368	0.1000	0.4517
0.0909	0.4777	0.0972	0.4679			0.0997	0.4377	0.1074	0.4517
0.0934	0.4792	0.1007	0.4658			0.1075	0.4377		
0.0984	0.4795	0.1072	0.4658						
0.1024	0.4771								
0.1075	0.4771								

Rough X = 4 m
Water Surface Elevation = 0.1294 m (5 point average)

Z = -0.030 m		Z = 0.0 m		Z = 0.030 m		Z = 0.091 m		Z = 0152 m	
y (m)	u (m/s)	y (m)	u (m/s)	y (m)	u (m/s)	y (m)	u (m/s)	y (m)	u (m/s)
0.0000	0.0000	0.0000	0.0000	0.0000	0.0000	0.0000	0.0000	0.0000	0.0000
0.0056	0.1813	0.0064	0.1952	0.0058	0.1861	0.0057	0.1311	0.0075	0.1700
0.0079	0.2187	0.0080	0.2226	0.0078	0.2147	0.0088	0.1586	0.0090	0.2040
0.0094	0.2419	0.0100	0.2495	0.0093	0.2388	0.0113	0.1806	0.0115	0.2287
0.0144	0.2828	0.0150	0.2880	0.0118	0.2603	0.0163	0.2187	0.0165	0.2608
0.0219	0.3307	0.0200	0.3337	0.0143	0.2797	0.0213	0.2352	0.0215	0.2880
0.0319	0.3681	0.0275	0.3678	0.0218	0.3295	0.0313	0.2706	0.0315	0.3184
0.0419	0.4024	0.0350	0.3952	0.0318	0.3657	0.0413	0.2999	0.0415	0.3476
0.0519	0.4357	0.0425	0.4164	0.0418	0.3892	0.0513	0.3284	0.0515	0.3620
0.0619	0.4489	0.0500	0.4368	0.0518	0.4112	0.0613	0.3602	0.0615	0.3794
0.0694	0.4658	0.0575	0.4464	0.0593	0.4223	0.0688	0.3778	0.0690	0.3983
0.0769	0.4724	0.0650	0.4604	0.0668	0.4279	0.0763	0.3901	0.0765	0.4048
0.0819	0.4758	0.0725	0.4655	0.0743	0.4345	0.0813	0.4115	0.0815	0.4146
0.0844	0.4779	0.0775	0.4708	0.0818	0.4436	0.0863	0.4158	0.0865	0.4202
0.0869	0.4797	0.0825	0.4714	0.0868	0.4489	0.0913	0.4252	0.0915	0.4290
0.0919	0.4821	0.0875	0.4735	0.0918	0.4525	0.0943	0.4305	0.0945	0.4342
0.0959	0.4813	0.0925	0.4758	0.0948	0.4571	0.0973	0.4351	0.0975	0.4354
0.0999	0.4852	0.0965	0.4756	0.0978	0.4574	0.1003	0.4382	0.1005	0.4399
0.1087	0.4852	0.1005	0.4732	0.1008	0.4569	0.1087	0.4382	0.1089	0.4399
		0.1084	0.4732	0.1082	0.4569				

Rough X = 4 m
Water Surface Elevation = 0.1294 m (5 point average)

Z = 0.213 m		Z = 0.274 m		Z = 0.335 m	
y (m)	u (m/s)	y (m)	u (m/s)	y (m)	u (m/s)
0.0000	0.0000	0.0000	0.0000	0.0000	0.0000
0.0050	0.1640	0.0065	0.1750	0.0065	0.1799
0.0058	0.1881	0.0101	0.2388	0.0101	0.2435
0.0083	0.2254	0.0151	0.2734	0.0151	0.2814
0.0133	0.2774	0.0201	0.2999	0.0201	0.3044
0.0183	0.3149	0.0301	0.3436	0.0301	0.3511
0.0283	0.3616	0.0401	0.3859	0.0401	0.3859
0.0383	0.3888	0.0501	0.4149	0.0501	0.4226
0.0483	0.4164	0.0576	0.4316	0.0601	0.4427
0.0558	0.4334	0.0651	0.4461	0.0701	0.4644
0.0633	0.4447	0.0701	0.4582	0.0776	0.4732
0.0708	0.4552	0.0751	0.4652	0.0826	0.4790
0.0783	0.4612	0.0801	0.4714	0.0876	0.4808
0.0833	0.4652	0.0851	0.4766	0.0901	0.4836
0.0883	0.4679	0.0876	0.4787	0.0941	0.4846
0.0923	0.4682	0.0901	0.4813	0.0981	0.4849
0.0953	0.4706	0.0931	0.4823	0.1011	0.4831
0.0983	0.4687	0.0941	0.4828	0.1100	0.4831
0.1092	0.4687	0.0981	0.4828		
		0.1011	0.4810		
		0.1098	0.4810		

Rough X = 5 m
Water Surface Elevation = 0.1282 m (5 point average)

Z = -0.335 m		Z = -0.274 m		Z = -0.213 m		Z = -0.152 m		Z = -0.091 m	
y (m)	u (m/s)	y (m)	u (m/s)	y (m)	u (m/s)	y (m)	u (m/s)	y (m)	u (m/s)
0.0000	0.0000	0.0000	0.0000	0.0000	0.0000	0.0000	0.0000	0.0000	0.0000
0.0075	0.1867	0.0075	0.1965	0.0055	0.1743	0.0075	0.1625	0.0080	0.1926
0.0091	0.2064	0.0100	0.2293	0.0085	0.2193	0.0092	0.1841	0.0104	0.2181
0.0116	0.2330	0.0150	0.2669	0.0120	0.2683	0.0127	0.2088	0.0129	0.2419
0.0166	0.2627	0.0200	0.2982	0.0170	0.2919	0.0177	0.2362	0.0179	0.2650
0.0216	0.2910	0.0275	0.3425	0.0245	0.3234	0.0252	0.2646	0.0254	0.3011
0.0291	0.3215	0.0375	0.3811	0.0345	0.3533	0.0352	0.2893	0.0354	0.3436
0.0391	0.3616	0.0475	0.4051	0.0445	0.3755	0.0452	0.3246	0.0454	0.3616
0.0491	0.3917	0.0575	0.4285	0.0545	0.3949	0.0552	0.3447	0.0554	0.3788
0.0566	0.4094	0.0675	0.4478	0.0645	0.4058	0.0652	0.3620	0.0654	0.3930
0.0641	0.4325	0.0775	0.4601	0.0745	0.4182	0.0752	0.3833	0.0754	0.4097
0.0716	0.4422	0.0850	0.4706	0.0820	0.4232	0.0827	0.3974	0.0829	0.4208
0.0791	0.4566	0.0925	0.4764	0.0895	0.4348	0.0902	0.4085	0.0904	0.4255
0.0841	0.4671	0.0975	0.4761	0.0945	0.4345	0.0952	0.4155	0.0954	0.4334
0.0891	0.4750	0.1000	0.4764	0.0975	0.4405	0.0987	0.4179	0.0994	0.4388
0.0916	0.4761	0.1020	0.4748	0.1005	0.4405	0.1017	0.4214	0.1024	0.4422
0.0941	0.4816	0.1081	0.4748	0.1082	0.4405	0.1092	0.4214	0.1091	0.4422
0.0966	0.4813								
0.0991	0.4836								
0.1011	0.4846								
0.1031	0.4849								
0.1081	0.4849								

Rough X = 5 m
Water Surface Elevation = 0.1282 m (5 point average)

Z = -0.030 m		Z = 0.0 m		Z = 0.030 m		Z = 0.091 m		Z = 0.152 m	
y (m)	u (m/s)	y (m)	u (m/s)	y (m)	u (m/s)	y (m)	u (m/s)	y (m)	u (m/s)
0.0000	0.0000	0.0000	0.0000	0.0000	0.0000	0.0000	0.0000	0.0000	0.0000
0.0070	0.2058	0.0067	0.2058	0.0070	0.2015	0.0080	0.1586	0.0070	0.1881
0.0093	0.2341	0.0089	0.2455	0.0088	0.2314	0.0090	0.1640	0.0094	0.2147
0.0118	0.2636	0.0114	0.2584	0.0113	0.2505	0.0115	0.1874	0.0144	0.2555
0.0143	0.2876	0.0164	0.3048	0.0163	0.2944	0.0165	0.2117	0.0219	0.2990
0.0193	0.3121	0.0214	0.3352	0.0238	0.3352	0.0240	0.2367	0.0319	0.3355
0.0243	0.3392	0.0264	0.3578	0.0338	0.3684	0.0340	0.2752	0.0419	0.3568
0.0293	0.3674	0.0339	0.3875	0.0438	0.3939	0.0440	0.2965	0.0519	0.3711
0.0343	0.3882	0.0439	0.4164	0.0538	0.4082	0.0540	0.3192	0.0619	0.3863
0.0443	0.4173	0.0539	0.4408	0.0638	0.4173	0.0640	0.3461	0.0719	0.3986
0.0543	0.4408	0.0639	0.4550	0.0738	0.4293	0.0740	0.3609	0.0794	0.4055
0.0643	0.4596	0.0739	0.4615	0.0813	0.4357	0.0815	0.3755	0.0869	0.4143
0.0743	0.4729	0.0814	0.4724	0.0888	0.4405	0.0890	0.4005	0.0919	0.4187
0.0818	0.4800	0.0889	0.4737	0.0938	0.4439	0.0940	0.4027	0.0949	0.4258
0.0893	0.4831	0.0939	0.4758	0.0978	0.4436	0.0970	0.4082	0.0979	0.4255
0.0943	0.4872	0.0979	0.4761	0.1018	0.4447	0.0990	0.4103	0.1009	0.4267
0.0983	0.4887	0.1019	0.4724	0.1101	0.4447	0.1030	0.4202	0.1101	0.4267
0.1023	0.4844	0.1097	0.4724			0.1102	0.4202		
0.1093	0.4844								

Rough X = 5 m
Water Surface Elevation = 0.1282 m (5 point average)

Z = 0.213 m		Z = 0.274 m		Z = 0.335 m	
y (m)	u (m/s)	y (m)	u (m/s)	y (m)	u (m/s)
0.0000	0.0000	0.0000	0.0000	0.0000	0.0000
0.0073	0.1939	0.0068	0.1841	0.0060	0.1820
0.0104	0.2383	0.0099	0.2210	0.0091	0.2221
0.0154	0.2738	0.0149	0.2608	0.0141	0.2734
0.0229	0.3121	0.0224	0.3056	0.0216	0.3085
0.0329	0.3501	0.0324	0.3458	0.0316	0.3522
0.0429	0.3814	0.0424	0.3846	0.0416	0.3863
0.0529	0.4106	0.0524	0.4109	0.0516	0.4094
0.0629	0.4302	0.0624	0.4351	0.0616	0.4365
0.0729	0.4433	0.0724	0.4580	0.0716	0.4577
0.0804	0.4511	0.0799	0.4671	0.0791	0.4684
0.0879	0.4544	0.0874	0.4803	0.0866	0.4790
0.0929	0.4574	0.0924	0.4810	0.0916	0.4854
0.0969	0.4593	0.0964	0.4854	0.0956	0.4870
0.0999	0.4596	0.1004	0.4867	0.0996	0.4887
0.1029	0.4569	0.1034	0.4877	0.1036	0.4905
0.1107	0.4569	0.1112	0.4877	0.1120	0.4905

Rough X = 6 m
Water Surface Elevation = 0.1271 m (5 point average)

Z = -0.335 m		Z = -0.274 m		Z = -0.213 m		Z = -0.152 m		Z = -0.091 m	
y (m)	u (m/s)	y (m)	u (m/s)	y (m)	u (m/s)	y (m)	u (m/s)	y (m)	u (m/s)
0.0000	0.0000	0.0000	0.0000	0.0000	0.0000	0.0000	0.0000	0.0000	0.0000
0.0068	0.1881	0.0065	0.1939	0.0065	0.1939	0.0068	0.1617	0.0060	0.1743
0.0086	0.2181	0.0077	0.2147	0.0083	0.2175	0.0078	0.1670	0.0066	0.1894
0.0136	0.2593	0.0117	0.2598	0.0108	0.2500	0.0103	0.1920	0.0091	0.2175
0.0186	0.2923	0.0167	0.2957	0.0158	0.2880	0.0128	0.2117	0.0141	0.2692
0.0261	0.3254	0.0242	0.3363	0.0233	0.3273	0.0153	0.2238	0.0216	0.3064
0.0361	0.3626	0.0342	0.3804	0.0333	0.3633	0.0188	0.2440	0.0316	0.3447
0.0461	0.3907	0.0442	0.4027	0.0433	0.3879	0.0228	0.2588	0.0416	0.3688
0.0561	0.4167	0.0542	0.4241	0.0533	0.4021	0.0328	0.2884	0.0516	0.3824
0.0636	0.4354	0.0642	0.4427	0.0633	0.4128	0.0428	0.3141	0.0616	0.3980
0.0711	0.4419	0.0742	0.4571	0.0733	0.4170	0.0528	0.3318	0.0716	0.4088
0.0786	0.4596	0.0817	0.4682	0.0808	0.4252	0.0628	0.3575	0.0791	0.4161
0.0861	0.4721	0.0892	0.4724	0.0883	0.4296	0.0728	0.3674	0.0866	0.4241
0.0911	0.4777	0.0942	0.4761	0.0933	0.4339	0.0803	0.3843	0.0916	0.4299
0.0961	0.4828	0.0972	0.4769	0.0973	0.4379	0.0878	0.3952	0.0941	0.4325
0.0991	0.4836	0.1002	0.4769	0.1008	0.4345	0.0928	0.4017	0.0966	0.4319
0.1021	0.4849	0.1067	0.4769	0.1068	0.4345	0.0953	0.4073	0.0996	0.4351
0.1067	0.4849					0.0978	0.4082	0.1076	0.4351
						0.1008	0.4128		
						0.1065	0.4128		

Rough X = 6 m
Water Surface Elevation = 0.1271 m (5 point average)

Z = -0.030 m		Z = 0.0 m		Z = 0.030 m		Z = 0.091 m		Z = 0.152 m	
y (m)	u (m/s)	y (m)	u (m/s)	y (m)	u (m/s)	y (m)	u (m/s)	y (m)	u (m/s)
0.0000	0.0000	0.0000	0.0000	0.0000	0.0000	0.0000	0.0000	0.0000	0.0000
0.0060	0.1920	0.0058	0.1939	0.0062	0.1887	0.0063	0.1481	0.0073	0.1894
0.0085	0.2293	0.0080	0.2221	0.0082	0.2221	0.0081	0.1655	0.0086	0.1984
0.0135	0.2871	0.0130	0.2850	0.0132	0.2711	0.0101	0.1861	0.0106	0.2249
0.0210	0.3322	0.0205	0.3333	0.0207	0.3180	0.0151	0.2158	0.0156	0.2598
0.0310	0.3830	0.0305	0.3781	0.0307	0.3592	0.0201	0.2394	0.0206	0.2836
0.0410	0.4128	0.0405	0.4149	0.0407	0.3885	0.0301	0.2734	0.0306	0.3207
0.0510	0.4374	0.0505	0.4368	0.0507	0.4045	0.0401	0.2957	0.0406	0.3479
0.0610	0.4550	0.0605	0.4497	0.0607	0.4122	0.0501	0.3117	0.0506	0.3671
0.0710	0.4666	0.0705	0.4588	0.0707	0.4164	0.0601	0.3355	0.0606	0.3768
0.0785	0.4737	0.0805	0.4609	0.0782	0.4226	0.0701	0.3508	0.0706	0.3882
0.0860	0.4761	0.0855	0.4639	0.0857	0.4296	0.0776	0.3647	0.0781	0.3952
0.0910	0.4787	0.0905	0.4631	0.0907	0.4299	0.0851	0.3761	0.0856	0.4017
0.0940	0.4787	0.0945	0.4663	0.0947	0.4354	0.0901	0.3888	0.0906	0.4067
0.0970	0.4816	0.0975	0.4684	0.0987	0.4348	0.0951	0.3911	0.0956	0.4094
0.1000	0.4779	0.1005	0.4658	0.1017	0.4351	0.0991	0.3983	0.0996	0.4143
0.1075	0.4779	0.1077	0.4658	0.1078	0.4351	0.1021	0.4030	0.1026	0.4131
						0.1081	0.4030	0.1081	0.4131

Rough X = 6 m
Water Surface Elevation = 0.1271 m (5 point average)

Z = 0.213 m		Z = 0.274 m		Z = 0.335 m	
y (m)	u (m/s)	y (m)	u (m/s)	y (m)	u (m/s)
0.0000	0.0000	0.0000	0.0000	0.0000	0.0000
0.0068	0.1952	0.0064	0.1907	0.0072	0.1971
0.0075	0.2106	0.0077	0.2164	0.0089	0.2221
0.0090	0.2287	0.0097	0.2341	0.0114	0.2445
0.0140	0.2756	0.0137	0.2715	0.0164	0.2823
0.0190	0.3048	0.0187	0.3089	0.0214	0.3207
0.0290	0.3454	0.0287	0.3582	0.0289	0.3504
0.0390	0.3811	0.0387	0.3920	0.0389	0.3794
0.0490	0.4051	0.0487	0.4103	0.0489	0.4109
0.0590	0.4217	0.0587	0.4302	0.0589	0.4325
0.0690	0.4342	0.0687	0.4519	0.0689	0.4483
0.0765	0.4433	0.0762	0.4631	0.0764	0.4703
0.0840	0.4464	0.0837	0.4764	0.0839	0.4756
0.0890	0.4514	0.0887	0.4813	0.0889	0.4849
0.0940	0.4541	0.0937	0.4857	0.0939	0.4890
0.0980	0.4544	0.0977	0.4862	0.0979	0.4928
0.1010	0.4533	0.1007	0.4870	0.1009	0.4941
0.1090	0.4533	0.1085	0.4870	0.1024	0.4938
				0.1093	0.4938

Z = -0.244 m		Z = -0.183 m		Z = -0.061 m		Z = 0.061 m		Z = 0.183 m	
y (m)	u (m/s)	y (m)	u (m/s)	y (m)	u (m/s)	y (m)	u (m/s)	y (m)	u (m/s)
0.0000	0.0000	0.0000	0.0000	0.0000	0.0000	0.0000	0.0000	0.0000	0.0000
0.0065	0.1926	0.0058	0.1750	0.0069	0.1996	0.0058	0.1570	0.0068	0.1920
0.0139	0.2801	0.0121	0.2555	0.0119	0.2545	0.0106	0.2232	0.0097	0.2232
0.0239	0.3352	0.0221	0.3109	0.0219	0.3295	0.0206	0.2836	0.0197	0.3036
0.0339	0.3731	0.0321	0.3337	0.0319	0.3721	0.0306	0.3133	0.0297	0.3385
0.0439	0.4082	0.0421	0.3616	0.0419	0.3983	0.0406	0.3396	0.0397	0.3761
0.0539	0.4214	0.0521	0.3781	0.0519	0.4173	0.0506	0.3568	0.0497	0.3939
0.0639	0.4377	0.0621	0.3814	0.0619	0.4285	0.0606	0.3647	0.0597	0.4088
0.0739	0.4489	0.0721	0.3986	0.0719	0.4359	0.0706	0.3817	0.0697	0.4199
0.0839	0.4574	0.0821	0.4067	0.0819	0.4436	0.0806	0.3866	0.0797	0.4305
0.0914	0.4631	0.0921	0.4103	0.0919	0.4536	0.0906	0.4045	0.0897	0.4357
0.0979	0.4609	0.0991	0.4173	0.0969	0.4472	0.0956	0.4103	0.0957	0.4331
0.1009	0.4620	0.1066	0.4173	0.1009	0.4514	0.1016	0.4176	0.1017	0.4396
0.1067	0.4620			0.1076	0.4514	0.1086	0.4176	0.1086	0.4396

Z = 0.244 m	
y (m)	u (m/s)
0.0000	0.0000
0.0069	0.1996
0.0096	0.2320
0.0196	0.3164
0.0296	0.3483
0.0396	0.3853
0.0496	0.4106
0.0596	0.4279
0.0696	0.4541
0.0796	0.4679
0.0896	0.4792
0.0956	0.4841
0.1016	0.4816
0.1087	0.4816

Extra profiles
Rough X = 6 m
Water Surface Elevation = 0.1271 m (5 point average)

Rough X = 7 m
Water Surface Elevation = 0.1260 m (5 point average)

Z = -0.335 m		Z = -0.274 m		Z = -0.213 m		Z = -0.152 m		Z = -0.091 m	
y (m)	u (m/s)	y (m)	u (m/s)	y (m)	u (m/s)	y (m)	u (m/s)	y (m)	u (m/s)
0.0000	0.0000	0.0000	0.0000	0.0000	0.0000	0.0000	0.0000	0.0000	0.0000
0.0060	0.1786	0.0060	0.1820	0.0060	0.1881	0.0060	0.1570	0.0055	0.1714
0.0075	0.1990	0.0081	0.2158	0.0074	0.2082	0.0094	0.2003	0.0075	0.2046
0.0095	0.2249	0.0106	0.2430	0.0099	0.2440	0.0144	0.2346	0.0125	0.2631
0.0120	0.2495	0.0156	0.2819	0.0149	0.2867	0.0219	0.2734	0.0200	0.3007
0.0170	0.2841	0.0231	0.3280	0.0224	0.3246	0.0319	0.3015	0.0300	0.3288
0.0245	0.3188	0.0331	0.3626	0.0324	0.3684	0.0419	0.3250	0.0400	0.3589
0.0345	0.3533	0.0431	0.3927	0.0424	0.3958	0.0519	0.3407	0.0500	0.3748
0.0445	0.3856	0.0531	0.4185	0.0524	0.4149	0.0619	0.3547	0.0600	0.3850
0.0545	0.4115	0.0631	0.4334	0.0624	0.4241	0.0719	0.3657	0.0700	0.3923
0.0645	0.4316	0.0731	0.4483	0.0724	0.4276	0.0794	0.3751	0.0775	0.3980
0.0745	0.4425	0.0806	0.4577	0.0799	0.4316	0.0869	0.3827	0.0850	0.4058
0.0820	0.4580	0.0881	0.4652	0.0874	0.4351	0.0919	0.3888	0.0900	0.4076
0.0895	0.4650	0.0931	0.4666	0.0924	0.4316	0.0959	0.3898	0.0940	0.4106
0.0945	0.4761	0.0971	0.4706	0.0964	0.4313	0.0989	0.3961	0.0980	0.4140
0.0975	0.4782	0.1006	0.4668	0.1014	0.4316	0.1019	0.3952	0.1010	0.4134
0.1005	0.4732	0.1075	0.4668	0.1086	0.4316	0.1084	0.3952	0.1086	0.4134
0.1072	0.4732								

Rough X = 7 m
Water Surface Elevation = 0.1260 m (5 point average)

Z = -0.030 m		Z = 0.0 m		Z = 0.030 m		Z = 0.091 m		Z = 0.152 m	
y (m)	u (m/s)	y (m)	u (m/s)	y (m)	u (m/s)	y (m)	u (m/s)	y (m)	u (m/s)
0.0000	0.0000	0.0000	0.0000	0.0000	0.0000	0.0000	0.0000	0.0000	0.0000
0.0065	0.2009	0.0060	0.1996	0.0068	0.2009	0.0055	0.1339	0.0065	0.1874
0.0080	0.2298	0.0082	0.2276	0.0075	0.2112	0.0064	0.1438	0.0073	0.1984
0.0125	0.2792	0.0117	0.2724	0.0095	0.2378	0.0079	0.1663	0.0083	0.2158
0.0200	0.3284	0.0192	0.3203	0.0120	0.2603	0.0104	0.1984	0.0108	0.2388
0.0300	0.3738	0.0292	0.3688	0.0145	0.2779	0.0129	0.2076	0.0133	0.2555
0.0400	0.4051	0.0392	0.4014	0.0195	0.3121	0.0179	0.2293	0.0183	0.2919
0.0500	0.4299	0.0492	0.4287	0.0295	0.3518	0.0279	0.2674	0.0283	0.3322
0.0600	0.4433	0.0592	0.4399	0.0395	0.3798	0.0379	0.2940	0.0383	0.3613
0.0700	0.4508	0.0692	0.4430	0.0495	0.3955	0.0479	0.3164	0.0483	0.3811
0.0775	0.4577	0.0767	0.4447	0.0595	0.4064	0.0579	0.3348	0.0583	0.3892
0.0850	0.4544	0.0842	0.4469	0.0695	0.4115	0.0679	0.3518	0.0683	0.4014
0.0900	0.4574	0.0892	0.4492	0.0795	0.4137	0.0779	0.3633	0.0783	0.4073
0.0950	0.4571	0.0942	0.4500	0.0870	0.4185	0.0879	0.3798	0.0858	0.4112
0.0990	0.4569	0.0982	0.4522	0.0945	0.4229	0.0929	0.3869	0.0933	0.4140
0.1020	0.4582	0.1012	0.4472	0.0995	0.4226	0.0979	0.3942	0.0983	0.4140
0.1083	0.4582	0.1083	0.4472	0.1025	0.4226	0.1009	0.3952	0.1013	0.4137
				0.1080	0.4226	0.1082	0.3952	0.1088	0.4137

Rough X = 7 m
Water Surface Elevation = 0.1260 m (5 point average)

Z = 0.213 m		Z = 0.274 m		Z = 0.335 m	
y (m)	u (m/s)	y (m)	u (m/s)	y (m)	u (m/s)
0.0000	0.0000	0.0000	0.0000	0.0000	0.0000
0.0065	0.1926	0.0055	0.1786	0.0060	0.1799
0.0080	0.2106	0.0068	0.2009	0.0072	0.1984
0.0105	0.2378	0.0093	0.2298	0.0097	0.2293
0.0130	0.2608	0.0118	0.2593	0.0122	0.2530
0.0180	0.2999	0.0168	0.2957	0.0172	0.2858
0.0280	0.3407	0.0268	0.3447	0.0272	0.3326
0.0380	0.3798	0.0368	0.3824	0.0372	0.3745
0.0480	0.4091	0.0468	0.4011	0.0472	0.4045
0.0580	0.4276	0.0568	0.4285	0.0572	0.4229
0.0680	0.4433	0.0668	0.4453	0.0672	0.4402
0.0780	0.4547	0.0768	0.4655	0.0772	0.4571
0.0855	0.4609	0.0843	0.4761	0.0847	0.4700
0.0930	0.4615	0.0918	0.4844	0.0922	0.4761
0.0980	0.4639	0.0968	0.4839	0.0972	0.4834
0.1010	0.4631	0.0998	0.4870	0.1002	0.4841
0.1089	0.4631	0.1096	0.4870	0.1097	0.4841

Rough X = 8 m
Water Surface Elevation = 0.1250 m (5 point average)

Z = -0.335 m		Z = -0.274 m		Z = -0.213 m		Z = -0.152 m		Z = -0.091 m	
y (m)	u (m/s)	y (m)	u (m/s)	y (m)	u (m/s)	y (m)	u (m/s)	y (m)	u (m/s)
0.0000	0.0000	0.0000	0.0000	0.0000	0.0000	0.0000	0.0000	0.0000	0.0000
0.0060	0.1793	0.0068	0.1939	0.0063	0.1926	0.0070	0.1757	0.0075	0.1806
0.0074	0.2070	0.0074	0.2015	0.0088	0.2293	0.0089	0.1971	0.0086	0.1996
0.0099	0.2325	0.0099	0.2341	0.0138	0.2724	0.0114	0.2193	0.0111	0.2135
0.0149	0.2788	0.0149	0.2756	0.0213	0.3322	0.0164	0.2480	0.0136	0.2346
0.0224	0.3188	0.0224	0.3101	0.0313	0.3585	0.0214	0.2819	0.0186	0.2711
0.0324	0.3511	0.0324	0.3578	0.0413	0.3974	0.0314	0.3168	0.0236	0.2914
0.0424	0.3804	0.0424	0.3850	0.0513	0.4112	0.0414	0.3403	0.0311	0.3261
0.0524	0.4082	0.0524	0.4103	0.0613	0.4276	0.0514	0.3543	0.0411	0.3414
0.0624	0.4235	0.0624	0.4337	0.0713	0.4339	0.0614	0.3620	0.0511	0.3674
0.0724	0.4425	0.0724	0.4425	0.0788	0.4405	0.0714	0.3775	0.0611	0.3725
0.0799	0.4464	0.0799	0.4566	0.0863	0.4433	0.0814	0.3898	0.0711	0.3923
0.0874	0.4612	0.0874	0.4615	0.0913	0.4399	0.0889	0.4017	0.0811	0.4021
0.0924	0.4682	0.0924	0.4666	0.0953	0.4408	0.0964	0.4045	0.0886	0.4082
0.0964	0.4719	0.0974	0.4706	0.0983	0.4458	0.0999	0.4079	0.0961	0.4128
0.0994	0.4743	0.1009	0.4671	0.1013	0.4433	0.1024	0.4058	0.1001	0.4140
0.1078	0.4743	0.1089	0.4671	0.1088	0.4433	0.1092	0.4058	0.1031	0.4173
								0.1098	0.4173

Rough X = 8 m
Water Surface Elevation = 0.1250 m (5 point average)

Z = -0.030 m		Z = 0.0 m		Z = 0.030 m		Z = 0.091 m		Z = 0.152 m	
y (m)	u (m/s)	y (m)	u (m/s)	y (m)	u (m/s)	y (m)	u (m/s)	y (m)	u (m/s)
0.0000	0.0000	0.0000	0.0000	0.0000	0.0000	0.0000	0.0000	0.0000	0.0000
0.0068	0.1939	0.0061	0.1793	0.0055	0.1685	0.0060	0.1438	0.0070	0.1714
0.0083	0.2170	0.0071	0.2058	0.0070	0.2021	0.0086	0.1750	0.0075	0.1861
0.0098	0.2287	0.0091	0.2320	0.0085	0.2265	0.0111	0.2052	0.0095	0.1984
0.0148	0.2779	0.0141	0.2765	0.0110	0.2515	0.0161	0.2238	0.0145	0.2440
0.0198	0.3105	0.0216	0.3269	0.0160	0.2902	0.0211	0.2584	0.0220	0.2889
0.0298	0.3595	0.0291	0.3620	0.0210	0.3176	0.0286	0.2792	0.0295	0.3133
0.0398	0.3898	0.0391	0.3920	0.0285	0.3486	0.0386	0.3089	0.0395	0.3374
0.0498	0.4179	0.0491	0.4170	0.0385	0.3798	0.0486	0.3172	0.0495	0.3620
0.0598	0.4290	0.0591	0.4331	0.0485	0.3993	0.0586	0.3392	0.0595	0.3698
0.0698	0.4374	0.0691	0.4396	0.0585	0.4103	0.0686	0.3497	0.0695	0.3853
0.0798	0.4425	0.0791	0.4408	0.0685	0.4202	0.0786	0.3664	0.0795	0.4005
0.0873	0.4436	0.0866	0.4458	0.0785	0.4185	0.0861	0.3738	0.0870	0.4036
0.0948	0.4475	0.0941	0.4461	0.0860	0.4229	0.0936	0.3843	0.0945	0.4112
0.0998	0.4486	0.0991	0.4450	0.0935	0.4244	0.0986	0.3933	0.0995	0.4152
0.1038	0.4469	0.1031	0.4453	0.0985	0.4255	0.1026	0.3955	0.1045	0.4167
0.1096	0.4469	0.1097	0.4453	0.1025	0.4276	0.1108	0.3955	0.1106	0.4167
				0.1099	0.4276				

Rough X = 8 m
Water Surface Elevation = 0.1250 m (5 point average)

Z = 0.213 m		Z = 0.274 m		Z = 0.335 m	
y (m)	u (m/s)	y (m)	u (m/s)	y (m)	u (m/s)
0.0000	0.0000	0.0000	0.0000	0.0000	0.0000
0.0070	0.1827	0.0065	0.1847	0.0069	0.1806
0.0091	0.2094	0.0082	0.2100	0.0081	0.2058
0.0111	0.2271	0.0132	0.2550	0.0106	0.2303
0.0141	0.2515	0.0182	0.2871	0.0156	0.2715
0.0216	0.2936	0.0232	0.3160	0.0206	0.2961
0.0291	0.3311	0.0282	0.3363	0.0281	0.3280
0.0391	0.3715	0.0382	0.3667	0.0381	0.3681
0.0491	0.3917	0.0482	0.4082	0.0481	0.3930
0.0591	0.4115	0.0582	0.4149	0.0581	0.4161
0.0691	0.4241	0.0682	0.4413	0.0681	0.4328
0.0791	0.4345	0.0782	0.4552	0.0781	0.4492
0.0866	0.4436	0.0882	0.4679	0.0856	0.4555
0.0941	0.4497	0.0932	0.4737	0.0931	0.4711
0.0991	0.4514	0.0982	0.4779	0.0981	0.4732
0.1016	0.4519	0.1012	0.4735	0.1021	0.4737
0.1041	0.4514	0.1042	0.4810	0.1051	0.4803
0.1111	0.4514	0.1108	0.4810	0.1107	0.4803

APPENDIX 3

Tabulation of Bauer(1954) and Delleur(1957) data

y	X = 0.621 m	X = 0.951 m	X = 1.265 m	X = 1.570 m	X = 1.881 m	X = 2.208 m	X = 2.510 m	X = 2.811 m	X = 3.119 m	X = 3.421 m	X = 3.726 m	X = 4.031 m
	u	u	u	u	u	u	u	u	u	u	u	u
(m)	(m/s)	(m/s)	(m/s)	(m/s)	(m/s)	(m/s)	(m/s)	(m/s)	(m/s)	(m/s)	(m/s)	(m/s)
0.00104	2.6584	2.9512	3.2221	3.4848	3.7119	3.9167	4.1149	4.3356	4.5220	4.6959	4.9121	5.0020
0.00152	2.8234	3.1596	3.4621	3.6505	3.8912	4.1509	4.3514	4.5881	4.6925	4.9228	5.1084	5.1831
0.00183	2.8814	3.2550	3.5281	3.7444	4.0233	4.2639	4.4439	4.6620	4.8028	4.9947	5.2019	5.3242
0.00213	2.9512	3.3074	3.5953	3.8019	4.0881	4.3419	4.5089	4.7681	4.9299	5.0825	5.2972	5.4335
0.00244	3.0315	3.3777	3.6931	3.8828	4.1509	4.4150	4.6216	4.8237	4.9947	5.2057	5.3981	5.5169
0.00274	3.0580	3.4321	3.7200	3.9625	4.1994	4.4536	4.6823	4.9156	5.0825	5.2627	5.4611	5.5976
0.00305	3.0915	3.4873	3.7635	4.0204	4.2762	4.4861	4.7611	4.9550	5.1307	5.3242	5.5209	5.6547
0.00366	3.1665	3.5563	3.8884	4.1690	4.3831	4.6283	4.8378	5.0531	5.2284	5.4413	5.6383	5.7792
0.00427	3.2338	3.6426	3.9567	4.2330	4.4828	4.7199	4.9658	5.1493	5.3590	5.5450	5.7249	5.9193
0.00488	3.3122	3.7119	4.0468	4.3105	4.5352	4.7923	5.0384	5.2474	5.4691	5.6342	5.8340	5.9928
0.00549	3.3509	3.7772	4.1059	4.3958	4.6350	4.8943	5.0899	5.3164	5.5049	5.6959	5.8893	6.0848
0.00610	3.3974	3.8324	4.1841	4.4796	4.7028	4.9407	5.1944	5.4572	5.5450	5.7624	5.9711	6.1559
0.00701	3.4672	3.9054	4.2949	4.5319	4.7923	5.0531	5.2780	5.5450	5.6918	5.8936	6.0804	6.2595
0.00792	3.5281	3.9481	4.3514	4.6620	4.8978	5.1718	5.3396	5.6220	5.7834	5.9711	6.1782	6.3648
0.00884	3.5460	4.0117	4.3894	4.7508	4.9514	5.2398	5.4335	5.6794	5.8893	6.0804	6.2640	6.4298
0.00975	3.5589	4.0380	4.4536	4.7785	5.0568	5.3164	5.5571	5.7666	5.9711	6.1559	6.3188	6.5239
0.01067	3.5641	4.0615	4.4796	4.8237	5.0973	5.3785	5.5976	5.8467	6.0320	6.2459	6.4345	6.6144
0.01189		4.0674	4.5352	4.8978	5.1718	5.4651	5.6877	5.9365	6.1425	6.3372	6.5144	6.7111
0.01311		4.0674	4.5682	4.9192	5.2436	5.5410	5.7834	6.0058	6.2187	6.4252	6.5857	6.7698
0.01433			4.5649	4.9478	5.2818	5.5854	5.8467	6.0804	6.3142	6.5049	6.6675	6.8738
0.01554				4.9586	5.3087	5.6220	5.8850	6.1559	6.3787	6.5714	6.7355	6.9390
0.01676				4.9514	5.3396	5.6424	5.9494	6.2007	6.4392	6.6289	6.8390	7.0149
0.01829					5.3552	5.6835	5.9754	6.2549	6.5097	6.7160	6.9138	7.0969
0.02134					5.3629	5.6835	6.0058	6.3188	6.5666	6.8192	7.0507	7.2268
0.02438							6.0145	6.3280	6.6096	6.8938	7.1227	7.3645
0.03048								6.3372	6.6192	6.9189	7.1797	7.4020
0.03658										6.9239	7.2006	7.4559
0.04267												7.4721

X	δ	Depth (m)
(m)	(m)	from
		continuity
0.621	0.0084	0.0973
0.951	0.0097	0.0855
1.265	0.0114	0.0766
1.570	0.0128	0.0709
1.881	0.0146	0.0659
2.208	0.0160	0.0624
2.510	0.0177	0.0593
2.811	0.0193	0.0565
3.119	0.0211	0.0544
3.421	0.0229	0.0524
3.726	0.0246	0.0507
4.031	0.0269	0.0492

Velocity profiles scaled off figure from Bauer(1954)
Smooth experiment

y	X = 0.532 m	X = 0.870 m	X = 1.176 m	X = 1.491 m	X = 1.797 m	X = 2.106 m	X = 2.416 m	X = 2.722 m	X = 3.028 m	X = 3.337 m	X = 3.643 m	X = 3.949 m
(m)	u (m/s)	u (m/s)	u (m/s)	u (m/s)	u (m/s)	u (m/s)	u (m/s)	u (m/s)	u (m/s)	u (m/s)	u (m/s)	u (m/s)
0.00061	1.8879	2.2134	2.2808	2.3375	2.4753	2.5975	2.7084	2.8472	2.8942	2.9959		3.1638
0.00091	1.9525	2.2114	2.3375	2.4131	2.6117	2.7731	2.8942	2.9959	3.0703	3.2043		3.3351
0.00122	2.0359	2.3164	2.4685	2.5414	2.7480	2.9312	3.0481	3.1552	3.2365	3.3625	3.4025	3.5381
0.00152	2.1578	2.4021	2.5880	2.6765	2.8706	3.0731	3.1927	3.2840	3.3686	3.5188	3.5899	3.7161
0.00183	2.2540	2.4911	2.6863	2.7832	2.9932	3.1725	3.3200	3.4118	3.5157	3.6458	3.7500	3.8642
0.00213	2.3164	2.6022	2.7656	2.8706	3.0703	3.2720	3.4335	3.5061	3.6791	3.7912	3.8748	4.0256
0.00244	2.3782	2.6523	2.8602	2.9959	3.1898	3.3932	3.5349	3.6128	3.7671	3.8502	3.9638	4.1331
0.00274	2.4551	2.7257	2.9473	3.0759	3.2750	3.4712	3.6161	3.7195	3.8293	4.0000	4.0920	4.2242
0.00305	2.5276	2.7908	2.9986	3.1210	3.3230	3.5285	3.7093	3.8154	3.9387	4.0623	4.1860	4.3489
0.00366	2.6499	2.8942	3.1097	3.2989	3.4870	3.6724	3.8293	3.9710	4.1069	4.2667	4.3608	4.5470
0.00427	2.7530	3.0095	3.2102	3.4056	3.6128	3.8015	3.9964	4.1143	4.2051	4.4126	4.5346	4.6558
0.00488	2.8446	3.1068	3.3473	3.4870	3.7296	3.9208	4.1143	4.2473	4.3648	4.5059	4.6473	4.7845
0.00549	2.9366	3.1956	3.4273	3.5801	3.8154	4.0219	4.1860	4.3489	4.4854	4.6642	4.7628	4.9346
0.00610	3.0095	3.3079	3.5188	3.6825	3.9173	4.0994	4.2551	4.4570	4.6136	4.7584	4.8722	5.0435
0.00701	3.1323	3.4304	3.6326	3.8572	4.0623	4.2551	4.4167	4.5885	4.7584	4.9078	5.0389	5.2018
0.00792	3.2307	3.5349	3.7705	3.9566	4.1708	4.3687	4.5387	4.7068	4.8590	5.0252	5.1594	5.3020
0.00884	3.3200	3.6425	3.8607	4.0586	4.2667	4.4814	4.6304	4.7801	4.9616	5.1081	5.2828	5.4140
0.00975	3.3809	3.6858	3.9674	4.1557	4.3648	4.5760	4.7326	4.9167	5.0618	5.2018	5.3553	5.5234
0.01067	3.4523	3.7981	4.0623	4.2667	4.4692	4.6727	4.8546	5.0343	5.1923	5.3310	5.4834	5.6145
0.01189	3.5125	3.8960	4.1670	4.4046	4.5885	4.8063	4.9616	5.1407	5.2876	5.4239	5.6094	5.7383
0.01311	3.5413	3.9783	4.2706	4.5018	4.6983	4.9123	5.0849	5.2636	5.4091	5.5789	5.6968	5.9077
0.01433	3.5704	4.0329	4.3489	4.5885	4.7975	5.0252	5.2350	5.3797	5.5034	5.6761	5.8277	5.9617
0.01554	3.5769	4.0586	4.4086	4.6897	4.8722	5.1081	5.2780	5.4436	5.6094	5.7592	5.8916	6.0380
0.01676		4.0771	4.4570	4.7369	4.9661	5.1923	5.3602	5.5334	5.7175	5.8543	5.9997	6.1937
0.01829		4.0994	4.5018	4.8325	5.0572	5.3020	5.4884	5.6452	5.7802	5.9238	6.1376	6.2958
0.02134		4.1031	4.5264	4.9167	5.1923	5.4784	5.6606	5.8543	6.0106	6.1824	6.3188	6.5053
0.02438			4.5511	4.9436	5.3117	5.5738	5.8013	6.0052	6.1993	6.3939	6.4934	6.6851
0.03048			4.5470	4.9436	5.3651	5.6813	5.9834	6.1937	6.4464	6.6427	6.8077	7.0534
0.03658					5.3748	5.7019	6.0216	6.3188	6.5706	6.8139	7.0342	7.2550
0.04267					5.3846	5.6968	6.0270	6.3476	6.6126	6.9201	7.1502	7.3948
0.04877							6.0325	6.3649	6.6367	6.9138	7.1894	
0.05486											7.1698	

X	δ	Depth (m)
(m)	(m)	from continuity
0.5325	0.0120	0.0981
0.8697	0.0137	0.0863
1.1758	0.0173	0.0786
1.4912	0.0199	0.0731
1.7973	0.0229	0.0662
2.1064	0.0249	0.0648
2.4156	0.0278	0.0620
2.7217	0.0305	0.0596
3.0277	0.0329	0.0578
3.3369	0.0352	0.0560
3.6429	0.0366	0.0547
3.9489	0.0393	0.0531

Velocity profiles scaled off figure from Bauer(1954)
Rough experiment

Velocity profiles scaled off Figure from Delleur(1957)

Z = 0 m		Z = 0.030 m		Z = 0.061 m		Z = 0.091 m		Z = 0.122 m	
y (m)	u (m/s)	y (m)	u (m/s)	y (m)	u (m/s)	y (m)	u (m/s)	y (m)	u (m/s)
0.0000	0.0000	0.0000	0.0000	0.0000	0.0000	0.0000	0.0000	0.0000	0.0000
0.0008	0.3246	0.0008	0.3115	0.0008	0.2957	0.0014	0.3292	0.0008	0.3200
0.0014	0.3459	0.0014	0.3414	0.0014	0.3216	0.0020	0.3444	0.0014	0.3414
0.0020	0.3688	0.0020	0.3734	0.0020	0.3383	0.0026	0.3627	0.0020	0.3597
0.0026	0.3871	0.0026	0.3850	0.0026	0.3545	0.0033	0.3719	0.0026	0.3764
0.0033	0.4023	0.0033	0.4039	0.0033	0.3597	0.0045	0.3901	0.0033	0.3856
0.0045	0.4298	0.0045	0.4237	0.0045	0.3801	0.0058	0.4060	0.0045	0.4048
0.0058	0.4481	0.0058	0.4359	0.0058	0.3901	0.0071	0.4176	0.0058	0.4188
0.0071	0.4633	0.0071	0.4502	0.0071	0.4054	0.0083	0.4298	0.0083	0.4420
0.0083	0.4764	0.0083	0.4663	0.0083	0.4145	0.0108	0.4459	0.0108	0.4602
0.0108	0.5014	0.0108	0.4846	0.0108	0.4328	0.0133	0.4633	0.0133	0.4785
0.0133	0.5182	0.0133	0.5060	0.0133	0.4450	0.0159	0.4755	0.0159	0.4862
0.0159	0.5319	0.0159	0.5151	0.0159	0.4542	0.0184	0.4846	0.0184	0.4968
0.0184	0.5395	0.0184	0.5243	0.0184	0.4663	0.0210	0.4892	0.0210	0.5060
0.0210	0.5425	0.0210	0.5364	0.0210	0.4785	0.0235	0.4990	0.0235	0.5121
0.0235	0.5456	0.0235	0.5425	0.0235	0.4816	0.0260	0.5008	0.0260	0.5197
0.0260	0.5471	0.0260	0.5517	0.0260	0.4877	0.0324	0.5121	0.0324	0.5249
0.0324	0.5486	0.0324	0.5544	0.0324	0.4968	0.0386	0.5258	0.0386	0.5331
0.0386	0.5486	0.0386	0.5550	0.0386	0.5060	0.0439	0.5334	0.0439	0.5364
0.0488	0.5465	0.0485	0.5560	0.0439	0.5151	0.0488	0.5364	0.0488	0.5395
				0.0480	0.5212				